CHARLES UNIVERSITY IN PRAGUE
MEDICAL FACULTY IN PILSEN
ŠIKLS' DEPARTMENT OF PATHOLOGY

DISSERTATION

CORRELATION OF IMMUNOHISTOCHEMISTRY AND MOLECULAR BIOLOGIC METHODS IN THE DIAGNOSIS OF TUMORS

MUDr. Michael MICHAL

Supervisor: Prof. MUDr. Alena Skálová, CSc.
Pilsen 2018

FOREWORD

While morphology is, and for many decades to come will remain the mainstay of the histopathological diagnosis, an accurate classification of neoplastic disorders is today in many cases impossible without the adjuvant methods of immunohistochemistry (IHC) and molecular genetics. Although there is a continuing effort to discover new sensitive and specific IHC antibodies that would be useful in laboratory practice, an even more intense effort is being exerted to widen our understanding of the molecular underpinnings of neoplastic diseases, particularly since the advent of next-generation sequencing (NGS) in the recent years. Such understanding can be later utilized in many ways. For instance, the knowledge of a rearrangement of a given tumor can later lead to the development of the very specific and sensitive antibody. Secondly, it can become itself diagnostically useful and be easily detected by some relatively cheap molecular genetic method such as fluorescence in situ hybridization (FISH), or by other methods that are becoming more widely available and affordable, including NGS itself. Thus, in both cases, it facilitates rendering of an accurate diagnosis. Thirdly, such rearrangement can lead to the development of novel, highly specific drugs which may target these rearrangements and improve patient's survival. Lastly, the knowledge of the molecular background of tumors allows for the refinement of the tumor classification which in turn leads to the availability of a better risk stratification groups for malignant tumors but also to an increase of pure academic knowledge. At first sight, for examples, when one type of a benign tumor is separated from a heterogeneous group of others, completely innocuous tumors, it may appear that mere academic progress has been achieved. However, such progress usually concomitantly leads to an increase of a deeper understanding of tumorigenesis whose impact and significance are impossible to predict.

Apart from hematopathology and perhaps neuropathology, there are very few areas of surgical pathology where IHC and molecular genetics play such a critical role as in the diagnosis of soft tissue tumors. In fact, it is our experience that today a diagnosis of any soft tissue tumor is rarely made without the use of a least a few IHC markers, and when rendering the diagnosis of sarcoma, IHC and increasingly, molecular genetics, is used almost invariably.

Since soft tissue tumors represent a highly complex group of usually very rare neoplasms whose diagnosis often necessitates advanced laboratory equipment, much of these lesions are usually concentrated in only a few large pathology centers. The author of this thesis is fortunate enough to work at an institution which receives arguably one the highest amount of both routine and consultation soft tissue tumor cases in the whole Central European region. In the last quarter of a century, this institution has also been very effective in the creation and administration of its tumor registry. In this archive of rare tumors, of which the soft tissue tumors represent a very significant part, all cases are precisely assorted using specific keywords. When necessary, any given case can be searched and obtained for review within few hours. For those interested, these circumstances along with the presence of several acknowledged soft tissue experts at the department, provide a unique environment to learn and study soft tissue tumors, as well as many other neoplasms. Therefore, the author of this thesis focused his research mostly (but not exclusively) on mesenchymal neoplasms. The intent of his publications was to study and find novel ways and clues which could help others to arrive at the correct diagnosis as well as to propose novel approaches and categories for classification of certain tumors. To achieve this goal, he and his colleagues approached every topic the same way a pathologist works in practice. With a novel hypothesis in mind, we first strived for a precise morphological assessment of the

material, followed by the IHC analysis. In cases where it was desirable and necessary, molecular genetic analysis followed.

Using this approach, the author of this thesis produced altogether 13 manuscripts as the main researcher, 11 of which focused on mesenchymal lesions. The remaining two studies reported one peculiar penile tumor and one head and neck neoplasm which, along with most of the 20 publications he co-authored, are dealing with the other areas of surgical pathology largely researched at his institution – head and neck pathology and the pathology of testicular and penile tumors. Apart from two contributions deliberately sent to non-impacted journals, all other studies were published in international journals with an impact factor, in many cases representing some of the best journals in this field of medicine.

The thesis is conceived as a collection of commentaries on each manuscript followed by a copy of every publication. It is divided into two main parts. In the initial one, the first authored manuscripts are discussed, the second summarizes the co-authored publications. Each of the two parts is then divided based on the body system it concerns.

STATEMENT

Hereby I confirm that I prepared this dissertation by myself and correctly cited all used sources. I agree with the storage of the digital version of this work in the database of Charles University in Prague, Medical Faculty in Pilsen.

Pilsen, 25th April 2018

SUMMARY

This thesis is a collection of commentaries on altogether 13 first-authored and 20 co-authored publications where morphology, immunohistochemistry (IHC) and molecular genetic methods were used to provide novel clues for arriving at an accurate diagnosis of tumors, as well as to propose novel approaches and refinement of classification of certain tumors. The presented manuscripts are the result of the postgraduate studies of MUDr. Michael Michal at the Charles University in Prague, Faculty of Medicine in Pilsen in the period between 2015-2018. The author focused the main part of his research, particularly his first-authored manuscripts, on soft tissue tumors but also largely participated in research activities focusing on other body systems. Over the course of his studies, four main areas of interests within the topic of soft tissue pathology emerged.

The first is oriented on soft tissue tumors of presumed (but unconfirmed) fibroblastic lineage. First two publications regard two related low-grade sarcomas called Myxoinflammatory fibroblastic sarcoma (MIFS) and Pleomorphic hyalinizing angiectatic tumor (PHAT). In the first manuscript, a high-grade variant of the former is described. The latter publication is focused on the morphological and IHC similarities between both MIFS and PHAT. The third and very recent publication describes 4 novel cases of an emerging entity provisionally called acral fibroblastic spindle cell neoplasm with *EWSR1-SMAD3* fusion. Only one previous report of this tumor has been published, and our contribution thus helps to further characterize this apparently very rare tumor.

The second group of publications concerns tumors of the peripheral nerve sheath origin. Overall three papers from this area are presented. One reports on a novel, so far undescribed morphological feature of a plexiform neurofibroma. Other presents a special, highly cellular variant of perineurioma which may be easily mistaken for monophasic fibrous synovial sarcoma. The last manuscript is a review of hybrid peripheral nerve sheath tumor pathology.

The third part concerns peculiar histiocytic proliferations. Although most of them do not primarily affect soft tissue structures, since they may be easily mistaken for a carcinoma and occur over a wide anatomic range, they are often signed out by the soft tissue pathologists. As mentioned, they occur in many different organs and tissues and in most of them they bear a different name. We proposed a unifying concept and a common name for all these lesions and also studied their expression of various IHC markers.

The fourth area of interest are tumors of adipose tissue which became the center of the author's research in one larger paper and two letters to the editor. First paper scrutinized the relatively common lipomatous tumor called spindle cell/pleomorphic lipoma for the presence of lipoblasts. Since general pathologists often consider the presence of lipoblasts as an important feature for rendering the diagnosis of liposarcoma, their presence in spindle cell/pleomorphic lipoma, a benign mimic of liposarcoma, may lead to overdiagnosis. The first letter to the editor reports another worrisome and commonly present feature of spindle cell/pleomorphic lipoma – the occurrence of atypical mitosis. The latter letter to the editor is a reply to a comment made by another group of investigators in a reaction to our studies of spindle cell/pleomorphic lipoma.

Due to a large number of co-authored manuscripts, their summary was omitted, and they will be introduced only at the particular section of the thesis.

CONTENT

LIST OF ABBREVIATIONS

APLT - Atypical pleomorphic lipomatous tumor

DDL – Dedifferentiated liposarcoma

dSIL - Differentiated squamous intraepithelial lesion

EFH – Epithelioid fibrous histiocytoma

FDC – Follicular dendritic cells

FDCS – Follicular dendritic cell sarcoma

FGF23 - Fibroblastic growth factor 23

HPNST - Hybrid peripheral nerve sheath tumor

HPV - Human Papillomavirus

IHC - Immunohistochemistry

ISMC - Invasive stratified mucin-producing carcinoma

LCA – Littoral cell angioma

MF - Myofibroma

MICE – Mesothelial/monocytic cardiac excrescences

MIFS – Myxoinflammatory fibroblastic sarcoma

MMFC - Multivacuolated mucin-filled cells

MPNST – Malignant peripheral nerve sheath tumor

MSS - Monophasic fibrous synovial sarcoma

NGS – Next-generation sequencing

PCR - Polymerase chain reaction

PHAT – Pleomorphic hyalinizing angiectatic tumor

PMT – Phosphaturic mesenchymal tumor

PNST - Peripheral nerve sheath tumor

RB-1 - Retinoblastoma-1

SAF – Superficial acral fibromyxoma

SCL/PL - Spindle cell and pleomorphic lipoma

SMILE - Stratified mucin-producing intra-epithelial lesion

SPN-P - Solid pseudopapillary neoplasm of the pancreas

SSTR2A - Somatostatin receptor 2A

TIO – Tumor induced osteomalacia

WCP - Whorling cellular perineurioma

WHO – World health organization

COMMENTED PUBLICATIONS

1. PART
FIRST-AUTHOR MANUSCRIPTS

1.1. SOFT TISSUES

1.1.1. HIGH-GRADE MYXOINFLAMMATORY FIBROBLASTIC SARCOMA: A REPORT OF 23 CASES.

Myxoinflammatory fibroblastic sarcoma (MIFS) is a low-grade sarcoma originally described in 1998 by three independent groups of authors [1-3]. These tumors have a high propensity for local recurrence and were initially thought to occur exclusively in the distal extremities. As further studies have shown, this tumor may not be restricted to acral sites, and apart from local recurrence, six cases with metastatic disease have been documented in the literature so far [3-7]. Nonetheless, despite these publications, MIFS is still generally considered a low-grade neoplasm with a very low metastatic potential [6].

In our group, we have noticed that some examples of this tumor do not always show the classical low-grade morphology but display highly atypical cellular features. Therefore, we searched the Pilsner tumor archive for such examples. Aside from the obvious prerequisite of blastic tumor cells with a high degree of pleomorphism notable at first sight with numerous atypical to bizarre mitoses and frequent foci of necrosis, the inclusion criteria in our series were exclusively based on the fulfilling of 4, in our view, highly specific histopathologic features of MIFS (also valid for low-grade tumors). The first one was characterized by mats of neoplastic cells with eosinophilic cytoplasm having accentuated cell membranes, often created a resemblance to a mosaic. These areas had gradual transitions to less cohesive foci, in which the extracellular mucous substance began to percolate between cells. In foci, where larger amounts of extracellular mucin were present, the cells further separated producing mucin pools with scattered individual cells bearing a resemblance to a “dilapidated brick wall.” The other 3 characteristic features of MIFS are the occurrence of 3 different types of cells, which in our view might represent different stages of the development of a single cell population, namely, (1) lipoblast-like cells with an ample, distended, mucin-filled cytoplasm, compartmentalized by a variable number of intracytoplasmic septa, thus remotely resembling soccer balls; (2) large, polygonal, bizarre ganglion-like, also called Reed-Sternberg (RS)–like cells which featured inclusion-like nucleolus. (3) cells with emperipolesis of variable sizes, ranging from very inconspicuous neoplastic cells containing only one or a few engulfed cells to conspicuous large ones having virtually hundreds of inflammatory cells, usually polymorphonuclear leukocytes admixed with various numbers of some lymphoid cells, within the cytoplasm. Quite often, we found large neoplastic cells that combined the histologic features of all these 3 characteristic tumor cell types. In one case, in addition to the typical histologic appearance of high-grade MIFS, not different from other cases in our series, there was an area of spindle cell type of undifferentiated sarcoma. Another case contained the same high-grade MIFS and spindle cell undifferentiated sarcoma and in addition also an area of a low-grade MIFS. Using these criteria, we collected 23 specimens of this tumor.

Clinically, the 23 cases of HG MIFS affected mostly older people, with a mean age of 64.3 years (age ranged from 39-93 years). Some of these tumors were located at the acral sites, but the majority affected the proximal parts of the extremities, especially the thigh. Follow-up was available for 18 patients, of whom 9 developed metastatic disease and 7 of these died. Therefore, it confirmed that this highly atypical variant has a much more ominous prognosis that the classical MIFS.

MIFS has an uncharacteristic immunoprofile showing variable positivity with antibodies such as CD34, keratins, Actin S, CD68, D2-40 [6]. In our study, we analyzed the reactivity of these tumors with a variety of other antibodies that have not been tested on these tumors so far. Eventually, we discovered a strong and usually diffuse positivity with Cyclin D1. Although very unspecific, we found this antibody very useful in highlighting the cells with emperipolesis since the stain is expressed by the neoplastic cells but not by the engulfed inflammatory cells which are then easier to recognize.

At the time of publication, the genetic background of these tumors was largely unknown. Some cases of low-grade MIFS were found to harbor TGFBR3 and MGEA5 gene rearrangements. However, we knew from another research group that this rearrangement is present in only a very small subset of cases (later confirmed by some studies [8]). Therefore we did not include these molecular genetic methods in our study. Recently, it was shown that BRAF rearrangements are present in about 25% of low-grade MIFS [9] and it will be interesting to see, how many cases in our cohort of HG MIFS have this rearrangement.

In summary, our study found that MIFS, being so far considered as a low-grade sarcoma occurring mostly on acral sites, is an entity that encompasses the whole spectrum of lesions ranging from low-grade and relatively indolent neoplasms to high-grade tumors or entirely undifferentiated spindle cell/pleomorphic sarcoma with aggressive biological behavior. Of note, another recent paper presented additional cases of HG MIFS including a case with dedifferentiation therefore independently confirming our observations [10].

Annals of Diagnostic Pathology 19 (2015) 157–163

Contents lists available at ScienceDirect

Annals of Diagnostic Pathology

High-grade myxoinflammatory fibroblastic sarcoma: a report of 23 cases ☆

Michael Michal, MD [a,*], Dmitry V. Kazakov, MD, PhD [a], Ladislav Hadravský, MD [a], Zdeněk Kinkor, MD, PhD [a], Naoto Kuroda, MD [a], Michal Michal, MD [b]

[a] Department of Pathology, Charles University, Medical Faculty and Charles University Hospital Plzen, Plzen, Czech Republic
[b] Red Cross Hospital Kochi, Kochi, Japan

ARTICLE INFO

Keywords:
High-grade myxoinflammatory fibroblastic sarcoma
Undifferentiated sarcoma
Pleomorphic hyalinizing angiectatic tumor
Chondrosarcoma
Soft tissues

ABSTRACT

We describe 23 cases of high-grade myxoinflammatory fibroblastic sarcoma (MIFS). The patients were 15 women and 8 men, with the age ranging at the time of diagnosis from 39 to 93 years (mean, 64.3 years; median, 66 years). Follow-up was available for 18 patients, of whom 9 developed metastatic disease; 7 of these died. Most tumors showed a predilection for the soft tissues of the extremities, with 14 cases involving the lower limb and 5 the upper extremity. However, in both sites, the acral parts were affected in only 1 case each. Of the 4 remaining tumors, 2 were found in axilla, 1 was found in sacral area, and 1 developed in the scar on the breast, 14 years after previous excision of a mammary carcinoma and subsequent local irradiation. The tumor size ranged from 1.3 cm to as much as 30 cm in the largest dimension with a mean size of 8.3 cm. Histologically, the tumors were characterized by occurrence of 3 types of characteristic cells, including (1) lipoblast-like cells with an ample, distended, mucin-filled cytoplasm compartmentalized by a variable number of intracytoplasmic septa, thus remotely resembling soccer balls; (2) large, polygonal, bizarre ganglion-like cells similar to those seen in the Hodgkin disease, also called Reed-Sternberg–like cells. Within an ample, deeply eosinophilic cytoplasm, there was an oval nucleus with vesicular chromatin and a large, inclusion-like nucleolus. Binucleated, multinucleated, or more pleomorphic forms of these cells were also present; (3) cells with emperipolesis of variable sizes, ranging from very inconspicuous neoplastic cells containing only one to a few engulfed cells to conspicuous large ones having many inflammatory cells, usually polymorphonuclear leukocytes admixed with various numbers of some lymphoid cells, within the cytoplasm. Quite often, we found elements that combined the histologic features of all the above 3 characteristic tumor cell types. In 2 tumors, we found an additional undifferentiated spindle cell sarcoma component, whereas in another tumor, a chondrosarcomatous moiety was evident. For comparison, we studied 10 cases of pleomorphic hyalinizing angiectatic tumor (PHAT) of soft tissues. Based on the identification of morphological changes typical for MIFS within most of the cases of PHAT, we suggest that most cases of PHAT represent examples of MIFS merely having hyaline ectatic vessels.

1. Introduction

Myxoinflammatory fibroblastic sarcoma (MIFS) is an entity simultaneously described in 1998 by 3 different groups of authors under various names [1-3] as a low-grade soft tissue tumor of distal extremities with a high propensity for local recurrence. As further studies have shown, this tumor may not be restricted to acral sites, and apart from local recurrence, 6 cases with metastatic disease have been documented in the literature so far [3-7]. Nonetheless, in spite of these publications, MIFS is still generally considered a low-grade neoplasm [6] with a very low metastatic potential.

In this study, we present the largest series of 23 cases of MIFS with a high-grade morphology, along with an extensive clinical and follow-up data in most cases and novel important immunohistochemical findings.

2. Materials and methods

The 23 cases constituting the subject of the study were retrieved from the Pilsen Tumor Registry; they came from the period between years 1993 and 2014. The clinical information was extracted from the registry records, and follow-up data were obtained from attending clinicians. To retrieve the cases, we searched our consultation registry files using key words, including “myxoinflammatory fibroblastic sarcoma,” “myxoid malignant fibrous histiocytoma,” “undifferentiated sarcoma,” “myxofibrosarcoma,” “emperipolesis,” and “inflammatory myxohyaline tumor.” The retrieved cases were reviewed to confirm the diagnosis. Seventeen cases were selected from the consultations files, further 3 cases were added from the routine practice, and another 3 neoplasms were accidentally discovered while reviewing biopsies for other

☆ The authors have no funding or conflicts of interest to disclose.
* Corresponding author at: Department of Pathology, Charles University, Medical Faculty and Charles University Hospital Plzen, Alej Svobody 80, 304 60 Plzen, Czech Republic. Tel.: +420 603792671.
E-mail address: michael.michal@medima.cz (M. Michal).

http://dx.doi.org/10.1016/j.anndiagpath.2015.03.012
1092-9134/

Table
Main clinicopathologic features and follow-up

	Age/sex	Size (cm)	Location	Therapy	Recurrence and therapy	Metastasis	Follow-up
1	47/M	Ø 5.5	Thigh	E, CH, A	N	Y—Subinguinal lymph node (discovered synchronously as the primary)	NED in 1-y follow-up
2	59/F	4.5 × 4.2 × 3	Lower leg	E	1× in 10 mo, E, A	N	NED in 1-y follow-up
3	81/M	30 × 15 × 10	Thigh	E	1× in 15 mo, E, A	Y—2 y after the first extirpation in the right acetabulum with the generalization into the lungs	DOMD in 2 y after the first extirpation
4	66/F	7.6 × 6 × 1.5	Elbow	E	3× in 1 y, E, A, CH, AMP	Y—1 y after the first extirpation in the left axillary lymph node, generalization into the lungs	DOMD in 2 y after the first extirpation
5	76/F	4.5 × 2 × 1.8	Lower leg	E	1× in 10 mo, AMP	Y—generalization into the lungs 1 y after the extirpation	DOMD in 2 y after the first extirpation
6	75/M	2.5 × 2 × 1.3	Forearm	E	N	N	NED in 3 y follow-up after the first extirpation
7	69/M	Ø 10	Axilla	NA	NA	NA	NA
8	53/F	Ø 4	Forearm	E	N	Y—generalization into the lungs 1 y after the extirpation	DOMD in 2 y after the first extirpation
9	82/F	ND	Thigh	NA	NA	NA	NA
10	54/M	Ø 9	Thigh	E	1× in 6 mo, E, CH, AMP	Y—14 mo after the first extirpation generalization into the both sides of axillary lymph nodes and lungs	DOMD in 2 y after the first extirpation
11	54/M	7 × 4 × 2	Knee	E	4× in 6 y, E, CH, AMP	N	NED in 4 y follow-up after the leg amputation
12	89/F	NA	Shank	NA	NA	NA	DONR 2 y after the diagnosis—generalization of colorectal cancer
13	47/F	Ø 8	Dorsal foot	CH, AMP	N	N	NED in 7 y follow-up after the leg amputation
14	69/F	4.5 × 3 × 3	Sacral area	E	NA	Y—into the lungs	DOMD in 1 mo after the first extirpation
15	93/F	ND	Lower leg	NA	NA	Y—into the lung	DONR in 11 y after the diagnosis
16	52/M	ND	Elbow	E	5× in 11 mo, E	N	NED in 16-y follow-up after the last re-extirpation
17	39/F	8 × 5.6 × 3.2	Dorsal hand	E	1× in 2 y, E, A	N	NED in 13-y follow-up after the last re-extirpation
18	76/F	Ø 3	Axilla	E	2× in 31 mo, E	N	NED in 7-y follow-up after the last re-extirpation
19	68/F	8 × 6 × 2.5	Breast—postirradiation	NA	NA	NA	Recent case
20	53/F	10 × 6 × 6	Gluteal region	E	4× in 4 y	Y—into the lung	DOMD 4 y after the first extirpation
21	53/F	26 × 15 × 10	Thigh	E, CH, A, AMP	N	N	NEORM in 9-y follow-up
22	59/M	Ø 4	Thigh	E	N	N	NEORM in 2-y follow-up
23	66/F	Ø 2	Lower leg	NA	NA	NA	Recent case

Abbreviations: DOMD, died of metastatic disease; DONR, died of nonrelated causes; NA, not available; NED, no evidence of disease; E, extirpation; CH, chemotherapy; A, actinotherapy; AMP, amputation; Y, yes; NEORM, no evidence of recurrence or metastasis.

purposes. In all but 1 case, paraffin blocks or unstained paraffin-embedded recuts were available.

For conventional microscopy, the excised tissues were fixed in formalin, routinely processed, embedded in paraffin, cut into 4-μm-thick sections, and stained with hematoxylin and eosin.

3. Immunohistochemistry

For immunohistochemical studies, 4-μm-thick sections were cut from paraffin blocks, mounted on slides coated with 3-aminopropyltriethoxysilane (Sigma, St Louis, MO), deparaffinized in xylene, and rehydrated in descending grades (100%-70%) of ethanol. Sections were then subjected to heat-induced epitope retrieval by immersion in a CC1 solution at pH 8.0 at 95°C. Endogenous peroxidase was blocked by a 5-minute treatment with 3% hydrogen peroxide in absolute methanol. The immunohistochemical analysis was performed using a Ventana BenchMark ULTRA (Ventana Medical System, Inc, Tucson, AZ).

The following primary antibodies were used: CD34 (monoclonal, QBEnd/10; Dako, Glostrup, Denmark), smooth muscle actin (monoclonal, 1A4; Dako), ALK (monoclonal, ALK-01; Ventana Medical Systems), cyclin D1 (polyclonal; Thermo Fisher Scientific, Fremont, CA; monoclonal), cyclin D1 (monoclonal, SP4; Dako), PRAME (polyclonal; Novus Biologicals, Littleton, CO). The primary antibodies were visualized using the enzymes alkaline phosphatase or peroxidase as detecting systems.

4. Results

The clinical features are summarized in Table. The patients were 15 women and 8 men, with the age at the time of diagnosis ranging from 39 to 93 years (mean, 64.3 years; median, 66 years). Follow-up was available for 18 patients, of whom 9 developed metastatic disease and 7 of these patients died. The average duration of follow-up was 6.6 years (range, 1-18 years). Most tumors showed a predilection for the soft tissues of the extremities, with 14 cases occurring on the lower limbs and 5 involving the upper extremity. However, in both sites, the acral parts were affected in only 1 case each, whereas a majority of tumors involved more proximal sites. Of the 4 remaining tumors, 2 were found in axilla, 1 was found in sacral area, and 1 developed in the scar on the breast, 14 years after previous excision of a mammary carcinoma and subsequent local irradiation. The tumor size ranged from 1.3 to 30 cm in the largest dimension, with a mean size of 8.3 cm.

Aside from the obvious prerequisite of blastic tumor cells with a high degree of pleomorphism notable at first sight with numerous atypical to

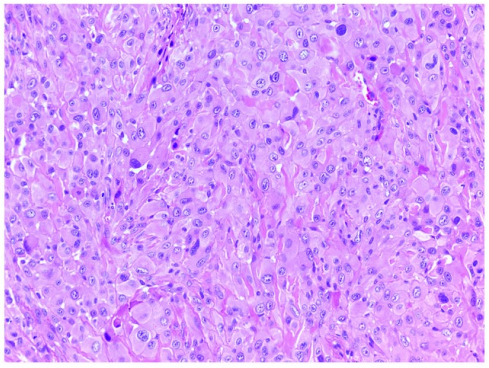

Fig. 1. Mats of neoplastic cells with eosinophilic cytoplasm and prominent cytoplasmic membranes. Note collagen fibers permeating between the neoplastic cells creating a resemblance of a mosaic (hematoxylin and eosin, original magnification ×200).

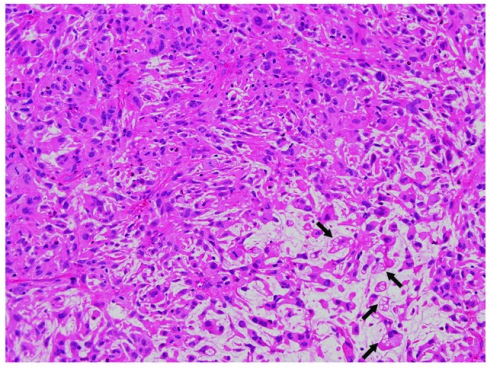

Fig. 3. Areas with copious mucin in which dyscohesive cell growth resulted in a scatter of individual cells in mucin pools remotely resembling a "dilapidated brick wall." Lipoblast-like cells with an ample, distended, mucin-filled cytoplasm, compartmentalized by a variable number of intracytoplasmic septa occasioning a resemblance to soccer balls (arrows). Nuclei of some cells are out of the plane of the section and, therefore, not visible. Note also numerous atypical mitotic figures (hematoxylin and eosin, ×200).

bizarre mitoses and frequent foci of necrosis, the inclusion criteria in our series were exclusively based on the fulfilling of 4, in our view, highly specific histopathologic features of MIFS. The first one was characterized by mats of neoplastic cells with eosinophilic cytoplasm having accentuated cell membranes, whereas thin collagen fibers permeating between the neoplastic cells often created a resemblance to a mosaic (Fig. 1). These areas had gradual transitions to less cohesive foci, in which the extracellular mucous substance began to percolate between cells (Fig. 2). In foci where larger amounts of extracellular mucin were present, the cells further separated producing mucin pools with scattered individual cells bearing a resemblance to a "dilapidated brick wall" (Fig. 3). The other 3 characteristic features of MIFS are the occurrence of 3 different types of cells, which in our view might represent different stages of the development of a single cell population, namely, (1) lipoblast-like cells with an ample, distended, mucin-filled cytoplasm, compartmentalized by a variable number of intracytoplasmic septa, thus remotely resembling soccer balls (Fig. 3); (2) large, polygonal, bizarre ganglion-like cells similar to those seen in Hodgkin disease, also called Reed-Sternberg (RS)–like cells. Within an ample deeply eosinophilic cytoplasm, there was an oval nucleus with vesicular chromatin and a large, inclusion-like nucleolus. Binucleated, multinucleated, or more pleomorphic forms of these cells were also present [8] (Fig. 4); (3) cells with emperipolesis of variable sizes, ranging from very inconspicuous neoplastic cells containing only one or a few engulfed cells to conspicuous large ones having many inflammatory cells, usually polymorphonuclear leukocytes admixed with various numbers of some lymphoid cells, within the cytoplasm (Fig. 5A). Sometimes these cells with emperipolesis contained virtually hundreds of engulfed polymorphonuclear leukocytes in their cytoplasm (Fig. 5B). Quite often, we found large neoplastic cells that combined the histologic features of all these 3 characteristic tumor cell types (Fig. 6).

Variations in the aforementioned specific histopathologic features as well as in the appearances of an inflammatory background were not striking, creating thus a relatively homogenous group. However, certain cases presented with additional microscopic features. In case 4, in addition to the typical histologic appearance of high-grade MIFS, not different from other cases in our series, there was an area of spindle cell type of undifferentiated sarcoma (Fig. 7). Case 19 contained the same high-grade MIFS and spindle cell undifferentiated sarcoma as in case 4, in addition to an area of a low-grade MIFS (Fig. 8A and B). A noteworthy clinical feature of case 19 was the location of the tumor in the scar 14 years after previous excision of a mammary carcinoma and subsequent local irradiation. In case 21, along with usual parts of high-grade MIFS (Fig. 9A), foci with malignant cartilaginous differentiation were encountered (Fig. 9B).

From the 9 metastatic cases in our study, the microscopic slide from a metastatic mass in the lungs was also available (case 14), showing an

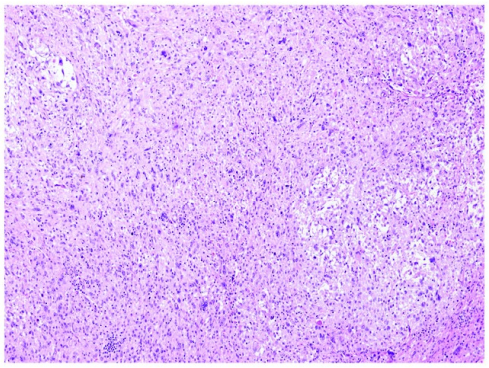

Fig. 2. Focal dyscohesive areas with the mucous substance between cells are present (hematoxylin and eosin, ×100).

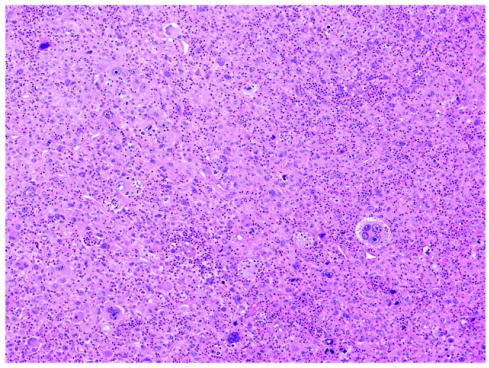

Fig. 4. Binucleated, multinucleated, and pleomorphic cells often with prominent nuclei resembling RS cells in Hodgkin disease can be seen (hematoxylin and eosin, ×100).

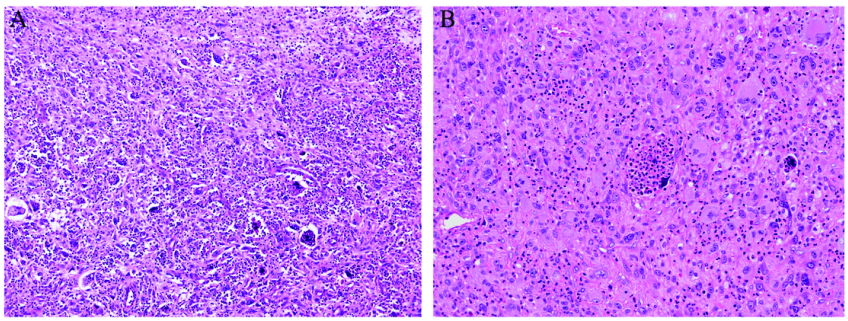

Fig. 5. Cells with emperipolesis of variable sizes, ranging from inconspicuous neoplastic cells containing one to only a few engulfed cells (A) to large conspicuous ones having many inflammatory cells within the cytoplasm (A and B). Some cells with emperipolesis contained virtually hundreds of engulfed polymorphonuclear leukocytes in their cytoplasm (B center) (hematoxylin and eosin, ×100 [A] and ×200 [B]).

undifferentiated high-grade spindle cell sarcoma containing occasional pleomorphic giant cells (Fig. 10). Other metastases were not available for histopathologic review. Interestingly, undifferentiated spindle cell component in cases 4 and 19 and metastatic undifferentiated high-grade spindle cell tumor to the lungs in case 14 were morphologically uncharacteristic, devoid of any of the above-described 3 cell types typical of MIFS.

5. Immunohistochemical finding

The most interesting feature was the overall positivity with antibodies (both polyclonal and monoclonal) to cyclin D1 in all cases. In most tumors, the cyclin D1 antibodies stained strongly the nuclei and less so the cytoplasm of most or all of the neoplastic cells. In a few cases, only the nuclei of the tumor cells were cyclin D1 positive with weak or no cytoplasmic staining. Cyclin D1 immunostaining was very helpful in disclosing cells with inconspicuous emperipolesis, revealing cyclin D1–negative nonneoplastic cells being engulfed by cyclin D1–positive tumor cells (Fig. 11). Positivity with PRAME was present in most cases, often revealing the cells with emperipolesis similar to cyclin D1. In contrast to cyclin D1, the reaction with PRAME was much weaker, and heavily stained background often hampered a reliable identification of neoplastic cells and their distinction from the background. Smooth muscle actin stained only a proportion of cells in 1 case, and CD34 stained the spindle cell sarcoma component in another tumor. ALK staining was always negative.

6. Discussion

To the best of our knowledge, the 23 cases of high-grade MIFS described in this article represent the first large series, although individual allusions to MIFS and its relation to a high-grade sarcoma can be rarely found in the literature. These 23 cases of high-grade MIFS were found beside approximately 50 low-grade MIFSs in our consultation of Pilsen Tumor Registry files. The large number of otherwise rare high-grade MIFSs can be explained by the selective bias caused by the consultation character of a majority of the included tumors.

There are on record more putative high-grade MIFS that were published all as case reports. In 2009, Hallor et al [7] included in their study myxoid spindle cell/pleomorphic sarcoma with MIFS features. Later, a case of myxofibrosarcoma recurring as MIFS was published [9]. Eventually, in 2013, Solomon et al [10] reported MIFS progressing to a highly anaplastic sarcoma, which metastasized. Metastatic cases of MIFS available in the literature were either described as having the same appearance as the primary tumor [4] or showed higher cytological atypia and cellularity [3]. Unfortunately, no representative microphotograph from a metastatic lesion was provided, precluding further comments.

As mentioned above, all specimens in our study exhibited all characteristics of conventional MIFS, along with a high-grade cytology. Aside from myxoid and inflammatory background, so-called RS-like cells and lipoblast-like cells, another feature that we consider specific is the gradual change in the cellular cohesion as depicted and described above. This change and variations thereof are seen in most of the

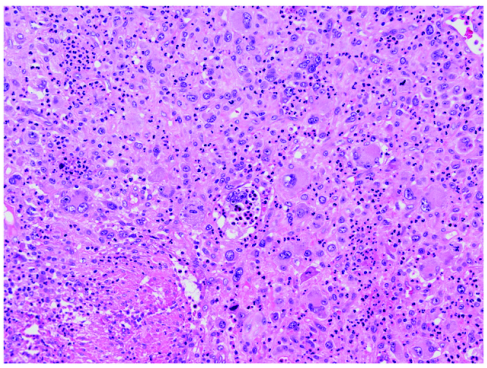

Fig. 6. The cell in the center of the picture combines all characteristics by manifesting emperipolesis, RS-like nuclei, and compartmentalization of the cytoplasm filled with mucin (hematoxylin and eosin, ×200).

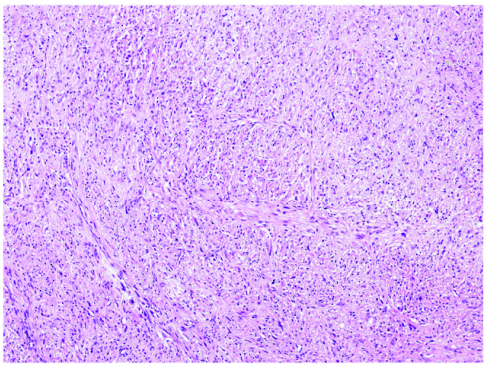

Fig. 7. Case 4. An area within a tumor featuring undifferentiated spindle cell sarcoma lacking any signs of MIFS present elsewhere in the specimens (hematoxylin and eosin, ×100).

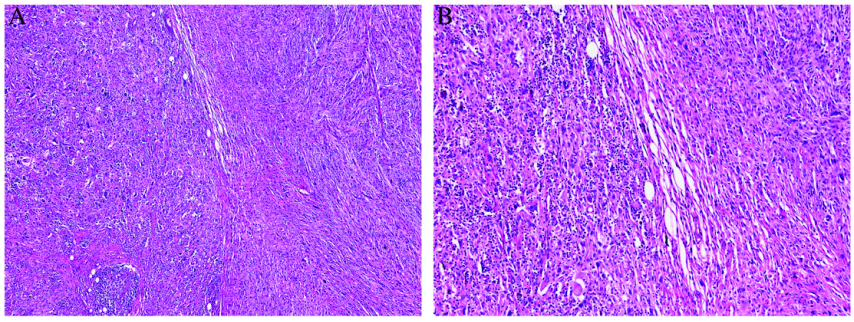

Fig. 8. An area showing high-grade MIFS (A and B, left side) in case 19 abruptly transforming into undifferentiated spindle cell sarcoma (A and B, right side) (hematoxylin and eosin, ×100 [A] and ×200 [B]).

high-grade lesions of our series and were present in all 50 cases of low-grade MIFS available in our registry as well (unpublished observation). However, one of the most specific hallmarks of this type of sarcoma is, in our opinion, the presence of emperipolesis. We think that the occurrence of this morphologic epiphenomenon is generally highly underestimated in MIFS among pathologists as well as in the publications. For example, Laskin et al [6] found cells with emperipolesis in only about 10% of their cases. Although large cells with high amount of engulfed inflammatory cells easily recognizable at the first sight are usually present only focally or may be absent, a meticulous search will almost invariably reveal at least few numbers of inconspicuous cells showing discrete emperipolesis of only one or a few individual cells. Notably, in our institution, we never make a diagnosis of MIFS, either low grade or high grade, if the cells with emperipolesis are not present in the tumor. In our experience, emperipolesis occurs rarely in soft tissue tumors, and inclusion of this diagnostic criterion into the histopathologic definition of MIFS makes the diagnosis highly specific. Interestingly, when we reviewed 7 cases in our files coded with the index word "emperipolesis" and for which no definitive diagnosis in the past was made, 5 cases were reclassified as MIFS; 1 lesion as Rosai-Dorfman disease; and only for the last remaining case, no definitive diagnosis was still rendered. Emperipolesis is much easier found with the help of immunohistochemistry. The recently introduced antibody PRAME and especially cyclin D1 are very useful in this regard. These immunostains easily reveal cyclin D1 intensely stained cells (and less often PRAME-positive cells) having in their cytoplasm engulfed cyclin D1–negative nonneoplastic inflammatory cells. Despite the fact that the constant presence of cyclin D1 is not unique for MIFS, as it was reported in other tumors such as chondroid lipoma [11], microcystic stromal tumor of the ovary [12], intranodal palisaded myofibroblastoma [13], endometrial stromal sarcomas with YWHAE-FAM22 rearrangement [14], mantle cell lymphoma [15], and others, we greatly advocate the use of these antibodies (especially cyclin D1) to visualize emperipolesis, which is a very important and according to us defining diagnostic feature, allowing one to differentiate MIFS from nearly all known soft tissue neoplasms. One of a very few relevant differential diagnoses in this area of pathology is extranodal, primary soft tissue Rosai-Dorfman disease, in which such emperipolesis is also invariably found. However, this histiocytic disorder presents with a different morphology, and the tumor cells are, in contrast to MIFS, practically always S-100 protein positive. The immunohistochemical positivity of MIFS with antibody to PRAME is important to have in mind because this antibody was introduced to soft tissue pathology as being relatively specific for myxoid liposarcomas [16].

The remarkable features of cases in our series, most of our tumors were not located on the acral parts of the extremities, as is usual for low-grade MIFS, and they were considerably larger than a majority of these neoplasms in acral locations, can be easily explained by the fact that a growing neoplastic mass involving hands and feet is usually noticed earlier by the patients, who due to growing discomfort seek the medical attention much sooner compared to cases when such a mass is localized more proximally. We observed a similar phenomenon with minute synovial sarcomas. Most small synovial sarcomas under the size of 1 cm in our registry involved hands and feet, especially the fingers [17]. Thus, theoretically, a more proximal location provides more time for a tumor to grow and to be noted and increase the chance of acquiring larger size. This may allow a low-grade MIFS time to evolve into a high-grade MIFS and occasionally produce even a completely undifferentiated sarcoma component.

The same patterns of both spindle cell dedifferentiation as seen in our cases 4 and 19 and even chondroid differentiation as seen in our case 21 can occur in liposarcomas [18], and indeed, case 21 was

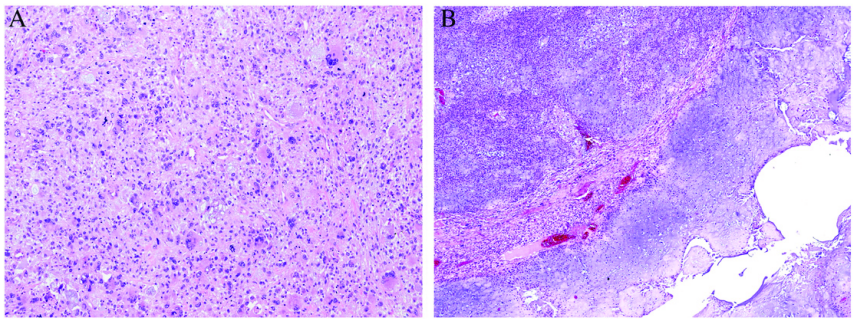

Fig. 9. In case 21, typical picture of high-grade MIFS (A) changes into areas with malignant cartilaginous differentiation (B) (hematoxylin and eosin, ×200 [A] and ×100 [B]).

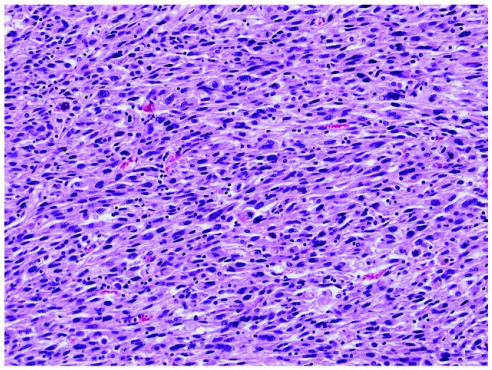

Fig. 10. In case 14, metastatic tumor in the lung showing undifferentiated high-grade spindle cell sarcoma containing occasional pleomorphic giant cells (hematoxylin and eosin, ×400).

identified by us while reviewing cases of myxoid liposarcomas associated with chondromatous differentiation retrieved from our consultation tumor registry recently.

Another very interesting case was added to our series after reexamining a case from our registry that was published in the past by 2 of the authors of this article (DVK and MM) in 2007 [19]. It was described as pleomorphic hyalinizing angiectatic tumor (PHAT) and later recurred under the diagnosis of myxofibrosarcoma grade 2. Interestingly, the same progression of PHAT to myxofibrosarcoma or its synchronous occurrence with other mesenchymal neoplasms has also been described by other authors [20-23]. However, thanks to our current better knowledge of MIFS's morphology, when we re-reviewed both biopsies again, it became obvious that both lesions show typical features of low-grade MIFS in the original excision, with the recurring high-grade lesion harboring additionally cytologic atypia. This surprising finding compelled us to review all 10 PHATs from our registry files, which resulted in further noteworthy observations. With the exception of 2 cases, all the remaining 8 lesions contained cells morphologically indistinguishable from MIFS on the background of predominant features of PHAT characterized by thin-walled angular ectatic vessels surrounded by perivascular hyaline material [24]. We performed the same immunohistochemical analysis as with our study of MIFS specimens, and it yielded a similar staining pattern, with cyclin D1 and PRAME being positive in all cases of PHAT. The fact that MIFS may contain areas similar to PHAT [6,25], both of them have a very similar clinical presentation and share certain genetic alterations [25], is already well known in the literature. Our findings suggest that most tumors diagnosed as PHAT might, in fact, represent the examples of MIFS that, in addition to a conventional MIFS morphology, produce aberrant angiectatic hyalinized vessels. This vascular change could be theoretically initiated by the tumor growth itself, possibly being more likely to occur at the lower extremities, where high hydrostatic pressure and often concomitant venous insufficiency are present, but this will remain a subject of further research. The possibility that vascular changes in PHAT represent solely a histologic pattern and not a true neoplasm or that MIFS and PHAT represent a different morphologic manifestation of a single entity has already been raised by other authors [6,20,25]. That would also explain why some authors described cases showing features of PHATs recurring as myxofibrosarcomas because the recurrence in most cases might, in fact, be high-grade MIFS and most of these reported lesions might have represented primarily a low-grade MIFS associated with morphologically prominent ectatic hyalinized vessels. We also assume that tumors depicted in several publications described as PHAT might, in fact, be examples of MIFS [21,23].

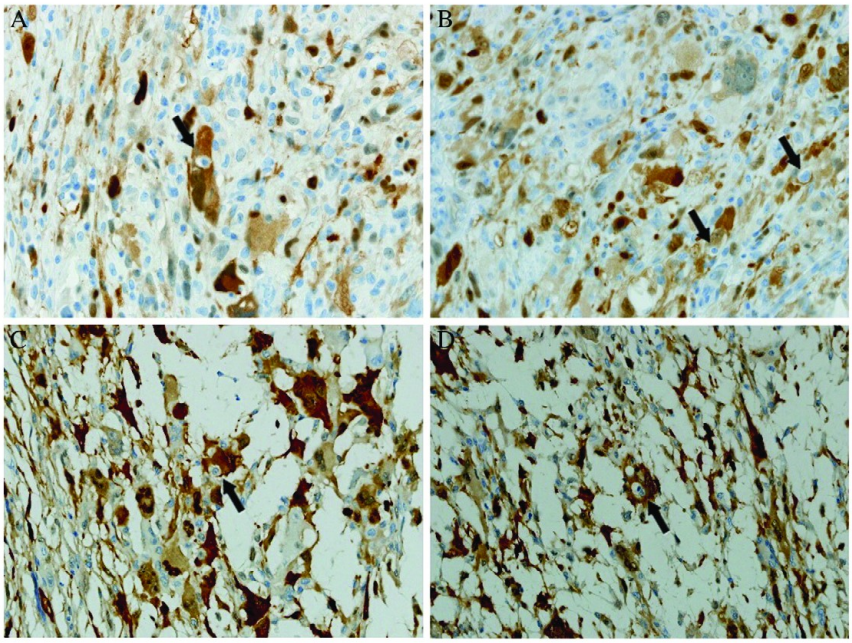

Fig. 11. Cyclin D1 immunostaining revealing cyclin D1–negative engulfed nonneoplastic cells within the cytoplasm of cyclin D1–positive neoplastic cells (arrows). Staining for cyclin D1 is very helpful in disclosing cells with emperipolesis in cases this feature is subtle and not readily appreciable (cyclin D1 counterstained with hematoxylin, ×200).

In summary, myxoinflammatory fibroblastic sarcoma, being so far considered as a low-grade sarcoma occurring mostly on acral sites, is an entity that encompasses the whole spectrum of lesions ranging from low-grade and relatively indolent neoplasms to high-grade tumors or entirely undifferentiated spindle cell/pleomorphic sarcoma with an aggressive biological behavior, examples of which used to be diagnosed in the past as high-grade myxofibrosarcomas or myxoid/pleomorphic malignant fibrous histiocytomas. Most cases of PHAT might represent a low-grade MIFS associated with morphologically prominent ectatic hyalinized vessels; ergo before the diagnosis of PHAT is made, wide sampling is mandatory, and a careful search for diagnostic features of MIFS should be performed. Immunostaining for cyclin D1 is recommended to identify emperipolesis typical for MIFS.

References

[1] Montgomery EA, Devaney KO, Giordano TJ, Weiss SW. Inflammatory myxohyaline tumor of distal extremities with virocyte or Reed-Sternberg–like cells: a distinctive lesion with features simulating inflammatory conditions, Hodgkin's disease, and various sarcomas. Mod Pathol 1998;11:384–91.

[2] Michal M. Inflammatory myxoid tumor of the soft parts with bizarre giant cells. Pathol Res Pract 1998;194:529–33.

[3] Meis-Kindblom JM, Kindblom LG. Acral myxoinflammatory fibroblastic sarcoma: a low-grade tumor of the hands and feet. Am J Surg Pathol 1998;22:911–24.

[4] Sakaki M, Hirokawa M, Wakatsuki S, Sano T, Endo K, Fujii Y, et al. Acral myxoinflammatory fibroblastic sarcoma: a report of five cases and review of the literature. Virchows Arch 2003;442:25–30.

[5] Hassanein AM, Atkinson SP, Al-Quran SZ, Jain SM, Reith JD. Acral myxoinflammatory fibroblastic sarcomas: are they all low-grade neoplasms? J Cutan Pathol 2008;35:186–91.

[6] Laskin WB, Fetsch JF, Miettinen M. Myxoinflammatory fibroblastic sarcoma: a clinicopathologic analysis of 104 cases, with emphasis on predictors of outcome. Am J Surg Pathol 2014;38:1–12.

[7] Hallor KH, Sciot R, Staaf J, Heidenblad M, Rydholm A, Bauer HC, et al. Two genetic pathways, t(1;10) and amplification of 3p11-12, in myxoinflammatory fibroblastic sarcoma, haemosiderotic fibrolipomatous tumour, and morphologically similar lesions. J Pathol 2009;217:716–27.

[8] Kinkor Z, Mukensnabl P, Michal M. Inflammatory myxohyaline tumor with massive emperipolesis. Pathol Res Pract 2002;198:639–42.

[9] Chiu HY, Chen JS, Hsiao CH, Tsai TF. Transformation of myxofibrosarcoma into myxoinflammatory fibroblastic sarcoma. J Dermatol 2012;39:422–4.

[10] Solomon DA, Antonescu CR, Link TM, O'Donnell RJ, Folpe AL, Horvai AE. Hemosiderotic fibrolipomatous tumor, not an entirely benign entity. Am J Surg Pathol 2013;37:1627–30.

[11] de Vreeze RS, van Coevorden F, Boerrigter L, Nederlof PM, Haas RL, Bras J, et al. Delineation of chondroid lipoma: an immunohistochemical and molecular biological analysis. Sarcoma 2011;2011 [Article ID 638403, 5 pages].

[12] Oliva E, Young RH. Stromal tumours of the ovary: an update. Diagn Histopathol 2014;20:376–84.

[13] Laskin WB, Lasota JP, Fetsch JF, Felisiak-Golabek A, Wang ZF, Miettinen M. Intranodal palisaded myofibroblastoma: another mesenchymal neoplasm with CTNNB1 (beta-catenin gene) mutations: clinicopathologic, immunohistochemical, and molecular genetic study of 18 cases. Am J Surg Pathol 2015;39:197–205.

[14] Lee CH, Ali RH, Rouzbahman M, Marino-Enriquez A, Zhu M, Guo X, et al. Cyclin D1 as a diagnostic immunomarker for endometrial stromal sarcoma with YWHAE-FAM22 rearrangement. Am J Surg Pathol 2012;36:1562–70.

[15] Bosch F, Jares P, Campo E, Lopez-Guillermo A, Piris MA, Villamor N, et al. PRAD-1/cyclin D1 gene overexpression in chronic lymphoproliferative disorders: a highly specific marker of mantle cell lymphoma. Blood 1994;84:2726–32.

[16] Hemminger JA, Toland AE, Scharschmidt TJ, Mayerson JL, Guttridge DC, Iwenofu OH. Expression of cancer-testis antigens MAGEA1, MAGEA3, ACRBP, PRAME, SSX2, and CTAG2 in myxoid and round cell liposarcoma. Mod Pathol 2014;27:1238–45.

[17] Michal M, Fanburg-Smith JC, Lasota J, Fetsch JF, Lichy J, Miettinen M. Minute synovial sarcomas of the hands and feet: a clinicopathologic study of 21 tumors less than 1 cm. Am J Surg Pathol 2006;30:721–6.

[18] Panoussopoulos D, Theodoropoulos G, Lazaris AC, Papadimitriou K. Focal divergent chondrosarcomatous differentiation in a primary pleomorphic liposarcoma and expression of transforming growth factor beta. Int J Surg Pathol 2004;12:79–85.

[19] Kazakov DV, Pavlovsky M, Mukensnabl P, Michal M. Pleomorphic hyalinizing angiectatic tumor with a sarcomatous component recurring as high-grade myxofibrosarcoma. Pathol Int 2007;57:281–4.

[20] Capovilla M, Birembaut P. Primary cutaneous myxofibrosarcoma mimicking pleomorphic hyalinizing angiectatic tumor (PHAT): a potential diagnostic pitfall. Am J Dermatopathol 2006;28:276–7 [author reply 277–278].

[21] Illueca C, Machado I, Cruz J, Almenar S, Noguera R, Navarro S, et al. Pleomorphic hyalinizing angiectatic tumor: a report of 3 new cases, 1 with sarcomatous myxofibrosarcoma component and another with unreported soft tissue palpebral location. Appl Immunohistochem Mol Morphol 2012;20:96–101.

[22] Folpe AL, Weiss SW. Pleomorphic hyalinizing angiectatic tumor: analysis of 41 cases supporting evolution from a distinctive precursor lesion. Am J Surg Pathol 2004;28:1417–25.

[23] Mitsuhashi T, Barr RJ, Machtinger LA, Cassarino DS. Primary cutaneous myxofibrosarcoma mimicking pleomorphic hyalinizing angiectatic tumor (PHAT): a potential diagnostic pitfall. Am J Dermatopathol 2005;27:322–6.

[24] Smith ME, Fisher C, Weiss SW. Pleomorphic hyalinizing angiectatic tumor of soft parts. A low-grade neoplasm resembling neurilemoma. Am J Surg Pathol 1996;20:21–9.

[25] Carter JM, Sukov WR, Montgomery E, Goldblum JR, Billings SD, Fritchie KJ, et al. TGFBR3 and MGEA5 rearrangements in pleomorphic hyalinizing angiectatic tumors and the spectrum of related neoplasms. Am J Surg Pathol 2014;38:1182–992.

1.1.2. PLEOMORPHIC HYALINIZING ANGIECTATIC TUMOR REVISITED: ALL TUMORS MANIFEST TYPICAL MORPHOLOGIC FEATURES OF MYXOINFLAMMATORY FIBROBLASTIC SARCOMA, FURTHER SUGGESTING 2 MORPHOLOGIC VARIANTS OF A SINGLE ENTITY.

Pleomorphic hyalinizing angiectatic tumor (PHAT) is locally aggressive sarcoma [11] that is generally considered to be somehow related to MIFS. The progression of PHAT to a myxofibrosarcoma-like sarcoma has been described in several cases [12]. Both PHAT and MIFS have a very similar clinical presentation, and prognosis and the morphological features of both tumors are also considered to be very much alike. However, these morphological similarities have never been precisely studied and defined in the literature. While searching for cases of HG MIFS, we came across a recurrent PHAT initially diagnosed as myxofibrosarcoma. Thanks to our better knowledge of the wide spectrum of MIFS's morphology, when we re-reviewed both biopsies again, it became obvious that both the original and the recurrent lesions show typical cytological features of MIFS, albeit the recurrent tumor harbored more prominent cytological atypia. This surprising finding compelled us to review all 9 cases filed as PHATs from our files that matched our cytological and histological criteria for MIFS used in our previous publication concerning the HG variety of this tumor. All the 9 lesions contained cells morphologically indistinguishable from MIFS on the background of predominant features of PHAT characterized by thin-walled angular ectatic vessels surrounded by perivascular hyaline material. This vascular change can be theoretically initiated by the tumor growth itself, possibly being more likely to occur at the lower extremities, where high hydrostatic pressure and often concomitant venous insufficiency are present.

The possibility that vascular changes in PHAT represent solely a histologic pattern and not a true neoplasm or that MIFS and most of the cases of PHAT represent a different morphologic manifestation of a single entity has already been raised by other authors [6, 11, 13]. That would also explain why some authors described cases showing features of PHATs recurring as myxofibrosarcomas because the recurrence in most cases might, in fact, be high-grade MIFS, and most of these reported lesions might have represented primarily a low-grade MIFS associated with morphologically prominent ectatic hyalinized vessels.

The identical gene rearrangement of TGFBR3 and MGEA5 in a subset of cases of PHAT and MIFS lends further support to the proposition that these 2 entities are likely morphologic variants of the same tumor [11]. As mentioned in the previous commentary, recently, BRAF rearrangements were reported in 25% of MIFS [9]. Since only 2 cases of PHAT were tested in this study, it will be interesting to see if this rearrangement will be found in a larger set of cases.

Annals of Diagnostic Pathology 20 (2016) 40–43

Contents lists available at ScienceDirect

Annals of Diagnostic Pathology

Pleomorphic hyalinizing angiectatic tumor revisited: all tumors manifest typical morphologic features of myxoinflammatory fibroblastic sarcoma, further suggesting 2 morphologic variants of a single entity☆,☆☆

Michael Michal, MD [a,*], Dmitry V. Kazakov, MD [b], Ladislav Hadravský, MD [b], Abbas Agaimy, MD [c], Marián Švajdler, MD [b,d], Naoto Kuroda, MD [e], Michal Michal, MD [b]

[a] Department of Pathology, Charles University, Biomedical Center, Faculty of Medicine in Plzen and Charles University Hospital Plzen, Czech Republic
[b] Department of Pathology, Charles University, Medical Faculty and Charles University Hospital Plzen, Czech Republic
[c] Institute of Pathology, Friedrich-Alexander University Erlangen-Nürnberg, Erlangen, Germany
[d] Department of Pathology, Louis Pasteur University Hospital, Kosice, Slovakia
[e] Red Cross Hospital Kochi, Kochi, Japan

ARTICLE INFO

Keywords:
Pleomorphic hyalinizing angiectatic tumor
Myxoinflammatory fibroblastic sarcoma
Soft tissues

ABSTRACT

We describe 9 cases of pleomorphic hyalinizing angiectatic tumor (PHAT). Recently described TGFBR3 and MGEA5 gene rearrangements in these tumors have confirmed the long-hypothesized link between PHAT and another soft tissue entity, the myxoinflammatory fibroblastic sarcoma (MIFS). Myxoinflammatory fibroblastic sarcoma and PHAT share the same translocation and in addition have a very similar clinical presentation. However, to our best knowledge, no study has ever addressed the striking morphologic similarities between MIFS and PHAT. Our findings based on histological criteria suggest that most, if not all, tumors diagnosed as PHAT might, in fact, represent examples of MIFS that, in addition to a conventional MIFS morphology, manifest aberrant angiectatic hyalinized vessels.

1. Introduction

Pleomorphic hyalinizing angiectatic tumor (PHAT), first described in 1996 by Smith et al [1], is currently considered a low-grade, locally aggressive neoplasm of uncertain lineage with a high predilection for the lower extremity. Although as much as 50% of lesions recur locally, no metastases have so far been documented. Nonetheless, the progression to a myxofibrosarcomalike sarcoma has been described in several cases [2–4]. While working on another project on a high-grade variant of myxoinflammatory fibroblastic sarcoma (MIFS) [5], we came across a recurrent PHAT initially diagnosed as myxofibrosarcoma. Thanks to our current better knowledge of the wide spectrum of MIFS's morphology, when we re-reviewed both biopsies again, it became obvious that both the original and the recurrent lesions show typical cytological features of MIFS, albeit the recurrent tumor harbored prominent cytological atypia. This surprising finding compelled us to review all 13 cases filed as PHATs from our files, which resulted in further noteworthy observations. With the exception of 4 cases, all the remaining 9 lesions contained cells morphologically indistinguishable from MIFS on the background of predominant features of PHAT characterized by thin-walled angular ectatic vessels surrounded by perivascular hyaline material.

In this study, we report a series of 9 lesions originally diagnosed as PHAT, which, based on our histological criteria for MIFS, all most likely represent examples of the latter tumor, merely having an additional component of aberrant angiectatic hyalinized vessels.

2. Materials and methods

The 9 cases of PHAT constituting the subject of this study were retrieved from the authors' files; they came from the period between the years 1993 and 2015. The clinical information was extracted from the registry records, and follow-up data were obtained from attending clinicians. To retrieve the cases, we searched our consultation registry files using keywords, including *pleomorphic hyalinizing angiectatic tumor*, *PHAT*, *myxoid malignant fibrous histiocytoma*, and *myxofibrosarcoma*. This search yielded altogether 13 specimens which were reviewed to confirm the diagnosis. Upon revision, 2 cases were excluded for their incompatible morphology, of which one was reminiscent of low-grade fibromyxoid sarcoma with prominent vessels rather than a PHAT and the second one was reclassified as myxofibrosarcoma, not otherwise specified. In another case, we were not able to render any final diagnosis, and the

☆ This study was supported by the National Sustainability Program I (NPU I) No. LO1503 provided by the Ministry of Education Youth and Sports of the Czech Republic.
☆☆ The authors have no funding or conflicts of interest to disclose.
* Corresponding author at: Department of Pathology, Charles University, Medical Faculty and Charles University Hospital Plzen, Alej Svobody 80, 304 60 Pilsen, Czech Republic. Tel.: +420 603792671.
E-mail address: michael.michal@medima.cz (M. Michal).

http://dx.doi.org/10.1016/j.anndiagpath.2015.10.006
1092-9134/

remaining excluded tumor lacked any clinical information. In all but 2 cases, paraffin blocks or unstained reserve slides were available for the study.

For conventional microscopy, tissues were fixed in formalin, routinely processed, embedded in paraffin, cut into 4-μm–thick sections, and stained with hematoxylin-eosin (H&E).

For immunohistochemical studies, 4-μm–thick sections were cut from paraffin blocks, mounted on slides coated with 3-aminopropyltriethoxy-silane (Sigma, St Louis, MO), deparaffinized in xylene, and rehydrated in descending grades (100% to 70%) of ethanol. Sections were then subjected to heat-induced epitope retrieval by immersion in a CC1 solution at pH 8.0 at 95°C. Endogenous peroxidase was blocked by a 5-minute treatment with 3% hydrogen peroxide in absolute methanol. The slides were then stained by immunostainer BenchMark ULTRA (Roche, Switzerland). The immunohistochemical analysis was performed using a Ventana BenchMark ULTRA (Ventana Medical System, Inc, Tucson, AZ).

The following primary antibodies were used: Cyclin D-1 (polyclonal, Thermo Fisher Scientific, Fremont, CA; monoclonal) and Cyclin D-1 (monoclonal, SP4, Dako, Glostrup, Denmark). The primary antibodies were visualized using the enzymes alkaline phosphatase or peroxidase as detecting systems (both purchased from Ventana Medical System, Inc, Tucson, AZ).

3. Results

The clinical features are summarized in Table 1. The patients were 5 women and 3 men, and in the remaining case, the sex was unknown. The age of the patients at the time of diagnosis ranged from 53 to 76 years (mean, 62.9 years). Follow-up was available for 4 patients, of whom 1 suffered multiple recurrences. No metastases occurred. The average duration of follow-up was 5.9 years (range, 0.4-14 years). Locations were available for 8 tumors and included soft tissues of the lower extremity [4] and 1 each of the axilla, forearm, inguinal area, and the abdomen. The patient with the inguinal lesion had a history of inguinal hernia, and the tumor was initially suspected to represent recurrent hernia. The patient with abdominal lesion had been operated on for a colorectal carcinoma 13 years ago; the PHAT developed 4 cm away from the colostoma scar. The tumor size ranged from 2 to 7. 5 cm in the largest dimension, with a mean size of 5.0 cm.

All PHATs in this series matched our cytological and histological criteria for MIFS used in our previous publication concerning this tumor [5], merely adding the hyalinized, ectatic vessel to the morphologic picture (Fig. 1). The inclusion morphologic criteria were as follows: (1) Presence of mats of neoplastic cells with eosinophilic cytoplasm having accentuated cell membranes, with thin collagen fibers

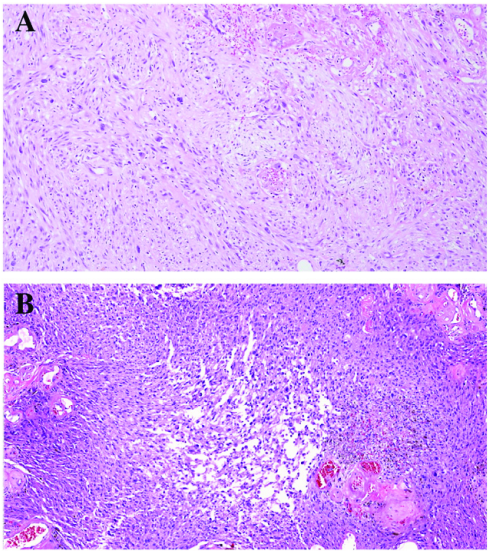

Fig. 1. Cell composition of tumor in between the ectatic vessels is identical to the myxoinflammatory fibroblastic sarcoma (A and B) (H&E, 100×).

permeating between the neoplastic cells often creating mosaiclike appearances (Fig. 1A). These areas had gradual transitions to less cohesive foci, in which the extracellular mucous substance began to percolate between cells, with appearances reminiscent of "dilapidated brick wall" in areas where larger amounts of extracellular mucin have produced pools containing scattered individual neoplastic cells (Fig. 1B). However, the above-described stroma so typical for MIFS differed slightly in 3 of our cases of PHAT where it was more hypocellular and edematous (Fig. 2.), usually with prominent hemosiderin deposition. In addition, in some cases, there were groups of foam cells present in the stroma. (2) Presence of lipoblastlike cells with an ample, distended, mucin-filled cytoplasm, compartmentalized by a variable number of intracytoplasmic bridges or septa, thus remotely resembling soccer balls (Fig. 3). (3) Occurrence of large, polygonal, bizarre ganglionlike cells similar to those seen in Hodgkin disease, also called *RS-like cells*. These cells possessed an oval nucleus with vesicular chromatin and a large, inclusionlike

Table 1
Main clinicopathologic features and follow-up.

	Age/sex	Size (cm)	Location	Therapy	Recurrence and therapy	Metastasis	Follow-up
1	57/F	5 cm	Scar on the abdomen	E	N	N	NED in 8-y follow-up after the extirpation
2	66/F	6 × 5.5 × 3.5 cm	Thigh	E	N	N	NED in 13-y follow-up after the extirpation
3	76/F	Ø 3.5 cm	Axilla	E	2× in 31 mo (as myxoinflammatory fibroblastic sarcoma), E	N	NED in 7-y follow-up after the last re-extirpation
4	62/F	4.5 × 4 × 2 cm	Ankle	E	N	N	NED in 3-y follow-up after the extirpation
5	63/M	4 × 3.5 × 2.5	Forearm	E	NA	NA	NA
6	64/F	3 × 3 × 2.2 cm	Instep	NA	NA	NA	NA
7	53/M	7.7 × 5.5 × 4.5 cm	Thigh	E	N	N	DONR (colorectal adenocarcinoma) 4 y after the extirpation
8	62/M	Ø 5.9 cm	Inguinal area, history of inguinal hernia	E	N	N	NED in 3 mo after the extirpation
9	NA	NA	Soft tissue, not specified	NA	NA	NA	NA

Abbreviations: DONR: died of nonrelated causes, NA: not available, NED: no evidence of disease, E: extirpation.

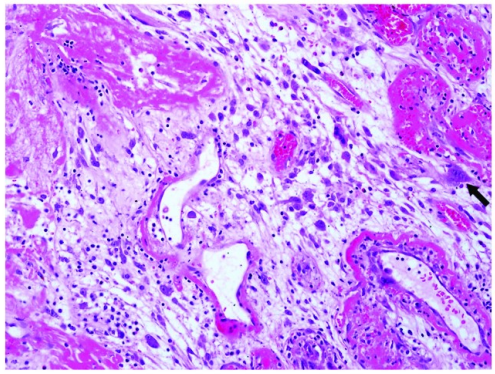

Fig. 2. The typical MIFS-like stroma differed slightly in 3 of our cases of PHAT where it was more hypocellular and edematous. Binucleated, multinucleated, and pleomorphic cells often with prominent nuclei resembling Reed-Sternberg cells in Hodgkin disease can be seen (arrow) (H&E, 200×).

nucleolus and an ample deeply eosinophilic cytoplasm; binucleated, multinucleated, or more pleomorphic forms of these cells were also present [6] (Fig. 2). (4) Presence of cells with emperipolesis of varying degree (Figs. 3 and 4.).

4. Immunohistochemical finding

The most interesting feature was the positivity with antibodies (both polyclonal and monoclonal) to Cyclin D1 in all but 1 case. In most tumors, the Cyclin D1 antibodies stained strongly the nuclei and less so the cytoplasm of most or all of the neoplastic cells. In a few cases, only the nuclei of the tumor cells were Cyclin D1 positive with week or no cytoplasmic staining. Cyclin D1 immunostaining was very helpful in disclosing cells with inconspicuous emperipolesis, revealing Cyclin D1-negative nonneoplastic cells being engulfed within Cyclin D1-positive cytoplasm of tumor cells [5].

5. Discussion

The fact that MIFS may contain areas similar to PHAT and both of them have a very similar clinical presentation has been addressed in the recent literature [7,8]. Moreover, Carter et al [8] recently proved that, in a significant proportion of cases, they also share the same

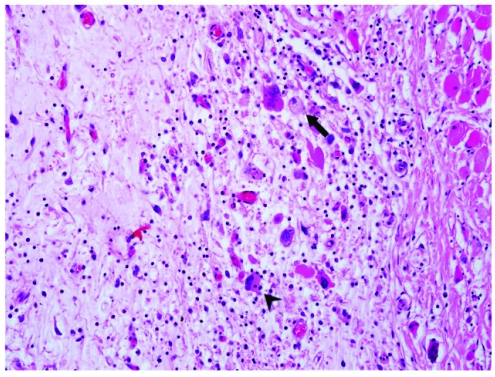

Fig. 3. Lipoblastlike cells with an ample, distended, mucin-filled cytoplasm, compartmentalized by a variable number of intracytoplasmic septa occasioning a resemblance to soccer balls (arrow). Cell with emperipolesis (arrowhead) (H&E, 200×).

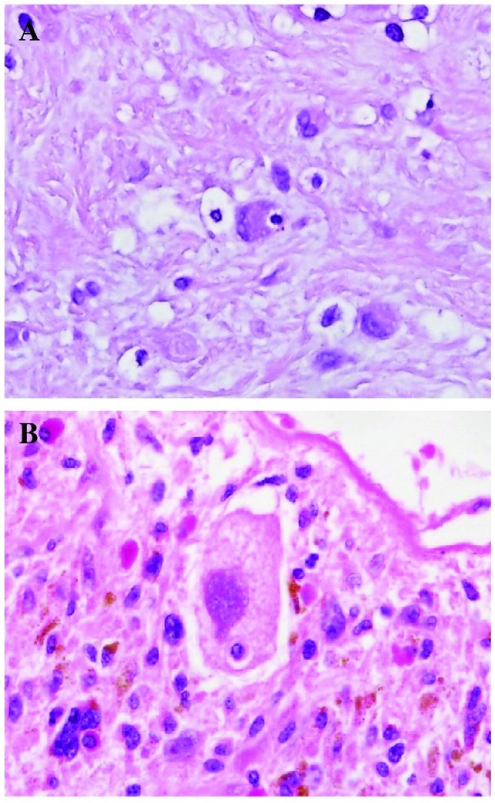

Fig. 4. One of the most specific hallmarks of MIFS/PHAT is, in our opinion, the presence of emperipolesis (A and B) (H&E, 400×).

TGFBR3 and MGEA5 gene rearrangements, further establishing a link between these 2 entities. Our findings based on histological criteria suggest that most if not all tumors diagnosed as PHAT might, in fact, represent examples of MIFS that, in addition to a conventional MIFS morphology, manifest aberrant angiectatic hyalinized vessels. This vascular change can be theoretically initiated by the tumor growth itself, possibly being more likely to occur at the lower extremities, where high hydrostatic pressure and often concomitant venous insufficiency are present, but this will remain a subject of further research. The possibility that vascular changes in PHAT represent solely a histologic pattern and not a true neoplasm or that MIFS and most of the cases of PHAT represent a different morphologic manifestation of a single entity has already been raised by other authors [7–9]. That would also explain why some authors described cases showing features of PHATs recurring as myxofibrosarcomas because the recurrence in most cases might, in fact, be high-grade MIFS, and most of these reported lesions might have represented primarily a low-grade MIFS associated with morphologically prominent ectatic hyalinized vessels. We also assume that tumors depicted in several publications described as PHAT might, in fact, be examples of MIFS [2,4].

As mentioned above, all specimens in our study exhibited all characteristics of conventional MIFS. Aside from the myxoinflammatory background, so-called RS-like cells, and lipoblastlike cells, another feature that we consider specific is the gradual loss of the cellular cohesion as depicted and described above. Interestingly, the presence of lipoblastlike cells typical of MIFS in the early PHAT was noticed already by Suarez-Vilela and Izquierdo-Garcia [10]. These features were observed in most

of the 50 cases of low-grade (our unpublished observations) and 23 cases of high-grade MIFS currently filed in our registry. However, the above-described stroma so typical for MIFS differed slightly in 3 of our cases of PHAT where it was more hypocellular and edematous, usually with prominent hemosiderin deposition. In addition, in some cases, there were groups of foam cells present in the stroma. All of these are in our view attributable to the common presence of stromal hemorrhage resulting from the traumatization of ectatic large vessels.

One of the most specific hallmarks of MIFS/PHAT is, in our opinion, the presence of emperipolesis. We think that the occurrence of this morphologic epiphenomenon is generally highly underestimated in MIFS. For example, Laskin et al [7] found cells with emperipolesis in only about 10% of their cases of MIFS. Emperipolesis in tumors so far designated as PHAT has in fact not been described, but a meticulous search will almost invariably reveal at least few numbers of inconspicuous cells showing discrete emperipolesis of only one or a few individual cells. Notably, in our institution, we never make a diagnosis of MIFS, either low grade or high grade, if the cells with emperipolesis are not present in the tumor. In our experience, emperipolesis occurs rarely in soft tissue tumors, and inclusion of this diagnostic criterion into the histopathologic definition of MIFS makes the diagnosis much more specific. Interestingly, when we reviewed 7 cases in our files coded with the index word *emperipolesis* and for which no definitive diagnosis in the past was made, 5 cases were reclassified as MIFS, 1 lesion was reclassified as Rosai-Dorfman disease, and only for the last remaining case was a definitive diagnosis still not rendered. Emperipolesis is much easier found with the help of immunohistochemistry. The antibody to Cyclin D1 is very useful in this regard. These immunostains easily reveal Cyclin D1 intensely stained cells having in their cytoplasm engulfed Cyclin D1-negative nonneoplastic inflammatory cells. Despite the fact that the constant presence of Cyclin D1 is by far not unique for MIFS, as it was reported in other tumors such as epithelioid sarcoma [11], chondroid lipoma [12], intranodal palisaded myofibroblastoma [13], microcystic stromal tumor of the ovary [14,15], endometrial stromal sarcomas with YWHAE-FAM22 rearrangement [16], clear cell sarcoma of the kidney [17], mantle cell lymphoma [18], and others, we strongly advocate the use of this antibody to better visualize emperipolesis. One of a very few relevant differential diagnoses in this area of pathology is extranodal, primary soft tissue Rosai-Dorfman disease, in which emperipolesis is also invariably found. However, this histiocytic disorder presents with a different morphology, and the tumor cells are, in contrast to MIFS, practically always S100 protein positive.

In summary, we report 9 cases of PHAT which, in our view, based on histomorphologic criteria, merely represent a morphologic variant of MIFS. Apart from the hyalinized vessels, the only difference between these 2 entities might be seen in the stromal component, which in about half of the cases of PHAT is more hypocellular and edematous. The identical gene rearrangement of TGFBR3 and MGEA5 in a significant proportion of cases of PHAT and MIFS lends further support to the proposition that these 2 entities are likely morphologic variants of the same tumor.

References

[1] Smith ME, Fisher C, Weiss SW. Pleomorphic hyalinizing angiectatic tumor of soft parts. A low-grade neoplasm resembling neurilemoma. Am J Surg Pathol 1996;20:21–9.

[2] Illueca C, Machado I, Cruz J, Almenar S, Noguera R, Navarro S, et al. Pleomorphic hyalinizing angiectatic tumor: a report of 3 new cases, 1 with sarcomatous myxofibrosarcoma component and another with unreported soft tissue palpebral location. Appl Immunohistochem Mol Morphol 2012;20:96–101.

[3] Kazakov DV, Pavlovsky M, Mukensnabl P, Michal M. Pleomorphic hyalinizing angiectatic tumor with a sarcomatous component recurring as high-grade myxofibrosarcoma. Pathol Int 2007;57:281–4.

[4] Mitsuhashi T, Barr RJ, Machtinger LA, Cassarino DS. Primary cutaneous myxofibrosarcoma mimicking pleomorphic hyalinizing angiectatic tumor (PHAT): a potential diagnostic pitfall. Am J Dermatopathol 2005;27:322–6.

[5] Michal M, Kazakov DV, Hadravský L, Kinkor Z, Kuroda N, Michal M. High-grade myxoinflammatory fibroblastic sarcoma: a report of 23 cases. Ann Diagn Pathol 2015;19:157–63.

[6] Kinkor Z, Mukensnabl P, Michal M. Inflammatory myxohyaline tumor with massive emperipolesis. Pathol Res Pract 2002;198:639–42.

[7] Laskin WB, Fetsch JF, Miettinen M. Myxoinflammatory fibroblastic sarcoma: a clinicopathologic analysis of 104 cases, with emphasis on predictors of outcome. Am J Surg Pathol 2014;38:1–12.

[8] Carter JM, Sukov WR, Montgomery E, Goldblum JR, Billings SD, Fritchie KJ, et al. TGFBR3 and MGEA5 rearrangements in pleomorphic hyalinizing angiectatic tumors and the spectrum of related neoplasms. Am J Surg Pathol 2014;38:1182–992.

[9] Capovilla M, Birembaut P. Primary cutaneous myxofibrosarcoma mimicking pleomorphic hyalinizing angiectatic tumor (PHAT): a potential diagnostic pitfall. Am J Dermatopathol 2006;28:276–7 [author reply 277–278].

[10] Suarez-Vilela D, Izquierdo-Garcia FM. Lipoblast-like cells in early pleomorphic hyalinizing angiectatic tumor. Am J Surg Pathol 2005;29:1257–9 [author reply 1259].

[11] Lin L, Hicks D, Xu B, Sigel JE, Bergfeld WF, Montgomery E. Expression profile and molecular genetic regulation of cyclin D1 expression in epithelioid sarcoma. Mod Pathol 2005;18:705–9.

[12] de Vreeze RS, van Coevorden F, Boerrigter L, Nederlof PM, Haas RL, Bras J, et al. Delineation of chondroid lipoma: an immunohistochemical and molecular biological analysis. Sarcoma 2011;2011:638403.

[13] Laskin WB, Lasota JP, Fetsch JF, Felisiak-Golabek A, Wang ZF, Miettinen M. Intranodal palisaded myofibroblastoma: another mesenchymal neoplasm with CTNNB1 (beta-catenin gene) mutations: clinicopathologic, immunohistochemical, and molecular genetic study of 18 cases. Am J Surg Pathol 2015;39:197–205.

[14] Oliva E, Young RH. Stromal tumours of the ovary: an update. Diagn Histopathol 2014;20:376–84.

[15] Irving JA, Lee CH, Yip S, Oliva E, McCluggage WG, Young RH. Microcystic stromal tumor: a distinctive ovarian sex cord-stromal neoplasm characterized by FOXL2, SF-1, WT-1, Cyclin D1, and beta-catenin nuclear expression and CTNNB1 mutations. Am J Surg Pathol 2015;39:1420–6.

[16] Lee CH, Ali RH, Rouzbahman M, Marino-Enriquez A, Zhu M, Guo X, et al. Cyclin D1 as a diagnostic immunomarker for endometrial stromal sarcoma with YWHAE-FAM22 rearrangement. Am J Surg Pathol 2012;36:1562–70.

[17] Mirkovic J, Calicchio M, Fletcher CD, Perez-Atayde AR. Diffuse and strong cyclin D1 immunoreactivity in clear cell sarcoma of the kidney. Histopathology 2015;67:306–12.

[18] Bosch F, Jares P, Campo E, Lopez-Guillermo A, Piris MA, Villamor N, et al. PRAD-1/cyclin D1 gene overexpression in chronic lymphoproliferative disorders: a highly specific marker of mantle cell lymphoma. Blood 1994;84:2726–32.

1.1.3. HISTIOCYTOSIS WITH RAISINOID NUCLEI: A UNIFYING CONCEPT FOR LESIONS REPORTED UNDER DIFFERENT NAMES AS NODULAR MESOTHELIAL/HISTIOCYTIC HYPERPLASIA, MESOTHELIAL/MONOCYTIC INCIDENTAL CARDIAC EXCRESCENCES, INTRALYMPHATIC HISTIOCYTOSIS, AND OTHERS: A REPORT OF 50 CASES.

Nodular mesothelial/histiocytic hyperplasia, nodular histiocytic aggregates, mesothelial/monocytic incidental cardiac excrescences (MICE), reactive eosinophilic pleuritis, histioeosinophilic granuloma of the thymus, and intralymphatic histiocytosis are all names for benign reactive histiocytic proliferations occurring in different body sites. Several previous publications have established a link between some of these conditions. However, no publication has ever comprehensively addressed all of these lesions together in one study in an attempt to explain and discuss their striking analogy.

We collected 50 cases of these proliferations from various body locations. To prove that all lesions represent the same process, we first analyzed their morphological features which were basically identical. However, based on the exact location, the histiocytes may be admixed with various other types of cells or tissues, and that was also the reason why most of them have not been linked to each other before. For example, lesions called nodular histiocytic hyperplasia occur on the serosal surfaces and therefore usually contain an additional admixture of mesothelial cells. On the other hand, probably due to the presence of air, the histiocytic lesions in the thymus (after pneumomediastinum was iatrogenically created) and in the lungs (after pneumothorax) contained an admixture of eosinophils.

Secondly, we used a fairly wide panel of histiocytic antibodies consisting of the following markers: CD68, CD163, CD4, Lysozyme, CD45, CD11c, CD64, CD14. The most sensitive markers turned out to be CD68, CD163, CD64 and also CD4. We also applied CD1a, Langerin and S100 protein to exclude the possibility of Langerhans cell histiocytosis which consistently yielded negative results.

Thirdly, besides analyzing the morphological and immunohistochemical features, we also performed a fairly exhaustive literature review. We pointed out the similarities between these processes and also found previous articles suggesting a potential link between some of the entities. Most of the evidence supports the concept that these proliferations occur as an unspecific reaction to an injury, that is, a trauma, inflammation, infiltratively growing malignancy, surgical procedure, etc. In most cases, they occur as an incidental finding during a diagnostic process for other purposes. Also, they are invariably benign and, with the exception of the skin, asymptomatic. These innocuous lesions can sometimes cause considerable differential diagnostic difficulties by resembling a metastatic carcinoma or Langerhans cell histiocytosis.

In summary, we studied 50 cases of peculiar histiocytic proliferations that occur in diverse body sites and bear various names based on the affected organ. These innocuous lesions can sometimes cause considerable differential diagnostic difficulties by resembling a metastatic carcinoma or Langerhans cell histiocytosis. We provided evidence that all of them share the same morphologic, immunohistochemical, and pathogenetic properties, thus they all represent the same pathologic process and should be referred to as such. Based on their typical nuclear features we proposed a collective term “histiocytosis with raisinoid nuclei” for them.

Histiocytosis With Raisinoid Nuclei: A Unifying Concept for Lesions Reported Under Different Names as Nodular Mesothelial/Histiocytic Hyperplasia, Mesothelial/Monocytic Incidental Cardiac Excrescences, Intralymphatic Histiocytosis, and Others

A Report of 50 Cases

Michael Michal, MD, Dmitry V. Kazakov, MD,† Pavel Dundr, MD,‡ Kvetoslava Peckova, MD,† Abbas Agaimy, MD,§ Heinz Kutzner, MD,‖ Frantisek Havlicek, MD,¶ Ondřej Daum, MD,† Magdalena Dubova, MD,† and Michal Michal, MD†*

Abstract: We report 50 cases of peculiar histiocytic proliferations occurring in diverse body sites that currently bear various names, including nodular mesothelial/histiocytic hyperplasia, nodular histiocytic aggregates, mesothelial/monocytic incidental cardiac excrescences, reactive eosinophilic pleuritis, histioeosinophilic granuloma of the thymus, and intralymphatic histiocytosis. They can sometimes cause considerable differential diagnostic difficulties by resembling a metastatic carcinoma or Langerhans cell histiocytosis. Several previous publications have established a link between some of these conditions, suggesting that these are merely variations within a histopathologic spectrum, affecting different organs and bearing different names based on a particular location. However, no publication has ever comprehensively addressed all of these lesions together in one study in an attempt to explain and discuss their striking analogy. Having studied a large series of cases we provide evidence that all these lesions share the same morphologic, immunohistochemical, and pathogenetic properties, thus they all represent the same pathologic process and should be referred to as such. Taking into account their typical nuclear features we propose a collective term "histiocytosis with raisinoid nuclei" for this spectrum of conditions.

Key Words: nodular mesothelial histiocytic hyperplasia, MICE, mesothelial monocytic incidental cardiac excrescences, histioeosinophilic granuloma, reactive eosinophilic pleuritis, intralymphatic histiocytosis, histiocytosis with raisinoid nuclei, Langerhans cell histiocytosis, histiocytes

(*Am J Surg Pathol* 2016;40:1507–1516)

Nodular mesothelial/histiocytic hyperplasia (NHMH), nodular histiocytic aggregates, mesothelial/monocytic incidental cardiac excrescences (MICE), reactive eosinophilic pleuritis (REP), histioeosinophilic granuloma (HEG) of the thymus, and intralymphatic histiocytosis (ILH) are all names for benign reactive histiocytic proliferations occurring in different body sites. Several previous publications have established a link between some of these conditions. However, no publication has ever comprehensively addressed all of these lesions together in one study in an attempt to explain and discuss their striking analogy.

Herein, we are offering a unifying concept for these peculiar histiocytic proliferations by presenting 50 cases from diverse body locations with a detailed immunohistochemical study, adding REP, HEG of the thymus, and mainly ILH to the spectrum of these lesions. On the basis of the characteristic nuclear features, we propose the name "histiocytosis with raisinoid nuclei" (HRN).

MATERIALS AND METHODS

The 50 cases constituting the subject of this study were retrieved from the authors' files. The clinical information was

From the *Department of Pathology, Charles University, Biomedical Center; †Department of Pathology, Charles University, Medical Faculty and Charles University Hospital Plzen, Plzen; ‡Department of Pathology, First Faculty of Medicine and General University Hospital, Charles University in Prague, Prague; ¶Department of Pathology, Regional Hospital Benesov, Benesov, Czech Republic; §Institute of Pathology, Friedrich-Alexander University Erlangen-Nürnberg, University Hospital, Erlangen; and ‖Dermatopathologische Gemeinschaftspraxis, Friedrichshafen, Germany.

Conflicts of Interest and Source of Funding: Supported by the National Sustainability Program I (NPU I) Nr. LO1503 provided by the Ministry of Education Youth and Sports of the Czech Republic. The authors have disclosed that they have no significant relationships with, or financial interest in, any commercial companies pertaining to this article.

Correspondence: Michael Michal, MD, Department of Pathology, Charles University, Medical Faculty and Charles University Hospital Plzen, Alej Svobody 80, 304 60 Pilsen, Czech Republic (e-mail: michael.michal@medima.cz).

extracted from the registry records. To retrieve the cases, we searched our consultation registry files using key words, including "nodular mesothelial hyperplasia," "nodular histiocytic hyperplasia," "nodular histiocytic aggregates," "mesothelial monocytic cardiac excrescences," "MICE," "intralymphatic histiocytosis," "histioeosinophilic granuloma," "Askin's pleuritis," and "reactive eosinophilic pleuritis." This search yielded altogether 50 specimens, which were reviewed. Cases 18, 21, and 34 to 49 have already been a subject of previous studies.[1–5]

For conventional microscopy, tissues were fixed in formalin, routinely processed, and stained. The immunohistochemical analysis was performed using a Ventana BenchMark ULTRA (Ventana Medical System Inc., Tucson, AZ). The primary antibodies used are shown in Table 1. They were visualized using the enzymes alkaline phosphatase or peroxidase as detecting systems (both purchased from Ventana Medical System Inc.).

RESULTS

Clinical Findings

The clinical features are summarized in Table 2. The patients were 32 women and 15 men; in the remaining cases the sex was unknown. The age of the patients at the time of diagnosis ranged from 4 to 85 years (mean: 50.1 y). In general, the lesions were frequently of microscopic size, consisting of few hundreds of cells, sometimes creating larger cellular nodules that measured up to 1 to 2 cm in diameter.

Histopathologic Findings

All histiocytic proliferations included in our study had a similar morphology, with some of the lesions showing an additional component. A very characteristic feature seen in the majority of the cases was the tendency to create nodular and well-circumscribed cellular aggregates that infrequently resembled an epithelial neoplasm (Fig. 1). These nodules consisted of compact aggregates of polygonal to ovoid histiocytes with a moderate amount of eosinophilic cytoplasm, which were enmeshed in a prominent fibrin deposition. Admixed with the histiocytes was a varying amount of other inflammatory cells. The histiocytes possessed a very characteristic nucleus that varied mildly in size and which, depending on the plane of section, was oval, irregular, or "shrunk" with a slight nuclear groove reminiscent of a raisin or, sometimes, of a coffee bean (Fig. 2). These raisinoid nuclei had 1 or 2 inconspicuous nucleoli. Mitotic figures were very scarce to absent. In cases in which the underlying condition was the air insufflation as in pneumothorax or in HEGs of the thymus, a prominent admixture of eosinophils was observed (Fig. 3). In the lesions situated on the peritoneal surfaces, a varying amount of clusters of mesothelial cells was present, sometimes creating strips, ribbons, or micropapillary structures.

Immunohistochemical Findings

The immunohistochemical findings are summarized in Table 3. The most sensitive markers were CD68, CD163, CD4, and CD64, which were expressed in all cases, yielding a strong and diffuse staining. Lysozyme and CD45 were also expressed in a great majority of cases, albeit the latter often weakly. Staining with CD11c and CD14 was insensitive, with positive expression in 52% and 29% of cases, respectively, but in almost a half of the positive cases, the staining was very weak or restricted to only few cells (Figs. 4C–H, 5). Staining with the Langerhans cell markers CD1a, Langerin, and S100 protein consistently yielded negative results.

DISCUSSION

In 1974, without the use of electron microscopy and in "preimmunohistochemistry era," Rosai and Dehner[6] presented a peculiar and characteristic lesion occurring in herniorrhaphy specimens consisting of solid nodules of atypical mesothelial cells for which they coined the term "nodular mesothelial hyperplasia in hernia sacs." With the advent of immunohistochemistry, the majority of cells constituting these tumor-like infiltrates was shown to represent histiocytes with only a minor admixture of mesothelial population,[7,8] eventually leading to the current designation "nodular histiocytic/mesothelial hyperplasia" (NHMH).[7] Since the initial description, identical histiocytic lesions intermixed with strips of mesothelial cells have been described at other body sites, for example, the pleura,[8,9] lungs,[7,10] on the peritoneum outside hernia sacs[7,9–12] in association with various pathologic states, or in the greater

TABLE 1. List of Antibodies

Antibody	Clone	Manufacturer	Dilution
CD68	KP1	Dako, Glostrup, Denmark	1:100
CD163	MRQ-26	Cell Marque, Rocklin, CA	Prediluted
CD4	SP35	Ventana, Tucson, AZ	Prediluted
CD45	2B11 + PD7/26	Dako	1:100
Lysozyme	Polyclonal	Cell Marque	Prediluted
CD11c	5D11	Zytomed Systems, Berlin, Germany	1:50
CD64	3D3	Abcam, Cambridge, UK	1:200
CD14	7	Novocastra, Newcastle, UK	1:50
CD1a	MTB1	Cell Marque	Prediluted
Langerin	12D6	Novocastra	1:100
S100	Polyclonal	Ventana	Prediluted
CD31	JC70A	Dako	1:40
Podoplanin	D2-40	Dako	Prediluted

TABLE 2. Clinical Features

Case No.	Age/Sex	Location	Clinical Information
1	61/M	Peritoneum	Severe peritoneal adhesions with multilocular peritoneal cyst
2	32/F	Peritoneum	Endometriosis in the wall of a ruptured ovarian cyst
3	69/M	Peritoneum	Deciduoid mesothelioma
4	48/F	Peritoneum	Cell block from a fluid from cavum Douglasi
5	33/F	Peritoneum	Hydrocele in inguinal canal
6	60/M	Peritoneum	Inguinal hernia
7	5/M	Peritoneum	Spermatocele of funiculus spermaticus
8	70/F	Peritoneum	Uterus myomatosus, diverticulitis and severe abdominal adhesions.
9	45/F	Peritoneum	Endosalpingiosis of omentum and ovarian cysts
10	36/F	Peritoneum	Multilocular mesothelial cyst
11	19/M	Peritoneum	Liver biopsy without any other remarkable finding
12	45/F	Peritoneum	Serous cystic tumor of borderline malignancy with peritoneal implants
13	29/F	Peritoneum	Excision from lesser pelvis without any other remarkable finding
14	22/M	Peritoneum	Excision of adipose tissue from terminal ileum with fat necrosis
15	31/F	Peritoneum	Excision from cavum Douglasi without any other remarkable finding
16	67/M	Peritoneum	Metastasis of hepatocellular carcinoma to the soft tissues of the umbilical area
17	58/F	Peritoneum	Hernia sac
18	55/F	Peritoneum	Umbilical hernia. Bilateral ovarectomy for ovarian fibromas, omentectomy
19	33/F	Peritoneum	Inflammation of an ovarian cyst with peritoneal abscess
20	28/F	Peritoneum	Endometriosis in the wall of a ruptured ovarian cyst
21	59/F	Fallopian tube and peritoneum	High grade serous carcinoma with peritoneal spread
22	51/F	Fallopian tube	High grade serous carcinoma without peritoneal involvement
23	55/F	Thyroid gland	Goiter, Post-fine-needle aspiration myofibroblastic proliferation
24	37/F	Thyroid gland	Goiter, Post-fine-needle aspiration myofibroblastic proliferation
25	4/F	Knee	Puncture of the knee effusion after a knee trauma few weeks before
26	65/F	Mediastinum	Cyst lined by mesothelium
27	67/M	Pleura	Parietal pleura with mesothelial proliferation
28	34/F	Pleura	Spontaneous pneumothorax, patient with bullous emphysema
29	71/F	Pleura	Fluidothorax of unknown etiology
30	48/F	Pleura	Iatrogenic pneumothorax, patient with bullous emphysema
31	33/F	Pericardium	Synchronous solitary fibrous tumor of pleura
32	59/F	Pericardium	Pericardial cyst
33	65/F	Pericardium	Pericardial cyst. History of metastatic ductal breast carcinoma in the lung with mastectomy
34	NA	Aorta	Aortic dissection
35	66/F	Aorta	Aortic dissection
36	58/M	Aorta	Aortic dissection
37	NA	Aorta	Aortic dissection
38	32/F	Thymus	Myasthenia gravis
39	52/M	Thymus	Myasthenia gravis
40	54/F	Thymus	Myasthenia gravis
41	NA	Thymus	Thymoma type B
42	68/M	Skin—eyelid	Melkersson-Rosenthal syndrome, unilateral eyelid swelling
43	65/M	Skin—thigh	Erythema on the surgical scar after hip joint replacement with a metal prosthesis
44	63/M	Skin—hip	Erythema on the surgical scar after hip joint replacement with a metal prosthesis
45	48/M	Skin—chest	NA
46	84/F	Skin—arm	Indurated plaque
47	79/M	Skin—abdomen	Multiple excoriated papules
48	85/F	Skin—arm	Livid erythema
49	78/F	Skin—elbow	Scaly induration
50	29/F	Skin—vulva	Bartholin gland cyst

omentum in patients with ovarian cancer.[13] Virtually identical proliferations, called nodular histiocytic hyperplasia or nodular histiocytic aggregates,[2,8,14–17] have also been reported in the endometrium[15–17] and fallopian tubes[2] (Figs. 2, 6), likewise occurring in association with medical intervention or some pathologic states (postcurettage, bleeding, infertility, inflammation, polyps, or carcinoma). Additional lesions that in our opinion belong to this spectrum are REP described by Askin et al,[18] HEG of the thymus reported by Havlicek and Rosai[4,19] (Fig. 3), histiocytoid hemangioma,[20]—later renamed "mesothelial/monocytic incidental cardiac excrescences" (MICE)[3,9,21–28] of the heart (Fig. 1)—and ILH.[5,29–33]

All the presented lesions have several substantial features in common. The morphology of the histiocytes is identical. They have a moderate amount of eosinophilic cytoplasm, and they reveal the same nuclear features, namely irregular, contorted shape, sometimes with a slight nuclear groove, that closely resembles that of a shrunken raisin or a coffee bean, which can alone provide a high level of suspicion for the correct diagnosis (Fig. 2). A very similar raisinoid shape can be seen in the nuclei of

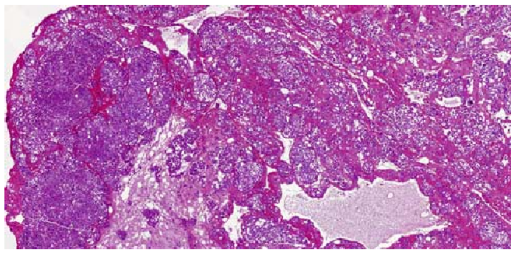

FIGURE 1. A very characteristic feature seen in the majority of the cases was the tendency to create nodular and well-circumscribed cellular aggregates that infrequently resembled an epithelial neoplasm. These nodules consisted of compact aggregates of polygonal to ovoid histiocytes with a moderate amount of eosinophilic cytoplasm, which were enmeshed in a prominent fibrin deposition. Admixed with the histiocytes was a varying amount of other inflammatory cells (case 31; hematoxylin and eosin).

poorly differentiated carcinomas of the thyroid or in the nuclei of chromophobe renal cell carcinomas, where the term "raisinoid" was introduced to the diagnostic pathology.[34] All

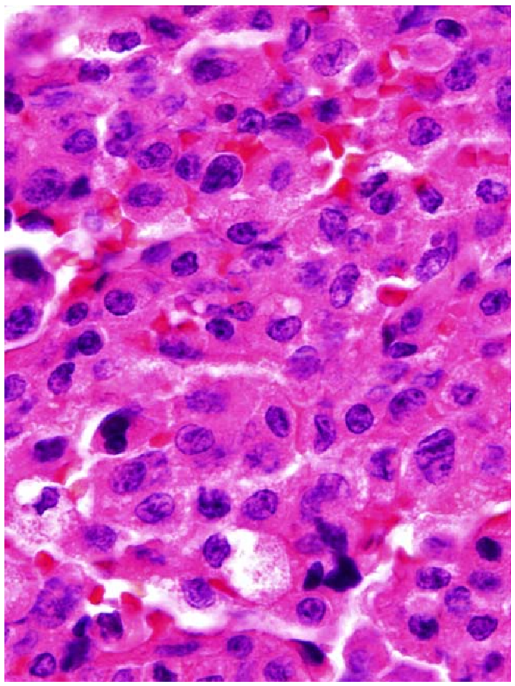

FIGURE 2. The histiocytes possessed a very characteristic nucleus that varied mildly in size and which, depending on the plane of section, was oval, irregular, or "shrunk" with a slight nuclear groove reminiscent of a raisin or, sometimes, of a coffee bean (case 21; hematoxylin and eosin).

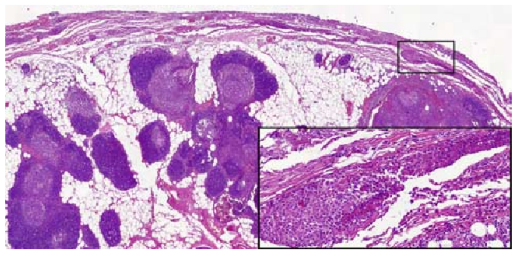

FIGURE 3. In cases in which the underlying condition was the air insufflation as in pneumothorax or in histioeosinophilic granulomas of the thymus, a prominent admixture of eosinophils (inset) was observed (case 38; hematoxylin and eosin).

these lesions tend to aggregate into nodules, often multiple, thus simulating an epithelial neoplasm. The mixture of cells constituting the nodules is also very similar, differing slightly on the basis of the anatomic site. The raisinoid histiocytes are found entrapped in fibrin, surrounded by a various number of other inflammatory cells. In cases of ILH, this cellular mixture is encountered in dilated dermal lymphatics (Figs. 4A, B). Interestingly, a virtually identical picture was seen in our cases 17 and 18 (the latter case was already published[1]). Besides the prototypical picture of NHMH in hernia showing a histiocytic proliferation located on the peritoneal surface, the neighboring lymphatic vessels were dilated, containing a prominent mixture of histiocytes and inflammatory cells identical to those seen in ILH (Figs. 7A, B). The lymphatics in these cases expressed CD31 and podoplanin. The latter stain also nicely highlighted the scattered mesothelial cells in the lumen, whereas most of the remaining luminal cells reacted strongly with CD163 (Figs. 7C, D). Moreover, in the sections taken from the skin overlying the hernia in case 18, the same cellular mixture was present even in the dermal lymphatics.[1] We believe that exactly the same phenomenon was also described in the paper by Suarez Vilela and Izquierdo Garcia.[35] The mechanism of passive lymphatic transport of all kinds of cellular and noncellular material is well described in the literature,[36] including the transport of mesothelial cells.[35,37–39] In a similar manner, provided the biopsy is taken from the surrounding skin, the lymphatic drainage of a pathologic process located, for example, in an inflamed rheumatic joint (ILH is most commonly associated with metal implants after joint replacement or with systemic inflammatory processes such as rheumatoid arthritis), where no mesothelial cells are present, may result in the histopathologic finding of mere histiocytes and other inflammatory cells as it is in cases of ILH. Another fact that lends credit to this concept is case 25, in which a biopsy was obtained by a puncture of knee effusion after a preceding trauma in this area, and it revealed a mixture of fibrin, inflammatory cells, and histiocytes characteristic for HRN arranged in variably sized nodules, thus providing evidence that HRN can also occur in the interarticular area. The mesothelial cell component in this area was obviously missing here, as it is missing in ILH. The

TABLE 3. Immunohistochemical Features

Case No.	Diagnosis	Location	CD68	CD163	CD4	Lysozyme	CD45	CD11c	CD64	CD14
1	NHMH	Peritoneum	++	++	+	–	++	–	++	–
2	NHMH	Peritoneum	++	++	++	++	++	+		
3	NHMH	Peritoneum	++	++	++	++	++	+	++	+
4	NHMH	Peritoneum	++	++	++	++	+	–		
5	NHMH	Peritoneum				NA				
6	NHMH	Peritoneum	++	++	++	++	++	++	++	++
7	NHMH	Peritoneum	++	++	++	NA	+	–		
8	NHMH	Peritoneum	++	++	++	++	+	–	++	–
9	NHMH	Peritoneum	++	++	++	++	+	–		
10	NHMH	Peritoneum	++	++	++	+	+	–	++	++
11	NHMH	Peritoneum	++	++	++	–	–	–		
12	NHMH	Peritoneum	++	++	++	++	++	–	++	–
13	NHMH	Peritoneum	++	++	++	++	++	+		
14	NHMH	Peritoneum	++	++	++	++	++	++		
15	NHMH	Peritoneum	++	++	++	++	–	–		
16	NHMH	Peritoneum				NA				
17	NHMH	Peritoneum	++	++	++	++	+	–	++	–
18	NHMH	Peritoneum	++	++	++	++	++	++	++	–
19	NHMH	Peritoneum	++	++	++	–	++	–		
20	NHMH	Peritoneum	++	++	++	++	++	++	++	–
21	NHMH	Fallopian tube and peritoneum	++	++	++	+	–	+		
22	NHMH	Fallopian tube	++	++	++	++	+	–		
23	NHMH	Thyroid gland	++	++	++	++	++	++		
24	NHMH	Thyroid gland	++	++	++	++	++	++		
25	NHMH	Knee	++	++	++	++	++	++		
26	NHMH	Mediastinum	++	++	++	++	++	+	++	–
27	REP	Pleura				NA				
28	REP	Pleura	++	++		++	+	++	++	+
29	REP	Pleura	++	++	++	++	+	–		
30	REP	Pleura	++	++	++	++	+	++	++	NA
31	MICE	Pericardium	++	++	++	++	–	–	++	–
32	MICE	Pericardium	++	++	++	+	++	–		
33	MICE	Pericardium	++	++	++	+	+	+		
34	MICE	Aorta	++	++	++	–	++	–		
35	MICE	Aorta	++	++	++	–	+	–		
36	MICE	Aorta	++	++	++	+	++	–		
37	MICE	Aorta	++	++	++	+	++	–		
38	HEG	Thymus	++	++	++	++	+	++	++	–
39	HEG	Thymus	++	++	++	++	+	–	++	–
40	HEG	Thymus	++	++	+	++	–	–		
41	HEG	Thymus	++	++	++	++	NA	++		
42	ILH	Skin	++	++	++	++	++	++		
43	ILH	Skin				NA				
44	ILH	Skin	++	++	++	++	+	++		
45	ILH	Skin	++	++	++	++	++	++		
46	ILH	Skin	++	++	+	++	+	+		
47	ILH	Skin	++	++	+	++	NA	+		
48	ILH	Skin				NA				
49	ILH	Skin	++	++	++	++	NA	NA		
50	ILH	Skin	++	++	++	++	++	++		
Overall (n [%])			45/45 (100)	45/45 (100)	45/45 (100)	39/44 (89)	37/42 (88)	23/44 (52)	15/15 (100)	4/14 (29)
			++45	++45	++41	++33	++21	++15	++15	++2
			+0	+0	+4	+6	+16	+8	+0	+2
			−0	−0	−0	−5	−5	−21	−0	−10

++Strong and diffuse staining.
+Weak or focal staining.
–Negative staining.
NA indicates not available/analyzable.

immunohistochemical features of ILH are of course identical to those of other discussed lesions (Figs. 4C–H, 5).

Another trauma-associated lesion was seen in cases 23 and 24, in which we have encountered a previously unreported association of HRN with a fine-needle aspiration procedure in the thyroid gland. Next to a typical example of a post–fine-needle aspiration spindle cell nodule as described by Baloch et al,[40] we found HRN located in a nearby follicle admixed with foamy cells and siderophages, further supporting its reactive origin.

If HRN is located on the serosal surfaces (or communicating with a serosal surface as in some cases of

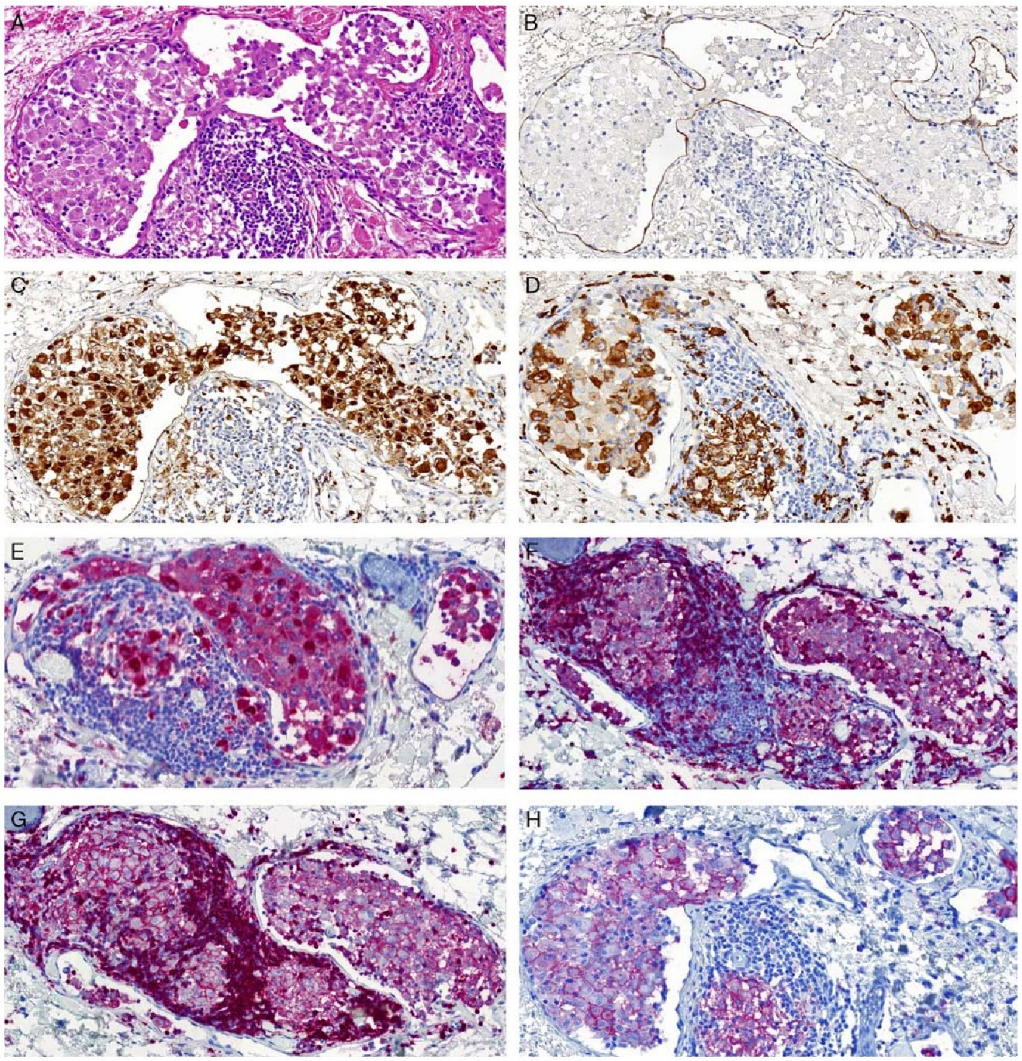

FIGURE 4. In cases of ILH, the typical cellular mixture is encountered in dilated dermal lymphatics (A, Hematoxylin and eosin. B, Podoplanin). The immunohistochemical features of ILH are identical to those of other discussed lesions: (C) CD68; (D) CD163; (E) lysozyme; (F) CD4; (G) CD45; (H) CD11c (case 42).

MICE), a varied amount of mesothelial cells is often present. The stripped mesothelium mostly creates ribbons or micropapillary structures, and infrequently they may be a dominant component. Such cases are the most deceptive for pathologists, inasmuch as they can be confused with a primary serosal tumor. However, as evident from cases 3, 12, 16, 21, and 22, HRN can be associated even with a carcinoma (Fig. 6), carcinoma metastasis, or mesothelioma.

We have seen a strong association of an increased number of eosinophils with a specific underlying cause.[4,18] The lesions in which the pleural surface came in contact with air, namely in cases of pneumothorax (cases 28 and 30) or when a pneumomediastinum was iatrogenically used (cases 38 to 41), the number of eosinophils sometimes overnumbered that of histiocytes. We think this is also one of the reasons why the original descriptions of REP and later of HEG missed the association with

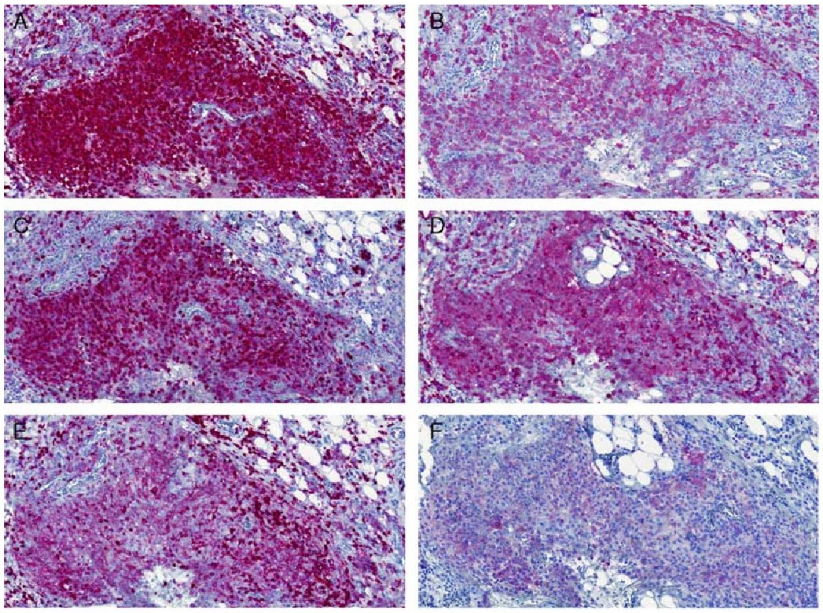

FIGURE 5. The immunohistochemical features of a typical case of HRN (case 14); (A) CD68; (B) CD163; (C) lysozyme; (D) CD4; (E) CD45; (F) CD11c.

NHMH described few years before. Another reason is the absence of stripped mesothelium in REP and HEG, which were in that time considered the defining constituent of NHMH.

In many cases, the auxiliary methods are the key to the correct diagnosis, and the immunohistochemical properties are also the second feature that links all discussed lesions together (Figs. 4C–H, 5). The classical histiocytic markers CD68, CD163, and lysozyme are well known to be expressed in each of these lesions, and they indeed were positive in all or most of our cases. CD64 and CD4 are other markers that were always positive in our series, which to our knowledge has not been reported so far in any of the discussed lesions. However, regarding CD4, it is sometimes difficult to distinguish between the positivity in the histiocytes and the surrounding T lymphocytes. CD45 positivity was briefly mentioned in 2 case reports and a small cohort.[10,41,42] We have studied the expression of this antibody in our large series, and, although CD45 was expressed in 88% of our cases, the staining was often weak. Moreover, it had the same disadvantage as CD4, labeling not only T lymphocytes but also a majority of other adjacent inflammatory cells. We also investigated the possible application of the antibody CD11c in the diagnostic process but found inconsistent results. The markers CD1a, Langerin, and S100 protein, which are commonly used for the diagnosis of the LCH, were negative in all our cases. For comparison, we

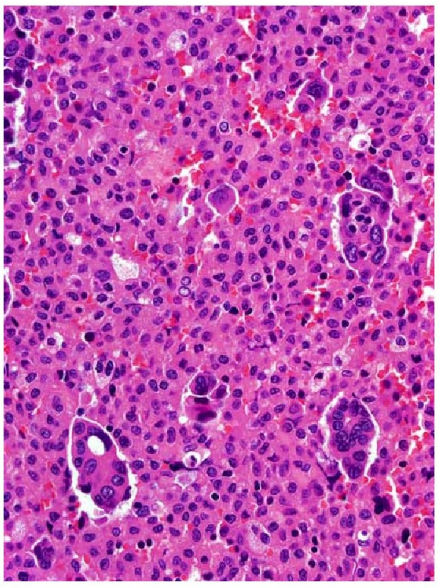

FIGURE 6. HRN can be associated even with a carcinoma. Therefore a careful search for additional malignant cells is warranted (case 21; hematoxylin and eosin).

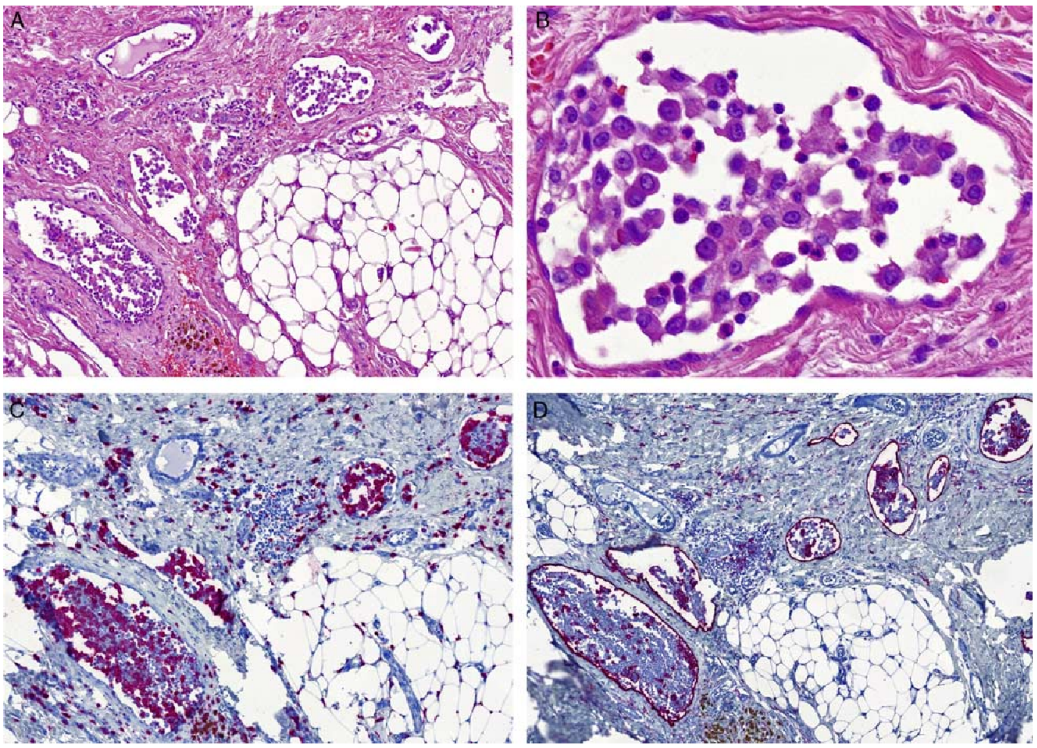

FIGURE 7. A and B, A virtually identical picture as in cases of ILH was seen in our case 17. Besides the prototypical picture of NHMH in hernia showing a histiocytic proliferation located on the peritoneal surface, the neighboring lymphatic vessels were dilated, containing a prominent mixture of histiocytes and inflammatory cells identical to those seen in ILH. D, The lymphatics in this case expressed podoplanin. This stain also nicely highlighted the scattered mesothelial cells in the lumen, whereas most of the remaining luminal cells reacted strongly with CD163 (C).

applied CD68, CD163, CD45, CD4, CD11c, and lysozyme on 4 cases of nodal LCH and found that Langerhans cells quite constantly, albeit sometimes only weakly, reacted with each antibody, a finding that is in concordance with the previously published literature.[43,44] On the basis of the immunohistochemical results, it seems that the lesional cells of HRN represent nonspecific histiocytes, as all other subtypes including Langerhans cells (S100+/CD1a+) and interdigitating dendritic cells (S100+) have been excluded by the appropriate markers.

Most of the presented evidence supports the concept that these proliferations occur as an unspecific reaction to an injury, that is, a trauma, inflammation, infiltratively growing malignancy, surgical procedure, etc. In most cases, they occur as an incidental finding during a diagnostic process for other purposes. Also, they are invariably benign and, with the exception of the skin, asymptomatic.

On the basis of the relatively small number of cases published in the literature, it seems that HRN might be a rare finding. However, thanks to our raised susceptibility to these lesions, only over the course of writing of this article, we came across 5 additional cases in our routine diagnostic practice. Hence, in our opinion, HRN is a fairly common, albeit an underrecognized and underreported lesion.

The differential diagnosis of reactive HRN depends on the specific location. In general, morphologically challenging cases, especially those containing stripped mesothelium, may mimic a carcinoma. When the pathologist is familiar with the existence of HRN, the latter can be usually readily diagnosed without the use of immunohistochemistry. In cases in which LCH is a differential diagnostic consideration, immunohistochemistry is needed. As mentioned before, most of the markers reacting with cells of HRN might overlap with those of LCH. Therefore we recommend the use of one of the LCH-specific markers such as S-100 protein, CD1a, or Langerin as a negative discriminator, when necessary. Also, morphologically, the cells of LCH and HRN are

slightly different in their nuclear features, with LCH showing greater size of nuclei and much more prominent nuclear grooves. Similarly, the raisinoid histiocytes of HRN should not be confused with the cerebroid nuclei of mycosis fungoides and lymphoblastic lymphoma or the cleaved nuclei of follicular lymphoma.

In summary, the last 40 years of research gave rise to a plethora of reactive histiocytic lesions occurring at diverse body sites, each having a different terminology. The literature review and the 50 cases we presented herein provide sufficient evidence for their similar origin and pathogenesis and a reason for consideration of these conditions as part of a single morphologic spectrum, allowing dropping out numerous puzzling terms and their unification under a collective name. On the basis of the characteristic nuclear features we propose the designation "histiocytosis with raisinoid nuclei."

REFERENCES

1. Agaimy A. Benign mesothelial nodules within dermal vessels associated with huge umbilical hernia: a potential mimicker of malignancy. *Am J Surg Pathol*. 2011;35:152–153.
2. Michal M, Rotter L, Kazakov DV. Nodular histiocytic aggregates in fallopian tube. *Int J Gynecol Pathol*. 2015;34:151.
3. Strecker T, Bertz S, Wachter DL, et al. Mesothelial/monocytic incidental cardiac excrescences (cardiac MICE) associated with acute aortic dissection: a study of two cases. *Int J Clin Exp Pathol*. 2015;8:3850–3856.
4. Halicek F, Rosai J. Histioeosinophilic granulomas in the thymuses of 29 myasthenic patients: a complication of pneumomediastinum. *Hum Pathol*. 1984;15:1137–1144.
5. Requena L, El-Shabrawi-Caelen L, Walsh SN, et al. Intralymphatic histiocytosis. A clinicopathologic study of 16 cases. *Am J Dermatopathol*. 2009;31:140–151.
6. Rosai J, Dehner LP. Nodular mesothelial hyperplasia in hernia sacs: a benign reactive condition simulating a neoplastic process. *Cancer*. 1975;35:165–175.
7. Chan JK, Loo KT, Yau BK, et al. Nodular histiocytic/mesothelial hyperplasia: a lesion potentially mistaken for a neoplasm in transbronchial biopsy. *Am J Surg Pathol*. 1997;21:658–663.
8. Ordonez NG, Ro JY, Ayala AG. Lesions described as nodular mesothelial hyperplasia are primarily composed of histiocytes. *Am J Surg Pathol*. 1998;22:285–292.
9. Walley VM, Peters HJ, Veinot JP, et al. The clinical and pathologic manifestations of iatrogenically produced mesothelium-rich fragments of operative debris. *Eur J Cardiothorac Surg*. 1997;11:328–332.
10. Chikkamuniyappa S, Herrick J, Jagirdar JS. Nodular histiocytic/mesothelial hyperplasia: a potential pitfall. *Ann Diagn Pathol*. 2004;8:115–120.
11. Clement PB. Reactive tumor-like lesions of the peritoneum. *Am J Clin Pathol*. 1995;103:673–676.
12. Ruffolo R, Suster S. Diffuse histiocytic proliferation mimicking mesothelial hyperplasia in endocervicosis of the female pelvic peritoneum. *Int J Surg Pathol*. 1993;1:101–106.
13. Lv Y, Li P, Zheng J, et al. Nodular histiocytic aggregates in the greater omentum of patients with ovarian cancer. *Int J Surg Pathol*. 2012;20:178–184.
14. Akhter S, Lawrence WD, Quddus MR. Polypoid nodular histiocytic hyperplasia associated with endometrioid adenocarcinoma of the endometrium: report of a case. *Diagn Pathol*. 2014;9:93.
15. Parkash V, Domfeh AB, Fadare O. Nodular histiocytic aggregates in the endometrium: a report of 7 cases. *Int J Gynecol Pathol*. 2014;33:52–57.
16. Kim KR, Lee YH, Ro JY. Nodular histiocytic hyperplasia of the endometrium. *Int J Gynecol Pathol*. 2002;21:141–146.
17. Fukunaga M, Iwaki S. Nodular histiocytic hyperplasia of the endometrium. *Arch Pathol Lab Med*. 2004;128:1032–1034.
18. Askin FB, McCann BG, Kuhn C. Reactive eosinophilic pleuritis: a lesion to be distinguished from pulmonary eosinophilic granuloma. *Arch Pathol Lab Med*. 1977;101:187–191.
19. Michal M, Havlicek F. Immunohistochemical phenotypes of histioeosinophilic granulomas of thymus and reactive eosinophilic pleuritis. *Acta Histochem*. 1993;94:97–101.
20. Rosai J, Gold J, Landy R. The histiocytoid hemangiomas. A unifying concept embracing several previously described entities of skin, soft tissue, large vessels, bone, and heart. *Hum Pathol*. 1979;10:707–730.
21. Luthringer DJ, Virmani R, Weiss SW, et al. A distinctive cardiovascular lesion resembling histiocytoid (epithelioid) hemangioma. Evidence suggesting mesothelial participation. *Am J Surg Pathol*. 1990;14:993–1000.
22. Veinot JP, Tazelaar HD, Edwards WD, et al. Mesothelial/monocytic incidental cardiac excrescences: cardiac MICE. *Mod Pathol*. 1994;7:9–16.
23. Chan JKC. Cardiac MICE: the dust settles. *Adv Anat Pathol*. 1995;2:48–51.
24. Argani P, Sternberg SS, Burt M, et al. Metastatic adenocarcinoma involving a mesothelial/monocytic incidental cardiac excrescence (cardiac MICE). *Am J Surg Pathol*. 1997;21:970–974.
25. Hu ZL, Lu H, Yin HL, et al. A case of mesothelial/monocytic incidental cardiac excrescence and literature review. *Diagn Pathol*. 2010;5:40.
26. Ton O, Polat N, Mansuroglu D, et al. Mesothelial/monocytic incidental cardiac excrescence in a patient with antiphospholipid syndrome. *Interact Cardiovasc Thorac Surg*. 2011;13:657–659.
27. Censi S, Dell'Amore A, Conti R, et al. Cardiac mesothelial/monocytic-incidental-excrescence: more than an artifactual lesion? *Interact Cardiovasc Thorac Surg*. 2008;7:1201–1203.
28. Courtice RW, Stinson WA, Walley VM. Tissue fragments recovered at cardiac surgery masquerading as tumoral proliferations. Evidence suggesting iatrogenic or artefactual origin and common occurrence. *Am J Surg Pathol*. 1994;18:167–174.
29. O'Grady JT, Shahidullah H, Doherty VR, et al. Intravascular histiocytosis. *Histopathology*. 1994;24:265–268.
30. Rieger E, Soyer HP, Leboit PE, et al. Reactive angioendotheliomatosis or intravascular histiocytosis? An immunohistochemical and ultrastructural study in two cases of intravascular histiocytic cell proliferation. *Br J Dermatol*. 1999;140:497–504.
31. Barba E, Colato C, Girolomoni G. Intralymphatic Histiocytosis: A case report and review of literature. *J Cutan Pathol*. 2015;42:593–599.
32. Grekin S, Mesfin M, Kang S, et al. Intralymphatic histiocytosis following placement of a metal implant. *J Cutan Pathol*. 2011;38:351–353.
33. Demirkesen C, Kran T, Leblebici C, et al. Intravascular/intralymphatic histiocytosis: a report of 3 cases. *Am J Dermatopathol*. 2015;37:783–789.
34. Tickoo SK, Amin MB. Discriminant nuclear features of renal oncocytoma and chromophobe renal cell carcinoma. Analysis of their potential utility in the differential diagnosis. *Am J Clin Pathol*. 1998;110:782–787.
35. Suarez Vilela D, Izquierdo Garcia FM. Embolization of mesothelial cells in lymphatics: the route to mesothelial inclusions in lymph nodes? *Histopathology*. 1998;33:570–575.
36. Pulitzer MP, Gerami P, Busam K. Solar elastotic material in dermal lymphatics and lymph nodes. *Am J Surg Pathol*. 2010;34:1492–1497.
37. Brooks JS, LiVolsi VA, Pietra GG. Mesothelial cell inclusions in mediastinal lymph nodes mimicking metastatic carcinoma. *Am J Clin Pathol*. 1990;93:741–748.
38. Clement PB, Young RH, Oliva E, et al. Hyperplastic mesothelial cells within abdominal lymph nodes: mimic of metastatic ovarian carcinoma and serous borderline tumor—a report of two cases associated with ovarian neoplasms. *Mod Pathol*. 1996;9:879–886.

39. Isotalo PA, Veinot JP, Jabi M. Hyperplastic mesothelial cells in mediastinal lymph node sinuses with extranodal lymphatic involvement. *Arch Pathol Lab Med*. 2000;124:609–613.
40. Baloch ZW, Wu H, LiVolsi VA. Post-fine-needle aspiration spindle cell nodules of the thyroid (PSCNT). *Am J Clin Pathol*. 1999; 111:70–74.
41. Suarez-Vilela D, Izquierdo-Garcia FM. Nodular histiocytic/mesothelial hyperplasia: a process mediated by adhesion molecules? *Histopathology*. 2002;40:299–300.
42. Jiao N, Zhang W, Wang W, et al. Mesothelial/monocytic incidental cardiac excrescence: a case report and review of literature. *Int J Clin Exp Pathol*. 2014;7:6219–6224.
43. Hage C, Willman CL, Favara BE, et al. Langerhans' cell histiocytosis (histiocytosis X): immunophenotype and growth fraction. *Hum Pathol*. 1993;24:840–845.
44. Ornvold K, Ralfkiaer E, Carstensen H. Immunohistochemical study of the abnormal cells in Langerhans cell histiocytosis (histiocytosis x). *Virchows Arch A Pathol Anat Histopathol*. 1990;416:403–410.

1.1.4. THE UNIFYING CONCEPT OF HISTIOCYTOSIS WITH RAISINOID NUCLEI: A NEW EVIDENCE THAT INTRAVASCULAR/INTRALYMPHATIC HISTIOCYTOSIS AND MICE BELONG IN THE SAME SPECTRUM OF LESIONS

Perhaps the most novel finding of the above-commented study was the provided evidence that intralymphatic histiocytosis and the other lesions are identical. Despite being the subject of myriad reports, until our publication, intralymphatic histiocytosis was a poorly understood entity. Now, when this lesion is set into a wider context, it is clear it represents the same unspecific body reaction to injury as any other of the above-mentioned proliferations.

Another evidence for our concept was presented in the study by Val-Bernal et al. [14] who reported two cases of intralymphatic histiocytosis in the dilated blood vessels of an aortic valve which represent the first two cases of intralymphatic histiocytosis reported outside the skin. For years there has been another lesion known to occur in this area which has been referred to as cardiac MICE. Both intralymphatic histiocytosis and MICE are included in our concept, and we consider these two lesions (along with the others) as identical processes consisting of CD68, CD163, CD4, Lysozyme, CD45 and CD64 positive histiocytes which merely occur at different body sites. In this location, their two cases could be alternatively diagnosed as intravascular examples of MICE. Their diagnosis of IVH occurring in the vessels of the aortic valve only proves that these two lesions are identical and therefore indistinguishable. In our series, we had several cases of MICE, but none of them occurred in the cardiac blood vessels, which would give us another persuasive evidence for our concept. In this letter to the editor, we commented on this unique and recently published example of this histiocytic proliferation which further supports one of the main theses of our work.

Pathology – Research and Practice 213 (2017) 292

Contents lists available at ScienceDirect

Pathology – Research and Practice

journal homepage: www.elsevier.com/locate/prp

Correspondence

The unifying concept of histiocytosis with raisinoid nuclei: A new evidence that intravascular/intralymphatic histiocytosis and MICE belong in the same spectrum of lesions☆

To the Editor,

We have with great interest read the article by Val-Bernal et al. [1] where the authors present two cases of intravascular histiocytosis (IVH) located in the dilated blood vessels of the aortic valve. They are the first two cases of this benign cutaneous lesion that has ever been reported outside of the skin.

In approximately the same time we have been preparing a manuscript on the same topic. In this lately published manuscript [2], we have provided a unifying concept for lesions currently reported under different names such as nodular mesothelial/histiocytic hyperplasia, nodular histiocytic aggregates, reactive eosinophilic pleuritis, histioeosinophilic granuloma of the thymus, mesothelial/monocytic incidental cardiac excrescences (MICE) and intravascular/intralymphatic histiocytosis (IVH). We have morphologically and immunohistochemically analyzed 50 such cases and undertaken an extensive literature review in order to provide sufficient evidence for a similar origin and pathogenesis of these lesions and a reason for consideration of these conditions as part of a single morphologic spectrum. This would allow dropping out numerous puzzling terms and unification of all these lesions under a collective name. On the basis of the characteristic nuclear features we proposed the designation "histiocytosis with raisinoid nuclei."

The article by Val-Bernal et al. provides further evidence for our concept. Their two cases of IVH occurred in the dilated blood vessels of an aortic valve. For years there has been another lesion known to occur in this area which has been referred to as cardiac MICE. Both IVH and MICE are included in our concept and we consider these two lesions (along with the others) as an identical processes consisting of CD68, CD163, CD4, Lysozyme, CD45 and CD64 positive histiocytes which merely occur at different body sites. In this location, their two cases could be alternatively diagnosed as intravascular examples of MICE. Their diagnosis of IVH occurring in the vessels of the aortic valve only proves that these two lesions are identical and therefore indistinguishable. In our series, we had several cases of MICE, unfortunately none of them occurred in the cardiac blood vessels, which would give us another persuasive evidence for our concept. Therefore we would like to thank the authors for their valuable contribution on this topic.

References

[1] J.F. Val-Bernal, M. Mayorga, N. Teran-Villagra, Extracutaneous intravascular histiocytosis of the aortic valve: report of two cases, Pathol. Res. Pract. 212 (2016) 258–263.

[2] M. Michal, D.V. Kazakov, P. Dundr, et al., Histiocytosis with raisinoid nuclei: a unifying concept for lesions reported under different names as nodular mesothelial/histiocytic hyperplasia, mesothelial/monocytic incidental cardiac excrescences, intralymphatic histiocytosis, and others: a report of 50 cases, Am. J. Surg. Pathol. 40 (November (11)) (2016) 1507–1516.

Michael Michal*
Department of Pathology, Charles University, Biomedical Center, Faculty of Medicine in Plzen and Charles University Hospital Plzen, Czech Republic

Michal Michal
Department of Pathology, Charles University, Medical Faculty and Charles University Hospital Plzen, Czech Republic

* Corresponding author.
E-mail address: michael.michal@medima.cz
(M. Michal)

18 October 2016

☆ The study was supported by the Biomedical center of the Faculty of Medicine in Pilsen, project number CZ.1.05/2.1.00/03.0076. The authors have no other funding or conflicts of interest to disclose.

http://dx.doi.org/10.1016/j.prp.2016.12.024

1.1.5. MULTIVACUOLATED MUCIN-FILLED CELLS: A UNIQUE CELL CHARACTERISTIC OF PLEXIFORM NEUROFIBROMA. A REPORT OF 11 CASES.

Neurofibroma is a benign peripheral nerve sheath tumor composed of a variable admixture of Schwann, perineurial-like, perineurial, mast and fibroblastic cells. Five neurofibroma subtypes are recognized, one of which is plexiform neurofibroma [15]. Its recognition is important since as much as 85% of cases plexiform neurofibroma are associated with neurofibromatosis type 1 [16], and in addition, they are more prone to undergo a malignant transformation than the remaining four subtypes .

While going through neural soft tissue tumors for the assortment into our soft tissue collection, we encountered several cases of plexiform neurofibroma, an extensively studied tumor type in the past, that exhibited a so-far unreported and highly distinctive type of cell. It typically featured a variably sized, multivacuolated cytoplasm divided by fine septa with a small polygonal nucleus that was dislodged to the periphery of the cells and was often compressed or slightly indented by the cytoplasmic mucous substance. Often the cells resembled a soccer ball or a jellyfish. Based on the appearance of these cells, we named them multivacuolated mucin-filled cells (MMFC). I further reviewed more than 100 plexiform neurofibroma cases and altogether collected 11 such examples. I also reviewed other (non-plexiform) neurofibroma subtypes, malignant neural tumors and some other entities and did not find this type of cell in any of them.

With the Alcian blue stain, the vacuoles of MMFC showed positive staining, providing evidence that they contain mucus. In all nine cases tested, the MMFC stained positively for CD34, which selectively highlighted their presence, with some plexiform neurofibromas containing hundreds of these elements. The immunostaining was usually strong, and it outlined the cytoskeleton of the MMFC. Out of the 9 tested cases, in 6 lesions MMFC were also positive for GLUT-1, with the staining pattern similar to that of CD34. Two cases also showed expression of Claudin-1 antibody, again in a pattern similar to that of the CD34 antibody. As expected, S-100 protein reacted in all 9 tested cases with the Schwann cell population but was consistently negative in all MMFC, as were all the remaining antibodies. The common combined positivity of MMFC with CD34 and GLUT-1 and, in few cases, Claudin-1 antibodies may point towards their intermediate lineage between perineurial cells and fibroblasts. The awareness of this cell type in plexiform neurofibroma may be helpful especially in small biopsy specimens where its recognition may provide a clue for recognition.

The correct diagnosis is clinically important since plexiform neurofibroma is a syndromic tumor. The same is true for some other differential diagnostic entities such as intramuscular myxomas. Moreover, other entities entering the differential diagnosis are malignant tumors, for example MIFS, myxofibrosarcoma or myxoid liposarcoma.

Human Pathology (2017) 60, 167–173

ELSEVIER

Human PATHOLOGY

www.elsevier.com/locate/humpath

Original contribution

Multivacuolated mucin-filled cells: a unique cell characteristic of plexiform neurofibroma. A report of 11 cases☆

Michael Michal MD[a,*], Dmitry V. Kazakov MD[b], Ladislav Hadravský MD[c], Květoslava Michalová MD[b], Boris Rychlý MD[d], Michal Michal MD[b]

[a]*Department of Pathology, Charles University, Biomedical Center, Faculty of Medicine in Plzen and Charles University Hospital Plzen, Alej Svobody 80, 304 60 Pilsen, Czech Republic*
[b]*Department of Pathology, Charles University, Medical Faculty and Charles University Hospital Plzen, Alej Svobody 80, 304 60 Pilsen, Czech Republic*
[c]*Department of Pathology, Charles University, Third Medical Faculty and Charles University Hospital Kralovske Vinohrady, Šrobárova 50, 100 34 Prague, Czech Republic*
[d]*Cytopathos, Limbová 5, 833 07, Bratislava 37, Slovakia*

Received 15 August 2016; revised 9 October 2016; accepted 14 October 2016

Keywords:
Soft tissue;
Plexiform neurofibroma;
Multivacuolated lipoblast-like cells;
Multivacuolated mucin-filled cells;
Perineurial cells

Summary The authors present 11 cases of plexiform neurofibroma (PN) that featured a very characteristic type of cell appearing as multivacuolated mucin-filled cells (MMFC). The 11 cases were obtained after reviewing 109 cases of PN. Six out of 10 patients showed clinical features of neurofibromatosis type 1. The size of PN ranged from 0.8 cm to 11.5 cm in the largest dimension. The lesions represented classical PN in all cases with myxoid, hypocellular stroma. The MMFC were found within the most myxoid tumorous nodules and were haphazardly located, typically featuring a variably sized, multivacuolated cytoplasm divided by fine septa with a small polygonal nucleus on one side, which was often compressed or slightly indented by the cytoplasmic mucous substances. In many cases, the cells resembled a soccer ball or a jellyfish. In all tested cases (n = 9), the MMFC stained for CD34; six cases were also positive with GLUT-1 antibody, and two cases expressed Claudin-1, whereas S-100 protein was negative. For comparison, we have reviewed a series of randomly selected non-PN, malignant peripheral nerve sheath tumors (MPNST) and of cases featuring non-neoplastic nerve trunks in our files, in which no MMFC were encountered. MMFC seem to be unique to myxoid areas of PN, where they occur in about 10% of cases. Their exact histogenesis is unclear but they might represent an intermediate type of cell between perineurial cells and fibroblasts. The awareness of this cell type in PN is especially important in limited (small) biopsy specimens where their recognition may provide a clue for the correct diagnosis.

☆ Ethics and Competing interests: The authors have no conflict of interest to disclose. When necessary, informed consent was obtained for experimentation with human subjects. This study was supported by the National Sustainability Program I (NPU I) Nr. LO1503 provided by the Ministry of Education Youth and Sports of the Czech Republic.

* Corresponding author: Department of Pathology, Charles University, Medical Faculty and Charles University Hospital Plzen, Alej Svobody 80, 304 60 Pilsen, Czech Republic.
E-mail address: michael.michal@medima.cz (M. Michal).

http://dx.doi.org/10.1016/j.humpath.2016.10.010
0046-8177/

1. Introduction

Neurofibroma is a benign peripheral nerve sheath tumor composed of a variable admixture of Schwann, perineurial-like, perineurial, mast and fibroblastic cells. Five neurofibroma subtypes are recognized, one of which is plexiform neurofibroma (PN) [1]. Its recognition is important since, according to some studies, as much as 85% of cases PNs are associated with neurofibromatosis type 1 (NF1) [2], and in addition, they are more prone to undergo a malignant transformation than the remaining four subtypes.

Recently, while reviewing a set of PN for other purposes, in a minority of the cases we have repeatedly encountered an unusual and highly distinctive type of cell, which appeared multivacuolated and mucin filled. This compelled us to review a larger series of PN in order to define the frequency of occurrence of these cells and to study their variations and immunoprofile. For comparison, we have reviewed a series of randomly selected non-PN, malignant peripheral nerve sheath tumors (MPNST) and of cases featuring non-neoplastic nerve trunks in our files to determine whether multivacuolated mucin-filled cells (MMFC) are unique to PN among all the neurofibromatous tumors.

We are presenting 11 cases of PN containing MMFC with an immunohistochemical (IHC) analysis and follow-up information. As far as we are aware, this type of cell in neurofibromas has not been described so far.

2. Materials and methods

The 11 cases of PN constituting the subject of this study were retrieved from the Pilsner consultation tumor registry and the routine biopsy archive; they came from the period between years 1993–2016. The clinical information was extracted from the registry records, and follow-up data obtained from attending clinicians. To retrieve these 11 cases, we searched our files using key words “plexiform neurofibroma”. This search yielded altogether 109 specimens (68 cases from the routine biopsy archive, 41 from the consultation registry), which were reviewed to confirm the diagnosis. MMFC were identified in 11 of the 109 cases. In all but 2 cases, paraffin blocks or unstained reserve slides were available for an immunohistochemical study. For conventional microscopy, tissues were fixed in formalin, routinely processed and stained. Alcian blue pH 2.5 staining was performed to highlight the intracellular mucin. The IHC features were analyzed using a Ventana BenchMark ULTRA (Ventana Medical Systems, Inc, Tucson, AZ). The primary antibodies employed are shown in the Table 1. They were visualized using the enzymes alkaline phosphatase or peroxidase as detecting systems (both purchased from Ventana Medical Systems, Inc).

3. Results

3.1. Clinical findings

The clinical features are summarized in Table 2. The patients were 9 women and 2 men. The age of the patients at the time of diagnosis ranged from 7 to 71 years (average, 21.7 years). Follow-up information was available for 10 patients, and 6 had clinical features of NF1. One patient developed a MPNST in another location (Table 2). The average duration of follow-up was 10.3 years (range, 1-17 years). The tumor size ranged from 0.8 cm to 11.5 cm in the largest dimension, with an average size of 3.4 cm.

3.2. Histopathological findings

In all cases, the histological appearance was very similar. The lesions represented classical PN, showing variably distended nerve fascicles in a plexiform arrangement with myxoid, hypocellular stroma composed of a typical admixture of Schwann cells, fibroblasts, mast cells and few perineurial cells along with intervening non-neoplastic nerve axons and collagen fibers. The MMFC were exclusively distributed within the most myxoid tumorous nodules among PNs (Fig. 1), where they were haphazardly or somewhat equidistantly located (Fig. 2). The cells typically featured a variably sized, multivacuolated cytoplasm divided by fine septa with a small polygonal nucleus that was dislodged to the periphery of the cells and was often compressed or slightly indented by the cytoplasmic mucous substance. In rare instances, the cells were binucleated. Often the cells resembled a soccer ball or a jellyfish (Fig. 3).

In Case 2, following the excision of the PN, the patient developed an MPNST in another location. After reviewing slides from all 33 block of the malignant lesion, we did not find any MMFC. In several cases, mature adipose tissue was present in the sections, showing no signs of lipoblastic differentiation.

In Case 1, 2 consecutive biopsies were available, both featuring PN with MLLCs. In Case 10, altogether five PN from various body sites were simultaneously excised from one patient, with 3 of them containing MMFC.

For comparison, we reviewed 30 randomly selected non-plexiform neurofibroma cases and 60 MPNST to determine if MMFC are unique to PN. Neither the non-PNs nor MPNST contained MMFC. We also reviewed 30 specimens from various conditions in which non-neoplastic nerve trunks were present. Similarly, none of the cases featured MMFC.

3.3. Histochemical and immunohistochemical findings

With the Alcian blue pH 2.5 stain, the vacuoles of MMFC showed positive staining, providing evidence that they contain mucus. In all nine cases with available blocks, the MMFC

Table 1 List of antibodies

Antibody	Clone	Manufacturer	Dilution
CD34	QBEnd/10	Dako, Glostrup, Denmark	1:200
GLUT-1	Polyclonal	Thermo Fischer Scientific, Freemont, CA	1:100
S-100 protein	Polyclonal	Ventana Medical System, Inc., Tucson, Arizona	Prediluted
Epithelial membrane antigen (EMA)	E29	Dako	1:400
Claudin-1	Polyclonal	Cell Marque, Rocklin, CA	Prediluted
GFAP	6F2	Dako	Prediluted
Claudin-5	Polyclonal	Abcam, Cambridge, UK	1:100
Cyclin D1	Polyclonal	Thermo Fisher Scientific	1:100
Factor XIIIa	AC-1A1	Ventana	Prediluted
Lysozyme	Polyclonal	Cell Marque	Prediluted
CD11c	5D11	Zytomed Systems, Berlin, Germany	1:50
CD68	KP1	Dako	1:100
CD163	MRQ-26	Cell Marque	Prediluted
CD4	SP35	Ventana	Prediluted

stained positively for CD34, which selectively highlighted their presence, with some myxoid nodules of PN containing hundreds of these elements (Fig. 4). The immunostaining was usually strong, and it outlined the cytoskeleton of the MMFC. In two cases, CD34 stained only few MMFC. Out of the 9 tested cases, in 6 lesions MMFC were also positive (3 strong, 3 weak) for GLUT-1, with the staining pattern similar to that of CD34, outlining the cytoskeleton of the cells, (Fig. 5). Of note, in these weakly staining cases, GLUT-1 antibody showed positivity almost exclusively in the areas situated close to the perineurial border. Two cases also showed expression of Claudin-1 antibody, again in a pattern similar to that of the CD34 antibody. As expected, S-100 protein reacted in all 9 tested cases with the Schwann cell population but was consistently negative in all MMFC, as were all the remaining antibodies listed in the Table 1.

Table 2 Clinicopathological features

Case	Gender/ Age	Location	Size	NF1	Number of plexiform neurofibromas	Café au lait spots; Lisch nodules	Tumors	Follow-up
1	F/7	Lip, face	0.8 and 0.7 cm in diameter	Yes	2	Multiple; none	0	AW
2	F/29	Soft tissue	2.5 × 2.0 × 1.5 cm	Yes	Multiple: head, neck, chest wall	Multiple; none	Malignant schwannoma – thigh (2002)	AW
3	M/18	Posterior chest wall	2 × 0.6 × 1	No	1	None	0	AW
4	M/14	Gluteal area	7 × 4.7 × 3.5 cm	Yes, combined form	Multiple	Multiple; none	Multiple CNS hamartomas	AW
5	F/10	Back	1.3 in diameter	Yes	2	Multiple: back and abdomen), bilateral Lisch nodules	Hamartomas of cerebellum, pons and retina	AW
6	F/20	Dorsum of hand	1 × 1 × 0.5 cm	NA				
7	F/9	Soft tissue	1.7 in diameter	No	1	None	0	AW
8	F/15	Arm	11.5 × 5 × 4 cm	Yes	Multiple	Multiple; bilateral Lisch nodules	0	AW
9	F/29	Labia majora	0.7 × 0.2 × 0.5 cm	No	1	None	0	AW
10	F/17	Various soft tissue locations	5.5; 2.5; 6; 3.3; 1.6 cm in the largest dimension	Yes	12	Multiple; none	0	AW
11	F/71	Soft tissue	NA	No	1	None	0	AW

Abbreviations: NF1, neurofibromatosis type 1; NA, not available; AW, alive and well.

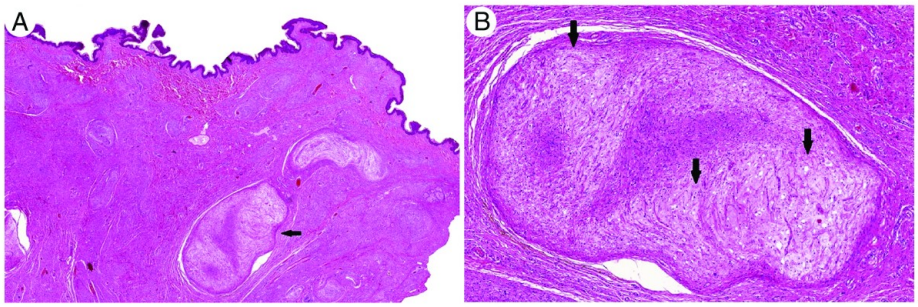

Fig. 1 A, The MMFC are exclusively distributed within the most myxoid tumorous nodules (arrow; H&E, original magnification ×20). B, MMFC are marked by arrows (H&E, original magnification ×50).

4. Discussion

The overall occurrence of MMFC in PN was about 10% (11/109). Although a large proportion of cases represented consultations (41/109), we do not think this factor biased the frequency of MMFC, since none of the submitting pathologists had mentioned the presence of MMFC in their report. To determine if MMFC are unique to PN, we have reviewed 30 specimens from various conditions containing non-neoplastic nerve trunks, 30 randomly selected non-PN and 60 MPNST and have not found a single case featuring MMFC; they thus seem to be a specific finding for benign PNs. Six of 10 (60%) patients from our cohort with known follow-up have a confirmed diagnosis of NF1. This is less than the 85% association of PN with NF1 indicated by some researchers [2]. Nevertheless, not all dermatologists and other physicians are perfectly familiar with the diagnostic criteria for NF1, and thus our follow-up data may be somewhat skewed.

Two reports are on record describing the presence of lipoblast-like cells in the peripheral nerve sheath tumors. In 2006, Plaza et al [3] reported 5 cases of lipoblastic nerve sheath tumors, one of which was a neurofibroma. However, these cells were entirely different from the MMFC encountered in our cases. By using electron microscopy, histochemical and IHC assays, the authors have proved that the cells in their study represented true immature S-100 protein-expressing adipocytes [3]. A virtually identical case to the one in the report of Plaza et al [3] was presented by Vecchio et al a few years later [4]. In contrast, the MMFC presented in the current study do not represent adipocytic lineage as shown by their constant negativity for S-100 protein and positivity for CD34. In addition, when present, the neighboring adipose tissue shows no signs of lipoblastic differentiation.

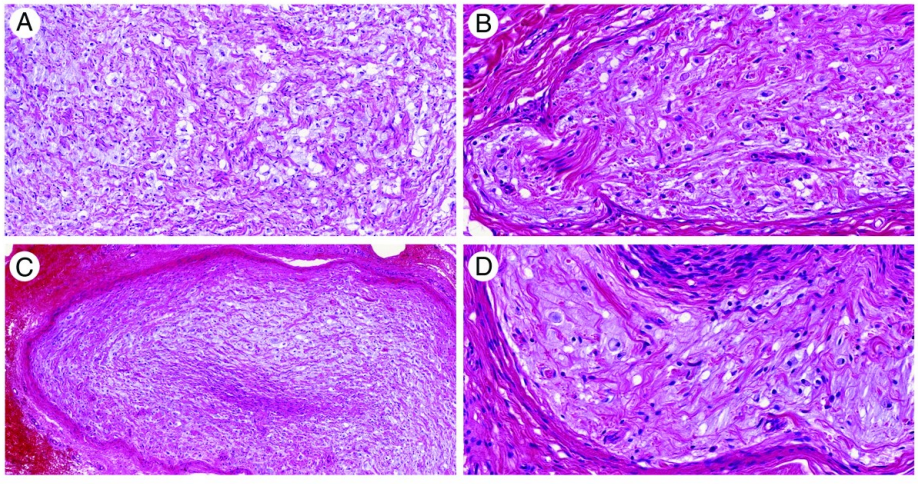

Fig. 2 MMFC are distributed either diffusely and more or less equidistantly (A and B; H&E, original magnification ×200 and ×380), or irregularly in the myxoid tumor nodules (C and D; H&E, original magnification ×120 and × 400).

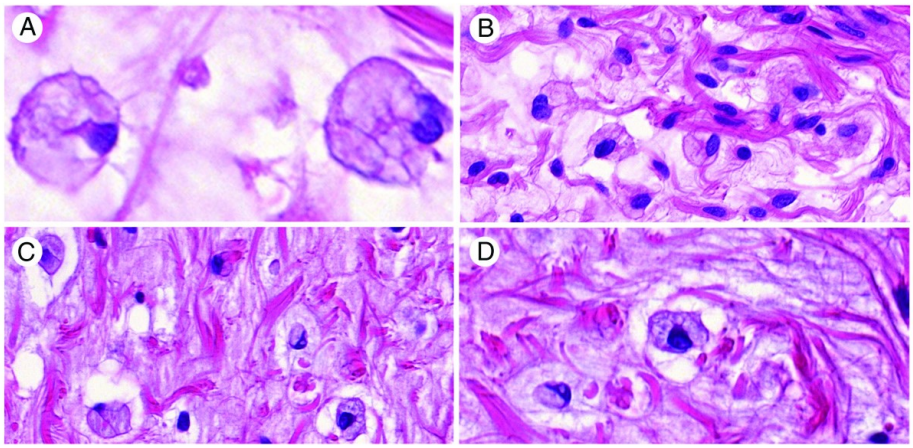

Fig. 3 High magnification of the MMFC shows multivacuolated cells filled with mucus occasioning a resemblance to a soccer ball or a jellyfish (H&E: A, original magnification ×3500; B, ×1300; C, ×1400; D, ×2000).

MMFC are strikingly similar to the cells occurring in myxoinflammatory fibroblastic sarcoma (MIFS) and called variously as for example lipoblast-like cells with multivacuolated cytoplasm [5-7], which also frequently resemble soccer balls [8]. Similar cells are also occasionally seen in conventional myxofibrosarcoma. In our experience, in both cases these multivacuolated cells are only rarely CD34 positive (in MIFS), and they are GLUT-1 and Claudin-1 negative.

MMFC also show certain similarities with the lipid-laden macrophages encountered in intramuscular myxomas [9]. However, these myxomas can be easily differentiated, because these tumors are usually non-plexiform S100 protein–negative intramuscular myxomas morphologically entirely different from PNs.

Another potential mimicker is the ring-shaped Schwann cells in nerve sheath myxomas (NSM) [10]. The multilobular architecture, myxoid background and, to some extent, also the tumor cells in some cases of NSM may appear similar. The main differentiating features are the lack of prominent collagen fibers in NSM and mainly the consistent reactivity of the ring-shaped Schwann cells with S-100 protein, whereas CD34 is not expressed by these cells.

The common combined positivity of MMFC with CD34 and GLUT-1 and, in few cases, Claudin-1 antibodies may point towards their intermediate lineage between perineurial cells and fibroblasts. The previously published ultrastructural studies of neurofibromas suggested the presence of perineurial cells, endoneurial fibroblasts, and intermediate cells, as well as Schwann cells [11,12]. Although this fact had for a long time remained immunohistochemically unsubstantiated, later several studies have confirmed the presence of perineurial cells in certain neurofibromas [13]. Eventually, using a highly

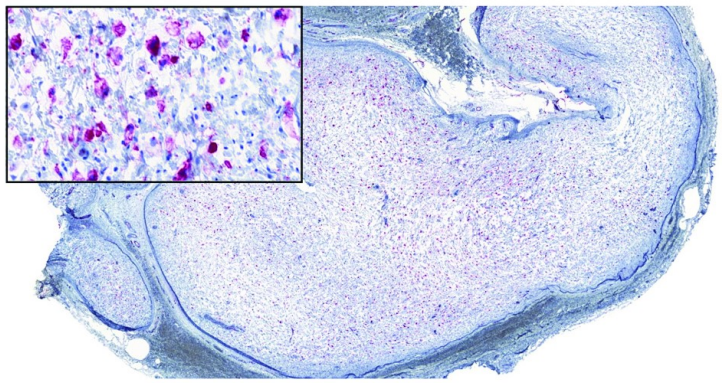

Fig. 4 CD34 highlighting MMFC. Note hundreds of these cells in some myxoid nodules (original magnification ×40).

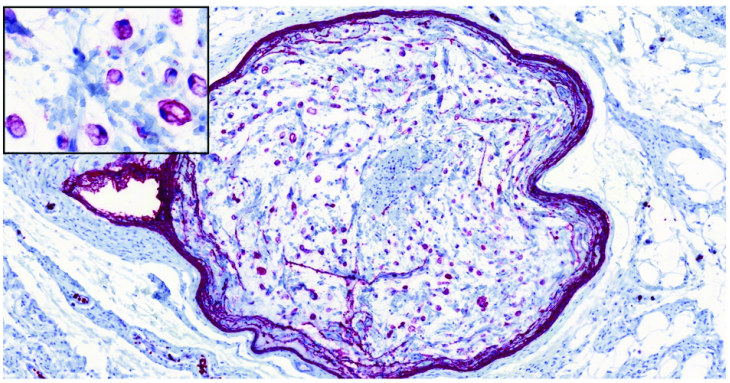

Fig. 5 The staining with GLUT-1 antibody outlining the cytoskeleton of MMFC (original magnification ×135).

sensitive detection system, Hirose et al proved that all neurofibromas contain EMA-positive perineurial cells. Using conventional IHC detection methods, they also proved the common presence of few GLUT-1–positive cells arranged in perineurial-like structures and also of CD34-positive endoneurial fibroblasts [14]. Interestingly, in the same study, while analyzing schwannomas, the authors found few cells exhibiting both perineurial (GLUT-1) and fibroblastic (CD34) immunophenotypes at the peripheral areas close to the perineurial capsule. In our study on PN, besides the three cases showing a strong GLUT-1 staining, we also encountered another three cases with only a weak GLUT-1 expression in MMFC, and this expression was also restricted to the subcapsular areas. Since the ultrastructural studies of neurofibromas indicated the presence of an intermediate type of cell between perineurial and fibroblast [11,12] (which by all means could also be present in schwannomas), it is plausible that the MMFC might represent a population of similar histogenesis. A low level of antigen expression probably explains the fact why the majority of perineurial cells in neurofibromas express EMA antibody only using highly sensitive detection methods [14] and also why the perineurial markers such as GLUT-1, Claudin-1 and especially EMA were expressed in only a small subset or none of our cases, respectively. On the other hand, it is also well known that GLUT-1 antibody is quite unspecific, as its expression has been demonstrated in a wide range of mesenchymal tumors, and therefore its positivity in our cases may have a completely different significance, unrelated to perineurial differentiation [15].

CD34 is a transmembrane glycoprotein expressed by human hematopoietic progenitor cells of lymphoid and myeloid lineage. Anti-CD34 antibodies also react with normal vascular endothelial cells, periadnexal spindle cells and dermal dendritic cells. Certain leukemias, benign and malignant vascular tumors, and dermatofibrosarcoma protuberans are typically immunoreactive for CD34. Other apparently unrelated neoplasms such as lipomatous tumors and solitary fibrous tumors are also CD34 positive [16]. Nonetheless, the exact nature of the CD34-positive cells in neurofibroma is not fully understood [17]. While some authors consider them as fibroblasts or endoneurial fibroblasts [14,18,19], there are in fact very few studies specifically addressing this topic. Apart from the above-mentioned study [14], there is work done by Weiss and Nickoloff [20], in which the authors concluded that the CD34-positive cells are cytologically and immunophenotypically distinct from Schwann and perineurial cells and also from "conventional" fibroblasts. Due to their slender dendritic processes, they were considered to be a variant of dendritic cells. Similar conclusions were drawn by Khalifa et al [16]. Weiss and Nickoloff found these CD34-positive cells most commonly in neurofibromas having a myxoid stroma. Notably, in their study, Hirose et al mentioned "multivacuolated cells floating in myxoid areas," which also showed CD34 positivity [14]. Although the authors did not provide any microphotographs, the description of the cells appears very similar to MMFC we report on and which were also encountered exclusively in the myxoid areas of PN. This exclusive occurrence in highly myxoid areas and the mucinous content of their vacuoles proved by the positive staining with Alcian blue pH 2.5 raises the question whether the MMFC themselves are not responsible for the production of the extracellular mucin. Additional studies are needed to precisely delineate the origin of MMFC.

The differential diagnosis of PN with MMFC should pose no major difficulties, provided the pathologist has enough diagnostic material, containing, besides the myxoid zones, the characteristic cellular composition of PN and the nerve fascicles themselves. The diagnosis of PN may be a quite challenging in a limited biopsy specimen. Under these circumstances, the differential diagnosis encompasses other myxoid tumors, especially MIFS, intramuscular myxomas and NSM in which, as already mentioned, very similar MMFC can also be encountered. Another differential diagnostic consideration is myxoid liposarcoma or conventional myxofibrosarcoma. In all cases, the correct diagnosis is clinically important. PN and intramuscular myxomas are both syndromic tumors [2,21], whereas

MIFS, myxofibrosarcoma and myxoid liposarcoma are malignant tumors [8,22]. In addition to the significant morphologic differences, staining with S-100 protein, CD34 and GLUT-1 may also be helpful. No other tumor than PN will show CD34, GLUT-1–positive MMFC on the background of S-100 protein-positive Schwann cells.

In conclusion, we have presented 11 cases of PN featuring CD34 and frequently GLUT-1–positive MMFC. Of all neurofibroma subtypes, these cells are unique to myxoid nodular areas of PN, where they occur in about 10% of cases and are never present in MPNST. Their exact histogenesis is unclear but they might represent an intermediate type of cell between perineurial cells and fibroblasts. The awareness of this cell type in PN may be helpful in small biopsy specimens where their recognition may provide a clue for the correct diagnosis.

References

[1] Antonescu CR, Scheithauer BW, Woodruff JM. AFIP atlas of tumor pathology (series 4): tumors of the peripheral nervous system. Silver Spring, MD: ARP Press; 2013.

[2] McCarron KF, Goldblum JR. Plexiform neurofibroma with and without associated malignant peripheral nerve sheath tumor: a clinicopathologic and immunohistochemical analysis of 54 cases. Mod Pathol 1998;11:612-7.

[3] Plaza JA, Wakely Jr PE, Suster S. Lipoblastic nerve sheath tumors: report of a distinctive variant of neural soft tissue neoplasm with adipocytic differentiation. Am J Surg Pathol 2006;30:337-44.

[4] Vecchio GM, Amico P, Leone G, Salvatorelli L, Magro G. Lipoblast-like signet-ring cells in neurofibroma: a potential diagnostic pitfall of malignancy. Pathologica 2010;102:108-11.

[5] Montgomery EA, Devaney KO, Giordano TJ, Weiss SW. Inflammatory myxohyaline tumor of distal extremities with virocyte or Reed-Sternberg-like cells: a distinctive lesion with features simulating inflammatory conditions, Hodgkin's disease, and various sarcomas. Mod Pathol 1998;11:384-91.

[6] Michal M. Inflammatory myxoid tumor of the soft parts with bizarre giant cells. Pathol Res Pract 1998;194:529-33.

[7] Meis-Kindblom JM, Kindblom LG. Acral myxoinflammatory fibroblastic sarcoma: a low-grade tumor of the hands and feet. Am J Surg Pathol 1998;22:911-24.

[8] Michal M, Kazakov DV, Hadravsky L, Kinkor Z, Kuroda N, Michal M. High-grade myxoinflammatory fibroblastic sarcoma: a report of 23 cases. Ann Diagn Pathol 2015;19:157-63.

[9] Goldblum JR, Folpe AL, Weiss SW. Enzinger and Weiss soft tissue tumors. Elsevier Saunders; 2014.

[10] Fetsch JF, Laskin WB, Miettinen M. Nerve sheath myxoma: a clinicopathologic and immunohistochemical analysis of 57 morphologically distinctive, S-100 protein- and GFAP-positive, myxoid peripheral nerve sheath tumors with a predilection for the extremities and a high local recurrence rate. Am J Surg Pathol 2005;29:1615-24.

[11] Erlandson RA, Woodruff JM. Peripheral nerve sheath tumors: an electron microscopic study of 43 cases. Cancer 1982;49:273-87.

[12] Hirose T, Sano T, Hizawa K. Ultrastructural localization of S-100 protein in neurofibroma. Acta Neuropathol 1986;69:103-10.

[13] Zamecnik M, Michal M. Perineurial cell differentiation in neurofibromas. Report of eight cases including a case with composite perineurioma-neurofibroma features. Pathol Res Pract 2001;197:537-44.

[14] Hirose T, Tani T, Shimada T, Ishizawa K, Shimada S, Sano T. Immunohistochemical demonstration of EMA/Glut1–positive perineurial cells and CD34-positive fibroblastic cells in peripheral nerve sheath tumors. Mod Pathol 2003;16:293-8.

[15] Ahrens WA, Ridenour III RV, Caron BL, Miller DV, Folpe AL. GLUT-1 expression in mesenchymal tumors: an immunohistochemical study of 247 soft tissue and bone neoplasms. Hum Pathol 2008;39:1519-26.

[16] Khalifa MA, Montgomery EA, Ismiil N, Azumi N. What are the CD34+ cells in benign peripheral nerve sheath tumors? Double immunostaining study of CD34 and S-100 protein. Am J Clin Pathol 2000;114:123-6.

[17] Rosai J. and Ackerman's surgical pathology 10th ed. New York:. Mosby Elsevier; 2011.

[18] Miettinen M. Modern soft tissue pathology. New York: Cambridge University Press; 2010.

[19] Requena L, Kutzner H. Cutaneous soft tissue tumors Philadelphia: Wolters Kluwer; 2015.

[20] Weiss SW, Nickoloff BJ. CD-34 is expressed by a distinctive cell population in peripheral nerve, nerve sheath tumors, and related lesions. Am J Surg Pathol 1993;17:1039-45.

[21] Carney JA, Headington JT, Su WP. Cutaneous myxomas. A major component of the complex of myxomas, spotty pigmentation, and endocrine overactivity. Arch Dermatol 1986;122:790-8.

[22] Kilpatrick SE, Doyon J, Choong PF, Sim FH, Nascimento AG. The clinicopathologic spectrum of myxoid and round cell liposarcoma. A study of 95 cases. Cancer 1996;77:1450-8.

1.1.6. WHORLING CELLULAR PERINEURIOMA: A PREVIOUSLY UNDESCRIBED VARIANT CLOSELY MIMICKING MONOPHASIC FIBROUS SYNOVIAL SARCOMA

Perineurioma is a benign peripheral nerve sheath tumor [17]. There are several subtypes including intraneural, retiform (reticular) and sclerosing perineurioma. Very recently, another putative and presumably very rare variant of PN was described and coined as pseudolipoblastic perineurioma. Perineurial cell differentiation is also frequently seen in hybrid peripheral nerve sheath tumors (HPNST), where a combination of various subtypes of perineurioma, schwannoma or neurofibroma can be found admixed together. In addition to the benign variants of perineurioma, rare cases of malignant peripheral nerve sheath tumors (MPNST) showing perineurial cell differentiation have been reported [18].

In our practice, we have encountered a distinctive tumor that, based on morphology, immunohistochemistry and electron microscopy was shown to consist of perineurial cells and that closely mimics monophasic fibrous synovial sarcoma (MSS). Due to its histopathological appearance, we designated this rare perineurioma variant as “whorling cellular perineurioma” (WCP). To our best knowledge, this perineurioma subtype has not been previously recognized.

Synovial sarcoma is a relatively common high-grade sarcoma of which the monophasic fibrous variant is the most frequent subtype. It typically arises on the extremities with approximately one third of cases involving the acral sites, where they are often of small size [19]. It features uniform, spindle-shaped cells with a small amount of cytoplasm and oval to tapered nuclei which are arranged in compact sheets. The absence of significant nuclear pleomorphism is typical for MSS [20].

Eventually, we collected 4 examples of this novel perineurial tumor. We performed immunohistochemical analysis using perineurial markers EMA, Claudin 1 and Glut-1, along with other markers to exclude the possibility of MSS such as keratins and TLE-1. Few other markers to rule out different PNST such as schwannoma were used as well. We also carried out FISH analysis using probes for SYT/SSX break to further exclude the possibility of MSS. Additionally, electron microscopy was used to confirm that the tumor has features of perineurial differentiation such as bipolar cytoplasmic processes with pinocytotic vesicles, tight-junctions and discontinuous external lamina.

The four cases of WCP presented in this study morphologically closely resembled the MSS. Three of the four tumors in our series were also located on the distal portion of extremities, with a mean size of 1.8 cm. The most essential similarity between our cases and MSS lies in the presence of a monotonous sheet-like growth of bland spindle-shaped cell with oval to round nuclei. Similar to WCP, a significant cellular pleomorphism and prominent mitotic activity can be absent in MSS as well as a prominent intervening stroma. However, in both tumors, foci of more prominent hyalinization may be encountered. Another potential pitfall is the immunohistochemical features of both neoplasms since the reactivity with the EMA antibody belongs to the typical characteristics of both MSS and perineurioma. Moreover, the expression of other antibodies frequently used to confirm the perineurial cell differentiation, namely Claudin-1 and GLUT-1, can be occasionally present in MSS as well [21].

Nevertheless, there are several histological as well as immunohistochemical differences between MSS and WCP which can be exploited in the differential diagnosis. One of the most helpful microscopic features is the whorling growth pattern which is not commonly seen in MSS.

The focally discernible long, slender cytoplasmic processes typical for perineurial differentiation can also help in rendering the correct diagnosis. Although the cells constituting both tumors are bland, with no or little cellular pleomorphism, MSS almost always exhibits some mitotic figures, but these were found only after a prolonged search or were absent altogether in our cases of WCP. Conversely, the various features frequently encountered in MSS such as the vaguely epithelioid areas, hemangiopericytoma-like vascular pattern, calcifications, mast cells, hemorrhage or necrosis were not found in WCP. The IHC, as misleading as it may appear with respect to EMA, Claudin-1 and Glut-1 staining, can be a very useful adjunct as well. Although positive in one third of cases of MSS, Claudin-1 expression in this neoplasm is confined primarily to the clusters of vaguely epithelioid cells [21] unlike the WCP where Claudin-1 expression was diffuse and, with the exception of one case, strong. The expression of EMA antibody, albeit noncontributory by the positivity itself, proved useful in highlighting the whorling growth pattern of WCP. When used in a panel, at least focal cytokeratin expression is found in most MSS, while OSCAR and CK7 were completely absent in all studied cases of WCP as was another of the most frequently used markers of synovial sarcomas, the TLE-1. When necessary and available, FISH (and of course EM) will provide the definite answer.

Taking into account similar clinicopathologic features, the relationship of WCP to the sclerosing perineurioma should be addressed. The latter perineurioma subtype also typically occurs on the hands and feet of predominantly male patients [22]. Some of the microscopic features such as the shape and bland appearance of the cells, and especially the frequent whorling pattern of growth are highly reminiscent of WCP. The main difference lies in the absence of abundant, hyalinized, thick collagen bundles between intervening tumor cells growing in corded or trabecular arrangement. However, it cannot be totally discarded that WCP represents a very cellular end of the morphological spectrum of sclerosing perineurioma with only a focal or completely absent areas of hyalinization.

In any case, this is a very rare perineurioma variant, as is evidenced by the fact that these 4 neoplasms were identified among 208 (~1.9%) cases of skin and soft tissue perineurioma and other lesions with perineurial differentiation stored in our files. Awareness of this PN variant is important in order to avoid its misinterpretation as MSS.

Annals of Diagnostic Pathology 27 (2017) 74–78

Contents lists available at ScienceDirect

Annals of Diagnostic Pathology

Whorling cellular perineurioma: A previously undescribed variant closely mimicking monophasic fibrous synovial sarcoma☆

Michael Michal [a,b,*], Dmitry V. Kazakov [a], Abbas Agaimy [c], Marta Hosova [d], Kvetoslava Michalova [a], Petr Grossmann [a], Petr Steiner [a], Faruk Skenderi [e], Semir Vranic [e,f], Michal Michal [a]

[a] Department of Pathology, Faculty of Medicine in Pilsen, Charles University, Alej Svobody 80, 304 60 Pilsen, Czech Republic
[b] Biomedical Center of the Faculty of Medicine in Pilsen, Alej Svobody 80, 304 60 Pilsen, Czech Republic
[c] Institute of Pathology, Friedrich-Alexander University Erlangen-Nürnberg, University Hospital, Krankenhausstrasse 8-10, 910 54, Erlangen, Germany
[d] Department of Pathology, Faculty Hospital, Budínova 67/2, 180 81 Prague, Czech Republic
[e] Department of Pathology, Clinical Center, University of Sarajevo, Bolnička 25, 710 00 Sarajevo, Bosnia and Herzegovina
[f] School of Medicine, Bolnička 25, 710 00 Sarajevo, Bosnia and Herzegovina

ARTICLE INFO

Available online xxxx
Keywords:
Soft tissue
Sclerosing
Whorling cellular perineurioma
Monophasic fibrous synovial sarcoma

ABSTRACT

The authors present a distinctive perineurioma (PN) variant which morphologically strongly resembles monophasic fibrous synovial sarcoma (MSS). The patients were 3 males and 1 female. The age ranged from 15 to 61 years (mean: 44 years). Locations included the sole, lower jaw, palm and foot. The tumor size ranged from 1.3 cm to 2.5 cm in the largest dimension (mean 1.8 cm). Morphologically, all tumors had an identical, monotonous appearance. The perineurial cells were closely packed and created a confluent cellular whorls and/or sheets in a scarce stroma, with only focally discernible long, slender cytoplasmic processes typical for perineurial differentiation. The nuclei were rounded or slightly elongated to tapered, without nuclear atypia. Mitoses were rare to completely absent. Atypical mitoses, hemorrhage, necrosis or calcifications were not present. The proliferative index (Ki-67) was 1–3%. All analyzed tumors were positive for EMA, Claudin-1, GLUT-1 and negative with S100 protein, CD34, OSCAR, CK7 and TLE-1. Two cases were tested by fluorescence in situ hybridization and neither showed alterations of the SYT gene. One case studied by electron microscopy showed characteristic features of perineurial differentiation. Follow-up was available for two patients both of which showed no evidence of disease at 8 years and 6 months, respectively. Based on their bland morphology, perineurial features and presumably benign clinical outcome we propose the term "whorling cellular perineurioma" for these tumors, which may represent an extremely cellular variant of sclerosing PN. Awareness of this PN subtype and its distinction from MSS is of utmost clinical significance.

1. Introduction

Synovial sarcoma (SS) is a malignant tumor most commonly arising in the soft tissue of extremities. Four histologic subtypes of SS are recognized, of which monophasic fibrous variant (MSS) consisting purely of spindled cells is the most frequent one. The differential diagnosis of this particular subtype is quite challenging, encompassing a broad spectrum of neoplasms [1]. In our consultation practice, we have encountered a potential mimicker of MSS which, based on morphology, immunohistochemistry (IHC) and electron microscopy (EM) was shown to consist of perineurial cells. Due to its histopathological appearance, we designated this rare perineurioma variant as "whorling cellular perineurioma". To our best knowledge, this perineurioma (PN) subtype has not been previously recognized.

2. Materials and methods

The 4 cases of WCP constituting the subject of this study were retrieved from the author's consultation files which currently contain 208 (~1.9%) tumors coded as perineurioma; they came from the period between years 1993–2016. One of the four cases was recently obtained in consultation with the particular request for molecular genetic confirmation of *SYT* gene break, as the submitting pathologist considered MSS. The clinical information was extracted from the medical records, and follow-up data obtained from the attending clinicians. Except for 1 case, paraffin blocks or unstained reserve slides were available for the study. For conventional microscopy, tissues were fixed in formalin,

☆ This study was supported by the National Sustainability Program I (NPU I) Nr. LO1503 provided by the Ministry of Education Youth and Sports of the Czech Republic. The authors have no conflicts of interest to disclose.

* Corresponding author at: Department of Pathology, Charles University, Medical Faculty and Charles University Hospital Plzen, Alej Svobody 80, 304 60 Pilsen, Czech Republic.
E-mail address: michael.michal@medima.cz (M. Michal).

http://dx.doi.org/10.1016/j.anndiagpath.2017.02.001
1092-9134/

Table 1

Case	Age/sex	Location	Size (cm)	EMA	Claudin-1	Glut-1	S100	TLE-1	CD34	OSCAR	CK7	SYT/SSX	Follow-up
1	61/M	Sole	1.3	+++	+++	+++	−	−	−	−	−	−	NED (6 months)
2	58/M	Lower Jaw	2	+++	+	+++	−	−	−	−	−	−	NA
3	40/M	Thenar											2.5 × 2.5 × 1
	+++	+++	+++	−	−	−	−	−	NA	NED (8 years)			
4	NA/F	Foot	1.5	+++	+++	NA	−	NA	NA	NA	NA	NA	NA

Legend: +++ strong staining; + weak staining; − negative staining; NA – not analyzable/available; NED – no evidence of disease.

routinely processed, embedded in paraffin, cut into 4 μm-thick sections, and stained with hematoxylin-eosin.

2.1. Immunohistochemistry

The immunohistochemical analysis was performed using a Ventana BenchMark ULTRA (Ventana Medical System, Inc., Tucson, AZ). The following primary antibodies were used: EMA (E29, Dako, Glostrup, Denmark, 1:400), Claudin-1 (polyclonal, Cell Marque, Rocklin, CA, prediluted), GLUT-1 (polyclonal, Thermo Fischer Scientific, Freemont, CA, 1:100), TLE-1 (M-101, Santa Cruz Biotechnology, Inc., Dallas, TX, 1:100), S100 (Polyclonal, Ventana Medical System, Inc., Prediluted), CD34 (QBEnd/10, Dako, 1:200), OSCAR (IgG2a, Covance, Emeryville, CA, 1:100), CK7 (OV-TL 12/30, Dako, 1:200), MIB (30-9, Ventana, Medical System, Inc., prediluted). The primary antibodies were visualized employing the enzymes alkaline phosphatase or peroxidase as detecting systems (both purchased from Ventana Medical System, Inc.).

2.2. Molecular genetic studies

2.2.1. Detection of SYT gene break by FISH

Molecular studies were performed to exclude synovial sarcoma, using a previously described method [2].

3. Results

The clinical features are summarized in Table 1. The patients were 1 woman and 3 men. The age of the patients at the time of diagnosis ranged from 15 to 61 years (mean, 44). Follow-up available for 2 patients was uneventful at 8 years and 6 months, respectively. The tumors were located on the sole, lower jaw, palm and foot and ranged in size from 1.3 cm to 2.5 cm in the largest dimension, with a mean size of 1.8 cm. Three cases presented as oval shaped, subcutaneous masses.

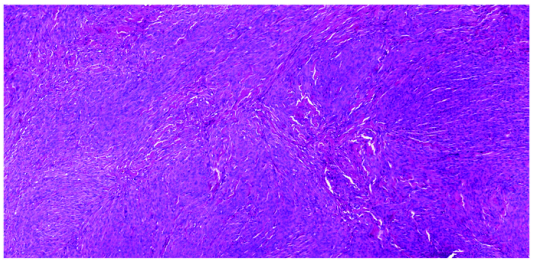

Fig. 1. The constituent cells were closely packed and created a confluent cellular whorls and/or sheets, with only focally discernible long, slender cytoplasmic processes typical for perineurial differentiation. The stroma between the cells was scarce and inconspicuous, but in some cases a more prominent area of hyalinization without intervening cells could be found. The overall microscopical picture was thus similar to monophasic fibrous variant of synovial sarcoma (Case 1; HE, ×100).

Case 2 involving the lower jaw was received fragmented, without any details concerning the depth of involvement.

3.1. Light microscopical findings

Microscopically, three neoplasms were rimmed by a thin capsule, whereas in the remaining case no capsule was discernible due to tissue fragmentation. The lesions were well-circumscribed and in none of the cases was an infiltrative growth evident. All tumors had an identical, monotonous appearance. The constituent cells were closely packed and created a confluent cellular whorls and/or sheets, with only focally discernible long, slender cytoplasmic processes typical for perineurial differentiation (Figs. 1 and 2). Focally, vague storiform arrangement of the cells was discernible. The shape of the nuclei ranged from rounded or slightly elongated to tapered, without a significant nuclear atypia. Mitoses were rare to completely absent. Atypical mitoses, hemorrhage, necrosis or calcifications were not present and neither mast cells were a prominent feature (Fig. 3). The stroma between the cells was scarce and inconspicuous, but in some cases a more prominent area of hyalinization without intervening cells could be found (Fig. 1).

3.2. Electron microscopical findings

In Case 3 a material for EM was available. It showed characteristic features of perineurial differentiation, including thin bipolar cytoplasmic processes with pinocytotic vesicles, tight-junctions and discontinuous external lamina. The cytoplasm contained a variable amount of rough endoplasmic reticulum, a few mitochondria, some glycogen particles and intermediate filaments.

3.3. Immunohistochemical finding

Immunohistochemical features are summarized in Table 1. All tumors reacted with the EMA and Claudin-1 antibodies. The EMA staining nicely highlighted the whorling growth pattern of tumor cells (Fig. 4). Three of the four cases were strongly positive for GLUT-1 antibody. All analyzed cases were negative with TLE-1, S100 protein, OSCAR, CK7

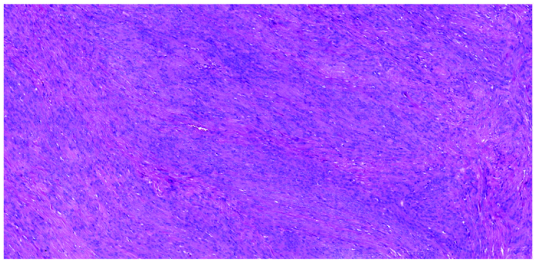

Fig. 2. The constituent cells were closely packed and created a confluent cellular sheets, with only focally discernible long, slender cytoplasmic processes typical for perineurial differentiation (Case 3; HE, ×100).

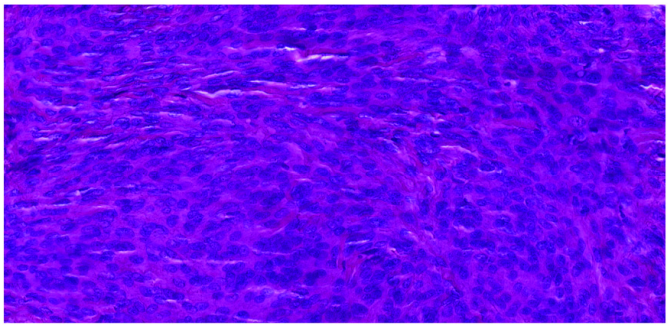

Fig. 3. The shape of the nuclei ranged from rounded or slightly elongated to tapered, without a significant nuclear atypia. Mitoses were rare to completely absent. Atypical mitoses, hemorrhage, necrosis or calcifications were not present and neither mast cells were a prominent feature (Case 1; HE, ×200).

and CD34 antibodies. The proliferative index (Ki-67), in spite of a high cellularity was very low (1–3%).

3.4. Molecular genetic findings

In 2 cases tested by FISH, none showed alterations of the SYT gene locus. In one instance the archival material was not suitable for analysis.

4. Discussion

Perineurioma (PN) was originally described in 1978 by Lazarus and Trombetta [3] as a tumor composed exclusively of neoplastic perineurial cells. From the morphological point of view, besides the usual type of soft tissue PN, there are several subtypes including intraneural [4], retiform (reticular) [5,6] and sclerosing PN [7]. Very recently, another putative and presumably very rare variant of PN was described and coined as pseudolipoblastic PN [8]. Perineurial cell differentiation is also frequently seen in hybrid peripheral nerve sheath tumors (PNST), where a combination of various subtypes of perineurioma, schwannoma or neurofibroma can be found admixed together [9-14]. In addition to the benign variants of PN, rare cases of malignant PNST (MPNST) showing perineurial cell differentiation have been reported [15-17].

When unassociated with the perineurium of normal nerve fascicles, perineurial cells cannot be identified with certainty using routine histochemical stains [18]. The evidence provided in the initial report [3] was therefore ultrastructural and only later were the observations of Lazarus and Trombetta confirmed by showing the immunoreactivity of these tumors with EMA antibody. In the meantime, additional IHC stains that can be utilized in the diagnosis of perineurial cell tumors including Claudin-1 (19) and GLUT-1 became available [20].

SS is a relatively common high-grade sarcoma of which the monophasic fibrous variant is the most frequent subtype. SS typically arises on the extremities with approximately one third of cases involving the acral sites [21], where they are often of small size [22]. Microscopically, MSS is often sharply circumscribed and may even form a pseudocapsule [22]. It features uniform, spindle-shaped cells with a small amount of cytoplasm and oval to tapered nuclei which are arranged in compact sheets. The absence of significant nuclear pleomorphism is typical for MSS. Mitotic activity is variable but mitotic figures are usually easily found. A hemangiopericytoma-type vascular pattern or cellular clusters of vaguely epithelioid cells may be encountered among the spindle cells. The intervening stroma is usually scarce. Mast cells and microscopic calcifications are a frequent finding in MSS. Immunohistochemically, most MSS are positive with EMA and cytokeratin antibodies. However, the expression of the latter is frequently limited in the monophasic variant, being present in only 79% (CK7), 60% (CK19) and 45% (CK8/18) of cases, respectively [23]. Interestingly, these epithelial markers are often positive in the vaguely epithelial areas of MSS, suggesting the possibility of focal early glandular differentiation.

The four cases presented herein morphologically closely resembled the MSS. Three of the four tumors in our series were also located on the distal portion of extremities, with a mean size of 1.8 cm. They also shared some microscopical features with MSS such as sharp circumscription and (pseudo-)capsule. The most essential similarity between WCP and MSS lies in the presence of a monotonous sheet-like growth of bland spindle-shaped cell with oval to round nuclei (Figs. 1 and 2). Similar to WCP, a significant cellular pleomorphism and prominent mitotic activity can be absent in MSS as well as a prominent intervening stroma. However, in both tumors, foci of more prominent hyalinization may be encountered. Another potential pitfall are the immunohistochemical features of both neoplasms since the reactivity with the EMA antibody belongs to the typical characteristics of both MSS and PN. Moreover, the expression of other antibodies frequently used to confirm the perineurial cell differentiation, namely Claudin-1 and GLUT-1, can be present in MSS in up to 27 and 30% of cases, respectively [24,25].

Nevertheless, there are several histological as well as immunohistochemical differences between MSS and WCP which can be exploited in the differential diagnosis. One of the most helpful microscopic features is the whorling growth pattern which is not commonly seen in MSS (Figs. 1 and 4). The focally discernible long, slender cytoplasmic processes typical for perineurial differentiation can also help in rendering the correct diagnosis. Although the cells constituting both tumors are bland, with no or little cellular pleomorphism, MSS almost always exhibits some mitotic figures, but these were found only after a prolonged search or were absent altogether in our cases of WCP. Conversely, the various features frequently encountered in MSS such as the vaguely epithelioid areas, hemangiopericytoma-like vascular pattern, calcifications, mast cells, hemorrhage or necrosis were not found in WCP. The IHC, as misleading as it may appear with respect to EMA, Claudin-1 and Glut-1 staining, can be a very useful adjunct as well. Although positive in one third of cases of MSS, Claudin-1 expression in this neoplasm is confined primarily to the clusters of vaguely epithelioid cells [19] unlike the WCP where Claudin-1 expression was diffuse and, with the exception of one case, strong. The expression of EMA antibody, albeit noncontributory by the positivity itself, proved useful in highlighting the whorling growth pattern of WCP (Fig. 4). When used in a panel, at least focal cytokeratin expression is found in most MSS, while OSCAR and CK7 were completely absent in all studied cases of WCP as was another of the most frequently used markers of SS, the TLE-1. When necessary and available, FISH (and

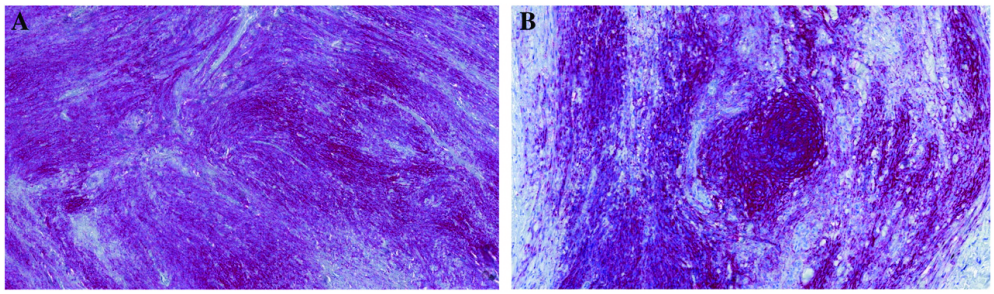

Fig. 4. (A, B.) All tumors reacted with the EMA antibody. The EMA staining nicely highlighted the whorling growth pattern of tumor cells. (A: Case 3; EMA, ×100; B: Case 1; EMA, ×200).

of course EM) will provide the definite answer. Although not entirely specific, cells with bipolar cytoplasmic processes having tight junctions and pinocytotic vesicles along the cell membrane are typical features in perineuriomas. In contrast, spindled cells of monophasic synovial sarcomas show only occasional randomly distributed, primitive intercellular junctions of uncertain type and no bipolar processes [26].

All the other relevant differential diagnostic considerations such as leiomyoma, leiomyosarcoma, fibrosarcoma, dermatofibrosarcoma protuberans etc. can be excluded based on morphology and IHC [27-29]. The rare perineurial cell MPNST [15-17] differs from WCP in several aspects. These are unencapsulated and usually infiltratively growing tumors consisting of pleomorphic cells with hyperchromatic often bizarre nuclei, commonly featuring atypical mitoses and/or areas of necrosis. However, obviously benign perineuriomas may also rarely manifest an infiltrative growth [30]. When considering a diagnosis of perineurial MPNST for lesions located in the area of hands and feet, it is important to note that such a case is currently not on record.

Taking into account similar clinicopathologic features, the relationship of WCP to the sclerosing perineurioma should be addressed [7]. The latter PN subtype also typically occurs on the hands and feet of predominantly male patients. Some of the microscopic features such as the shape and bland appearance of the cells, and especially the frequent whorling pattern of growth are highly reminiscent of WCP. The main difference lies in the absence of abundant, hyalinized, thick collagen bundles between intervening tumor cells growing in corded or trabecular arrangement. However, it cannot be totally discarded that WCP represents a very cellular end of the morphological spectrum of sclerosing perineurioma with only a focal or completely absent areas of hyalinization.

In summary, we presented 4 cases of a distinct variant of perineurial cell tumor that closely mimics MSS. Based on the bland morphological features, perineurial origin and presumably benign clinical outcome (although the follow-up information is admittedly limited), we propose the term “whorling cellular perineurioma” for these tumors and suggest that they may represent an extremely cellular variant of sclerosing perineurioma. This is a very rare perineurioma variant, as is evidenced by the fact that these 4 neoplasms were identified among 208 (~1.9%) cases of skin and soft tissue perineurioma and other lesions with perineurial differentiation stored in our files. Awareness of this PN variant is important in order to avoid its misinterpretation as MSS.

References

[1] Goldblum JR, Folpe AL, Weiss SW. Enzinger and Weiss soft tissue tumors. 6th ed. Elsevier Saunders; 2014 1052–70.
[2] Shelekhova KV, Calonje E, Grossmann P, et al. Superficial soft tissue biphasic synovial sarcoma with apocrine differentiation in the glandular component: a report of two cases. Am J Dermatopathol 2014;36:847–52.
[3] Lazarus SS, Trombetta LD. Ultrastructural identification of a benign perineurial cell tumor. Cancer 1978;41:1823–9.
[4] Emory TS, Scheithauer BW, Hirose T, et al. Intraneural perineurioma. A clonal neoplasm associated with abnormalities of chromosome 22. Am J Clin Pathol 1995; 103:696–704.
[5] Michal M. Extraneural retiform perineuriomas. A report of four cases. Pathol Res Pract 1999;195:759–63.
[6] Graadt van Roggen JF, McMenamin ME, Belchis DA, et al. Reticular perineurioma: a distinctive variant of soft tissue perineurioma. Am J Surg Pathol 2001;25:485–93.
[7] Fetsch JF, Miettinen M. Sclerosing perineurioma: a clinicopathologic study of 19 cases of a distinctive soft tissue lesion with a predilection for the fingers and palms of young adults. Am J Surg Pathol 1997;21:1433–42.
[8] Torres-Mora J, Ud Din N, Ahrens WA, et al. Pseudolipoblastic perineurioma: an unusual morphological variant of perineurioma that may simulate liposarcoma. Hum Pathol 2016;57:22–7.
[9] Kacerovska D, Michal M, Kazakov DV. Hybrid epithelioid schwannoma/perineurioma. Am J Dermatopathol 2016;38:e90–2.
[10] Kazakov DV, Pitha J, Sima R, et al. Hybrid peripheral nerve sheath tumors: schwannoma-perineurioma and neurofibroma-perineurioma. A report of three cases in extradigital locations. Ann Diagn Pathol 2005;9:16–23.
[11] Michal M, Kazakov DV, Belousova I, et al. A benign neoplasm with histopathological features of both schwannoma and retiform perineurioma (benign schwannoma-perineurioma): a report of six cases of a distinctive soft tissue tumor with a predilection for the fingers. Virchows Arch 2004;445:347–53.
[12] Shelekhova KV, Danilova AB, Michal M, et al. Hybrid neurofibroma-perineurioma: an additional example of an extradigital tumor. Ann Diagn Pathol 2008;12:233–4.
[13] Hornick JL, Bundock EA, Fletcher CD. Hybrid schwannoma/perineurioma: clinicopathologic analysis of 42 distinctive benign nerve sheath tumors. Am J Surg Pathol 2009;33:1554–61.
[14] Kacerovska D, Michal M, Kuroda N, et al. Hybrid peripheral nerve sheath tumors, including a malignant variant in type 1 neurofibromatosis. Am J Dermatopathol 2013; 35:641–9.
[15] Zamecnik M, Michal M. Malignant peripheral nerve sheath tumor with perineurial cell differentiation (malignant perineurioma). Pathol Int 1999;49:69–73.
[16] Hirose T, Sumitomo M, Kudo E, et al. Malignant peripheral nerve sheath tumor (MPNST) showing perineurial cell differentiation. Am J Surg Pathol 1989;13: 613–20.
[17] Hirose T, Scheithauer BW, Sano T. Perineurial malignant peripheral nerve sheath tumor (MPNST): a clinicopathologic, immunohistochemical, and ultrastructural study of seven cases. Am J Surg Pathol 1998;22:1368–78.
[18] Antonescu CR, Scheithauer BW, Woodruff JM. AFIP atlas of tumor pathology (series 4): tumors of the peripheral nervous system. , 265Silver Spring, Maryland: ARP Press; 2013.
[19] Folpe AL, Billings SD, McKenney JK, et al. Expression of claudin-1, a recently described tight junction-associated protein, distinguishes soft tissue perineurioma from potential mimics. Am J Surg Pathol 2002;26:1620–6.
[20] Hirose T, Tani T, Shimada T, et al. Immunohistochemical demonstration of EMA/Glut1-positive perineurial cells and CD34-positive fibroblastic cells in peripheral nerve sheath tumors. Mod Pathol 2003;16:293–8.
[21] Miettinen M. Modern soft tissue pathology. , 778Cambridge University Press; 2010.
[22] Michal M, Fanburg-Smith JC, Lasota J, et al. Minute synovial sarcomas of the hands and feet: a clinicopathologic study of 21 tumors less than 1 cm. Am J Surg Pathol 2006;30:721–6.
[23] Miettinen M, Limon J, Niezabitowski A, et al. Patterns of keratin polypeptides in 110 biphasic, monophasic, and poorly differentiated synovial sarcomas. Virchows Arch 2000;437:275–83.
[24] Billings SD, Walsh SV, Fisher C, et al. Aberrant expression of tight junction-related proteins ZO-1, claudin-1 and occludin in synovial sarcoma: an immunohistochemical study with ultrastructural correlation. Mod Pathol 2004;17:141–9.
[25] Ahrens WA, Ridenour 3rd RV, Caron BL, et al. GLUT-1 expression in mesenchymal tumors: an immunohistochemical study of 247 soft tissue and bone neoplasms. Hum Pathol 2008;39:1519–26.

[26] Erlandson RA, Woodruff JM. Role of electron microscopy in the evaluation of soft tissue neoplasms, with emphasis on spindle cell and pleomorphic tumors. Hum Pathol 1998;29:1372–81.
[27] Mentzel T. Cutaneous mesenchymal tumours: an update. Pathology 2014;46:149–59.
[28] Zamecnik M, Michal M. EMA + cells in dermatofibrosarcoma protuberans. A study of 11 tumors suggesting perineurial cell differentiation. Cesk Patol 2002;38:55–62.
[29] Massi D, Franchi A, Alos L, et al. Primary cutaneous leiomyosarcoma: clinicopathological analysis of 36 cases. Histopathology 2010;56:251–62.
[30] Shelekhova K, Kazakov DV, Michal M. Infiltrating retiform perineurioma: a case report. Ann Diagn Pathol 2005;9:293–4.

1.1.7. HYBRID PERIPHERAL NERVE SHEATH TUMORS: A REVIEW

Hybrid peripheral nerve sheath tumors (HPNST) represent a group of several entities, most of which were first described by my colleagues, professor Michal and Kazakov. Accordingly, these tumors are very often consulted at our department and thanks to this, our registry contains hundreds of examples of these rare tumors. Since I had the privilege to review virtually all of them with the two leading experts in this field, I felt confident to write the first review of this beautiful chapter of pathology in the literature.

Briefly, the issue of HPNST, i.e. tumors containing areas of schwannoma, perineurioma and neurofibroma in various combinations is a relatively new chapter in the pathology of both soft tissue and nervous system. Although the existence of tumors showing hybrid features between neurofibroma and schwannoma has already been mentioned in earlier literature, it was only 18 years ago when the first major work on this topic was published by Feany et al [23].

Three main cell types constitute the normal connective tissue sheath of a peripheral nerve, namely Schwann cells, perineurial cells, and fibroblasts. Schwannomas are believed to consist of a nearly pure population of cells showing schwannian differentiation which can be confirmed by ultrastructural examination of these tumors. Perineuriomas, the rarest lesion of the main triad of PNST, are similarly composed exclusively of one cell type: the neoplastic perineurial cell [17]. The situation is not so straightforward with respect to neurofibromas in which a more complex cellular mixture is present. The ultrastructural studies published previously suggested the presence of Schwann cells, perineurial cells, endoneurial fibroblasts [24], intermediate cells (Schwann cell - fibroblast and Schwann - perineurial cells), scattered axons and mast cells in neurofibromas [15, 25, 26]. Although this fact had for a long time remained immunohistochemically unsubstantiated, later several studies confirmed the presence of perineurial cells in neurofibromas

In general, our experience and that of others shows that the diverse types of biphasic lesions may manifest either abrupt transition of the 2 components or the two cellular components schwannomaare closely intermingled. In the latter situation, it is frequently possible to determine the biphasic composition only by IHC. Interestingly, in cases in which the biphasic composition is evident on H&E-stained slides, the individual areas may occasionally display patterns encountered in the less usual subtypes of "monophasic" PNST such as retiform (reticular) perineurioma or epithelioid schwannoma.

Although the whole topic of HPNST may appear of mere academic interest, considerable progress in this field has been accomplished since the initial reports, yielding important clinical implications. Hence, the ability to accurately recognize and classify HPNST proves to be substantial with respect to the management of the patient, and in some cases, to the management of the patients' whole family. For this purpose, the various combinations of HPNST consisting of schwannomas, neurofibromas and perineuriomas were addressed separately in this review, focusing mainly on the morphology and their association with tumor syndromes

Summarizing the collective knowledge of HPNST, hybrid neurofibromas – schwannomas show a very strong association with tumor syndromes called neurofibromatosis type 2 and schwannomatosis and, to a lesser degree, with neurofibromatosis type 1. It is important not to confuse these tumors with a malignant transformation in neurofibroma. Neurofibromatosis type 1 may further provide the genetic background for the development of neurofibromas – perineuriomas. Attention must be paid to accurately interpret the non-perineuriomatous part of these tumors and not to mistake them for schwannomas – perineuriomas which seem to be non-

syndromic tumors. However, occasionally, the distinction may be extremely difficult and there seem to be rare cases, where all three components can coexist in one specimen. Further research, especially with respect to the genetic background of these tumors is needed, as the exact molecular events occurring in these tumors remain largely unknown.

REVIEW ARTICLE

Hybrid peripheral nerve sheath tumors: A review

Michael Michal [1,2], Dmitry V. Kazakov [1], Michal Michal [1]

[1] *Department of Pathology, Faculty of Medicine in Pilsen, Charles University, Prague, Czech Republic*
[2] *Biomedical Center of the Faculty of Medicine in Pilsen, Charles University, Prague, Czech Republic*

SUMMARY

Hybrid peripheral nerve sheath tumors (HPNST) are relatively recently described tumors. With ongoing research, a considerable amount of important findings have been made, much of which has substantial clinical implications. However, a comprehensive review of the whole topic has not been published in the literature so far. In the presented manuscript, the various hybrid tumors are discussed separately with a special emphasis on the morphological and immunohistochemical findings as well as on their association with tumor syndromes.

Keywords: Hybrid peripheral nerve sheath tumors – schwannoma – perineurioma – neurofibroma – neurofibromatosis – schwannomatosis

Hybridní nádory z obalů periferních nervů: přehledový článek

SOUHRN

Hybridní nádory z obalů periferních nervů jsou poměrně nedávno popsanými jednotkami. S postupujícím výzkumem bylo v této oblasti dosaženo značného množství důležitých poznatků, z nichž mnohé jsou významné i z klinického hlediska. V literatuře však dosud chybí kompexní souhrn tohoto tématu. V předkládaném přehledovém článku jsou probrány jednotlivé typy hybridních tumorů se zvláštním zaměřením na jejich morfologické a imunohistochemické vlastnosti, přičemž důraz je rovněž kladen na jejich vztah k nádorovým syndromům.

Klíčová slova: Hybridní nádory z obalů periferních nervů – schwannom – perineuriom – neurofibrom – neurofibromatóza – schwannomatóza

Cesk Patol 2017; 53(2): 81–88

The issue of hybrid peripheral nerve sheath tumors (HPNST), i.e. tumors containing areas of schwannoma, perineurioma and neurofibroma in various combinations is a relatively new chapter in the pathology of both soft tissue and nervous system. Although the existence of tumors showing hybrid features between neurofibroma and schwannoma has already been mentioned in earlier literature, it was only 18 years ago when the first major work on this topic was published by Feany et al (1). Three years later, the first published case of HPNST showing perineuriomatous differentiation (hybrid perineurioma - schwannoma) was presented by Zamecnik and Michal (2).

Three main cell types constitute the normal connective tissue sheath of a peripheral nerve, namely Schwann cells, perineurial cells, and fibroblasts. Schwannomas are believed to consist of a nearly pure population of cells showing schwannian differentiation which can be confirmed by ultrastructural examination of these tumors (3). Perineuriomas, the rarest lesion of the main triad of peripheral nerve sheath tumors (PNST), are similarly composed exclusively of one cell type: the neoplastic perineurial cell (4). The situation is not so straightforward with respect to neurofibromas in which a more complex cellular mixture is present. The ultrastructural studies published previously suggested the presence of Schwann cells, perineurial cells, endoneurial fibroblasts (5), intermediate cells (Schwann cell - fibroblast and Schwann - perineurial cells), scattered axons and mast cells in neurofibromas (6-8). Although this fact had for a long time remained immunohistochemically unsubstantiated, later several studies confirmed the presence of perineurial cells in some neurofibromas (2,9). Eventually, using a highly sensitive detection system, Hirose et al. proved that all neurofibromas contain a small number of EMA positive perineurial cells (5).

Briefly, from the genetic perspective, both neurofibromas and schwannomas originate from either somatic or germline biallelic gene mutations. *NF1* gene (17q11.2) mutations with a functional loss of the protein neurofibromin are found in neurofibromas (10), whereas schwannomas typically harbor biallelic loss of the *NF2* gene (22q12.2) function leading to loss of merlin (schwannomin) protein activity (11). Similarly, perineuriomas have been shown to have a pathogenic relationship to the loss of *NF2* gene function (8,12,13). In tumors that arise in patients with neurofibromatosis type 1 or 2 (NF1, NF2), one allele contains a germline mutation of *NF1* or *NF2* gene respectively, whereas the second allele becomes mutated later in life (somatic mutation). In sporadic tumors, both mutations are somatic. Schwannomatosis is a disease defined by multiple nondermal schwannomas and a lack of vestibular schwannoma. Schwannomatosis-associated schwannomas exhibit four genetic events: non-germline biallelic inactivation of the NF2 gene and mutations of the SWI/SNF chromatin remodeling subunit SMARCB1/INI1 (22q11.23) on both alleles (8,14).

In general, our experience and that of others shows that the various types of biphasic lesions may manifest either abrupt transition of the 2 components or the two cellular components

✉ ***Correspondence address:***
Michael Michal M.D.
Department of Pathology,
Charles University, Medical Faculty and
Charles University Hospital Plzen
Alej Svobody 80, 304 60 Pilsen, Czech Republic.
tel.: +420 603 792 671
e-mail: michael.michal@medima.cz

are closely intermingled (15). In the latter situation, it is frequently possible to determine the biphasic composition only by immunohistochemistry (IHC). In fact, the routine use of IHC has been suggested to increase the frequency of HPNST detection (16). Interestingly, in cases in which the biphasic composition is evident on H&E-stained slides, the individual areas may occasionally display patterns encountered in the less usual subtypes of "monophasic" PNST such as retiform (reticular) perineurioma (2,17,18) or epithelioid schwannoma (19,20).

When approaching HPNST it is always essential to combine morphology with immunohistochemical results. Due to the available antibodies for perineurial differentiation (epithelial membrane antigen (EMA)/Claudin-1/Glut-1), which may be considered quite specific in the context of HPNST, the detection of this line of differentiation is usually not a problem. The most challenging task is to differentiate between a schwannoma and neurofibroma component, especially because hybrid schwannomas - perineuriomas do not exhibit other classical features of schwannomas (hyalinized vessels, Antoni A and B zonation etc.) (21). Although both are S100 protein positive, the Schwann cells in schwannomas are large spindle cells with plump nuclei. In contrast, the Schwann cells in neurofibromas are much smaller (21) and the nuclei have a more elongated, curved (8) or wavy appearance. Moreover, S100 protein positivity in schwannomas is much more diffuse and is present in practically 100% of tumor cells, while in neurofibromas the expression is more limited (approximately 50% of tumor cells). Schwannomas usually contain only focal intratumoral axons, whereas these are often readily identifiable by IHC or by histochemical stain in neurofibromas (3). Although CD34 labels a fibroblastic population in neurofibromas, it may, in up to 50% of cases, also highlight the perineurial cells of perineuriomas (22). Thus again, careful attention must be paid to the morphology of the stained cells. While fibroblasts in neurofibromas have a bland round to oval nuclei, featuring long multipolar cytoplasmic processes (23), the perineurial cells are composed of very thin spindle cells with wavy nuclei and delicate, elongated bipolar or multipolar cytoplasmic processes (22). Most reported examples of hybrid neurofibroma – perineurioma are not morphologically much different from plexiform neurofibroma (15). This architectural trait was encountered in only one sporadic case of hybrid schwannoma – perineurioma (21). Also, based on the published data, the hybrid neurofibroma – perineurioma variant seems to be the by far least frequently encountered. The remaining two groups occur with comparable frequency. Nevertheless, as will be further discussed, in some cases, a clear distinction cannot be made with certainty.

Although the whole topic of HPNST may appear of mere academic interest, significant progress in this field has been accomplished since the initial reports, yielding important clinical implications. Hence, the ability to accurately recognize and classify HPNST proves to be substantial with respect to the management of the patient, and in some cases, to the management of the patients' whole family.

To our knowledge, this is the first comprehensive review of this topic in the literature. For this purpose, the various combinations of HPNST consisting of schwannomas, neurofibromas and perineuriomas will be addressed separately, focusing mainly on the morphology and their association with tumor syndromes. Since most of the hybrid tumors occur in a superficial (dermal or subcutaneous) soft tissue over a wide anatomic distribution, we will specify the tumor location only in cases which show deviation from this scheme.

NEUROFIBROMA - SCHWANNOMA

Due to the morphological similarities between schwannomas and neurofibromas, the only arrangement of hybrid schwannomas – neurofibromas reported so far and also probably the only one histologically recognizable, is in the form of two clearly separated tumor populations. They exhibit the typical features of ordinary neurofibroma enclosing distinct, small (usually less than 1 cm in size), often multiple areas with larger cells containing more ample and eosinophilic cytoplasm, significantly higher cellularity and palisading nuclei corresponding to the Antoni A regions of schwannomas (1,11) (Figure 1A and B). Alternatively, some authors categorize these tumors as neurofibromas with Schwann cell nodules (8). Only a minority of some larger nodules may additionally contain Antoni B regions (11). The Antoni A areas frequently feature hyalinized vessels, which is in contrast to the surrounding neurofibromatous regions, where such vessels are not found. Both Antoni A and B regions are strongly and diffusely positive for S100 protein. While an increased proliferation index (Ki-67) reaching as much as 18% is not uncommon in the schwannomatous area (1,11), the mitotic activity is either very focal or absent. In the less dense neurofibromatous parts, the tumor cells show the characteristic elongated and wavy appearance, with abundant collagen fibers and there is frequent myxoid change in the surrounding stroma. These neurofibromatous parts show virtually no mitoses, stain strongly with CD34 antibody and also react with S100 protein, but the expression is not as diffuse when compared to the schwannomatous areas (11).

There are two reasons why it is crucial to be familiar with this type of HPNST. The first lies in the fact that the more cellular and prominent schwannomatous areas could be mistaken for foci of malignant degeneration in a neurofibroma. Although more cellular, often with an increased proliferation index and occasional mitoses, the Schwann cell component in these tumors does not show other atypical features such as hyperchromasia, prominent mitotic activity, atypical mitoses, necrosis en mass etc. Moreover, early malignant PNSTs (MPNSTs) normally do not grow in a nodular arrangement, as these hybrid tumors in question do (8).

Putting together the data of the two largest studies on this topic, in almost 30% (20/69) of these hybrid tumors, the neurofibroma was of the plexiform type. Knowing that this kind of neurofibroma is almost pathognomonic for NF1 (24) it is not surprising to learn that such hybrid tumors arising in this setting may also be associated with this syndrome. Much more surprising are the facts recently reported by Harder et al (11) who found that NF1 is the least frequently encountered among the three inheritable genetic syndromes causing the development of PNST, namely NF1, NF2 and schwannomatosis. The authors reviewed PNSTs from 14 schwannomatosis patients and found that 71% (10/14) of them had either single or multiple hybrid neurofibromas - schwannomas. Separately, they also studied 23 patients with hybrid neurofibromas – schwannomas whose clinical information were initially unknown. After review of their clinical data, the most common genetic syndrome recorded was NF2 (6/23) followed by schwannomatosis (4/23), whereas only 2 patients showed the stigmata of NF 1. Additionally, the remaining 11 patients showed either signs of an inherited syndrome which could not be accurately specified (2/11) or no clinical data were available for review, thus precluding further classification. Hence, based on this study, a clear conclusion can be drawn that hybrid neurofibromas – schwannomas are very frequently, if not always, associated with a hereditary tumor syndrome.

Very recently, using molecular genetic methods, Stahn et al analyzed 22 cases of hybrid neurofibromas – schwannomas and among other molecular events, one of the most prominent findings was the uncovered monosomy of the chromosome 22 identified in almost half of the tumors tested (14). Biallelic but not germline inactivation of this gene is found in all schwannomas, including those diagnosed in patients with schwannoma-

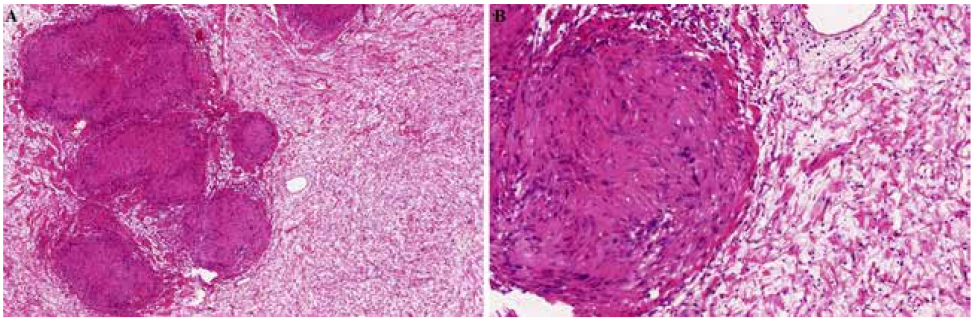

Figure 1. Hybrid neurofibroma – schwannoma. **A, B:** These tumors exhibit the typical features of ordinary neurofibroma enclosing small often multiple areas with larger cells containing more ample and eosinophilic cytoplasm, significantly higher cellularity and palisading nuclei corresponding to the Antoni A regions of schwannomas. In the less dense neurofibromatous parts, the tumor cells show the characteristic elongated and wavy appearance, with abundant collagen fibers and there is frequent myxoid change in the surrounding stroma.

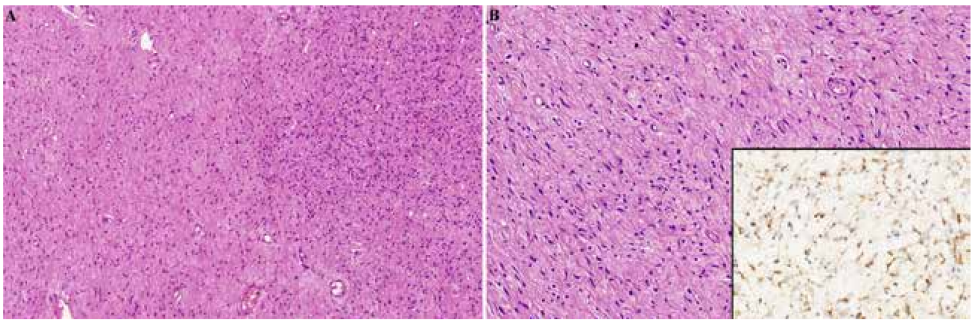

Figure 2. Hybrid neurofibroma – perineurioma with retiform arrangement. **A:** Lesion with a biphasic pattern produced by areas with a retiform perineurioma appearance (on the left - mosaic-like arrangement of interconnected spindle-shaped cells with bipolar or stellate nuclei) which gradually merge into areas which look like an ordinary neurofibroma (on the right - Schwann cells with spindled wavy nuclei). **B:** Higher power view of the retiform perineurioma area with a strong claudin-1 staining (inset).

tosis. On the contrary, patients with NF2 have germline mutations found in this gene (8,25).

NEUROFIBROMA – PERINEURIOMA

As mentioned above, the ultrastructural studies have for a long time indicated the presence of perineurial cell subpopulation in neurofibromas. Nevertheless, this had remained immunohistochemically unproven until 2001, when Zamecnik and Michal analyzed 99 neurofibromas and demonstrated EMA positive perineurial cells being present in 7 of these lesions in a sparse, but quite diffuse manner (2). However, although no exact criteria exist, the amount of perineuriomatous tissue in these neurofibromas was not significant enough as to warrant the designation of HPNST.

The first two cases of hybrid neurofibroma – perineurioma were presented four years later by Kazakov et al (18). Both tumors had a unique appearance but differed from one another. The first was a lesion with a biphasic pattern produced by areas with a retiform perineurioma appearance (Figure 2B; mosaic-like arrangement of interconnected spindle-shaped cells with bipolar or stellate nuclei) which gradually merged into areas which looked like an ordinary neurofibroma (Figure 2A; Schwann cells with spindled wavy nuclei). Immunohistochemically, the tumor showed abundant S-100 protein positive wavy Schwann cells and CD34 positive fibroblasts in the neurofibromatous areas. EMA was negative in these parts. Conversely, antibodies to EMA and claudin-1 stained the perineuriomatous areas strongly (Figure 2B - inset) and reacted negatively with the spindled wavy Schwann cells. No CD34-positive fibroblasts and very scarce S-100 protein positive wavy cells were present in the perineuriomatous compartments.

The second tumor showed a different arrangement of the two components that mostly merged together imperceptibly within a lesion: individual spindled cells with wavy nuclei identical to those found in neurofibroma were closely intermingled with spindled cells with bipolar or stellate nuclei corresponding to the perineurial cell differentiation. Thus the biphasic pattern was poorly discernable on HE-stained slides but was appreciable on immunohistochemical slides, with the spindled cells having wavy nuclei manifesting S-100 protein+/EMA-/claudin-1- phenotype surrounded by EMA+/claudin-1+/S-100 protein- stellate cells. CD34 labeled plentiful fibroblasts distributed evenly within the lesion (18). Notably, this case was shown to contain a point mutation in the *NF2* gene (18). This group of authors later reported an additional and virtually identical case (26). A similar example is depicted in Figure 3.

In 2013, Kacerovska et al published a series of 5 patients with NF1 who presented with hybrid neurofibromas – perineuriomas. In four cases, the tumors at first glance represented ordinary plexiform neurofibromas. The perineuriomatous component was admixed in a very discreet, intermingled fashion and was not apparent on H&E-stained slides (Figure 4A-C). In the last

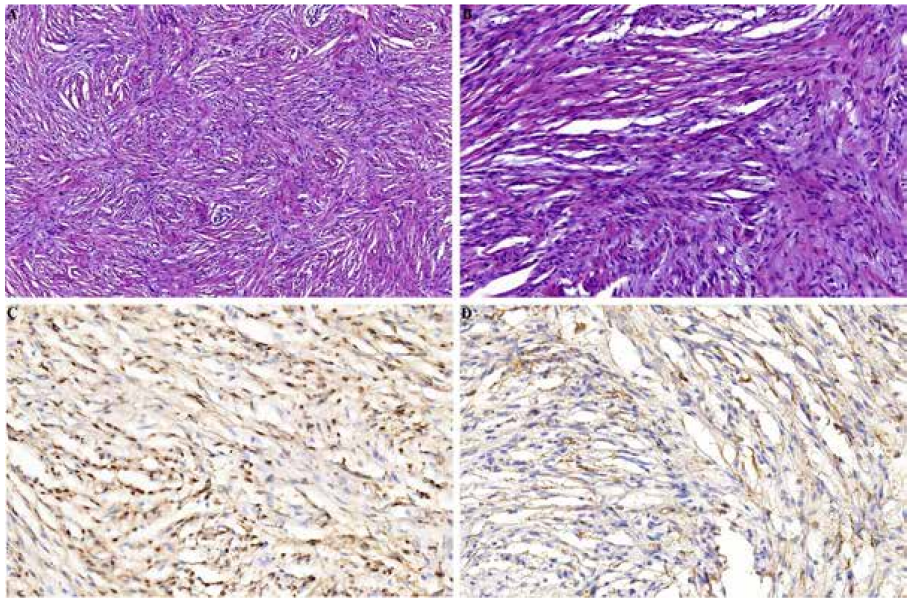

Figure 3. Hybrid neurofibroma – perineurioma. **A, B:** Different arrangement of the two components that mostly merge together imperceptibly within a lesion: individual spindled cells with wavy nuclei identical to those found in neurofibroma are closely intermingled with spindled cells with bipolar or stellate nuclei corresponding to the perineurial cell differentiation. **C:** The biphasic pattern is poorly discernible on HE-stained slides but is appreciable on immunohistochemical slides, with the spindled cells having wavy nuclei manifesting S-100 protein positivity. **D:** They are surrounded by EMA positive bipolar or stellate cells.

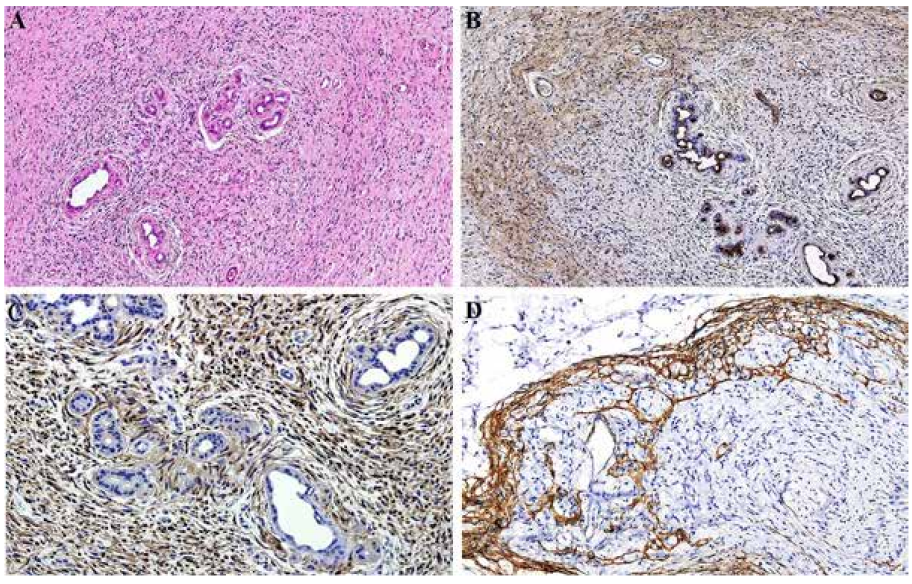

Figure 4. Hybrid neurofibroma – perineurioma in a patient with NF1. **A:** The tumors at first glance represent ordinary neurofibromas. The perineuriomatous component is admixed in a very discreet, intermingled fashion and is not apparent on H&E-stained slides. **B:** However, it is easily discernible on immunohistochemical staining with EMA. **C:** EMA negative parts are usually S100 protein positive. **D:** Several nerve fibers in the vicinity show prominent reticular networks of GLUT-1-positive perineurial cells. Among PNSTs, these intraneural lesions are restricted only to cases harboring hybrid neurofibroma - perineurioma. This finding supports the role of these intraneural lesions as precursors of hybrid neurofibroma – perineurioma.

case, areas with perineuriomatous differentiation were clearly visible on H&E-stained slides as spindled cells with bipolar or stellate nuclei arranged in short fascicles or whorls. The neurofibromatous element resembled diffuse neurofibroma and the 2 components were segregated from one another. In addition to the bland-looking neurofibromatous and perineuriomatous areas, there were multifocal hypercellular areas showing numerous mitotic figures and closely packed epithelioid and spindled pleomorphic cells arranged in nests and fascicles which were classified as features of MPNST. The neoplastic cells in the malignant areas stained for S-100 protein and were negative for EMA, GLUT-1, and Claudin-1 (15). Although neurofibroma can on rare occasion be a benign precursor to MPNST and several tumors classified as MPNST with perineurial differentiation have also been described (27-29), this was the first and so far the only case of MPNST reported in any type of HPNST.

Interesting observations regarding the relationship between hybrid neurofibromas – perineuriomas and NF1 have recently been reported by Agaimy (30). Employing immunohistochemical antibodies for perineurial differentiation (EMA, Claudin-1, GLUT- 1) he analyzed histologically normal-looking nerve fibers in resections specimens harboring PNSTs from NF1 patients. Of these, several nerve fibers showed prominent reticular networks of EMA/claudin-1/GLUT-1-positive perineurial cells. These intraneural lesions were restricted practically only to cases harboring hybrid neurofibroma – perineurioma and were not present in other PNSTs. This finding supports the role of these intraneural lesions as precursors of hybrid neurofibroma - perineurioma (30). Identical intraneural proliferations of perineurial cells were also present in our series of NF1 associated hybrid neurofibromas – perineuriomas (15) (Figure 4D).

Perineuriomas have shown a pathogenic relationship to loss of NF2 gene function (8,12,13) and are generally not considered a part of the NF1-associated spectrum of tumors. However, two case reports of perineuriomas arising in the setting of NF1 are on record (31,32). While knowing that a large proportion of HPNST is overlooked in routine practice, the findings reported by Kacerovska et al and by Agaimy suggest that tumors exhibiting perineurial cell differentiation in the setting of underlying NF1 may not be as uncommon as previously thought. Nevertheless, this by no means excludes the possibility that similarly to normal soft tissue perineuriomas, some HPNST with perineurial differentiation may still contain mutations of the NF2 gene as exemplified in the aforementioned study by Kazakov et al (18).

SCHWANNOMA – PERINEURIOMA

Quite similarly to the described examples of neurofibroma – perineurioma, the two populations found in schwannomas – perineuriomas can be either closely intermingled or occur in a segregated manner. The cells in the perineuriomatous component in the latter cases often also resemble retiform (reticular) perineurioma. As was mentioned previously, rare cases of non-hybrid PNST exist, where it is extremely difficult to precisely classify the tumor as either schwannoma or neurofibroma, an opinion shared by others as well (3,33). Accordingly, the non-perineuriomatous component in hybrid tumors can also have ambivalent features of both schwannoma and neurofibroma (18). Hence, admittedly, the final classification of HPNST as hybrid neurofibroma - perineurioma or hybrid schwannoma - perineurioma may be quite subjective in certain cases. This fact was best illustrated in the aforementioned study by Zamecnik and Michal (2). In addition to the examples of neurofibroma with focal perineuriomatous differentiation, one unique case where the latter moiety was much more prominent was identified by the authors who described this tumor as having features

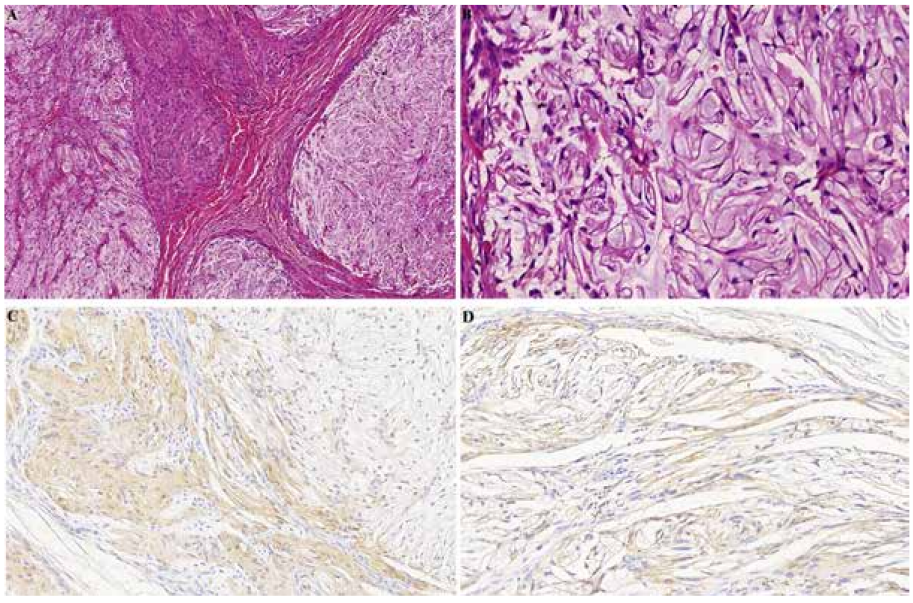

Figure 5. Hybrid schwannoma – retiform perineurioma. **A:** The lesions feature a multilobular architecture. The variably sized and shaped lobules are separated by variably thick collagenous septae. The schwannomatous component (central part) consists of elongated cells with tapered, spindled nuclei, mostly arranged in a compact Antoni A pattern and the cells, in contrast to the perineurial cells, have deeply eosinophilic cytoplasm. **B:** The perineuriomatous component has the appearance of retiform perineurioma and is EMA positive. **C:** S100 protein is positive in the schwannomatous areas and negative in the perineuriomatous parts. **D:** EMA staining of the perineuriomatous area.

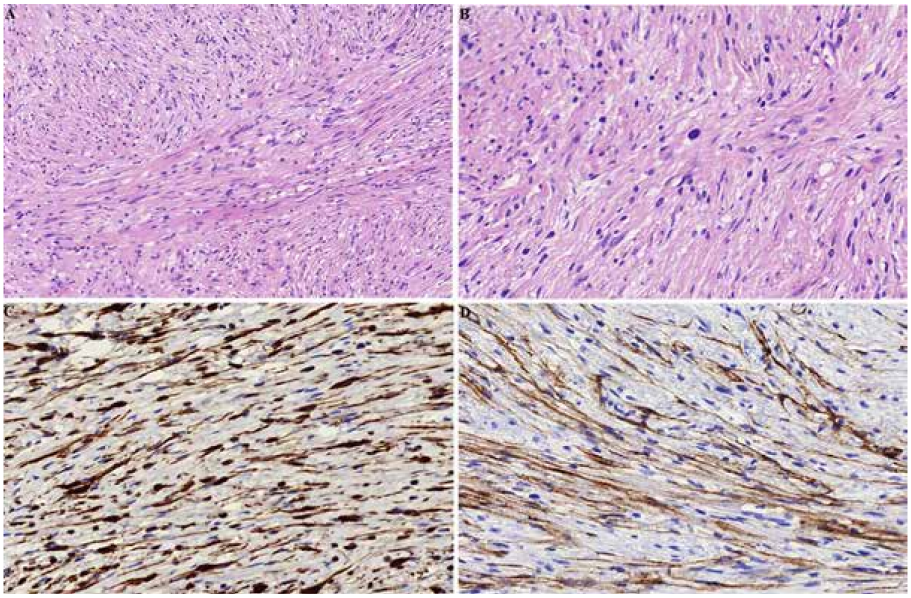

Figure 6. Hybrid schwannoma – perineurioma. **A:** On low magnification, the first impression of these tumors is rather that of a perineurioma, mainly due to the prominent storiform, lamellar and whorled growth patterns. **B:** However, on higher magnification, the dominant cytology is schwannian, with the slender, elongated perineurial cells being obscured by the more numerous and large Schwann cells. Notably, nuclear atypia in the form of scattered pleomorphic cells with hyperchromatic, smudged nuclei is often present and does not herald malignant behavior in such cases. **C:** By IHC, the dual cell population is again readily appreciable with positive staining for S100 protein in the larger cells. **D:** Conversely, the more slender and elongated perineurial cells stain with EMA.

of both neurofibroma and retiform perineurioma. In 2004, while preparing another study on hybrid schwannomas - retiform perineuriomas, this case was re-reviewed by the authors and together with five other similar cases, it was immunohistochemically studied for the presence of neurofilament protein and CD34 expression, which label axons and fibroblasts in neurofibromas respectively (5). The nonperineuriomatous parts of all tested tumors were found to be devoid of axons, and only a few CD34-positive cells were detected. Based upon these findings the tumor was reclassified as hybrid schwannoma – perineurioma (34), thus representing the first published example of this kind. Overall, this tumor as well as all other 5 lesions included in the study occurred on the hands, with a predilection for the fingers. Importantly, no association with any syndrome was noted. Microscopically, the lesions featured a multilobular architecture. The variably sized and shaped lobules were separated by variably thick collagenous septae (Figure 5A). The schwannomatous component (Figure 5C; S-100 protein +/EMA and CD34 -) consisted of elongated cells with tapered, spindled nuclei, mostly arranged in a compact Antoni A pattern and the cells, in contrast to the perineurial cells, had deeply eosinophilic cytoplasm (Figure 5A). The perineuriomatous component had the appearance of retiform perineurioma (Figure 5B) and was S-100 protein/CD34 negative and EMA positive (Figure 5D). These two components either formed separate nodules or the schwannomatous tissue surrounded the perineurial parts located in the centers of the lobules (Figure 5A) (34).

The largest series of hybrid schwannomas – perineuriomas was published by Hornick et al, first in an abstract form at the annual USCAP meeting in 2004 (35), and then, several years later, as a full article (21). Unlike the previous studies on this topic, the authors presented tumors composed purely of an intimate admixture of the two cell types. The tumors showed a wide anatomic distribution, and no association with NF1 was recorded, both findings being confirmed later in an additional study on this topic by different authors (36). Microscopically, on low magnification, the first impression of these tumors was that of perineurioma, mainly due to the prominent storiform, lamellar and whorled growth patterns (Figure 6A). However, on higher magnification, the dominant cytology was schwannian, with the slender, elongated perineurial cells being obscured by the more numerous and large Schwann cells. Notably, degenerative nuclear atypia in the form of scattered pleomorphic cells with hyperchromatic, smudged nuclei was present in one quarter of the cases (Figure 6B) (21). By IHC, the dual cell population was again readily appreciable. Using the elegant method of double immunostaining, the authors clearly illustrated that these tumors are composed of two separate populations of cells arranged in parallel arrays. Usually constituting 60-70% of the lesion, the larger cells were stained with S100 protein (Figure 6C), whereas the second type of cell expressed the EMA antibody (Figure 6D). Although practically all the cases were diffusely labeled with CD34, the authors did not interpret this feature as fibroblastic staining. Instead, they concluded, that this staining was present in the perineurial cells, a feature that may occur in more than 50% of perineuriomas (22).

Included in this series and also reported earlier in a separated case report (37) was hybrid schwannoma – perineurioma occurring in the colon, the first ever reported HPNST of the GI tract. Later, additional GI cases were reported in other parts of the GI tract (36,38). All lesions were morphologically analogous to the schwannoma – perineurioma of soft tissue as described by Hornick et al (21), thus having features very different from conventional GI schwannomas. The differentiating traits include dif-

ferent growth patterns, an absence of peripheral lymphoid cuff, more prominent and diffuse CD34 expression and the presence of alternating fascicles of schwannian and perineurial cells, as again confirmed by double immunostaining (38).

Finally, very recently, Kacerovska et al. reported a case where the schwannomatous moiety showed prominent epithelioid features and was thus classified as hybrid epithelioid schwannoma – perineurioma. These epithelioid cells were arranged singly or in small aggregates or short cords and although closely admixed, due to the larger size of the Schwann cells in this case, the biphasic composition was well apparent already on the H&E-stained slides (20).

SCHWANNOMA - NEUROFIBROMA - PERINEURIOMA

As repeatedly discussed in this review, some tumors are remarkably difficult to fit not only into one specific category of schwannoma, neurofibroma or perineurioma, but even into the various categories of hybrid tumors. One tumor, arising on a sporadic basis and classified as a hybrid tumor containing all three PNST types was reported in the nasopharyngeal area by Kuroda et al (39). Another such lesion was encountered in a patient with NF1 and is illustrated in the Figure 8 in the review by Rodriguez et al (40). Furthermore, as mentioned in one of our publications (15), due to the quite pronounced and illustrated presence of perineurial cells in some cases reported by Harder et al (11), some of them might in fact represent HPNST containing neurofibromatous, schwannomatous, and perineuriomatous differentiation. However, admittedly, at present no quantitative criteria for such a classification exists.

CONCLUSION

The research of HPNST has yielded several important findings, especially with respect to the clinical management of the patients and their kindred. Hybrid neurofibromas – schwannomas show a very strong association with NF2 and schwannomatosis and, to a lesser degree, with NF1. It is important not to confuse these tumors with a malignant transformation in neurofibroma. NF1 may further provide the genetic background for the development of neurofibromas – perineuriomas. Attention must be paid to accurately interpret the non-perineuriomatous part of these tumors and not to mistake them for schwannomas – perineuriomas which seem to be non-syndromic tumors. However, occasionally, the distinction may be extremely difficult and there seem to be rare cases, where all three components can coexist in one specimen. Further research, especially with respect to the genetic background of these tumors is needed, as the exact molecular events occurring in these tumors remain largely unknown.

ACKNOWLEDGEMENTS

This study was supported by the National Sustainability Program I (NPU I) Nr. LO1503 provided by the Ministry of Education Youth and Sports of the Czech Republic. The authors have no conflicts of interest to disclose.

CONFLICT OF INTEREST

The authors declare that there is no conflict of interest regarding the publication of this paper.

REFERENCES

1. **Feany MB, Anthony DC, Fletcher CD.** Nerve sheath tumours with hybrid features of neurofibroma and schwannoma: a conceptual challenge. *Histopathology* 1998; 32(5): 405-410.
2. **Zámečník M, Michal M.** Perineurial cell differentiation in neurofibromas. Report of eight cases including a case with composite perineurioma-neurofibroma features. *Pathol Res Pract* 2001; 197(8): 537-544.
3. **Nascimento AF, Fletcher CD.** The controversial nosology of benign nerve sheath tumors: neurofilament protein staining demonstrates intratumoral axons in many sporadic schwannomas. *Am J Surg Pathol* 2007; 31(9): 1363-1370.
4. **Lazarus SS, Trombetta LD.** Ultrastructural identification of a benign perineurial cell tumor. *Cancer* 1978; 41(5): 1823-1829.
5. **Hirose T, Tani T, Shimada T, Ishizawa K, Shimada S, Sano T.** Immunohistochemical demonstration of EMA/Glut1-positive perineurial cells and CD34-positive fibroblastic cells in peripheral nerve sheath tumors. *Mod Pathol* 2003; 16(4): 293-298.
6. **Erlandson RA, Woodruff JM.** Peripheral nerve sheath tumors: an electron microscopic study of 43 cases. *Cancer* 1982; 49(1): 273-287.
7. **Hirose T, Sano T, Hizawa K.** Ultrastructural localization of S-100 protein in neurofibroma. *Acta Neuropathol* 1986; 69(1-2): 103-110.
8. **Antonescu CR, Scheithauer BW, Woodruff JM**. AFIP atlas of tumor pathology (Series 4): Tumors of the peripheral nervous system. Silver Spring, Maryland: ARP Press; 2013.
9. **Michal M, Kazakov DV, Hadravský L, Michalový K, Rychlý B, Michal M.** Multivacuolated mucin-filled cells: a unique cell characteristic of plexiform neurofibroma. A report of 11 cases. *Hum Pathol* 2017; 60(2): 167-173.
10. **Petrák B, Bendová Š, Lisý J, et al.** Neurofibromatosis von Recklinghausen typ 1 (NF1) - klinický obraz a molekulárně-genetická diagnostika. *Cesk Patol* 2015; 51(1): 34-40.
11. **Harder A, Wesemann M, Hagel C, et al.** Hybrid neurofibroma/schwannoma is overrepresented among schwannomatosis and neurofibromatosis patients. *Am J Surg Pathol* 2012; 36(5): 702-709.
12. **Giannini C, Scheithauer BW, Jenkins RB, et al.** Soft-tissue perineurioma. Evidence for an abnormality of chromosome 22, criteria for diagnosis, and review of the literature. *Am J Surg Pathol* 1997; 21(2): 164-173.
13. **Lasota J, Fetsch JF, Wozniak A, Wasag B, Sciot R, Miettinen M.** The neurofibromatosis type 2 gene is mutated in perineurial cell tumors: a molecular genetic study of eight cases. *Am J Pathol* 2001; 158(4): 1223-1229.
14. **Stahn V, Nagel I, Fischer-Huchzermeyer S, et al.** Molecular Analysis of Hybrid Neurofibroma/Schwannoma Identifies Common Monosomy 22 and alpha-T-Catenin/CTNNA3 as a Novel Candidate Tumor Suppressor. *Am J Pathol* 2016; 186(12): 3285-3296.
15. **Kacerovská D, Michal M, Kuroda N, et al.** Hybrid peripheral nerve sheath tumors, including a malignant variant in type 1 neurofibromatosis. *Am J Dermatopathol* 2013; 35(8): 641-649.
16. **Pusiol T, Zorzi MG, Morichetti D, Piscioli F.** Routine use of immunohisto-chemistry may increase the frequency of hybrid peripheral nerve sheath tumors. *Am J Dermatopathol* 2011; 33(8): 634-636.
17. **Michal M.** Extraneural retiform perineuriomas. A report of four cases. *Pathol Res Pract* 1999; 195(11): 759-763.
18. **Kazakov DV, Piťha J, Šíma R, et al.** Hybrid peripheral nerve sheath tumors: Schwannoma-perineurioma and neurofibroma-perineurioma. A report of three cases in extradigital locations. *Ann Diagn Pathol* 2005; 9(2): 16-23.
19. **Kindblom LG, Meis-Kindblom JM, Havel G, Busch C.** Benign epithelioid schwannoma. *Am J Surg Pathol* 1998; 22(6): 762-770.
20. **Kacerovská D, Michal M, Kazakov DV.** Hybrid Epithelioid Schwannoma/Perineurioma. *Am J Dermatopathol*. 2016; 38(7): e90-92.
21. **Hornick JL, Bundock EA, Fletcher CD.** Hybrid schwannoma/perineurioma: clinicopathologic analysis of 42 distinctive benign nerve sheath tumors. *Am J Surg Pathol* 2009; 33(10): 1554-1561.
22. **Hornick JL, Fletcher CD.** Soft tissue perineurioma: clinicopathologic analysis of 81 cases including those with atypical histologic features. *Am J Surg Pathol* 2005; 29(7): 845-858.
23. **Weiss SW, Nickoloff BJ.** CD-34 is expressed by a distinctive cell population in peripheral nerve, nerve sheath tumors, and related lesions. *Am J Surg Pathol* 1993; 17(10): 1039-1045.
24. **McCarron KF, Goldblum JR.** Plexiform neurofibroma with and without associated malignant peripheral nerve sheath tumor: a clinicopathologic and immunohistochemical analysis of 54 cases. *Mod Pathol* 1998; 11(7): 612-617.
25. **Rodriguez FJ, Stratakis CA, Evans DG.** Genetic predisposition to peripheral nerve neo-

plasia: diagnostic criteria and pathogenesis of neurofibromatoses, Carney complex, and related syndromes. *Acta Neuropathol* 2012; 123(3): 349-367.
26. **Shelekhova KV, Danilova AB, Michal M, Kazakov DV.** Hybrid neurofibroma-perineurioma: an additional example of an extradigital tumor. *Ann Diagn Pathol* 2008; 12(6): 233-234.
27. **Zámečník M, Michal M.** Malignant peripheral nerve sheath tumor with perineurial cell differentiation (malignant perineurioma). *Pathol Int* 1999; 49(1): 69-73.
28. **Hirose T, Sumitomo M, Kudo E, et al.** Malignant peripheral nerve sheath tumor (MPNST) showing perineurial cell differentiation. *Am J Surg Pathol* 1989; 13(7): 613-620.
29. **Hirose T, Hasegawa T, Kudo E, Seki K, Sano T, Hizawa K.** Malignant peripheral nerve sheath tumors: an immunohistochemical study in relation to ultrastructural features. *Hum Pathol* 1992; 23(8): 865-870.
30. **Agaimy A.** Microscopic intraneural perineurial cell proliferations in patients with neurofibromatosis type 1. *Ann Diagn Pathol* 2014; 18(4): 95-98.
31. **Schaefer IM, Strobel P, Thiha A, et al.** Soft tissue perineurioma and other unusual tumors in a patient with neurofibromatosis type 1. *Int J Clin Exp Pathol* 2013; 6(12): 3003-3008.
32. **Ausmus GG, Piliang MP, Bergfeld WF, Goldblum JR.** Soft-tissue perineurioma in a 20-year-old patient with neurofibromatosis type 1 (NF1): report of a case and review of the literature. *J Cutan Pathol* 2007; 34(9): 726-730.
33. **Zámečník M.** Hybrid neurofibroma/schwannoma versus schwannoma with Antoni B areas. *Histopathology* 2000; 36(5): 473-474.
34. **Michal M, Kazakov DV, Belousova I, Bisceglia M, Zamecnik M, Mukensnabl P.** A benign neoplasm with histopathological features of both schwannoma and retiform perineurioma (benign schwannoma-perineurioma): a report of six cases of a distinctive soft tissue tumor with a predilection for the fingers. *Virchows Arch* 2004; 445(10): 347-353.
35. **Bundock EA FC.** Nerve sheath tumors with hybrid features of perineurioma and schwannoma [abstract]. *Modern Pathology* 2004; 17(suppl 1):12A.
36. **Yang X, Zeng Y, Wang J.** Hybrid schwannoma/perineurioma: report of 10 Chinese cases supporting a distinctive entity. *Int J Surg Pathol* 2013; 21(2): 22-28.
37. **Emanuel P, Pertsemlidis DS, Gordon R, Xu R.** Benign hybrid perineurioma-schwannoma in the colon. A case report. *Ann Diagn Pathol* 2006; 10(12): 367-370.
38. **Agaimy A, Michal M.** Hybrid schwannoma-perineurioma of the gastrointestinal tract: a clinicopathologic study of 2 cases and reappraisal of perineurial cells in gastrointestinal schwannomas. *Appl Immunohistochem Mol Morphol* 2011; 19(10): 454-459.
39. **Kuroda N, Kazakov DV, Hes O, et al.** Hybrid peripheral nerve sheath tumor of the nasal cavity showing schwannomatous, neurofibromatous, and perineuriomatous areas. *Med Mol Morphol* 2010; 43(6): 82-85.
40. **Rodriguez FJ, Folpe AL, Giannini C, Perry A.** Pathology of peripheral nerve sheath tumors: diagnostic overview and update on selected diagnostic problems. *Acta Neuropathol* 2012; 123(3): 295-319.

1.1.8. LIPOBLASTS IN SPINDLE CELL AND PLEOMORPHIC LIPOMAS: A CLOSE SCRUTINY

Spindle cell and pleomorphic lipomas (SCL/PL) are benign lipomatous tumors considered as opposite ends in a morphological spectrum of one single entity. We investigated the presence and frequency of lipoblasts, an immature form of fat cell, in these tumors. By many general pathologists, lipoblasts are incorrectly considered as a diagnostic criterion for atypical lipomatous tumor/well differentiated liposarcoma - a malignant adipocytic tumor - where they very often occur. The presence of lipoblasts in SCL/PL has been reported in the past, but contemporary reports often fail to mention this frequent and important feature of SCL/PL which often leads to diagnostic difficulties or errors. Our goal was to illustrate how common lipoblasts in these benign tumors are.

Overall, we collected 129 cases of SCL/PL. Then we started to morphologically review all the cases again, searching for lipoblasts. When more than 3 unequivocal fat cells having hyperchromatic, indented, or sharply scalloped nuclei (i.e. lipoblasts) were found, the case was regarded as positive for the presence of lipoblasts. The 129 cases selected consisted of 91 SCL and 38 PL. Lipoblasts were found in 37 cases (41%) of SCL. Of the 38 PL cases, 25 (66%) contained lipoblasts. While in the majority of SCL cases, only a few lipoblasts were found after a meticulous search, PL showed single or several lipoblasts in a much more diffuse manner. Nevertheless, a significant subset of cases of both SCL and PL contained several foci with a highly prominent lipoblastic admixture, which was easy to be found.

After this step, we stained all the lipoblasts containing cases with CD34 and RB protein antibodies, both of which yielded results compatible with the diagnosis. Then we performed FISH analysis using probes for FUS gene to exclude myxoid liposarcoma and MDM2 and CDK4 genes to rule out the possibility of atypical lipomatous tumor/well differentiated liposarcoma.

Since many of these cases were sent to us for consultation, we also collected the referring diagnoses. For all the cases we also obtained follow up information. Overall, the most common referring diagnosis was that of ALT or another type of liposarcoma, which was listed in 6 of 15 SCL and in 8 of 13 PL cases. Follow-up was available for 44 patients, of whom 2 suffered recurrence of SCL.

Summarizing our findings, this study emphasized the fact that lipoblasts are very frequent findings in both SCL (41%) and PL (66%), and it shows that their presence is not a distinguishing feature of these tumors from liposarcomas. Even more importantly, in many SCL/PL, lipoblasts constitute a component so prominent as to cause diagnostic difficulties to the unaware as illustrated by the referral diagnoses which commonly listed liposarcoma as the possibility. In order to prevent a misdiagnosis it is therefore important to base the diagnosis on different, diagnostically more relevant clinicopathological features such as the most common occurrence of SCL/PL in the subcutis of shawl area or histological features such as the presence of ropey collagen bundles in SCL/PL. A useful byproduct of our study is also the confirmed low recurrence rate of immunohistochemically and molecular genetically validated set of SCL/PL.

Human Pathology (2017) 65, 140–146

ELSEVIER

Human PATHOLOGY

www.elsevier.com/locate/humpath

Original contribution

Lipoblasts in spindle cell and pleomorphic lipomas: a close scrutiny☆,☆☆

Michael Michal MD[a,b,*], Dmitry V. Kazakov MD[a], Ladislav Hadravsky MD[c], Kvetoslava Michalova MD[a], Petr Grossmann PhD[a], Petr Steiner PhD[a], Tomas Vanecek PhD[a], Valentina Renda MD[d], Saul Suster MD[d], Michal Michal MD[a]

[a]*Department of Pathology, Faculty of Medicine in Pilsen, Charles University, 323 00 Pilsen, Czech Republic*
[b]*Biomedical Center, Faculty of Medicine in Pilsen, Charles University, 323 00 Pilsen, Czech Republic*
[c]*Department of Pathology, Third Medical Faculty in Prague, Charles University, 100 34 Prague, Czech Republic*
[d]*Department of Pathology and MCW Cancer Center, Medical College of Wisconsin, Milwaukee, WI, USA 53226-3522*

Received 26 January 2017; revised 27 April 2017; accepted 5 May 2017

Keywords:
Soft tissues;
Spindle cell;
Pleomorphic lipoma;
Liposarcoma;
Lipoblasts

Summary The presence and frequency of lipoblasts (LPB) in spindle cell lipomas (SCL) and pleomorphic lipomas (PL) has never been studied in detail on a histologically, immunohistochemically and molecular genetically validated set of tumors. The authors investigated this feature by reviewing 91 cases of SCL and 38 PL. When more than 3 unequivocal LPB were found, the case was regarded as positive for the presence of LPB. All positive cases were then stained with CD34 and retinoblastoma (Rb) protein antibodies and tested by fluorescence in situ hybridization for *MDM2* and *CDK4* amplifications and the *FUS* gene rearrangements. The patients with SCL and PL containing LPB were 14 women and 47 men, the rest were of unknown gender. The cases usually presented as superficial, well-circumscribed soft tissue masses and most commonly occurred in the upper back and neck. CD34 was expressed in all cases, while Rb protein was consistently absent in all. Molecular genetic results, when available, were in concordance with the morphological diagnosis of SCL/PL. LPB were found in 37 (41%) cases of SCL and 25 cases of PL (66%). While in many cases they are inconspicuous, in some others they constitute a very prominent component of the tumor. It is important to be aware of this fact in order to avoid misinterpretation as liposarcoma.

1. Introduction

Spindle cell lipomas (SCL) and pleomorphic lipomas (PL) are distinctive soft tissue tumors, originally described as 2 separate entities by Enzinger et al [1,2]. Based on similar clinicopathological, immunohistochemical as well as molecular genetic features, these neoplasms are today considered as opposite ends in a morphological spectrum of one single entity [3]. This is further supported by a frequent occurrence of cases showing characteristic morphological features of both SCL and PL in the same specimen. In their seminal paper by

☆ Competing interests: The authors have no conflict of interest to disclose. Neither ethics approval nor informed consent was required for our study.

☆☆ Funding/Support: This study was supported by the National Sustainability Program I (NPU I) Nr. LO1503 provided by the Ministry of Education Youth and Sports of the Czech Republic.

* Corresponding author at: Department of Pathology, Charles University, Medical Faculty and Charles University Hospital Plzen, Alej Svobody 80, 323 00 Pilsen, Czech Republic.
E-mail address: michael.michal@medima.cz (M. Michal).

http://dx.doi.org/10.1016/j.humpath.2017.05.006
0046-8177/

Shmookler and Enzinger in 1981, it was noted that almost one half of PL exhibited lipoblasts (LPB). Two years later, this finding was confirmed by another group [4]. However, contemporary reports often fail to mention this frequent and important feature of PL; and with respect to SCL, this feature is clearly underrecognized. After a review of the literature, including the major soft tissue pathology textbooks, we have found only 3 publications [3,5,6] acknowledging the presence of LPB in SCL. This situation is in stark contrast with our own experience. Over the years, we have encountered many cases of both SCL and PL with a prominent admixture of LPB. Since many of these cases were sent to us because of the concern for liposarcoma by the submitting pathologist, we decided to undertake this study on a large series of cases. To our knowledge, this is the first study which attempts to rigorously assess the frequency of LPB on a histologically, immunohistochemically, and molecular genetically validated set of SCL/PL.

2. Materials and methods

The 129 cases of SCL/PL constituting the subject of this study were retrieved from the routine biopsy archive and the authors' consultation files; they came from the period between years 1993 and 2016. The clinical information was extracted from the medical records, and follow-up data were obtained from the attending clinicians. To identify cases, we searched our consultation registry files for tumors diagnosed as SCL, PL or SCL/PL. This search yielded altogether 151 specimens, which were reviewed to confirm the diagnosis. Upon revision, 5 cases were excluded because they did not meet the diagnostic criteria for SCL/PL [3]. Another 11 cases of SCL were not included because they featured a prominent myxoid change, which made a reliable recognition of LPB very difficult. Five cases were omitted because they represented the fat-free variant of these tumors. One case diagnosed as PL was removed from the series due to the presence of *MDM2* amplification.

The 129 cases were divided into categories of SCL and PL based on the presence of PL component. If present even in a small amount, the case was already considered as PL. When more than 3 unequivocal fat cells having hyperchromatic, indented, or sharply scalloped nuclei were found, the case was regarded as positive for the presence of LPB. Areas where it was difficult to ascertain whether fat necrosis was present were not evaluated. Similarly, adipocytes showing Lochkerne, Ringkerne, and Kerbenkerne [7,8] (ie, different variations of an intranuclear vacuole) were disregarded. All tumors were reviewed without the knowledge of clinical features (ie, localization, gender, age). In negative cases, all available blocks of tissue were reviewed. When a case was scored as positive, the remaining blocks were not further assessed. This was also the reason why one case was misdiagnosed as PL and where later *MDM2* amplification was found. When reviewed again, the remaining blocks revealed characteristic features of atypical lipomatous tumor/well-differentiated liposarcoma (ALT/WDL).

Except for 8 cases (Cases 5, 10, 26, 30, and 34 of SCL and 19, 20, and 21 of PL), paraffin blocks or unstained reserve slides were available for the study. For conventional microscopy, tissues were fixed in formalin, routinely processed, embedded in paraffin, cut into 4-μm-thick sections, and stained with hematoxylin-eosin.

2.1. Immunohistochemistry

The immunohistochemical analysis was performed using a Ventana BenchMark ULTRA (Ventana Medical System, Inc, Tucson, AZ). The following primary antibodies were used: CD34 (QBEnd/10, 1:200; Dako, Glostrup, Denmark) and Rb protein (G3–245, 1:50; BD Biosciences, Franklin Lakes, NJ). The primary antibodies were visualized employing the enzymes alkaline phosphatase or peroxidase as detecting systems (both purchased from Ventana Medical System, Inc, Tucson, AZ).

2.2. Molecular genetic studies

2.2.1. Detection of amplifications of MDM2 and CDK4 and break of *FUS* by fluorescence in situ hybridization

Specimens representing 4-μm-thick FFPE section on positively charged slides were routinely deparaffinized and processed. An appropriate amount of probe mix, Probe Vysis *FUS* Break Apart fluorescence in situ hybridization (FISH) Probe Kit (Abbott Molecular, Abbott Park, IL), mixed according to the manufacturer's protocols and factory premixed probes ZytoLight® SPEC *MDM2*/CEN 12 Dual Color Probe and ZytoLight® SPEC *CDK4*/CEN 12 Dual Color Probe (ZytoVision GmbH, Bremerhaven, Germany) were applied to the specimens. The slides were then routinely incubated, washed, and counterstained with 4′,6′-diamidino-2-phenylindole DAPI (Abbott).

2.2.2. Fluorescence in situ hybridization interpretation

One hundred randomly selected nonoverlapping tumor cell nuclei were evaluated in all analyzed samples. Samples were considered positive for amplification [9] when the ratio of signals of *MDM2* and *CDK4* probes to corresponding chromosome 12 centromeric probe signals was ≥2.0. The cut-off value of *FUS* break-apart probe was set to 10% of nuclei with chromosomal break.

3. Results

The clinical features are summarized in Tables 1 (SCL) and 2 (PL). The patients were 14 women and 47 men; and in one case, the gender was unknown. The age of the patients at the time of diagnosis ranged from 27 to 90 years (mean, 60.1 years). Twenty-two cases were retrieved from the routine

Table 1 Spindle cell lipomas

Case	Available methods	Age/sex	Location	Size (cm)	Referring diagnosis
1	All 3	70/M	Back of the neck	7 × 4 × 4	SCL/PL *vs* ALT
2	All 3	76/M	Back of the neck	Ø2	Routine case
3	*CDK4*; *MDM2*	61/M	Back of the neck	2.5 × 1.5 × 10	SCL
4	All 3	62/M	Back of the neck	6 × 5 × 3.5	Routine case
5	NT	69/F	NA	NA	Not listed
6	*CDK4*; *MDM2*	55/M	Back of the neck	6 × 4 × 2.5	Routine case
7	None	77/M	Back of the neck	Ø5	Routine case
8	None	63/M	3rd toe	3 × 2 × 2	SCL
9	None	59/M	Buccal mucosa	Ø2	Exclude ALT
10	NT	27/F	Head	Ø2	Probably SCL, uncertainty due to the clinical setting
11	None	39/M	NA	NA	NA
12	All 3	72/M	Shoulder	3 × 1.7 × 1.7	Routine case
13	All 3	57/M	Back of the neck	Ø1.5	Routine case
14	All 3	49/M	Scapula	3 × 2.5 × 1.5	Routine case
15	*CDK4*; *MDM2*	61/M	Scapula	3 × 2.5 × 1.5	NA
16	*CDK4*; *MDM2*	87/M	Back	NA	Routine case
17	*CDK4*; *MDM2*	65/M	Back	NA	Routine case
18	None	71/F	Buccal mucosa	1.5 × 1 × 1	Myxoid liposarcoma
19	None	61/F	Nose	NA	Routine case
20	All 3	62/M	Parotid gland	NA	Myoepithelioma *vs* ALT *vs* schwannoma
21	None	61/M	Back of the neck	NA	Routine case
22	*CDK4*; *MDM2*	73/M	Hypogastrium	Ø4.5	Routine case
23	All 3	62/M	Clavicle	NA	Routine case
24	All 3	55/M	Upper back	3 × 3 × 2	SCL
25	*CDK4*; *MDM2*	49/M	Upper back	15 × 14 × 4.5	Exclude liposarcoma
26	NT	59/M	Back of the neck	0.8	Angiolipoma *vs* SCL with focal regressive cellular changes
27	None	55/M	Upper back	4 × 3 × 2	Routine case
28	None	65/M	Scalp	NA	Routine case
29	None	76/M	Upper back	Ø2	Fibrolipoma
30	NT	NA	Back	NA	NA
31	None	73/M	NA	8 × 4 × 2.5	Neurofibroma
32	CDK4	90/M	Shoulder	10 × 9 × 4	Lipoma
34	NT	50/M	Back	6.5 × 6 × 5	Fibrolipoma
35	None	49/M	Forehead	NA	Routine case
36	None	87/M	NA	NA	Routine case
37	All 3	53/M	Back	1.5 × 1.5 × 0.8	Spindle cell tumor with univacuolated and focally multivacuolated lipoblasts (reminiscent of lipoblastoma but in incompatible setting).

Abbreviations: All 3, available (negative) result for *FUS*, *MDM2* and *CDK4* FISH; None, all 3 FISH methods not analyzable; NT, not tested; NA, not available; NL, not listed; ALT, atypical lipomatous tumor; Ø, diameter.

biopsy archive, and the remaining 40 cases were sent to us for a second opinion. When provided, the referral diagnoses of the consult cases are summarized in Tables 1 and 2. Overall, the most common referring diagnosis was that of ALT or another type of liposarcoma, which was listed in 6 of 15 SCL and in 8 of 13 PL cases. Follow-up was available for 44 patients, of whom 2 suffered recurrence of SCL (cases 6 and 25). No metastases occurred. The average duration of follow-up was 7.5 years (range, 1 month to 20 years). The cases presented as superficial, well-circumscribed soft tissue masses, with a few cases growing into the underlying muscle tissue. Locations were available for 55 tumors and most commonly included upper back and neck. The tumor size ranged from 0.5 cm to 24 cm in the largest dimension, with a mean size of 4.44 cm.

Table 2 Pleomorphic lipomas

Case	Available methods	Age/sex	Location	Size (cm)	Referring diagnosis
1	All 3	66/M	Nuchal area	No	NL
2	All 3	46/M	Upper back	6 × 3 × 3	NL
3	All 3	27/F	NA	Ø0.6	Pleomorphic fibroma, stromal areas raising concerns about ALT
4	None	66/M	Back of the neck	2.2 × 2 × 1.2	LG sarcoma—myxoid or angiomatoid variant of ALT
5	All 3	81/M	Arm	7 × 5.5 × 2	PL
6	All 3	55/M	Back of the neck	Ø2.5	PL
7	All 3	66/M	Back of the neck	2.4 × 2 × 1.4	ALT—focally more cellular but without dedifferentiation
8	All 3	63/F	Popliteal area	Ø1.3	NL
9	FUS	76/F	Back of the neck	1.5 × 0.5 × 0.5	Fibrolipoma—some nuclei irregular and hyperchromatic—probably a reactive posttraumatic change
10	All 3	62/F	Shoulder	Ø4.5	Routine case
11	None	46/F	Upper back	6 × 6 × 4	Routine case
12	All 3	40/F	Upper back	24 × 16 × 8	Atypical lipoma *vs* ALT
13	All 3	58/M	Back of the neck	3 × 3 × 3	Routine case
14	All 3	42/M	Back of the neck	8 × 6 × 2	Routine case
15	All 3	53/F	Upper back	3.5 × 3 × 3	ALT
16	All 3	60/F	Elbow	Ø2.5	PL *vs* ALT
17	None	75/M	Back of the neck	Ø2	Spindle cell liposarcoma
18	*CDK4*; *MDM2*	53/F	Back of the neck	NA	Routine case
19	NT	70/M	Back of the neck	7 × 4 × 4	PL *vs* ALT
20	NT	41/M	Parotid gland	Ø1.5	PL
21	NT	65/M	NA	Ø2	PL
22	All 3	56/F	NA	2.1	NA
23	All 3	69/M	Neck	7	NA
24	All 3	58/M	Shoulder	3.8	NA
25	All 3	71/M	Neck	12.2	NA

Abbreviations: All 3, available (negative) result for *FUS*, *MDM2* and *CDK4* FISH; None, all 3 FISH methods not analyzable; NT, not tested; NA, not available; NL, not listed; ALT, atypical lipomatous tumor; Ø, diameter.

The 129 cases selected consisted of 91 SCL and 38 PL. LPB were found in 37 cases (41%) of SCL. Of the 38 PL cases, 25 (66%) contained LPB, while in the majority of SCL cases, only a few LPB were found after a meticulous search; PL showed single or several LPB in a much more diffuse manner. Nevertheless, a significant subset of cases of both SCL and PL contained several foci with a highly prominent admixture of LPB, which was easy to be found (Figs. 1-3). Moreover, some cases of PL even occasionally featured a multivacuolated LPB (Fig. 1B).

3.1. Immunohistochemical findings

All tested cases (n = 55) reacted with the CD34 antibody (Fig. 3A), albeit in 5 cases of SCL the expression was fairly

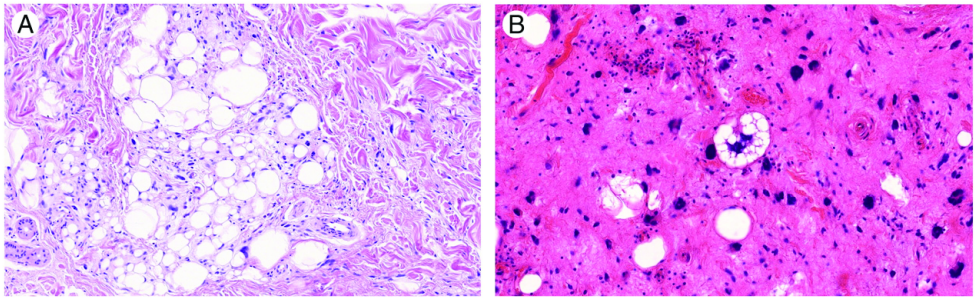

Fig. 1 A, Significant subset of cases of both SCL and PL contained several foci with a highly prominent admixture of LPB, which was easy to be found (PL, Case 16; HE ×17). B, Moreover, some cases of PL even occasionally featured a multivacuolated LPB (PL, Case 2; HE ×20).

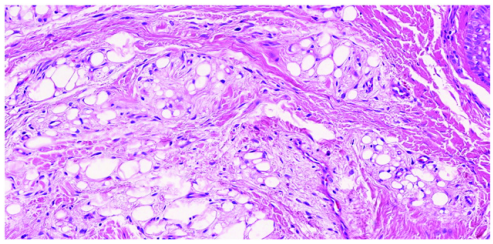

Fig. 2 In both SCL/PL there were also many cases featuring a very prominent LPB-containing component in a number usually found in liposarcomas (SCL, Case 19; HE ×30).

weak. Conversely, all tested cases (n = 54) consistently showed Rb protein deficiency.

3.2. Molecular genetic findings

The molecular genetic findings are summarized in Tables 1 and 2. One case was excluded based on the presence of *MDM2* and *CDK4* amplification. Seventeen cases were not analyzable due to the poor quality of the archival tissue. For the same reason, not all three assays were analyzable in the subsequent 10 cases. The rest of the cases showed neither *MDM2* or *CKD4* amplification nor a break of the *FUS* gene.

4. Discussion

Since Stout described liposarcoma as a malignant tumor of lipoblasts (LPB), their identification has been overemphasized by pathologists as an indispensable criterion of malignancy. The morphologic definition of LPB may vary, but in a narrow sense, LPB are cells having hyperchromatic nuclei that are indented or sharply scalloped due to lipid-rich mono- or multivacuolated cytoplasmic droplets [6,10]. Although the histologic background on which the LPB are encountered is far more important for diagnosis than the occurrence of LPB per se [3], when present, LPB may lead the pathologist to overdiagnosis. While it surely is an essential task for a pathologist to search for LPB while rendering a diagnosis of liposarcoma, even more crucial is not to forget that there are many types of cells simulating LPB in various neoplastic as well as non-neoplastic conditions [6,10]. Conversely, in very rare cases, LPB may also be inconspicuous or totally absent in ALT/WDL. This is mirrored in the current World Health Organization diagnostic criteria for ALT/WDL, where LPB are considered as a helpful clue for the diagnosis but are not included among the prerequisites for it [3]. Moreover, true LPB also occur in benign lipogenic tumors, including lipoblastoma, lipoblastoma-like tumor of the vulva [11,12] and chondroid lipoma. SCL/PL represent another not as widely acknowledged member of this group of tumors. [6].

In our series, LPB were found in 37 (41%) of 91 cases classified as SCL and in 25 (66%) of 38 cases of PL. The frequency of LPB in our series of PL cases is only slightly higher than 50%, the number found in the prior reports [2,4]. To the best of our knowledge, the frequency of LPB in SCL has never been assessed. In addition, except for 3 publications that we have found after a review of major pathology textbooks and other pertinent literature [3,5,6], we were not able to find any other report even recognizing the presence of LPB in SCL. Admittedly, in some cases of PL in our cohort and particularly in many cases of SCL, the LPB were scant and found only after a concentrated search. However, the great majority of the 25 PL positive for LPB contained LPB in a diffuse manner, making their recognition an easy task. Rarely, some cases of PL even occasionally showed a multivacuolated LPB (Fig. 1B). Most importantly, in both groups, there were also many cases featuring a very prominent LPB-containing component in a number usually found in liposarcomas (Figs. 1-3).

It is important to note that most of our cases (~ 2/3) were referrals and therefore, the proportion of cases containing LPB may be slightly higher in our series than in routine practice. Nevertheless, without the knowledge that LPB do routinely occur in SCL/PL, the finding of LPB may lead to an unnecessary use of expensive ancillary techniques or, in a worst case scenario, to overdiagnosis. Of note, when the referring diagnoses were reviewed, the most common diagnostic consideration was that of ALT or another type of liposarcoma, which was listed in 6/15 SCL and in 8/13 PL cases with available data (Tables 1 and 2).

SCL/PL typically occur in middle-aged to older men in superficial soft tissues of the posterior neck, back or shoulder. Although these tumors may occur at other body sites as well, when present in the posterior neck/back/shoulder, it can be a helpful distinguishing feature since it is an uncommon location for any type of liposarcoma. However, as usual, there are notable exceptions to this rule, which is also exemplified in our study. The case excluded due to the *MDM2* amplification was located in the nuchal area. Conversely, several cases of SCL/PL in our study grew into the underlying muscle tissue. Therefore, the most important clues for the correct diagnosis lie in the characteristic morphology of SCL/PL. As evident from our current series, where all the cases were reviewed without knowing the clinical information (including location), a great majority of cases can be distinguished from liposarcoma variants merely on the basis of the histological features (thorough sampling is, however, warranted). In cases of SCL, bland, spindle cells and especially the thick, ropey-type collagen fibers are the most helpful clues for the correct diagnosis. Myxoid change and prominent plexiform vascular pattern may be rarely present in SCL to such an extent that the diagnosis of myxoid liposarcoma (ML) must be considered. However, SCL are usually more circumscribed and more superficially located than ML, and ropey-like collagen fibers are characteristic only for SCL. IHC for CD34 and Rb protein [13] or, in the most challenging cases, FISH analysis for rearrangements of *FUS* or *DDIT3* genes may prove helpful [10].

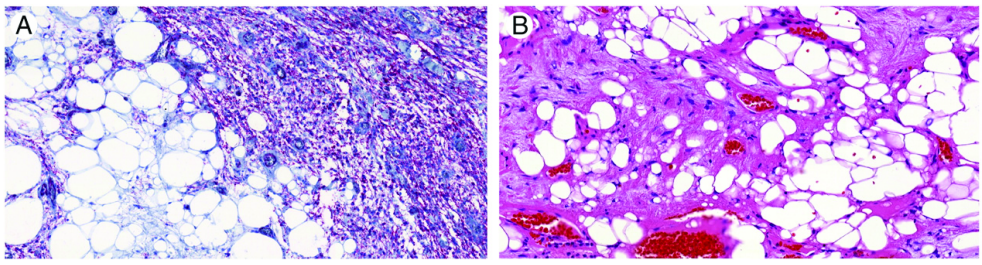

Fig. 3 A, All cases reacted with the CD34 antibody (SCL, Case 13; CD34 ×20). B, In both SCL/PL there were also many cases featuring a very prominent LPB-containing component in a number usually found in liposarcomas (SCL, Case 1; HE ×30).

Another potential differential diagnosis of a lesion with LPB in superficial soft tissues may represent atrophic fat tissue or fat necrosis. In atrophic fat tissue, the adipocytes appear to be of uniform size and maintain their arrangement in lobules. Areas of fat necrosis contain granular or vacuolated macrophages located in the vicinity of damaged fat, characterized by diminished cell size, dropout of adipocytes, and chronic inflammation. Unlike LPB, macrophages are of uniform size and have small, evenly dispersed vacuoles that do not indent the rounded nucleus [10].

Another differential diagnosis represents the so called fibrosarcoma-like lipomatous neoplasm as reported by Deyrup et al [14]. These distinct tumors have a wide anatomic distribution and are composed of nodules of differentiated fibroblastic cells resembling well-differentiated, slightly myxoid fibrosarcoma showing varying degrees of lipoblastic differentiation reminiscent of the early stages of embryonic fat development. The distinct appearance of these LPB, which is reminiscent of an ice cream cone, may be a helpful diagnostic clue in some cases. They also do not show the typical molecular alterations of SCL/PL nor of any other lipomatous tumor. SCL can be generally distinguished based on the usual clinical presentation and the typical morphology of parallel groups of bland spindled cells admixed with dense collagen bundles. However, SCL arising in atypical sites and especially those cases containing a significant amount of LPB are more challenging, and IHC for Rb protein or molecular testing may be necessary.

In 2014 Creytens et al described so called atypical spindle cell lipomas [15]. According to the authors, the following features distinguish them from classical SCL: (1) wider anatomical distribution; (2) unencapsulation and frequent infiltrative growth; (3) presence of atypical lipogenic tumor cells with numerous mono- and/or multivacuolated LPB with scalloped, hyperchromatic nuclei; (4) spindle-shaped tumor cells with often hyperchromatic nuclei that are set in a collagenous stroma, which lacks the typical ropey-like collagen fibers; (5) molecular genetic profile with more complex deletions of functionally important *RB1* exons [15].

In our view, classical SCL can infrequently occur at unusual sites, are usually well circumscribed but do not necessarily have to be encapsulated (also noted by Enzinger [1]) and of course frequently contain LPB. Therefore, the only differences we see between classical SCL and the above-described cases lie in the presence of spindle-shaped tumor cells with hyperchromatic nuclei (which is a quite subjective feature), the absence of ropey collagen fibers and probably some relatively minor molecular genetic differences. It is uncertain whether these subtle differences merit the designation "atypical" for such tumors, especially when considering that SCL creates a continuum with PL, which per se contain pleomorphic cells. Moreover, so far there seems to be no prognostic relevance of such categorization since the (limited) follow-up of their eight cases was marked by only a single recurrence and no metastasis.

Cases falling into the spectrum of PL additionally show pleomorphic cells, as well as the very characteristic floret-like multinucleated giant cells, which are intimately associated with the same dense collagen bundles as in SCL [2,3]. Such pleomorphic cells may be occasionally present in the sclerosing type of ALT/WDL but usually are less numerous. The most helpful distinguishing feature in this differential diagnosis is again the presence of characteristic collagen fibers. ALT/WDL show a more uniform network of much more delicate collagen fibers than PL. Importantly, ALT/WDL are very rarely encountered in the superficial soft tissue. In the recent study by Clay et al, only 1 in 61 superficial cases of problematic lipomatous tumors (ie, >10 cm in size, equivocal atypia, recurrent lesions, worrisome radiologic features) showed amplification of *MDM2* [16]. IHC for Rb protein can again be helpful [13]. In any case, when necessary, molecular genetic testing for *MDM2* and *CDK4* amplifications is the most reliable diagnostic tool [16].

In summary, this study emphasizes the fact that LPB are very frequent findings in both SCL (41%) and PL (66%), and it shows that the presence of LPB is not a distinguishing feature of these tumors from liposarcomas. Even more importantly, in many SCL/PL, LPB constitute a component so prominent as to cause diagnostic difficulties to the unaware. It is therefore important to base the diagnosis on different, diagnostically more relevant clinicopathological and histological features of SCL/PL, in order to prevent a misdiagnosis.

References

[1] Enzinger FM, Harvey DA. Spindle cell lipoma. Cancer 1975;36:1852-9.

[2] Shmookler BM, Enzinger FM. Pleomorphic lipoma: a benign tumor simulating liposarcoma. A clinicopathologic analysis of 48 cases. Cancer 1981;47:126-33.

[3] Fletcher CDM, Bridge JA, Hogendoorn PCW, Mertens F. WHO classification of tumors of soft tissue and bone. Lyon, France: International Agency for Research on Cancer (IARC); 2013.

[4] Azzopardi JG, Iocco J, Salm R. Pleomorphic lipoma: a tumour simulating liposarcoma. Histopathology 1983;7:511-23.

[5] French CA, Mentzel T, Kutzner H, Fletcher CD. Intradermal spindle cell/pleomorphic lipoma: a distinct subset. Am J Dermatopathol 2000;22:496-502.

[6] Hisaoka M. Lipoblast: morphologic features and diagnostic value. J UOEH 2014;36:115-21.

[7] Resnik KS, Kutzner H. Original observation to rediscovery: nuclear findings in adipocytes as example. Am J Dermatopathol 2004;26:493-8.

[8] Kazakov DV, Belousova IE, Bisceglia M, et al. Apocrine mixed tumor of the skin ("mixed tumor of the folliculosebaceous-apocrine complex"). Spectrum of differentiations and metaplastic changes in the epithelial, myoepithelial, and stromal components based on a histopathologic study of 244 cases. J Am Acad Dermatol 2007;57:467-83.

[9] Ware PL, Snow AN, Gvalani M, Pettenati MJ, Qasem SA. MDM2 copy numbers in well-differentiated and dedifferentiated liposarcoma: characterizing progression to high-grade tumors. Am J Clin Pathol 2014;141:334-41.

[10] Goldblum JR, Folpe AL, Weiss SW. Enzinger & Weiss's Soft Tissue Tumors. Philadelphia: Elsevier Saunders; 2014.

[11] Lae ME, Pereira PF, Keeney GL, Nascimento AG. Lipoblastoma-like tumour of the vulva: report of three cases of a distinctive mesenchymal neoplasm of adipocytic differentiation. Histopathology 2002;40:505-9.

[12] Mirkovic J, Fletcher CD. Lipoblastoma-like tumor of the vulva: further characterization in 8 new cases. Am J Surg Pathol 2015;39:1290-5.

[13] Chen BJ, Marino-Enriquez A, Fletcher CD, Hornick JL. Loss of retinoblastoma protein expression in spindle cell/pleomorphic lipomas and cytogenetically related tumors: an immunohistochemical study with diagnostic implications. Am J Surg Pathol 2012;36:1119-28.

[14] Deyrup AT, Chibon F, Guillou L, Lagarde P, Coindre JM, Weiss SW. Fibrosarcoma-like lipomatous neoplasm: a reappraisal of so-called spindle cell liposarcoma defining a unique lipomatous tumor unrelated to other liposarcomas. Am J Surg Pathol 2013;37:1373-8.

[15] Creytens D, van Gorp J, Savola S, Ferdinande L, Mentzel T, Libbrecht L. Atypical spindle cell lipoma: a clinicopathologic, immunohistochemical, and molecular study emphasizing its relationship to classical spindle cell lipoma. Virchows Arch 2014;465:97-108.

[16] Clay MR, Martinez AP, Weiss SW, Edgar MA. MDM2 amplification in problematic Lipomatous tumors: analysis of FISH testing criteria. Am J Surg Pathol 2015;39:1433-9.

1.1.9. ATYPICAL MITOSES IN PLEOMORPHIC LIPOMAS

The above-commented study which analyzed the presence and frequency of lipoblasts in SCL/PL was also presented at the poster session during the congress of United States and Canadian Academy of Pathology in 2017 in San Antonio. At this poster I met Dr. Kemal Kosemehmetoglu from Turkey who raised the question whether we found any atypical mitotic figures (another worrisome histological feature usually speaking in favor of malignancy) in our cases of PL. Since we did not deliberately search for this feature, I was unsure about the answer. After the congress, I re-reviewed the entire set of 25 PL and found atypical mitotic figures in 4 of them (16%). After a review of the literature, I have found only 3 monographs briefly mentioning this histologic feature of PL, which may be very confusing and misleading. For this reason, we decided to write a letter to the editor to make this observation more widely recognized and prevent erroneous overdiagnosis of these lesions, especially as atypical lipomatous tumor/well-differentiated liposarcoma.

[4] Xu K, Shen K, Liang X, et al. MiR-139-5p reverses CD44+/CD133+-associated multidrug resistance by downregulating NOTCH1 in colorectal carcinoma cells. Oncotarget 2016;7:75118-29.
[5] Mo Y, Lu Y, Wang P, et al. Long non-coding RNA XIST promotes cell growth by regulating miR-139-5p/PDK1/AKT axis in hepatocellular carcinoma. Tumour Biol 2017;39:1010428317690999. http://dx.doi.org/10.1177/1010428317690999 [in press].
[6] Sannigrahi MK, Sharma R, Singh V, Panda NK, Rattan V, Khullar M. Role of host-microRNA Hsa-miR-139-3p in HPV-16 induced carcinomas. Clin Cancer Res 2017;23:3884-95.
[7] Chen Z, Yu T, Cabay RJ, et al. miR-486-3p, miR-139-5p, and miR-21 as biomarkers for the detection of oral tongue squamous cell carcinoma. Biomark Cancer 2017;9:1-8.
[8] Krowiorz K, Ruschmann J, Lai C, et al. MiR-139-5p is a potent tumor suppressor in adult acute myeloid leukemia. Blood Cancer J 2016;6:e508.
[9] Miyoshi J, Toden S, Yoshida K, et al. MiR-139-5p as a novel serum biomarker for recurrence and metastasis in colorectal cancer. Sci Rep 2017;7:43393.

Atypical mitoses in pleomorphic lipomas

To the Editor:

In our recent article published in this journal, we evaluated the presence and frequency of lipoblasts in spindle cell and pleomorphic lipomas (SCL/PL). Overall, lipoblasts were found in 66% of PL. These cases, which mostly occurred in the typical clinical setting of PL, were also molecular genetically tested to exclude *MDM2* and *CDK4* amplifications, and stained for CD34 and retinoblastoma protein to further validate the diagnosis [1].

Recently, we have been contacted by Dr Kosemehmetoglu who presented to us cases of PL that displayed unquestionable atypical mitoses and thus led to erroneous diagnosis of liposarcoma. After a review of the literature, we have found only 3 monographs briefly mentioning this histologic feature of PL, which may be very confusing and misleading [2-4]. The frequency of atypical mitoses in PL is virtually unknown. Because it might represent an important diagnostic pitfall, we again reviewed our histologically, immunohistochemically, and molecular genetically validated cohort of 25 PL to assess the frequency of atypical mitoses in PL and found them in 4 cases (16%; Figure). A larger subset of cases also contained typical mitoses, which are, however, a more widely acknowledged feature of PL. Thus, besides the routine presence of lipoblasts, we would also additionally like to highlight the possibility of encountering atypical mitosis in PL, which may lead to erroneous overdiagnosis of these lesions, especially as atypical lipomatous tumor/well-differentiated liposarcoma.

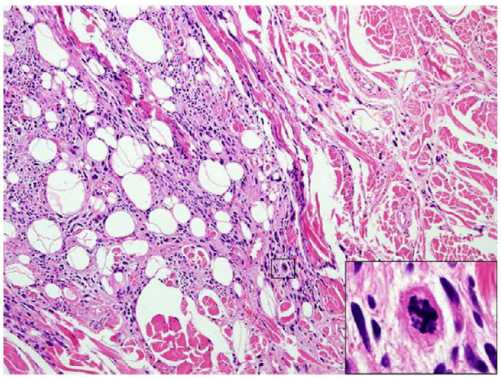

Figure Four (16%) of 25 pleomorphic lipomas contained an unequivocal atypical mitosis (inset). Hematoxylin and eosin, original magnification ×100.

Michael Michal, MD
Department of Pathology, Faculty of Medicine in Pilsen, Charles University, 32300 Pilsen, Czech Republic
Biomedical Center, Faculty of Medicine in Pilsen, Charles University, 32300 Pilsen, Czech Republic
E-mail address: michael.michal@seznam.cz (M. Michal)

Berrin Babaoglu, MD
Kemal Kosemehmetoglu, MD
Department of Pathology, Faculty of Medicine, Hacettepe University, 06230 Ankara, Turkey

Dmitry V. Kazakov, MD
Michal, MD
Department of Pathology, Faculty of Medicine in Pilsen, Charles University, 32300 Pilsen, Czech Republic

http://dx.doi.org/10.1016/j.humpath.2017.06.024

References

[1] Michal M, Kazakov DV, Hadravsky L, et al. Lipoblasts in spindle cell and pleomorphic lipomas: a close scrutiny. Hum Pathol 2017;65:140-6.
[2] Fletcher CDM. Diagnostic histopathology of tumors. Philadelphia: Elsevier Saunders; 2013.
[3] Miettinen M. Modern soft tissue pathology. New York: Cambridge University Press; 2010.
[4] Lindberg MR. Diagnostic histopathology: soft tissue tumors. Philadelphia: Elsevier; 2016.

1.1.10. ATYPICAL MULTIVACUOLATED LIPOBLASTS AND ATYPICAL MITOSES ARE NOT COMPATIBLE WITH THE DIAGNOSIS OF SPINDLE CELL/PLEOMORPHIC LIPOMA—REPLY

As a response to the two previously commented studies, the journal Human Pathology published a letter to the editor from a group of distinguished European soft tissue pathologists who are currently proposing a novel lipomatous tumor entity called Atypical pleomorphic lipomatous tumor (APLT) [27]. According to this group, APLT should have partially overlapping features with PL but in addition show several atypical traits such as lipoblasts, atypical mitoses, atypical spindle cells and infiltrative growth. As a result, they oppose our notion that lipoblasts and atypical mitoses are a common feature of ordinary/benign PL. However, as we noted in a consequent reply to their letter, using their criteria, up to about one-half of tumors currently classified as PL would fall into the category of APLT although these cases showed no signs of aggressive behavior over a long follow-up period.

We think the morphological spectrum of SCL/PL is broad with a minimal risk of aggressive behavior. On the other hand, true sarcomatous PL do very rarely occur and may have a higher risk of local recurrence. However, until more accurate criteria for the distinction between "classical" PL and APLT are defined (perhaps larger size and infiltrative growth), we advocate a very conservative use of the term APLT to avoid overtreatment. We believe it is better to treat a few sporadic recurrences than to trigger confusion among pathologists and surgeons (caused by the addition of adjective "atypical") and unnecessarily aggressive surgical treatments for benign tumors.

References

[1] Michal M, Kazakov DV, Hadravsky L, et al. Lipoblasts in spindle cell and pleomorphic lipomas: a close scrutiny. Hum Pathol 2017;65:140-6.
[2] Michal M, Babaoglu B, Kazakov DV, Michal, Kosemehmetoglu K. Atypical mitoses in pleomorphic lipomas. Hum Pathol 2017;70:143.
[3] Fletcher CD, Bridge JA, Hogendoorn PC, Mertens F, editors. World Health Organization classification of tumours. Pathology and genetics. Tumours of soft tissue and bone. 4th ed. Lyon: IARC Press; 2013.
[4] Creytens D, Mentzel T, Ferdinande L, et al. "Atypical" pleomorphic lipomatous tumor. A clinicopathologic, immunohistochemical and molecular study of 21 cases, emphasizing its relationship to atypical spindle cell lipomatous tumor and suggesting a morphologic spectrum (atypical spindle cell/pleomorphic lipomatous tumor). Am J Surg Pathol 2017;41:1443-55.
[5] Mariño-Enríquez A, Nascimento AF, Ligon AH, et al. Atypical spindle cell lipomatous tumor: clinicopathologic characterization of 232 cases demonstrating a morphologic spectrum. Am J Surg Pathol 2017;41:234-44.

Atypical multivacuolated lipoblasts and atypical mitoses are not compatible with the diagnosis of spindle cell/pleomorphic lipoma—reply

To the Editor,

We thank Dr Creytens et al for their comments on our articles [1,2]. We would like to make some additional comments in response to their letter.

The authors disagree with our notion that atypical multivacuolated lipoblasts, mitotic figures (both atypical and typical) and infiltration of the underlying skeletal muscle are compatible with a histological diagnosis of classical pleomorphic lipoma (PL). For cases showing such features, they propose the term "atypical" pleomorphic lipomatous tumor (APLT) [3].

Typical mitotic figures are a very common feature of PL, found in about half of the lesions. In our study, atypical mitoses were detected in 16% of cases (4/25) of PL. The PL with atypical mitoses and atypical spindle cells illustrated in our paper [2] occurred in the classical clinical setting, showed sharp circumscription, was of a relatively small size (3 cm) and demonstrated no recurrence in 2 years of follow-up (case 13 of our previous study [1]). Similarly, the remaining 3 PL with atypical mitoses (cases 8, 10, 16 [1]) were also relatively small, circumscribed tumors without recurrence with 3, 10 and 1 years of follow-up. Besides the univacuolated lipoblasts (LPB), occasional PL also contain multivacuolated LPB, a feature with absolutely no impact on the clinical course and prognosis. For example, the PL depicted in figure 1B of our manuscript (Case 2 [1]) showed multivacuolated LPB. However, it was again a sharply circumscribed tumor occurring in the classical setting with no recurrence in 17 years post-removal.

Our study did not specifically focus on the presence of atypical spindle cells with hyperchromatic nuclei. However, even such cells have no impact on the prognosis, as again illustrated by case 13 of our publication. Moreover, despite the fact that some of the abovementioned "atypical" features occurred in a considerable number of our cases, there have been only 2 recurrences in the 44 patients with available follow-up. Interestingly, both recurrent cases (cases 6 and 25 [1]) represented SCL with none of the aforementioned "atypical" features (except univacuolated LPB). In fact, these 2 "recurrences" likely represent incomplete excisions, allowing the neoplasms to regrow. It is also true that several cases showed infiltration into the underlying skeletal muscle. When reviewed, all such tumors (SCL cases 18, 20, and 35 [1]) were located on the face, where muscle "infiltration" is often encountered in various benign proliferations including SCL/PL [4] due to the lack of well-defined fascial planes and superficial location of the mimic muscles. Taken together, if the stringent criteria proposed by Creytens et al were applied, up to about one-half of tumors currently classified as PL would be diagnosed as APLT. On the other hand, we agree with Creytens et al that "sarcomatous" transformation of PL may very rarely occur, but the diagnostic criteria for these neoplasms must be better defined.

In conclusion, the morphological spectrum of SCL/PL is broad with a minimal risk of aggressive behavior. On the other hand, true sarcomatous PL do very rarely occur and may have a higher risk of local recurrence. Until more accurate criteria for the distinction between "classical" PL and APLT are defined, we advocate a very conservative use of the term APLT to avoid overtreatment. We believe it is better to treat a few sporadic recurrences than to trigger confusion among pathologists and surgeons and unnecessarily aggressive surgical treatments for benign tumors.

Michael Michal, MD
Department of Pathology, Faculty of Medicine in Pilsen Charles University, 30460 Pilsen Czech Republic and Biomedical Center, Faculty of Medicine in Pilsen, Charles University, 30460 Pilsen, Czech Republic
E–mail address: michael.michal@medima.cz

Dmitry V. Kazakov, MD
Kvetoslava Michalova, MD
Michal Michal, MD
Department of Pathology, Faculty of Medicine in Pilsen Charles University, 30460 Pilsen, Czech Republic

https://doi.org/10.1016/j.humpath.2017.11.024

References

[1] Michal M, Kazakov DV, Hadravsky L, et al. Lipoblasts in spindle cell and pleomorphic lipomas: a close scrutiny. Hum Pathol 2017;65:140-6.
[2] Michal M, Babaoglu B, Kazakov DV, Michal M, Kosemehmetoglu K. Atypical mitoses in pleomorphic lipomas. Hum Pathol 2017;70:143.
[3] Creytens D, Mentzel T, Ferdinande L, et al. "Atypical" pleomorphic lipomatous tumor. A clinicopathologic, immunohistochemical and molecular study of 21 cases, emphasizing its relationship to atypical spindle cell lipomatous tumor and suggesting a morphologic spectrum (atypical spindle cell/pleomorphic lipomatous tumor). Am J Surg Pathol 2017;41:1443-55.
[4] Cheah A, Billings S, Goldblum J, Hornick J, Uddin N, Rubin B. Spindle cell/pleomorphic lipomas of the face: an under-recognized diagnosis. Histopathology 2015;66:430-7.

1.1.11. EWSR1-SMAD3-REARRANGED FIBROBLASTIC TUMOR: AN EMERGING ENTITY IN AN INCREASINGLY MORE COMPLEX GROUP OF FIBROBLASTIC/MYOFIBROBLASTIC NEOPLASMS.

The purpose of this study was to report 4 cases of the very recently described soft tissue tumor provisionally called *EWSR1-SMAD3* acral fibroblastic spindle cell tumor [28]. It has a very characteristic morphology and can be distinguished from its mimics by a (so far) consistent expression of ERG antibody and also by the *EWSR1-SMAD3* fusion. To assess how specific is the ERG expression among the pertinent differential diagnostic entities, we also analyzed the staining characteristics of several such examples.

To find the particular tumors with *EWSR1-SMAD3* gene fusion, we have searched our soft tissue consultation files using a combination of pertinent keywords. Also, we reviewed all cases collected in a separate box of slides over the last 30 years and designated as "uncharacterized tumors of soft tissues". After review of more than 300 cases, we have found 3 tumors compatible with the diagnosis. Another case was recently received for a consultation at Cleveland Clinic, USA and was added to our study.

We scrutinized the tumors using light microscopy, IHC, FISH and NGS. Clinical information, including follow-up, were obtained, when possible.

All cases in our cohort occurred in women aged 5 to 68 years (mean: 36.5 years). Two were located on the hand, 1 on foot and the last case arose on the calf. The tumor size ranged from 1 to 1.5 cm in the greatest dimension, with a mean size of 1.2 cm. Except for one recent case, follow-up was available, ranging from 7 to 18 years (mean, 11.7 years), with a recurrence noted in one case after 10 years. All tumors were subcutaneous and showed two main components. One consisted of bland, spindled cells with elongated nuclei which were round when observed on the cross-section. These cells mostly grew in relatively hypercellular, well-organized and intersecting fascicles. The second component was prominently hyalinized and paucicellular, resembling hyalinizing-type necrosis, but lacked calcifications. Both components showed either a distinct zonation pattern or they were randomly intermingled with each other. In all 3 analyzable tumors, NGS showed *EWSR1-SMAD3* gene fusion in each case. By FISH, one tested case also revealed unbalanced rearrangement of the EWSR1 gene. All 4 cases showed strong, diffuse nuclear expression of ERG, whereas none of the mimics stained with this antibody except for weak to moderate staining in calcifying aponeurotic fibromas (9/10 cases). Two tumors showed focal weak to moderate expression of SAT-B2.

The 4 cases presented in our study further broadened the clinicopathologic spectrum of tumors with *EWSR1-SMAD3* gene fusion. They also confirmed that they represent a novel entity for which we proposed the name *EWSR1-SMAD3*-rearranged fibroblastic Tumor. Our study also proved that in the context of fibroblastic/myofibroblastic tumors, ERG IHC is a relatively specific marker for these neoplasms.

This paper is currently accepted for publication pending minor revision in the American Journal of Surgical Pathology.

American Journal of Surgical Pathology

EWSR1-SMAD3-rearranged Fibroblastic Tumor: An Emerging Entity in an Increasingly More Complex Group of Fibroblastic/Myofibroblastic Neoplasms.

--Manuscript Draft--

Manuscript Number:	
Full Title:	EWSR1-SMAD3-rearranged Fibroblastic Tumor: An Emerging Entity in an Increasingly More Complex Group of Fibroblastic/Myofibroblastic Neoplasms.
Article Type:	Original Article
Keywords:	Soft tissues; Acral Fibroblastic Spindle Cell Neoplasm; EWSR1-SMAD3-rearranged fibroblastic Tumor; ERG; Lipofibromatosis; Lipofibromatosis-like Neural Tumor; Myofibroma; Fibromatosis; Calcifying Aponeurotic Fibroma
Corresponding Author:	Michael Michal Charles University, Biomedical Center, Faculty of Medicine in Plzen and Charles University Hospital Plzen Pilsen, CZECH REPUBLIC
Corresponding Author Secondary Information:	
Corresponding Author's Institution:	Charles University, Biomedical Center, Faculty of Medicine in Plzen and Charles University Hospital Plzen
Corresponding Author's Secondary Institution:	
First Author:	Michael Michal
First Author Secondary Information:	
Order of Authors:	Michael Michal
	Ryan S. Berry
	Brian P. Rubin, Professor
	Scott E. Kilpatrick
	Abbas Agaimy, Professor
	Dmitry V. Kazakov, Professor
	Petr Steiner
	Nikola Ptakova
	Petr Martinek, PhD.
	Ladislav Hadravsky, PhD.
	Kvetoslava Michalova, PhD.
	Zoltan Szep, PhD.
	Michal Michal, Professor
Order of Authors Secondary Information:	
Abstract:	Three cases of superficial acral fibroblastic spindle cell neoplasms with EWSR1-SMAD3 fusion have been recently reported. Their differential diagnosis is broad, primarily comprising rare tumors from the fibroblastic/myofibroblastic category. The aim of this report is to present 4 new cases of this entity and to discuss the appropriate differential diagnosis. Also, since the ERG antibody seems to be a characteristic marker for these tumors, we analyzed ERG immunostaining characteristics in potential mimics of this entity. All cases in our cohort occurred in women aged 5 to 68 years (mean: 36.5 years). Two were located on the hand, 1 on foot and the last case arose on the calf. The tumor size ranged from 1 to 1.5 cm in the greatest dimension, with a

	mean size of 1.2 cm. Except for one recent case, follow-up was available, ranging from 7 to 18 years (mean, 11.7 years), with a recurrence noted in one case after 10 years. All tumors were subcutaneous and showed two main components. One consisted of bland, spindled cells with elongated nuclei which were round when observed on the cross-section. These cells mostly grew in relatively hypercellular, well-organized and intersecting fascicles. The second component was prominently hyalinized and paucicellular, resembling hyalinizing-type necrosis, but lacked calcifications. Both components showed either a distinct zonation pattern, or they were randomly intermingled with each other. In all 3 analyzable tumors, NGS showed EWSR1-SMAD3 gene fusion in each case. By FISH, one tested case also revealed unbalanced rearrangement of the EWSR1 gene. All 4 cases showed strong, diffuse nuclear expression of ERG, whereas none of the mimics stained with this antibody except for weak to moderate staining in calcifying aponeurotic fibromas (9/10). Two tumors showed focal weak to moderate nuclear expression of SAT-B2. The 4 herein presented cases further broaden the clinicopathologic spectrum of tumors with EWSR1-SMAD3 gene fusion. They also confirm that they represent a novel entity for which we propose the name EWSR1-SMAD3-rearranged fibroblastic Tumor. Our study also proves that in the context of fibroblastic/myofibroblastic tumors, ERG IHC is a relatively specific marker for these neoplasms.

Dear editor in chief, April 13, 2018

we are submitting our paper named „**EWSR1-SMAD3-rearranged Fibroblastic Tumor: An Emerging Entity in an Increasingly More Complex Group of Fibroblastic/Myofibroblastic Neoplasms.**“ which we would like to publish in American Journal of Surgical Pathology.

Ethics and conflict of interest: The authors have no conflict of interest to disclose. Informed consent was not required for our study. Supported in parts by the National Sustainability Program I (NPU I) Nr. LO1503 and by the grant SVV–2017 No. 260 391 provided by the Ministry of Education Youth and Sports of the Czech Republic.

Michael Michal M.D.

Department of Pathology, Charles University, Medical Faculty and Charles University Hospital Plzen, Alej Svobody 80, 323 00 Pilsen, Czech Republic.
Email: michael.michal@medima.cz, cellular phone: +420603792671

EWSR1-SMAD3-rearranged Fibroblastic Tumor: An Emerging Entity in an Increasingly More Complex Group of Fibroblastic/Myofibroblastic Neoplasms.

Running head: EWSR1-SMAD3-rearranged Fibroblastic Tumor

Michael Michal[1, 2, 3]; Ryan S. Berry[4]; Brian P. Rubin[4]; Scott E. Kilpatrick[4]; Abbas Agaimy[5]; Dmitry V. Kazakov[1, 3]; Petr Steiner[1, 3]; Nikola Ptakova[1, 3], Petr Martinek[1, 3]; Ladislav Hadravsky[6]; Kvetoslava Michalova[1, 3]; Zoltan Szep[7]; Michal Michal[1, 3];

[1]Department of Pathology, Charles University, Faculty of Medicine in Pilsen, Pilsen, Czech Republic

[2]Biomedical Center, Charles University, Faculty of Medicine in Pilsen, Pilsen, Czech Republic

[3]Bioptical Laboratory, Ltd., Pilsen, Czech Republic

[4]Department of Pathology, Robert J. Tomsich Pathology and Laboratory Medicine Institute, Cleveland Clinic, Cleveland, OH, USA

[5] Institute of Pathology, Friedrich-Alexander University Erlangen-Nürnberg, Erlangen, Germany

[6]Department of Pathology, First Faculty of Medicine, Charles University in Prague, Czech Republic

[7]Cytopathos, Ltd., Bratislava, Slovakia

Address for correspondence: Michael Michal M.D. Department of Pathology, Charles University, Medical Faculty and Charles University Hospital Plzen, Alej Svobody 80, 323 00 Pilsen, Czech Republic. Email: michael.michal@medima.cz, cellular phone: +420603792671

Ethics and conflict of interest: The authors have no conflict of interest to disclose. Informed consent was not required for our study. Supported in parts by the National Sustainability Program I (NPU I) Nr. LO1503 and by the grant SVV–2017 No. 260 391 provided by the Ministry of Education Youth and Sports of the Czech Republic.

Abstract

Three cases of superficial acral fibroblastic spindle cell neoplasms with *EWSR1-SMAD3* fusion have been recently reported. Their differential diagnosis is broad, primarily comprising rare tumors from the fibroblastic/myofibroblastic category. The aim of this report is to present 4 new cases of this entity and to discuss the appropriate differential diagnosis. Also, since the ERG antibody seems to be a characteristic marker for these tumors, we analyzed ERG immunostaining characteristics in potential mimics of this entity. All cases in our cohort occurred in women aged 5 to 68 years (mean: 36.5 years). Two were located on the hand, 1 on foot and the last case arose on the calf. The tumor size ranged from 1 to 1.5 cm in the greatest dimension, with a mean size of 1.2 cm. Except for one recent case, follow-up was available, ranging from 7 to 18 years (mean, 11.7 years), with a recurrence noted in one case after 10 years. All tumors were subcutaneous and showed two main components. One consisted of bland, spindled cells with elongated nuclei which were round when observed on the cross-section. These cells mostly grew in relatively hypercellular, well-organized and intersecting fascicles. The second component was prominently hyalinized and paucicellular, resembling hyalinizing-type necrosis, but lacked calcifications. Both components showed either a distinct zonation pattern, or they were randomly intermingled with each other. In all 3 analyzable tumors, NGS showed *EWSR1-SMAD3* gene fusion in each case. By FISH, one tested

case also revealed unbalanced rearrangement of the *EWSR1* gene. All 4 cases showed strong, diffuse nuclear expression of ERG, whereas none of the mimics stained with this antibody except for weak to moderate staining in calcifying aponeurotic fibromas (9/10). Two tumors showed focal weak to moderate nuclear expression of SAT-B2. The 4 herein presented cases further broaden the clinicopathologic spectrum of tumors with *EWSR1-SMAD3* gene fusion. They also confirm that they represent a novel entity for which we propose the name *EWSR1-SMAD3*-rearranged fibroblastic Tumor. Our study also proves that in the context of fibroblastic/myofibroblastic tumors, ERG IHC is a relatively specific marker for these neoplasms.

Key words: Soft tissues; Acral Fibroblastic Spindle Cell Neoplasm; EWSR1-SMAD3-rearranged fibroblastic Tumor; ERG; Lipofibromatosis; Lipofibromatosis-like Neural Tumor; Myofibroma; Fibromatosis; Calcifying Aponeurotic Fibroma

Introduction

Although several new entities have been defined or redefined during the last few decades, still there are mesenchymal neoplasms which elude precise classification. This is particularly true for soft tissue neoplasms featuring undifferentiated-looking spindled or round cells. Next-generation sequencing (NGS) represents a very effective tool for further characterization and classification of such tumors. Using this technology, Kao et al. recently reported three cases of a novel acral fibroblastic spindle cell neoplasm with recurrent *EWSR1-SMAD3* gene fusion (1). Prompted by the characteristic histologic features of these tumors, we have searched our tumor registry files for further examples. Using immunohistochemistry (IHC), fluorescence in situ hybridization (FISH) and NGS as ancillary techniques, we identified 4 cases having very similar to identical features as the recently reported cases. This confirms that these tumors clearly represent a novel neoplastic entity for which we, for practical purposes, propose the name *EWSR1-SMAD3*-rearranged fibroblastic Tumor (ESFT). ERG immunostaining appears to be a helpful marker distinguishing ESFT from its mimics. However, the differential diagnosis contains many rare entities and their reactivity with ERG antibody is currently unknown. For this reason, we also investigated ERG expression in these rare tumors.

Materials and Methods

The 4 cases described in this study were retrieved from the consultation files of the authors. The clinical information was extracted from the medical records, and follow-up data obtained from the patients' medical records. To retrospectively identify appropriate cases, we searched the Pilsner Tumor Registry files using the following key-words and their combinations: soft tissues + unknown, fibromatosis + unusual, lipofibromatosis, and myofibroma. This search yielded more than 300 cases, which were morphologically reviewed. Three cases fulfilled the criteria as reported recently and hence were included for further studies. The fourth case was a recent consultation case. All 4 cases were stained with ERG antibody, and after yielding positive results, they were submitted for FISH and NGS testing. For the analysis of ERG immunostaining in potential mimics of ESFT, 3 cases of lipofibromatosis, 10 cases of calcifying aponeurotic fibroma (CAF), 1 case of infantile digital fibroma/fibromatosis, 6 cases of superficial fibromatosis and 8 myofibromas were included in the study. In all cases, paraffin blocks were available. For conventional microscopy, tissues were fixed in formalin, routinely processed, embedded in paraffin, cut into 4 μm-thick sections, and stained with hematoxylin-eosin.

Immunohistochemistry

IHC analysis was performed using a Ventana BenchMark ULTRA (Ventana Medical System, Inc., Tucson, Arizona). The following primary antibodies were

used: ERG (for ESFT: EPR3864, prediluted, Ventana Medican Systems, Inc; calcifying aponeurotic fibromas were stained at a different institution using the clone EP111, 1:500, Epitomic), SOX10 (Polyclonal, 1:100, Cell Marque), S100 (Polyclonal, Prediluted, Ventana), EMA (E29, 1:400, Dako), CD34 (QBEnd/10, 1:200, Dako), SMA (1A4, 1:500, Dako), Desmin (D33, 1:200, Dako), OSCAR (IsoType:IgG2a, 1:100, Covance), AE1/3 (AE1/AE3&PCK26, prediluted, Ventana), Pan-TRK (A7H6R, 1:20, Cell Signaling), SAT-B2 (CL0276, 1:100; Sigma-Aldrich), HMB45 (HMB45, 1:400, Dako), β-Catenin (Polyclonal, 1:150, Thermo Fischer Scientific), MUC4 (8G7, 1:200, Santa Cruz Biotechnology), Synaptophysin (SP11, prediluted, Ventana), Chromogranin (DAK-A3, 1:400, Dako), CD117 (polyclonal, 1:800, Dako), DOG1 (SP31, prediluted, Cell Marque). The primary antibodies were visualized employing the enzymes alkaline phosphatase or peroxidase as detecting systems (both purchased from Ventana Medical System, Inc., Tucson, Arizona).

Molecular genetic studies

Detection of EWSR1 rearrangement by FISH

The dual color, break apart probe consisting of a mixture of FISH DNA probes on the centromeric and the telomeric sides of the EWSR1 gene breakpoints (Abbott Molecular, Des Plaines, IL), was used in this interphase FISH assay to detect the presence of an EWSR1 (22q12) rearrangement. 200 nuclei were scored, using the reference range of 0-11%.

Detection of EWSR-SMAD3 fusion by next generation sequencing

Fusion Plex Solid Tumor kit (ArcherDX Inc., Boulder, CO, USA) was used to construct a cDNA library for detecting fusion transcripts in 52 genes. All steps were performed according to the manufacturer's instructions (version of the protocol LA135.F), and the library was sequenced on an Illumina platform as described previously (2).

Results

Clinical findings

The clinical features are summarized in Table 1. All 4 patients were women with age ranging from 5 to 68 years (mean: 36.5 years). All tumors presented in the subcutaneous soft tissues of the extremities and were equally distributed between upper and lower extremity. While three tumors were found at acral sites, one arose on the calf. The tumor sizes ranged from 1 to 1.5 cm in greatest dimension, with a mean size of 1.2 cm. Follow-up was available for 3 patients; one case is recent. The average duration of follow-up was 11.7 years (range 7 to 18 years). After 10 years, one patient had a recurrence; none had metastatic disease. The cases were initially diagnosed as lipofibromatosis, fibromatosis, myofibroma or descriptively as "unusual benign spindle cell tumor". In the former 3 cases, the diagnosing pathologists always mentioned that the tumors do not represent a typical example of any entity as defined by the WHO classification of soft tissue tumors.

Pathological findings

The overall histopathological appearance of ESFT varied a little from case to case. Cases 1 and 3 were vaguely lobulated or plexiform (Figure 1A, 3A), whereas the 2 others created a single tumorous nodule (Figure 2A, 4A), as did the recurrence in Case 1 (1E). Case 4 was circumscribed, showing a thin fibrous capsule (Figure 4A), while the remaining cases had an infiltrative growth pattern, at least focally, occasionally engulfing a small amount of the surrounding subcutaneous adipose tissue (Figure 1A-F, 2A). The tumors showed two main components. One consisted of bland spindled cells with elongated, focally wavy nuclei (Figure 1D, 2B, 2D, 3D), which were round when observed on cross-section (Figure 2D, 3C) and did not show conspicuous nucleoli. A moderate amount of eosinophilic fibrillary cytoplasm surrounded the nuclei. These cells mostly grew in relatively hypercellular and well-organized fascicles of intermediate length that frequently intersected with each other at different angles. Pleomorphism, atypia or mitoses were absent (Figure 1D, 2B, 2D). The second component had an identical cellular composition and architecture. However, these areas were prominently hyalinized, resembling hyalinizing-type necrosis, and lacked calcifications with only a few viable spindled cells (Figure 2C). Both components showed either a distinct zonation pattern with the spindle cell component located at the periphery and central hyalinization (Figure 1B-C, 4A-B), or they randomly intermingled with each other (Figure 2B, 3B,). The

primary tumor in Case 1 was excised with positive surgical margins and recurred 10 years after surgery. The recurrence showed similar morphology, without increased cellularity or pleomorphism (Figure 1E-F). Despite again leaving positive surgical margins after re-excision, no recurrence was noted with an additional 8 years of follow-up. Similarly, in Case 2 the surgical margins were positive. However, the tumor did not recur with 10 years of follow-up. In Case 3, the tumor was successfully removed in toto after one immediate re-excision (suggested by the pathologist due to the incompleteness of the initial removal) with no signs of recurrence 7 years after diagnosis. The fourth case was completely excised with narrow margins, but the case is too recent for any meaningful follow-up evaluation.

Immunohistochemical findings

The IHC results are summarized in Table 1. All cases showed strong nuclear staining for ERG (Figure 2A inset, 3E, 4C). The recurrent tumor in Case 1 and Case 2 showed focal weak to moderate nuclear staining with SAT-B2 (Figure 2F). Despite employing a broad IHC panel including OSCAR, CD34, Pan-TRK, along with muscle, neuroendocrine and melanoma markers, no other expression of any antibody was noted. From the analyzed mimics, 9/10 cases of CAF showed a weak to moderate ERG staining in most cells. None of other mimics stained with this marker.

Molecular genetic findings

The molecular genetic results are summarized in Table 1. Due to suboptimal quality of archival tissue, FISH analysis was successfully carried out only in the most recent Case 4, where it confirmed unbalanced rearrangement involving *EWSR1* gene in 72% of nuclei. The material quality issues precluded the NGS analysis in Case 3. However, we believe that despite missing molecular genetic proof for this case, both the typical ESFT morphology and strong nuclear ERG expression (with all other markers being negative) warrant inclusion of this case into the study. In the remaining cases, the characteristic *EWSR1-SMAD3* gene fusion, resulting from a t(15;22)(q22.33;q12.2) was confirmed by NGS.

Discussion

The group of fibroblastic/myofibroblastic tumors encompass a broad spectrum of entities that demonstrate overlapping morphological and immunohistochemical features, frequently defying their accurate classification. Due to the recent vast expansion of NGS-based techniques, the molecular underpinnings of these tumors are gradually being discovered, and this knowledge may be utilized in difficult cases. Moreover, it also represents an invaluable tool for a potential delineation of novel entities from hitherto unclassifiable fibroblastic tumors. An example of the latter application is the three cases recently reported by Kao et al. who described a novel spindle cell tumor with recurrent *EWSR1-SMAD3* fusion (referred to as ESFT in this article) that, based on all available evidence, exhibits fibroblastic differentiation (1).

Combining both the current and initial report, altogether 7 cases of ESFT have now been described. While most findings from the original series were confirmed by us, several novel features emerged in the current series, and despite the persisting need for more substantial patient numbers, some preliminary general observations can now be made.

The first 3 cases reported were all located at acral sites of lower extremities. Besides one of our cases that arose at the dorsal aspect of the foot, 2 other lesions were found on the acral aspects of the hand. Additionally, one of the tumors in our series affected the calf, thereby representing the first non-acral case. With respect to the gender, ESFT seems to have a distinct gender predilection for women (6/7 cases). The age range is wide, with some cases arising in infants or young children, others affecting patients up to the seventh decade. Since these tumors usually grow infiltratively, they are prone to recur locally. Of the 5 cases with available follow up, 3 (60%) have recurred after a variable time interval ranging from 5 months to as late as 10 years. On the other hand, the remaining 2 cases have not recurred after long follow-up despite having positive surgical margins.

Microscopically, the low power arrangement of ESFT varied a little from the initial 3 reported cases, showing, in addition to nodular growth (1), vaguely lobular or slightly plexiform tumors that infiltrated into the surrounding tissue and showed two main components. The first was represented by intersecting,

relatively hypercellular and well-organized fascicles of bland spindled cells. The second component had a similar cellular composition and architecture but was prominently hyalinized, resembling hyalinizing-type necrosis and contained a small number viable cells. In a single previously reported case, this area also featured focal stippled calcifications. The components showed either a distinct zonation pattern as reported by Kao et al., with the spindle cell component located at the periphery and the hyalinized area in the center (1). Additionally, in our two cases, the components were intermingled throughout the tumor without distinct zonation. All reported cases showed strong nuclear positivity for ERG. Although a relatively wide panel of antibodies was used in both studies, the only other reactivity observed was weak, equivocal staining with both keratins and EMA in one case of Kao et at. (1), and focal weak to moderate nuclear staining with SAT-B2 in the current Case 2 and in the recurrent tumor in Case 1.

ERG is a widely used vascular endothelial marker and is also expressed in Ewing sarcomas or prostate carcinomas with ERG fusions (3-5). Also, it was shown to be a reliable marker for chondrogenic tumors and a useful marker for phosphaturic mesenchymal tumors (6-8). Its expression in fibroblastic/myofibroblastic tumors has, to our knowledge, not been described and in the right context, strong ERG expression seems to be quite specific and sensitive for ESFT. The differential diagnosis of ESFT is broad, primarily comprising rare tumors from the fibroblastic/myofibroblastic category such as

lipofibromatosis (LPF), calcifying aponeurotic fibroma (CAF), lipofibromatosis-like neural tumor (LFLNT), myofibroma/myofibromatosis (MF), infantile digital fibroma/fibromatosis and palmar/plantar fibromatosis. Nevertheless, due to the rarity of these tumors, their ERG expression has not been studied. One of the aims of this study was thus to evaluate ERG staining in potential ESFT mimics as well.

LPF is a rare pediatric mesenchymal tumor with a predilection for the hands and feet (9). ESFT frequently infiltrates the surrounding fatty tissue and may therefore be mistaken for LPF as illustrated by Case 1. However, LPF does not feature the prominent hyalinized component, the fascicles do not show the prominent intersecting pattern and are composed of rather oval than fusiform cells. The fat component is also more abundant and usually present throughout the entire tumor. In contrast, the fatty component in ESFT is limited and is usually present only at the tumor margins. LPF usually stains with CD34, and about 1/3 of cases express S100 protein (9). Although it may show variable staining with several other IHC markers, it does not express ERG as evidenced by our analysis carried out on 3 cases. Until recently, the molecular underpinnings of LPF were mostly unknown (discussed below).

CAF is a tumor primarily affecting children or young adults with a strong predilection for the hands and feet, although occasional examples may occur outside this typical location (10). The chondroid foci of CAF bear a superficial

resemblance to the hyalinized component of ESFT. However, only one case of the latter tumor was reported to contain a limited amount of calcific material. The cellularity of CAF varies, depending on the age of the lesion. However, the tumor fascicles of CAF, when present, are more haphazardly arranged than in ESFT. Recently, *FN1–EGF* gene fusions were reported as a recurrent molecular event in the majority of CAF (11), and the tumor also shows a simultaneous elevation of *FN1* mRNA levels (1). ERG expression in CAF has not been reported in the literature. While confirming the specificity of strong ERG expression for ESFT among lesions in its differential diagnosis, our study also demonstrated frequent, albeit weak to moderate, expression of ERG in most (90%) of cases of CAF.

Like LPF, LPFLNT does not contain the hyalinized zones, the spindled cells are more atypical and hyperchromatic and do not show such prominent intersecting fascicles as in ESFT. Most cases stain with S100 protein and CD34, whereas ERG staining has not been reported. Recurrent *NTRK1* gene rearrangements were identified in 10/14 cases, with another 2 cases harboring *ROS1* and *ALK* gene rearrangements respectively (12). LPFLNT with *NTRK1* rearrangement is also positive with NTRK1 IHC, which did not react in the several ESFT tested.

Interestingly, even in the absence of *FN1* fusion, one case of LPLNT with *TPR-NTRK1* fusion showed an increased *FN1* mRNA overexpression, and even higher *FN1* mRNA upregulation was observed in ESFT. Moreover, based on

unsupervised clustering of the whole transcriptome RNA data of more than 100 various soft tissue tumors performed by Kao et al., CAF and ESFT clustered together with LPF and LPFLNT in one group of related tumors (1). *FN1* mRNA upregulation (in the presence of *FN1* fusions) is further present in phosphaturic mesenchymal tumors which concurrently shows ERG expression (1, 7, 8, 13, 14)

Very interesting findings regarding this topic were presented at the 2018 USCAP Annual Meeting in Vancouver. Prompted by a typical case of LPF that recurred showing morphological features of CAF, Al-Ibraheemi et al. studied 16 cases of LPF for the CAF-associated fusion or other genetic events. They found a subset of LPF harboring the CAF-associated *FN1-EGF* fusion, or a related *FN1-TGFA* fusion, suggesting that some "LPF" may instead represent CAF lacking the hallmark calcifications. Other LPF showed alterations involving kinase-encoding genes *TPR-ROS1* and *SPARC-PDGFRB*, suggesting a possible link to LPFLNT. A third subset of LPF showed novel gene fusions *HBEGF-RBM27* and *EGR1-GRIA1,* and six cases lacked identifiable genetic events. Therefore, LPF appears to be a genetically heterogeneous tumor, despite stereotypical morphologic features (15). Finally, it seems that ESFT, LPF, CAF, and LPFLNT represent a group of benign or locally aggressive tumors that, besides sharing overlapping morphological features, are also related at the molecular and/or transcriptomic level. Although morphologically relatively

dissimilar, phosphaturic mesenchymal tumor also seems to be vaguely related to these neoplasms.

MF frequently contain myointimal-like nodular proliferations (also called myoid or vascular balls) (16). These areas may show a variable level of hyalinization, and when well developed, they may closely mimic the hyalinized areas of ESFT. Especially in the cellular variants of MF, the surrounding spindle cells sometimes additionally acquire a hypercellular fascicular arrangement (17) and may thus also resemble similar areas of ESFT. Nevertheless, the spindled cells of MF are plumper, and the hemangiopericytoma-like vessels and pericytic arrangement of the surrounding cells are usually present and offer a helpful diagnostic clue. Although with variable intensity, virtually all MF express smooth muscle actin and the cellular examples also co-express desmin (18). However, they do not stain with ERG as documented by our analysis of 8 cases and by the literature data (3). Genetically, classic MF show *PDGFRB* mutation in most cases (16), while a subset of what appears to be the cellular variant of MF was reported to show *SRF-RELA* fusion (18).

Infantile digital fibroma/fibromatosis has a cellular arrangement that varies in any given tumor from whorled bundles or interlacing short fascicles to broad storiform arrays and is thus slightly different from the uniformly fascicular architecture of ESFT. Moreover, the hyalinized areas typical for ESFT are absent. The spindled tumor cells in infantile digital fibromatosis possess an

elongated nucleus, lightly eosinophilic cytoplasm and mainly, the very characteristic paranuclear inclusion. They are present in most examples, and on standard hematoxylin and eosin (HE) sections appear as a small, rounded, pale pink body. The tumors uniformly stain with muscle markers (19), but ERG expression was not found in our single tested case.

Although superficial fibromatosis may, particularly in the cellular examples, closely resemble ESFT, larger hyalinizing-type necrosis-like areas are not found. ESFT is much more cellular than examples of superficial fibromatoses, and cytologically the nuclei of ESFT are less curved, wavy, and plumper than in any type of fibromatosis. Expression of smooth muscle actin, uniformly present in fibromatosis, is not a feature of ESFT. ERG staining has been studied in desmoid-type fibromatosis and was negative (3), as was the staining of 6 cases of superficial fibromatosis in our study.

It is known that *EWSR1* is a highly promiscuous gene that is rearranged in many different tumor types. In the context of dermal-based spindle cell neoplasms with *EWSR1* rearrangement, the diagnosis of cutaneous forms of myoepithelioma (20, 21) or clear cell sarcoma (22) may also be considered. However, their overall morphology and immunoprofile differ significantly from ESFT. Lastly, a small number of spindle cell sarcomas with prominent myopericytic/hemangiopericytic growth pattern have been reported to harbor *LMNA-NTRK1* and *TPM3-NTRK1* gene fusions (23). Identical fusions are

present in LPLNT, and the latter fusion has also been described in one case of pediatric spindle cell sarcoma resembling infantile fibrosarcoma (24). This underscores the complexity and overlapping features within the group of fibroblastic/myofibroblastic tumors. Also, it once again proves that not only tumors with the same fusion partner but even with an identical gene fusion may be morphologically and biologically completely different and that the clinical and histological context remains crucial for establishing the correct diagnosis.

In this article, we presented 4 cases of a recently described fibroblastic mesenchymal tumor with *EWSR1-SMAD3* gene fusion, further extending its clinicopathologic spectrum. All reported examples demonstrate highly reproducible morphologic features that allow classification of this tumor on H&E slides with a high level of certainty, confirming that they represent a novel and distinct entity within the otherwise highly complex group of fibroblastic/myofibroblastic tumors. We also proved that in the right clinicopathological context, strong ERG staining is a sensitive and relatively specific immunohistochemical marker for these tumors. For practical purposes, we propose the name *EWSR1-SMAD3*-rearranged Fibroblastic Tumor for these neoplasms.

Legends to figures

Figure 1. The original tumor in Case 1 was vaguely lobulated or plexiform (A). It showed a distinct zonation pattern with central hyalinization and the spindle cell component located at the periphery, engulfing a small amount of the surrounding subcutaneous adipose tissue (B, C). Higher power view of the bland spindled cells with elongated, focally wavy nuclei growing in relatively hypercellular and well-organized fascicles of intermediate length that frequently intersected with each other at different angles (D). The recurrence created a single tumorous nodule (1E), engulfing a small amount of the surrounding fat and showing the characteristic hyalinization (1F).

Figure 2. The tumor in Case 2 created a single tumorous nodule. A small amount of engulfed adipose tissue is seen on the right (A). The hypercellular fascicles frequently intersected with each other at different angles, and in this case, randomly intermingled with the hyalinized component (B). High power view of the prominently hyalinized component, which resembled hyalinizing-type necrosis, and lacked calcifications with only a few viable spindled cells (C). The bland spindled cell component with elongated, focally wavy nuclei, which were round when observed on cross-section and did not show conspicuous nucleoli (D). Strong nuclear staining with ERG (E). This tumor also showed focal weak to moderate nuclear staining with SAT-B2 (F).

Figure 3. The tumor in Case 3 was vaguely plexiform (A). In this case, both components randomly intermingled with each other (B, C). Bland spindled cells with elongated, focally wavy nuclei (D). Strong nuclear staining with ERG (E).

Figure 4. The tumor in Case 4 created a single tumorous nodule which featured a distinct zonation pattern with the spindle cell component located at the periphery and central hyalinization (A). The prominently hyalinized component, which resembled hyalinizing-type necrosis gradually merged with the more peripherally located spindle cell proliferation (B). Strong nuclear staining with ERG (C). Pleomorphism, atypia or mitoses were absent in the spindled cell component (D).

References

1. Kao YC, Flucke U, Eijkelenboom A, et al. Novel EWSR1-SMAD3 Gene Fusions in a Group of Acral Fibroblastic Spindle Cell Neoplasms. *Am J Surg Pathol.* 2018;42:522-528.
2. Skalova A, Vanecek T, Martinek P, et al. Molecular Profiling of Mammary Analog Secretory Carcinoma Revealed a Subset of Tumors Harboring a Novel ETV6-RET Translocation: Report of 10 Cases. *Am J Surg Pathol.* 2018;42:234-246.
3. Miettinen M, Wang ZF, Paetau A, et al. ERG transcription factor as an immunohistochemical marker for vascular endothelial tumors and prostatic carcinoma. *Am J Surg Pathol.* 2011;35:432-441.
4. Wang WL, Patel NR, Caragea M, et al. Expression of ERG, an Ets family transcription factor, identifies ERG-rearranged Ewing sarcoma. *Mod Pathol.* 2012;25:1378-1383.
5. Furusato B, Tan SH, Young D, et al. ERG oncoprotein expression in prostate cancer: clonal progression of ERG-positive tumor cells and potential for ERG-based stratification. *Prostate Cancer Prostatic Dis.* 2010;13:228-237.
6. Shon W, Folpe AL, Fritchie KJ. ERG expression in chondrogenic bone and soft tissue tumours. *J Clin Pathol.* 2015;68:125-129.
7. Tajima S, Takashi Y, Ito N, et al. ERG and FLI1 are useful immunohistochemical markers in phosphaturic mesenchymal tumors. *Med Mol Morphol.* 2016;49:203-209.
8. Agaimy A, Michal M, Chiosea S, et al. Phosphaturic Mesenchymal Tumors: Clinicopathologic, Immunohistochemical and Molecular Analysis of 22 Cases Expanding their Morphologic and Immunophenotypic Spectrum. *Am J Surg Pathol.* 2017;41:1371-1380.
9. Fetsch JF, Miettinen M, Laskin WB, et al. A clinicopathologic study of 45 pediatric soft tissue tumors with an admixture of adipose tissue and fibroblastic elements, and a proposal for classification as lipofibromatosis. *Am J Surg Pathol.* 2000;24:1491-1500.
10. Fetsch JF, Miettinen M. Calcifying aponeurotic fibroma: a clinicopathologic study of 22 cases arising in uncommon sites. *Hum Pathol.* 1998;29:1504-1510.
11. Puls F, Hofvander J, Magnusson L, et al. FN1-EGF gene fusions are recurrent in calcifying aponeurotic fibroma. *J Pathol.* 2016;238:502-507.
12. Agaram NP, Zhang L, Sung YS, et al. Recurrent NTRK1 Gene Fusions Define a Novel Subset of Locally Aggressive Lipofibromatosis-like Neural Tumors. *Am J Surg Pathol.* 2016;40:1407-1416.
13. Lee JC, Jeng YM, Su SY, et al. Identification of a novel FN1-FGFR1 genetic fusion as a frequent event in phosphaturic mesenchymal tumour. *J Pathol.* 2015;235:539-545.
14. Lee JC, Su SY, Changou CA, et al. Characterization of FN1-FGFR1 and novel FN1-FGF1 fusion genes in a large series of phosphaturic mesenchymal tumors. *Mod Pathol.* 2016;29:1335-1346.
15. Al-Ibraheemi A, Perez-Atayde A, Perry KD, et al. Lipofibromatosis (LPF): A Clinicopathological and Molecular Genetic Study of 16 Cases Suggesting a Link to Calcifying Aponeurotic Fibroma (CAF) and LPF-like Neural Tumor (LPFLNT). *Mod Pathol.* 2018;31:18.
16. Agaimy A, Bieg M, Michal M, et al. Recurrent Somatic PDGFRB Mutations in Sporadic Infantile/Solitary Adult Myofibromas But Not in Angioleiomyomas and Myopericytomas. *Am J Surg Pathol.* 2017;41:195-203.
17. Linos K, Carter JM, Gardner JM, et al. Myofibromas with atypical features: expanding the morphologic spectrum of a benign entity. *Am J Surg Pathol.* 2014;38:1649-1654.
18. Antonescu CR, Sung YS, Zhang L, et al. Recurrent SRF-RELA Fusions Define a Novel Subset of Cellular Myofibroma/Myopericytoma: A Potential Diagnostic Pitfall With Sarcomas With Myogenic Differentiation. *Am J Surg Pathol.* 2017;41:677-684.
19. Laskin WB, Miettinen M, Fetsch JF. Infantile digital fibroma/fibromatosis: a clinicopathologic and immunohistochemical study of 69 tumors from 57 patients with long-term follow-up. *Am J Surg Pathol.* 2009;33:1-13.
20. Jo VY, Antonescu CR, Zhang L, et al. Cutaneous syncytial myoepithelioma: clinicopathologic characterization in a series of 38 cases. *Am J Surg Pathol.* 2013;37:710-718.

21. Flucke U, Palmedo G, Blankenhorn N, et al. EWSR1 gene rearrangement occurs in a subset of cutaneous myoepithelial tumors: a study of 18 cases. *Mod Pathol.* 2011;24:1444-1450.
22. Hantschke M, Mentzel T, Rutten A, et al. Cutaneous clear cell sarcoma: a clinicopathologic, immunohistochemical, and molecular analysis of 12 cases emphasizing its distinction from dermal melanoma. *Am J Surg Pathol.* 2010;34:216-222.
23. Haller F, Knopf J, Ackermann A, et al. Paediatric and adult soft tissue sarcomas with NTRK1 gene fusions: a subset of spindle cell sarcomas unified by a prominent myopericytic/haemangiopericytic pattern. *J Pathol.* 2016;238:700-710.
24. Kao YC, Fletcher CDM, Alaggio R, et al. Recurrent BRAF Gene Fusions in a Subset of Pediatric Spindle Cell Sarcomas: Expanding the Genetic Spectrum of Tumors With Overlapping Features With Infantile Fibrosarcoma. *Am J Surg Pathol.* 2018;42:28-38.

Tables

Table 1. Clinical, immunohistochemical and molecular genetic features

Case	Sex/ Age	Location	Duration	Size (cm)	FISH	NGS	IHC +	IHC -	Recurrence	Length of FU (years)	Original diagnosis	Comment
1	F/5 and 15	Hand - palm	3 years	1,2 and 0,3	NA	EWSR1-SMAD3	ERG in both; Focal SAT-B2 staining in the 2nd tumor, neg. in the first tumor	SOX-10; S100; EMA; CD34; SMA; Actin E; Desmin; SAT-B2; OSCAR; Pan-TRK ; SAT-B2;	Yes -in 10 years	18	Unusual lipofibromatosis	Incomplete excision in both the original tumor and the re-excision
2	F/68	Interphalangeal joint of the thumb	10 months	1,5x0,7 x0,5	NA	EWSR1-SMAD3	ERG, focal SAT-B2 staining	SOX-10; S100; CD34; EMA; Desmin; OSCAR; HMB45;	No	10	Unusual fibromatosis	Incomplete excision but no recurrence
3	F/39	Calf	NA	1x0,5 x0,5	NA	NA	ERG	S100; EMA; CD34; SMA; Desmin; OSCAR; AE1/3 Synaptophysin; Chromogranin; CD117; DOG-1	No	7	Benign plexiform spindle cell tumor	Early re-excision - no additional tumor tissue
4	F/34	Left foot – dorsal metatarsal aspect	NA	1.1x0.8 x 0.5	Positive	EWSR1-SMAD3	ERG	SOX-10; S100; EMA; CD34; SMA; Desmin; Caldesmon; AE1/3; Beta Catenin; MUC4	Recent case	Recent	Unusual myofibroma	Slowly enlarging, painful, no history of trauma

NA – not available; FU – follow-up

Figure 1

Click here to download Figure Figure 1.jpg

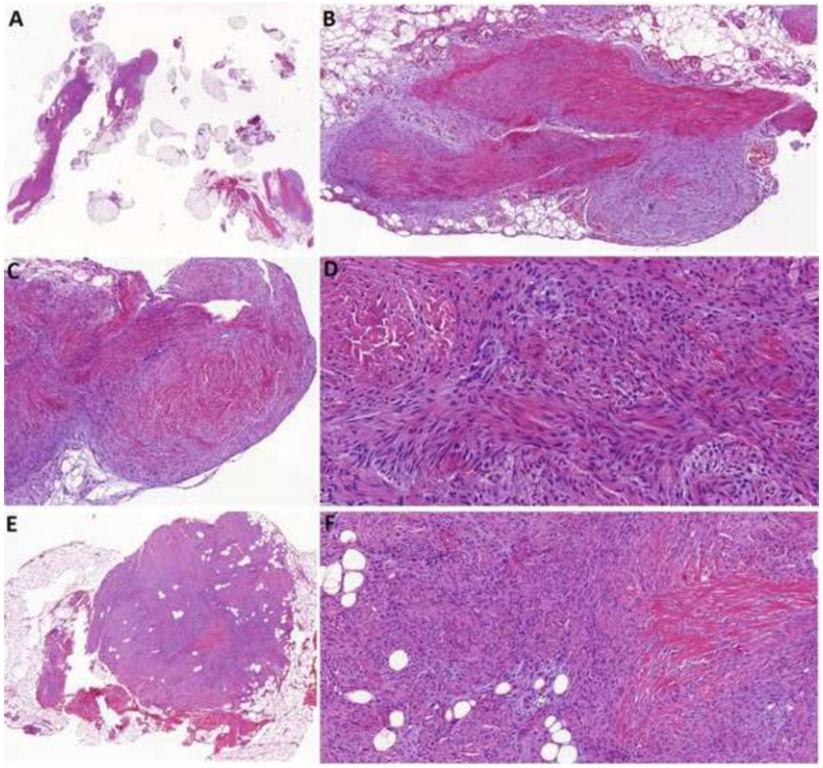

Figure 2

Click here to download Figure Figure 2.jpg

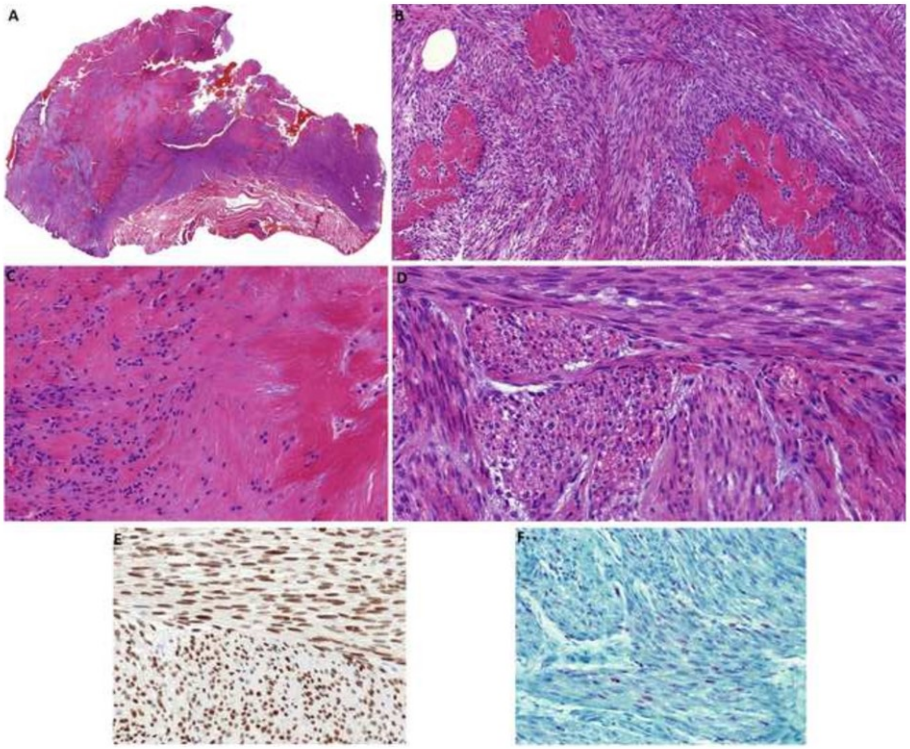

Figure 3

Click here to download Figure Figure 3.jpg

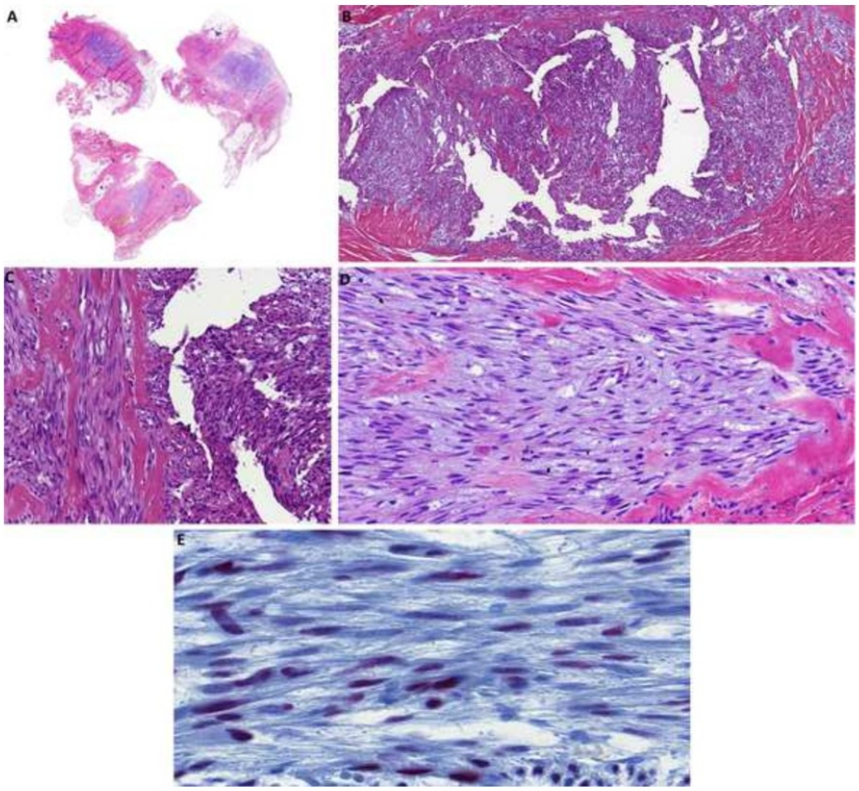

Figure 4

Click here to download Figure Figure 4.jpg

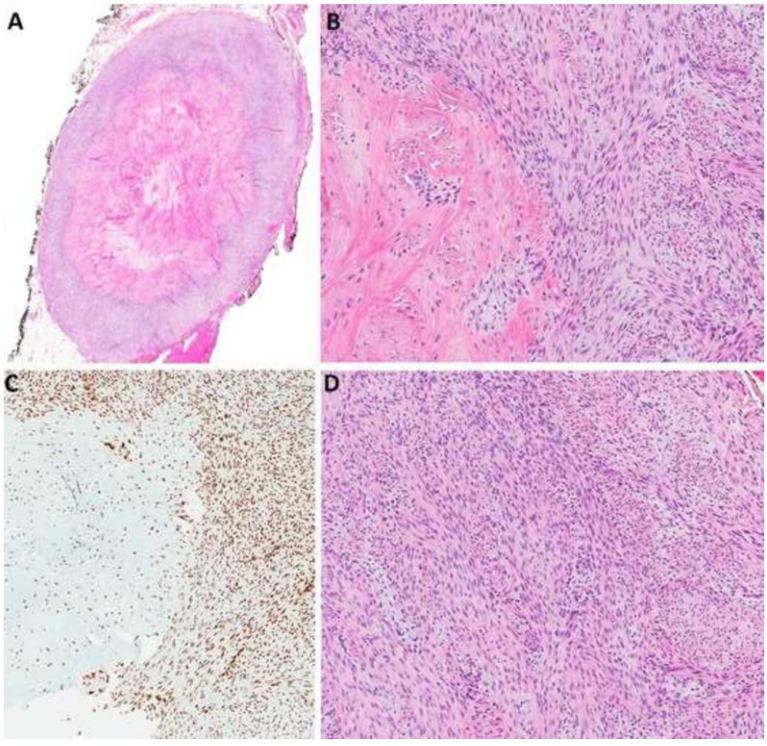

1.2. Others

1.2.1. PENILE ANALOGUE OF STRATIFIED MUCIN-PRODUCING INTRAEPITHELIAL LESION OF THE CERVIX: THE FIRST DESCRIBED CASE. A DIAGNOSTIC PITFALL

Stratified mucin-producing intraepithelial lesion (SMILE) has originally been described in the cervix as a rare neoplastic intraepithelial process affecting the transformation zone of the uterine cervix and showing features of both cervical intraepithelial neoplasia and adenocarcinoma in situ. Histopathologically, the stratified epithelium contains mitotically active cells with atypical and hyperchromatic nuclei, involving the surface epithelium and/or the underlying endocervical glands. Simultaneously, in the absence of gland formation, mucin vacuoles are present throughout the full-thickness of the squamous epithelium [29]. Two similar lesions have later been described on the vulva, where collections of cells with intracytoplasmic mucin present at all epidermal layers occurred concomitantly with changes corresponding to classic vulvar intraepithelial neoplasia [30]. These lesions, on both the cervix and the vulva, have been shown to be caused by high-risk Human Papillomavirus (HPV).

In this case report, we presented a unique case of classic intraepithelial neoplasia with goblet cells encountered on the penis, which subsequently progressed into an invasive carcinoma featuring both squamous and glandular components. This was the first description of such a lesion occurring on the penis, which can be considered the penile analogue of cervical SMILE.

The lesion occurred in a 56-year-old HIV-positive man and evolved in three consecutive biopsies from only surface epithelium occupying numerous goblet cells in the first to variably sized solid nodules in the dermis composed of atypical squamous and/or basaloid cells intermixed with numerous goblet cells in the third biopsy. The initial biopsy was misinterpreted as extramammary Paget disease. The correct diagnosis was rendered retrospectively, after recognition of the existence of the vulvar lesion resembling cervical SMILE [30].ref2 After coming across the latter article, we stained the tumor with p16 antibody which yielded diffuse block type positivity in a full thickness of the epithelium, e.i. a staining pattern characteristic for the presence of a high risk HPV infection. This prompted the HPV genotyping which disclosed the presence of HPV type 16 infection thereby confirming our hypothesis.

As evident in our case, the main pitfall in the differential diagnosis of penile (or vulvar) SMILE is extramammary Paget disease. Another important differential diagnosis is penile/vulvar mucinous metaplasia. The finding of atypical squamous epithelial cells positive for p16 associated with mucinous cells present throughout the full epithelial thickness is a clue to the diagnosis of penile SMILE.

Penile Analogue of Stratified Mucin-Producing Intraepithelial Lesion of the Cervix: The First Described Case. A Diagnostic Pitfall

Michael Michal, MD, Michal Michal, MD,† Marketa Miesbauerova, MD,† Jana Hercogova, MD,‡ Barbora Skopalikova, MD,§ and Dmitry V. Kazakov, MD†*

Abstract: The authors report a case where undifferentiated (classic) penile intraepithelial neoplasia was associated with the presence of goblet cells throughout the full epithelial thickness and which later progressed into an invasive carcinoma. The lesion evolved in three consecutive biopsies from only surface epithelium occupying numerous goblet cells in the first to variably sized solid nodules in the dermis composed of atypical squamous and/or basaloid cells intermixed with numerous goblet cells in the third biopsy. Both cellular components expressed CK7 and p16 protein. Human Papillomavirus (HPV) genotyping revealed high risk HPV type 16. To the best of our knowledge, this is the first description of such a lesion occurring on the penis, which can be considered the penile analogue of cervical stratified mucin-producing intraepithelial lesion (SMILE). The correct diagnosis was rendered retrospectively, after recognition of the existence of a vulvar lesion resembling cervical SMILE. The initial biopsy was misinterpreted as extramammary Paget disease, which also constitutes the main pitfall in the differential diagnosis. Another important differential diagnosis is penile/vulvar mucinous metaplasia. The finding of atypical squamous epithelial cells positive for p16 associated with mucinous cells present throughout the full epithelial thickness is a clue to the diagnosis of penile SMILE.

Key Words: penis, stratified mucin-producing intraepithelial lesion, SMILE, penile intraepithelial neoplasia, PeIN, mucinous metaplasia, Paget disease

(*Am J Dermatopathol* 2016;38:e64–e67)

From the *Department of Pathology, Charles University, Biomedical Center, Faculty of Medicine in Plzen and Charles University Hospital Plzen, Pilsen, Czech Republic; †Department of Pathology, Charles University, Medical Faculty and Charles University Hospital Plzen, Pilsen, Czech Republic; ‡Department of Dermatovenereology, Charles University, 2nd Faculty of Medicine and Bulovka Hospital, Prague, Czech Republic; and §Department of Pathology, Charles University, 2nd Faculty of Medicine, Prague, Czech Republic.

Supported by the National Sustainability Program I (NPU I) Nr. LO1503 provided by the Ministry of Education Youth and Sports of the Czech Republic.

The authors declare no conflicts of interest.

Reprints: Michael Michal, MD, Department of Pathology, Charles University, Medical Faculty and Charles University Hospital Plzen, Alej Svobody 80, 304 60 Pilsen, Czech Republic (e-mail: michael.michal@medima.cz).

INTRODUCTION

Stratified mucin-producing intraepithelial lesion (SMILE) has originally been described in the cervix as a rare neoplastic intraepithelial process affecting the transformation zone of the uterine cervix and showing features of both cervical intraepithelial neoplasia (CIN) and adenocarcinoma in situ (AIS). Histopathologically, the stratified epithelium contains mitotically active cells with atypical and hyperchromatic nuclei, involving the surface epithelium and/or the underlying endocervical glands. Simultaneously, in the absence of gland formation, mucin vacuoles are present throughout the full-thickness of the squamous epithelium.[1] Two similar lesions have later been described on the vulva, where collections of cells with intracytoplasmic mucin present at all epidermal layers occurred concomitantly with changes corresponding to classic vulvar intraepithelial neoplasia (VIN).[2] These lesions, on both the cervix and the vulva, have been shown to be caused by high-risk Human Papillomavirus (HPV).

Herein, we present a unique case of classic intraepithelial neoplasia with goblet cells encountered on the penis, which subsequently progressed into an invasive carcinoma featuring both squamous and glandular components. To the best of our knowledge, this is the first description of such a lesion occurring on the penis, which can be considered the penile analogue of cervical SMILE. The correct diagnosis was rendered retrospectively, after recognition of the existence of a vulvar lesion resembling cervical SMILE.[2] The initial biopsy was misinterpreted as extramammary Paget disease (EMPD).

CASE REPORT

Clinical Findings

The patient was a 56-year-old HIV-positive man, who presented with a painless, bleeding, nonitching, erosive solitary lesion, measuring 25 mm, involving the inner foreskin and the glans of the penis. The clinical differential diagnostic considerations included erosive balanitis, precancerous lesion, or penile carcinoma. After the initial histological diagnosis of EMPD, the patient was treated with Aldara, Efudix, and 7 rounds of photodynamic therapy. Due to persistence of the lesion (Fig. 1), repeated biopsies were taken 32 and 34 months later.

Histopathological and Immunohistochemical Findings

The initial biopsy of the tumor showed focally atypical, basaloid surface epithelium containing numerous goblet cells filled

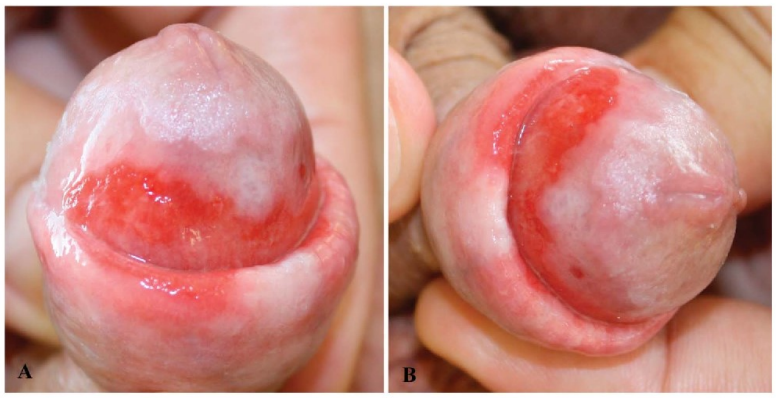

FIGURE 1. The persistent lesions after unsuccessful treatment with Aldara, Efudix, and photodynamic therapy (A, B).

with Periodic acid-Schiff-positive, alcian blue-positive mucin, some of which resembled signet ring cells (Figs. 2A–C). Immunohistochemically, they were positive for CK7 (monoclonal, clone OV-TL 12/30; Dako, Glostrup, Denmark).

The second biopsy performed 32 months later revealed only a minor surface epithelial component with appearances similar to those seen in the original biopsy, and, in addition, there were a few tiny glandlike structures in the dermis containing mucin-filled goblet cells. Focally, destruction of these structures and extrusion of the mucus into the corium has resulted in mucin pools (Figs. 3A, B).

Two months later, a large specimen was sampled, revealing microscopically an invasive process, with variably sized solid nodules and glandlike structures composed of atypical squamous and/or basaloid cells intermixed with numerous goblet cells, filled with mucus (Figs. 4A–C). Both components expressed CK7 and p16 protein (monoclonal, clone E6H4, CINtech, Heidelberg, Germany) (Fig. 4D). Retrospectively, immunostaining for p16 was performed on the previous biopsy specimens, revealing positivity in the dysplastic areas (Fig. 2D).

HPV Genotyping

HPV genotyping was performed using the following primer systems: CPSGB, GP5+/GP6+ and type specific primers for HPV

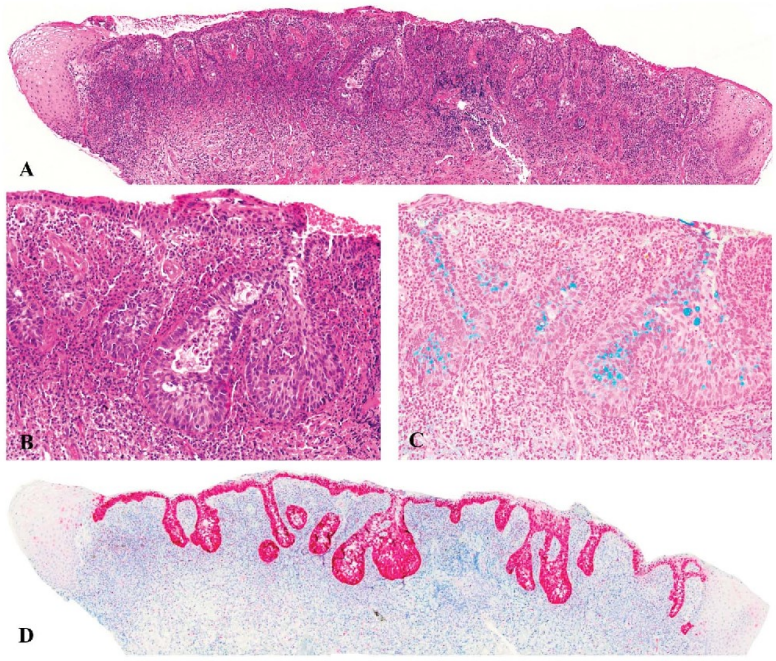

FIGURE 2. The initial biopsy of the tumor showed focally atypical, basaloid surface epithelium containing numerous goblet cells (A, B) filled with alcian blue-positive mucin (C). Immunostaining for p16 (D) performed retrospectively.

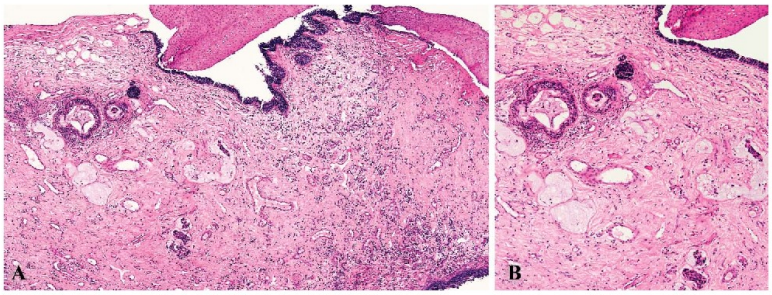

FIGURE 3. The second biopsy: a few tiny glandlike structures and pools of mucin can be recognized (A, B).

16, 18, 31, 33, 35, 45, as described elsewhere.[3] HPV type 16 was detected in the last biopsy specimen and, retrospectively, in the original specimen. The lesion was thus reclassified as the penile analogue of cervical SMILE with an invasive component of both squamous and glandular phenotype.

DISCUSSION

We report a case, where undifferentiated (classic, basaloid) penile intraepithelial neoplasia was associated with the presence of goblet cells throughout the full epithelial thickness and which later progressed into an invasive carcinoma. Similar HPV-induced epithelial lesions, termed SMILE, occurring at the transformation zone of uterine cervix, with a potential progression into an invasive carcinoma have been recognized for many years. The first comprehensive study of SMILE was published by Park et al,[4] who described it as a variant of CIN combining squamous and columnar differentiation, which was manifested by the presence of mucin production in the absence of gland formation. The mucin-producing cells were diffusely distributed throughout the whole thickness of the epithelium in lesions otherwise exhibiting squamous phenotype, with nuclear atypia, hyperchromasia, and a high proliferative index. In that study, SMILE has been found to coexist frequently with another type of intraepithelial neoplasia, either CIN or AIS, or even with an invasive carcinoma. Similar findings have recently been reported in an extensive study by McCluggage et al.[1] The cervical malignancies arising in association with SMILE were described as being either squamous in type, glandular in type, or a combination of both. Overall, SMILE was present in 0.6% of cervical specimens.[1] Both authors suggested that these lesions originate from HPV-infected stem or reserve cells with the potential for multidirectional differentiation. Thus, according to them, SMILE should be regarded as a form of high-grade reserve

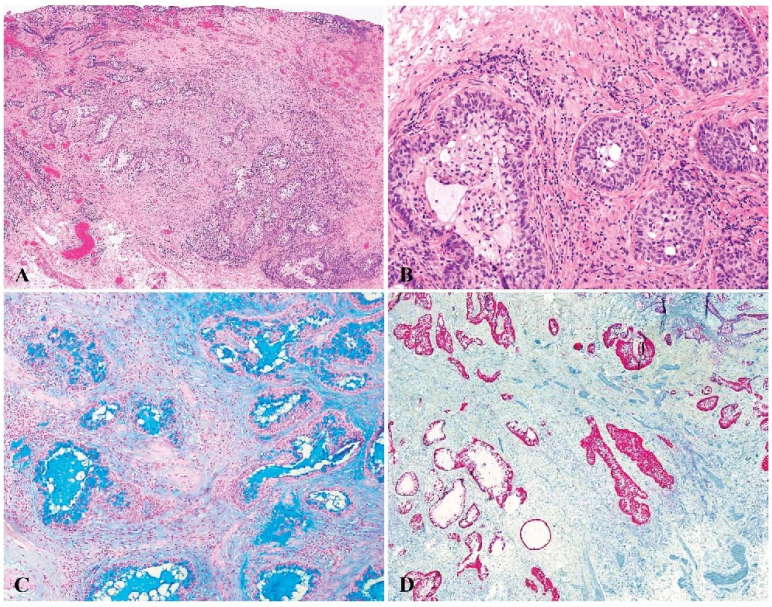

FIGURE 4. An invasive lesion manifesting variably sized solid nodules and glandular structures composed of atypical squamous and/or basaloid cells intermixed with numerous goblet cells (A, B). Staining for alcian blue (C) and immunostaining for p16 (D).

cell dysplasia with the potential to coexist with CIN, AIS, or an invasive carcinoma. However, in the recent 2014 World Health Organization classification, it is considered to be a variant pattern of AIS.

In 2009, McCluggage et al[2] reported 2 cases of classic (basaloid) VIN with collections of cells containing intracytoplasmic mucin throughout the full epithelial thickness and especially within epithelial downgrowths, which are commonly seen in VIN. The histological description and accompanying microphotographs are virtually identical to the changes seen in cervical SMILE and to those we report in our case on the penis, the only exception being the presence of an invasion in our patient during the progress of the disease.

Although the precise histogenesis of the vulvar and penile analogue of cervical SMILE remains unknown, HPV may be implicated in the etiopathogenesis of the conditions. It is well known that HPV infection may affect the morphology of squamous lesions in other anatomic locations. For example, HPV-related oropharyngeal carcinomas significantly differ from the conventional squamous cell counterparts in their histological profile.[5] It is well known that the HPV infection in the anal area similarly diverts the differentiation pathway into an aberrant direction, eventually producing goblet cells.[6]

As evident in our case, the main pitfall in the differential diagnosis of penile (or vulvar) SMILE is EMPD. It is a rare condition, representing approximately 1% of neoplasms in the anogenital area, most commonly occurring in white postmenopausal women, with the median age being 70–75 years. It can be classified into primary and secondary variants, with the latter representing secondary involvement from an underlying carcinoma, most commonly originating in gastrointestinal or urinary tract. EMPD manifests a typical pattern of an intraepithelial proliferation of carcinoma cells having vesicular nuclei with prominent nucleoli and abundant pale, clear, basophilic, or amphophilic cytoplasm. Several cytological variations in EMPD, including signet ring cells, have been reported.[7] Neoplastic cells in EMPD usually stain positively with alcian blue, Periodic acid-Schiff, and CK7. The latter is often used to confirm the diagnosis but as demonstrated by our case, CK7 cannot be used as a discriminator alone, as this marker was positive in all biopsy specimens in our patient. Also, squamous cell carcinoma in situ, including lesions in the anogenital area, is rarely immunoreactive for CK7.[8] The absence of cells containing mucin and positivity for p63 exclude EMPD in such cases. The presence of atypical squamous epithelial cells positive for p16 associated with mucinous cells is a clue to penile (vulvar) SMILE. However, one should keep in mind that, rarely, carcinoma cells in EMPD may express p16.[9] On the other hand, in such cases of EMPD, no dysplasia of the squamous epithelium is seen.

Another important differential diagnosis is penile/vulvar mucinous metaplasia[10–15] characterized by the presence of mucin containing goblet cells. The latter however predominantly occur singly (or rarely form small aggregates) in the upper part of the epithelium, which is otherwise normal. Mucinous metaplasia often occurs in association with an inflammatory process such as Zoon balanitis or some other nonspecific balanitis or vulvitis.[12] Its histogenesis is unknown but the association with inflammatory changes strongly suggests a reactive metaplastic process.[12]

The invasive lesion in our case resembled to some degree mucoepidermoid carcinoma. However, in the skin, in our view, cutaneous tumors revealing simultaneous squamous cell and glandular differentiation, in contrast to those in salivary glands, represent a heterogeneous group of tumors, for which the unifying term mucoepidermoid carcinoma cannot be used. Most reported cases of cutaneous "mucoepidermoid carcinoma" occurring in the skin can be categorized as hidradenocarcinoma or nodular hidradenoma, squamous cell carcinoma with mucinous metaplasia or mucoepidermoid carcinoma of the salivary gland secondarily involving the skin. Notably, HPV has been detected in squamous cell carcinoma with mucinous metaplasia occurring outside the anogenital area.[16]

In summary, we have described a lesion which we believe represents the first case of the penile analogue of cervical SMILE. The lesion is HPV induced. Further studies are warranted to validate the existence of this entity in the penile and vulvar locations.

REFERENCES

1. Boyle DP, McCluggage WG. Stratified mucin-producing intraepithelial lesion (SMILE): report of a case series with associated pathological findings. *Histopathology*. 2015;66:658–663.
2. McCluggage WG, Jamison J, Boyde A, et al. Vulval intraepithelial neoplasia with mucinous differentiation: report of 2 cases of a hitherto undescribed phenomenon. *Am J Surg Pathol.* 2009;33:945–949.
3. Kazakov DV, Nemcova J, Mikyskova I, et al. Human papillomavirus in lesions of anogenital mammary-like glands. *Int J Gynecol Pathol.* 2007; 26:475–480.
4. Park JJ, Sun D, Quade BJ, et al. Stratified mucin-producing intraepithelial lesions of the cervix: adenosquamous or columnar cell neoplasia? *Am J Surg Pathol.* 2000;24:1414–1419.
5. Bishop JA. Histopathology of human papillomavirus-related oropharyngeal carcinoma: a review of classic and variant forms. *Diagn Histopathol.* 2015;21:70–76.
6. Williams GR, Talbot IC. Anal carcinoma—a histological review. *Histopathology*. 1994;25:507–516.
7. Kazakov DV, Michal M, Kacerovska D, et al. *Cutaneous Adnexal Tumors*. Philadelphia, PA: Lippincott Williams & Wilkins; 2012.
8. Sah SP, Kelly PJ, McManus DT, et al. Diffuse CK7, CAM5.2 and BerEP4 positivity in pagetoid squamous cell carcinoma in situ (pagetoid Bowen's disease) of the perianal region: a mimic of extramammary Paget's disease. *Histopathology*. 2013;62:511–514.
9. Sah SP, McCluggage WG. Florid vulval Paget disease exhibiting p16 immunoreactivity and mimicking classic VIN. *Int J Gynecol Pathol.* 2013;32:221–227.
10. Ruiz-Genao DP, Dauden-Tello E, Adrados M, et al. Mucinous metaplasia of the glans penis. *Histopathology*. 2004;44:90–91.
11. Fang AW, Whittaker MA, Theaker JM. Mucinous metaplasia of the penis. *Histopathology*. 2002;40:177–179.
12. Garcia-Abos M, Fraga J, Dauden E. Mucinous metaplasia of the penis associated with Zoon's balanitis [Article in Spanish]. *Actas Dermosifiliogr.* 2010;101:362–364.
13. Val-Bernal JF, Hernandez-Nieto E. Benign mucinous metaplasia of the penis. A lesion resembling extramammary Paget's disease. *J Cutan Pathol.* 2000;27:76–79.
14. Mathew M, Joshi A, Roy A. Mucinous metaplasia of the prepuce–a case report and review of literature—a case report. *Indian J Pathol Microbiol.* 2006;49:263–264.
15. Coghill SB, Tyler X, Shaxted EJ. Benign mucinous metaplasia of the vulva. *Histopathology*. 1990;17:373–375.
16. Caputo V, Colombi R, Ribotta M, et al. Cutaneous squamous cell carcinoma with mucinous metaplasia on the sole associated with high-risk human papillomavirus type 18. *Am J Dermatopathol.* 2011;33:317–322.

1.2.2. MIXED EPITHELIAL AND STROMAL TUMOR OF THE MIDDLE EAR THE FIRST CASE REPORT

There are tumors occurring outside the female genital tract which, in addition to an epithelial component, contain a stroma identical to that one seen in the ovary. Such tumors have been documented in the pancreas liver, biliary tract, retroperitoneum, spleen, mesentery, kidney and in the paratesticular location. Except for the latter location, these neoplasms mostly affect middle-aged women. In this case report we presented a unique case of a tumor arising in the middle ear of an adult woman that featured both ovarian type stroma and an epithelial component. By analogy to its renal counterpart, we designated the neoplasm benign mixed epithelial and stromal tumor of the middle ear. We believe it is the first such case reported in this location.

The patient was a 65-year-old woman with chronic inflammation of the middle ear. On otoscopy, the upper part of her right tympanic membrane showed a prominent bulging. Middle ear polyp was suspected, and the patient was scheduled for an operation. During the operation, a rounded polypoid tissue which occupied the entire middle ear cavity and separated the auditory bones was resected. The histological diagnosis which was rendered in 2009 was chronic hyperplastic medial otitis with prominent metaplastic changes.

Eventually, while reviewing various archival cases from the middle ear region, we stumbled upon this case. Since the members of our research group were the first to describe mixed epithelial stromal tumor of the kidney (REF), the morphological resemblance was instantly noted. We performed a wide panel of immunomarkers to exclude other potential diagnoses. FISH to rule out *SYT* gene break characteristic for synovial sarcoma was performed. Also, polymerase chain reaction (PCR) for the detection of *NAB2-STAT6* fusion to exclude solitary fibrous tumor was carried out. Moreover, one of the reviewers demanded clonality analysis using X-chromosomal inactivation pattern and human androgen receptor locus to prove the tumor is indeed a neoplastic process. This method yielded a positive result which eventually led to the acceptance of this article.

Human Pathology (2017) 61, 199–204

ELSEVIER

Human PATHOLOGY

www.elsevier.com/locate/humpath

Case study

Mixed epithelial and stromal tumor of the middle ear. The first case report☆,☆☆

Michael Michal MD[a,*], Alena Skálová MD[b], Dmitry V. Kazakov MD, PhD[b], Květoslava Pecková MD[b], Filip Heidenreich MD[c], Petr Grossmann PhD[d], Michal Michal MD[b]

[a]*Department of Pathology, Faculty of Medicine in Pilsen, Charles University, Prague and Biomedical Center of the Faculty of Medicine in Pilsen, Czech Republic 30460*
[b]*Department of Pathology, Faculty of Medicine in Pilsen, Charles University, Prague, Czech Republic 30460*
[c]*Department of Radiology, Faculty of Medicine in Pilsen, Charles University, Czech Republic 30460*
[d]*Bioptical Laboratory Ltd., Pilsen, Czech Republic 32600*

Received 1 June 2016; revised 1 September 2016; accepted 23 September 2016

Keywords:
Middle ear;
Mixed epithelial and stromal tumor;
Ovarian stroma;
Corpus albicans like scar;
Head and neck

Summary We report a tumor arising in the middle ear of a 65-year-old female patient that was composed of an ovarian-type stroma (OS) and an epithelial component. The tumor consisted of irregular, polypoid masses containing multiple variably sized cystic spaces, which were invariably surrounded by the OS. The cystic spaces were lined by flat, cuboidal, or columnar epithelial cells, in most parts showing mucinous differentiation. The epithelial lining of the cysts strongly expressed cytokeratins AE1-3, CK7, CK8, CK18, CK19, EMA, and S100 protein. The stroma expressed CD34 and smooth muscle actin. No cytological atypia or mitoses were present, and the proliferative activity was less than 1% in both components. The clonality analysis proved the clonal nature of the neoplasm. We believe that this tumor is a new member in the family of neoplasms containing the OS, and therefore we propose the term *mixed epithelial and stromal tumor of the middle ear*.

1. Introduction

It is well known that ovarian-type stroma (OS) (along with an epithelial component) may occur in a variety of tumors outside the ovary. The best known examples are mucinous cystic neoplasms of the pancreas, liver, and biliary system [1-4]. Rarely, similar tumors can also develop in the retroperitoneum [5,6], spleen, mesentery [7], or vicinity of the testis [8,9]. Another example include the mixed epithelial and stromal tumor (MEST) of the kidney, originally described by one of the authors (Michal M.) [10,11]. The tumors containing OS show a striking female predilection.

Herein we present a unique case of a tumor arising in the middle ear of an adult woman that featured both OS and an epithelial component. By analogy to its renal counterpart, we designated the neoplasm benign *mixed epithelial and stromal tumor of the middle ear* (MESTME). We are unaware of any published reports of a similar neoplasm in this location.

☆ Competing interests: The authors have no conflicts of interest to disclose.
☆☆ Funding/Support: The study was supported by the Biomedical Center of the Faculty of Medicine in Pilsen (Pilsen, Czech Republic), project no. CZ.1.05/2.1.00/03.0076.
* Corresponding author at: Department of Pathology, Faculty of Medicine in Pilsen, Charles University, Prague, Alej Svobody 80, 304 60, Pilsen, Czech Republic.
E-mail address: michael.michal@medima.cz (M. Michal).

http://dx.doi.org/10.1016/j.humpath.2016.09.020
0046-8177/

2. Case report

2.1. Clinical findings

A 65-year-old woman suffering from chronic inflammation of the middle ear and a long-standing partial hearing loss complained of further rapid decline in the quality of perception in her right ear and occasional vertigo. The phoniatric and vestibular testing proved that her right ear is completely nonfunctioning in both auditory and vestibular components. On otoscopy, the upper part of her right tympanic membrane showed a prominent bulging. Middle ear polyp was suspected, and the patient was scheduled for an explorative tympanotomy. During the operation, a rounded polypoid tissue that occupied the entire middle ear cavity and separated the auditory bones was resected. The histological diagnosis of chronic hyperplastic medial otitis with prominent metaplastic changes was rendered.

In the following 3½ years, the patients' clinical course was unremarkable. Eventually, at a regular ear-nose-throat examination, the right tympanic membrane otoscopically showed similar recurring exophytic bulgings, which were excised. The subsequent histological diagnosis was identical to the original one.

Three years after the second operation, the patient remains without any signs of recurrence.

2.2. Radiologic findings

The preoperative computed tomographic (CT) scan from 2009 showed in bone window complete obliteration of right mastoid air cells and cavum tympani with a dense content. There was no destruction or reactive sclerosis of the surrounding bone. The septa between the air cells were slightly thickened (Fig. 1A). The preoperative CT scan from 2013 showed a mild thickening of the residual septa in the right mastoid after a middle ear surgery and mastoidectomy. Again, the presence of a dense content in residual mastoid air cells and cavum tympani can be seen. However, it could not be reliably distinguished whether it was a tumorous or a mucous mass. There was no destruction of the surrounding bone, and the very subtle sclerosis was most likely postoperative (Fig. 1B).

2.3. Pathological findings

Macroscopically, the first specimen consisted of 3 irregular, partially fragmented samples of tissue, each of them no larger than 1 cm in the largest dimension. The second specimen obtained 3½ years later was grossly composed entirely of fragmented tissue, together measuring 2 cm in the largest dimension. Histologically, both tumors were identical (Figs. 2 and 3). They consisted of irregular, polypoid masses containing multiple variably sized cystic spaces lined by flat, cuboidal, or columnar epithelial cells, in most parts showing mucinous differentiation with occasional goblet cells. The lumina of many cysts were filled with an eosinophilic secretion. The cysts were invariably surrounded by the OS, focally with variably pronounced hyalinization. In several parts of the stroma, areas strongly resembling corpora albicantia were encountered (Fig. 3C). Clusters of variably sized mucinous or seromucinous glands were scattered throughout the OS. In some parts, the tumor featured a squamous epithelium. As a rule, no cytological atypia or mitoses were present.

Immunohistochemical features are summarized in the Table. The epithelial lining of the cysts strongly expressed cytokeratins AE1-3, CK7, CK8, CK18, and CK19 and epithelial membrane antigen (EMA). Epithelial cells in a small proportion of the cysts expressed S100 protein. The stromal cells were reactive with CD34 protein and in some parts expressed smooth muscle actin. Scattered, weak expression of progesterone receptors (PRs) was noted focally (Fig. 3D). Estrogen receptors (ERs), calponin, inhibin, desmin, CD56, HMB45, TLE-1, CK20, CD-X2, MUC 2, MUC 5AC, MUC 6, antimucin monoclonal antibody, and PAX-8 were completely negative. MIB1 antibody was positive only in exceptional cells (less than 1% in both components).

2.4. Molecular genetic findings

2.4.1. *SYT* gene break

Molecular studies were performed to exclude biphasic synovial sarcoma using a previously described method [12], and the neoplastic sample was negative for an *SYT* gene break.

2.4.2. Clonality analysis using X-chromosomal inactivation pattern and human androgen receptor locus

The clonality analysis was performed according to a previously described method [13]. Analysis of tumor tissue revealed clonality ratio of 0.15 indicating its monoclonal pattern.

2.4.3. Detection of the NAB2-STAT6 fusion transcript by reverse-transcription polymerase chain reaction

RNA was extracted using the RecoverAll Total Nucleic Acid Isolation Kit (Ambion, Austin, TX). cDNA was synthesized using the Transcriptor First Strand cDNA Synthesis Kit (RNA input 500 ng) (Roche Diagnostics, Mannheim, Germany). All procedures were performed according to the manufacturer's protocols. Amplification of a 105– and 133–base pair product of the *B2M* gene and 247–base pair product of the *PGK* gene was used to test the quality of the extracted RNA as previously described [14,15]. For the detection of the *NAB2-STAT6* fusion transcript using reverse-transcription polymerase chain reaction (PCR), the same combination of the primers in *NAB2* and *STAT6* genes as described previously was applied [16].

For PCR, 2 mL of cDNA was added to reaction consisting of 12.5 mL of HotStar Taq PCR Master Mix (Qiagen, Hilden, Germany), 10 pmol of each primer, and distilled water up to 25 mL. The amplification program comprised denaturation at 95°C for 14 minutes and then 45 cycles of denaturation at 95°C for 1 minute, annealing at 60°C for 1 minute, and extension at 72°C for 1 minute. The program was finished

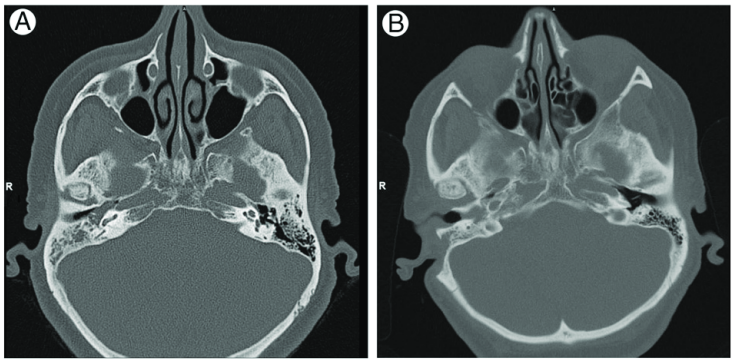

Fig. 1 A, CT scan from 2009. A complete obliteration of right mastoid air cells and cavum tympani with a dense content. No destruction or reactive sclerosis of the surrounding bone. B, CT scan from 2013. The presence of some dense content in residual mastoid air cells and cavum tympani can be seen. No destruction of the surrounding bone.

by incubation at 72°C for 7 minutes. The PCR products were analyzed by agarose gel electrophoresis.

Using this method, the tumorous tissue was negative for *NAB2-STAT6* fusion.

3. Discussion

There are tumors occurring outside the female genital tract, which contain a stroma identical to that seen in the ovary. Such tumors have been documented in the pancreas [1,3], liver, biliary tract [2,4], retroperitoneum [5,6], spleen, mesentery [7], and kidney [10,11] and in the paratesticular location [9]. Except for the latter location, these neoplasms affect mostly middle-aged women.

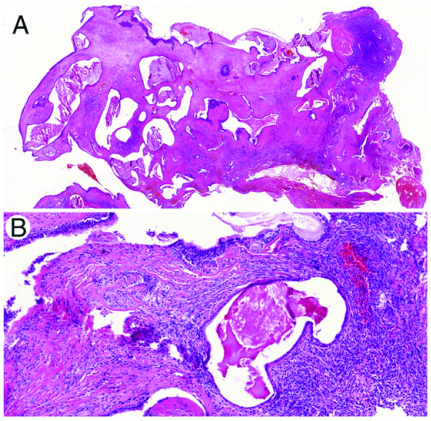

Fig. 2 A, The tumor consisted of irregular, polypoid masses containing multiple variably sized cystic spaces. The lumina of many cysts were filled with an eosinophilic secretion. The cysts were surrounded by the OS. B, The cystic spaces were lined by flat, cuboidal, or columnar epithelial cells, in many parts showing mucinous differentiation. Clusters of variably sized mucinous or seromucinous glands were scattered throughout the OS. As a rule, no cytological atypia or mitoses were present.

The tumor we report herein appeared histologically as a cyst-forming epithelial neoplasm featuring a prominent OS (Figs. 2 and 3). The inner surface of the cysts was lined by a flattened, cuboidal to columnar, in parts mucin-producing epithelium, and the neoplasm thus was microscopically most similar to the mucinous cystic neoplasms (MCNs) of the liver from the OS-containing family of tumors. In contrast, the pancreatic examples of MCN mostly present with tall, columnar, in most parts mucin-producing cells [17]. Similar to both pancreatic and liver counterparts, the epithelial cells of the neoplasm in our case expressed CK7, CK8, CK18, CK19, and EMA and were negative for CK20. The lining cells were immunonegative for mucin markers, including MUC2, MUC5AC, and MUC6, sharing thus the same bile duct immunophenotype as MCN of the liver and differing in this regard from MCNs of the pancreas that usually stain with MUC5AC [4,17]. There was expression of smooth muscle actin in the stromal component similar to the above-mentioned intra-abdominal neoplasms. The OS in our case was negative for ER, with only weak and very focal immunoreaction for PR (Fig. 3D). Nevertheless, positive immunoreaction for both receptors in the OS component of pancreatic MCNs is not a constant feature, seen in only 30% (ER) and 60%-90% (PR) of cases [4]. The same inconsistent results are also found in cases of MEST of the kidney [11] and MCNs at other sites. The stroma also reacted positively with the CD34 antibody. However, in our long experience with these tumors, we have repeatedly encountered CD34 positivity in the MEST of the kidney (unpublished observation, Michal M.).

The MEST of the kidney is a well-circumscribed, multilocular tumor showing variably sized cysts and glands separated by the OS. The epithelial component consists mostly of medium-sized cysts and glands/tubules lined by flat to

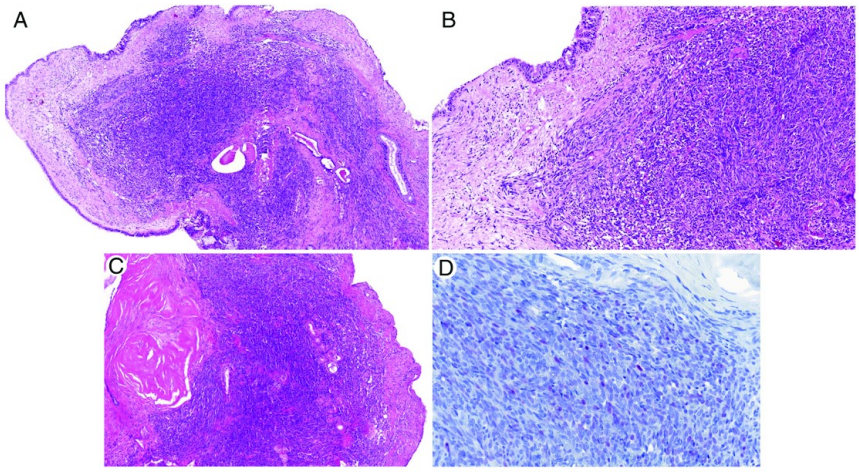

Fig. 3 A, The cysts were surrounded by the OS, focally with variably pronounced hyalinization. B, Higher magnification of the OS. C, Scarring of the stromal tissue resembling corpora albicantia. D, Focal and weak positivity with the antibody against PRs (alkaline phosphatase).

Table Immunohistochemical features

Antibody	Reactivity	Clone	Dilution	Manufacturer
PR	Positive—very focal and weak stromal staining	1E2	RTU	Ventana Medical Systems, Inc, Tucson, AZ
Actin S	Positive—stroma	1 A4	1:500	Dako, Glostrup, Denmark
Calponin	Negative	EP798Y	RTU	Ventana Medical Systems, Inc
CD34	Positive—stroma	QBEnd/10	1:200	Dako
S-100	Positive—lining of some cysts	Polyclonal	RTU	Ventana Medical Systems, Inc
AE1-3	Positive—epithelial lining diffusely	AE1/AE3 & PCK26	RTU	Ventana Medical Systems, Inc
CK7	Positive—epithelial lining diffusely	OV-TL12/30	1:200	Dako
CK8	Positive—epithelial lining diffusely	35ßH11	1:400	Ventana Medical Systems, Inc
CK18	Positive—epithelial lining diffusely	DC 10	RTU	Dako
CK19	Positive—epithelial lining diffusely	A53-B/A2.26	RTU	Ventana Medical Systems, Inc
EMA	Positive—epithelial lining diffusely	E29	1:400	Dako
Estrogen receptor	Negative	SP1	RTU	Ventana Medical Systems, Inc
Inhibin	Negative	R1	RTU	Ventana Medical Systems, Inc
Desmin	Negative	D33	1:200	Dako
CD56	Negative	MRQ-42	RTU	Ventana Medical Systems, Inc
HMB 45	Negative	HMB45	1:400	Dako
CK20	Negative	Ks20.8	1:100	Dako
CD-X2	Negative	EPR2764Y	RTU	Ventana Medical Systems, Inc
MUC 2	Negative	MRQ-18	RTU	Ventana Medical Systems, Inc
MUC 5AC	Negative	MRQ-19	RTU	Ventana Medical Systems, Inc
MUC 6	Negative	MRQ-20	RTU	Ventana Medical Systems, Inc
Antimucin monoclonal antibody	Negative	HIK1083	1:50	Cosmo Bio Co, Tokyo, Japan
PAX-8	Negative	Polyclonal	1:50	Cell Marque, Rocklin, CA
TLE-1	Negative	M-101	1:100	Santa Cruz Biotechnology, Inc, Dallas, TX

Abbreviation: RTU, ready to use.

cuboidal, hobnail, or rarely columnar cells that are positive with antibodies to cytokeratins AE1-3 [10]. Focally, the epithelium has Müllerian-type features, including endometrioid and tubal appearances; rarely, it may be pyloric and/or intestinal or urothelial [18]. The stromal properties of MEST of the kidney are virtually identical to those seen in the current case, including the presence of corpora albicantia–like areas (Fig. 3C). The occurrence of this feature in the OS-containing family of tumors represents, in our opinion, a type of nonspecific pattern of scarring with hyalinization as a reaction to trauma, identical to the reaction seen in ovaries after a rupture of primordial follicle. The broader variations in the microscopic appearances of the epithelial component are thus the only disparate feature of renal MEST. However, it is quite likely that with the recognition of new cases of MESTME, a similar diversity of the lining cells, which may be attributed to a metaplastic process, can be appreciated. Metaplasia was presumably also an important factor in the current tumor that featured various types of the epithelium, including a squamous epithelium, which is known to occur in this area because of metaplasia. It is also possible that the tumor growth itself was initiated by the long-standing chronic inflammation. To prove that the herein presented tumor is indeed of a neoplastic nature, we performed clonality analysis with an unequivocally positive result. Similarly to such tumors in other locations, the histogenesis of MESTME is unclear. Tumors with OS occur almost exclusively in middle-aged, perimenopausal women, which points to the importance of hormonal factors in the pathogenesis. The absence of mitoses and atypia, low rate of proliferation as measured by the staining of the MIB1 antibody (less than 1%), and the overall indolent clinical course marked only by a single recurrence during 7 years of follow-up indicate the benign nature of the tumor.

The only 2 reasonable differential diagnoses of the MESTME are synovial sarcoma and solitary fibrous tumor. Synovial sarcoma can be easily distinguished by means of immunohistochemistry. In this regard, TLE-1 appears to be the most useful because cytokeratins stained the adenomatous component in our case. Apart from TLE-1 negativity, negative immunoreaction of the stromal component for EMA, AE1-3, or other cytokeratins and the overall benign cytology along with a very low proliferative activity are features excluding synovial sarcoma. In ambiguous cases or in small tissue specimens, molecular genetic studies can be used. Although the tumor reacted with CD34 protein, the unlikely possibility of a solitary fibrous tumor with entrapped epithelial elements was ruled out based on the negative *NAB2-STAT6* fusion analysis.

Regarding the terminology, in spite of the very similar histopathologic features that the presented case shares with mucinous cystic neoplasms of the liver and to a lesser degree the pancreas, we would prefer the term *mixed epithelial and stromal tumor of the middle ear*. It is known that, in the past, tumors of various locations that did not show the defining OS component were often referred to as *mucinous cystic neoplasms* [19]. It was confusing, and it often created discrepancies concerning their clinicopathological features [3]. On the contrary, in MEST of the kidney, since its first description, the OS was a required diagnostic feature.

In summary, we described a benign tumor occurring in the middle ear of an elderly woman, which contained both epithelial and stromal components, with the latter being entirely composed of an OS. The morphological and immunohistochemical features of our case are similar to those seen in other OS-containing tumors occurring at different anatomic locations [4,17]. We therefore propose the term *mixed epithelial and stromal tumor of the middle ear*.

References

[1] Compagno J, Oertel JE. Mucinous cystic neoplasms of the pancreas with overt and latent malignancy (cystadenocarcinoma and cystadenoma). A clinicopathologic study of 41 cases. Am J Clin Pathol 1978;69:573-80.

[2] Devaney K, Goodman ZD, Ishak KG. Hepatobiliary cystadenoma and cystadenocarcinoma. A light microscopic and immunohistochemical study of 70 patients. Am J Surg Pathol 1994;18:1078-91.

[3] Jang KT, Park SM, Basturk O, et al. Clinicopathologic characteristics of 29 invasive carcinomas arising in 178 pancreatic mucinous cystic neoplasms with ovarian-type stroma: implications for management and prognosis. Am J Surg Pathol 2015;39:179-87.

[4] Zen Y, Pedica F, Patcha VR, et al. Mucinous cystic neoplasms of the liver: a clinicopathological study and comparison with intraductal papillary neoplasms of the bile duct. Mod Pathol 2011;24:1079-89.

[5] Roma AA, Malpica A. Primary retroperitoneal mucinous tumors: a clinicopathologic study of 18 cases. Am J Surg Pathol 2009;33:526-33.

[6] Matsubara M, Shiozawa T, Tachibana R, et al. Primary retroperitoneal mucinous cystadenoma of borderline malignancy: a case report and review of the literature. Int J Gynecol Pathol 2005;24:218-23.

[7] Shiono S, Suda K, Nobukawa B, et al. Pancreatic, hepatic, splenic, and mesenteric mucinous cystic neoplasms (MCN) are lumped together as extra ovarian MCN. Pathol Int 2006;56:71-7.

[8] Axiotis CA. Intratesticular serous papillary cystadenoma of low malignant potential: an ultrastructural and immunohistochemical study suggesting mullerian differentiation. Am J Surg Pathol 1988;12:56-63.

[9] Michal M, Kazakov DV, Kacerovska D, et al. Paratesticular cystadenomas with ovarian stroma, metaplastic serous mullerian epithelium, and male adnexal tumor of probable wolffian origin: a series of 5 hitherto poorly recognized testicular tumors. Ann Diagn Pathol 2013;17:151-8.

[10] Michal M, Syrucek M. Benign mixed epithelial and stromal tumor of the kidney. Pathol Res Pract 1998;194:445-8.

[11] Michal M, Hes O, Bisceglia M, et al. Mixed epithelial and stromal tumors of the kidney. A report of 22 cases. Virchows Arch 2004;445:359-67.

[12] Shelekhova KV, Calonje E, Grossmann P, et al. Superficial soft tissue biphasic synovial sarcoma with apocrine differentiation in the glandular component: a report of two cases. Am J Dermatopathol 2014;36:847-52.

[13] Hes O, de Souza TG, Pivovarcikova K, et al. Distinctive renal cell tumor simulating atrophic kidney with 2 types of microcalcifications. Report of 3 cases. Ann Diagn Pathol 2014;18:82-8.

[14] Gaffney R, Chakerian A, O'Connell JX, et al. Novel fluorescent ligase detection reaction and flow cytometric analysis of SYT-SSX fusions in synovial sarcoma. J Mol Diagn 2003;5:127-35.

[15] Antonescu CR, Kawai A, Leung DH, et al. Strong association of SYT-SSX fusion type and morphologic epithelial differentiation in synovial sarcoma. Diagn Mol Pathol 2000;9:1-8.

[16] Vogels RJ, Vlenterie M, Versleijen-Jonkers YM, et al. Solitary fibrous tumor—clinicopathologic, immunohistochemical and molecular analysis of 28 cases. Diagn Pathol 2014;9:224.

[17] Bosman FT, Carneiro F, Hruban RH, Theise ND. WHO classification of tumours of the digestive system. Lyon: IARC; 2010.
[18] Moch H, Humphrey PA, Ulbright TM, Reuter VE. WHO classification of tumours of the urinary system and male genital organs. Lyon: IARC; 2016.
[19] Gao ZH, Urbanski SJ. The spectrum of pulmonary mucinous cystic neoplasia: a clinicopathologic and immunohistochemical study of ten cases and review of literature. Am J Clin Pathol 2005; 124:62-70.

2. PART
CO-AUTHORED MANUSCRIPTS

2.1. SOFT TISSUES

2.2.1. FOLLICULAR DENDRITIC CELL SARCOMA: CLINICOPATHOLOGICAL STUDY OF 15 CASES WITH EMPHASIS ON NOVEL EXPRESSION OF MDM2, SOMATOSTATIN RECEPTOR 2A AND PD-L1

Follicular dendritic cell sarcoma (FDCS) is a rare neoplasm whose cells show phenotypic features of normal follicular dendritic cells (FDC). Only few larger series of this entity have been published since the description [31-35]. Being initially considered a low-grade malignancy, later series suggested a higher rate of aggressiveness and recommended considering FDCS a neoplasm of intermediate grade. Approximately half of the cases recurred locally after initial excision, whereas metastasis and death from the tumor were reported in half of cases [34, 36]. Diagnosis of FDCS mainly relies on characteristic histologic appearance supplemented by IHC and, if necessary, electron microscopy [37]. Due to rarity and hence limited familiarity with the histologic features of FDCS, this entity is known for being frequently misdiagnosed as other neoplasms of epithelial, mesenchymal, meningeal, or hematolymphoid origin [38]. In addition to the classical FDC markers such as CD21, CD23, CD35, and CNA.42, the list of markers found to be frequently expressed in FDCS is ever increasing. In this study, we reviewed clinicopathologic features of 15 FDCS and stained them for novel markers in addition to survey of conventional FDC markers. Based on observations (by the first author) of somatostatin receptor type 2A (SSTR2A) expression in native lymphoid follicles surrounding a metastatic neuroendocrine tumor and of an MDM2-positive FDCS submitted for second opinion as dedifferentiated liposarcoma, we assumed that these 2 markers might be expressed in FDCS.

Altogether we collected 15 cases. Patients were 7 men and 7 women (1 unspecified), with a mean age of 47 years (20-75 years). The tumor site was lymph nodes (6) or spleen (2), both (1) and extranodal sites of head and neck (4) or abdominal cavity (2). Treatment was variable combinations of surgery and aggressive chemotherapy/radiotherapy. Four of 8 patients with follow-up died of disease within 1 to 10 years.

To confirm the diagnosis, we performed a wide panel of antibodies, whose expression have been reported in FDCS. Additionally, to further analyze the cases, we stained them for newly reported or novel markers (PD-L1, Rb1, MDM2, and somatostatin receptor 2A [SSTR2A]) and performed MDM2 FISH to assess the presence of this gene's amplification.

Eventually, all tumors expressed at least 1 FDC marker. Most importantly, five of 14 cases (36%) stained strongly for SSTR2A with a distinctive membranous pattern. Seven (54%) of 13 assessable cases showed moderate to strong membranous staining for PD-L1 in greater than 5% of the neoplastic cells. The Rb1 antigen was lost in 4 (28%) of 14 cases. MDM2 stained less than 5% to 20% of the tumor cells in 5 (36%) of 14 cases; 2 of them showed amplification by FISH. CDK4 was negative except for weak staining in 1 of 14 cases.

This study adds to the existing few clinicopathologic series on FDCS and represents the first study to show MDM2 amplification in this entity. Our results regarding frequent SSTR2A expression in FDCS are novel and might be of potential diagnostic and therapeutic relevance. Expression of SSTR2A in any neoplasm has the potential relevance of being of value as a biomarker used in imaging examination to detect tumors and their metastases (as a tracer for scintigraphy), but might also be of value for specific treatment such as radioactive peptide

receptor therapy as in neuroendocrine neoplasms. FDCS occurring within the retroperitoneum and/or the abdominal cavity may closely mimic dedifferentiated liposarcoma, particularly if MDM2 positive and/or amplified and should thus be carefully assessed for expression of FDC markers.

Annals of Diagnostic Pathology 23 (2016) 21–28

Contents lists available at ScienceDirect

Annals of Diagnostic Pathology

Follicular dendritic cell sarcoma: clinicopathologic study of 15 cases with emphasis on novel expression of MDM2, somatostatin receptor 2A, and PD-L1☆

Abbas Agaimy, MD [a,*], Michael Michal, MD [b], Ladislav Hadravsky, MD [c,d], Michal Michal, MD [c]

[a] Institute of Pathology, University Hospital, Erlangen, Germany
[b] Department of Pathology, Charles University, Biomedical Center, Faculty of Medicine in Plzen and Charles University Hospital Plzen, Plzen, Czech Republic
[c] Department of Pathology, Faculty of Medicine, Charles University, Plzen, Czech Republic
[d] Department of Pathology, Charles University, 3rd Medical Faculty and Charles University Hospital Royal Vineyards, Prague, Czech Republic

ARTICLE INFO

Keywords:
Follicular dendritic cell sarcoma
FDC tumor
MDM2
Somatostatin receptor
PD-L1
Head and neck
Spleen

ABSTRACT

Follicular dendritic cell sarcoma (FDCS) is a rare low-grade neoplasm with the phenotype of FDC cells. This rare sarcoma has been well known for being mistaken for a variety of neoplasms (mainly meningioma), particularly at extranodal sites. Diagnosis of FDCS mainly relies on characteristic histologic appearance supplemented by immunohistochemistry and electron microscopy. In this study, we reviewed 15 FDCSs retrieved from our consultation files and stained them for newly reported or novel markers (PD-L1, Rb1, MDM2, and somatostatin receptor 2A [SSTR2A]) in addition to conventional FDC markers. Patients were 7 men and 7 women (1 unspecified) with a mean age of 47 years (20-75 years). The tumor site was lymph nodes (6) or spleen (2), both (1) and extranodal sites of head and neck (4) or abdominal cavity (2). Treatment was variable combinations of surgery and aggressive chemotherapy/radiotherapy. Four of 8 patients with follow-up died of disease within 1 to 10 years. All tumors expressed at least 1 FDC marker: CD21 (8/13), CD23 (2/13), CD35 (8/12), CNA.42 (13/14), Clusterin (8/13), Fascin (15/15) and D2-40/podoplanin (7/14). Epstein-Barr virus (EBER-1/2 in situ hybridization) was performed successfully in 10 conventional variants; all were negative. Five of 14 cases (36%) stained strongly for SSTR2A with a distinctive membranous pattern. Residual lymphoid follicles surrounding some of the tumors stained similarly for SSTR2A. Seven (54%) of 13 assessable cases showed moderate to strong membranous staining for PD-L1 in greater than 5% of the neoplastic cells. The Rb1 antigen was lost in 4 (28%) of 14 cases. MDM2 stained less than 5% to 20% of the tumor cells in 5 (36%) of 14 cases; 2 of them showed amplification by fluorescence in situ hybridization (FISH). CDK4 was negative except for weak staining in 1 of 14 cases. This study adds to the existing few clinicopathologic series on FDCS and represents the first study to show MDM2 amplification in this entity. Our results regarding frequent SSTR2A expression in FDCS are novel and might be of potential diagnostic and therapeutic relevance. SSTR2A expression in FDCS represents a further confusing factor when thinking of meningioma which uniformly expresses this receptor. FDCS occurring within the retroperitoneum and/or the abdominal cavity may closely mimic dedifferentiated liposarcoma, particularly if MDM2 positive and/or amplified and should thus be carefully assessed for expression of FDC markers.

1. Introduction

Follicular dendritic cell sarcoma (FDCS) is a rare neoplasm whose cells show phenotypic features of normal FDCs. Since first description in 1986 [1], only a few case series have been published on this entity [2–5]. Follicular dendritic cell sarcoma has been well known for being mistaken for a variety of neoplasms (mainly meningioma), particularly at extranodal sites. Diagnosis of FDCS mainly relies on characteristic histologic appearance supplemented by immunohistochemistry (IHC) and, if necessary, electron microscopy [6]. Reported cases suggested a behavior that is more akin to sarcoma than lymphoma [2–5]. Being initially considered a low-grade malignancy, later series suggested a higher rate of aggressiveness and recommended considering FDCS a neoplasm of intermediate grade [4,7]. Approximately half of the cases recurred locally after initial excision, whereas metastasis and death from the tumor were reported in half of cases. This tumor has been increasingly recognized at extranodal sites including in particular head and neck organs and intra-abdominal structures. Distinctive variant of FDCS has been reported including "hepatosplenic inflammatory pseudotumor (IPT)–like FDCS," which is uniformly associated with

☆ Conflict of interest: None.

* Corresponding author at: Pathologisches Institut, Universitätsklinikum Erlangen, Krankenhausstrasse 8-10, 91054 Erlangen, Germany. Tel.: +49 9131 85 22288; fax: +49 9131 85 24745.
E-mail address: abbas.agaimy@uk-erlangen.de (A. Agaimy).

http://dx.doi.org/10.1016/j.anndiagpath.2016.05.003
1092-9134/

Table 1
Clinicopathologic features of FDCSs (n = 15)

No.	Age (y)/sex	Site	Size (cm)	Associated disease?	Treatment	MTS (time and site)	Follow-up duration and outcome
1[a]	58/M	LN and spleen	1-7	Polyclonal gammopathy (2 subsets of IgG/lambda-and 1 subset of IgA/lambda-positive paraproteins)	Repeated excisions	Multiple (5) recurrences in cervical LN	DOD 10 y after the first occurrence, generalization into the right cervical, paratracheal lymph nodes and spleen
2	36/M	LN subclavicular	2	None	Excision	Recurrence same location (4 y), excised	4 mo after recurrence NED
3	29/F	Spleen (332 g)	4	Sideropenic anemia	Splenectomy	None	NED (16 y)
4	28/M	Mesenteric root and mesenteric nodes	11	None (FDCS initially misdiagnosed as HL)	CT (COPP, 6xBEACOPP), resection	Retroperitoneal and cervical node MTS (1 y)	DOD 11 mo after MTS
5	58/M	LN supraclavicular	3	None	Excision, CH (COPP, doxorubicin, ifosfamide, gemcitabin, docetaxel)	Brain MTS (4 y)	DOD 5 mo after brain MTS
6	69/F	LN submandibular	NA	None	Excision and CT (6xCOEP21)	None	NED (4 y)
7	21/F	Soft tissue cheek	NA	None	NA	NA	NA
8	NA	Parapharyngeal region	NA	None	NA	NA	NA
9	26/M	Processus frontalis maxilla, spread to nasopharynx, skull base, and parapharyngeal	8.5	None	Resection + CT (ifosfamide, adriamycin) + RT (55.6 Gy)	Lung (5 y) treated by CT + RT	NED (14 y after MTS)
10	58/F	LN	NA	NA	NA	NA	NA
11	51/F	LN cervical	NA	NA	NA	NA	NA
12	66/M	LN	NA	NA	NA	None	Recent case
13	20/F	Pelvic retroperitoneum/mesentery	13.5	Extensive extramedullary hemopoesis in the liver	Ifosfamide + doxorubicin, then radical surgery	Synchronous liver MTS	DOD 12 mo
14	69/M	Spleen	5.3 cm	Synchronous ccRCC	Surgery	Local recurrence + liver MTS (4 mo)	AWD under chemotherapy
15	75/F	Posterior oropharynx + nasopharynx	NA	NA	Partial excision, very recent case	None	Recent case

Abbreviations: AWD, alive with disease; ccRCC, clear cell renal cell carcinoma; DOD, died of disease; F, female; HL, Hodgkin lymphoma; LN, lymph node; M, male; MTS, metastasis; NA, not available; NED, no evidence of disease.
[a] Case published previously [15].

clonal Epstein-Barr virus (EBV) infection of the tumor cells [8], "eosinophil-rich granulomatous variant" of the latter [9], "folliculocentric FDCS" mimicking a lymphoproliferative neoplasm [10], "FDCS showing features of sinus lining cells" [11], and other rare features.

Due to rarity and hence limited familiarity with the histologic features of FDCS, this entity is known for being frequently misdiagnosed as other neoplasms of epithelial, mesenchymal, meningeal, or hematolymphoid origin [12]. In addition to the classical FDC markers such as CD21, CD23, CD35, and CNA.42, the list of markers found to be frequently expressed in FDCS is ever increasing to include clusterin [13], fascin [13], D2-40 (podoplanin) [14], and others. In this study, we reviewed clinicopathologic features of 15 FDCS and stained them for novel markers in addition to survey of conventional FDC markers. Based on recent observations (by the first author) of somatostatin receptor type 2A (SSTR2A) expression in native lymphoid follicles surrounding a metastatic neuroendocrine tumor and of an MDM2-positive FDCS submitted for second opinion as *dedifferentiated liposarcoma*, we assumed that these 2 markers might be expressed in FDCS.

2. Material and methods

Cases were retrieved from our consultation files. A tumor was accepted as FDCS if it showed characteristic histology as defined for this entity, expressed at least 1 of 4 definitional FDC markers (CD21, CD23, CD35, CNA42), did not reveal any features of another definable entity other than FDCS and, if negative for FDC markers, showed ultrastructural features of FDCS (only 1 case was included by the latter definition). Case 1 has been reported before [15]. Interestingly, this case which predated the original description of the entity by Monda et al [1] was sent initially to Professor Karl Lennert (Kiel, Germany) for second opinion, who classified it as a "sinus-lining cell tumor". The tumor specimens were generally fixed in buffered formalin and embedded routinely for light microscopic examination. However, because some cases were retrieved as a consultation material from different countries through the globe, the tissue preservation and quality of fixation seem to vary greatly. Therefore, if both the tumor cells and the surrounding native lymphoid follicles seemed to be nonreactive for any of the FDC markers, the results were considered equivocal (no results; see Table 2). Immunohistochemical studies were performed on 3- to 4-μm sections cut from paraffin blocks using a fully automated system ("Benchmark XT System"; Ventana Medical Systems Inc, Tucson, Arizona) and the following antibodies: CD21 (clone 1F8, 1:100; Dako, Hamburg, Germany), CD23 (clone SP23, 1:100; Thermo Scientific, Waltham, MA), CD35 (clone Ber-MAC-DRC, 1:50; Dako), CNA.42 (clone CNA.42, 1:100; Dako), Fascin (clone 55 k-2, ready-to-use; Ventana), Clusterin (clone 41D, 1:100; Biocare Medical, Concord, CA), podoplanin (clone D2-40, 1:50; Zytomed, Berlin, Germany), SSTR2A (polyclonal, 1:100; Zytomed), PD-L1 (clone 28-8, 1:200; Abcam, Cambridge, UK), retinoblastoma antigen 1 (Rb1, clone G3-245, 1:200; BD-Pharmingen, Heidelberg, Germany), MDM2 (clone IF1, 1:50; CalBiochem, San Diego, CA) and CDK4 (clone DCS-156, 1:100; Zytomed).

2.1. Evaluation and scoring of SSTR2A and PD-L1 in FDCS

Expression of the SSTR2A was scored according to the proposal published by Volante et al [16], that is, score 0 (no staining at all), score 1+ (only cytoplasmic staining independent of extent), score 2+ (membranous staining in <50% of tumor cells irrespective of cytoplasmic staining), and score 3+ (membranous staining in ≥50% of tumor cells irrespective of cytoplasmic staining). For PD-L1, the scoring

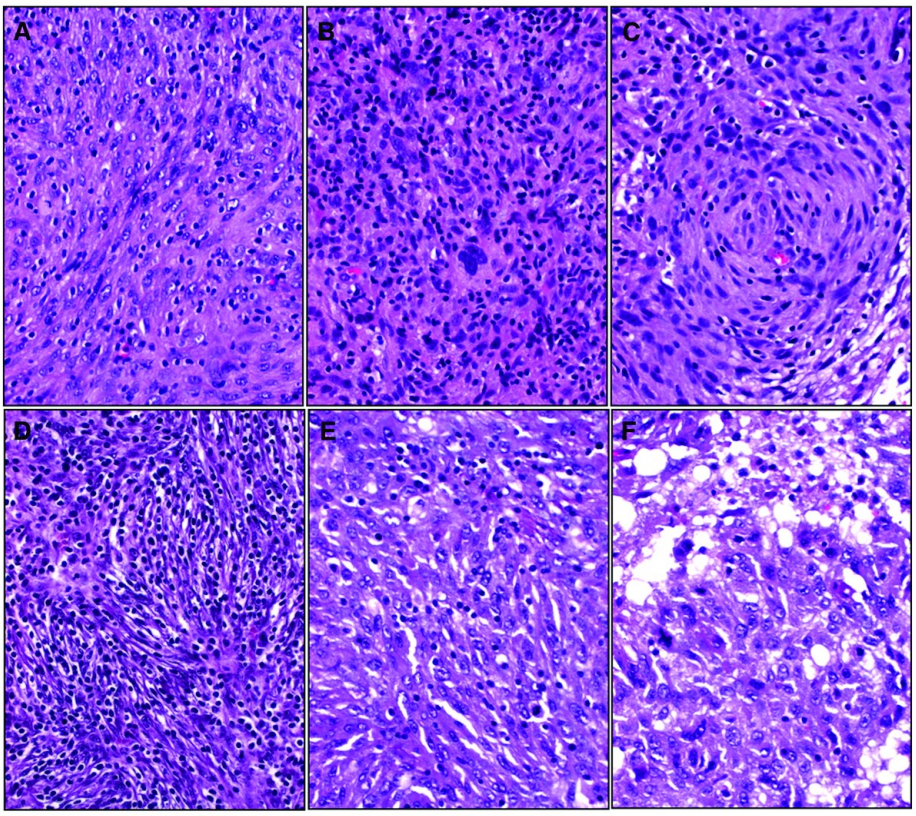

Fig. 1. Representative examples of FDCS illustrating sweeping fascicles of plump ovoid cells with fascicular nuclei and sprinkling of small mature lymphocytes (A) that were occasionally very prominent (B; note binucleated pleomorphic larger cells). (C) Meningothelial-like whorls were occasionally seen. Splenic FDCS showed either IPT-like pattern (D) or conventional features of FDCS (E). (F) Sarcomatous features with focal necrosis, atypical mitoses, and vacuolated cells (possibly artifact) might be mistaken for dedifferentiated liposarcoma if MDM2-positive. Images A-C from case 15, D from case 3, and E/F from case 14.

system used recently by Xu et al [17] has been adopted in this study; that is, distinctive membranous staining in at least 5% of tumor cells showing either moderate (2+) or strong (3+) staining was scored PD-L1 positive as opposed to those with either less than 5% staining irrespective of intensity or pattern and those with absent (0) or weak (1+) staining irrespective of the extent of staining tumor cells.

In addition to IHC as described above, assessment of the MDM2 gene locus was performed by fluorescence in situ hybridization (FISH) on freshly cut sections prepared from formalin-fixed, paraffin-embedded tumor tissue blocks using ZytoLight Dual Color Probes (ZytoVision, Bremerhaven, Germany) with standard protocols according to the manufacturer's instructions. Fifty tumor cell nuclei were assessed and cases with a ratio greater than 2 were considered amplified. Epstein-Barr virus status was evaluated with the in situ hybridization method using EBER 1/2 probes (ZytoVision) according to the manufacturer instructions.

3. Results

3.1. Clinical features

Patients were 7 men and 7 women (sex was not specified in 1 patient; Table 1). Their age range was 20 to 75 years (mean, 47 years; median, 54 years). Median age was 51 and 58 years for women and men, respectively. The tumor originated in lymph nodes in 6 cases, within the spleen in 2 cases, involved both in 1 case and within extranodal nonsplenic sites in the head and neck region in 4 cases and the intra-abdominal and retroperitoneal soft tissue in 2 patients. Treatment was a variable combination of surgical excision, aggressive chemotherapy, and radiotherapy but varied from case to case. Follow-up was available in 9 patients and ranged from 4 months to 19 years. Local recurrence developed in 3 patients; one of them developed generalized disease 10 years later and died and another developed liver metastasis at same time as local recurrence. In total, 4 of 8 patients with follow-up died of disease within 1 to 10 years. Of note, 3 of 4 patients who died of their disease had intra-abdominal tumors.

3.2. Pathological findings

Tumor size ranged from 2 to 13.5 cm (mean, 6.8 cm). Grossly, tumors were described as well-circumscribed fleshy tan masses of soft consistency. Histologic examination showed characteristic features of FDCS as reported earlier in case series on this entity. The tumor cells were elongated with tapered nuclei, vesicular chromatin with small nucleoli, and pale-eosinophilic cytoplasm with indistinct cell borders (Fig. 1A, B). Most tumors showed sweeping fascicles and storiform pattern occasionally closely mimicking that of meningioma and fibrous histiocytomas (Fig. 1C). The background showed variably vascularized fibrocollagenous stroma with sprinkling of small mature lymphocytes

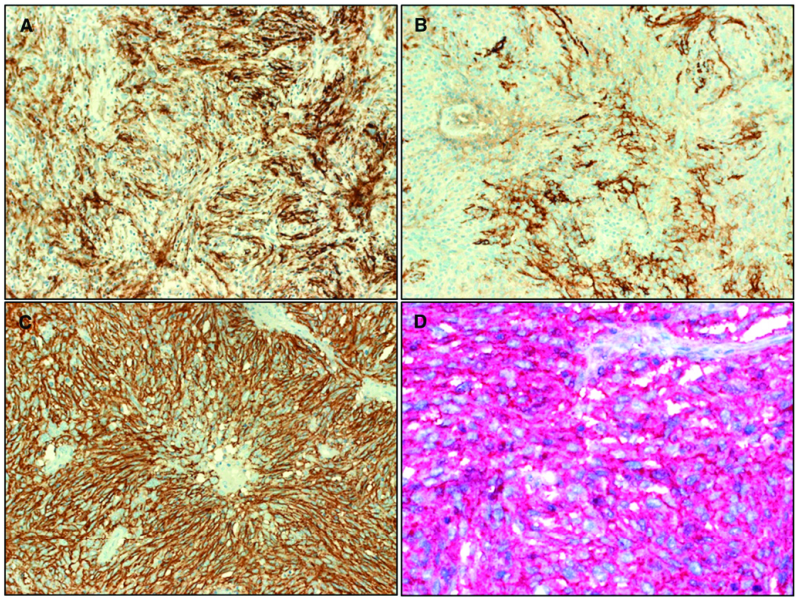

Fig. 2. Representative examples of FDC marker expression. Prominent CD21 (A) and variable CD23 (B) expression in case 15. Case 14 showed very strong and diffuse CD23 (C) and CNA.42 (D) expression.

between the tumor cells. The numbers of background lymphocytes varied greatly from case to case and within the same tumor (Fig. 1A-F). Scattered pleomorphic tumor cells with enlarged occasionally bilobated nuclei were a frequent feature in most of tumors (Fig. 1B), but diffuse high-grade or pleomorphic nuclei were uncommon, except in one splenic tumor (Fig. 1F). The latter showed frequent foci of coagulative necrosis and focal frankly sarcomatous features with paucity of lymphocytes. Mitotic figures were seen but were usually infrequent, although some tumors showed brisk and atypical mitoses (Fig. 1F). In the nodal cases, residual lymphoid follicles were seen frequently at the periphery of the neoplasm. One splenic tumor showed features of IPT-like FDCS with abundance of background mononuclear cells, mainly lymphocytes, with scattered slender FDCs showing elongated communicating dendritic cytoplasmic processes (Fig. 1D). The other splenic case showed features of conventional FDCS with variable sarcomatous areas. One retroperitoneal tumor presented initially with hepatic metastasis that closely mimicked the IPT-like variant associated with extensive extramedullary hematopoesis but lacked EBV infection by in situ hybridization. However, later resection of the hepatic metastases and the primary retroperitoneal tumor showed conventional FDCS.

3.3. Immunohistochemical findings

By IHC, all tumors expressed at least 1 FDC markers used in this study: CD21 (8/13; Fig. 2A), CD23 (2/13; Fig. 2B, C), CD35 (8/12), CNA42 (13/14; Fig. 2D), Clusterin (8/13), Fascin (15/15) and D2-40/podoplanin (7/14; Table 2). The staining was variable but usually homogenous within the tumors in cases with well-preserved tumor tissue, in particular in the most recent cases, possibly due to better fixation properties. CD23 varied from focal (Fig. 2B) to extensive strong staining (Fig. 2C). The residual lymphoid follicles of lymph nodes or spleen were similarly stained. Regarding expression of SSTR2A, variable staining was seen in 7 cases; of them 5 cases were scored positive with moderate to strong distinctive membranous staining in the tumor cells (2+/3+). Pure cytoplasmic staining was seen in 2 tumors, but in these 2 tumors, it was difficult to reliably distinguish pure cytoplasmic staining from membranous staining due to scarcity of the tumor cell cytoplasm (Fig. 3A). Thus, 5 (36%) of 14 assessable FDCS cases were unequivocally positive for the SSTR2A in this study (Fig. 3B, C). Notably, residual lymphoid follicles surrounding some of the tumors within lymph nodes or spleen showed similar staining pattern for SSTR2A indicating an inherent property of the FDCs and excluding an aberrant expression confined to neoplastic cells (Fig. 3B, inset).

All of 10 cases successfully evaluated for EBV status by in situ hybridization (all were conventional FDCS) were EBV negative.

Regarding PD-L1, 7 (54%) of 13 assessable cases showed moderate to strong membranous staining in more than 5% of the neoplastic cells. The remainder were either completely negative (2 cases) or showed weak or pure cytoplasmic staining. The different patterns of PD-L1 are shown in Fig. 3D-F).

The Rb1 antigen was successfully evaluated in 14 cases. Four tumors (28%) showed complete loss of RB1 in the neoplastic cells with retained expression in the background inflammatory and lymphoid cells (Fig. 3G), whereas additional 2 cases showed hybrid or mosaic pattern. The remaining 8 cases were intact (Fig. 3G, inset).

MDM2 IHC showed moderate to strong nuclear expression in 5 (36%) of 14 tumors ranging from less than 5% to 20% of the tumor cells. The MDM2-positive tumor cells were evenly distributed within the tumor and no focal aggregation or clustering was observed (Fig. 3H). Fortunately, all 5 MDM2-positive tumors could be assessed successfully by FISH; 2 of 5 cases showed amplification of the MDM2 gene locus, one of them also with evidence of polyploidy. Consistent with the MDM2 IHC, the amplified cells were scattered among a background of cells having normal signals (Fig. 3I). Thus, no diffuse high-level amplification affecting all or most of neoplastic cells as would be expected in dedifferentiated liposarcoma was seen. On the other hand, only a single case among 14 cases stained with CDK4 showed weak expression in the tumor cell nuclei. This case was negative for MDM2 alterations both by IHC and by FISH. Of the 4 cases

Table 2
Immunohistochemical and molecular findings in FDCSs (n = 15)

No.	histology	CD21	CD23	CD35	CNA42	D2-40	Clusterin	Fascin	EBV (EBER CISH)	SSTR2A	PD-L1	Rb1	MDM2 IHC	MDM2 FISH	CDK4 IHC
1	Conventional	−	NR	−	+	+	+	+	−	1+	−	Intact	NR	NR	−
2	Conventional	+	NR	+	+	−	−	+	−	NR	NR	NR	−	NR	−
3	IPT-like	+	−	−	NR	−	NR	+	NR	1+	−	Loss	−	NR	−
4	Conventional	+	−	+	+	+	+	+	NR	2+	+ (20%/3+)	Intact	5%+	Normal	−
5	Conventional	NR	−	−	+	NR	−	+	−	0 (V + LF+)	+ (10%/2+)	Intact	−	Normal	Weak diffuse
6	Conventional	−	−	−	+	−	−	+	−	0 (V+)	+ (30%/2+)	Hybrid	−	Normal	−
7	Conventional	NR	−	+	+ (wk)	+	−	+ (wk)	−	2+	+ (40%/2+)	Loss	10%+	Amplified	−
8	Conventional	+	−	+	−	+	+	+	NR	3+	NR	Loss	−	Normal	−
9	Conventional	+	−	+	+	+	+	+	NR	0 (V+)	− (70%/1+) cytoplasmic	Hybrid	5%-10%+	Normal	NR
10	Conventional	+	−	+ (wk)	+	+	NR	+ (wk)	−	0 (V+)	+ (50%/2+)	Intact	−	NR	NR
11	Conventional	−	−	NR	+	+	+	+	−	0 (V+)	−(<5%/1+)	Intact	−	Normal	NR
12	Conventional	−	−	NR	+	−	−	+	−	0 (V + LF+)	+ (20%/2+)	Intact	−	Normal	−
13	Conventional	+	−	+ (wk)	+	−	+	+	−	0	− (60%/1+)	Loss	−	NR	−
14	Conventional	−	+	NR	+	−	+ (wk)	+	−	3+	− (10%/1+), cytoplasmic	Intact	20+	Amplified + polyploidy	−
15	Conventional	+	+	+	+	−	+	+	NR	3+	+ (70%/3+)	Intact	<5+	Normal	−

Abbreviations: CISH, chromogenic in situ hybridization; LF+, lymphoid follicles positive; NR, no results due to poor staining quality or suboptimal tissue preservation; V+, vessels positive.

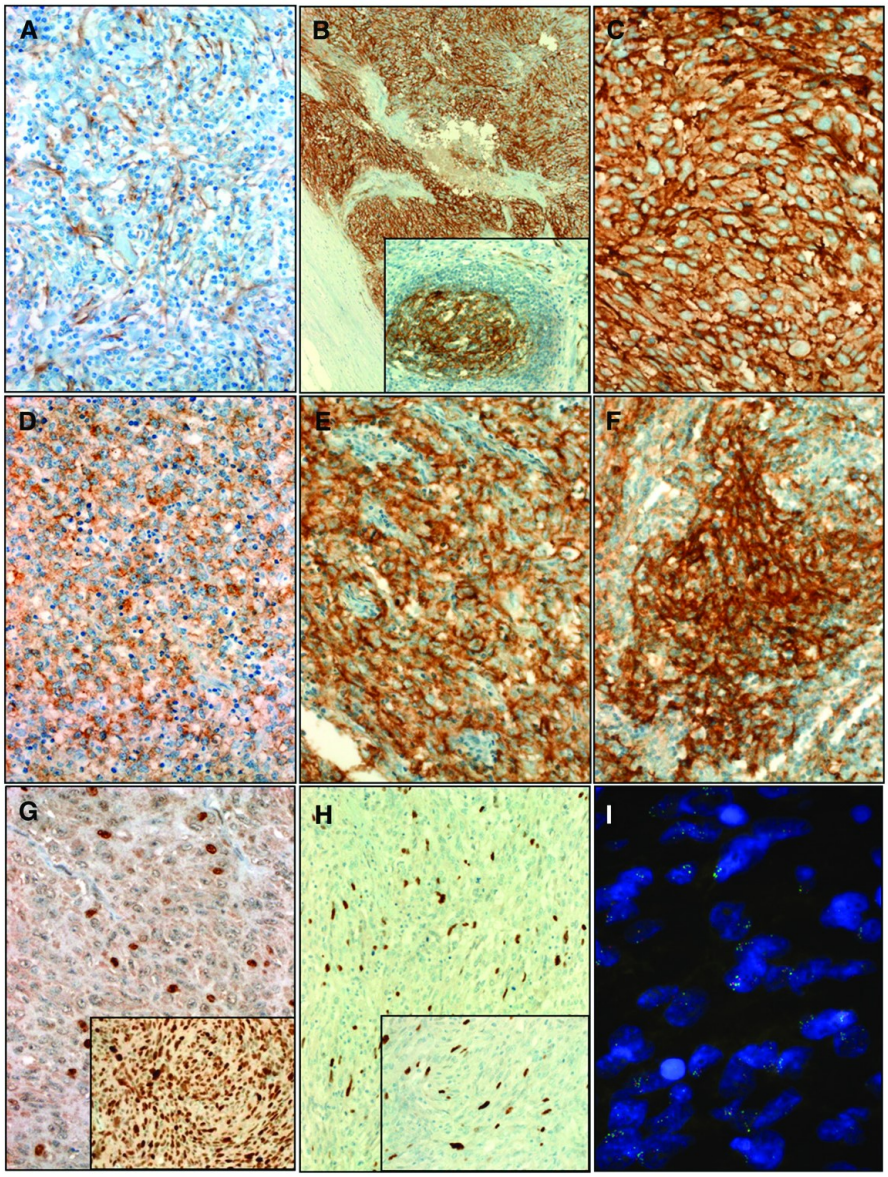

Fig. 3. Expression of novel markers in FDCS. SSTR2A expression highlighting the delicate dendritic cell processes in case 3 (A) and showing distinctive membranous reactivity (3+) in all of tumor cells in case 14 (B, C). (B) Inset: normal lymphoid follicle expresses SSTR2A; note also weak staining in vessels. Expression of PD-L1 in FDCS ranged from weak cytoplasmic (D; case 9) to moderate membranous (E; case 6) to strong membranous (F; case 4). The latter 2 patterns are considered positive. Four cases showed Rb1 loss (G; case 7). (G) Inset: intact Rb1 was seen in 8 cases (image case 15). MDM2 was expressed in a subset of tumor cells ranging from less than 5% to 20% (H; image case 7). (G) Inset: higher magnification showed nuclear staining of tumor cells. (I) MDM2-FISH probe showed several tumor cells with more than 5 green MDM2 signals indicating amplification in a subpopulation of tumor cells (image case 7).

with Rb1 loss, only 1 case showed MDM2 expression by IHC. This case was also MDM2 amplified by FISH.

4. Discussion

Follicular dendritic cell sarcoma is a rare neoplasm that is well known for its differential diagnostic confusion with a variety of other neoplasms of epithelial, mesenchymal, meningeal, and melanocytic origin. Since the first description of this enigmatic neoplasm by Monda et al [1] in 1986, only very few case series have been published [2–5].

Our series is consistent with previous series that a considerable fraction of FDCS originates at extranodal sites and that at least 50% of patients with extended follow-up died of their disease after experiencing local disease recurrence, distant metastasis, or both [4–6]. Our study also

highlights the significant variation in the frequency of expression of the different FDC markers with significantly variable pattern from one tumor to another. This fact underlines the need for an extended FDC marker panel for confirming diagnosis.

A novel aspect in our study is the observation of a frequent specific (membranous) expression of the SSTR2A in at least 36% of the cases. We observed the more extensive and strong SSTR2A expression in 2 recent cases that we encountered during preparation of this study. Both cases showed better antigen preservation and reactivity for all markers so that one would speculate about a possibly higher frequency of SSTR2A expression in this entity. Future studies on more cases are going to illuminate this point. SSTR2A has been increasingly recognized to be expressed in a variety of nonneuroendocrine neoplasms including meningioma [18,19], phosphaturic mesenchymal tumors [20], and other entities. Of note, a case of intra-abdominal FDCS showed aberrant expression of neuroendocrine markers (synaptophysin and NSE) [21]. This rare finding and also the frequent expression of SSTR2A we describe herein should not lead to an erroneous diagnosis of neuroendocrine neoplasm metastatic to lymph node.

From a differential diagnostic point of view, meningioma is the most relevant among these SSTR2A-positive entities, given the fact that the classical histomorphology of FDCS has been traditionally likened to that of meningioma so that a meningioma-like whorled pattern in a neoplasm should always alert to the possibility of FDCS. This topic has been further complicated by the uniform expression of EMA in meningioma [18] and in up to 87% of FDCS [4]. In the current study, we add a new aspect in the differential diagnosis "meningioma vs FDCS" by reporting a novel expression of SSTR2A in a subset of FDCS (≥36%). In a recent study, 87% of meningiomas of different types expressed strongly SSTR2A, whereas a single case (5%) of soft tissue perineurioma did [18]. The pattern of SSTR2A expression in meningioma is membranous with or without cytoplasmic staining and is essentially identical to that we describe herein for FDCS. Expression of SSTR2A in any neoplasm has the potential relevance of being of value as a biomarker used in imaging examination to detect tumors and their metastases (as a tracer for scintigraphy), but might also be of value for specific treatment such as radioactive peptide receptor therapy as in neuroendocrine neoplasms. Our observation that surrounding normal lymphoid follicles showed similar staining for SSTR2A as their tumors points to a consistent expression, thus highlighting this receptor as a potential additional FDC marker, but extended future studies evaluating larger case series and including other variants of accessory cell neoplasms are mandatory for validation of this finding.

In this study, we observed expression of the programmed cell death 1 ligand PD-L1 in 54% of FDCS. Our findings are consistent with 2 very recent studies. Increased expression of PD-L1 (ie, ≥2 +/≥5% of tumor cells) was reported in all 3 FDCSs examined in the study by Gatalica et al [22]. In addition, Xu et al [17] reported strong membranous expression of PD-L1 in 10 of 20 FDCSs, whereas reactive lymphoid follicles did not show any expression indicating a novel tumor-associated biomarker. These studies indicate a potential benefit of immune therapy using checkpoint inhibitors in treating these tumors.

The molecular pathogenesis of FDCS remains largely obscure. BRAF V600E mutations were found in 19% of cases in a recent study [24], but none was detected in another study [23]. More recently, Griffin et al [23] analyzed 13 FDCSs using a panel of 309 genes well known to be frequently associated with different cancers. They detected loss-of-function alterations in tumor suppressor genes known to be involved in the regulation of NF-κB (38%) and cell cycle (31%) pathway. Loss of Rb1 by IHC was noted in 2 of 13 cases; both showed genetic alterations of Rb1 [23]. Four cases showed copy number gains of MDM2 and CDK4, but IHC of these 2 markers was not mentioned. Our results are consistent with these results concerning Rb1 loss, which we detected in 4 of 14 cases in addition to 2 cases with mosaic pattern for Rb1.

Recently, Creytens [25] described 5 FDCSs arising in the abdominal cavity (3 in the mesentery and 2 in the retroperitoneum). All 5 cases showed strong diffuse nuclear expression of MDM2, but all lacked MDM2 amplification by FISH. However, CDK4 was not mentioned. The findings in the Creytens series differ from our current study in 2 aspects: (1) MDM2 positivity in our series is limited to a subpopulation of neoplastic cells (<5%-20%) as opposed to diffuse staining in his series, and (2) we detected unequivocal amplification of MDM2 locus by FISH in 2 of 5 positive cases, whereas all of his cases lacked amplification. Notably, our cases (with one exception) were all negative with CDK4 antibody, a finding not expected in liposarcoma.

It is noteworthy in this regard to point out the observation of Cokelaere et al. [26], who detected rearrangement of the high mobility group I-C (HMGIC) in a case of hyaline vascular Castleman disease, which is known to be a potential precursor for a subset of FDCS [27,28]. HGMIC is known to be rearranged in ordinary lipoma and it is amplified in atypical lipomatous tumors as well [29]. Italiano et al [30] showed that in well-differentiated/dedifferentiated liposarcoma CDK4 (12q14.1) belongs to a different amplicon than MDM2 (12q15) and that CDK4 is not overexpressed/amplified in 13% of the cases as opposed to 100% overexpression/amplification of MDM2. Taken together, these findings of HMGI-C, CDK4, and MDM2 protein overexpression in atypical lipomatous tumors and the observation of HMGIC in the FDCs of hyaline-vascular Castleman disease and of MDM2 expression/amplification in a subset of FDCS suggest involvement of the 12q14-15 locus in a subset of FDCS.

In summary, we reported herein detailed clinicopathologic features of a larger series of FDCS, hereby illuminating frequent expression of novel potential therapeutic biomarkers including SSTR2A and PD-L1 and highlighting frequent expression of MDM2 and occasional MDM2 amplification in a subset of cases. Our results are of potential value regarding diagnosis, differential diagnosis, and treatment of these rare aggressive sarcomas, for which no specific treatment strategies are established yet.

References

[1] Monda L, Warnke R, Rosai J. A primary lymph node malignancy with features suggestive of dendritic reticulum cell differentiation. A report of 4 cases. Am J Pathol 1986;122:562–72.

[2] Perez-Ordonez B, Erlandson RA, Rosai J. Follicular dendritic cell tumor: report of 13 additional cases of a distinctive entity. Am J Surg Pathol 1996;20:944–55.

[3] Raymond I, Al Saati T, Tkaczuk J, Chittal S, Delsol G. CNA.42, a new monoclonal antibody directed against a fixative-resistant antigen of follicular dendritic reticulum cells. Am J Pathol 1997;151:1577–85.

[4] Chan JK, Fletcher CD, Nayler SJ, Cooper K. Follicular dendritic cell sarcoma. Clinicopathologic analysis of 17 cases suggesting a malignant potential higher than currently recognized. Cancer 1997;79:294–313.

[5] Soriano AO, Thompson MA, Admirand JH, Fayad LE, Rodriguez AM, Romaguera JE, et al. Follicular dendritic cell sarcoma: a report of 14 cases and a review of the literature. Am J Hematol 2007;82:725–8.

[6] Perez-Ordoñez B, Rosai J. Follicular dendritic cell tumor: review of the entity. Semin Diagn Pathol 1998;15:144–54.

[7] Pang J, Mydlarz WK, Gooi Z, Waters KM, Bishop J, Sciubba JJ, et al. Follicular dendritic cell sarcoma of the head and neck: case report, literature review, and pooled analysis of 97 cases. Head Neck 2016(38 Suppl 1):E2241–9.

[8] Cheuk W, Chan JK, Shek TW, Chang JH, Tsou MH, Yuen NW, et al. Inflammatory pseudotumor-like follicular dendritic cell tumor: a distinctive low-grade malignant intra-abdominal neoplasm with consistent Epstein-Barr virus association. Am J Surg Pathol 2001;25:721–31.

[9] Li XQ, Cheuk W, Lam PW, Wang Z, Loong F, Yeong ML, et al. Inflammatory pseudotumor–like follicular dendritic cell tumor of liver and spleen: granulomatous and eosinophil-rich variants mimicking inflammatory or infective lesions. Am J Surg Pathol 2014;38:646–53.

[10] Lorenzi L, Lonardi S, Petrilli G, Tanda F, Bella M, Laurino L, et al. Folliculocentric B-cell–rich follicular dendritic cells sarcoma: a hitherto unreported morphological variant mimicking lymphoproliferative disorders. Hum Pathol 2012;43:209–15.

[11] Krokowski M, Merz H, Thoms C, Bernd HW, Schade U, Le Tourneau A, et al. Sarcoma of follicular dendritic cells with features of sinus lining cells—a new subtype of reticulum cell sarcoma? Virchows Arch 2008;452:565–70.

[12] Pai VD, Desai S, Desouza A, Saklani AP. Extranodal follicular dendritic cell sarcoma: a frequently misdiagnosed entity. J Postgrad Med 2015;61:55–6.

[13] Grogg KL, Macon WR, Kurtin PJ, Nascimento AG. A survey of clusterin and fascin expression in sarcomas and spindle cell neoplasms: strong clusterin immunostaining is highly specific for follicular dendritic cell tumor. Mod Pathol 2005;18:260–6.

[14] Yu H, Gibson JA, Pinkus GS, Hornick JL. Podoplanin (D2-40) is a novel marker for follicular dendritic cell tumors. Am J Clin Pathol 2007;128:776–82.

[15] Michal M, Koza V, Jindra P. Spindle cell tumor of lymph node of probable reticulum origin associated with multiclonal gammopathy. Zentralbl Pathol 1994;140:165–72.
[16] Volante M, Brizzi MP, Faggiano A, La Rosa S, Rapa I, Ferrero A, et al. Somatostatin receptor type 2A immunohistochemistry in neuroendocrine tumors: a proposal of scoring system correlated with somatostatin receptor scintigraphy. Mod Pathol 2007;20:1172–82.
[17] Xu J, Sun HH, Fletcher CD, Hornick JL, Morgan EA, Freeman GJ, et al. Expression of programmed cell death 1 ligands (PD-L1 and PD-L2) in histiocytic and dendritic cell disorders. Am J Surg Pathol 2016;40:443–53.
[18] Agaimy A, Buslei R, Coras R, Rubin BP, Mentzel T. Comparative study of soft tissue perineurioma and meningioma using a five-marker immunohistochemical panel. Histopathology 2014;65:60–70.
[19] Menke JR, Raleigh DR, Gown AM, Thomas S, Perry A, Tihan T. Somatostatin receptor 2a is a more sensitive diagnostic marker of meningioma than epithelial membrane antigen. Acta Neuropathol 2015;130:441–3.
[20] Houang M, Clarkson A, Sioson L, Elston MS, Clifton-Bligh RJ, Dray M, et al. Phosphaturic mesenchymal tumors show positive staining for somatostatin receptor 2A (SSTR2A). Hum Pathol 2013;44:2711–8.
[21] Padilla-Rodríguez AL, Bembassat M, Lazaro M, Ortiz-Hidalgo C. Intra-abdominal follicular dendritic cell sarcoma with marked pleomorphic features and aberrant expression of neuroendocrine markers: report of a case with immunohistochemical analysis. Appl Immunohistochem Mol Morphol 2007;15:346–52.
[22] Gatalica Z, Bilalovic N, Palazzo JP, Bender RP, Swensen J, Millis SZ, et al. Disseminated histiocytoses biomarkers beyond BRAFV600E: frequent expression of PD-L1. Oncotarget 2015;6:19819–25.
[23] Griffin GK, Sholl LM, Lindeman NI, Fletcher CD, Hornick JL. Targeted genomic sequencing of follicular dendritic cell sarcoma reveals recurrent alterations in NF-κB regulatory genes. Mod Pathol 2016;29(1):67–74.
[24] Go H, Jeon YK, Huh J, Choi SJ, Choi YD, Cha HJ, et al. Frequent detection of BRAF(V600E) mutations in histiocytic and dendritic cell neoplasms. Histopathology 2014;65:261–72.
[25] Creytens D. MDM2 expression in extranodal abdominal and retroperitoneal follicular dendritic cell sarcomas, mimicking dedifferentiated liposarcomas. Appl Immunohistochem Mol Morphol 2016;24:e25–7 [Epub ahead of print].
[26] Cokelaere K, Debiec-Rychter M, De Wolf-Peeters C, Hagemeijer A, Sciot R. Hyaline vascular Castleman's disease with HMGIC rearrangement in follicular dendritic cells: molecular evidence of mesenchymal tumorigenesis. Am J Surg Pathol 2002;26:662–9.
[27] Chan JK, Tsang WY, Ng CS. Follicular dendritic cell tumor and vascular neoplasm complicating hyaline-vascular Castleman's disease. Am J Surg Pathol 1994;18:517–25.
[28] Kazakov DV, Morrisson C, Plaza JA, Michal M, Suster S. Sarcoma arising in hyaline-vascular Castleman disease of skin and subcutis. Am J Dermatopathol 2005;27:327–32.
[29] Tallini G, Dal Cin P, Rhoden KJ, Chiapetta G, Manfioletti G, Giancotti V, et al. Expression of HMGI-C and HMGI(Y) in ordinary lipoma and atypical lipomatous tumors: immunohistochemical reactivity correlates with karyotypic alterations. Am J Pathol 1997;151:37–43.
[30] Italiano A, Bianchini L, Keslair F, Bonnafous S, Cardot-Leccia N, Coindre JM, et al. HMGA2 is the partner of MDM2 in well-differentiated and dedifferentiated liposarcomas whereas CDK4 belongs to a distinct inconsistent amplicon. Int J Cancer 2008;122:2233–41.

2.2.2. LITTORAL CELL ANGIOMA OF THE SPLEEN: A STUDY OF 25 CASES WITH CONFIRMATION OF FREQUENT ASSOCIATION WITH VISCERAL MALIGNANCIES

In this paper we have studies the largest series of rare splenic tumors called Littoral cell angioma (LCA). This tumor has two fairly unique features. Firstly, it seems to be associated with malignancies as there are numerous literature reports regarding this association. Secondly, the cell of origin, i.e. the littoral cell, has a unique immunophenotype, expression both endothelial and histiocytic markers. Our study focused on both of these aspects.

Regarding the first facet, we have collected a detailed follow-up information for 11 of our cases. Additionally, an extensive literature review was undertaken to summarize all the known tumor associations published in the literature.

To further analyze the immunophenotype, we applied an extensive panel of both reported and novel endothelial and histiocytic markers including LYVE-1, factor VIII, FLI-1, vascular endothelial growth factor receptor 2, VEGFR-3, claudin-5, ERG, LMO2, CD31, CD163, lysozyme, WT-1, CD4, D2-40, CD8, and factor XIIIa. Although a wide spectrum of these markers (except for the latter four) were expressed in the LCA, many of them more or less also reacted with the surrounding splenic parenchyma. Eventually, the three antibodies we found most useful in the diagnosis of LCA were Claudin-5, Vascular endothelial growth factor receptor 2 and CD11c which were expressed exclusively in the LCA areas and not in the splenic tissue.

The result of this study is the expanded spectrum of immunohistochemical features of LCA, which may facilitate the diagnosis, especially in ambiguous cases. For practical purposes, we recommended the combined use of the vascular markers vascular endothelial growth factor receptor 2, claudin-5, and the more widely available factor VIII, together with the histiocytic markers CD163, CD4, and CD11c. Such a combination of vascular and histiocytic markers is highly specific for LCA. To add even more specificity, the absence of staining of WT-1 in LCA, which is very rare among splenic vascular tumors, can be also exploited. Finally, we confirmed frequent associations of LCA with various visceral malignancies (>60%), and showed that the associated malignancies are not always epithelial, as suggested previously [39], but comprise a whole spectrum of neoplastic diseases.

Based on the marked presence with malignant tumors, one is tempted to speculate whether the development of these two, or sometimes even multiple (!!) seemingly unrelated tumors might be the result of some kind of tumor syndrome. We plan to further investigate such possibility.

Histopathology

Histopathology 2016, **69**, 762–774. DOI: 10.1111/his.13026

Littoral cell angioma of the spleen: a study of 25 cases with confirmation of frequent association with visceral malignancies

Kvetoslava Peckova,[1] Michael Michal,[1,2] Ladislav Hadravsky,[1] Saul Suster,[3] Ivan Damjanov,[4] Marketa Miesbauerova,[1] Dmitry V Kazakov,[1] Zdenka Vernerova[5] & Michal Michal[1]

[1]*Department of Pathology, Charles University, Medical Faculty and Charles University Hospital Plzen, Pilsen, Czech Republic,* [2]*Biomedical Centre, Faculty of Medicine in Plzen and Charles University Hospital Plzen, Pilsen, Czech Republic,* [3]*Department of Pathology and MCW Cancer Center, Medical College of Wisconsin, Milwaukee, WI, USA,* [4]*Department of Pathology and Laboratory Medicine, The University of Kansas School of Medicine, Kansas City, KS, USA, and* [5]*Department of Pathology, Charles University, Third Medical Faculty and Charles University Hospital Kralovske Vinohrady, Prague, Czech Republic*

Date of submission 1 March 2016
Accepted for publication 30 June 2016
Published online *Article Accepted* 4 July 2016

Peckova K, Michal M, Hadravsky L, Suster S, Damjanov I, Miesbauerova M, Kazakov D V, Vernerova Z & Michal M

(2016) *Histopathology* **69**, 762–774. DOI: 10.1111/his.13026

Littoral cell angioma of the spleen: a study of 25 cases with confirmation of frequent association with visceral malignancies

Aims: Littoral cell angioma (LCA) is a rare primary splenic tumour that is frequently associated with internal malignancies. Immunohistochemistry can demonstrate a distinct hybrid endothelial–histiocytic phenotype of littoral cells, and is a helpful adjunct for making the correct diagnosis. The aims of this study were to present a series of 25 LCAs, with an emphasis on the frequent association of the neoplasm with visceral malignancies, and to provide a detailed immunohistochemical analysis by employing new markers.

Methods and results: All 25 cases with available tissue blocks were immunohistochemically stained for endothelial and histiocytic markers. Clinical and follow-up data were retrieved from the respective institutions. The tumours were obtained from 16 males and nine females, whose age ranged from 32 to 86 years (mean 56.2 years). Clinical information was available for 24 of 25 patients, and follow-up for 11 of 25 patients (range 2–19 years; mean 11.6 years). Immunohistochemically, all cases were positive for LYVE-1, factor VIII, FLI-1, vascular endothelial growth factor receptor (VEGFR)-2, VEGFR-3, claudin-5, ERG, LMO2, CD31, CD163, lysozyme, and CD4, but negative for D2-40, CD8, and factor XIIIa. Fifteen of 25 cases were associated with various malignancies, including epithelial, mesenchymal and haematological tumours.

Conclusions: The cohort of 25 patients is the largest series of LCAs published to date. By using antibodies against recently introduced endothelial markers, we have expanded the immunoprofile of LCA. We have further highlighted the clinical significance of LCA, as more than half of the patients in this study also harboured a coexisting visceral malignancy. Therefore, we conclude that the finding of splenic LCA mandates a thorough clinical evaluation for a concomitant malignancy.

Keywords: immunohistochemistry, littoral cell angioma, spleen, vascular tumours, visceral malignancies

Address for correspondence: Kvetoslava Peckova, MD. Department of Pathology, Charles University, Medical Faculty and Charles University Hospital Plzen, Alej Svobody 80, 304 60 Pilsen, Czech Republic. e-mail: peckova.kveta@gmail.com

Introduction

Littoral cell angioma (LCA) is a rare primary tumour of the spleen that originates from the cells lining the splenic red pulp sinuses. These littoral cells are characterized by a distinct hybrid endothelial–histiocytic immunophenotype, and the correct diagnosis is thus established with immunohistochemical methods, which prove this dual differentiation.

Since the initial description of 17 cases of LCA in 1991,[1] only scattered case reports and a few series of LCA have been published.[2–26] A striking association between LCA and internal malignancies has been postulated in a small series of four cases in the past.[4] As a point of reference, we have reviewed all previously published malignancies from patients with LCA, and tabulated these published data for future use.

The rarity of LCA prompted us to collect as many cases as possible and to address two critical questions: how often are LCAs associated with other neoplastic conditions, and can the dual differentiation of the littoral cells be immunohistochemically confirmed by the use of some novel and/or recently developed antibodies against endothelial and histiocytic markers?

Materials and methods

The 25 cases constituting the subject of this study were retrieved from the author's files; they came from the period between 1993 and 2015. Two of the included cases have been previously published.[4] The clinical information was extracted from the registry records, and follow-up data were obtained from the attending clinicians. For 17 of 25 cases, paraffin tissue blocks were available. For conventional microscopy, tissues were fixed in formalin, routinely processed, embedded in paraffin, cut into 4-μm-thick sections, and stained with haematoxylin and eosin.

The immunohistochemical analysis was performed with a Ventana BenchMark ULTRA (Ventana Medical Systems, Tucson, AZ, USA). Antibodies were used against the following: factor VIII (polyclonal; Cell Marque, Rocklin, CA, USA) ready to use (RTU), CD31 (monoclonal, JC70A; Dako, Glostrup, Denmark) 1:40, FLI-1 (monoclonal, MRQ-1; Cell Marque, Rocklin, CA, USA), ERG (monoclonal, EPR3864; Ventana Medical Systems), LMO2 (monoclonal, SP51; Spring Bioscience, Pleasanton, CA, USA) 1:100, vascular endothelial growth factor receptor (VEGFR) (monoclonal, 55B11; Cell Signaling Technology, Danvers, MA, USA) 1:50, claudin-5 (monoclonal, 4C3C2; Invitrogen, Camarillo, CA, USA) 1:100, LYVE-1 (polyclonal; Abcam, Cambridge, UK) 1:50, podoplanin (monoclonal, D2-40; Dako) RTU, anti-WT-1 (monoclonal, 6F-H2; Dako) 1:50, CD4 (monoclonal, SP35; Ventana Medical Systems) RTU, CD8 (monoclonal, SP57; Ventana Medical Systems) RTU, CD11c (monoclonal, 5D11; Zytomed Systems, Berlin, Germany) 1:50, CD163 (monoclonal, MRQ-26; Cell Marque), lysozyme (polyclonal; Cell Marque) RTU, and factor XIIIa (monoclonal, clone AC-1A1; Cell Marque).

The primary antibodies were visualized with alkaline phosphatase or peroxidase as the detection system (both from Ventana Medical Systems). Only slides with positive controls were evaluated, which explains the slight variation in the number of evaluated slides. Immunohistochemical slides were considered to be positive when they showed clear and diffuse staining of the LCA luminal cells. When only focal LCA cells expressed a given marker or only the cells underlying the tall, plump LCA-lining cells were reactive, the result was regarded as negative.

Results

The clinical features are summarized in Table 1. There were 16 males and nine females, with ages ranging from 32 to 86 years (mean 56.2 years, median 51 years). Clinical information was available for 24 of 25 patients, and follow-up was available for 11 of 25 patients, ranging from 2 to 19 years (mean 11.6 years, median 15 years). Fifteen of 125 cases were associated with various malignancies, including epithelial, mesenchymal and haematological neoplasms.

GROSS DESCRIPTION

Grossly, the lesions always led to splenomegaly with the presence of multiple variably sized spongy and cystic nodules on the cut section. The tumours were well demarcated and compressed the adjacent splenic parenchyma but were not encapsulated. The colour of the lesions varied from dark red to brown and black, because of blood products of varying chronicity.

MORPHOLOGY

Tumour size ranged from only small foci in an otherwise unremarkable splenic parenchyma to large lesions almost completely replacing most of the splenic parenchyma. All lesions comprised multiple nodules ranging from 2 to 40 mm in diameter.

Table 1. Clinicopathological features

Case	Age (years)	Sex	Size of the spleen (mm)	Weight of the spleen (g)	Size of the tumour (mm)	Clinical information and FU
1	62	F	190 × 110 × 50	310	Multiple nodules 4–10	Endometrioid endometrial adenocarcinoma. Died of unknown cause 6 years after splenectomy
2	63	F	NA	NA	NA	Surgery for rupture of the spleen. Chronic lymphocytic leukaemia. Bone marrow biopsy in 2011 without leukaemic infiltration. AW at 19-year FU
3	53	F	NA	NA	Multiple nodules 10–30	Surgery for pancreatic adenocarcinoma with multiple distant metastases, at the same time as splenectomy. LFU
4	74	M	NA	NA	Multiple nodules, variable size	Colorectal adenocarcinoma. DOD
5	44	M	200 × 130 × 50	1450	Multiple nodules up to 25	Malignant lymphoma. LFU
6	83	M	140 × 100 × 60	200	Multiple nodules 4–12	Renal cell carcinoma resected in 2005, splenectomy in 2006, multiple myeloma diagnosed in 2011, adenocarcinoma of ascending colon (not known when). Died of multiple myeloma
7	55	M	130 × 90 × 60	NA	Multiple nodules up to 20	Clear-cell renal cell carcinoma. AW at 18-year FU
8	70	M	140 × 110 × 40	220	Multiple nodules 2–14	PH of prostate cancer and gastric spindle-cell tumour. At time of splenectomy, diagnosed with gastric GIST, low grade. LFU
9	49	M	150 × 140 × 20	500	Multiple nodules 10–40	Idiopathic thrombocytopenia. LFU
10	61	M	95 × 70 × 30	180	Multiple nodules 3–25	Colonic cancer diagnosed in 1997. Surgery performed for positive lymph nodes on PET/CT. LFU
11	49	M	160 × 100 × 35	720	Multiple nodules up to 12	Thyroid gland cancer. Surgery performed for suspicious nodules of the spleen detected on CT scan. LFU
12	48	F	NA	NA	Two small samples of the spleen, each measuring 13 × 5 × 1	Breast cancer. AW at 2-year FU
13	63	F	NA	180	Multiple nodules 3–8	Malignant melanoma removed in 1999. Splenectomy for suspicious splenic nodules at the same time. AW at 17-year FU
14	86	M	100 × 60 × 80	NA	NA	Colonic adenocarcinoma removed together with the tumour of the spleen. Died of sepsis
15	43	M	NA	NA	Multiple nodules up to 15	Splenomegaly. AW at 15-year FU
16	51	F	NA	NA	Multiple nodules 6–18	Splenomegaly. Chronic hepatitis C. AW at 6-year FU

Table 1. *(Continued)*

Case	Age (years)	Sex	Size of the spleen (mm)	Weight of the spleen (g)	Size of the tumour (mm)	Clinical information and FU
17	51	F	NA	NA	Multiple nodules, unknown size	Splenomegaly. AW at 2-year FU
18	45	M	NA	NA	Multiple nodules 5–20	Splenomegaly. AW at 9-year FU
19	32	M	NA	734	NA	NA
20	61	M	NA	NA	NA	Colonic adenocarcinoma resected in 1997. Splenectomy in 2005. LFU
21	64	M	220 × 180 × 100	3700	NA	Splenectomy for the tumour diagnosed as partially littoral cell angioma, and partially littoral cell haemangioendothelioma. Recurrence after 8 years, with an abdominal mass and multiple liver metastases. DOD
22	74	F	NA	240	Multiple nodules 5–40	Haemolytic anaemia, autoimmune thrombocytopenia (Evans syndrome). LFU
23	37	M	NA	720	Multiple nodules 5–30	Splenomegaly. Anaemia, thrombocytopenia. AW at 17-year FU
24	55	F	NA	370	Multiple nodules up to 25	Splenomegaly. Ulcerative colitis. AW at 17-year FU
25	50	M	NA	400	Multiple nodules, unknown size	Surgery for clear-cell renal cell carcinoma, at the same time as splenectomy. LFU

AW, Alive and well; CT, Computed tomography; DOD, Died of disease; F, Female; FU, follow-up; GIST, Gastrointestinal stromal tumour; LFU, Lost to follow-up; M, Male; NA, not available; PET, Positron emission tomography; PH, Personal history.

Histologically, all tumours in our study were consistent with the typical morphological pattern of LCA described previously in the literature.[4]

All angiomas were characterized by blood-filled, anastomosing vascular spaces reminiscent of normal splenic sinuses. The vascular channels varied in width; some were cystically dilated, whereas others presented with narrow lumina only slightly wider than normal splenic sinuses. Vascular spaces were lined with flat and tall endothelial cells, which sloughed off into the lumina (Figures 1 and 2) and focally showed haemophagocytosis. In some areas, papillary fronds were also evident, whereas no truly solid growth and necrosis were seen anywhere. No atypia was found and the proliferative activity was unremarkable in all cases, with only occasional mitotic figures being observed. Additionally, some cases featured a few foci of extramedullary haematopoiesis with sparse megakaryocytes and islands of haematopoietic precursors within the vascular tumour bed. Normal splenic sinuses were present at the periphery of lesions in the splenic red pulp.

IMMUNOHISTOCHEMISTRY

Immunohistochemical findings for all of the vascular and histiocytic markers employed are summarized in Table 2. All staining results refer to LCA cells only. Of the vascular markers, factor VIII showed, in each case, strong cytoplasmic staining of the luminal cells lining both the normal splenic sinuses and LCA. A very similar staining pattern was observed with CD31, although the positivity was stronger in LCA cells than in splenic sinuses. LYVE-1 also showed cytoplasmic positivity in both normal sinuses and, even more strongly, in LCA-lining cells, but also (and sometimes strongly) stained a high number of lymphocytes of the white and red pulp. In two cases, LYVE-1 showed no reactivity. ERG, LMO2 and FLI-1 showed a very similar staining pattern, with nuclear positivity in both LCA and normal splenic sinuses and capillaries. The only two vascular markers that stained almost exclusively LCA-lining cells were claudin-5 (Figure 3) and VEGFR-2 (Figure 4), which otherwise reacted only in small splenic capillaries.

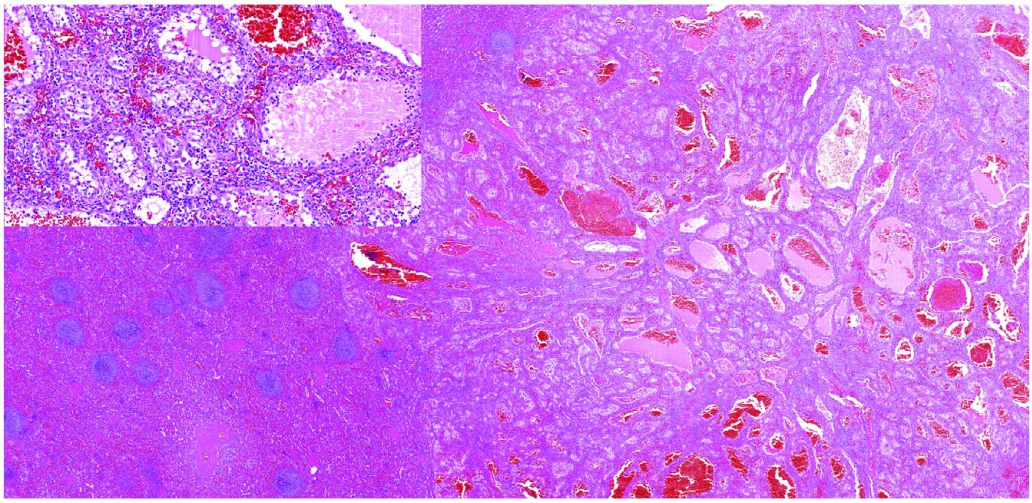

Figure 1. Characteristic multinodular growth, in this case partially replacing the normal splenic parenchyma. There are anastomosing vascular channels of varying width, separated by stromal septa. The inset figure shows a detailed view of vascular spaces reminiscent of splenic sinuses.

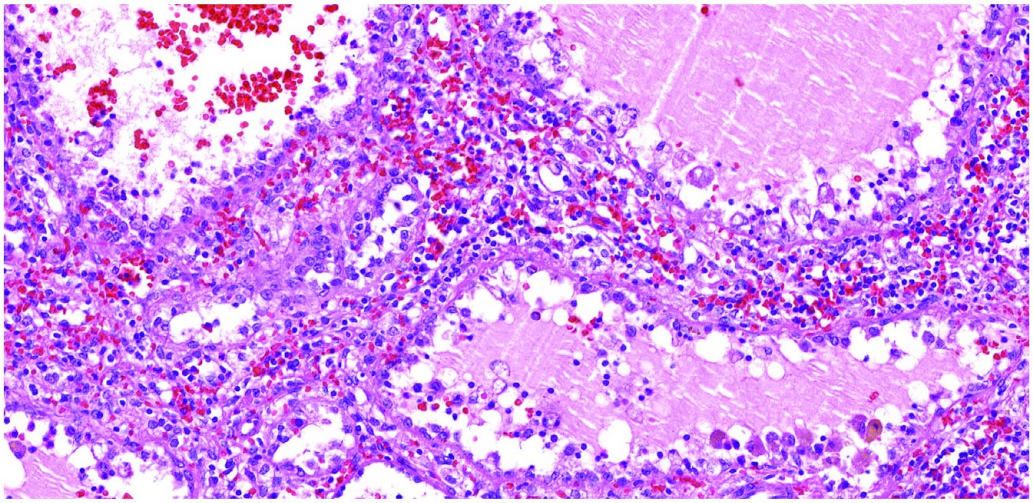

Figure 2. Single layer of bland-looking plump lining cells of the littoral phenotype sloughing off into the blood-filled vascular spaces.

Although the intensity varied considerably, both markers showed clear cytoplasmic staining in all cases of LCA. WT-1 was strongly expressed in the cytoplasm of unaltered splenic sinusoids, but was absent in the LCA endothelium. With the exception of splenic lymphatic channels, podoplanin showed no expression.

Most of the histiocytic markers used in our study, i.e. CD163, CD11c, CD4, and lysozyme, showed a very similar pattern of staining, namely cytoplasmic

Table 2. Immunohistochemical results

Factor VIII	16/16 (100%)	Claudin-5	17/17 (100%)
++	16	++	12
+	0	+	5
–	0	–	0
CD31	15/15 (100%)	CD4	16/16 (100%)
++	15	++	16
+	0	+	0
–	0	–	0
CD163	17/17 (100%)	CD11c	14/16 (88%)
++	16	++	7
+	1	+	7
–	0	–	2
Lysozyme	15/15 (100%)	Podoplanin	0/15 (0%)
++	15	++	0
+	0	+	0
–	0	–	15
VEGFR2	17/17 (100%)	LYVE-1	13/13 (100%)
++	9	++	13
+	8	+	0
–	0	–	0
FLI-1	15/15 (100%)	Factor XIIIa	0/17 (0%)
++	11	++	0
+	4	+	0
–	0	–	17
ERG	16/16 (100%)	WT-1	0/17 (0%)
++	15	++	0
+	1	+	0
–	0	–	17
LMO2	17/17 (100%)	CD8	0/15 (0%)
++	15	++	0
+	2	+	0
–	0	–	15

VEGFR, Vascular endothelial growth factor receptor; ++, strong and diffuse staining; +, weak or focal staining; –, absence of staining.

positivity of the tall, plump, LCA-lining cells, and varying degrees of positivity in ubiquitous splenic histiocytic cells of the red pulp. Lysozyme stained the highest number of non-LCA cells, whereas CD11c appeared to be the most specific marker for LCA. However, CD11c was entirely absent in two cases, and in several other lesions the expression was fairly weak. Factor XIIIa and CD8 did not react in any cells.

Discussion

Littoral cell angioma is a rare primary tumour of presumed vascular origin, and was first described in 1991 by Falk *et al.*, who reported a series of 17 cases.[1] Since then, ~150 cases of LCA have been reported. This lesion is unique to the spleen, and does not appear to possess a soft tissue or lymph node counterpart. LCA shows neither a gender nor an age predilection. The exact prevalence of LCA is unknown, partly because of the rarity of these tumours.[27]

Most LCAs are clinically latent. Symptomatic cases may manifest with fever of unknown origin, abdominal pain, and, relatively often, with splenomegaly and clinical evidence of hypersplenism, including anaemia, thrombocytopenia, or pancytopenia.[28] LCA is usually discovered incidentally on imaging studies or after a splenectomy performed for splenomegaly of unknown aetiology. Although the radiological features of LCA have been well described, there is a lack of specificity in differentiating this tumour from other primary and more common vascular splenic neoplasms, metastases, disseminated infections, or sarcoidosis. The diagnosis is only possible after microscopic examination,[29] as a characteristic feature of LCA is considered to be multinodular growth partially or even totally replacing the normal splenic parenchyma. The splenic involvement is distinguished by anastomosing monotonous vascular channels resembling splenic sinuses, but lined by tall endothelial cells with variable degrees of haemophagocytosis.[4] The Ki67 index tends to be very low (<1%), as repeatedly described in previous reports.[1,9,10,30]

Littoral cells show dual endothelial and histiocytic differentiation, and are considered to be different from common endothelial cells. The immunoprofile of positive staining for factor VIII, CD31, ERG, CD68, CD163, CD21, cathepsin D, and vimentin, accompanied by an absence of staining for CD34, CD8, and

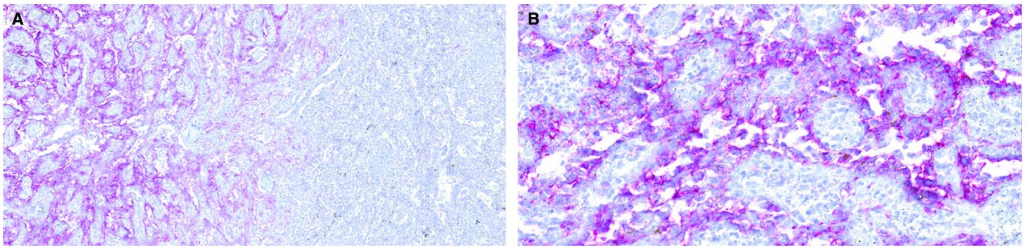

Figure 3. Claudin-5 stains only the cells of littoral cell angioma (**B**), and not the normal splenic red and white pulp cells (**A**).

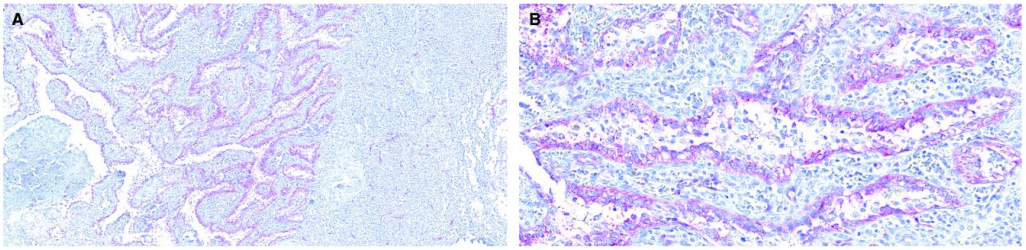

Figure 4. Vascular endothelial growth factor receptor 2 (VEGFR2) stains only the cells of littoral cell angioma (LCA) (**B**), and not the normal splenic red and white pulp cells (**A**).

WT-1, is considered to be typical for LCA.[9,31] In addition, endothelial differentiation of the LCA cells was proven at the ultrastructural level by the finding of cytoplasmic Weibel–Palade bodies, subcellular structures characteristic of endothelial cells.[32] The coexpression of histiocytic markers and some endothelial markers is thought to be specific for LCA.

In the current study, besides using previously known diagnostic markers of LCA, we also investigated the expression of novel endothelial and histiocytic markers, which have not been examined in the diagnostic process for LCA to date. Of these novel markers, the positive staining for VEGFR-2, FLI-1, claudin-5, CD4, CD11c, and LYVE-1, and the absence of staining for podoplanin and factor XIIIa, has produced a new expanded immunoprofile that is more specific for LCA.

FLI-1 is a member of the ETS family of transcription factors. In the haematopoietic system, FLI-1 plays an important role in megakaryocytic differentiation, and has been implicated in myelomonocytic, erythroid and natural killer cell development. In addition, FLI-1 has been shown to be involved in the embryonic development of blood vessels. In normal tissues, FLI-1 is preferentially expressed by lymphatic and blood vessel endothelial cells and by some haematopoietic cells, such as T lymphocytes and megakaryocytes, but it has also been reported in the breast, prostate, colon, and squamous epithelium. As FLI-1 is a transcription factor, its immunoreactivity is nuclear in location. This marker has been reported to be commonly expressed by all types of benign and malignant endothelial tumours, including haemangiomas, epithelioid haemangioendotheliomas, angiosarcomas, and Kaposi sarcomas. It is also frequently expressed by lymphoblastic lymphoma.[33]

VEGFR-2 is mainly expressed by endothelial cells, embryonic tissue, and megakaryocytes. It plays an important role in the regulation of angiogenesis, vasculogenesis, and vascular permeability.[33] Miettinen *et al.*[34] demonstrated that, in normal adult tissues, VEGFR-2 expression is restricted to the cytoplasm or the cytoplasmic membrane of endothelial and mesothelial cells. The authors found that VEGFR-2 was consistently expressed by angiosarcomas, Kaposi sarcomas, and retiform haemangioendotheliomas, but only half of the epithelioid haemangioendotheliomas expressed this marker, and the staining was usually focal. VEGFR-2 was strongly expressed by most capillary haemangiomas, and weakly or focally expressed in cavernous, venous and spindle-cell haemangiomas.

Claudin-5 is a member of the claudin family, which consists of at least 24 members. Claudins are integral membrane proteins and components of tight junction strands. Claudin-5 is highly expressed in vascular endothelial cells, and plays an important role in the maintenance of the tight junction strand integrity of the vascular endothelium.[33] Miettinen *et al.*[35] recently investigated claudin-5 expression in a large number of vascular endothelial tumours. The results of this study indicate that this marker is expressed by the vast majority of Kaposi sarcomas, kaposiform haemangioendotheliomas, angiosarcomas, epithelioid haemangioendotheliomas, capillary and cavernous haemangiomas, and lymphangiomas. The expression varied from cytoplasmic to membranous, depending on the particular tumour.

LYVE-1 is expressed by lymphatic endothelial cells, the sinusoidal endothelium of liver and spleen, and discrete populations of activated tissue macrophages, but not by the blood vascular endothelium. It was found that the large majority of spindle cells in both early and late Kaposi sarcomas express this marker. LYVE-1 has also been reported to be consistently expressed in multifocal lymphangioendotheliomatosis and infantile haemangiomas, where it shows cytoplasmic and membranous expression.[33,36,37]

CD4 is a preferential T-cell marker that is also expressed by a subset of monocyte/macrophage cells, including plasmacytoid monocytes and a variety of rare associated malignancies, including blastic plasmacytoid dendritic cell neoplasms. CD4 expression is either cytoplasmic or membranous.[38–40]

CD11c is a type I transmembrane protein found on most human dendritic cells, but also on monocytes, macrophages, neutrophils, and some B cells. It is involved in a variety of cellular functions, including adherence to activated endothelial cells and complement-mediated phagocytosis. CD11c can be expressed either in the cytoplasm or in the cytoplasmic membrane.[39,41]

Antibodies against all of the broad-spectrum endothelial markers[33] employed in our study reacted with LCA cells. However, antibodies against most markers, namely factor VIII, CD31, FLI-1, ERG, and LMO2, were reactive not only in LCA, but also in the non-neoplastic red pulp. The only two vascular markers that were expressed almost exclusively in LCA were VEGFR-2 and claudin-5, which, besides LCA, were expressed only by small splenic capillaries, thus very clearly delineating the extent of LCA from the whole neighbouring splenic parenchyma. Of the lymphatic endothelium-associated markers,[33] LYVE-1 again was expressed by both LCA and normal sinusoidal endothelium. However, it is known that LYVE-1 is not entirely specific for lymphatics, as it is normally expressed not only in the splenic sinuses but also by histiocytes (tissue macrophages) and some other cells.[37] Considering the results of previous immunohistochemical studies, it is therefore more likely that LYVE-1 positivity points towards histiocytic/macrophage differentiation of LCA cells rather than differentiation towards the lymphatic endothelium. In addition, podoplanin, which is perhaps the most specific lymphatic endothelial marker, was never seen in LCA. WT-1 is another marker that was not expressed in LCA. However, it may still be of some diagnostic use as a negative discriminator, as many other splenic vascular tumours and the normal splenic vasculature are WT-1-positive.[31]

Besides VEGFR-2 and claudin-5, the most useful markers for diagnosing LCA are, in our opinion, the histiocytic markers CD4, CD11c, and CD163. In spite of their synchronous staining diffusely distributed histiocytes in the spleen, they still clearly highlighted LCA-lining cells. Lysozyme, another histiocytic marker, was also strongly expressed by the tumour cells. However, probably because of its broader spectrum, it also stained non-tumorous splenic cells with much greater intensity, which makes it diagnostically less helpful. Factor XIIIa is the only histiocytic/macrophage marker that was expressed neither by LCA nor by the rest of the splenic parenchyma.

The morphology of LCA is not specific, and may resemble that of other vascular tumours of the spleen, namely hamartoma, sclerosing angiomatoid nodular transformation (SANT), lymphangioma, haemangioma, haemangioendothelioma, or angiosarcoma.[42–44] The most useful feature favouring LCA in this differential diagnostic dilemma is the already mentioned hybrid endothelial and histiocytic phenotype of LCA, which can be confidently established with immuohistochemistry and differentiated from other splenic vascular tumours.[43]

Splenic hamartoma is a tumour-like malformation composed of an anomalous mixture of normal splenic red pulp elements. An association of splenic hamartoma with visceral malignancy has been documented.[45] Endothelial cells that are positive for CD8 constitute a key feature that differentiates hamartoma from other vascular lesions of the spleen.[46]

SANT is a distinctive entity that is unique to the spleen. Its main characteristic is a striking multinodular growth pattern, with the concentric hyaline shells surrounding individual angiomatoid nodules, and inflamed fibrotic to sclerotic stroma between the nodules.[44] Immunostaining typically reveals three

distinct types of vessel in the lesion, recapitulating the composition of the normal splenic red pulp: cord capillaries (CD34+/CD8−/CD31+), sinusoids (CD34−/CD8+/CD31+), and small veins (CD34−/CD8−/CD31−). The heterogeneous morphology/immunoprofile of vessels composing the SANT differs from that of the monotonous type of vessels present in LCA.

Lymphangioma of the spleen is composed of thin-walled cystic structures lined by predominantly flat endothelium and filled with pink proteinaceous fluid rich in lymphocytes and devoid of erythrocytes. It tends to be located in the subcapsular region, but may involve the entire organ.[43] The endothelial cells of lymphangioma react with markers typical of lymphatic endothelium, including CD31, CD34, and factor VIII. These cells do not express CD68, a histiocytic marker, and are only rarely positive for lysozyme.[43]

Regarding haemangioma, it is mainly the cavernous type that enters the differential diagnosis of LCA. This most common primary splenic vascular neoplasm is usually a small, inconspicuous lesion, but occasionally it can be large and/or multiple, and may involve the entire spleen.[43] Haemangioma is histologically composed of large, interconnected, dilated, blood-filled spaces identical to those seen in haemangiomas of soft tissue and other sites.[44] The endothelial lining represents one distinct morphological line, which can be supported by immunohistochemical positivity of solely endothelial markers.

Haemangioendothelioma of the spleen is a vascular neoplasm with morphological and clinical features intermediate between those of haemangioma and angiosarcoma.[43] It is composed of ill-defined vascular spaces lined by cells with mild to moderate cellular atypia and a low mitotic rate. In contrast, the lack of atypia and the well-formed anastomosing vascular channels resembling splenic sinuses are morphological properties in keeping with the diagnosis of LCA. A correct diagnosis is then confidently established with immunohistochemistry. Splenic angiosarcoma is a very rare and highly aggressive lesion, with extremely variable histomorphology, even within a single tumour. Solid, papillary or freely anastomosing vascular channels lined by atypical, hyperchromatic cells with intracytoplasmic hyaline globules, together with frequent haemorrhage and necrosis, are considered to be characteristics of splenic angiosarcoma.[43] The differentiation of LCA from angiosarcoma is determined by the absence of cytological atypia or necrosis, the lack of significant mitotic activity in LCA, and the unique immunophenotype of littoral cells.

In 1998, Bisceglia *et al.* presented four cases of LCA that occurred along with other malignancies, and pointed to the striking association with visceral organ cancers.[4] This observation was supported by subsequent studies, as approximately one-third of LCAs reported to date were accompanied by an internal malignant neoplasm.[27] However, the study of Falk *et al.* showed entirely different results, with only two of 17 cases of LCA being associated with malignancy (12%). This may be explained by the fact that the study article was more focused on the description and introduction of the new tumour entity from a morphological point of view than on obtaining detailed clinical information. Moreover, the majority of cases in that study were from the files of The Armed Forces Institute of Pathology in Washington DC, and mainly represented consultation cases for which the acquisition of thorough follow-up and clinical information was difficult.

Initially, it was thought that LCA is associated predominantly with epithelial malignancies.[4] After extensive research of the literature on LCA from its initial description to date, it has become apparent that LCA has relationships with a broad spectrum of internal malignancies, including epithelial, mesenchymal and haematological malignancies. The coexisting malignancies reported to date are summarized in Table 3.[1–26,47]

In our series, visceral malignancy occurred in 15 of 25 cases of LCA. The malignant associations in our series included colorectal carcinoma (five cases), renal cell carcinoma (three cases), endometrioid endometrial adenocarcinoma (one case), chronic lymphocytic leukaemia (one case), malignant lymphoma (one case), pancreatic adenocarcinoma (one case), multiple myeloma (one case), prostate cancer (one case), gastrointestinal stromal tumour of the stomach (one case), carcinoma of the thyroid gland (one case), breast cancer (one case), and melanoma (one case).

Additionally, LCA seems to be associated with immune dysregulation. To date, the reported systemic diseases associated with LCA include Crohn disease, Wiskott–Aldrich syndrome, Gaucher disease, Epstein syndrome, lymphocytic colitis, ankylosing spondylitis, myelodysplastic syndrome, chronic glomerulonephritis, aplastic anaemia, pulmonary sarcoidosis, post-renal transplantation, hepatitis B and C, psoriasis, chemotherapy, cytostatic treatment, autoimmune thrombocytopenia (Evan's syndrome), and systemic lupus erythematosus.[9,48–51] Quite a number of our cases showed associations of LCA with diseases of presumed immune origin or systemic diseases known

Table 3. Associated malignancies

Year	Author	Number of malignant cases	Associated malignancy
2016	Peckova *et al.*	15	Colorectal adenocarcinoma
			Colorectal adenocarcinoma
			Colorectal cancer
			Adenocarcinoma of lienal flexure
			Adenocarcinoma of ascending colon, renal carcinoma, multiple myeloma
			Clear-cell renal cell carcinoma
			Clear-cell renal cell carcinoma
			Endometroid endometrial adenocarcinoma
			Chronic lymphocytic leukaemia
			Malignant lymphoma
			Pancreatic adenocarcinoma with multiple distant metastases
			Prostate cancer, yolk sack tumour, GIST
			Thyroid gland cancer
			Breast cancer
			Malignant melanoma
2014	Sarandria *et al.*	1	Papillary thyroid carcinoma
2013	Mokhtari *et al.*	1	Non-Hodgkin B-cell lymphoma
2012	Melzer	1	Non-metastatic prostate cancer, plasmablastic B-cell lymphoma
2011	Shah	2	Renal cell carcinoma
			Giant-cell tumour of the right femur
2011	Pilz	1	Melanoma of the left jaw
2010	Hansen	1	Adenocarcinoma of the sigmoid colon
2008	Priego	1	Osteogenic sarcoma
2007	Bhatt	1	Melanoma, thigh leiomyosarcoma
2006	Harmon *et al.*	1	Transitional cell carcinoma of the urinary bladder
2005	Floyd *et al.*	1	Diffuse large B-cell lymphoma, Hodgkin's disease, diffuse large T-cell lymphoma
2005	Mohan *et al.*	1	Papillary thyroid cancer metastatic to lymph nodes
2005	Lin *et al.*	1	Hepatocellular carcinoma
2004	Levy *et al.*	1	Bronchial adenocarcinoma
2003	Collins *et al.*		Poorly differentiated adenocarcinoma of the lung
2003	Yano *et al.*	1	Seminoma of the left testis
2002	Chatelain *et al.*	1	Splenic marginal zone lymphoma, villous lymphocyte leukaemia
2001	Gorg *et al.*	1	Breast cancer

Table 3. *(Continued)*

Year	Author	Number of malignant cases	Associated malignancy
2000	Veillon *et al.*	1	Malignant cystic neuroendocrine neoplasm of the pancreas
2000	Heese and Bocklage	1	CNS lymphoma
2000	Shneider *et al.*	1	Cutaneous malignant melanoma
2000	Steensma and Morice	1	Caecal adenocarcinoma
1999	Sauer *et al.*	2	Seminoma
			Cutaneous malignant melanoma
1998	Bisceglia *et al.*	4	Differentiated carcinoma of the descending colon
			Renal carcinoma, angiomatous meningioma
			Rectal adenocarcinoma with metastasis to the colic lymph nodes
			Cystadenocarcinoma of the pancreas with metastases to ovaries, colon, mesentery
1997	Arber *et al.*	2	Gastric leiomyosarcoma
			Renal cell carcinoma
1997	Sallah *et al.*	1	Non-small-cell lung cancer
1993	Tsang/Chan	1	Disseminated ovarian adenocarcinoma
1991	Falk *et al.*	2	Malignant lymphoma
			Malignant lymphoma

CNS, Central nervous system; GIST, Gastrointestinal stromal tumour.

to cause immune disturbances, such as idiopathic thrombocytopenia, chronic hepatitis C, hemolytic anaemia, autoimmune thrombocytopenia (Evan's syndrome), ulcerative colitis, and ankylosing spondylitis. Some LCA patients had both an immune disorder and visceral malignancy.

Although several explanations regarding the relationship between LCA, malignancy and immune disorders have been postulated, the aetiology and pathogenetic mechanisms still remain to be elucidated.[16] Immune system dysregulation probably plays a role in the pathogenesis, considering the fact that some of the above-mentioned immune-mediated diseases are very rare entities, much like LCA, and the synchronous occurrence of two rare disorders is highly improbable.[52]

Summary

We have presented 25 cases of LCA, and this is, to our knowledge, the largest series reported to date. We have expanded the spectrum of immunohistochemical features of LCA by using novel endothelial and histiocytic markers, which may facilitate the diagnosis, especially in ambiguous cases. For practical purposes, we recommend the combined use of the vascular markers VEGFR-2, claudin-5, and the more widely available factor VIII, together with the histiocytic markers CD163, CD4, and CD11c. Such a combination of vascular and histiocytic markers is highly specific for LCA. To add even more specificity, the absence of staining of WT-1 in LCA, which is very rare among splenic vascular tumours, can be also exploited.

Finally, we confirmed frequent associations of LCA with various visceral malignancies (>60%), and showed that the associated malignancies are not always epithelial, as suggested previously, but comprise a whole spectrum of neoplastic diseases.

Author contributions

K. Peckova and Michael Michal planned, conducted and reported the work. L. Hadravsky and M.

Miesbauerova obtained the follow-up data. S. Suster, I. Damjanov and Z. Vernerova supplied a proportion of the cases. D. Kazakov and Michal Michal planned and reported the work.

Ethics and conflicts of interest

The authors have no conflicts of interest to disclose. Neither ethics approval nor informed consent were required for our study.

References

1. Falk S, Stutte HJ, Frizzera G. Littoral cell angioma. A novel splenic vascular lesion demonstrating histiocytic differentiation. *Am. J. Surg. Pathol.* 1991; **15**; 1023–1033.
2. Arber DA, Strickler JG, Chen YY *et al.* Splenic vascular tumors: a histologic, immunophenotypic, and virologic study. *Am. J. Surg. Pathol.* 1997; **21**; 827–835.
3. Bhatt S, Huang J, Dogra V. Littoral cell angioma of the spleen. *AJR Am. J. Roentgenol.* 2007; **188**; 1365–1366.
4. Bisceglia M, Sickel JZ, Giangaspero F *et al.* Littoral cell angioma of the spleen: an additional report of four cases with emphasis on the association with visceral organ cancers. *Tumori* 1998; **84**; 595–599.
5. Collins GL, Morgan MB, Taylor FM 3rd. Littoral cell angiomatosis with poorly differentiated adenocarcinoma of the lung. *Ann. Diagn. Pathol.* 2003; **7**; 54–59.
6. Floyd JD, Kaplan PA, Sauter ER *et al.* Patients with unusual bladder malignancies and a rare cause of splenomegaly. Case 3. Littoral cell angioma of the spleen in a patient with previous lymphoma. *J. Clin. Oncol.* 2005; **23**; 4460–4462.
7. Gorg C, Barth P, Backhus J *et al.* Sonographic patterns of littoral cell angioma: case report and review of the literature. *Ultraschall Med.* 2001; **22**; 191–194.
8. Hansen T, Habekost M, Flieger D *et al.* Littoral cell angioma of the spleen. Association with colon and hepatocellular carcinoma. *Pathologe* 2010; **31**; 290–292.
9. Harmon RL, Cerruto CA, Scheckner A. Littoral cell angioma: a case report and review. *Curr. Surg.* 2006; **63**; 345–350.
10. Heese J, Bocklage T. Specimen fine-needle aspiration cytology of littoral cell angioma with histologic and immunohistochemical confirmation. *Diagn. Cytopathol.* 2000; **22**; 39–44.
11. Chatelain D, Bonte H, Guillevin L *et al.* Small solitary littoral cell angioma associated with splenic marginal zone lymphoma and villous lymphocyte leukaemia in a patient with hepatitis C infection. *Histopathology* 2002; **41**; 473–475.
12. Levy AD, Abbott RM, Abbondanzo SL. Littoral cell angioma of the spleen: CT features with clinicopathologic comparison. *Radiology* 2004; **230**; 485–490.
13. Lin CH, Yu JC, Shih ML *et al.* Littoral cell angioma of the spleen in a patient with hepatocellular carcinoma. *J. Formos. Med. Assoc.* 2005; **104**; 282–285.
14. Melzer N, Barth PJ, Muller KM *et al.* Rapidly progressive B-cell dominated inflammatory neuropathy and littoral cell angioma of the spleen associated with plasmablastic B-cell lymphoma. *Leuk. Lymphoma* 2012; **53**; 1242–1244.
15. Mohan V, Jones RC, Drake AJ 3rd *et al.* Littoral cell angioma presenting as metastatic thyroid carcinoma to the spleen. *Thyroid* 2005; **15**; 170–175.
16. Mokhtari N, Hamidian Jahromi A, Dela Cruz N *et al.* Littoral cell angioma: review of the literature and case report. *J. La State Med. Soc.* 2013; **165**; 329–333.
17. Priego P, Rodriguez Velasco G, Griffith PS *et al.* Littoral cell angioma of the spleen. *Clin. Transl. Oncol.* 2008; **10**; 61–63.
18. Sallah S, Gonzalez P, Maia DM *et al.* Littoral cell angioma in a patient with Epstein syndrome. *Acta Haematol.* 1997; **98**; 113–115.
19. Sarandria JJ, Escano M, Kamangar F *et al.* Littoral cell angioma: gastrointestinal associations. *Gastrointest. Cancer Res.* 2014; **7**; 63–64.
20. Sauer J, Treichel U, Kohler HH *et al.* Littoral-cell angioma—a rare differential diagnosis on splenic tumors. *Dsche Med. Wochenschr.* 1999; **124**; 624–628.
21. Shah S, Wasnik A, Pandya A *et al.* Multimodality imaging findings in image-guided biopsy proven splenic littoral cell angioma: series of three cases. *Abdom. Imaging* 2011; **36**; 735–738.
22. Schneider G, Uder M, Altmeyer K *et al.* Littoral cell angioma of the spleen: CT and MR imaging appearance. *Eur. Radiol.* 2000; **10**; 1395–1400.
23. Steensma DP, Morice WG. Littoral cell angioma associated with portal hypertension and resected colon cancer. *Acta Haematol.* 2000; **104**; 131–134.
24. Tsang WY, Chan JK. Splenic littoral cell angioma, not bacillary angiomatosis. *Pathology* 1994; **26**; 347.
25. Veillon DM, Williams RB, Sardenga LJ *et al.* 'Little' littoral cell angioma of the spleen. *Am. J. Surg. Pathol.* 2000; **24**; 306–307.
26. Yano H, Imasato M, Monden T *et al.* Hand-assisted laparoscopic splenectomy for splenic vascular tumors: report of two cases. *Surg. Laparosc Endosc. Percutan. Tech.* 2003; **13**; 286–289.
27. Johansson J, Bjornsson B, Ignatova S *et al.* Littoral cell angioma in a patient with Crohn's disease. *Case Rep. Gastrointest. Med.* 2015; **2015**; 474969.
28. Ziske C, Meybehm M, Sauerbruch T *et al.* Littoral cell angioma as a rare cause of splenomegaly. *Ann. Hematol.* 2001; **80**; 45–48.
29. Tatli S, Cizginer S, Wieczorek TJ *et al.* Solitary littoral cell angioma of the spleen: computed tomography and magnetic resonance imaging features. *J. Comput. Assist. Tomogr.* 2008; **32**; 772–775.
30. Matuszczak E, Reszec J, Debek W *et al.* Is littoral cell angioma of the spleen as rare as previously believed in the pediatric population? *Folia Histochem. Cytobiol.* 2012; **50**; 480–485.
31. O'Malley DP, Kim YS, Weiss LM. Distinctive immunohistochemical staining in littoral cell angioma using ERG and WT-1. *Ann. Diagn. Pathol.* 2015; **19**; 143–145.
32. Michal M, Skalova A, Fakan F *et al.* Littoral cell angioma of the spleen. A case report with ultrastructural and immunohistochemical observations. *Zentralbl. Pathol.* 1993; **139**; 361–365.
33. Ordonez NG. Immunohistochemical endothelial markers: a review. *Adv. Anat. Pathol.* 2012; **19**; 281–295.
34. Miettinen M, Rikala MS, Rys J *et al.* Vascular endothelial growth factor receptor 2 as a marker for malignant vascular tumors and mesothelioma: an immunohistochemical study of 262 vascular endothelial and 1640 nonvascular tumors. *Am. J. Surg. Pathol.* 2012; **36**; 629–639.
35. Miettinen M, Sarlomo-Rikala M, Wang ZF. Claudin-5 as an immunohistochemical marker for angiosarcoma and hemangioendotheliomas. *Am. J. Surg. Pathol.* 2011; **35**; 1848–1856.

36. Dadras SS, North PE, Bertoncini J *et al.* Infantile hemangiomas are arrested in an early developmental vascular differentiation state. *Mod. Pathol.* 2004; **17**; 1068–1079.
37. Jackson DG. The lymphatics revisited: new perspectives from the hyaluronan receptor LYVE-1. *Trends Cardiovasc. Med.* 2003; **13**; 1–7.
38. Kraus MD, Haley JC, Ruiz R *et al.* 'Juvenile' xanthogranuloma: an immunophenotypic study with a reappraisal of histogenesis. *Am. J. Dermatopathol.* 2001; **23**; 104–111.
39. Sandell RF, Carter JM, Folpe AL. Solitary (juvenile) xanthogranuloma: a comprehensive immunohistochemical study emphasizing recently developed markers of histiocytic lineage. *Hum. Pathol.* 2015; **46**; 1390–1397.
40. Wood GS, Warner NL, Warnke RA. Anti-Leu-3/T4 antibodies react with cells of monocyte/macrophage and Langerhans lineage. *J. Immunol.* 1983; **131**; 212–216.
41. Jang SJ, Jeon HM, Kim D, Yang W-L. Myeloperoxidase positive histiocytes in subacute necrotizing lymphadenitis express both CD11c and CD163. *Basic Appl. Pathol.* 2011; **4**; 110–115.
42. Katz JA, Mahoney DH, Shukla LW *et al.* Endovascular papillary angioendothelioma in the spleen. *Pediatr. Pathol.* 1988; **8**; 185–193.
43. Kutok JL, Fletcher CD. Splenic vascular tumors. *Semin. Diagn. Pathol.* 2003; **20**; 128–139.
44. Martel M, Cheuk W, Lombardi L *et al.* Sclerosing angiomatoid nodular transformation (SANT): report of 25 cases of a distinctive benign splenic lesion. *Am. J. Surg. Pathol.* 2004; **28**; 1268–1279.
45. Abbott RM, Levy AD, Aguilera NS *et al.* From the archives of the AFIP: primary vascular neoplasms of the spleen: radiologic–pathologic correlation. *Radiographics* 2004; **24**; 1137–1163.
46. Sim J, Ahn HI, Han H *et al.* Splenic hamartoma: a case report and review of the literature. *World J. Clin. Cases* 2013; **1**; 217–219.
47. Pilz JB, Sperschneider T, Lutz T *et al.* Littoral cell angioma in main and accessory intrapancreatic spleen presenting as splenic rupture. *Am. J. Surg.* 2011; **201**; e15–e17.
48. Cappello M, Bravata I, Cocorullo G *et al.* Splenic littoral cell hemangioendothelioma in a patient with Crohn's disease previously treated with immunomodulators and anti-TNF agents: a rare tumor linked to deep immunosuppression. *Am. J. Gastroenterol.* 2011; **106**; 1863–1865.
49. Cordesmeyer S, Putzler M, Titze U *et al.* Littoral cell angioma of the spleen in a patient with previous pulmonary sarcoidosis: a TNF-alpha related pathogenesis? *World J. Surg. Oncol.* 2011; **9**; 106.
50. MacNew HG, Fowler CL. Partial splenectomy for littoral cell angioma. *J. Pediatr. Surg.* 2008; **43**; 2288–2290.
51. Muhlfeld AS, Eitner F, Perez-Bouza A *et al.* Littoral cell angioma of the spleen mimicking posttransplantation lymphoma in a 63-year-old renal transplant patient. *Am. J. Kidney Dis.* 2008; **52**; e11–e14.
52. Gupta MK, Levin M, Aguilera NS *et al.* Littoral cell angioma of the spleen in a patient with Gaucher disease. *Am. J. Hematol.* 2001; **68**; 61–62.

2.2.3. RECURRENT SOMATIC PDGFRB MUTATIONS IN SPORADIC INFANTILE/SOLITARY ADULT MYOFIBROMAS BUT NOT IN ANGIOLEIOMYOMAS AND MYOPERICYTOMAS

Infantile myofibroma (MF) represents an uncommon proliferative mesenchymal lesion of infancy and early childhood that shows myofibroblastic differentiation. The disease occurs in 3 main clinicopathologic settings: solitary MF, multicentric MF/myofibromatosis, and generalized myofibromatosis [40, 41]. This study utilized the knowledge of the recently reported presence of activating germline PDGFRB mutations in familial infantile myofibroma (MF) [42-44]. Since the molecular pathogenesis of sporadic infantile and adult solitary MF remained unclear, we undertook this study.

Overall, we collected and analyzed 25 non-familial solitary MFs (of which 9 were infantile and 16 were adult MFs), in order to find out, whether somatic PDGFRB mutations might be responsible for the sporadic form of the disease as well. Given the presumed histogenetic link of MF to myopericytoma and angioleiomyoma, we additionally analyzed a control group of 6 myopericytomas and 9 angioleiomyomas for PDGFRB mutations. We also tested the utility of the PDGFRB antibody in the distinction between these three entities.

We detected PDGFRB mutations in 6/8 (75%) analyzable infantile and in 11/16 (69%) adult MFs but in none of the angioleiomyomas or myopericytomas. Additional sequencing of the germline confirmed the somatic nature of PDGFRB mutations. The staining pattern of the PDGFRB antibody did not differ significantly between any of the three groups and thus currently seems not useful in the diagnostic practice.

Further studies are needed to uncover the genetic background of the fraction of cases that tested negative in our series as well as that of angioleiomyoma. Interestingly, probably due to a more sensitive molecular genetic method used, another group recently reported the presence of PDGFRB mutations in myopericytoma/myopericytomatosis as well [45].

Recurrent Somatic *PDGFRB* Mutations in Sporadic Infantile/Solitary Adult Myofibromas But Not in Angioleiomyomas and Myopericytomas

Abbas Agaimy, MD, Matthias Bieg, MSc,† Michael Michal, MD,‡ Helene Geddert, MD,§ Bruno Märkl, MD,‖ Jan Seitz,* Evgeny A. Moskalev, PhD,* Matthias Schlesner, PhD,† Markus Metzler, MD,¶ Arndt Hartmann, MD,* Stefan Wiemann, PhD,#** Michal Michal, MD,†† Thomas Mentzel, MD,‡‡ and Florian Haller, MD**

Abstract: Infantile myofibroma (MF) is an uncommon benign myofibroblastic tumor of infancy and childhood. Solitary adult MF shares similar features with infantile MF. The lesions occur in 3 clinicopathologic settings: solitary, multicentric, and generalized and can be either sporadic or familial. Traditionally, infantile MF has been included in the spectrum of infantile hemangiopericytoma. The recent World Health Organization classification listed MF, angioleiomyoma, and myopericytoma under the general heading of *perivascular tumors* in the sense of a morphologic spectrum of *perivascular myoid cell neoplasms*. Although activating germline *PDGFRB* mutations have recently been linked to familial infantile MF, the molecular pathogenesis of sporadic infantile and adult solitary MF remained unclear. In this study, we analyzed 25 solitary MFs without evidence of familial disease (9 infantile and 16 adult MFs) to address the question whether somatic *PDGFRB* mutations might be responsible for the sporadic form of the disease. Given the presumed histogenetic link of MF to myopericytoma and angioleiomyoma, we additionally analyzed a control group of 6 myopericytomas and 9 angioleiomyomas for *PDGFRB* mutations. We detected *PDGFRB* mutations in 6/8 (75%) analyzable infantile and in 11/16 (69%) adult MFs but in none of the angioleiomyomas or myopericytomas. In 2 infantile MFs, additional sequencing of the germline confirmed the somatic nature of *PDGFRB* mutations. To our knowledge, this is the first study reporting apparently somatic recurrent *PDGFRB* mutations as molecular driver events in the majority of sporadic infantile and adult solitary MFs. Our results suggest molecular distinctness of MF as compared with angioleiomyoma/myopericytoma. Investigation of more cases including those with atypical and worrisome features, as well as other mimickers in the heterogenous morphologic spectrum of MF, is mandatory for validating the potential diagnostic value of *PDGFRB* mutation testing as a possible surrogate in difficult-to-classify lesions.

Key Words: infantile myofibroma, infantile myofibromatosis, myopericytoma, angioleiomyoma, *PDGFRB* mutations, sporadic

(*Am J Surg Pathol* 2017;41:195–203)

Infantile myofibroma (MF) represents an uncommon proliferative mesenchymal lesion of infancy and early childhood that shows myofibroblastic differentiation with variable features overlapping with what has traditionally been named infantile hemangiopericytoma.[1,2] The disease occurs in 3 main clinico-pathologic settings: solitary MF, multicentric MF/myofibromatosis, and generalized myofibromatosis.[1,2] The sex distribution of the 3 disease variants differs as well. In particular, whereas the solitary disease shows a predilection for male individuals, multicentric MF tends to affect mainly females.[1,2] The lesions are characterized by a distinctive biphasic growth pattern, being composed of alternating bundles of mature eosinophilic spindled myoid cells and primitive darker staining small round to spindled mesenchymal cells associated with frequent myointimal-like nodular proliferations (vascular balls), numerous thin-walled hemangiopericytoma-like vessels, and occasional calcification.[1,2] Solitary MF represents the adult counterpart of infantile MF with a wide age range and varying localization.[2–4]

In addition to classical MF, the histomorphologic spectrum of infantile myofibroblastic proliferative lesions encompasses so-called atypical MF and infantile/congenital fibrosarcoma, 2 biologically distinctive lesions

From the *Institute of Pathology; ¶Department of Paediatrics, University Hospital, Friedrich-Alexander University Erlangen-Nuremberg, Erlangen; †Division of Theoretical Bioinformatics (B080); #Division Molecular Genome Analysis; **Genomics & Proteomics Core Facility, German Cancer Research Center (DKFZ), Heidelberg; §Institute of Pathology, St. Vincent's Hospital, Karlsruhe; ‖Institute of Pathology, Klinikum Augsburg, Augsburg; ‡‡Dermatopathologische Gemeinschaftspraxis, Friedrichshafen, Germany; ‡Department of Pathology, Faculty of Medicine in Plzen and Charles University Hospital, Biomedical Center; and ††Department of Pathology, Faculty of Medicine, Charles University, Plzen, Czech Republic.

Conflicts of Interest and Source of Funding: The authors have disclosed that they have no significant relationships with, or financial interest in, any commercial companies pertaining to this article.

Correspondence: Abbas Agaimy, MD, Pathologisches Institut, Universitätsklinikum Erlangen, Krankenhausstrasse 8-10, 91054 Erlangen, Germany (e-mail: abbas.agaimy@uk-erlangen.de).

with significant morphologic overlap that may, on occasion, make their distinction impossible on morphologic ground alone.[5–7] However, the recent introduction of specific genetic alterations enabled a clear classification for many of these lesions. In particular, congenital/infantile fibrosarcoma has been defined by recurring gene fusions involving the *ETV6* and *NTRK3* gene loci.[8] Detection of this translocation proved helpful in difficult cases and in cases in which only limited tissue sample is available.

Between the benign end of the spectrum (conventional infantile MF) and infantile/congenital fibrosarcoma, there exists a heterogenous group of neoplasms showing highly overlapping features with infantile MF, but with several atypical and worrisome features. For the former the term "MF with atypical features" has been used by some authors.[7] However, the histologically or clinically malignant counterpart of MF still remains an issue of controversy. This still emerging category seems to include neoplasms with prominent features of the so-called infantile hemangiopericytoma and *ETV6* fusion–negative congenital fibrosarcoma-like neoplasms, in addition to adult sarcomas with myopericytic features.[9] Very recent comprehensive genomic profiling studies revealed a new variant of infantile hemangiopericytic sarcoma harboring a novel translocation involving the *NTRK1* gene locus, which can be addressed therapeutically.[10,11]

A few recent studies uncovered germline mutations in the *platelet-derived growth factor receptor beta* (*PDGFRB*) in familial infantile MF, which were inherited in an autosomal-dominant manner.[12–14] However, until now, the molecular pathogenesis of the sporadic form of MF is unknown. In particular, the justified question whether the same molecular mechanisms (activating mutations in the *PDGFRB* gene) involved in the pathogenesis of the familial form of the disease do apply to the sporadic form remained unanswered. In the study by Cheung and colleagues, 5 individuals with sporadic MF did not harbor *PDGFRB* mutations in their tumors nor in the germline.[12] In this study, we analyzed a series of apparently sporadic MFs, angioleiomyomas, and myopericytomas to: (1) explore the potential rule of somatic *PDGFRB* mutations in the pathogenesis of sporadic MF; and (2) to verify any potential histogenetic link of MF to angioleiomyoma and myopericytoma, as the current World Health Organization classification has listed these lesions under the general heading of perivascular tumors in the sense of a histogenetic continuum.[15]

MATERIALS AND METHODS

Patients and Tumor Samples

This study has been approved by the local ethics committee of the University Hospital Erlangen, Germany (No. 217_12 B, 19.09.2012). Cases have been retrieved from the routine surgical pathology files of the Institute of Pathology in Erlangen, the Department of Pathology in Plzen, the Dermatopathologische Gemeinschaftspraxis Friedrichshafen, and from consultation files of the authors (A.A., M.M., T.M.). Diagnosis of a lesion as MF, angioleiomyoma, or myopericytoma was done using strict morphologic criteria in accordance with the 2013 World Health Organization classification of soft tissue neoplasms.[15] Of 49 tumors with original diagnosis of MF, angioleiomyoma, or myopericytoma, 9 cases were excluded after critical review either due to equivocal features or due to limited tissue on the block. Thus the remaining 40 cases were used for this study. Cases of MF were classified as either *classical* or *atypical* according to the presence of one of the following features: hypercellularity; absent or inconspicuous, poorly demarcated myoid nodules; infiltrative growth pattern; perineural invasion.[7] For the purpose of this study, lesions with atypical features but also clear-cut classical areas were classified as *mixed*. All tumor specimens had been fixed in buffered formalin overnight and processed routinely for histologic assessment. Signed informed consent was obtained from the index patient's parents (case 5) for whole-genome sequencing analysis of the tumor and a peripheral blood sample. Signed informed consent for sequencing of the *PDGFRB* germline status was also obtained from the parents of another patient (case 1). Local ethical guidelines (Statement of ethics committee, University Hospital Erlangen, January 2012) were followed during the retrospective use of tissue samples in all other cases. None of the patients had clinical features of metacentric or familial form of the disease.

Immunohistochemistry

Immunohistochemical analysis was performed on 3-μm-thick sections cut from paraffin blocks using a fully automated system (Benchmark XT System, Ventana Medical Systems Inc., Tucson, AZ) and the following antibodies: desmin (clone D33, 1:250, Dako), alpha smooth muscle actin (clone 1A4, 1:200, Dako), h-caldesmon (clone h-CD, 1:100, Dako), protein S-100 (polyclonal, 1:2500, Dako), and CD34 (clone BI-3C5, 1:200, Zytomed). To assess the potential usefulness of PDGFRB immunostaining, we stained a subset of the tumors using an anti-PDGFRB antibody (clone C82A3, 1:200, Cell Signaling).

Whole-genome and RNA Sequencing of the Index Case

Tumor DNA and normal DNA for control were isolated from fresh-frozen tumor tissue and blood of the index patient (case 5) with the DNeasy Blood and Tissue Kit (Qiagen, Hilden, Germany), whereas RNA was isolated from the tumor tissue using the RNeasy Plus Mini Kit (Qiagen). Quality of the DNA was analyzed using an Agilent 2200 Tapestation (Agilent, Waldbronn, Germany), and quality of the RNA was assessed with an Agilent Bioanalyzer 2100 (Agilent). Libraries for sequencing were prepared using the TruSeq Nano DNA Library Prep Kit (Illumina Inc., San Diego, CA) for DNA and the Illumina TruSeq RNA Sample Preparation Kit v2 (Illumina) for RNA. For whole-genome sequencing,

paired-end sequencing (2 × 150 bp) was performed using 1 lane of a HiSeqX (Illumina) for every sample, whereas RNA-seq was done with paired-end sequencing (2 × 100 bp) using a HiSeq2000 (Illumina). Bioinformatic analysis of whole-genome sequencing and RNA sequencing data was performed as described previously in detail elsewhere.[11,16]

PDGFRB Mutation Analysis

DNA was isolated from FFPE tumor samples using the QIAamp DNA FFPE Tissue Kit (Qiagen), and polymerase chain reaction amplification of *PDGFRB* exons 12 and 14 was carried out in 50 μL reactions containing 200 ng DNA, 7.5 mM $MgCl_2$, 200 μM dNTP, 500 nM primers (Table 1), and 2 U/μL Phusion Hot Start Flex Polymerase (Biolabs, Frankfurt am Main, Germany). An amplification program was used with initial activation phase at 95°C for 15 minutes, followed by 40 cycles of annealing at 95°C for 30 seconds, amplification at 57.6°C for 45 seconds, and elongation at 72°C for 1 minute. About 5 μL of each reaction was examined on 2% agarose gels, and polymerase chain reaction products were purified using the Qiagen Purification Kit (Qiagen). The sequencing reactions were performed at an external facility (Seqlab Sequencing Laboratories, Göttingen, Germany).

TABLE 1. Primer Sequences for *PDGFRB* Mutation Analysis

Primer	Sequence
PDGFRB exon 12 forward	TGTCCTAGACGGACGAACCT
PDGFRB exon 12 reverse	CATGGGGTCCACGTAGATGT
PDGFRB exon 14 forward	CATTTTCCTCAGCCACAGC
PDGFRB exon 14 reverse	GGTGGGCACTTTCCCTGA

RESULTS

Clinicopathologic and Demographic Features

The main clinicopathologic features of the patients are summarized in Table 2. The 9 infantile MF cases affected 5 female and 3 male patients (1 case of unknown sex) aged 10 days to 17 years (median, 6 y). The 16 adult MFs occurred in 5 female and 11 male patients at a median age of 53 years (range, 22 to 87 y). The median age of patients with angioleiomyoma was 63 years (range, 22 to 77 y), and the median age of patients with myopericytoma was 68 years (range, 44 to 91 y). The mean size of the tumors was 1.6 (± 1.1), 1.0 (± 0.8), 1.4 (± 0.9), and 0.8 cm (± 0.3 cm) for infantile MFs, adult MFs, angioleiomyomas, and myopericytomas, respectively. There were no significant differences considering age and size comparing adult MFs, angioleiomyomas, and myopericytomas.

Histologically, infantile MFs showed variable proportions of pink staining spindle myoid cells alternating with darker staining primitive mesenchymal cells in a fibrovascular stroma that varied from delicate and sparse to prominent hemangiopericytoma-like with occasional foci of hyaline necrosis (Figs. 1A–C). The periphery of the lesions varied from irregular/infiltrative (Fig. 1D) to well circumscribed (Fig. 1E). Myxohyaline (intima-like) "balls" were uniformly present but varied significantly in extent (Figs. 1A, B, F). Of the 25 MFs, 15 lesions belonged to the classical category, 5 to the atypical, and another 5 to the mixed group (Table 2). Immunohistochemistry showed uniform expression of smooth muscle actin in the myoid cells (Fig. 1G), but other markers listed above including CD34 were negative (Fig. 1H). The PDGFRB antibody showed expression of PDGFRB mainly in the myoid cells with diffuse cytoplasmic and occasionally paranuclear dot-like pattern (Fig. 1I).

The myopericytomas and angioleiomyomas all affected adults with expectedly frequent location of angioleiomyoma on the extremities, mainly the elbow (Table 2). They showed prototypical histologic features (Figs. 2A, C) with diffuse expression of smooth muscle markers but not CD34. PDGFRB antibody showed variable cytoplasmic reactivity that was mainly confined to the vascular channels and less prominent in the intervening cells (Figs. 2B, D). No difference in the PDGFRB staining was seen between MFs and the group of angioleiomyomas/myopericytomas.

Identification of Activating *PDGFRB* Mutations in Sporadic MF

Whole-genome sequencing of the index case (case 5) revealed 2 somatic gain-of-function mutations in exons 12 and 14 of the *PDGFRB* gene (c.1681C > T; p.R561C and c.1998C > A, p.N666K). The comparison of RPKM values as indicator of gene expression showed a >3-fold higher value for PDGFRB compared with 2 other soft tissue tumors of the pericytic tumor spectrum recently analyzed by RNA-seq (data not shown).[11,16] Comprehensive analysis of the tumor DNA and RNA revealed no further relevant genetic alterations including copy number alterations, gene fusions, somatic missense mutations, or small insertions/deletions. Both somatic *PDGFRB* mutations were confirmed by Sanger sequencing in the index patient's tumor DNA but were absent in the patient's germline DNA (Figs. 3A–D). Another patient (case 1) with sporadic infantile MF harbored almost identical *PDGFRB* mutations in the tumor DNA (c.1681C > T; p.R561C and c.1998C > G, p.N666K), which were also not present in the patient's germline DNA (Figs. 3E–H).

Sanger sequencing of *PDGFRB* exons 12 and 14 in the whole cohort revealed a total of 22 *PDGFRB* mutations in 17 MFs, whereas 7 MFs were of wild-type status (Table 2 and Fig. 4). One tumor (Case 3) with a size of 0.3 cm was not analyzable due to limited material. Interestingly, 5 tumors harbored 2 *PDGFRB* mutations (all but 1 of them had a combination of a *PDGFRB* exon 12 mutation with the exon 14 p.N666K mutation), whereas 12 tumors harbored a single mutation. Mutations in *PDGFRB* exon 12 were distributed in a region covering amino acid positions R561 to I569, with 2 single amino acid changes at position R561, 3 at position Y562, 1 at

TABLE 2. Summary of Clinicopathologic and Molecular Data of All Cases

Case	Diagnosis	Age/Sex	Location	Size (cm)	PDGFRB Exon 12	PDGFRB Exon 14
	Infantile MF					
1	MF—classical	3 mo/m	Knee	1.0	c.1681C > T; p.R561C	c.1998C > G; p.N666K
2	MF—classical	11 y/f	Skin	0.5	Wild type	c.1998C > G; p.N666K
3	MF—classical	14 y/	Forehead	0.3	NA	NA
4	MF—classical	17 y/m	Paranasal skin	0.7	Wild type	c.1998C > A; p.N666K
5	MF—mixed	6 y/f	Thyroid	3.7	c.1681C > T; p.R561C	c.1998C > A; p.N666K
6	MF—mixed	12 y/f	Masticator space	1.8	c.1685A > G; pY562C	c.1998C > G; p.N666K
7	MF—atypical	10 d/f	Thoracic	1.5	Wild type	Wild type
8	MF—atypical	2 mo/f	Shoulder	2.5	c.1697G > C; p.W566S; c.1706T > A; I569N	Wild type
9	MF—atypical	1 y/m	Breast	2.6	Wild type	Wild type
	Adult MF					
10	MF—classical	28 y/f	Skin	0.6	Wild type	Wild type
11	MF—classical	30 y/m	Forearm	0.6	Wild type	Wild type
12	MF—classical	32 y/f	Buttock	0.5	Wild type	Wild type
13	MF—classical	37 y/m	Calf	0.3	c.1705A > G; p.I569V	Wild type
14	MF—classical	53 y/f	Buccal	0.9	c.1685A > G; pY562C	c.1998C > G; p.N666K
15	MF—classical	54 y/m	Soft tissue	0.7	c.1691_1696del6; p.I564_W566delinsR	Wild type
16	MF—classical	56 y/f	Lower leg	0.4	Wild type	c.1998C > A; p.N666K
17	MF—classical	64 y/m	Ankle	2.5	Wild type	c.1998C > A; p.N666K
18	MF—classical	74 y/f	Popliteal area	1.3	Wild type	Wild type
19	MF—classical	77 y/m	Knee	0.7	c.1698_1706del9; p.W566_I569delinsC	Wild type
20	MF—classical	87 y/m	Knee	0.6	Wild type	c.1998C > A; p.N666K
21	MF—mixed	31 y/m	Neck	0.9	c.1684T > G; p.Y562D	Wild type
22	MF—mixed	37 y/m	Forehead	1.2	Wild type	Wild type
23	MF—mixed	65 y/m	Testis	3.5	Wild type	c.1998C > A; p.N666K
24	MF—atypical	22 y/m	Temple	0.8	Wild type	c.1998C > A; p.N666K
25	MF—atypical	73 y/m	Upper leg	0.4	Wild type	c.1998C > G; p.N666K
	Angioleiomyoma					
26	Angioleiomyoma	22 y/f	Elbow	3.2	Wild type	Wild type
27	Angioleiomyoma	58 y/f	Elbow	1.1	Wild type	Wild type
28	Angioleiomyoma	59 y/f	Ear	0.8	Wild type	Wild type
29	Angioleiomyoma	61 y/f	Unknown	0.7	Wild type	Wild type
30	Angioleiomyoma	63 y/m	Elbow	1.9	Wild type	Wild type
31	Angioleiomyoma	65 y/f	Knee	0.5	Wild type	Wild type
32	Angioleiomyoma	67 y/m	Shoulder	2.2	Wild type	Wild type
33	Angioleiomyoma	70 y/m	Ear	0.6	Wild type	Wild type
34	Angioleiomyoma	77 y/f	Unknown	1.5	Wild type	Wild type
	Myopericytoma					
35	Myopericytoma	44 y/m	Lower leg	0.7	Wild type	Wild type
36	Myopericytoma	48 y/m	Elbow	1.3	Wild type	Wild type
37	Myopericytoma	63 y/f	Lower leg	0.9	Wild type	Wild type
38	Myopericytoma	73 y/f	Unknown	0.8	Wild type	Wild type
39	Myopericytoma	73 y/m	Nose	0.5	Wild type	Wild type
40	Myopericytoma	91 y/m	Nose	0.5	Wild type	Wild type

f indicates female; m, male; NA, not available.

position W566, and 2 at position I569. Two other mutations were small deletions insertions affecting positions I564 to W566 and W566 to I569, respectively. All 12 *PDGFRB* exon 14 mutations resulted in the amino acid change N666K, although there were 2 different types of mutations at the DNA level, including 7 tumors with c.1998C > A and 5 tumors with c.1998C > G. There were no significant differences in the frequency and distribution of PDGFRB mutations comparing sporadic infantile and adult MFs, or comparing classical, mixed, and atypical cases of MF (Table 2 and Fig. 4). In contrast to the high frequency of *PDGFRB* mutations in MFs (17/24; 77%), none of the 9 angioleiomyomas and 6 myopericytomas harbored a mutation in *PDGFRB* exons 12 and 14.

DISCUSSION

The histopathologic classification of pediatric myofibroblastic tumors, in particular those lesions with a predominant hemangiopericytic pattern, has been a subject of controversy. The spectrum of these uncommon neoplasms encompasses infantile MF/myofibromatosis and variants, congenital/infantile fibrosarcoma, and neoplasms with atypical or intermediate features. Currently, infantile fibrosarcoma is defined by recurrent *ETV6-NTRK3* gene fusions.[8] Recently, a subgroup of *ETV6* fusion–negative infantile fibrosarcomas and infantile hemangiopericytic sarcomas were shown to harbor an alternative gene fusion involving the *NTRK1* gene.[10,11] The same gene fusion was very recently reported in distinctive

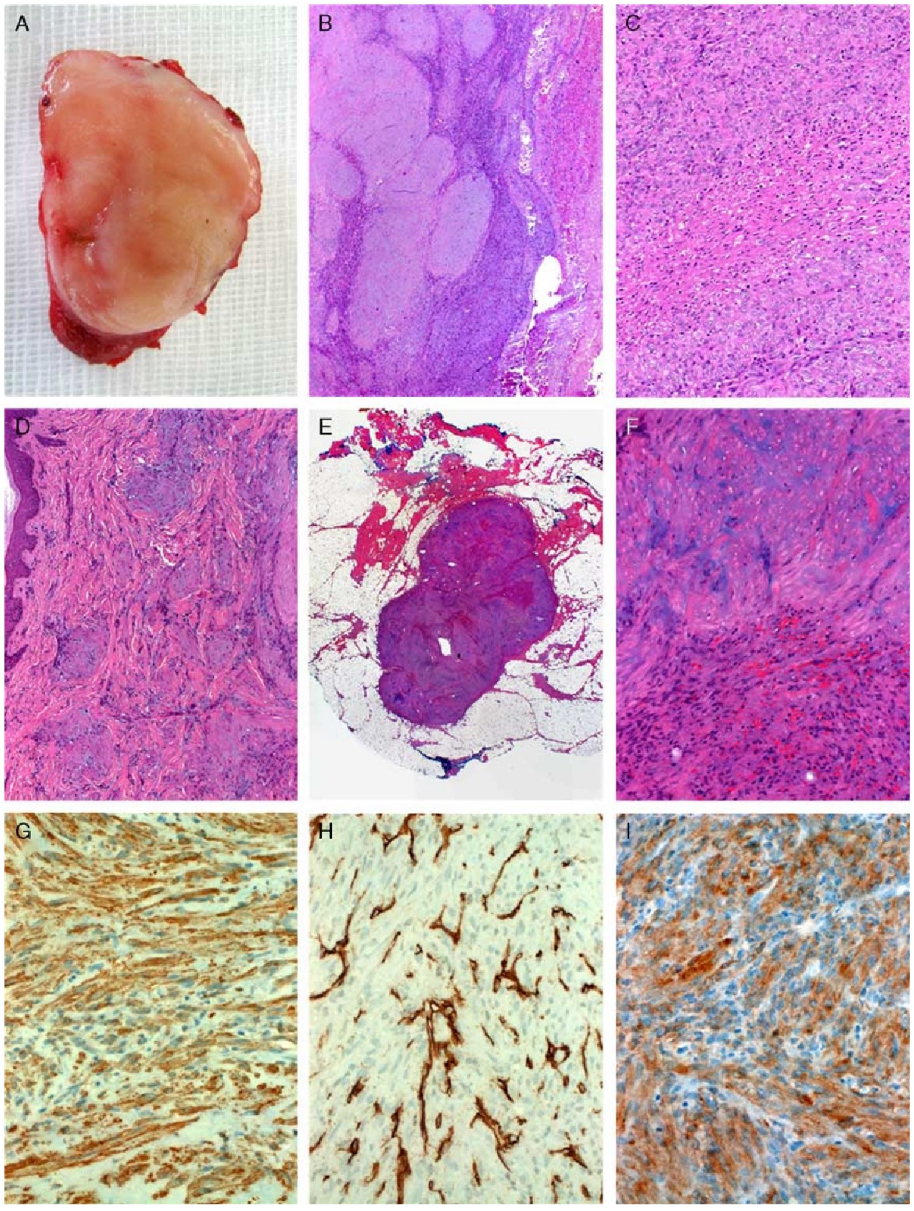

FIGURE 1. Histomorphologic features of sporadic infantile and adult MF. A, This large infantile MF (case 1) originated within the thyroid gland (note remnant of thyroid tissue at the lower border of the specimen). B, The same case showed prominent myxohyaline myointimal-like balls of classical MF. C, Other areas of same case showed atypical features with high cellularity, diffuse fascicular pattern, and focal hyaline necrosis. The periphery of the MF lesions varied from irregular (D; case 2) to well circumscribed (E; case 3). F, Higher magnification of E showed myxohyaline areas abutting cellular primitive spindle cells. Immunohistochemistry showed prominent expression of smooth muscle actin (G), negative staining with CD34 (H), and diffuse cytoplasmic and occasionally paranuclear dot-like pattern of PDGFRB (I). G–I are from case 1.

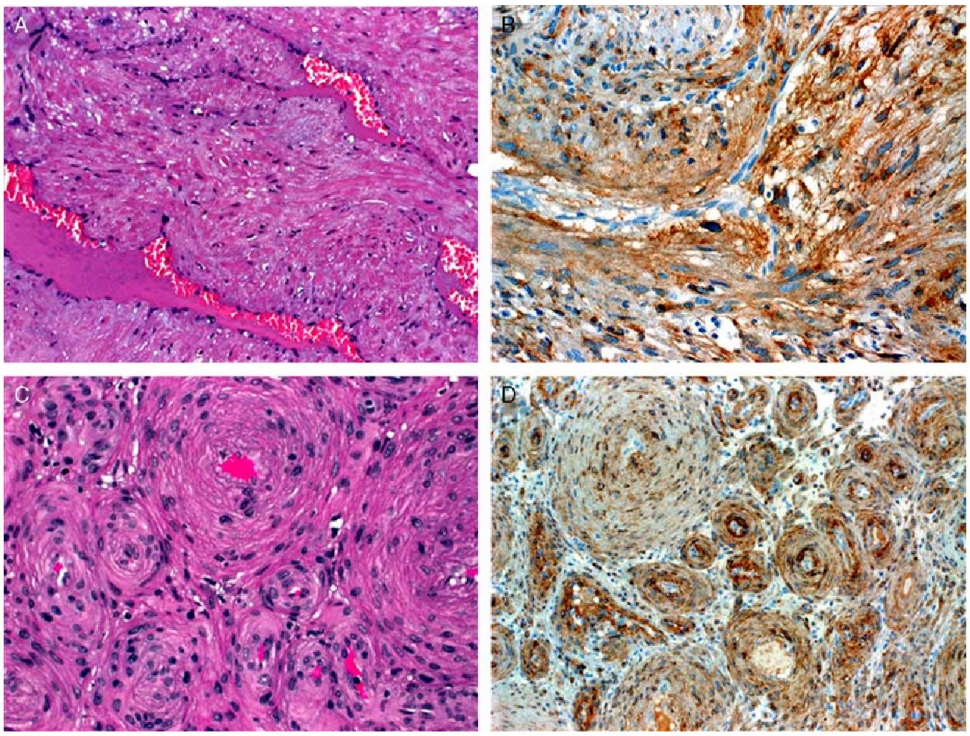

FIGURE 2. Histomorphologic features of angioleiomyoma and myopericytoma. Cases of angioleiomyoma (A) and myopericytoma (C) showed characteristic prototypical features distinctive from those of MF. PDGFRB immunostaining showed comparable cytoplasmic expression that is more evident in the vascular wall cells and less prominent in the intervening cells (B, angioleiomyoma; D, myopericytoma).

soft tissue lesions resembling lipofibromatosis but showing a neural immunophenotype.[17] However, the molecular pathogenesis of MF remains unclear. In this study, we show for the first time somatic gain-of-function *PDGFRB* mutations occurring at a high frequency in sporadic MFs (75% in infantile and 69% in adult cases). In contrast, there were no *PDGFRB* mutations in angioleiomyomas and myopericytomas tested in this study, suggesting molecular distinctness of MFs as *PDGFRB* mutation–driven neoplasms on one side and myopericytoma/angioleiomyoma as histologically overlapping lesions lacking these mutations on the other side.[18,19] Interestingly, we could not find any significant difference in PDGFRB immunostaining patterns of MF, angioleiomyoma, and myopericytoma highlighting the uselessness of the PDGFRB immunostaining in their distinction. In contrast, *PDGFRB* mutation analysis seems to be a promising novel adjunct tool to separate MF from angioleiomyoma and myopericytoma in cases with equivocal histomorphologic appearance or with limited tissue material. Whether myopericytoma and angioleiomyoma also represent genetically distinct, albeit morphologically overlapping, lesions remains to be evaluated in larger future studies. In this context, it is noteworthy that a subset of myopericytomas (15%) reportedly harbors *BRAF* mutations, but available data are still limited and do not allow for definite conclusion.[20] Furthermore, *ACTB-GLI* gene fusions have been described in some morphologically distinctive lesions in the pericytoma group.[21] Admittedly, our results regarding absence of *PDGFRB* mutations in angioleiomyoma and myopericytoma are limited by the low case numbers indicating the need to analyze larger series in future studies in order to address this point more reliably. The PDGFRB immunoexpression observed in all angioleiomyoma and myopericytoma cases in the absence of PDGFRB mutations is difficult to explain, but PDGFRB activation by alternative mechanisms other than mutations is possible, although a nonspecific reactivity or cross-reactivity with other cellular antigens cannot be ruled out with certainty.

The *PDGFRB* mutations in our current series are different from those reported in familial infantile MF.[12–14] Cheung et al[12] observed the p.R561C mutation

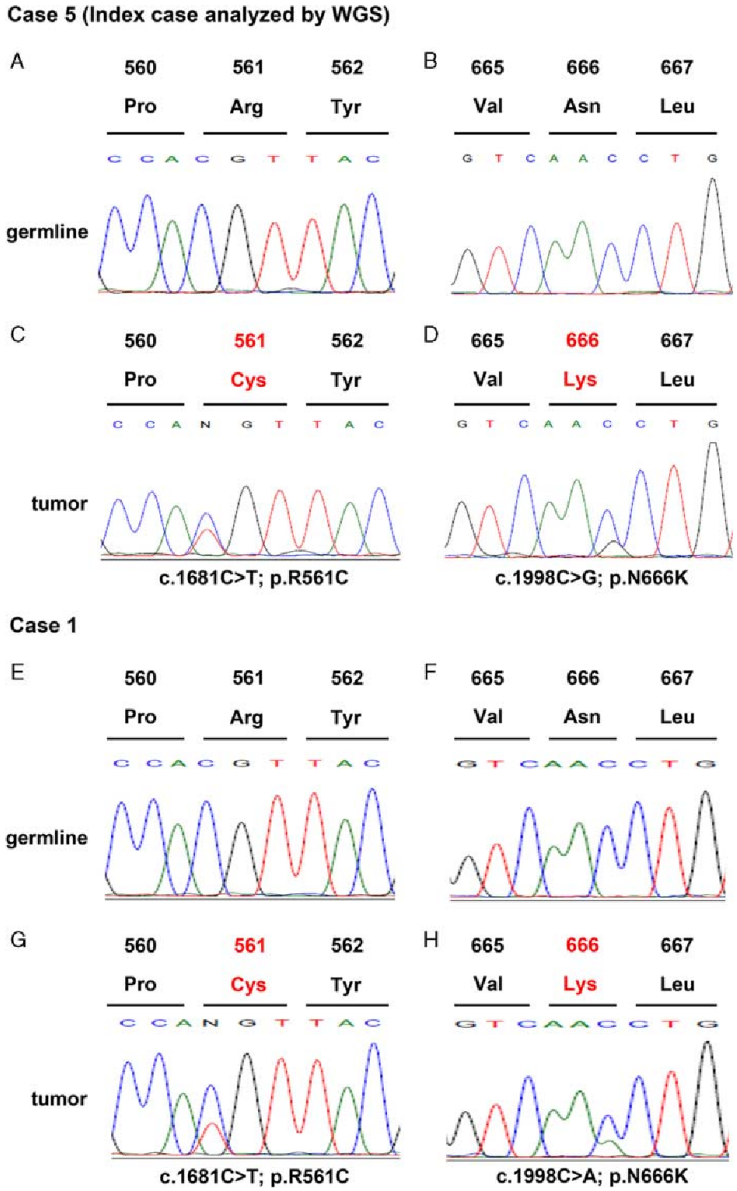

FIGURE 3. Somatic gain-of-function *PDGFRB* mutations in 2 cases of sporadic infantile MF. A–D, Case 5 (Index case): Sanger sequencing demonstrates a wild-type status in the germline DNA (A and B), compared with somatic gain-of-function mutations p.R561C (C) and p.N666K (D) in the tumor DNA. E–H, Case 1. Wild-type status in the germline DNA (E and F) compared with mutations p.R561C (G) and p.N666K (H) in the tumor DNA. Note the different nucleotide exchanges at position c.1998C in the 2 cases (C > G in case 5 vs. C > A in case 1), both resulting in the identical amino acid change p.N666K.

		fMF														PFBC		fMF					PS				
	Codon	559	560	561	562	563	564	565	566	567	568	569	570	571	572	... 658	659	660	661	662	663	664	665	666	667	668
	Amino acid	K	P	R	Y	E	I	R	W	K	V	I	E	S	V	L	G	P	H	L	N	V	V	N	L	L
Case	Diagnosis																									
	Infantile MF																									
1	Myofibroma - classical	K	P	C	Y	E	I	R	W	K	V	I	E	S	V	L	G	P	H	L	N	V	V	K	L	L
2	Myofibroma - classical	K	P	R	Y	E	I	R	W	K	V	I	E	S	V	L	G	P	H	L	N	V	V	K	L	L
4	Myofibroma - classical	K	P	R	Y	E	I	R	W	K	V	I	E	S	V	L	G	P	H	L	N	V	V	K	L	L
5	Myofibroma - mixed	K	P	C	Y	E	I	R	W	K	V	I	E	S	V	L	G	P	H	L	N	V	V	K	L	L
6	Myofibroma - mixed	K	P	R	C	E	I	R	W	K	V	I	E	S	V	L	G	P	H	L	N	V	V	K	L	L
7	Myofibroma - atypical	K	P	R	Y	E	I	R	W	K	V	I	E	S	V	L	G	P	H	L	N	V	V	N	L	L
8	Myofibroma - atypical	K	P	R	Y	E	I	R	S	K	V	N	E	S	V	L	G	P	H	L	N	V	V	N	L	L
9	Myofibroma - atypical	K	P	R	Y	E	I	R	W	K	V	I	E	S	V	L	G	P	H	L	N	V	V	N	L	L
	Adult MF																									
10	Myofibroma - classical	K	P	R	Y	E	I	R	W	K	V	I	E	S	V	L	G	P	H	L	N	V	V	N	L	L
11	Myofibroma - classical	K	P	R	Y	E	I	R	W	K	V	I	E	S	V	L	G	P	H	L	N	V	V	N	L	L
12	Myofibroma - classical	K	P	R	Y	E	I	R	W	K	V	I	E	S	V	L	G	P	H	L	N	V	V	N	L	L
13	Myofibroma - classical	K	P	R	Y	E	I	R	W	K	V	V	E	S	V	L	G	P	H	L	N	V	V	N	L	L
14	Myofibroma - classical	K	P	R	C	E	I	R	W	K	V	I	E	S	V	L	G	P	H	L	N	V	V	K	L	L
15	Myofibroma - classical	K	P	R	Y	E	R	-	-	K	V	I	E	S	V	L	G	P	H	L	N	V	V	N	L	L
16	Myofibroma - classical	K	P	R	Y	E	I	R	W	K	V	I	E	S	V	L	G	P	H	L	N	V	V	K	L	L
17	Myofibroma - classical	K	P	R	Y	E	I	R	W	K	V	I	E	S	V	L	G	P	H	L	N	V	V	K	L	L
18	Myofibroma - classical	K	P	R	Y	E	I	R	W	K	V	I	E	S	V	L	G	P	H	L	N	V	V	N	L	L
19	Myofibroma - classical	K	P	R	Y	E	I	R	C	-	-	-	E	S	V	L	G	P	H	L	N	V	V	N	L	L
20	Myofibroma - classical	K	P	R	Y	E	I	R	W	K	V	I	E	S	V	L	G	P	H	L	N	V	V	K	L	L
21	Myofibroma - mixed	K	P	R	D	E	I	R	W	K	V	I	E	S	V	L	G	P	H	L	N	V	V	N	L	L
22	Myofibroma - mixed	K	P	R	Y	E	I	R	W	K	V	I	E	S	V	L	G	P	H	L	N	V	V	N	L	L
23	Myofibroma - mixed	K	P	R	Y	E	I	R	W	K	V	I	E	S	V	L	G	P	H	L	N	V	V	K	L	L
24	Myofibroma - atypical	K	P	R	Y	E	I	R	W	K	V	I	E	S	V	L	G	P	H	L	N	V	V	K	L	L
25	Myofibroma - atypical	K	P	R	Y	E	I	R	W	K	V	I	E	S	V	L	G	P	H	L	N	V	V	K	L	L

FIGURE 4. Summary of *PDGFRB* mutations in a cohort of 25 infantile and adult sporadic MFs. Mutations clustered in the region R561 to I549 in PDGFRB exon 12, but were restricted to amino acid position N666 in exon 14. Notice that (except for codon 561) there was no overlap with amino acid positions reported to be involved in familial infantile MF (fMF), primary familial brain calcification (PFBC), and Penttinen Syndrom (PS). There were no significant differences in the distribution of PDGFRB mutations among cases of infantile versus adult MF or classical versus atypical or mixed histomorphology.

in the germline of 11 individuals from 4 different families. Martignetti et al[13] reported on 40 individuals from 8 families with the p.R561C germline mutation and 4 individuals from 1 family with a germline p.P660T mutation. Linhares et al[14] observed 3 individuals from 1 family with the p.R561C germline mutation, with 2 of the 3 affected individuals carrying a *PDGFRB* germline mutation developing infantile MFs.

In our series of 25 sporadic MFs, only 2 cases (both infantile MFs) harbored the p.R561C mutation involved in the vast majority of familial MFs (54 reported patients from 13 families). Notably, we were able to exclude a familial *PDGFRB* mutation in both patients by germline analysis. The p.P660T mutation reported in another family with familial MF was not detected in our samples. The p.N666K mutation, which constituted the most frequent mutation (12 cases) among our cohort of sporadic MFs, was reported as an additional somatic *PDGFRB* mutation in 2 tumors from 2 patients with p.R561C germline mutation[12] but was never found as a germline mutation. Moreover, we observed single amino acid substitutions at positions Y562, W566, and I569, as well as 2 deletions insertions in the same region, which have not been reported in familial infantile MF.

Apart from the familial form of infantile MF, *PDGFRB* germline mutations at specific amino acid positions have also been reported in other familial conditions. The activating *PDGFRB* germline mutation p.V665A is the cause of Penttinen Syndrome.[22] Loss-of-function mutations at positions p.L658P, p.R695C, and p.R987W are associated with primary familial brain calcification.[23–25] These amino acid positions were not involved in the spectrum of *PDGFRB* mutations among our sporadic MF cases.

There is some clinical and experimental evidence that activated PDGFRB can be targeted by tyrosine kinase inhibitors such as imatinib[26] and regorafenib.[27] However, the vast majority of sporadic/solitary MFs are successfully treated by simple surgical excision alone. Thus, the need for tyrosine kinase inhibitor therapy would be reserved for those rare cases with advanced and clinically problematic multicentric or visceral infantile myofibromatosis as well as rare cases with presumed malignant transformation.[28]

In summary, we herein describe for the first time frequent *PDGFRB* mutations in sporadic infantile and solitary adult MF, which differ significantly from the mutations described in familial infantile MF. Investigation of more cases, in particular those with atypical and worrisome features, as well as other mimickers in the heterogenous morphologic spectrum of MF is mandatory for validating the potential diagnostic value of *PDGFRB* mutation testing as a genotypic adjunct in difficult-to-classify lesions ("atypical MF" vs. "low-grade sarcomas").

ACKNOWLEDGMENTS

The authors thank Dr Irma Gresshoff, Simone Hebele, and Daniela Renner (Institute of Pathology, University Hospital Erlangen, Germany) for excellent technical assistance.

REFERENCES

1. Chung EB, Enzinger FM. Infantile myofibromatosis. *Cancer*. 1981;48:1807–1818.
2. Oudijk L, den Bakker MA, Hop WC, et al. Solitary, multifocal and generalized myofibromas: clinicopathological and immunohistochemical features of 114 cases. *Histopathology*. 2012;60:1–11.
3. Daimaru Y, Hashimoto H, Enjoji M. Myofibromatosis in adults (adult counterpart of infantile myofibromatosis). *Am J Surg Pathol*. 1989;13:859–865.
4. Beham A, Badve S, Suster S, et al. Solitary myofibroma in adults: clinicopathological analysis of a series. *Histopathology*. 1993;22:335–341.
5. Mentzel T, Calonje E, Nascimento AG, et al. Infantile hemangiopericytoma versus infantile myofibromatosis. Study of a series suggesting a continuous spectrum of infantile myofibroblastic lesions. *Am J Surg Pathol*. 1994;18:922–930.
6. Granter SR, Badizadegan K, Fletcher CD. Myofibromatosis in adults, glomangiopericytoma, and myopericytoma: a spectrum of tumors showing perivascular myoid differentiation. *Am J Surg Pathol*. 1998;22:513–525.
7. Linos K, Carter JM, Gardner JM, et al. Myofibromas with atypical features: expanding the morphologic spectrum of a benign entity. *Am J Surg Pathol*. 2014;38:1649–1654.
8. Knezevich SR, McFadden DE, Tao W, et al. A novel ETV6-NTRK3 gene fusion in congenital fibrosarcoma. *Nat Genet*. 1998;18:184–187.
9. McMenamin ME, Fletcher CD. Malignant myopericytoma: expanding the spectrum of tumours with myopericytic differentiation. *Histopathology*. 2002;41:450–460.
10. Wong V, Pavlick D, Brennan T, et al. Evaluation of a congenital infantile fibrosarcoma by comprehensive genomic profiling reveals an LMNA-NTRK1 gene fusion responsive to crizotinib. *J Natl Cancer Inst*. 2015;108:1(1–3).
11. Haller F, Knopf J, Ackermann A, et al. Pediatric and adult soft tissue sarcomas with NTRK1 gene fusions: a subset of spindle cell sarcomas unified by prominent myo-/hemangiopericytic pattern. *J Pathol*. 2016;238:700–710.
12. Cheung YH, Gayden T, Campeau PM, et al. A recurrent PDGFRB mutation causes familial infantile myofibromatosis. *Am J Hum Genet*. 2013;92:996–1000.
13. Martignetti JA, Tian L, Li D, et al. Mutations in PDGFRB cause autosomal-dominant infantile myofibromatosis. *Am J Hum Genet*. 2013;92:1001–1007.
14. Linhares ND, Freire MC, Cardenas RG, et al. Modulation of expressivity in PDGFRB-related infantile myofibromatosis: a role for PTPRG? *Genet Mol Res*. 2014;13:6287–6292.
15. Fletcher CDM, Bridge JA, Lee JC. Extrapleural solitary fibrous tumour. In: Fletcher CDM, Bridge JA, Hogendoorn PCW, Mertens F, eds. *World Health Organisation classification of Tumours of Soft Tissue and Bone*, 4th edn. Lyon: IARC Press; 2013:118–121.
16. Haller F, Bieg M, Moskalev EA, et al. Recurrent mutations within the amino-terminal region of β-catenin are probable key molecular driver events in sinonasal hemangiopericytoma. *Am J Pathol*. 2015;185:563–571.
17. Agaram NP, Zhang L, Sung YS, et al. Recurrent NTRK1 gene fusions define a novel subset of locally aggressive lipofibromatosis-like neural tumors. *Am J Surg Pathol*. 2016;40:1407–1416.
18. Matsuyama A, Hisaoka M, Hashimoto H. Angioleiomyoma: a clinicopathologic and immunohistochemical reappraisal with special reference to the correlation with myopericytoma. *Hum Pathol*. 2007;38:645–651.
19. Mentzel T, Dei Tos AP, Sapi Z, et al. Myopericytoma of skin and soft tissues: clinicopathologic and immunohistochemical study of 54 cases. *Am J Surg Pathol*. 2006;30:104–113.
20. Sadow PM, Priolo C, Nanni S, et al. Role of BRAFV600E in the first preclinical model of multifocal infiltrating myopericytoma development and microenvironment. *J Natl Cancer Inst*. 2014;106:8(1-7).
21. Dahlén A, Fletcher CD, Mertens F, et al. Activation of the GLI oncogene through fusion with the beta-actin gene (ACTB) in a group of distinctive pericytic neoplasms: pericytoma with t(7;12). *Am J Pathol*. 2004;164:1645–1653.
22. Johnston JJ, Sanchez-Contreras MY, Keppler-Noreuil KM, et al. A point mutation in PDGFRB causes autosomal-dominant penttinen syndrome. *Am J Hum Genet*. 2015;97:465–474.
23. Nicolas G, Charbonnier C, de Lemos RR, et al. Brain calcification process and phenotypes according to age and sex: Lessons from SLC20A2, PDGFB, and PDGFRB mutation carriers. *Am J Med Genet B Neuropsychiatr Genet*. 2015;168:586–594.
24. Sanchez-Contreras M, Baker MC, Finch NA, et al. Genetic screening and functional characterization of PDGFRB mutations associated with basal ganglia calcification of unknown etiology. *Hum Mutat*. 2014;35:964–971.
25. Vanlandewijck M, Lebouvier T, Andaloussi Mäe M, et al. Functional characterization of germline mutations in PDGFB and PDGFRB in primary familial brain calcification. *PLoS One*. 2015;10:e0143407.
26. Arts FA, Chand D, Pecquet C, et al. PDGFRB mutants found in patients with familial infantile myofibromatosis or overgrowth syndrome are oncogenic and sensitive to imatinib. *Oncogene*. 2016;35:3239–3248.
27. Rechsteiner M, Wild P, Kiessling MK, et al. A novel germline mutation of PDGFR-β might be associated with clinical response of colorectal cancer to regorafenib. *Ann Oncol*. 2015;26:246–248.
28. Dictor M, Elner A, Andersson T, et al. Myofibromatosis-like hemangiopericytoma metastasizing as differentiated vascular smooth-muscle and myosarcoma. Myopericytes as a subset of "myofibroblasts". *Am J Surg Pathol*. 1992;16:1239–1247.

2.2.4. SUPERFICIAL ACRAL FIBROMYXOMA: CLINICOPATHOLOGIC, IMMUNOHISTOCHEMICAL AND MOLECULAR STUDY OF 11 CASES HIGHLIGHTING FREQUENT RB1 LOSS/DELETIONS

This study was focused on benign and predominantly acrally located fibroblastic tumors called Superficial acral fibromyxoma (SAF). Histologically, SAF have a fairly non-specific morphology and often elude confident diagnosis Moreover, the IHC profile of SAF is also unspecific, usually expressing only CD34.

In a cohort of 11 cases, we studied the Retinoblastoma-1 (RB-1) protein expression as well as *RB1* gene deletion by FISH. Except for one case, all 9 analyzable cases showed a complete loss of RB-1 immunoexpression. Moreover, all 7 tested cases had *RB1* gene deletion by FISH. These results highlight frequent RB1 deficiency as possible driver molecular event in SAF and indicate relationship of SAF to the RB1-deleted tumor family. This group includes, besides spindle cell and pleomorphic lipoma as the prototypes [46], also mammary-type myofibroblastoma [47] and cellular angiofibroma [48]. All these lesions are unified by consistent expression of CD34, RB1 loss by IHC, as a consequence of RB1 gene deletions, and a benign clinical course with a low recurrence rate. In this study, we added another lesion to this family of RB1-deficient neoplasms, the SAF. The loss of RB1 IHC staining and perhaps even more importantly, the *RB1* gene deletions detectable by FISH provide a very useful adjuvant methods especially in difficult to diagnose cases, as some SAF are occasionally confused for low-grade sarcomas.

Human Pathology (2017) 60, 192–198

ELSEVIER

Human PATHOLOGY

www.elsevier.com/locate/humpath

Original contribution

Superficial acral fibromyxoma: clinicopathological, immunohistochemical, and molecular study of 11 cases highlighting frequent Rb1 loss/deletions☆

Abbas Agaimy MD[a,*], Michael Michal MD[b], Johannes Giedl MD[a], Ladislav Hadravsky MD[c,d], Michal Michal MD[c]

[a]*Institute of Pathology, Friedrich-Alexander University Erlangen-Nuremberg, University Hospital, 91054 Erlangen, Germany*
[b]*Department of Pathology, Charles University, Biomedical Center, Faculty of Medicine in Plzen and Charles University Hospital Plzen, 304 60 Plzen, Czech Republic*
[c]*Department of Pathology, Charles University, Faculty of Medicine, 304 60 Plzen, Czech Republic*
[d]*Department of Pathology, Charles University, 3rd Medical Faculty and Charles University Hospital Royal Vineyards, 100 00 Prague, Czech Republic*

Received 2 September 2016; revised 30 September 2016; accepted 14 October 2016

Keywords:
Superficial acral fibromyxoma;
Digital fibromyxoma;
Rb1;
Deletion;
Angiofibroma;
Angiomyxoma

Summary Superficial acral fibromyxoma (SAF) is an uncommon benign dermal mesenchymal lesion of adults with predilection for acral sites, in particular the nail region. To date, less than 300 cases have been reported. SAFs consistently express CD34, but other diagnostic markers or specific genetic alterations have not been established yet. We describe 11 SAFs occurring in 7 men and 4 women aged 37 to 86 years (median, 48 years). Mean size was 6 mm (range, 4-20 mm). Affected sites were fingers (n = 5), toes (n = 3), heel (n = 1), calf (n = 1), and unspecified digit (n = 1). None of 10 patients with available follow-up (2-60 months; median, 24 months) developed recurrence. Histology showed relatively hypocellular vaguely lobulated nodules composed of bland-looking spindled or stellate fibroblast-like cells arranged into storiform or loose fascicles within a variably myxoid, fibromyxoid, or collagenous vascularized stroma. Immunohistochemistry showed expression of CD34 (9/10) and focal weak reactivity for epithelial membrane antigen (2/11). None of the lesions expressed protein S100 (0/11), MUC4 (0/11), or STAT6 (0/11). Loss of Rb1 immunoexpression was observed in 9 (90%) of 10 cases. All 7 cases with successful *RB1* fluorescence in situ hybridization testing showed *RB1* gene deletions, which was variably associated with co-loss of the corresponding 13q12 signal (monosomy at the 13q region). To our knowledge, this is the first study investigating the expression status of the tumor suppressor Rb1 in SAF by immunohistochemistry and fluorescence in situ hybridization. Our results showed frequent Rb1 deficiency as a possible driver molecular event in SAF (seen in 90% of cases) indicating relationship of SAF to the *RB1*-deleted tumor family.

1. Introduction

Superficial acral fibromyxoma (SAF; synonym: digital fibromyxoma) is a relatively uncommon benign mesenchymal soft tissue lesion with a significant predilection for acral sites, in

☆ Competing interests: None.

* Corresponding author at: Pathologisches Institut, Universitätsklinikum Erlangen, Krankenhausstrasse 8-10, 91054 Erlangen, Germany.
E-mail address: abbas.agaimy@uk-erlangen.de (A. Agaimy).

http://dx.doi.org/10.1016/j.humpath.2016.10.016
0046-8177/

particular the nail region of fingers and toes. Adults are affected with a wide age range [1]. Since the first description in a series of 37 cases by Fetsch et al [2] in 2001, a total of ≈300 cases have been reported in the English literature (260 cases in 5 major series of 12-124 cases published during the last 7 years [2-7] and 36 cases as single case reports or small series of up to 4 patients [1,8]). Although the tumor is essentially dermal based, variable extension into the subcutaneous tissue and even rarely into underlying bone may be seen, particularly in larger lesions [9].

The histogenesis of SAF remained unclear, although the immunohistochemical and histologic features are considered consistent with a fibroblastic origin/phenotype [2]. In this study, we describe our experience with 11 SAFs identified from our files during the last 5 years. In addition to CD34 and other relevant markers, we investigated SAF for the first time for expression of the retinoblastoma antigen 1 (Rb1) and verified the status of the *RB1* gene by fluorescence in situ hybridization (FISH).

2. Materials and methods

Cases were retrieved from our surgical pathology files and from the consultation files of 2 of the authors (A. A. and M. M.). Immunohistochemistry (IHC) was performed on 3-μm sections cut from paraffin blocks using a fully automated system ("Benchmark XT System," Ventana Medical Systems, Tucson, AZ) and the following antibodies: CD34 (clone BI-3C5, 1:200; Zytomed, Berlin, Germany), α-smooth muscle actin (clone 1A4, 1:200; Dako, Hamburg, Germany), MUC4 (clone 8G7, 1:500; Santa Cruz Biotechnology, Santa Cruz, CA), protein S100 (polyclonal, 1:2500; Dako), STAT6 (clone sc-621, 1:1000; Santa Cruz Biotechnology), epithelial membrane antigen (EMA; clone E29, 1:200; Dako), and Rb1 (1:200; BD Biosciences, Heidelberg, Germany). Rb1 loss was defined as complete loss of nuclear Rb1 immunoexpression restricted to the tumor cells in the presence of unequivocal nuclear reactivity in endothelial cells in the background stroma.

2.1. *RB1* FISH testing

To detect copy number alterations of the *RB1* gene locus, FISH was performed on 1- to 2-μm-thick sections cut from formalin-fixed, paraffin-embedded tissue blocks using the ZytoLight SPEC *RB1/13q12* Dual Color Probe (ZytoVision, Bremerhaven, Germany) with standard protocols according to the manufacturer's instructions. Fifty tumor cells were visually inspected using a fluorescence microscope. The presence or absence of the *RB1* gene locus (orange signal) and of the green signal indicating intact 13q12 region is assessed and reported. The variable alterations detected are described as follows: absence of one or both of *RB1* orange signal/s but intact 13q12 green signals is reported as monoallelic and biallelic deletion of *RB1*, respectively. Absence of 1 orange and 1 green signal is reported as monosomy 13q or at least part of it spanning both *RB1* gene locus and 13q12 region. Variable combinations were observed as well and reported accordingly. A cutoff of greater than 22% was used to define positive FISH results [10].

3. Results

3.1. Clinical features

The main clinical and demographic features of the patients are summarized in Table 1. The patients were 4 women and 7 men aged 37 to 86 years (median, 48 years). Lesions were located mainly to the fingers (n = 5) and toes (n = 3). One case each originated in the heel, calf, and the nail bed of unspecified digit. Follow-up information was available for 10 patients and ranged from 2 to 60 months (median, 24 months). No recurrence was recorded at last follow-up. Although no detailed clinical history was available in most of cases, no special associated diseases or neoplasms have been recorded.

3.2. Pathological findings

Size of the lesions ranged from 4 to 20 mm (median, 6 mm). At low power, most lesions were seen as relatively small polypoid or dome-shaped nodules (Fig. 1A) that were either located immediately beneath the epidermis (Fig. 1B) or separated from it by a narrow compressed fibrous *Grenzzone* (Fig. 1C and D). The periphery of the lesions was usually well delineated, but not encapsulated (Fig. 1A and E). The deeper borders of the tumors were irregular in 4 and well circumscribed in 5 cases. In 2 lesions, the deeper margin was not recognizable in the specimen. A vaguely lobular architecture was fairly common and is more prominent in larger lesions (Fig. 1F). At higher magnification, the tumors were composed of bland-looking spindled or stellate-shaped fibroblast-like mesenchymal cells arranged into vague storiform or poorly formed loose fascicles set within a variably myxoid to fibromyxoid or heavily collagenous well-vascularized stroma (Fig. 2A-D). The stroma was vascular and highly myxoid in some lesions to warrant the descriptive alternate term *angiomyxoma* (Fig. 2B and E). Special histologic features that are worth mentioning include higher cellularity (seen in 3 cases; Fig. 2F), desmoplastic features and/or heavily collagenized stroma seen focally in 1 case each (Fig. 2C), and significant myxoid background seen in 1 case (Fig. 2B). Numerous mast cells were seen in the background in most of cases. Multinucleated giant cells were not observed in this series.

Results of the IHC are summarized in Table 2. The tumor cells showed consistent expression of CD34, which is usually strong and diffuse, highlighting the lesion at low power (9/10 cases; Fig. 3A). EMA was expressed in 2 of 11 cases but usually focal and weak (Fig. 3B). Focal α-smooth muscle actin

Table 1 Clinicopathological features of SAFs (n = 11)

No	Age (y)/sex	Site/duration	Size mm	Initial diagnosis	Circumscribed/margin status	Special histologic features	Outcome
1	86/F	Right thumb (ulcerated)	5	Myxoid fibroma	Irregular margin complete excision	Focal desmoplastic features	NA
2	38 M	Tip of 3rd toe	6	Digital fibromatosis	Circumscribed margin, complete excision		NER (7 mo)
3	39/M	Nail bed, first digit (7 y)	20	SAF	Irregular, infiltrative into subcutis, complete excision	Cellular	NER (4 mo)
4	50/M	Heel left	6	Angiofibroma	Deep border not seen	Moderately cellular	NER (3 mo)
5	76/M	Finger distal	20	Myxoma *vs* LGFMS	Irregular, infiltrative into subcutis, complete excision	Cellular	NER (2 mo)
6	84/M	3rd toe right foot	10	NA	Circumscribed margin complete excision		NER (36 mo), DOOC
7	42/M	3rd finger right hand	10	NA	Irregular margin complete excision	Highly myxoid	NER (60 mo)
8	39/F	Right thumb	6	LGFMS	Circumscribed margin complete excision		NER (12 mo)
9	48/F	5th toe left foot	5	NA	Deeper margin not included		NER (24 mo)
10	37/M	Left calf	4	NA	Circumscribed margin complete excision	Focal epidermal induction	NER (24 mo)
11	53/F	4th finger left hand	10	NA	Circumscribed margin complete excision	Densely collagenized	NER (48 mo)

Abbreviations: DOOC, died of other cause; F, female; LGFMS, low-grade fibromyxoid sarcoma; M, male; NA, not available; NER, no evidence of recurrence.

expression was seen in 1 of the 11 cases. None of the lesions expressed protein S100 (0/11), MUC4 (0/11), or STAT6 (0/11).

3.3. Rb1 expression status and *RB1* FISH results

By IHC, 9 (90%) of 10 evaluable cases showed loss of Rb1, whereas the background stromal fibroblasts and endothelial cells showed intact expression (Fig. 3C). Using FISH methods, assessable results were obtained in 7 cases; all showed *RB1* gene locus alterations (Fig. 4). Two cases had monoallelic deletion of *RB1* as the sole detected abnormality. Three cases had monoallelic deletion of *RB1* with co-loss of the corresponding 13q12 signal resulting in a 13q12 monosomy, and 2 cases had more complex findings (Table 2). The latter contained an admixture of cells with loss of one or both *RB1* signals, frequently accompanied by loss of one 13q12 signal.

4. Discussion

SAF (synonym: digital fibromyxoma) is an uncommon but possibly underreported benign cutaneous mesenchymal tumor of unknown pathogenesis. Since the original description by Fetsch et al [2] in 2001, ≈300 cases have been reported in variably sized major case series and as case reports [1-8]. Although no true statistical studies on the frequency and/or incidence of SAF are available, a recent study from the United Kingdom showed 5% of all acral lesions coded as fibroma, myxoma, or dermatofibroma to represent SAF [4].

Most SAFs present as small polypoid or dome-shaped lesions measuring 2 cm or less, but lesions as large as 5 cm have been reported [2,7]. A significant subset of cases presented as subungual or periungual lesions [2-7]. The histologic spectrum of SAF varies but most lesions have in common a proliferation of spindled or stellate-shaped fibroblast-like cells within a myxocollagenous stroma. Rare reported variants include cellular lesions [5] and those with a lipomatous component [11]. SAFs occasionally contain multinucleated cells that may have a floret-like appearance, reminiscent of those encountered in pleomorphic lipoma. Although in most of cases, only mild nuclear atypia is seen, a small subset of cases may display substantial atypia [2].

To date, immunohistochemical analysis showed consistent expression of CD34 and occasional reactivity with EMA [2-7]. In this study, we analyzed a series of 11 SAFs not reported before. Our findings are consistent with current knowledge on the clinicopathological and demographic features of this distinctive lesion. We included a single case from the heel, which is an uncommon site reported previously in only very few cases [3]. In addition, one of our cases presented in the calf, which also represents a rare location for this lesion.

Rb1 is a chromatin-associated protein that acts as a tumor suppressor protein [12]. The gene encoding Rb1 is mapped to chromosome 13q14.2. Rb1 plays a crucial role in the regulation of the cell cycle processes [12]. Deletion of *RB1* associated with loss of the protein expression by IHC was originally observed in retinoblastoma (hence the name), but later studies showed frequent loss of expression of this tumor suppressor protein either as a secondary event related to biological tumor progression in a variety of aggressive malignancies [12] or as a sole driver event in a family of benign mesenchymal neoplasms [13]. The latter family of Rb1-deficient benign mesenchymal lesions includes, besides

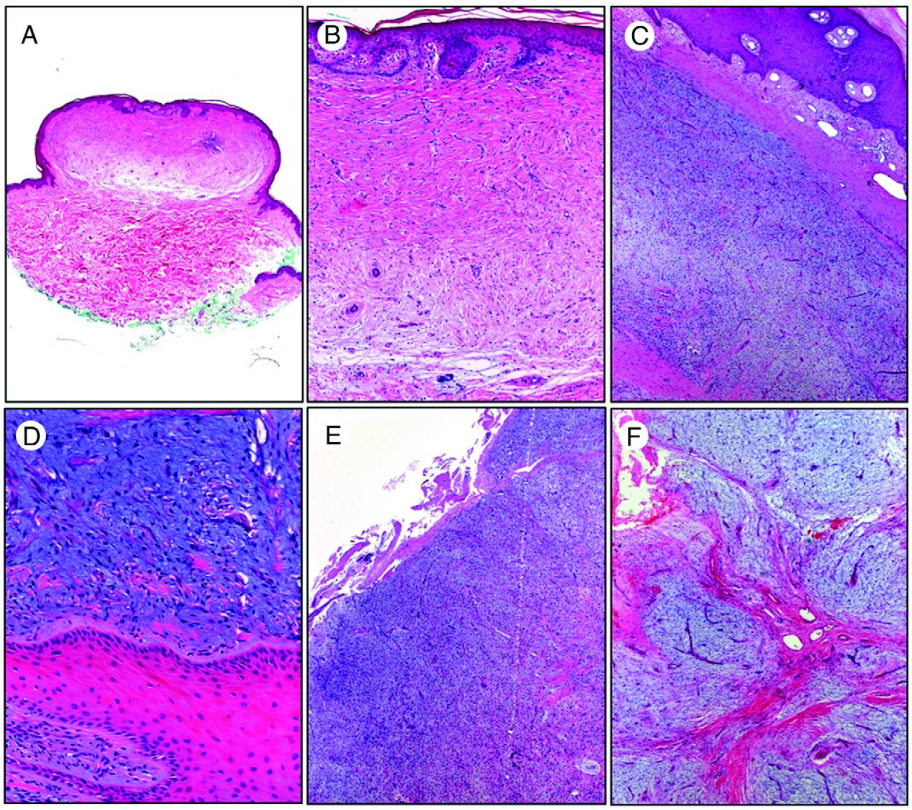

Fig. 1 At low power, SAF is a well-circumscribed dermal dome-shaped nodule (A; original magnification ×50) with infrequent signs of epidermal induction (B; ×100). Most lesions showed a narrow rim of *grenzzone* connective tissue separating them from the epidermis (C; ×100), which is frequently hyperplastic and hyperkeratotic (D; ×200). E, The deep and lateral lesional margins are usually well circumscribed but nonencapsulated (×100). F, A vague lobular architecture is characteristic (×100).

spindle cell and pleomorphic lipoma as the prototypes [13], also mammary-type myofibroblastoma [14] and cellular angiofibroma [15]. All these lesions are unified by consistent expression of CD34, Rb1 loss by IHC as a consequence of *RB1* gene deletions, and a benign clinical course with a low recurrence rate. In this study, we added another lesion to this family of Rb1-deficient neoplasms, the SAF.

To our knowledge, this is the first study investigating the expression status of the tumor suppressor protein Rb1 in SAF by IHC and complemented by FISH analysis using an *RB1* FISH probe. Our results showed loss of Rb1 immunoexpression in 90% of SAF. Consistent with this immunohistochemical loss of Rb1 expression, *RB1* deletion was confirmed by FISH in all 7 cases with assessable results using both tools. These results highlight frequent Rb1 deficiency as possible driver molecular event in SAF and indicate relationship of SAF to the *RB1*-deleted tumor family [13]. In this context, it is noteworthy that multiple acral myxoid fibromas (with features consistent with SAF) have been described in a patient with familial retinoblastoma syndrome caused by a germline *RB1* mutation [16]. This reported case is consistent with our current study and illustrates that multiple SAFs may rarely occur in a hereditary background, whereas sporadic SAF as a solitary lesion is driven by somatic *RB1* deletion.

In addition to SAF, the differential diagnostic spectrum of CD34-positive dermal-based mesenchymal lesions at acral sites is heterogeneous and includes plaque-like dermal fibroma [17], myxoid dermatofibrosarcoma protuberans [18], soft tissue perineurioma and acquired digital fibrokeratoma, cutaneous myxoma (superficial angiomyxoma [19,20]), and others. As seen in the current study, due to the highly variable histologic appearance of SAF, many other entities may enter the differential diagnosis as well. Our impression is that SAF seems still to be underrecognized as a specific entity as most of our consult cases were submitted with alternative diagnoses other than SAF. The original diagnosis in some of our cases included, in addition to other benign diagnoses, low-grade fibromyxoid sarcoma and fibromatoses. This highlights the potential hazard

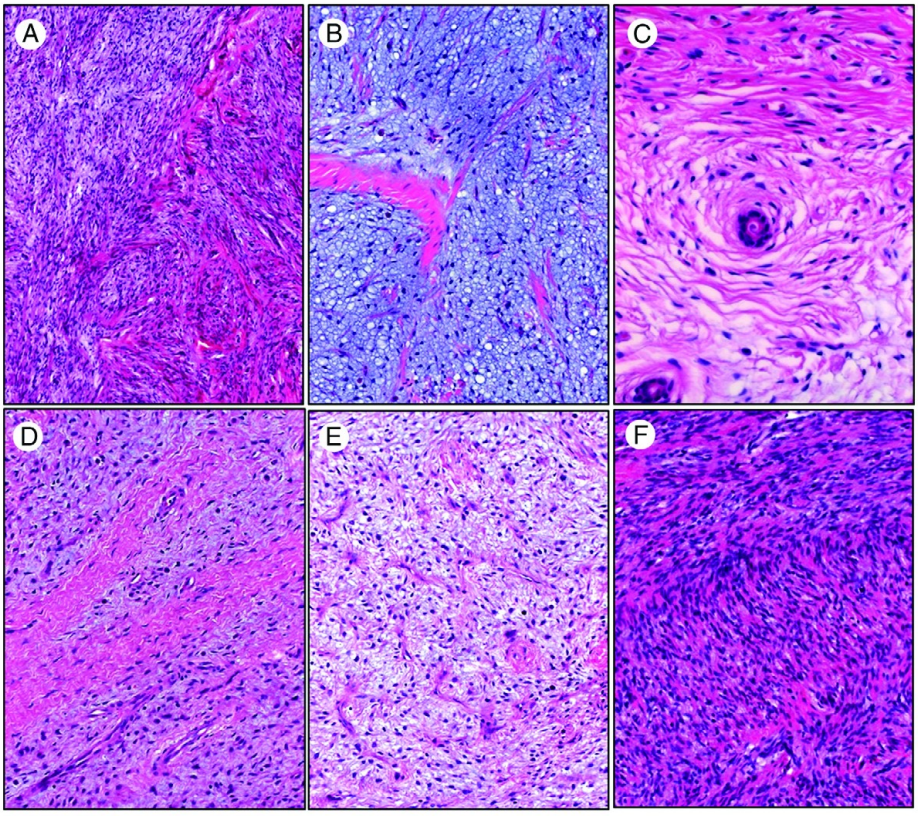

Fig. 2 Histologically, SAF ranged from myxocollagenous (A; ×200) to highly myxoid (B; ×400) or significantly collagenized (C; ×400) lesions with variable cellularity (note entrapment of adnexa in panel C). D, Myxoid areas were frequently traversed by wavy hyaline tendinous connective tissue imparting a biphasic pattern (×200). E, Some highly vascularized lesions closely mimicked soft tissue angiofibroma (×200). F, This otherwise typical SAF showed areas with significant cellularity but no atypia or mitoses (×400).

Table 2 IHC and molecular findings in SAFs (n = 11)

No	CD34	S100	SMA	MUC4	EMA	STAT6	Rb1 IHC	*RB1* FISH	Other markers tested negative
1	+++	−	−	−	−	−	Loss	NR	
2	+++	−	−	−	−	−	Loss	Monoallelic deletion	TLE1, GLUT1, claudin-1, GFAP
3	−	−	−	−	+	−	Loss	Monoallelic deletion, many cells with 13q12 monosomy = loss of both Rb1 signals	
4	+++	−	−	−	−	−	Loss	Monoallelic deletion, many cells with 13q12 monosomy = loss of both Rb1 signals	Ki-67 < 1%
5	+++	−	−	−	−	−	Loss	Monoallelic deletion	TLE1, GFAP, claudin-1, Ki-67 < 1%
6	+++	−	F+	−	−	−	Loss	NR	
7	+++	−	−	−	−	−	Loss	Monoallelic deletion (monosomy 13q12)	
8	++wk	−	−	−	−	−	Loss	Monoallelic deletion (monosomy 13q12)	MiB1 < 1%
9	NR	−	−	−	F+	−	Intact	NR	
10	+++	−	−	−	−	−	Loss	Monoallelic deletion (monosomy 13q12)	
11	++	−	−	−	−	−	NR	NR	Claudin-1, GLUT-1

Abbreviations: F, focal; NR, no results due to artifacts or suboptimal tissue preservation; wk, weak.

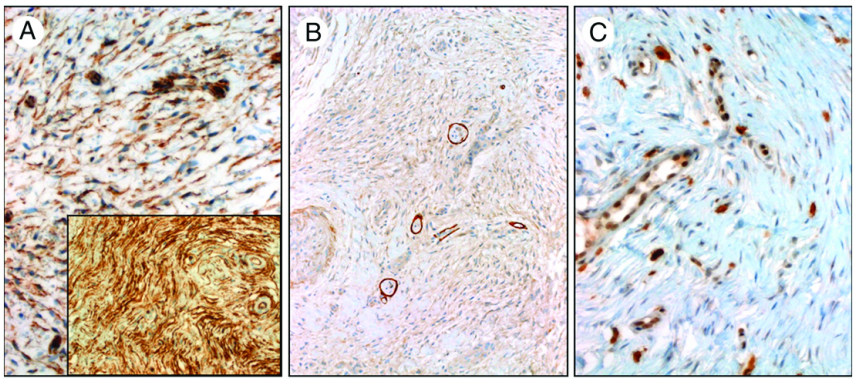

Fig. 3 A, IHC showed consistent expression of CD34 with delicate (main image) to strong diffuse (×400; inset, ×100) cytoplasmic pattern. B, EMA was negative in most cases (note staining in small nerve twigs within the lesion; ×100). C, Rb1 was lost in the neoplastic cells while being retained in endothelial cells, a few fibroblasts and numerous scattered mast cells in the background (×400).

of misinterpreting SAF as a malignancy if one is not familiar with this distinctive lesion. The distinctive acral and/or peri/subungual location, the characteristic biphasic myxocollagenous stroma, the bland-looking fibroblast-like cells lacking significant atypia or mitotic figures supplemented by CD34 expression, and loss of Rb1 are almost pathognomonic to SAF as opposed to other lesions in the differential diagnostic category. The rare atypical SAF variants with pleomorphism and/or mitoses should be carefully assessed to exclude alternative diagnoses, in particular low-grade sarcomas [2].

Absent CD34 immunoreactivity in otherwise typical SAF (seen in one of our cases) indicates that genuine SAF might rarely lack CD34 expression. In this study, we observed intact Rb1 expression in a single case, but unfortunately, the FISH results and CD34 immunostaining were inconclusive in this case due to suboptimal tissue preservation. Either this Rb1-intact variant might be related to alternative yet unidentified molecular alterations other than Rb1 loss, or it does represent other yet undefined lesions falling into the morphologic spectrum of SAF. In this context, soft tissue angiofibroma is particularly prone to be mistaken for SAF and vice versa. This is due to the overlapping morphologic features and IHC (expression of CD34 and variable expression of EMA) in both entities [1,21]. However, angiofibroma of soft tissue presents only rarely at acral sites (only 2/37 lesions originated in the digits), and it shows a female preponderance in contrast to the male predilection seen in SAF [21]. Also, the mean size of angiofibroma is much larger than that of SAF (3.5 versus 1.7 cm) [21]. Notably, soft tissue angiofibroma was related to recurrent gene fusions resulting in expression of the AHRR/NCOA2 transcripts [22]. In this regard, it should be pointed out that analysis of Rb1 status would be contributory to the precise classification of acral lesions with features of soft tissue angiofibroma and SAF, which are overlapping histologically and immunophenotypically.

In summary, we herein described 11 cases of SAF, uncovering frequent *RB1* deletions as the possible pathogenetic alteration in this uncommon but likely underreported benign dermal tumor. Our results highlight the value of adding Rb1 IHC to the marker panel used to classify CD34-positive dermal spindle cell myxoid lesions.

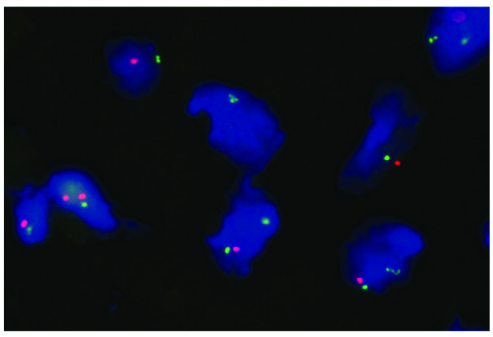

Fig. 4 FISH findings in SAF (case 3). Loss of 1 orange *RB1* signal and 1 green 13q12 signal was seen in several tumor cells indicating monosomy at the 13q region.

References

[1] Ashby-Richardson H, Rogers GS, Stadecker MJ. Superficial acral fibromyxoma: an overview. Arch Pathol Lab Med 2011;135:1064-6.

[2] Fetsch JF, Laskin WB, Miettinen M. Superficial acral fibromyxoma: a clinicopathologic and immunohistochemical analysis of 37 cases of a distinctive soft tissue tumor with a predilection for the fingers and toes. Hum Pathol 2001;32:704-14.

[3] Al-Daraji WI, Miettinen M. Superficial acral fibromyxoma: a clinicopathological analysis of 32 tumors including 4 in the heel. J Cutan Pathol 2008;35:1020-6.

[4] Prescott RJ, Husain EA, Abdellaoui A, et al. Superficial acral fibromyxoma: a clinicopathological study of new 41 cases from the U.K.:

should myxoma (NOS) and fibroma (NOS) continue as part of 21st-century reporting? Br J Dermatol 2008;159:1315-21.
[5] Luzar B, Calonje E. Superficial acral fibromyxoma: clinicopathological study of 14 cases with emphasis on a cellular variant. Histopathology 2009;54:375-7.
[6] Fanti PA, Dika E, Piraccini BM, Infusino SD, Baraldi C, Misciali C. Superficial acral fibromyxoma: a clinicopathological and immunohistochemical analysis of 12 cases of a distinctive soft tissue tumor with a predilection for the fingers and toes. G Ital Dermatol Venereol 2011;146:283-7.
[7] Hollmann TJ, Bovée JV, Fletcher CD. Digital fibromyxoma (superficial acral fibromyxoma): a detailed characterization of 124 cases. Am J Surg Pathol 2012;36:789-98.
[8] Grigore LE, Baican CI, Botar-Jid C, et al. Clinico-pathologic, dermoscopic and ultrasound examination of a rare acral tumour involving the nail—case report and review of the literature. Clujul Med 2016;89:160-4.
[9] Carranza C, Molina-Ruiz AM, Pérez de la Fuente T, Kutzner H, Requena L, Santonja C. Subungual acral fibromyxoma involving the bone: a mimicker of malignancy. Am J Dermatopathol 2015;37:555-9.
[10] Cohen JA, Geradts J. Loss of RB and MTS1/CDKN2 (p16) expression in human sarcomas. Hum Pathol 1997;28:893-8.
[11] Tardío JC, Butrón M, Martín-Fragueiro LM. Superficial acral fibromyxoma: report of 4 cases with CD10 expression and lipomatous component, two previously underrecognized features. Am J Dermatopathol 2008;30:431-5.
[12] Dyson NJ. RB1: a prototype tumor suppressor and an enigma. Genes Dev 2016;30:1492-502.
[13] Chen BJ, Mariño-Enríquez A, Fletcher CD, Hornick JL. Loss of retinoblastoma protein expression in spindle cell/pleomorphic lipomas and cytogenetically related tumors: an immunohistochemical study with diagnostic implications. Am J Surg Pathol 2012;36:1119-28.
[14] Howitt BE, Fletcher CD. Mammary-type myofibroblastoma: clinicopathologic characterization in a series of 143 cases. Am J Surg Pathol 2016;40:361-7.
[15] Iwasa Y, Fletcher CD. Cellular angiofibroma: clinicopathologic and immunohistochemical analysis of 51 cases. Am J Surg Pathol 2004;28:1426-35.
[16] Dereure O, Savoy D, Doz F, Junien C, Guilhou JJ. Multiple acral fibromas in a patient with familial retinoblastoma: a cutaneous marker of tumour-suppressor gene germline mutation? Br J Dermatol 2000;143:856-9.
[17] Kutzner H, Mentzel T, Palmedo G, et al. Plaque-like CD34-positive dermal fibroma ("medallion-like dermal dendrocyte hamartoma"): clinicopathologic, immunohistochemical, and molecular analysis of 5 cases emphasizing its distinction from superficial, plaque-like dermatofibrosarcoma protuberans. Am J Surg Pathol 2010;34:190-201.
[18] Mentzel T, Schärer L, Kazakov DV, Michal M. Myxoid dermatofibrosarcoma protuberans: clinicopathologic, immunohistochemical, and molecular analysis of eight cases. Am J Dermatopathol 2007;29:443-8.
[19] McNiff JM, Subtil A, Cowper SE, Lazova R, Glusac EJ. Cellular digital fibromas: distinctive CD34-positive lesions that may mimic dermatofibrosarcoma protuberans. J Cutan Pathol 2005;32:413-8.
[20] Calonje E, Guerin D, McCormick D, Fletcher CD. Superficial angiomyxoma: clinicopathologic analysis of a series of distinctive but poorly recognized cutaneous tumors with tendency for recurrence. Am J Surg Pathol 1999;23:910-7.
[21] Mariño-Enríquez A, Fletcher CD. Angiofibroma of soft tissue: clinicopathologic characterization of a distinctive benign fibrovascular neoplasm in a series of 37 cases. Am J Surg Pathol 2012;36:500-8.
[22] Jin Y, Möller E, Nord KH, et al. Fusion of the AHRR and NCOA2 genes through a recurrent translocation t(5;8)(p15;q13) in soft tissue angiofibroma results in upregulation of aryl hydrocarbon receptor target genes. Genes Chromosomes Cancer 2012;51:510-20.

2.2.5. PHOSPHATURIC MESENCHYMAL TUMORS CLINICOPATHOLOGIC, IMMUNOHISTOCHEMICAL AND MOLECULAR ANALYSIS OF 22 CASES EXPANDING THEIR MORPHOLOGIC AND IMMUNOPHENOTYPIC SPECTRUM

Phosphaturic mesenchymal tumor (PMT) is a rare neoplasm of uncertain lineage. The hallmark of this tumor is the ability to induce osteomalacia as a result of inappropriate production of fibroblastic growth factor 23 (FGF23) by the neoplastic cells. FGF23 leads to increased loss of phosphate in the urine resulting in phosphaturic hypophosphatemia.

The diagnosis of PMT has traditionally been a difficult one to make, especially in cases when the tumor induced ostemalacia (TIO) or phosphaturia was absent as there were almost no IHC or molecular markers to support the diagnosis. Morphologically, besides the already rare classical form [49], there are numerous other, even rarer morphological subvariants that make this tumor prone to misclassification. Given the highly variable morphologic spectrum of these tumors and lack of defining phenotypic and/or genetic criteria, it remained controversial whether these tumors, particularly those lacking the classical PMT features, even belong to the same histogenetic group of neoplasms.

For this reason, it has been the aim of several research groups to find a useful IHC stain for the diagnosis of PMT. In last several years, various studies reported the utility of markers such as ERG, somatostatin receptor 2A (SSTR2A), CD56 or DOG1. Of note, recently, another group discovered a characteristic fusion in PMT, consisting of FN1 gene that is fused either with FGF1 (in 42% of cases) or FGFR1 (6%) [50, 51]. However, the rearrangement in the other half of cases still remains obscure.

In our study, we analyzed a cohort of 22 cases for the presence of special morphological patterns and the expression of multiple IHC markers including a novel (in the context of PMT) marker SAT-B2. Also, we carried out FGFR1 FISH analysis to support the diagnosis of PMT.

Eventually, we confirmed the uniform expression of SSTR2A, ERG, and CD56 in the vast majority of cases. In addition, we described a novel consistent expression of SATB2 and confirmed the uniform reactivity for SSTR2A in the majority of in PMTs irrespective of the histologic variant. Furthermore, we describe a distinctive ERG expression that is essentially weak compared with normal endothelial cells and slightly weaker or comparable with that seen in normal cartilage cells [52]. Notably, expression of these immunomarkers is independent of the histologic pattern seen in PMT. Thus, taken together, it seems that in the majority of cases, PMTs are characterized by a distinctive combined immunophenotype showing positivity with SATB2, SSTR2A, CD56 and ERG and negativity with S100 protein and DOG1. Although all these markers are known to have limited general specificity and none is reliable in isolation to detect or confirm PMT, it seems promising that the combined expression of these markers is peculiar to PMT. It may be of particular value in supporting diagnosis in unusual looking cases and in those without TIO but this needs validation in larger future studies comprising and comparing several entities in the differential diagnosis of PMT. In our view, this immunophenotype is a strong argument for the notion that these tumors indeed represent a polymorphous neoplasm with many faces that is unified by prototypic immunophenotype of the neoplastic cells. Accordingly, the possibility that some variant lesions might have represented distinctive non-PMT lesions that happened to be incidentally associated with TIO seems unlikely.

Phosphaturic Mesenchymal Tumors

Clinicopathologic, Immunohistochemical and Molecular Analysis of 22 Cases Expanding their Morphologic and Immunophenotypic Spectrum

Abbas Agaimy, MD, Michael Michal, MD,†‡ Simion Chiosea, MD,§ Fredrik Petersson, MD,‖ Ladislav Hadravsky, MD,¶ Glenn Kristiansen, MD,** Raymund E. Horch, MD,†† Jan Schmolders, MD,‡‡ Arndt Hartmann, MD,* Florian Haller, MD,* and Michal Michal, MD†*

Abstract: Phosphaturic mesenchymal tumor (PMT) is a rare neoplasm of uncertain histogenesis that has been linked to tumor-induced osteomalacia (TIO) since 1959. The neoplastic cells produce increased amount of FGF23 which results in TIO via uncontrolled renal loss of phosphate (phosphaturia), and consequently diminished bone mineralization. To date, ~300 cases have been reported. Although there is increasing evidence that PMT can be diagnosed by reproducible histopathologic features, firm diagnosis has been often restricted to cases associated with TIO and, hence, diagnosis of "nonphosphaturic variants" remained challenging. Recently, *FGFR1*/*FN1* gene fusions were detected in roughly half of cases. We herein reviewed the clinicopathologic features of 22 PMTs (15 cases not published before), stained them with an extended immunohistochemical marker panel and examined them by fluorescence in situ hybridization for *FGFR1* gene fusions. Patients were 12 males and 9 females (one of unknown sex) aged 33 to 83 years (median: 52 y). Lesions affected the soft tissues (n = 11), bones (n = 6), sinonasal tract (n = 4), and unspecified site (n = 1). Most lesions originated in the extremities (9 in the lower and 4 in the upper extremities). Acral sites were involved in 10 patients (6 foot/heel, 3 fingers/hands, and 1 in unspecified digit). Phosphaturia and TIO were recorded in 10/11 and 9/14 patients with detailed clinical data, respectively. Limited follow-up (5 mo to 14 y; median: 16 mo) was available for 14 patients. Local recurrence was noted in one patient and metastasis in another patient. Histologically, 11 tumors were purely of conventional mixed connective tissue type, 3 were chondromyxoid fibroma-like, 2 were hemangio-/glomangiopericytoma-like with giant cells, and 1 case each angiomyolipoma-like and reparative giant cell granuloma-like. Four tumors contained admixture of patterns (predominantly cellular with variable conventional component). Immunohistochemistry showed consistent expression of CD56 (11/11; 100%), ERG (19/21; 90%), SATB2 (19/21; 90%), and somatostatin receptor 2A (15/19; 79%), while other markers tested negative: DOG1 (0/17), beta-catenin (0/14), S100 protein (0/14), and STAT6 (0/7). *FGFR1* fluorescence in situ hybridization was positive in 8/17 (47%) evaluable cases. These results add to the phenotypic delineation of PMT reporting for the first time consistent expression of SATB2 and excluding any phenotypic overlap with solitary fibrous tumor or sinonasal glomangiopericytoma. The unifying immunophenotype of the neoplastic cells irrespective of the histologic pattern suggests a specific disease entity with diverse morphotypes/variants rather than different neoplasms unified by TIO.

Key Words: phosphaturic mesenchymal tumor, FGF23, SATB2, SSTR2A, ERG, osteomalacia

(*Am J Surg Pathol* 2017;41:1371–1380)

Phosphaturic mesenchymal tumor (PMT) is a rare neoplasm of uncertain histogenesis characterized by the presence of clinical features of osteomalacia resulting from inappropriate production of fibroblastic growth factor 23 (FGF23) by the neoplastic cells. FGF23 leads to increased loss of phosphate in the urine resulting in phosphaturic hypophosphatemia.[1] The concept of tumor-induced osteomalacia (TIO; also called oncogenic osteomalacia) was proposed early in 1959.[2] However, it is not until 1972 when Evans and Azzopardi[3] and Olefsky et al[4] pointed to the existence of distinctive lesions associated with TIO that is different from all other well known soft tissue and bone neoplasms. In 1987, Weidner and Santa Cruz[5] proposed the concept of PMT, polymorphous or mixed connective tissue type (PMT-MCT) as a novel entity. By the year 2004, a total of 109 cases have been reported in the English literature (extensively reviewed by Folpe et al[1]). Since then, some additional 200 cases have

From the *Institute of Pathology; ††Department of Hand & Plastic Surgery, University Hospital, Erlangen; **Institute of Pathology; ‡‡Department of Orthopedic & Traumatology, Section for Tumor Orthopedics, University Hospital, Bonn, Germany; †Department of Pathology, Faculty of Medicine in Pilsen, Charles University, Prague; ‡Biomedical Center of the Faculty of Medicine in Pilsen, Pilsen, Czech Republic; §Department of Pathology, University of Pittsburgh Medical Center, Presbyterian Hospital, Pittsburgh, PA; ‖Department of Pathology, National University Health System, Singapore; and ¶Department of Pathology, 3rd Medical Faculty in Prague, Charles University, Prague, Czech Republic.

Conflicts of Interest and Source of Funding: The authors have disclosed that they have no significant relationships with, or financial interest in, any commercial companies pertaining to this article.

Correspondence: Abbas Agaimy, MD, Pathologisches Institut, Universitätsklinikum Erlangen, Krankenhausstrasse 8-10, Erlangen 91054, Germany (e-mail: abbas.agaimy@uk-erlangen.de).

been reported in case reports and a few series, but most of them in poorly illustrated clinical papers (most were reviewed in Honda et al[6] and Qari et al[7]).

The majority of PMT-MCT cases originate in soft tissue and bones while the remainder mainly affect the head and neck area, in particular the maxillofacial sinuses.[1] Histologically malignant PMT-MCT comprised < 10% of cases in the largest series published to date.[1] However, given the highly variable morphologic spectrum of these tumors and lack of defining phenotypic and/or genetic criteria, it remained controversial whether these tumors, particularly those lacking the classical PMT features, belong to the same histogenetic group of neoplasms. In this study, we reviewed our experience with 22 PMTs including 15 unpublished cases and applied an extended immunohistochemical panel selected on the basis of previous observations and own experience with these lesions. Our results uncovered a distinctive immunophenotype suggestive of a deranged osteochondroid (osteochondroblastic) cell phenotype.

MATERIALS AND METHODS

Cases were retrieved from our surgical pathology files and from the consultation files of 2 of the authors (M.M. and A.A.). Seven cases have been published previously (case 6,[8] case 7,[9] cases 17 to 18,[10] and cases 19 to 21[11]). As most of these previously reported cases were associated with TIO, we included them with the intention to enhance the power of immunohistochemical evaluation by including more TIO-positive cases. Tumors were included on the basis of classical PMT-MCT morphology, the presence of phosphaturia/TIO or both. Notably, all of the nonclassical cases were associated with phosphaturia/TIO. Seven cases without phosphaturia/TIO and without *FGFR1* translocation were included on the basis of classical PMT-MCT morphology which is identical to their classical hormonally active counterparts.[1] Immunohistochemistry (IHC) was performed on 3-μm sections cut from paraffin blocks using a fully automated system ("Benchmark XT System," Ventana Medical Systems Inc, 1910 Innovation Park Drive, Tucson, AZ) and the following antibodies: CD34 (clone BI-3C5, 1:200; Zytomed), S100 protein (polyclonal, 1:2500; Dako), STAT6 (clone sc-621, 1:1000; Santa Cruz Biotechnology), ERG (clone EP111, 1:500; Epitomic), SSTR2A (polyclonal, 1:100; Zytomed), SATB2 (clone EPNCIR130A, 1:200; Abcam), CD56 (clone MRQ-42, 1:100; Cell Marque), beta-catenin (clone 14, 1:50; BD Biosciences), and DOG1 (clone K9, 1:200; Novocastra). As a control group we tested cohorts of molecularly confirmed sinonasal hemangiopericytomas (HPC) (n = 8) and solitary fibrous tumors (SFT) from pleural and different extrapleural sites (n = 48) for expression of SATB2 as well.

FGFR1 Fluorescence In Situ Hybridization Testing

To detect gene translocation involving the *FGFR1* gene locus, fluorescence in situ hybridization (FISH) was performed on sections cut from formalin-fixed paraffin-embedded tissue blocks using the ZytoLight *SPEC FGFR1* dual color break-apart probe (ZytoVision, Bremerhaven, Germany) with standard protocols according to the manufacturer's instructions. Fifty tumor cells were visually inspected using a fluorescence microscope. The presence of 2 pairs of fused green and orange signals was considered normal findings. In contrast, translocation-positive nuclei showed 1 fused orange/green signal and 1 separate orange and green signal. A cutoff of > 20% was considered translocation-positive.

RESULTS

Clinical Features

The main clinical and demographic features of the patients are summarized in Table 1. The patients were 12 males and 9 females (one of unknown sex) aged 33 to 83 years (median: 52 y). Lesions affected the skin/soft tissues (n = 11), bone structures (n = 6), and sinonasal tract (n = 4). The site was not known in 1 case. The tumors were located mainly on the extremities (9 in the lower and 4 in the upper extremities). In total, acral sites were involved in 10 patients (6 in the foot/heel, 3 in the fingers/hands, and 1 in unspecified digit) (Figs. 1A–C). All 4 tumors in the head and neck area originated in the sinonasal cavities.

Limited follow-up ranging from 5 months to 14 years (median: 16 mo) was available for 14 patients. Local recurrence was noted in 1 patient (8 y later). One tumor with primary diagnosis in the distal radius metastasized later to the lung, nasal cavity, tongue, and lip. All other patients remained disease-free at last follow-up. Phosphaturia and TIO were recorded in 10/11 and 9/14 patients with detailed clinical data, respectively.

Pathologic Findings

Grossly, the tumors were described as well circumscribed and some had focal cystic changes (Fig. 1D). Their cut-surface ranged from tan and fleshy to glistening myxoid with characteristic brownish discoloration corresponding to the hemorrhagic giant cell areas (Fig. 1E). Histologically, 11 cases were purely conventional PMT-MCT being composed of fibroblastic-like spindled or stellate undifferentiated mesenchymal cells set irregularly into prominent sclerotic matrix with characteristic bluish to hyaline smudgy/grungy appearance (Figs. 2A–F). A variable component of scattered osteoclastic giant cells was noted in practically all cases as well as foci of hemorrhage (Fig. 2D). Unusual features were multiple oxalate-like crystals (seen in 1 case; Fig. 2E), foci of mature-looking hyaline cartilage (seen in 2 cases; Fig. 2F) and extensive hemorrhage that largely obscured the neoplastic nature of the lesion (seen in 1 case). The stroma occasionally showed pericytoma-like vasculature (Fig. 2G) or sieve-like clefts (Fig. 2H). One case each showed a prominent fatty component with interspersed tumor cells admixed with thick-walled vessels closely mimicking angiomyolipoma in addition to focal matrix formation (Fig. 3). Three tumors were chondromyxoid fibroma-like (Fig. 4A) while another case closely mimicked reparative giant cell granuloma (Fig. 4B).

TABLE 1. Clinicopathologic Features of Phosphaturic Mesenchymal Tumors (n = 22)

No.	Age/Sex	Location	Histology Pattern	Phosphaturia	Osteomalacia	Outcome
1	NA	NA	Classical (MCT)	NA	NA	NA
2	67F	Finger	Classical (MCT)	NA	NA	NA
3	45F	Heel	Classical (MCT)	NA	No	NED (14 y)
4	34M	Distal femur	Giant cell rich hemangiopericytoma-like + aneurysmal features	Yes	Yes, deformities, muscle weakness	NED (36 mo)
5	60F	Toe	Classical (MCT)	NA	No	NED (11 y)
6	42M	Inguinal area	Classical (MCT)	Yes	Yes, multiple fractures	NED (13 y)
7	53M	Frontal sinus	Classical (MCT)	NA	NA	DOUC (8 mo)
8	76M	Hip bone	Classical (MCT) + cellular	NA	NA	DOUR (< 1 y)
9	75F	Finger	Chondromyoxid-fibroma-like + classical	No	No	NED (96 mo)
10	72M	Toe	Classical (MCT)	NA	No	DOOC (36 mo)
11	49M	Left hand thenar	Classical (MCT)	Yes	Yes	NED (3 y)
12	73M	Quadriceps muscle right thigh	Angiolipoma-like	Yes	Yes	NA
13	52M	Heel	Classical (MCT)	Yes	Yes	NED (3 mo)
14	52M	Left ethmoid sinuses	Hemangiopericytoma + cellular glomoid	Yes	NA	NED (7 mo)
15	52M	Foot 3.metatarsal bone	Spindle sarcomatous + minor classical	Yes (multiple fractures over 10 y)	NA	NED (5 mo)
16	83F	D2 left (NOS)	Classical (MCT)	NA	NA	Recent case
17	45F	Left frontal sinus	Highly cellular + classical	NA	NA	NA
18	33F	Distal radius	Giant cell granuloma-like	NA	Yes	Later metastasis to nasal cavity, lip, tongue lungs
19	61F	Right ant inf iliac spine	Chondromyxoid fibroma-like	Yes	No	NA
20	49M	Right hip/ proximal femur	Chondromyxoid fibroma-like	Yes	Yes	NED (12 mo)
21	48M	Nasal cavity	Cellular, nondescript	Yes	Yes	NED (12 mo)
22	59F	Big toe	Classical (MCT)	NA	NA	Very recent case

DOOC indicates died of other cause; DOUR, died of unknown reason; F, female; M, male; MCT, mixed connective tissue type; NA, not available; NED, no evidence of disease; NOS, not otherwise specified.

Remarkably, sinonasal tract tumors tended to show variant histology with no or only minimal characteristic matrix (Fig. 4C). They were generally more cellular with nondescript pattern (Fig. 4D) with a variable component of hyaline matrix-like sclerosis entrapping the tumor cells (Fig. 4E) as well as hemangio-/glomangiopricytoma-like features (Fig. 4F). Five tumors showed remarkable cellularity, particularly in the sinonasal cases with focal glomoid features. One acral lesion showed highly cellular undifferentiated spindle cell neoplasm closely mimicking high-grade spindle cell sarcoma abutting a minute focus of dense bluish matrix (Figs. 4G–I).

IHC (Table 2) showed consistent expression of ERG (19/21; 90%; Fig. 5A), SATB2 (19/21; 90%; Figs. 3D, 5B, C), somatostatin receptor 2A (15/19; 79%; Fig. 5D) and CD56 (11/11; 100%; Fig. 5E), while other markers tested negative: DOG1 (0/17), beta-catenin (0/14), S100 protein (0/14) and STAT6 (0/7). CD34 showed variable reactivity in 2/11 cases. S100 protein highlighted foci of cartilage in 2 cases (Fig. 5F). None of the 8 sinonasal-type hemangiopericytomas or the 48 SFTs expressed SATB2 (data not shown).

FGFR1 FISH Results

Of 17 cases tested successfully using the dual color break-apart FISH probe targeting the *FGFR1* gene locus, 8 tumors (47%) showed clear-cut translocation signals (Fig. 6).

DISCUSSION

PMT is an uncommon mesenchymal neoplasm of uncertain histogenesis that seems to be significantly under-recognized, both by clinicians and pathologists. Under-recognition by clinicians is reflected by frequent significant delay of diagnosis with many patients suffering from disability related to their tumors for several years.[12] On the other hand the relative rarity of PMT makes pathologists unfamiliar with its characteristic histologic appearance. Accordingly, diagnosis proved difficult if not impossible at all in many cases if the clinical presentation of the lesion is not known to the pathologist at the time of biopsy assessment and/or if the pathologist is not aware of the entity. This problem is further enhanced by the fact that several variants of PMT exist and even if one thought of PMT as a possibility, to date no consistent or defining immunophenotype has been established for this tumor to confirm this suspicion. Together these factors are likely responsible for the underreporting of the hormonally inactive (nonphosphaturic) variant of the neoplasm.[6]

The confusion regarding diagnosis and nosologic classification of PMTs is reflected by the plethora of names and terminologies applied to this entity in previous

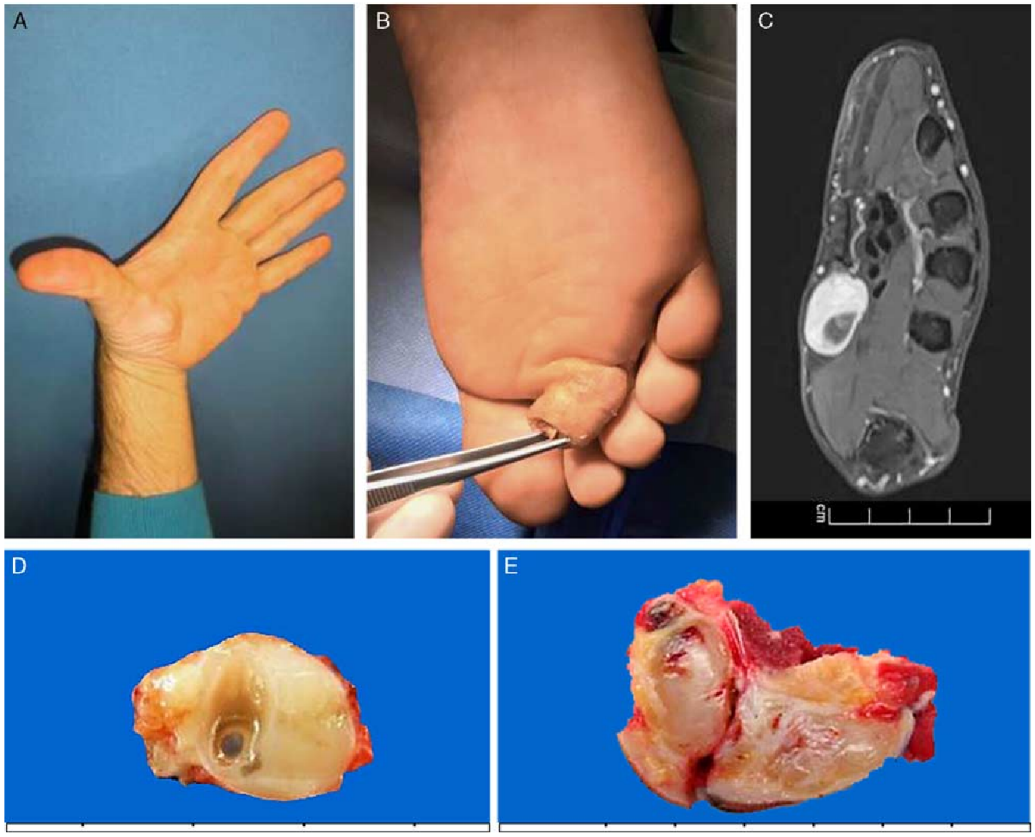

FIGURE 1. Examples of clinical, imaging, and gross features of PMT. A, This patient (case 11) presented with a subcutaneous nodule bulging on his hand (thenar) while being disabled (due to TIO) for years. B, Patient 15 presented with this foot lesion after having multiple recurrent fractures due to TIO for 10 years. C, Imaging of case 11 showed contrast-enhancing tumor with central cystic portion. D, Gross specimen of same case showed whitish glistening cut-surface with cystic degeneration. E, Another PMT (case 13) showed fibrous whitish cut-surface with focal brownish discoloration due to recurrent hemorrhage.

reports in the literature or as original diagnoses in consult cases. The latter encompass mesenchymal chondrosarcomas, osteosarcoma, osteoblastoma, atypical enchondroma, and atypical giant cell tumor of bone for the intraosseous lesions and spindle cell lipoma, angiolipoma, sclerosing hemangioma, hemangiopericytoma with osteoclastic giant cells, atypical/tenosynovial giant cell tumor, and sinonasal hemangiopericytoma-like tumor for soft tissue and sinonasal cases, respectively.[1] In the series by Folpe et al,[1] even after expert review, 5 cases remained unclassifiable as PMT and they were more consistent with a morphologic diagnosis of sinonasal hemangiopericytoma-like tumor (2 cases), HPC/SFT with osteoclast-like giant cells (1 case), sclerosing osteosarcoma (1 case), and atypical enchondroma (1 case).[1] This confusing terminology is a reflection of the varying histologic patterns and is because of lack of defining phenotype of the underlying neoplastic cells and lack of pathognomonic genetic markers.

Recent studies showed presence of mutually exclusive gene translocations involving the *FN1-FGFR1* and *FN1-FGF1* gene loci with a frequency of 42% and 6%, respectively.[13,14] In the current study, we detected *FN1-FGFR1* gene fusions with a comparable frequency (47%). FGFR1 was expressed by immunohistochemistry in 82% of the cases irrespective of the translocation status detected by FISH.[14] In the study by Lee et al,[14] however, FGFR1 IHC was positive in SFT (40%), chondroblastomas (40%) and giant cell tumor of bone (38%).[14] These data underlines the limited sensitivity of FISH (as almost half of cases would be negative) and of FGFR1 IHC (as many mimics such as SFT, giant cell tumor and chondroblastoma express this marker) in confirming PMT.

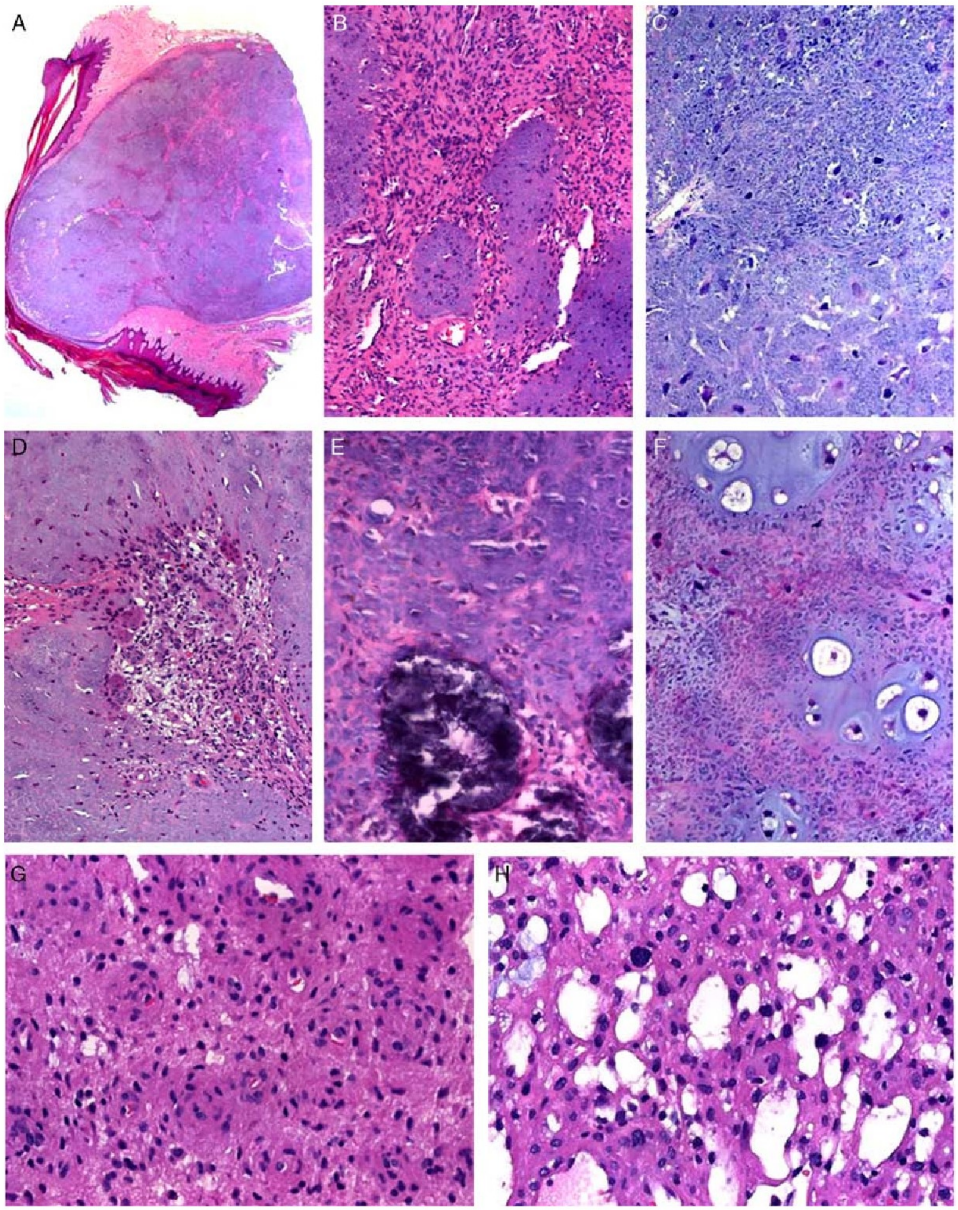

FIGURE 2. Representative examples of the histologic features of classical PMT. A, Well circumscribed cutaneous mass in the toe (case 22) with characteristic bluish appearance due to extensive grungy matrix. B, Prominent spindle cell component entrapping typical matrix and imparting a biphasic pattern. C, Higher magnification of the matrix. D, Osteoclastic giant cells are frequently seen at the interface between tumor matrix and stromal component. Unusual features seen were oxalate-like crystals (prominent in 1 case; E) and foci of mature cartilage seen in 2 cases (F). Focal pericytoma-like vessels (G) and characteristic sieve-like stromal changes (H) from case 11.

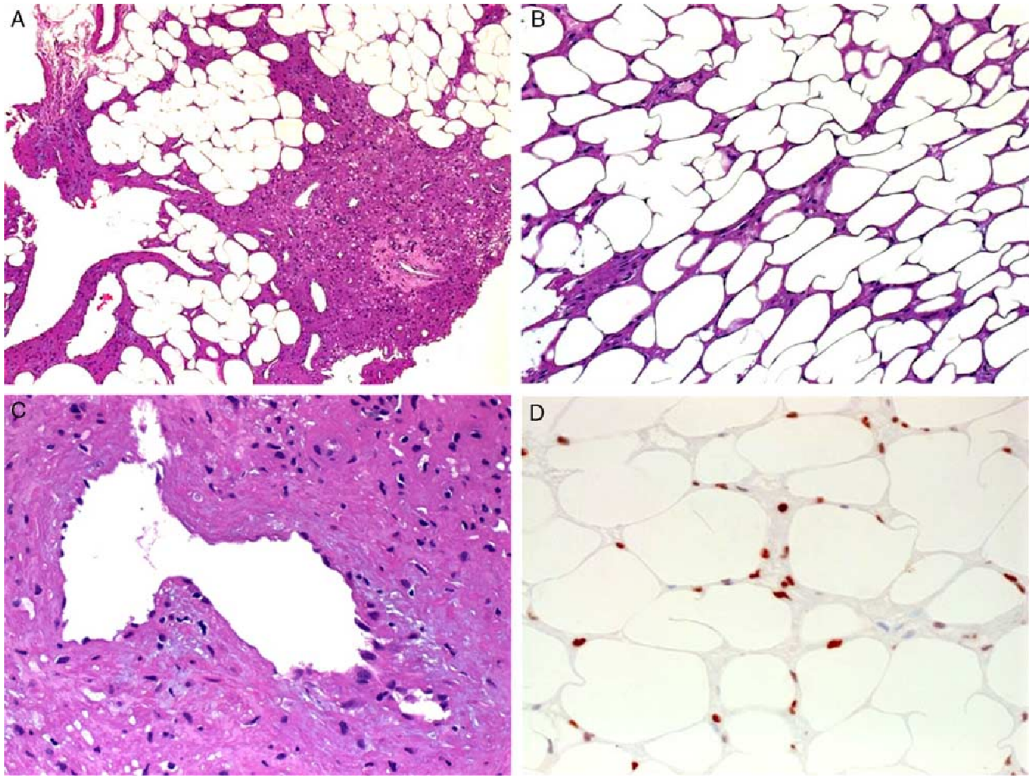

FIGURE 3. A, This angiomyolipoma-like variant PMT contained prominent fatty component imparting biphasic pattern, note prominent thick-walled vessels. B, Tumor cells were intermingled between adipocytic cells. C, thick-walled veins embedded within sclerotic matrix. D, The scattered neoplastic cells are highlighted by SATB2 immunostaining.

Immunohistochemical data on PMT has been scarce except for complementary studies performed to exclude other differential diagnoses. In the Folpe et al's[1] study, all tumors analyzed were consistently negative with desmin, S100 protein, CD34, and cytokeratins while 3 cases (25%) showed focal reactivity for alpha smooth muscle actin.[1] Although expression of FGF23 by immunohistochemistry and/or using mRNA methods is expected in PMTs, recent studies showed a high sensitivity but limited specificity.[15–17] The FGF23 antibody stained the majority of PMTs, but also stained 50% of SFT/HPC lacking phosphaturia and stained some endothelial cells and normal tissues as well indicating limited specificity.[1] Other markers found to be expressed in PMTs include SSTR2A,[18] ERG,[19] FLI-1,[19] CD56,[20] D2-40[21], and DOG1.[22] In the current study, we confirm uniform expression of SSTR2A, ERG, and CD56 in the vast majority of cases. In addition, we describe a novel consistent expression of SATB2 in PMTs irrespective of the histologic variant. SATB2 has been recently identified as useful marker of osteoblastic and chondroblastic differentiation.[23–25]

In addition to SATB2, we confirm the uniform reactivity for SSTR2A in the majority of PMTs with some cases showing no or limited expression, possibly due to the excessive matrix sclerosis or poor tissue preservation in old archival material. Furthermore, we describe a distinctive ERG expression that is essentially weak compared with normal endothelial cells and slightly weaker or comparable with that seen in normal cartilage cells.[26] Notably, expression of these immunomarkers is independent of the histologic pattern seen in PMT. Thus taken together, it seems that in the majority of cases, PMTs are characterized by a distinctive wired immunophenotype (SATB2 + /SSTR2A + /CD56 + /ERG + /S100 protein − /DOG1 −). This immunophenotype helps to distinguish them from the vast majority of their mimics in bones and their SATB2 + /SSTR2A + /STAT6 − /beta-catenin – phenotype distinguishes them from SFT and sinonasal-type HPC.

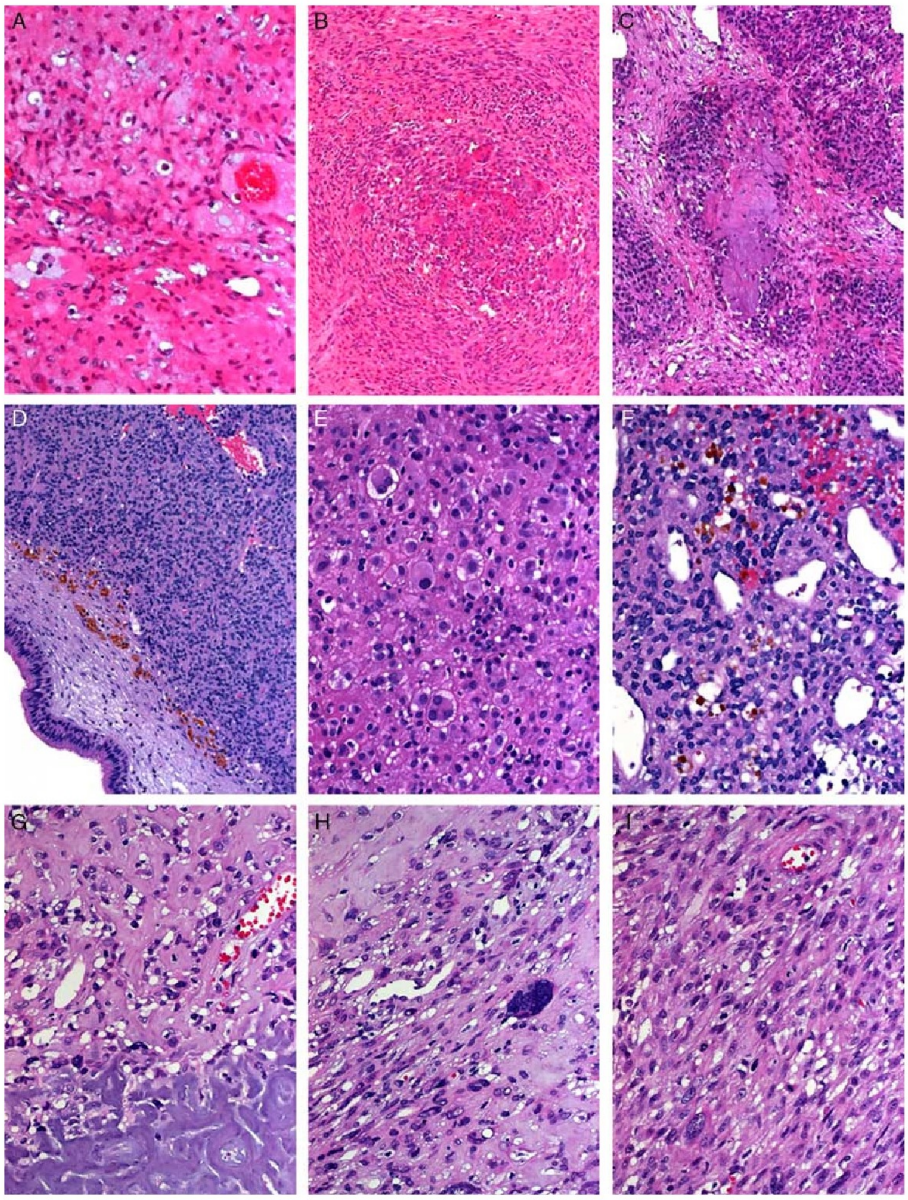

FIGURE 4. Other variants of PMT included chondromyxoid fibroma-like (A) and giant cell granuloma-like (B). C, Head and neck cases only rarely contained minor foci of matrix amid hypercellular tumor tissue. This ethmoid sinus case (case 14) showed high cellularity with glomoid features (D) and variable hyalinized matrix containing large binucleated and multinucleated histiocytoid cells (likely chondroblasts; E) in addition to HPC-like areas (F). One TOI-associated tumor from the foot (case 15) showed transition from sclerotic matrix (G) to pleomorphic (H) and highly cellular sarcomatous growth of spindle cells with brisk mitotic activity (I).

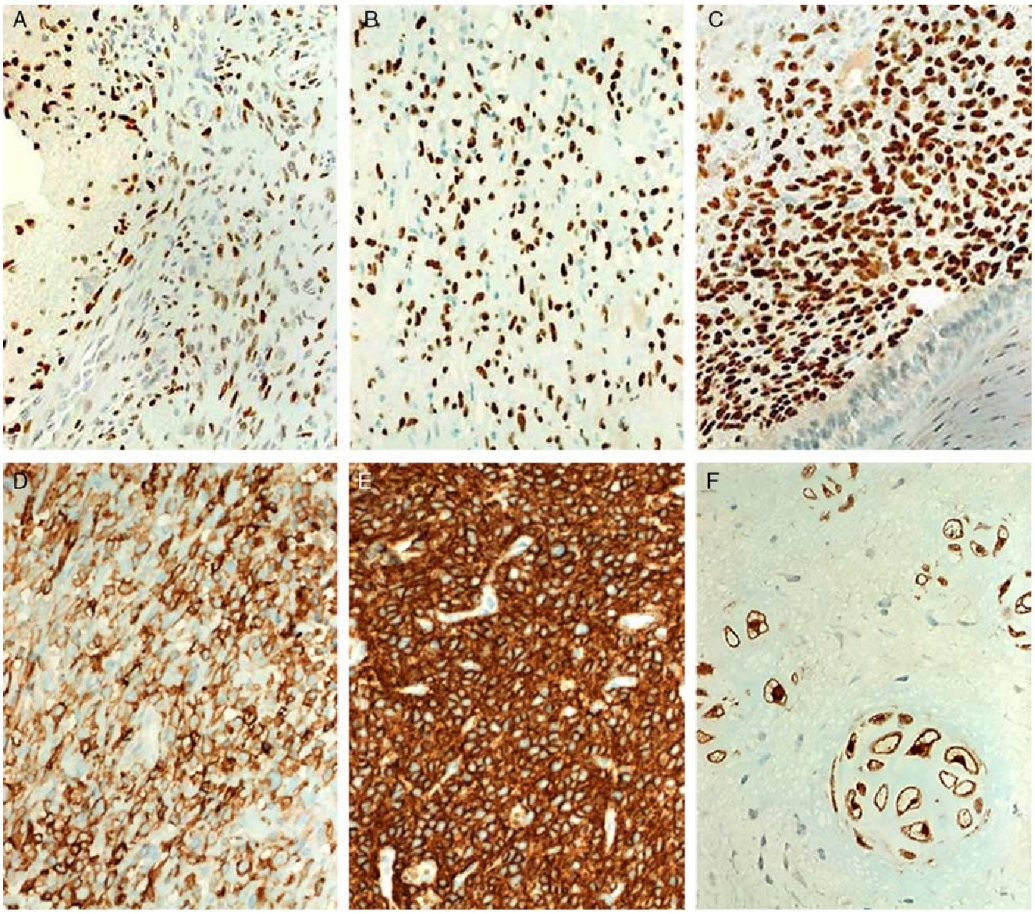

FIGURE 5. By IHC, PMT showed variable expression of ERG ranging from weak to moderate (A), but still weaker than that of normal endothelial cells. In contrast, SATB2 was strongly expressed in a subpopulation of tumor cells (B) or diffusely (C). Consistent expression was seen with somatostatin receptor 2A (D) and CD56 (E). S100 protein was expressed only in the cartilage foci seen in 2 cases (F).

The pathogenesis of this unusual immunophenotype remains obscure. It seems as if the neoplastic cells tend to show combined features of or intermediate features between osteoblastic (SATB2+/S100 protein−) and chondroblastic (SATB2+/ERG+) cells. Although all of these markers are known to have limited general specificity and none is reliable in isolation to detect or confirm PMT, it seems promising that the combined expression of these markers is peculiar to PMT and may be of value in supporting diagnosis in unusual looking cases[27] and in those without TIO[6] but this needs validation in larger future studies comprising and comparing several entities in the differential diagnosis of PMT.

The inherent tendency of PMT cells for osteoblastic differentiation is reflected in several features of these peculiar neoplasms: (1) presence of a prominently calcified matrix with occasional osteoid like material mimicking sclerosing osteosarcoma in some reported cases,[1] (2) presence of numerous osteoclastic giant cells associated with areas of plump or spindled cells in storiform or fascicular pattern closely mimicking giant cell tumor of bone, (3) presence of mature bone in some of the cases, and (4) presence of large blood-filled lakes associated with giant cells suggesting mimicry to aneurysmal bone cyst-like pattern. In contrast, chondroblast-like cells with eccentric eosinophilic cytoplasm and grooved folded nuclei were a prominent component in one of our cases as well as in previous studies.[1] These observations may explain the uniform reactivity of the neoplastic cells with SATB2 as a marker of osteoblastic differentiation. An important

TABLE 2. Immunohistochemical and Molecular Findings in Phosphaturic Mesenchymal Tumors (n = 22)

No.	SSTR2A	SATB2	ERG	CD56	S100	CD34	DOG1	STAT6	Beta-catenin	*FGFR1* FISH
1	+ +	+ + +	+ +	NA	NA	NA	NA	NA	–	–*
2	+ +	–	+ +	NA	NA	NA	NA	NA	–	–*
3	–	+ + +	–	NA	NA	NA	–	NA	NA	+
4	+ +	+ + +	+ +	NA	–	NA	–	NA	NA	+
5	+(F)	–	+ +	NA	–	NA	–	NA	NA	–
6	+ +	+ +	–	NA	NA	NA	NA	NA	–	NA
7	NA	NA	NA	NA	NA	NA	NA	NA	–	NA
8	+ +	+ + +	+(F)	NA	NA	NA	–	NA	NA	–*
9	NA	+	+ +	NA	NA	NA	–	NA	NA	NR
10	–	+ + +	+ +	NA	–	NA	NA	NA	NA	+
11	+ +	+ + +	+ +	+ + +	–	+	–	–	–	–*
12	+ +	+ + +	+ +	+ + +	–	–	–	–	NA	–*
13	+ +	+ + +	+ +	+ + +	–	–	–	NA	–	–*
14	+ +	+ + +	+ +	+ + +	–	–	–	–	–	–
15	+ + +	+ + +	+ +	+ + +	–	–	–	–	–	+
16	–	+	+ +	+(F)	–	+	–	–	–	NR
17	+ +(wk)	+ + +	+ +	+ + +	–	–	–	–	–	+
18	+ +(wk)	+ + +	+(F)	NA	–	NA	–	NA	–	+
19	NR	+ +	+ +	+ + +	–	–	–	NA	NA	+
20	–	+ +	+ +	+ + +	NA	–	–	NA	–	NR
21	+ +	+ + +	+ +	+ + +	–	–	–	NA	–	–
22	+ +(wk)	+ + +	+ +	+ + +	–	–	–	–	–	+

*Limited assessability due to poor signal quality.

F indicates focal; NA, not available; NR, no results due to poor tissue preservation; wk, weak; –, negative; +, positive in < 25% tumor cells; + +, positive in 26–50% tumor cells; + + +, positive in > 50% tumor cells.

point to stress is the uniform expression of these immunomarkers in the majority of cases including also those angiomyolipoma-like and HPC-like variant tumors that lacked the specific PMT matrix. In our view, this immunophenotype is a strong argument for the notion that these tumors indeed represent a polymorphous neoplasm with many faces that is unified by prototypic immunophenotype of the neoplastic cells. Accordingly, the possibility that some variant lesions might have represented distinctive non-PMT lesions that happened to be incidentally associated with TIO seems unlikely.

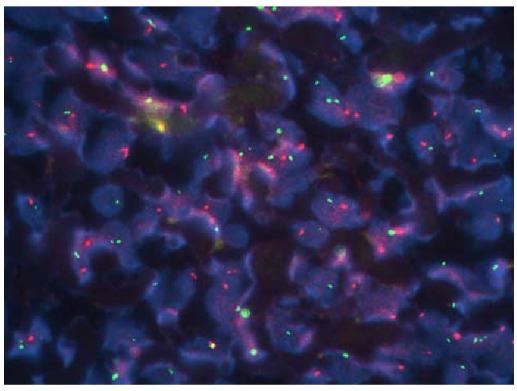

FIGURE 6. FISH analysis using the ZytoLight *SPEC FGFR1* dual color break-apart probe showed split signals in the majority of tumor cells indicating a translocation (case 15).

From a differential diagnostic perspective, it should be emphasized that sinonasal PMTs are histologically more akin to variant HPC than to PMT-MCT, being devoid of the classical grungy or chondromyxoid matrix seen in majority of bony and soft tissue PMTs.[1] Also, their cells were more similar to myoid perivascular cells with prominently hyalinized thick-walled vessels. This makes the differential diagnosis of sinonasal PMTs and their distinction from HPC and SFT rather complicated. Thus, our study is novel in showing consistent expression of another potentially useful marker, SATB2, in almost all of PMTs and its absence in tumors in the differential diagnosis, particularly of sinonasal PMTs including sinonasal HPC and SFT. Furthermore, for the first time we analyzed a subset of PMTs for STAT6 and beta-catenin; none was positive for either. These findings underline the histogenetic distinctness of sinonasal PMTs on one side and their HPC/SFT mimics on the other side.[28,29]

One issue regarding the power of our immunohistochemical results might be the fact that clinical evidence of phosphaturia and/or TIO was available only in half of the cases raising the question whether the remainder are genuine PMTs. In our opinion and based on available studies in the literature, our cases are acceptable as PMTs on the basis of either phosphaturia and/or TIO (n = 11), detectable *FGFR1* gene fusion in the appropriate (classical) tumor morphology (n = 4) or presence of classical PMT-MCT histology. Notably, all 7 cases lacking the former 2 criteria were identical to classical PMT as reported in the literature.[1] This third criteria has been accepted by Folpe et al[1] in their large series where 3/32 cases lacked phosphaturia and/or TIO, but were

identical to classical PMTs. Thus taken together, we are convinced that our immunohistochemical results are valid for the whole series.

In summary, we herein highlighted additional immunophenotypic features of PMTs with consistent coexpression of SATB2, SSTR2A, ERG, and CD56 suggesting a valuable and emerging role of IHC in supporting a diagnosis of PMT in difficult-to-diagnose tumors, particularly those hormonally inactive (nonphosphaturic) variants. These results add to the phenotypic delineation of PMT reporting for the first time consistent expression of SATB2 and excluding any phenotypic overlap with solitary fibrous tumors and sinonasal-type hemangiopericytoma, the main differential diagnosis for many cases.

REFERENCES

1. Folpe AL, Fanburg-Smith JC, Billings SD, et al. Most osteomalacia-associated mesenchymal tumors are a single histopathologic entity: an analysis of 32 cases and a comprehensive review of the literature. *Am J Surg Pathol*. 2004;28:1–30.
2. Prader A, Illig R, Uehlinger RE, et al. Rachitis infolge knochentumors [Rickets caused by bone tumor]. *Helv Pediatr Acta*. 1959;14:554–565.
3. Evans DJ, Azzopardi JG. Distinctive tumours of bone and soft tissue causing acquired vitamin-D-resistant osteomalacia. *Lancet*. 1972;1:353–354.
4. Olefsky J, Kempson R, Jones H, et al. Tertiary hyperparathyroidism and apparent "cure" of vitamin-D-resistant rickets after removal of an ossifying mesenchymal tumor of the pharynx. *N Engl J Med*. 1972;286:740–745.
5. Weidner N, Santa Cruz D. Phosphaturic mesenchymal tumors: a polymorphous group causing osteomalacia or rickets. *Cancer*. 1987;59:1442–1454.
6. Honda R, Kawabata Y, Ito S, et al. Phosphaturic mesenchymal tumor, mixed connective tissue type, non-phosphaturic variant: report of a case and review of 32 cases from the Japanese published work. *J Dermatol*. 2014;41:845–849.
7. Qari H, Hamao-Sakamoto A, Fuselier C, et al. Phosphaturic mesenchymal tumor: 2 new oral cases and review of 53 cases in the head and neck. *Head Neck Pathol*. 2016;10:192–200.
8. Shelekhova KV, Kazakov DV, Hes O, et al. Phosphaturic mesenchymal tumor (mixed connective tissue variant): a case report with spectral analysis. *Virchows Arch*. 2006;448:232–235.
9. Shelekhova KV, Kazakov DV, Michal M. Sinonasal phosphaturic mesenchymal tumor (mixed connective tissue variant): report of 2 cases. *Am J Surg Pathol*. 2010;34:596–597.
10. Wasserman JK, Purgina B, Lai CK, et al. Phosphaturic mesenchymal tumor involving the head and neck: a report of five cases with FGFR1 fluorescence in situ hybridization analysis. *Head Neck Pathol*. 2016;10:279–285.
11. Mok Y, Lee JC, Lum JH, et al. From epistaxis to bone pain-report of two cases illustrating the clinicopathological spectrum of phosphaturic mesenchymal tumour with fibroblast growth factor receptor 1 immunohistochemical and cytogenetic analyses. *Histopathology*. 2016;68:925–930.
12. Ledford CK, Zelenski NA, Cardona DM, et al. The phosphaturic mesenchymal tumor: why is definitive diagnosis and curative surgery often delayed? *Clin Orthop Relat Res*. 2013;471:3618–3625.
13. Lee JC, Jeng YM, Su SY, et al. Identification of a novel FN1-FGFR1 genetic fusion as a frequent event in phosphaturic mesenchymal tumour. *J Pathol*. 2015;235:539–545. Erratum in: *J Pathol* 2015;236:131.
14. Lee JC, Su SY, Changou CA, et al. Characterization of FN1-FGFR1 and novel FN1-FGF1 fusion genes in a large series of phosphaturic mesenchymal tumors. *Mod Pathol*. 2016;29:1335–1346.
15. Graham R, Krishnamurthy S, Oliveira A, et al. Frequent expression of fibroblast growth factor-23 (FGF23) mRNA in aneurysmal bone cysts and chondromyxoid fibromas. *J Clin Pathol*. 2012;65:907–909.
16. Carter JM, Caron BL, Dogan A, et al. A novel chromogenic in situ hybridization assay for FGF23 mRNA in phosphaturic mesenchymal tumors. *Am J Surg Pathol*. 2015;39:75–83.
17. Shiba E, Matsuyama A, Shibuya R, et al. Immunohistochemical and molecular detection of the expression of FGF23 in phosphaturic mesenchymal tumors including the non-phosphaturic variant. *Diagn Pathol*. 2016;11:26.
18. Houang M, Clarkson A, Sioson L, et al. Phosphaturic mesenchymal tumors show positive staining for somatostatin receptor 2A (SSTR2A). *Hum Pathol*. 2013;44:2711–2718.
19. Tajima S, Takashi Y, Ito N, et al. ERG and FLI1 are useful immunohistochemical markers in phosphaturic mesenchymal tumors. *Med Mol Morphol*. 2016;49:203–209.
20. Tajima S, Fukayama M. CD56 may be a more useful immunohistochemical marker than somatostatin receptor 2A for the diagnosis of phosphaturic mesenchymal tumors. *Int J Clin Exp Pathol*. 2015;8:8159–8164.
21. Tajima S, Fukayama M. Possibility of D2-40 as a diagnostic and tumor differentiation-suggestive marker for some of phosphaturic mesenchymal tumors. *Int J Clin Exp Pathol*. 2015;8:9390–9396.
22. Creytens D, Van Dorpe J. DOG1 expression in phosphaturic mesenchymal tumour. *J Clin Pathol*. 2016. pii: jclinpath-2016-203893. Doi:10.1136/jclinpath-2016-203893. [Epub ahead of print].
23. Conner JR, Hornick JL. SATB2 is a novel marker of osteoblastic differentiation in bone and soft tissue tumours. *Histopathology*. 2013;63:36–49.
24. Machado I, Navarro S, Picci P, et al. The utility of SATB2 immunohistochemical expression in distinguishing between osteosarcomas and their malignant bone tumor mimickers, such as Ewing sarcomas and chondrosarcomas. *Pathol Res Pract*. 2016;212:811–816.
25. Ordóñez NG. SATB2 is a novel marker of osteoblastic differentiation and colorectal adenocarcinoma. *Adv Anat Pathol*. 2014;21:63–67.
26. Shon W, Folpe AL, Fritchie KJ. ERG expression in chondrogenic bone and soft tissue tumours. *J Clin Pathol*. 2015;68:125–129.
27. Suryawanshi P, Agarwal M, Dhake R, et al. Phosphaturic mesenchymal tumor with chondromyxoid fibroma-like feature: an unusual morphological appearance. *Skeletal Radiol*. 2011;40:1481–1485.
28. Lasota J, Felisiak-Golabek A, Aly FZ, et al. Nuclear expression and gain-of-function β-catenin mutation in glomangiopericytoma (sinonasal-type hemangiopericytoma): insight into pathogenesis and a diagnostic marker. *Mod Pathol*. 2015;28:715–720.
29. Haller F, Bieg M, Moskalev EA, et al. Recurrent mutations within the amino-terminal region of β-catenin are probable key molecular driver events in sinonasal hemangiopericytoma. *Am J Pathol*. 2015;185:563–571.

2.2.6. DEDIFFERENTIATED LIPOSARCOMA COMPOSED PREDOMINANTLY OF RHABDOID/EPITHELIOID CELLS: A FREQUENTLY MISDIAGNOSED HIGHLY AGGRESSIVE VARIANT

After the recognition that most malignant fibrous histiocytomas of the retroperitoneum contain *MDM2* gene amplification most characteristic (but not exclusive to) well differentiated liposarcomas, most of these tumors started to be classified as dedifferentiated liposarcomas [53] (DDL) and today DDLs are considered to be the most frequent undifferentiated sarcomas in the retroperitoneum. They also occur in other sites including the paratesticular area, the extremities, the head and neck and the trunk [54]. DDL is defined as a non-lipogenic sarcoma that develops within a well differentiated liposarcoma (WDL) as a recurrence of the former or, more commonly (90% of cases), de novo as an undifferentiated sarcoma showing amplification of *MDM2* and *CDK4* (both mapping to chromosome 12q14-15) and occurring at anatomic sites where DDL typically occurs [54]. Since FISH testing for MDM2 amplification became widely available, numerous morphological patterns of DDLs have been reported.

In this study, we described our experience with DDL showing a striking predominance of small to medium-sized cells with rhabdoid, epithelioid or non-descript round cell morphology. They closely mimicked a variety of other neoplasms, in particular undifferentiated carcinoma, mesothelioma, malignant melanoma, anaplastic large cell lymphoma, epithelioid leiomyosarcoma, epithelioid variant of pleomorphic rhabdomyosarcoma, PEComa, high grade epithelioid myxofibrosarcoma and others.

Five of our 6 cases originated in the retroperitoneum (3 in the psoas muscle) and one in the deep soft tissue of the thigh. All 3 patients with follow-up died of metastatic disease within 4 to 8 months.

One of the aims of this study was to analyze their IHC profile, in order to find staining patterns overlapping with the differential diagnostic entities. Our cohort showed expression of MDM2 (6/6), CDK4 (5/6) but also of pancytokeratin AE/1AE3 (4/6) and diffuse desmin and myogenin (2/6) reactivity. Therefore, these tumors might potentially mimic undifferentiated carcinoma or pleomorphic rhabdomyosarcoma unless one thinks of DDL as a possible diagnosis. On the other hand, the SWI/SNF complex components (SMARCB1, SMARCA2, SMARCA4, ARID1A and PBRM1) were intact in all cases, therefore excluding the possibility of an alternative diagnosis from the heterogeneous spectrum of SWI/SNF-deficient malignancies [55]. Most importantly, all cases showed high-level co-amplification of MDM2/CDK4 by FISH.

As our follow-up shows, it is a very aggressive liposarcoma variant with a very short median survival. The molecular background of these tumors may also be a potential target to novel therapeutic modalities (i.e. Nutlins [56]) in a close future. Therefore, the separation from other differential diagnostic entities is warranted.

Unfortunatelly, few months before finishing our study, another group published a series of very similar tumors [57] which slightly diminished the impact of our work.

Dedifferentiated liposarcoma composed predominantly of rhabdoid/epithelioid cells: a frequently misdiagnosed highly aggressive variant

Abbas Agaimy, Michael Michal, Ladislav Hadravsky, Michal Michal

PII: S0046-8177(17)30496-3
DOI: https://doi.org/10.1016/j.humpath.2017.12.025
Reference: YHUPA 4445

To appear in:

Received date: 6 November 2017
Revised date: 15 December 2017
Accepted date: 16 December 2017

Please cite this article as: Abbas Agaimy, Michael Michal, Ladislav Hadravsky, Michal Michal , Dedifferentiated liposarcoma composed predominantly of rhabdoid/epithelioid cells: a frequently misdiagnosed highly aggressive variant. The address for the corresponding author was captured as affiliation for all authors. Please check if appropriate. Yhupa(2018), https://doi.org/10.1016/j.humpath.2017.12.025

Dedifferentiated Liposarcoma Composed Predominantly of Rhabdoid/Epithelioid Cells: A Frequently Misdiagnosed Highly Aggressive Variant.

Abbas Agaimy, MD[1], Michael Michal, MD[2, 3], Ladislav Hadravsky, MD[4], Michal Michal, MD[2]

[1] Institute of Pathology, University Hospital, Erlangen, Germany
[2] Department of Pathology, Faculty of Medicine in Pilsen, Charles University, Prague
[3]Biomedical Center, Faculty of Medicine in Pilsen, Charles University, Czech Republic
[4] Department of Pathology, First Faculty of Medicine, Charles University in Prague, Czech Republic

Address page proofs, correspondence, and requests for reprints to
Abbas Agaimy, MD
Pathologisches Institut
Universitätsklinikum Erlangen
Krankenhausstrasse 8-10
91054 Erlangen, Germany
Phone: +49-9131-85-22288
Fax: +49-9131-85-24745
Email: abbas.agaimy@uk-erlangen.de

Short running title: Rhabdoid Dedifferentiated Liposarcoma

SUMMARY

Dedifferentiated liposarcoma is one of the most common sarcoma types in adults with a predilection for the retroperitoneum. We have recently encountered 6 cases of DDL composed predominantly of rounded, rhabdoid or epithelioid cells mimicking rhabdoid melanoma, epithelioid rhabdomyosarcoma or undifferentiated carcinoma. Patients were 5 males and one female aged 64 to 81 years (median, 68). Tumors originated in the retroperitoneum (n=5; 3 in the psoas muscle) and deep soft tissue of the thigh (n=1). All 3 patients with follow-up died of metastatic disease within 4 to 8 months. Preoperative biopsy diagnoses never suggested dedifferentiated liposarcoma as a possibility; instead carcinoma, rhabdomyosarcoma and lymphoma were on top of suggestions. Five resected tumors were composed predominantly (70-100%) of anaplastic rounded to oval rhabdoid cells with prominent central nucleoli and paranuclear rhabdoid inclusions. Bi- and multinucleation was a constant feature. The background stroma showed variable myxoid changes and minor mixed inflammatory cells. Two cases showed homologous dedifferentiation and another had sclerosing spindle cell nodule but a well differentiated lipomatous component was not seen in any. One biopsied case showed solely monotonous small round blue cells with scattered rhabdoid cells. Immunohistochemistry showed expression of MDM2 (6/6), CDK4 (5/6), pancytokeratin AE/1AE3 (4/6) and diffusely desmin + myogenin (2/6). All cases showed high-level co-amplification of *MDM2/CDK4* by in-situ-hybridization. The SWI/SNF complex components (SMARCB1, SMARCA2, SMARCA4, ARID1A and PBRM1) were intact in all cases. This highly aggressive liposarcoma variant needs to be distinguished from a variety of neoplasms including undifferentiated carcinoma, melanoma, lymphoma, rhabdomyosarcoma and others.

Key words: dedifferentiated liposarcoma; retroperitoneum; rhabdoid; epithelioid; SWI/SNF; rhabdomyosarcoma; melanoma.

INTRODUCTION

Dedifferentiated liposarcoma (DDL) is the most frequent undifferentiated sarcoma in the retroperitoneum but it also occurs in other sites including the paratesticular area, the extremities, the head and neck and the trunk [1,2]. It is defined as a non-lipogenic sarcoma that develops within a well differentiated liposarcoma (WDL), as a recurrence of the former or de novo as an undifferentiated sarcoma showing amplification of *MDM2* and *CDK4* (both mapping to chromosome 12q14-15) and occurring at anatomic sites where DDL typically occurs [1,2]. Dedifferentiation occurs in approximately 10% of WDL, but 90% of DDL arise de novo without detectable WDL component [1,2]. Mainly middle-aged adults are affected with equal gender distribution [2].

The morphological spectrum of DDL has been ever growing to include in addition to the most frequent undifferentiated pleomorphic sarcoma (MFH/UPS-like) and spindle cell sarcoma not otherwise specified/NOS [3] unusual patterns such as low-grade dedifferentiation [4], heterologous dedifferentiation (corresponding to any of the other mesenchymal lineage such as bone, cartilage, smooth muscle, rhabdomyoblastic) [3-5], meningothelial-like whorls [6], inflammatory myofibroblastic tumor-like [7], myxofibrosarcoma-like [3], myxoid liposarcoma-like [1] and homologous dedifferentiation mimicking pleomorphic liposarcoma [8]. In this study, we describe our experience with DDL with a striking predominance of small to medium-sized cells showing rhabdoid, epithelioid or non-descript round cell morphology closely mimicking a variety of other neoplasms.

MATERIALS AND METHODS

Cases were retrieved from our surgical pathology files (n=1) and from the consultation files of two of the authors (n=5; A.A. & M.M.). None has been published before.

Immunohistochemistry (IHC) was performed on 3-µm sections cut from paraffin blocks using a fully automated system ("Benchmark XT System", Ventana Medical Systems Inc, 1910 Innovation Park Drive, Tucson, Arizona, USA) and the following antibodies: pancytokeratin (clone AE1/AE3, 1:40, Zytomed Systems, Berlin, Germany), MDM2 (clone IF1, 1:50, CalBiochem), CDK4 (clone DCS-156, 1:100, Zytomed), desmin (clone D33, 1:250, Dako), myogenin (clone F5D, 1:50, Dako), SMARCA4 (anti-BRG1 antibody, clone EPNCIR111A, dilution, 1:100, Abcam, Cambridge, UK), SMARCA2 (polyclonal antibody, 1:100, Atlas Antibodies AB, Stockholm, Sweden), SMARCB1/INI1, clone MRQ-27, dilution, 1:50, Zytomed), ARID1A (rabbit polyclonal antibody, ab97995, 1:100; Abcam) and PBRM1 (clone CL0331, 1:50, Atlas Antibodies). Several other mesenchymal, epithelial and hematolymphoid markers were used in a routine setting to exclude other differential diagnoses according to our routine laboratory staining protocol (details available upon request; see table 2). Assessment of the SWI/SNF markers was done the same way as reported previously, i.e. only unequivocal absent staining in the nuclei of viable tumor tissue (away from necrotic areas) was considered "deficient or lost" as opposed to "intact" expression (intense expression in the tumor cells that is equivalent to the staining of non-neoplastic cells in the background). As a control, the presence of homogeneous strong nuclear staining of stromal fibroblasts, inflammatory cells, vascular endothelial cells or other normal cells in the background was a prerequisite for assessable staining in the tumor. A "reduced expression" was assigned if viable tumor cells displayed homogenous very weak but still recognizable staining as opposed to stronger staining in normal cells in the background. Specimens lacking strong staining in the background non-neoplastic cells were considered not assessable.

MDM2 and CDK4 fluorescent in-situ-hybridization (FISH) testing

To detect copy number variations in the *MDM2* and/or *CDK4* gene loci, fluorescent in-situ-hybridization (FISH) was performed on sections cut from formalin-fixed paraffin-embedded tissue blocks using the Zyto*Light*® *SPEC MDM2/CEN12* and Zyto*Light*® *SPEC CDK4/CEN12* Dual Color Break Apart Probes (ZytoVision, Bremerhaven, Germany) with standard protocols according to the manufacturer`s instructions. Fifty tumor cells were visually inspected using a fluorescence microscope. The presence of two pairs of green and orange signals was considered normal findings. On the other hand, clusters of green *MDM2* or *CDK4* signals are considered indicative of amplification. The *MDM2* gene locus was assessed in Case 1 to 3 also using a chromogenic ISH probe (CISH method) from same manufacturer.

RESULTS

Clinical features

The main clinical and demographic features of the patients are summarized in table 1. The patients were 5 males and one female aged 64 to 81 years (median, 68). Tumors originated in the retroperitoneum (n=5) and the deep soft tissue of the thigh (n=1). Three of the 5 retroperitoneal tumors were located in the psoas muscle/iliac fossa. Imaging diagnoses were non-liposarcoma in all cases and included psoas abscess, lymphoma and sarcoma (Fig. 1).

Follow-up was available for 4 patients. Three died of metastatic disease at 4, 6 and 8 months (median: 6). One patient was alive with progressive disease under palliative chemotherapy after R2 resection 6 months after surgery. Metastases affected the GI tract (one stomach and one vermiform appendix), peritoneum (2) and wide-spread bone sites (1).

Pathological findings

Preoperative image-guided biopsy was obtained in three patients and was interpreted as poorly differentiated rhabdoid carcinoma (1) and pleomorphic rhabdomyosarcoma (1). One case was interpreted initially as probable aggressive lymphoma and diagnosis was then shifted to probable alveolar rhabdomyosarcoma based on immunohistochemistry (IHC). Grossly, the tumors were described as fleshy with brown cut-surface with extensive areas of necrosis that in most of cases took half of the mass or even more. Some tumors had a yellowish periphery indicating entrapped fat. Case 1 showed sclerosing spindled morphology in the appendiceal and peritoneal nodules with firm whitish whorled cut-surface.

All tumors were characterized by a significant proportion of anaplastic looking rounded to oval rhabdoid cells with vesicular chromatin and prominent centrally located nucleoli with a moderate rim of eosinophilic cytoplasm that was condensed to form paranuclear filamentous rhabdoid inclusion displacing the nucleus to the cell periphery. Bi- and multinucleation was a constant feature in all cases (Fig. 2A, B). The size of the neoplastic cells varied greatly with some being small or medium-sized while other cells had copious eosinophilic cytoplasm with distinctive cell borders (Fig. 2C, D). The background stroma was very sparse but frequently showed variable degree of myxoid change (Fig. 2E). The periphery of the tumors varied from well circumscribed (focally) to diffuse sieve-like and septal infiltration of surrounding fat and muscle (Fig. 2F). A minor component of scattered mononuclear inflammatory cells was observed in all cases occasionally admixed with a few scattered polymorph-nuclear granulocytes but a significant inflammation was not seen nor was there any prominent emperipolesis. One case was composed solely of monotonous small blue looking rounded cells with minor cytoplasmic rim arranged in a diffuse solid pattern within delicate fibrous stroma with

very few scattered rhabdoid cells (Fig. 2G). This case was biopsied only and resection was not available. However, the imaging suggested a diagnosis of either lymphoma or sarcoma as fatty component was not evident. This case was sent for consultation as alveolar rhabdomyosarcoma due to extensive expression of desmin and myogenin (Fig. 2H, I).

The lipomatous differentiation varied greatly from one tumor to another and within same tumor. Two cases showed a component of homologous dedifferentiation that occupied one third of the tumor mass (in one case; Fig. 3A) or represented incidental microscopic finding (<1%) in the other case (Fig. 3B). Other cases contained very few scattered signet-ring like lipoblastic cells amid the rhabdoid cell population (Fig. 3C). A sclerosing pattern closely mimicking sclerosing liposarcoma was seen in a few peritoneal nodules in Case 1, focally associated with epithelioid features reminiscent of sclerosing epithelioid fibrosarcoma (Fig. 3D). A conventional well differentiated lipomatous component was otherwise not seen in any of the cases.

Immunohistochemistry (table 2) showed consistent expression of CDK4 (5/6) and MDM2 (6/6) (Fig. 4A, B). Notably, 4/6 cases showed variable reactivity for pancytokeratin AE/1AE3 usually within numerous but scattered cells with focal paranuclear dot-like pattern (Fig. 4C, D). Indeed, this suggested a diagnosis of poorly differentiated carcinoma on core needle biopsy in case 1 leading to extensive clinical investigations looking for a primary but without success. Two cases showed uniform expression of desmin and myogenin in almost all of the neoplastic cells (Fig. 2H, I). One of these cases was composed of uniform small round cells suggestive of solid alveolar rhabdomyosarcoma but the latter was ruled out on the basis of high level amplification of *MDM2* and *CDK4* and absence of *FOXO1* translocation by FISH. All cases showed high level amplification of *MDM2* (Fig. 4E) and *CDK4* (Fig. 4F).

DISCUSSION

In this series, we described an underreported variant of DDL characterized by a remarkable predominance of undifferentiated rhabdoid, epithelioid or round cell morphology that can be mistaken for a variety of undifferentiated malignancies of epithelial, mesothelial, melanocytic, hematolymphoid or mesenchymal origin. The morphology of most of these tumors is nondescript and does not allow for their recognition as DDL unless DDL is included in the differential diagnosis and careful search done for evidence of subtle lipogenic features supported by relevant immunomarkers and genetic testing. The cytology and the architecture closely recapitulated that reported for a variety of undifferentiated and dedifferentiated rhabdoid malignancies, in particular carcinomas and melanomas [9-12]. This is reflected in the presence of vesicular nuclei, prominent nucleoli and frequent bi-and multinucleation.

To our knowledge, this variant of DDL has not been reported before in details except for a series published by Makise et al during preparation of this study [13]. Rhabdoid/epithelioid DDL seems to affect mainly middle-aged and elderly patients similar to DDL in general. Our study is comparable to the recent report by Makise et al [13] with similar site and gender distribution. However, Makise et al mentioned that rhabdoid cells represented a focal feature in many of their cases in contrast to our series. Compared to conventional DDL with a distant metastatic rate of <15-30% [1], the variant reported herein seems to pursue a more aggressive course (4/4 cases with detailed information had distant metastasis).

Makise et al´s series showed a WDL component either synchronously or metachronously in 6/8 cases. For two cases lacking this, they suggested the termed "*MDM2-amplified undifferentiated epithelioid neoplasms"* [13]. The adipocytic nature was evident in two of our cases featuring unequivocal areas of homologous dedifferentiation. Another case showed sclerosing component similar to retroperitoneal liposarcomas. This case and another two cases showed only subtle signet ring lipoblast-like cells histologically and one case lacked any lipogenic differentiation (the latter had only core needle biopsies available). The main hint to these cases being possible DDLs was their retroperitoneal location, their similar clinicopathological features as DDL of retroperitoneum (all presenting as huge masses) and the detection of *CDK4*/*MDM2* amplification. Thus, proving them as DDLs was only possible by immunophenotyping analysis to exclude other diagnoses (mainly melanoma and carcinoma) and demonstrating MDM2 and CDK4 expression/amplification.

Admittedly, some controversy still exists regarding the classification of *MDM2*/*CDK4*-amplified sarcomas. This is mainly due to the observation of *MDM2* and/or *CDK4* amplification in other sarcoma subsets including parietal osteosarcomas [14], intimal sarcomas of large vessels [15] and possibly other yet undefined neoplasms. However, there is a growing acceptance to classify *MDM2*/*CDK4*-co-amplified but otherwise undifferentiated sarcomas in the retroperitoneum as DDL. As a consequence, a diagnosis of undifferentiated pleomorphic sarcoma (so-called MFH) is not made any more in the retroperitoneum if *MDM2*/*CDK4* amplification is detected [16].

Based on the unusual large anaplastic looking non-descript epithelioid and rhabdoid cells the differential diagnosis includes in particular undifferentiated carcinoma, mesothelioma, malignant melanoma, anaplastic large cell lymphoma, epithelioid

leiomyosarcoma, epithelioid variant of pleomorphic rhabdomyosarcoma, PEComa, high-grade epithelioid myxofibrosarcoma and others.

Of note, none of 16 cases of epithelioid variant of pleomorphic rhabdomyosarcoma reported recently by Jo et al originated in the retroperitoneum [17]. Three of the 16 cases showed rhabdoid cell features that were very similar to our current cases. Strong and diffuse desmin expression in conjunction with myogenin expression should help to distinguish this variant from rhabdoid DDL. However, DDL may show a variable component of desmin and rarely myogenin positive cells as in our current study. Retroperitoneal location is probably the best hint to the possibility of heterologous rhabdomyoblastic differentiation in DDL when such a neoplasm is encountered. Moreover, DDL shows amplification of MDM2 and CDK4 while both are not expected in epithelioid rhabdomyosarcoma.

The second and probably most important group in the differential diagnosis is metastatic neoplasms with undifferentiated rhabdoid morphology as a predominant pattern. The latter encompass different tumors and entities in the heterogeneous spectrum of SWI/SNF-deficient malignancies. In particular, metastatic rhabdoid carcinomas from the GI tract including the pancreatobiliary system [10,11], the genitourinary system including kidney [12], urinary bladder [18] and uterus [19] as well as undifferentiated thoraco-pulmonary malignancies [20]. In addition, extra-renal malignant rhabdoid tumors of soft tissue and frankly rhabdoid proximal-type epithelioid sarcoma are important differential considerations; all of them are SMARCB1-deficient [21]. This differential can largely be solved based on a detailed clinicopathological correlation, imaging studies to define or rule out another primary and immunohistochemical workup using appropriate markers. In contrast to all these

rhabdoid malignancies listed above, rhabdoid/epithelioid DDL lacks phenotypic features of melanoma, PEComa, and lymphoma. Partial expression of cytokeratins in up to 66% of epithelioid DDL represents a pitfall and should be thought of. Furthermore, DDL in our and Makise et al´s series showed intact expression of SMARCB1, SMARCA2 and SMARCA4 thus ruling out a majority of the rhabdoid entities above [10-12,18-21].

Dedifferentiated malignant melanoma may occasionally present as pleomorphic epithelioid "or rhabdoid" rhabdomyoblastic malignancy within the GI tract and other sites, show variable cytokeratin immunoreactivity and lack any other defining melanocytic immunophenotype. However, they lack expression and/or amplification of MDM2 and CDK4 in contrast to DDL [22]. Genotyping (BRAF/NRAS) may be helpful in problematic cases [22]. Epithelioid pleomorphic liposarcoma as another important consideration lacks MDM2/CDK4 alterations [23]. Other differential diagnostic considerations including mesothelioma and others can be ruled out based on defined diagnostic criteria of these entities. As one of our cases displayed a non-descript monotonous round cell pattern, high-grade myxoid liposarcoma (s-called round cell liposarcoma) and other round cell sarcomas should be considered as well in the differential.

A last point to address is the prominent small round cell morphology seen in one case that turned out to represent uniform rhabdomyoblastic differentiation indistinguishable from solid alveolar rhabdomyosarcoma. Indeed, DDL was considered solely on the basis of the advanced patient age (81 yrs), the retroperitoneal location and huge size of the tumor. Although this tumor has been only biopsied and a lipogenic component cannot be verified or excluded, the imaging appearance was similar to other cases and thus liposarcoma was not considered radiologically. Diagnosis of DDL was rendered based on

the high-level amplification of MDM2 and CDK4 and the absence of the FOXO1 gene fusion characteristic of alveolar rhabdomyosarcoma. Rhabdomyoblastic dedifferentiation of any extent was observed in 7/92 cases (7%) in a recent series and significantly impacted adverse outcome (5/6 patients died within 8 months [24]). Thus, it is mandatory to stain with rhabdomyogenic markers in DDL featuring small round cell or epithelioid/rhabdoid cell morphology as rhabdomyoblastic differentiation seems to be overrepresented in this subgroup of DDL (one third of our cases).

In summary, we herein described 6 cases of dedifferentiated liposarcoma composed predominantly or almost exclusively of undifferentiated small to medium-sized rhabdoid or round/epithelioid cells associated with frequent co-reactivity with pancytokeratin and rhabdomyoblastic differentiation. This more aggressive variant of dedifferentiated retroperitoneal liposarcoma needs to be distinguished from a variety of neoplasms including undifferentiated carcinoma, mesothelioma, melanoma, lymphoma and rhabdomyosarcoma.

Compliance with Ethical Standards

The authors confirm that the study has been performed in accordance with accepted principles of ethical and professional conduct for biomedical scientific research. The study is covered by ethical vota of the medical faculty of the University of Erlangen for retrospective translational research activities.

Sources of grants or funding to this study: None.

Disclosure of potential conflicts of interest:

The authors have no financial or non-financial conflicts of interest to disclose.

REFERENCES

1. Thway K, Jones RL, Noujaim J, Zaidi S, Miah AB, Fisher C. Dedifferentiated Liposarcoma: Updates on Morphology, Genetics, and Therapeutic Strategies. Adv Anat Pathol. 2016;23:30-40.

2. Dei Tos AP, Marino-Enriquez A, Pedeutour F, Rossi S. Dedifferentiated liposarcoma. In: Fletcher CDM, Bridge JA, Hogendoorn PCW, Mertens F. *World Health Organisation classification of Tumours of Soft Tissue and Bone (4th edn)*. Lyon: IARC Press; 2013:37-38.

3. Hasegawa T, Seki K, Hasegawa F, et al. Dedifferentiated liposarcoma of retroperitoneum and mesentery: varied growth patterns and histological grades--a clinicopathologic study of 32 cases. Hum Pathol 2000;31:717-27.

4. Henricks WH, Chu YC, Goldblum JR, Weiss SW. Dedifferentiated liposarcoma: a clinicopathological analysis of 155 cases with a proposal for an expanded definition of dedifferentiation. Am J Surg Pathol. 1997;21:271-81.

5. Binh MB, Guillou L, Hostein I, et al. Dedifferentiated liposarcomas with divergent myosarcomatous differentiation developed in the internal trunk: a study of 27 cases and comparison to conventional dedifferentiated liposarcomas and leiomyosarcomas. Am J Surg Pathol. 2007;31:1557-66.

6. Fanburg-Smith JC, Miettinen M. Liposarcoma with meningothelial-like whorls: a study of 17 cases of a distinctive histological pattern associated with dedifferentiated liposarcoma. Histopathology. 1998;33:414-24.

7. Lucas DR, Shukla A, Thomas DG, Patel RM, Kubat AJ, McHugh JB. Dedifferentiated liposarcoma with inflammatory myofibroblastic tumor-like features. Am J Surg Pathol. 2010;34:844-51.

8. Mariño-Enríquez A, Fletcher CD, Dal Cin P, Hornick JL. Dedifferentiated liposarcoma with "homologous" lipoblastic (pleomorphic liposarcoma-like) differentiation: clinicopathologic and molecular analysis of a series suggesting revised diagnostic criteria. Am J Surg Pathol. 2010;34:1122-31.

9. Bittesini L, Dei Tos AP, Fletcher CD. Metastatic malignant melanoma showing a rhabdoid phenotype: further evidence of a non-specific histological pattern. Histopathology. 1992;20:167-70.

10. Agaimy A, Daum O, Märkl B, Lichtmannegger I, Michal M, Hartmann A. SWI/SNF Complex-deficient Undifferentiated/Rhabdoid Carcinomas of the Gastrointestinal Tract. A Series of 13 Cases highlighting Mutually Exclusive Loss of SMARCA4 and SMARCA2 and Frequent Co-inactivation of SMARCB1 and SMARCA2. Am J Surg Pathol 2016;40:544-53.

11. Agaimy A, Haller F, Frohnauer J, et al. Pancreatic Undifferentiated Rhabdoid Carcinoma: *KRAS* Alterations and SMARCB1 Expression Status Define Two Subtypes. Mod Pathol 2015;28:248-60.

12. Agaimy A, Cheng L, Egevad L, et al. Rhabdoid and Undifferentiated Phenotype in Renal Cell Carcinoma: Analysis of 32 Cases Indicating a Distinctive Common Pathway of Dedifferentiation Frequently Associated With SWI/SNF Complex Deficiency. Am J Surg Pathol. 2017;41:253-262.

13. Makise N, Yoshida A, Komiyama M, et al. Dedifferentiated Liposarcoma With Epithelioid/Epithelial Features. Am J Surg Pathol. 2017;41:1523-1531.

14. Dujardin F, Binh MB, Bouvier C, Gomez-Brouchet A, MDM2 and CDK4 immunohistochemistry is a valuable tool in the differential diagnosis of low-grade osteosarcomas and other primary fibro-osseous lesions of the bone. Mod Pathol. 2011;24:624-37.

15. Neuville A, Collin F, Bruneval P, et al. Intimal sarcoma is the most frequent primary cardiac sarcoma: clinicopathologic and molecular retrospective analysis of 100 primary cardiac sarcomas. Am J Surg Pathol. 2014 Apr;38(4):461-9.

16. Coindre JM, Mariani O, Chibon F, et al. Most malignant fibrous histiocytomas developed in the retroperitoneum are dedifferentiated liposarcomas: a review of 25 cases initially diagnosed as malignant fibrous histiocytoma. Mod Pathol. 2003;16:256-62.

17. Jo VY, Mariño-Enríquez A, Fletcher CD. Epithelioid rhabdomyosarcoma: clinicopathologic analysis of 16 cases of a morphologically distinct variant of rhabdomyosarcoma. Am J Surg Pathol. 2011;35:1523-30.

18. Agaimy A, Bertz S, Cheng L, et al. Loss of expression of the SWI/SNF complex is a frequent event in undifferentiated/dedifferentiated urothelial carcinoma of the urinary tract. Virchows Arch 2016;469:321-30.

19. Ramalingam P, Croce S, McCluggage WG. Loss of expression of SMARCA4 (BRG1), SMARCA2 (BRM) and SMARCB1 (INI1) in undifferentiated carcinoma of the endometrium is not uncommon and is not always associated with rhabdoid morphology. Histopathology 2017;70:359-366.

20. Le Loarer F, Watson S, Pierron G, et al. SMARCA4 inactivation defines a group of undifferentiated thoracic malignancies transcriptionally related to BAF-deficient sarcomas. Nat Genet. 2015;47:1200-5.

21.Hollmann TJ, Hornick JL. INI1-deficient tumors: diagnostic features and molecular genetics. Am J Surg Pathol. 2011;35:e47-63.

22. Agaimy A, Specht K, Stoehr R, et al. Metastatic Malignant Melanoma With Complete Loss of Differentiation Markers (Undifferentiated/ Dedifferentiated Melanoma): Analysis of 14 Patients Emphasizing Phenotypic Plasticity and the Value of Molecular Testing as Surrogate Diagnostic Marker. Am J Surg Pathol. 2016;40:181-91.

23. Miettinen M, Enzinger FM. Epithelioid variant of pleomorphic liposarcoma: a study of 12 cases of a distinctive variant of high-grade liposarcoma. Mod Pathol 1999;12:722-8.

24. Gronchi A, Collini P, Miceli R, et al. Myogenic differentiation and histologic grading are major prognostic determinants in retroperitoneal liposarcoma. Am J Surg Pathol 2015;39:383–393.

FIGURES

Figure 1

CT scan (Case 1) showed large non-fatty retroperitoneal mass with extensive necrosis.

Figure 2

Dedifferentiated liposarcoma composed of poorly cohesive undifferentiated rhabdoid cells in nests and packages (**A**, Case 1) and trabeculae (**B**, Case 2) within scant stroma. . Other features included solid pattern resembling poorly differentiated carcinoma (**C**, Case 1), small lymphocyte-like nuclei with copious eosinophilic cytoplasm (**D**, Case 5), myxoid stromal changes (**E**, Case 5) and septal infiltration of fat by ganglion-like rhabdoid cells mimicking proliferative fasciitis (**F**, Case 1). Case 3 featured monotonous small round cells with clear cytoplasm and a few rhabdoid cells (**G**) and expression diffusely desmin (**H**) and myogenin (**I**).

Figure 3

Homologous dedifferentiated foci were seen in Case 6 (**A**) and Case 1 (**B**). Scattered signet ring lipoblasts (thin arrows) and rare multivacuolated cells (thick arrow) were seen in Case 2 (**C**). A sclerosing component with focal features reminiscent of sclerosing epithelioid fibrosarcoma was seen in Case 1 (**D**).

Figure 4

Strong expression of CDK4 (**A**) and MDM2 (**B**) was seen in all cases (images: Case 2). AE1/AE3 was positive in scattered numerous cells (**C**) with focally prominent dot-like

pattern highlighting rhabdoid morphology (**D**; images Case 1). **E**: Amplification of MDM2 (CISH, Case 3) and CDK4 (**F**; FISH, Case 6) was a constant feature.

Table 1: Clinicopathologic features of rhabdoid/epithelioid dedifferentiated liposarcoma (n=6).

No	Age/ Gender	Site	Size cm	Histology	% Rhabdoid / epithelioid	Lipogenic component?	Treatment	Distant MTS?	Follow-up
1	65 M	Right psoas muscle	11 +3.5	Small to medium-sized rhabdoid/ epithelioid cells	90%	Sclerosing nodules, scattered signet ring lipoblasts, microscopic homologous dedifferentiation	Surgery+ CT	Multiple peritoneal (synchronous), lung (1 mo)	DOD (4 mo)
2	77 M	Left psoas muscle	Large, NS	Small to medium-sized rhabdoid/ epithelioid cells	100%	Scattered signet ring lipoblasts,	R2 Surgery+ palliative CT	Lower left abdominal cavity	AWD progressive under palliative CT (6 mo)
3	81 M	Left retroperitoneum	Large, NS	Small blue round cells, scattered rhabdoid cells	100% of core needle biopsies	None (only biopsied)	NA	NA	Recent case
4	64 F	Retroperitoneum	15	Large rhabdoid cells	100%	Scattered signet ring lipoblasts	NA	NA	NA
5	67 M	Iliac fossa	11.5	Small to medium-sized rhabdoid/ epithelioid cells	100%	Scattered signet ring lipoblasts	RT	Stomach	DOD (6 mo)
6	69 M	Thigh	7	Small to medium-sized epithelioid cells/ scattered huge rhabdoid cells	70%	Homologous dedifferentiation (30%)	Surgery+ RCT	Cranial vault, ribs, vertebrae, pelvic skeleton	DOD (8 mo)

CT, chemotherapy; DOD, died of disease; mo, months; MTS, metastases; NA, not available; NS, not specified; RCT, radiochemotherapy; RT, radiotherapy;

Table 2: Immunohistochemical and molecular features of rhabdoid/epithelioid dedifferentiated liposarcoma (n=6).

No	Desmin	Myogenin	AE1/AE3	MDM2 IHC	CDK IHC	MDM2 FISH	CDK4 FISH	SWI/SNF markers tested	Other negative markers
1	-	-	+	+	+	+	+	SMARCB1, SMARCA4 & ARID1A intact	CD2, CD20, CD30, CD31,ERG, S100, SOX10, pan-melanoma, CK7, CK20, h-caldesmon, MUC4
2	-	-	-	+	+	+	+	SMARCB1, SMARCA2, SMARCA4, ARID1A, PBRM1 all intact	S100, SOX10, STAT6, EMA, PAX8, ERG
3	+	+	+	+	+	+	+	SMARCB1, SMARCA4 & ARID1A intact	S100, synaptophysin, pan-melanoma, CD3, CD20, CD30, FOXO1 FISH negative
4	+	+	+	+	+	+	+	SMARCB1, SMARCA4 & ARID1A intact	S100, CD34
5	-	-	+	+	-	+	-	SMARCB1, SMARCA4 & ARID1A intact	S100, HMB45, Actin E, Actin S, CD34
6	-	-	-	+	+	+	+	SMARCB1, SMARCA4 & ARID1A intact	Actin S, Synaptophysin, Chromogranin, CD34

IHC, immunohistochemistry; FISH, fluorescent in-situ hybridization

Figure 1

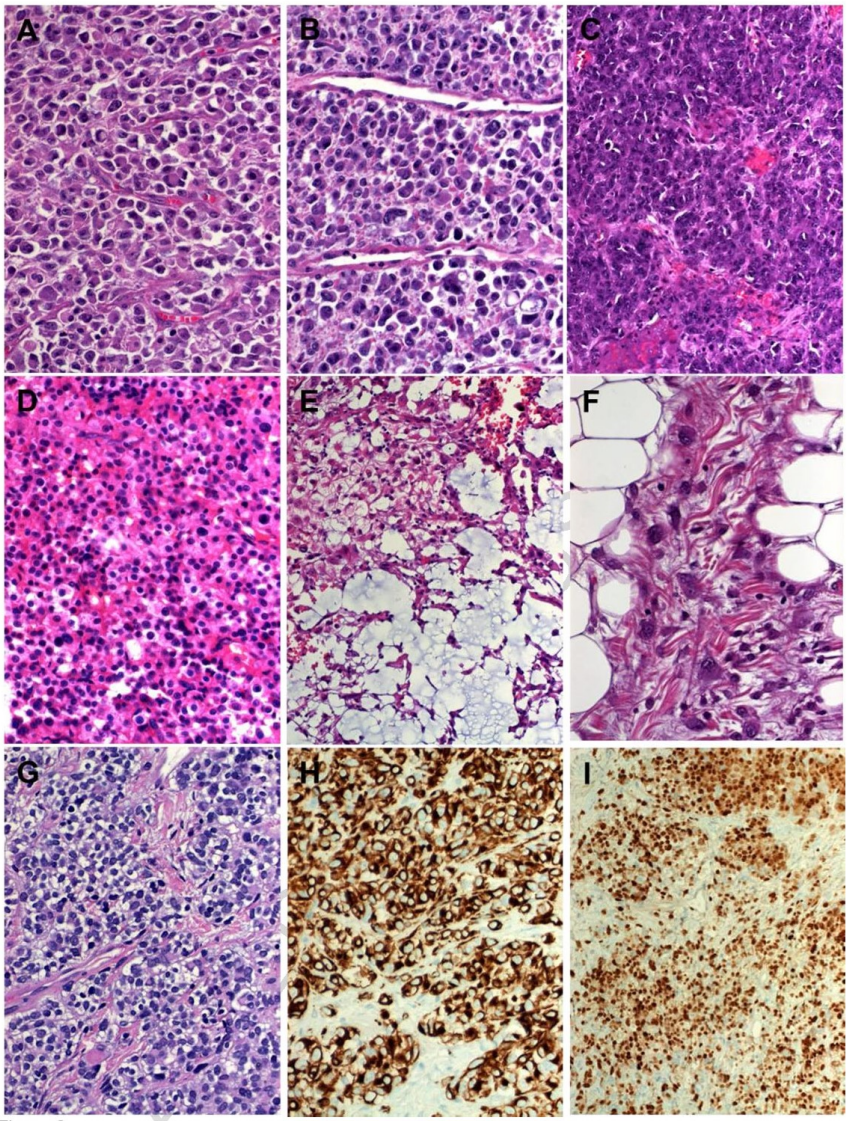

Figure 2

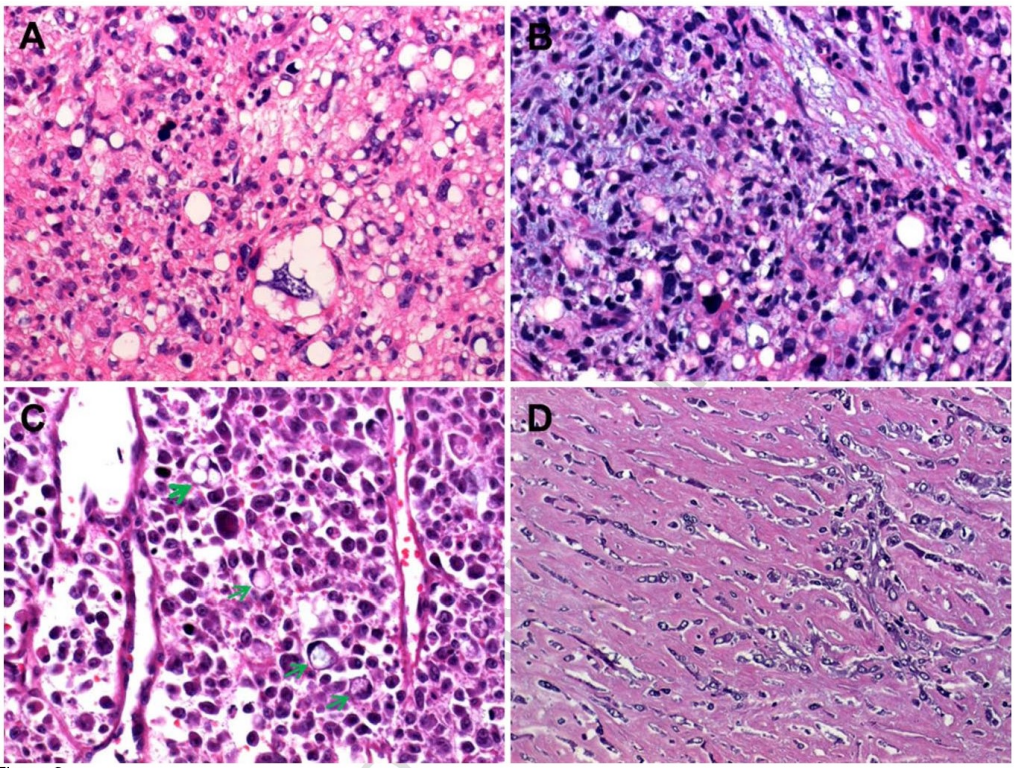

Figure 3

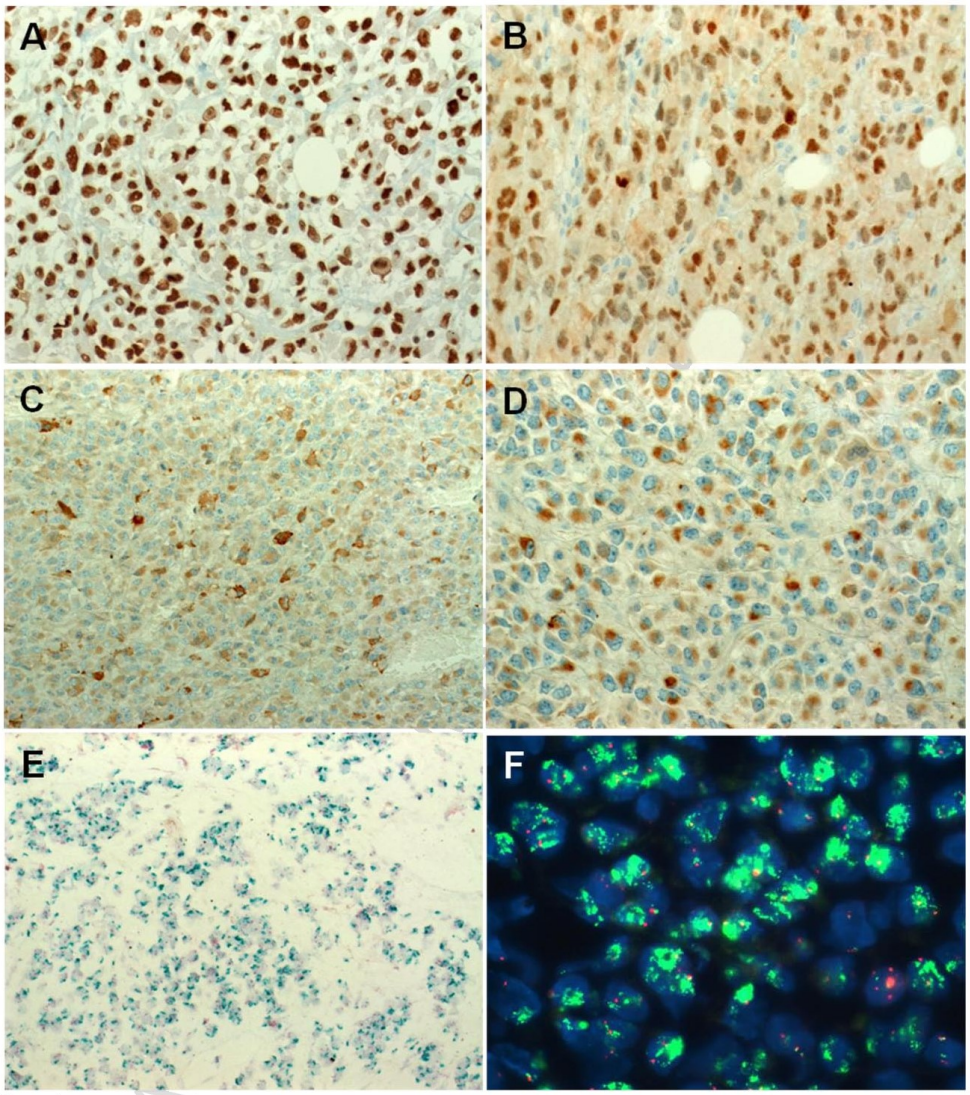

Figure 4

Highlights

- Dedifferentiated epithelioid liposarcoma closely mimics a variety of other malignancies.
- It shows a significantly higher distant metastatic rate than conventional DDL.
- Heterologous rhabdomyoblastic differentiation seems to be a frequent feature.
- Careful assessment detects at least subtle lipogenic cells.
- Immunohistochemistry and molecular analysis are mandatory for diagnosis.

2.2.7. ALK GENE FUSIONS IN EPITHELIOID FIBROUS HISTIOCYTOMA: A STUDY OF 14 CASES, WITH NEW HISTOPATHOLOGICAL FINDINGS

Fibrous histiocytoma is a benign tumor occurring in the dermis, superficial subcutis or rarely, in deep soft tissues over a wide anatomic range. When this tumor consists of more than 50% of epithelioid cells it is referred to as epithelioid fibrous histiocytoma (EFH). In 88% of cases, this subtype shows immunoreactivity with ALK antibody and even most of the immunonegative cases show *ALK* gene rearrangements [58]. Another study found that a subset of these ALK rearranged lesions harbor *VCL-ALK* and *SQSTM1-ALK* gene fusions [59]. However, the majority of *ALK* fusion partners remained unknown. This led us to analyze all EFH stored in our files to further characterize the molecular underpinnings and also, to look for novel, yet unreported morphological features of these tumors. Moreover, since we observed a frequent TFE3 immunoreactivity in these tumors, we analyzed all our samples for the expression of this antibody.

After morphological review, 14 well characterized examples of EFH were included in the study. All ALK immunonegative cases were excluded. Then, we further morphologically scrutinized the cases and performed ALK and TFE3 FISH to confirm or exclude the gene break. After only the ALK gene break was confirmed by FISH, the cases were submitted for next generation sequencing(NGS)-based panel analysis of 195 targets in 40 genes [The Comprehensive Thyroid Lung kit (ArcherDX Inc, Boulder, CO)].

Morphologically, two lesions were composed of closely packed, plexiform, or fascicular proliferations of pale to clear spindled cells and thus resembled PEComa or leiomyoma. The typical epithelioid cell component was absent and in both cases, the original diagnosis of EFH was rendered as an “exclusion” diagnosis after a broad spectrum of antibodies had been performed to exclude possible tumors of other lineages. We consider these lesions EFH, as we have noted similar cytological features, albeit never prominent, in more conventional EFH. ALK positivity and ALK gene fusion support the classification of these lesions as EFH. Thus, PEComa and leiomyoma can be added to the list of the differential diagnosis of EFH. We also found some minor novel cytological variations, including cells with multilobulated nuclei, nuclear grooves, and mucinous cells. In a subset of cases, we identified cells with intranuclear pseudoinclusions and eccentric nuclei. In 3 cases, occasional areas with emperipolesis of single lymphocytes were noted, which is another hitherto unreported feature in EFH. The break apart test for ALK was positive in all 11 analyzable cases. ALK genes fusions were found in all but 3 cases and included SQSTM1-ALK (3), VCL-ALK (3), TMP3-ALK (2), PRKAR2A-ALK (1), MLPH-ALK (1), and EML4-ALK (1). No correlation between histological features and type of ALK fusion was found. TFE-3 break apart test was negative.

Summarizing these results, ALK-positive EFH shows frequently ALK gene fusions that involve various protein-coding genes, implicated in a variety of biological processes. Rare variants of EFH rather consist of spindled “non-epithelioid” cells, thus occasioning a resemblance to PEComa or leiomyoma. Inclusion of such lesions into the spectrum of EFH must be validated by further observations. TFE-3 is expressed in a majority of ALK-positive EFH; however, TFE-3 rearrangement is not a feature.

Our study was published ahead of print several days before a similar study appeared online in another journal, mostly confirming our results [60].

ALK Gene Fusions in Epithelioid Fibrous Histiocytoma: A Study of 14 Cases, With New Histopathological Findings

Dmitry V. Kazakov, MD, PhD,*† Liubov Kyrpychova, MD,*† Petr Martinek, PhD,*† Petr Grossmann, PhD,*† Petr Steiner,*† Tomas Vanecek, PhD,*† Michal Pavlovsky, MD,‡ Vladimir Bencik, MD,§ Michael Michal, MD,*† and Michal Michal, MD*†

Abstract: Previous studies showed that ALK is often positive in epithelioid fibrous histiocytoma (EFH). Two cases of EFH with *ALK* gene fusions have been recorded. Our objective was to study a series of EFH to present histopathological variations of EFH, identify novel *ALK* gene fusions, and determine whether there is a correlation between histopathological features and particular gene. We investigated 14 cases of EFH, all ALK immunopositive. The cases were assessed histopathologically as well as for *ALK* and *TFE-3* rearrangements using FISH and *ALK* gene fusions using next-generation sequencing. The analysis of the sequencing results was performed using the Archer Analysis software (v5; ArcherDX Inc). The study group consisted of 8 female and 6 male patients, ranging in age from 18 to 79 years (mean 42 years; median 37.5 years). All presented with a solitary lesion. Microscopically, most lesions were polypoid and composed of epithelioid cells with ample cytoplasm. In addition, a variable number of bi-, tri-, or multinucleated, spindled, multilobated, cells with eccentric nuclei, cells with nuclear pseudoinclusions, mucinous, and grooved cells were admixed. In 5 cases, the predominant epithelioid cell component consisted of rather small cells, whereas spindled cells dominated in 3 cases. Of these, 2 lesions were composed rather of pale eosinophilic to clear cells, occasioning a resemblance to PEComa or leiomyoma. Immunohistochemically, all cases expressed ALK and 11 were positive for TFE-3. The break apart test for *ALK* was positive in 11 cases, whereas specimens from the remaining 3 cases were not analyzable. *ALK* genes fusions were found in all but 3 cases and included *SQSTM1-ALK* (3), *VCL-ALK* (3), *TMP3-ALK* (2), *PRKAR2A-ALK* (1), *MLPH-ALK* (1), and *EML4-ALK* (1). No correlation between histological features and type of *ALK* fusion was found. *TFE-3* break apart test was negative. It is concluded that ALK-immunopositive EFH shows *ALK* gene fusions that involve various protein-coding genes, implicated in a variety of biological processes. Rare variants of EFH rather consist of spindled "non-epithelioid" cells.

Key Words: epithelioid fibrous histiocytoma, ALK, TFE-3, gene fusions, Spitz nevus

From the *Sikl's Department of Pathology, Medical Faculty in Pilsen, Charles University in Prague, Pilsen, Czech Republic; †Bioptical Laboratory, Pilsen, Czech Republic; ‡Department of Pathology, Regional Hospital Most, Czech Republic; and §Ben Labor, Ostrava, Czech Republic.

Supported in part by a Charles University project (SVV 260 391/2017).
The authors declare no conflicts of interest.

Reprints: Dmitry V. Kazakov, MD, PhD, Sikl's Department of Pathology, Charles University Medical Faculty Hospital, Alej Svobody 80, 304 60 Pilsen, Czech Republic (e-mail: kazakov@medima.cz).

(*Am J Dermatopathol* 2018;0:1–10)

INTRODUCTION

Epithelioid fibrous histiocytoma (EFH) is considered as a variant of benign fibrous histiocytoma in which more than 50% of cells are epithelioid.[1,2] In contrast to benign fibrous histiocytoma (dermatofibroma), EFH usually lacks collagen entrapment at the periphery of the lesion, xanthomatized cells and epidermal hyperpigmentation above the lesion. EFH usually presents as a polypoid lesion, often with an epidermal collarette. Previously published material and our own experience indicate certain histopathological heterogeneity of EFH, regarding cytological features, architectural features and immunoprofile.[3–6] With respect to the latter, a subset of EFH shows ALK expression on immunohistochemistry.[7,8] Doyle et al detected this feature in 29 of 33 cases, and in all 13 studied ALK-positive lesions, FISH demonstrated *ALK* rearrangements.[9] Two cases of EFH with *ALK* gene fusions have been recently recorded.[10] Our objective was to study a series of EFH to present histopathological variations of EFH, identify potentially novel *ALK* gene fusions, and determine whether there is a correlation between the histopathological features and a particular gene fusion.

MATERIAL AND METHODS

Case Selection

A search in the joint consultation files of 2 authors (M. M. and D.V.K.) yielded 46 cases coded as EFH and lesions in which EFH was a diagnostic consideration. Cases with available blocks were retrieved and reviewed. Apart from tissue availability, included in the study were only ALK-immunopositive lesions. A total of 14 cases meeting the selection criteria were included for a further investigation.

Immunohistochemical Studies

A new staining for ALK was performed for all selected cases. In most cases, 2 clones, namely ALK01 and D5F3 (both prediluted; Ventana, Tuscon, AZ), were used. Also, all lesions were stained for TFE-3 (MRQ-37, prediluted; Cell Marque, Rocklin, CA), as we have previously noted frequently positivity of EFH for TFE-3. In most cases, other various markers, including melanocytic, epithelial, vascular, neural, follicular dendritic, Langerhans cell, and others were performed at the time of the original diagnosis; these were not repeated.

TABLE 1. Summary of the Main Clinicopathological, Immunohistochemical, and Molecular Biological Features

Case	Sex/Age	Location	Clinical Data/Size (mm)	Architecture	Cell Arrangement	Cells
1	F/49	Back	Tumor, 2 yrs duration/5	Polypoid with epidermal collaret	Sheets	Small epithelioid cells*; multilobated cells; cells with eccentric nuclei; spindled cells; intranuclear pseudoinclusions
2	M/38	Shin	Fibrous tumor/8	Polypoid with epidermal collaret	Sheets, nests	Large epithelioid cells with ample cytoplasm*; multinucleated cells; grooved cells; intranuclear pseudoinclusions
3	M/35	Chest wall	Nevus/10	Polypoid with epidermal collaret	Sheets	Large epithelioid cells with ample cytoplasm*; multinucleated cells; grooved cells; mucinous; intranuclear pseudoinclusions
4	F/45	Thigh	Nodule/8	Polypoid with epidermal collaret	Sheets, fascicles	Spindled cells*; large epithelioid cells with ample cytoplasm; grooved cells; intranuclear pseudoinclusions
5	F/79	Thigh	Fibroma/17	Polypoid, ulcerated	Sheets, perivascular cuffs	Small epithelioid cells*; multilobated cells; multinucleated cells; spindled cells; grooved cells
6	M/18	Back	Bleeding pyogenic granuloma, 1-mo duration/12	Polypoid, ulcerated	Sheets, perivascular cuffs	Small epithelioid cells*; spindled cells; multinucleated cells; mucinous cells
7	F/37	Flank	Dermatofibroma? Keratoacanthoma? 1-yr duration/5	Intradermal, nonpolypoid	Nested, focally fascicular	Small epithelioid cells*; cells with eccentric nuclei; spindled cells; grooved cells; intranuclear pseudoinclusions
8	M/48	Thigh	Amelanotic melanoma? BCC? 3-mo duration/10	Polypoid	Sheets, focally storiform with vague whorling	Large epithelioid cells with ample cytoplasm*; multinucleated cells; spindled cells; cells with eccentric nuclei; intranuclear pseudoinclusions
9	M/74	Back	BCC/10	Polypoid with epidermal collaret	Fascicular, single cell files, nested	Small epithelioid and spindled cells*; multinucleated cells; intranuclear pseudoinclusions
10	F/31	Thigh	Nodule/10	Polypoid with epidermal collaret	Sheets, focally nested	Large epithelioid cells with ample cytoplasm*; cells with eccentric nuclei mucinous cells; spindled cells; multinucleated cells; grooved cells; intranuclear pseudoinclusions
11	F/55	Earlobe	Tumor/7	Polypoid	Sheets	Large epithelioid cells with ample cytoplasm*; multinucleated cells; cells with eccentric nuclei; spindled cells; grooved cells; intranuclear pseudoinclusions
12	M/21	Trunk	Wart/20	Intradermal	Sheets, focally plexiform, fascicular	Clear spindled cells*; spindled cells; nuclear pseudoinclusions
13	F/28	Shin	Verrucous nevus/8	Polypoid with epidermal collaret	Sheets, fascicular	Clear spindled cells*; cigar-like cells
14	F/28	Chest wall	Nodule, 6-mo duration/8	Polypoid with epidermal collaret	Sheets	Large epithelioid cells with ample cytoplasm*; multinucleated cells; cells with eccentric nuclei; mucinous cells

Case	Stroma	Vasculature	Reactive Cells	IHC ALK/TFE-3	FISH *ALK/TFE-3* Ba	Gene Fusion
1	Scant	Inconspicuous	Lymphocytes	+/+	+/−	*SQSTM1-ALK*
2	Focally collagenous	Inconspicuous	Lymphocytes	+/+	+/−	*SQSTM1-ALK*
3	Scant, focally fibrotic	Focally prominent	Lymphocytes	+/+	+/−	*VCL-ALK*
4	Focally fibrotic	Focally prominent	Lymphocytes	+/+	+/−	*TPM3-ALK*
5	Scant, focally myxoid	Prominent	Lymphocytes; neutrophils	+/+	+/−	*VCL-ALK*

TABLE 1. (*Continued*) Summary of the Main Clinicopathological, Immunohistochemical, and Molecular Biological Features

Case	Stroma	Vasculature	Reactive Cells	IHC ALK/TFE-3	FISH *ALK/TFE-3* Ba	Gene Fusion
6	Scant	Prominent	Lymphocytes; neutrophils	+/+	+/−	*VCL-ALK*
7	Collagenous, focally myxoid	Inconspicuous	Lymphocytes	+/-	NA	*SQSTM1-ALK*
8	Scant	Inconspicuous	Lymphocytes; emperiopolesis	+/+	+/−	NA
9	Collagenous	Inconspicuous	Lymphocytes	+/-	+/−	*PRKAR2A-ALK*
10	Collagenous, especially perivascular	Prominent	Lymphocytes; emperiopolesis	+/+	NA	NA
11	Scant, focally myxoid	Focally prominent	Lymphocytes; plasma cells; emperiopolesis	+/+	+/−	*MLPH-ALK*
12	Scant, focally collagenous	Inconspicuous	Lymphocytes; plasma cells	+/+	+/−	*TMP3-ALK*
13	Scant	Focally prominent	Lymphocytes	+/+	+/−	*EML4-ALK*
14	Scant	Focally prominent	Lymphocytes; plasma cells	+/−	NA	NA

*Predominant cell type.
ba, break apart; NA, not analyzable.

FISH for *ALK* and *TFE3* Rearrangements

Four-micrometer thick formalin-fixed paraffin-embedded sections were placed onto positively charged slides. The unstained slides were routinely deparaffinized and incubated in the 1× Target Retrieval Solution Citrate pH 6 (Dako, Glostrup, Denmark) at 95°C for 40 minutes and subsequently cooled for 20 minutes at a room temperature in the same solution. The slides were washed in deionized water for 5 minutes and digested in protease solution with Pepsin (0.5 mg/mL; Sigma Aldrich, St. Louis, MO) in 0.01 M HCl at 37°C for 35–60 minutes, according the sample conditions. The slides were then placed into deionized water for 5 minutes, dehydrated in a series of ethanol solution (70%, 85%, and 96% for 2 minutes each) and air-dried. For the detection of *ALK* and *TFE3* breaks, the Vysis ALK Break Apart Probe Kit (Vysis/Abbott Molecular, Des Plaines, IL) and ZytoLight SPEC TFE3 Dual Color Break Apart Probe (ZytoVision GmbH, Bremerhaven, Germany) were used, respectively. An appropriate amount of factory premixed probe was applied on a specimen, covered with a glass coverslip, and sealed with rubber cement. The slides were incubated in the ThermoBrite instrument (StatSpin/Iris Sample Processing, Westwood, MA) with co-denaturation at 85°C for 8 minutes and hybridization at 37°C for 16 hours. The rubber cemented coverslip was then removed and the slide was placed in post-hybridization wash solution (2xSSC + 0.3% NP-40) at 72°C for 2 minutes. The slides were air-dried in the dark, counterstained with 4′,6′-diamidino-2-phenylindole DAPI (Vysis/Abbott Molecular), coverslipped and immediately examined with an Olympus BX51 fluorescence microscope (Olympus Corporation, Tokyo, Japan) using a 100× objective and filter sets triple band pass (DAPI/SpectrumGreen/SpectrumOrange), dual band pass (SpectrumGreen/SpectrumOrange), and single band pass (SpectrumGreen or SpectrumOrange). A minimum of 100 randomly selected nonoverlapping tumor cell nuclei were counted. For both the *ALK* break apart and *TFE-3* break apart tests, the presence of yellow (normal) and separated (break) orange and/or green fluorescent signals was evaluated. Samples were considered positive when more than 10% of nuclei showed break signals (mean + 3 standard deviation in normal nonneoplastic control tissues).

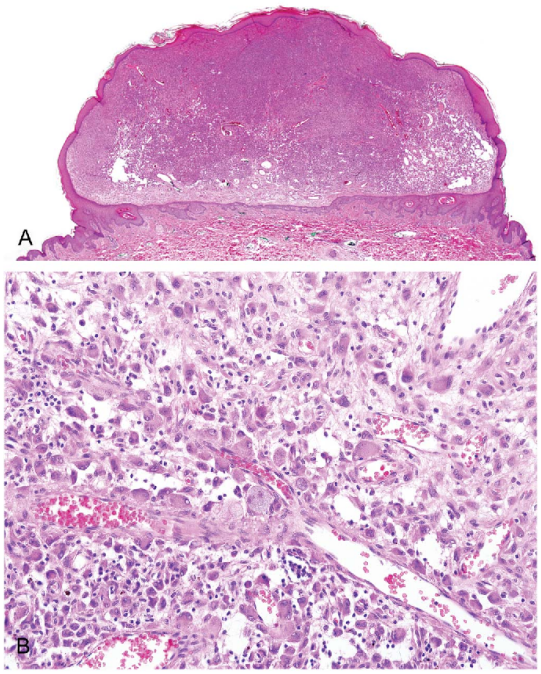

FIGURE 1. EFH (case 13). A polypoid lesion with epidermal collarette and prominent vasculature at the periphery (A) composed of large epithelioid cells with ample cytoplasm, with focal accentuation around the vessels (B). Note binucleated cells and occasional cells with mucinous cytoplasm (B).

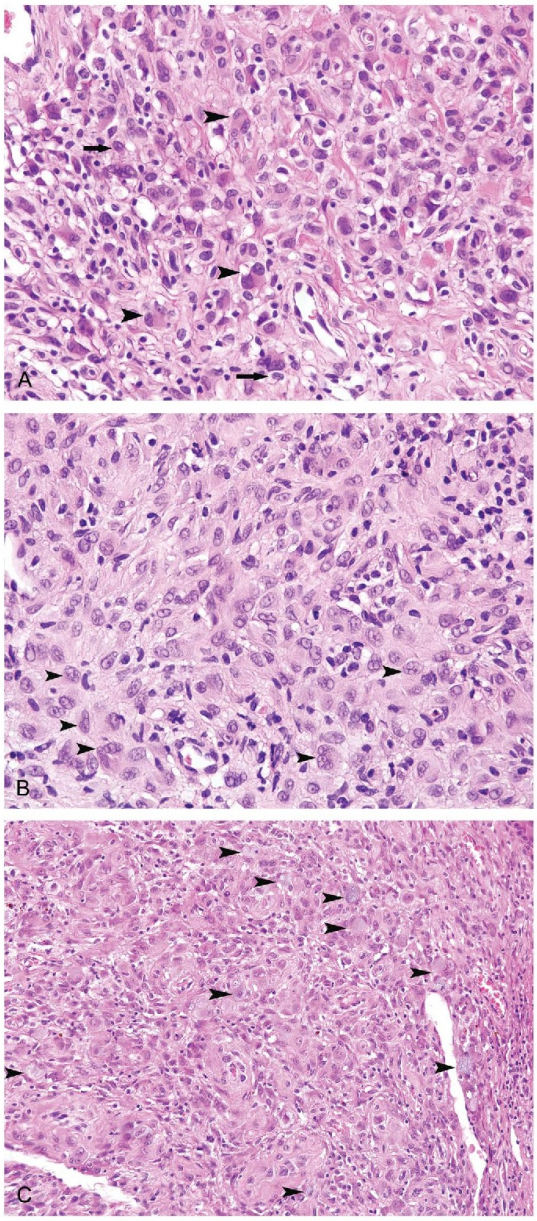

FIGURE 2. Cytological variations in EFH. Note cells with nuclear grooves (arrows) and numerous bi- or tri-nucleated cells (arrowheads) (A), cells with lobulated nuclei (arrowheads, B), and numerous mucinous cells (arrowheads, C).

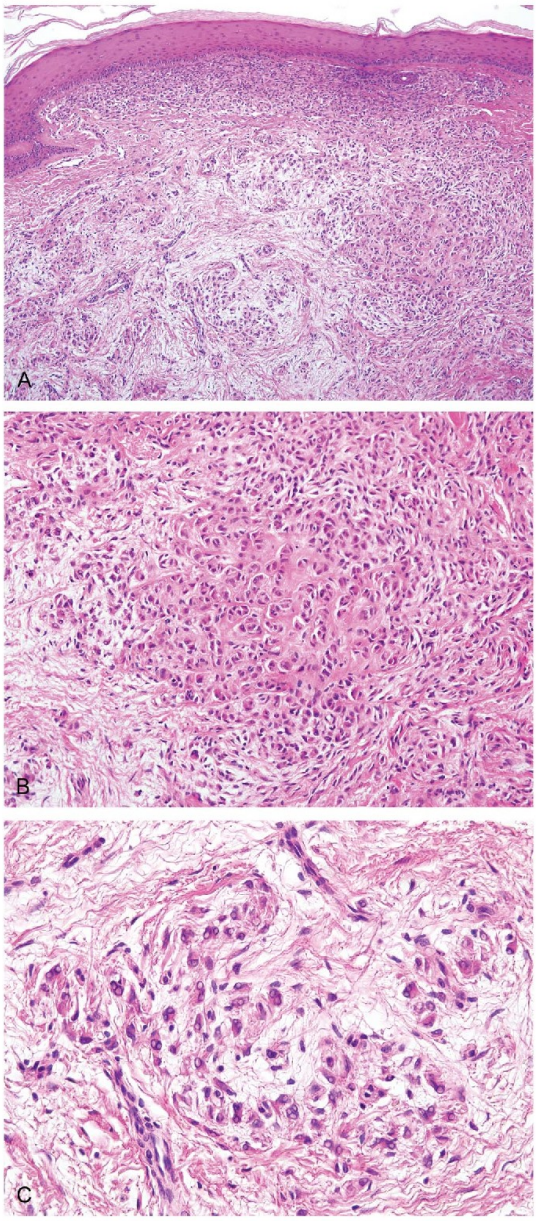

FIGURE 3. EFH (case 7) with nested pattern (A, B), focally resembling a melanocytic lesion. Note plentiful cells with intranuclear pseudoinclusions in less cellular (C) compared with the nested area (B).

Gene Fusion Detection Using Next-Generation Sequencing

Depending on the sample size, up to 3 formalin-fixed paraffin-embedded sections (10 μm thick) were macrodissected and total nucleic acid was extracted using the Agencourt FormaPure Kit (Beckman Coulter, Brea, CA) with modifications recommended by ArcherDX (ArcherDX Inc, Boulder, CO). Total nucleic acid was quantified using the Qubit Broad Range RNA Assay Kit (ThermoFisher Scientific, Waltham, MA) and input for each sample's library preparation was set to 250 ng. The PreSeq RNA QC Assay using iTaq Universal SYBR Green Supermix (Biorad, Hercules, CA) was performed to assess sample quality. Samples with the cycle threshold value smaller than 30 continued with target enrichment. The Comprehensive Thyroid Lung kit (ArcherDX Inc, Boulder, CO) containing 195 targets in 40 genes was used, and all steps were performed following the Archer's Fusion Plex Protocol for Illumina (ArcherDX Inc). Final libraries were quantified following the Library Quantification for Illumina Libraries protocol (KAPA, Wilmington, MA) assuming a 200 bp fragment length. Up to 32 samples were multiplexed per run on a NextSeq sequencer (Illumina, San Diego, CA) spiked with 20% PhiX control. The analysis of the sequencing results was performed using the Archer Analysis software (v5; ArcherDX Inc). Fusion parameters were set to a minimum of 5 valid fusion reads with a minimum of 3 unique start sites within the valid fusion reads.

RESULTS

Clinical Data

There were 8 female and 6 male patients, ranging in age from 18 to 79 years (mean 42 years; median 37.5 years). All presented with a solitary lesion. The clinical diagnoses included a melanocytic nevus, pyogenic granuloma, dermatofibroma, basal cell carcinoma, wart, keratoacanthoma, or mere description as a nodule or tumor. The locations included the trunk (7 cases), lower extremities (6 cases), and face (1 case). Grossly, the lesions varied in sized from 5 to 20 mm (mean 9.9 mm; median 9 mm) (Table 1).

Histopathological Findings

The lesions were mostly polypoid, with (n = 8) or without (n = 4) an epidermal collarette (Fig. 1A). Two cases exhibited a nonpolypoid architecture with an intradermal proliferation of the neoplastic cells. The predominant cell types were mononucleated medium-sized to large epithelioid cells with ample eosinophilic to amphophilic cytoplasm. In addition, a variable number of bi-, tri-, or multinucleated (rarely), spindled, multilobated, cells with eccentric nuclei, cells with nuclear pseudoinclusions, mucinous, and grooved cells, likely representing a variation of a single cell type were admixed (Figs. 1B, 2–4) The cells were usually arranged in well-demarcated sheets, rarely with a focal nested/whirling pattern, fascicular areas, and perivascular cuffs. Subtle variations of cell arrangement were noted in some cases within a single lesion. In cases, where focal stromal edema was prominent, the cells were arranged in a more dyscohesive fashion (Figs. 1B, 2–4). In 5 cases, the predominant epithelioid cell component consisted of rather small cells, whereas spindled cells dominated in 3 cases (Fig. 5). Of these, 2 lesions were composed of pale eosinophilic to clear cells, occasioning a resemblance to PEComa or leiomyoma (Fig. 6). The stroma was usually scant, focally myxoid, or sclerotic. In 7 cases, a vascular component was conspicuous. Admixed with the neoplastic cells were occasional lymphocytes, plasma cells, and, rarely,

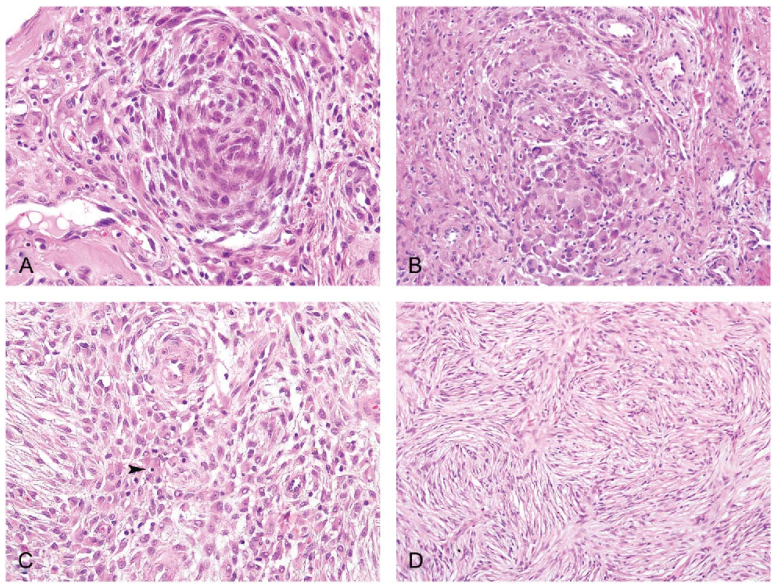

FIGURE 4. Pattern variation in EFH. A nest with vague whorling of the neoplastic cells with some spindling (A) and a more sharply circumscribed nodule composed of large round epithelioid cells (B). Both areas (A, B) are from the same lesion (case 10). Solid and vague storiform patterns with slender spindled cells occurring in the same lesion (case 8) (C, D). Note intracytoplasmic lymphocyte (emperipolesis, C, arrowhead).

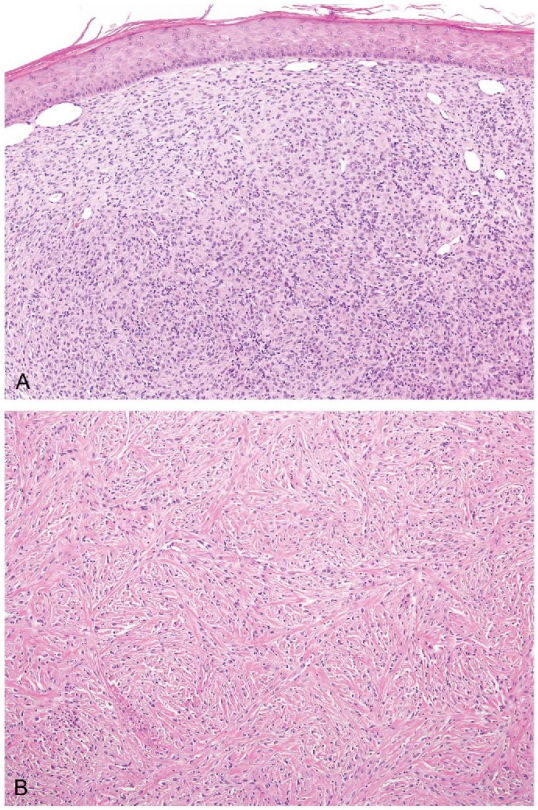

FIGURE 5. EFH composed predominantly of small epithelioid (A) (case 1) and small, spindled cells on a fibrous background (B) (case 9).

neutrophils. In 3 cases, single intracytoplasmic lymphocytes were identified, a feature consistent with emperipolesis (Fig. 4C).

Immunohistochemical Findings

ALK was positive in all 14 cases, whereas TFE-3 was positive in 11 lesions (>50% of cells). In the 3 cases labeled as negative for TFE-3, only focal nuclear positivity was noted.

FISH Findings

A break apart test for *ALK* was positive in 11 cases, whereas specimens from the remaining 3 cases were not analyzable (Table 1). Of the 11 positive cases, 10 manifested the classical break apart pattern, whereas one case (case 1) showed a FISH positive pattern with deletion of the 5′-*ALK* probe that hybridizes centromerically of the breakpoint (Fig. 7). *TFE-3* rearrangements were not found in none of the 11 analyzable cases.

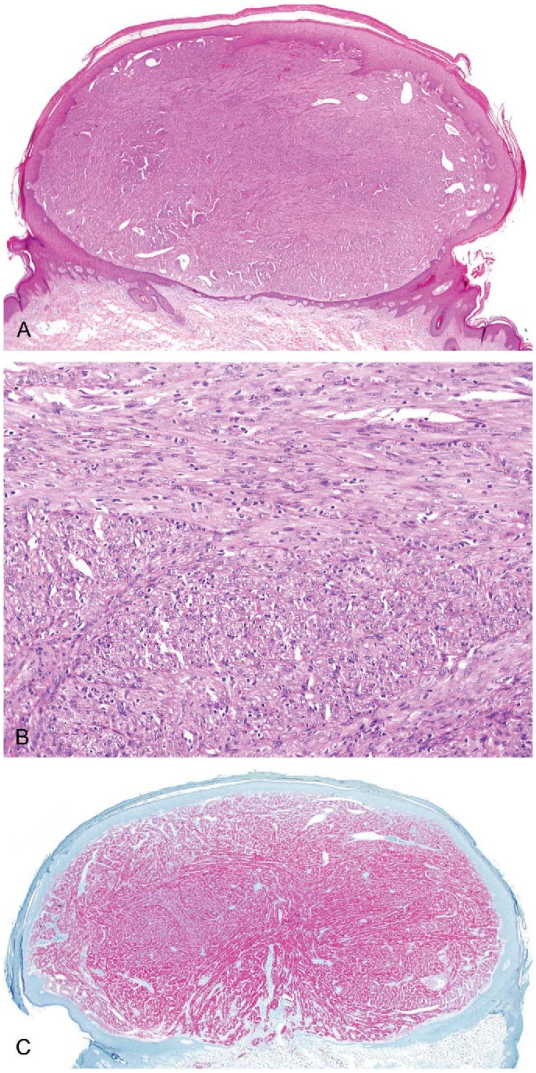

FIGURE 6. This example (case 13) manifests a typical polypoid architecture (A) but is composed of densely packed pale to clear spindled cells arranged in fascicles resembling a leiomyoma (B). ALK staining (C).

ALK Gene Fusions

Genes fusions were found in all 11 analyzable samples and included *SQSTM1-ALK* (n = 3), *VCL-ALK* (n = 3), *TMP3-ALK* (n = 2), *PRKAR2A-ALK* (n = 1), *MLPH-ALK* (n = 1), and *EML4-ALK* (n = 1) (Fig. 8, Tables 1 and 2).

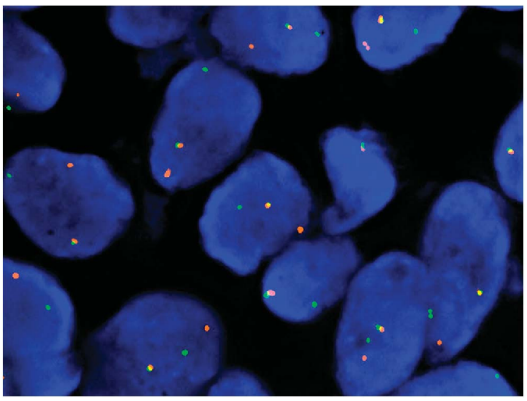

FIGURE 7. FISH analysis of the *ALK* locus using Vysis ALK break apart probe. Nuclei with 1 normal yellow fusion and separated 1 orange and 1 green signal pattern indicates the rearrangement (break) of 1 copy in the *ALK* gene region.

TABLE 2. Details of Next-Generation Sequencing Analysis

Case	Fusions	Exons	Reads	%	Start Sites
1	*SQSTM1-ALK*	5–20	1389	88	155
2	*SQSTM1-ALK*	5–20	672	93.2	138
3	*VCL-ALK*	16–20	2959	43.4	205
4	*TPM3-ALK*	6–20	1200	69.2	202
5	*VCL-ALK*	16–20	102	83.6	50
6	*VCL-ALK*	16–20	41	75.9	9
7	*SQSTM1-ALK*	5–20	21	53.9	6
8	NA				
9	*PRKAR2A-ALK*	2–20	112	100	25
10	NA	NA	NA	NA	NA
11	*MLPH-ALK*	11–20	277	58.9	54
12	*TMP3-ALK*	6–20	17	94.4	7
13	*EML4-ALK*	2–20	80	88.9	33
14	NA				

%, percentage of the reads supporting the fusion; exons, number of exons involved in the fusion, respectively; NA, not analyzable; reads, number of reads supporting the fusion; start sites, number of unique start sites of reads supporting the fusion.

DISCUSSION

Our study confirms the finding of Doyle et al[9] that all ALK-immunopositive cases manifest *ALK* gene rearrangements as detected by FISH. Also, in all analyzable cases, we detected *ALK* gene fusions. Six fusion types were identified, including 2 previously reported by Jedrych et al and 4 being novel fusions in EFH. Table 3 summarizes the main characteristics of the involved genes, proteins encoded by these genes, and their role and conditions in which these gene fusions or gene mutations have previously been detected.[10–31]

Our study revealed no correlation between the histopathological features and a particular fusion type, but we have found some hitherto unreported microscopic features in EFH. Two lesions were composed of closely packed, plexiform, or fascicular proliferations of pale to clear spindled cells and thus resembled PEComa or leiomyoma. The typical epithelioid cell component was absent and in both cases, the original diagnosis of EFH was rendered as an "exclusion" diagnosis after a broad spectrum of antibodies had been performed to exclude possible tumors of other lineages. We consider these lesions EFH, as we have noted similar cytological features, albeit never prominent, in more conventional EFH. ALK positivity and *ALK* gene fusion support the classification of these lesions as EFH. Both cases were more cellular and in this respect resemble those reported by Glusac et al as the cellular variant of EFH.[6] Thus, PEComa and leiomyoma can be added to the list of the differential diagnosis of EFH, which at present also include perineurioma,

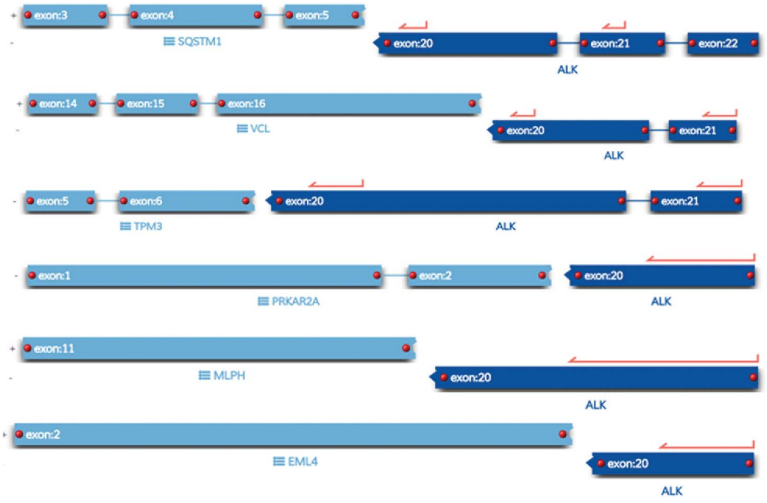

FIGURE 8. Schematic visualization of the detected fusion transcripts: (1) *SQSTM1-ALK*, (2) *VCL-ALK*, (3) *TPM3-ALK*, (4) *PRKAR2A-ALK*, (5) *MLPH-ALK*, and (6) *EML4-ALK*. In all cases, a 5′ fusion partner is joined with exons 20–29 of *ALK* containing the tyrosine kinase domain.

TABLE 3. Brief Overview of Location of the Involved Genes, Encoded Proteins, Their Function, and Roles and Conditions Associated With Fusions and Gene Mutations

Gene	Location/Type	Protein Function	Role	Conditions with Gene Fusions and Mutations Tumors/Diseases
VCL; Vinculin	10q22/protein coding	A cytoskeletal protein (vinculin) is associated with cell–cell and cell–matrix junctions, functioning as one of several interacting proteins involved in anchoring F-actin to the membrane	Regulates cell adhesion and migration; links extracellular matrix to the actomyosin cytoskeleton	*VCL-ALK*: renal cell carcinoma, EFH; *VCL* mutations: dilated cardiomyopathy
SQSTM1; Sequestosome	5q35/protein coding	A multifunctional protein that binds ubiquitin and regulates activation of the nuclear factor kappa-B (NF-κB) signaling pathway, functioning as a scaffolding/adaptor protein in concert with TNF receptor-associated factor 6 to mediate activation of NF-κB in response to upstream signals	Participate in processes of autophagy, cell signalling and differentiation	*SQSTM1-ALK*: diffuse large B-cell lymphoma, EFH; *SQSTM1* mutations: sporadic and familial Paget disease of bone
TPM3; Tropomyosin 3	1q21.3/protein coding	Tropomyosin family of actin-binding proteins are dimers of coiled-coil proteins that provide stability to actin filaments	Regulates access of other actin-binding proteins	*TPM3-ALK*: inflammatory myofibroblastic tumor, TFE3-positive renal cell carcinoma, spitzoid melanocytic leisons; gene mutations: nemaline myopathy and other muscle disorders
PRKAR2A; Protein kinase cAMP-dependent type II regulatory subunit alpha	3p21.31/protein coding	cAMP activates the cAMP-dependent protein kinase, which transduces the signal through phosphorylation of different target proteins. The protein encoded by this gene is one of the regulatory subunits of the inactive kinase holoenzyme	Participates in a variety of cellular functions, including regulation of protein transport from endosomes to the Golgi apparatus and further to the endoplasmic reticulum	*PRKAR2A-ALK*: not reported
MLPH; Melanophilin	2q37.3/protein coding	A member of the exophilin subfamily of Rab effector proteins that forms a ternary complex with the small Ras-related GTPase Rab27A in its GTP-bound form and the motor protein myosin Va	Ties melanosomes to the actin cytoskeleton in melanocytes	*MLPH-ALK*: not reported; *MLPH* mutations: Griscelli syndrome type 3
EML4; Echinoderm microtubule-associated protein like 4	2p21/protein coding	Echinoderm microtubule-associated protein (EMAP)-like (EML) family proteins are microtubule-associated proteins that have a conserved hydrophobic EMAP-like protein (HELP) domain and multiple WD40 domains	May be involved in microtubule formation; participates in mitotic spindle organization and for microtubule-kinetochore attachment	*EML4-ALK*: nonsmall cell lung carcinomas, esophageal carcinoma, breast and colorectal carcinomas, epithelioid inflammatory myofibroblastic sarcoma, large-cell neuroendocrine carcinoma

melanocytic tumors and other entities as discussed in details elsewhere.[1–3,32]

We also found some minor novel cytological variations, including cells with multilobulated nuclei, nuclear grooves, and mucinous cells. The latter appear similar to the elements described and depicted by Singh et al as foamy cells. In a subset of cases, we identified cells with intranuclear pseudoinclusions and eccentric nuclei. Although these cells were never emphasized on in the previously published material, they can be found in several illustrations (Figs. 2, 3 in Ref. 6; Fig. 4 in Ref. 2). In 3 cases, occasional areas with emperiopolesis of single lymphocytes were noted, which is another hitherto unreported feature in EFH. With respect to the skin, emperipolesis is a typical finding in Rosai-Dorfman

disease, granulomatous slack skin, and myxoinflammatory fibroblastic sarcoma.[33,34] In the latter, it can be very conspicuous with numerous engulfed cells easily recognizable at first glance or discrete, requiring a meticulous search.[35] Cyclin D1 has been shown to be useful for identification of cells with such a discrete single cell emperiopolesis by leaving the engulfed intracytoplasmic cells unstained.[36] We stained 3 cases of EFH with Cyclin D1 and observed a similar feature in one case with positive immunostaining.

A remarkable feature was TFE-3 immunopositivity of EFH in a majority of cases. TFE-3 positive mesenchymal tumors include epithelioid hemangioma, visceral PEComa alveolar soft part sarcoma, to name but a few.[37–39] The significance of this feature in EFH is unclear but, given frequent immunopositivity, this marker can additionally be used in the diagnosis of this neoplasm. Parenthetically, while selecting cases for inclusion, we observed more lesions with a TFE-3 +/ALK-phenotype compared with TFE-3+/ALK+ lesions. Despite frequent TFE-3 imunopositivity, the molecular analysis by FISH with *TFE3* break apart probe and by ArcherDX next-generation sequencing detecting all possible *TFE3* transcript partners, revealed neither gene alterations nor fusion transcripts. The most probable explanation of TFE-3 immunopositivity, if we exclude false positivity, is the activation of some upstream gene(s). Of note, concurrent *ALK* and *TFE-3* rearrangements are seen in some renal cell carcinoma, and remarkably these neoplasms are characterized by an epithelioid cell morphology.[13,31]

In conclusion, ALK-positive EFH shows frequently *ALK* gene fusions that involve various protein-coding genes, implicated in a variety of biological processes. Rare variants of EFH rather consist of spindled "non-epithelioid" cells, thus occasioning a resemblance to PEComa or leiomyoma. Inclusion of such lesions into the spectrum of EFH must be validated by further observations. TFE-3 is expressed in a majority of ALK-positive EFH; however, *TFE-3* rearrangement is not a feature.

REFERENCES

1. Jones EW, Cerio R, Smith NP. Epithelioid cell histiocytoma: a new entity. *Br J Dermatol*. 1989;120:185–195.
2. Singh Gomez C, Calonje E, Fletcher CD. Epithelioid benign fibrous histiocytoma of skin: clinico-pathological analysis of 20 cases of a poorly known variant. *Histopathology*. 1994;24:123–129.
3. Doyle LA, Fletcher CD. EMA positivity in epithelioid fibrous histiocytoma: a potential diagnostic pitfall. *J Cutan Pathol*. 2011;38:697–703.
4. Mehregan AH, Mehregan DR, Broecker A. Epithelioid cell histiocytoma. A clinicopathologic and immunohistochemical study of eight cases. *J Am Acad Dermatol*. 1992;26:243–246.
5. Glusac EJ, McNiff JM. Epithelioid cell histiocytoma: a simulant of vascular and melanocytic neoplasms. *Am J Dermatopathol*. 1999;21:1–7.
6. Glusac EJ, Barr RJ, Everett MA, et al. Epithelioid cell histiocytoma. A report of 10 cases including a new cellular variant. *Am J Surg Pathol*. 1994;18:583–590.
7. Walther C, Hofvander J, Nilsson J, et al. Gene fusion detection in formalin-fixed paraffin-embedded benign fibrous histiocytomas using fluorescence in situ hybridization and RNA sequencing. *Lab Invest*. 2015;95:1071–1076.
8. Creytens D, Ferdinande L, Van Dorpe J. ALK rearrangement and overexpression in an unusual cutaneous epithelioid tumor with a peculiar whorled "perineurioma-like" growth pattern: epithelioid fibrous histiocytoma. *Appl Immunohistochem Mol Morphol*. 2017;25:e46–e48.
9. Doyle LA, Marino-Enriquez A, Fletcher CD, et al. ALK rearrangement and overexpression in epithelioid fibrous histiocytoma. *Mod Pathol*. 2015;28:904–912.
10. Jedrych J, Nikiforova M, Kennedy TF, et al. Epithelioid cell histiocytoma of the skin with clonal ALK gene rearrangement resulting in VCL-ALK and SQSTM1-ALK gene fusions. *Br J Dermatol*. 2015;172:1427–1429.
11. Debelenko LV, Raimondi SC, Daw N, et al. Renal cell carcinoma with novel VCL-ALK fusion: new representative of ALK-associated tumor spectrum. *Mod Pathol*. 2011;24:430–442.
12. Zhang H, Erickson-Johnson M, Wang X, et al. Malignant high-grade histological transformation of inflammatory myofibroblastic tumour associated with amplification of TPM3-ALK. *J Clin Pathol*. 2010;63:1040–1041.
13. Thorner PS, Shago M, Marrano P, et al. TFE3-positive renal cell carcinomas are not always Xp11 translocation carcinomas: report of a case with a TPM3-ALK translocation. *Pathol Res Pract*. 2016;212:937–942.
14. Takeuchi K, Soda M, Togashi Y, et al. Identification of a novel fusion, SQSTM1-ALK, in ALK-positive large B-cell lymphoma. *Haematologica*. 2011;96:464–467.
15. d'Amore ES, Visco C, Menin A, et al. STAT3 pathway is activated in ALK-positive large B-cell lymphoma carrying SQSTM1-ALK rearrangement and provides a possible therapeutic target. *Am J Surg Pathol*. 2013;37:780–786.
16. Ali SM, Hensing T, Schrock AB, et al. Comprehensive genomic profiling identifies a subset of crizotinib-responsive ALK-rearranged non-small cell lung cancer not detected by fluorescence in situ hybridization. *Oncologist*. 2016;21:762–770.
17. Lin E, Li L, Guan Y, et al. Exon array profiling detects EML4-ALK fusion in breast, colorectal, and non-small cell lung cancers. *Mol Cancer Res*. 2009;7:1466–1476.
18. Jiang Q, Tong HX, Hou YY, et al. Identification of EML4-ALK as an alternative fusion gene in epithelioid inflammatory myofibroblastic sarcoma. *Orphanet J Rare Dis*. 2017;12:97.
19. Xia N, An J, Jiang QQ, et al. Analysis of EGFR, EML4-ALK, KRAS, and c-MET mutations in Chinese lung adenocarcinoma patients. *Exp Lung Res*. 2013;39:328–335.
20. Sokai A, Enaka M, Sokai R, et al. Pulmonary inflammatory myofibroblastic tumor harboring EML4-ALK fusion gene. *Jpn J Clin Oncol*. 2014;44:93–96.
21. Lawrence B, Perez-Atayde A, Hibbard MK, et al. TPM3-ALK and TPM4-ALK oncogenes in inflammatory myofibroblastic tumors. *Am J Pathol*. 2000;157:377–384.
22. van de Krogt JA, Vanden Bempt M, Finalet Ferreiro J, et al. ALK-positive anaplastic large cell lymphoma with the variant RNF213-, ATIC- and TPM3-ALK fusions is characterized by copy number gain of the rearranged ALK gene. *Haematologica*. 2017;102:1605–1616.
23. Cools J, Wlodarska I, Somers R, et al. Identification of novel fusion partners of ALK, the anaplastic lymphoma kinase, in anaplastic large-cell lymphoma and inflammatory myofibroblastic tumor. *Genes Chromosomes Cancer*. 2002;34:354–362.
24. Bayliss R, Choi J, Fennell DA, et al. Molecular mechanisms that underpin EML4-ALK driven cancers and their response to targeted drugs. *Cell Mol Life Sci*. 2016;73:1209–1224.
25. Woo CG, Seo S, Kim SW, et al. Differential protein stability and clinical responses of EML4-ALK fusion variants to various ALK inhibitors in advanced ALK-rearranged non-small cell lung cancer. *Ann Oncol*. 2017;28:791–797.
26. Soda M, Choi YL, Enomoto M, et al. Identification of the transforming EML4-ALK fusion gene in non-small-cell lung cancer. *Nature*. 2007;448:561–566.
27. Choi YL, Takeuchi K, Soda M, et al. Identification of novel isoforms of the EML4-ALK transforming gene in non-small cell lung cancer. *Cancer Res*. 2008;68:4971–4976.
28. Busam KJ, Kutzner H, Cerroni L, et al. Clinical and pathologic findings of Spitz nevi and atypical Spitz tumors with ALK fusions. *Am J Surg Pathol*. 2014;38:925–933.
29. Wiesner T, He J, Yelensky R, et al. Kinase fusions are frequent in Spitz tumours and spitzoid melanomas. *Nat Commun*. 2014;5:3116.
30. Omachi N, Shimizu S, Kawaguchi T, et al. A case of large-cell neuroendocrine carcinoma harboring an EML4-ALK rearrangement with resistance to the ALK inhibitor crizotinib. *J Thorac Oncol*. 2014;9:e40–e42.

31. Cajaiba MM, Jennings LJ, Rohan SM, et al. ALK-rearranged renal cell carcinomas in children. *Genes Chromosomes Cancer*. 2016;55:442–451.
32. Busam KJ, Granter SR, Iversen K, et al. Immunohistochemical distinction of epithelioid histiocytic proliferations from epithelioid melanocytic nevi. *Am J Dermatopathol*. 2000;22:237–241.
33. Rosai J, Dorfman RF. Sinus histiocytosis with massive lymphadenopathy: a pseudolymphomatous benign disorder. Analysis of 34 cases. *Cancer*. 1972;30:1174–1188.
34. Belousova IE, Nikonova SM, Sima R, et al. Granulomatous slack skin with clonal T-cell receptor-gamma gene rearrangement in skin and lymph node. *Br J Dermatol*. 2007;157:405–407.
35. Kinkor Z, Mukensnabl P, Michal M. Inflammatory myxohyaline tumor with massive emperipolesis. *Pathol Res Pract*. 2002;198:639–642.
36. Michal M, Kazakov DV, Hadravsky L, et al. High-grade myxoinflammatory fibroblastic sarcoma: a report of 23 cases. *Ann Diagn Pathol*. 2015;19:157–163.
37. Flucke U, Vogels RJ, de Saint Aubain Somerhausen N, et al. Epithelioid Hemangioendothelioma: clinicopathologic, immunhistochemical, and molecular genetic analysis of 39 cases. *Diagn Pathol*. 2014;9:131.
38. Llamas-Velasco M, Mentzel T, Requena L, et al. Cutaneous PEComa does not harbour TFE3 gene fusions: immunohistochemical and molecular study of 17 cases. *Histopathology*. 2013;63:122–129.
39. Kacerovska D, Michal M, Nemcova J, et al. Crystal-deficient alveolar soft-part sarcoma with cutaneous involvement: a case report. *Am J Dermatopathol*. 2009;31:272–277.

2.2. HEAD AND NECK

2.2.1. ANGIOLEIOMYOMA OF THE SINONASAL TRACT: ANALYSIS OF 16 CASES AND REVIEW OF THE LITERATURE

The purpose of this manuscript was to analyze the clinicopathological features of sinonasal angioleiomyoma, a rare mesenchymal tumor which even more rarely occurs in this anatomic location. Altogether we analyzed 16 cases from our files using light microscopy and immunohistochemistry.

Histologically, all lesions were well circumscribed but non-encapsulated and most (12/16) were of the compact solid type superficially mimicking conventional leiomyoma but contained numerous compressed muscular veins. The remainder were of venous (2) and cavernous (2) type. Variable amounts of mature fat were observed in four cases (25 %). Atypia, necrosis, and mitotic activity were absent. Immunohistochemistry showed consistent expression of smooth muscle actin (12/12), h-caldesmon (9/9), muscle-specific actin (4/4), variable expression of desmin (11/14) and CD56 (4/6), and absence of HMB45 expression (0/11). The covering mucosa was ulcerated in 6 cases and showed squamous metaplasia in one case. There were no recurrences after local excision. Submucosal sinonasal ALMs are rare benign tumors similar to their reported cutaneous counterparts with frequent adipocytic differentiation. They should be distinguished from renal-type angiomyolipoma. Simple excision is curative.

Head and Neck Pathol (2015) 9:463–473
DOI 10.1007/s12105-015-0636-y

ORIGINAL PAPER

Angioleiomyoma of the Sinonasal Tract: Analysis of 16 Cases and Review of the Literature

Abbas Agaimy[1] · Michael Michal[2] · Lester D. R. Thompson[3] · Michal Michal[2]

Received: 7 April 2015 / Accepted: 30 May 2015 / Published online: 6 June 2015

Abstract Angioleiomyoma (ALM; synonyms: angiomyoma, vascular leiomyoma) is an uncommon benign tumor of skin and subcutaneous tissue. Most arise in the extremities (90 %). Head and neck ALMs are uncommon (~10 % of all ALMs) and those arising beneath the sinonasal tract mucosa are very rare (<1 %) with 38 cases reported so far. We herein analyzed 16 cases identified from our routine and consultation files. Patients included seven females and nine males aged 25–82 years (mean 58; median 62). Symptoms were intermittent nasal obstruction, sinusitis, recurrent epistaxis, and a slow-growing mass. Fifteen lesions originated within different regions of the nasal cavity and one lesion was detected incidentally in an ethmoid sinus sample. Size range was 6–25 mm (mean 11). Histologically, all lesions were well circumscribed but non-encapsulated and most (12/16) were of the compact solid type superficially mimicking conventional leiomyoma but contained numerous compressed muscular veins. The remainder were of venous (2) and cavernous (2) type. Variable amounts of mature fat were observed in four cases (25 %). Atypia, necrosis, and mitotic activity were absent. Immunohistochemistry showed consistent expression of smooth muscle actin (12/12), h-caldesmon (9/9), muscle-specific actin (4/4), variable expression of desmin (11/14) and CD56 (4/6), and absence of HMB45 expression (0/11). The covering mucosa was ulcerated in 6 cases and showed squamous metaplasia in one case. There were no recurrences after local excision. Submucosal sinonasal ALMs are rare benign tumors similar to their reported cutaneous counterparts with frequent adipocytic differentiation. They should be distinguished from renal-type angiomyolipoma. Simple excision is curative.

Keywords Angioleiomyoma · Sinonasal tract · Angiomyolipoma · Vascular leiomyoma · Angiomyoma · PEComa · Nasal

✉ Abbas Agaimy
abbas.agaimy@uk-erlangen.de

[1] Pathologisches Institut, Universitätsklinikum Erlangen, Krankenhausstrasse 8-10, 91054 Erlangen, Germany

[2] Sikl's Department of Pathology, Faculty of Medicine, Charles University, Pilsen, Czech Republic

[3] Department of Pathology, Woodland Hills Medical Center, 5601 De Soto Avenue, Woodland Hills, CA 91367, USA

Introduction

Mesenchymal tumors of the sinonasal tract are rare. They encompass benign tumors (benign peripheral nerve sheath tumors, angioleiomyoma and hemangiomas), lesions of low-grade or uncertain biological potential (sinonasal hemangio/glomangiopericytoma, solitary fibrous tumor, desmoid fibromatosis, low-grade malignant peripheral nerve sheath tumors and low-grade sinonasal sarcoma with neural and myogenic features) and frankly malignant aggressive neoplasms (conventional malignant peripheral nerve sheath tumors, leiomyosarcoma, rhabdomyosarcoma and other rare sarcoma types) [1–5]. Due to the rarity of sinonasal mesenchymal neoplasms, many pathologists are not familiar with their broad phenotypic spectrum.

Angioleiomyoma (ALM; synonyms: angiomyoma, vascular leiomyoma) is an uncommon benign tumor of skin and subcutaneous tissue composed of well differentiated smooth muscle proliferations associated with variable but usually prominent vascular component [6]. The latter may consist of thick-walled collapsed vascular channels (solid type), predominant thick-walled venous vessels with well

recognizable lumens within smooth muscle background (venous type), or display ectatic muscular venous channels mimicking venous hemangioma but with variable smooth muscle component in-between (cavernous type) [6]. The majority of lesions originate in the extremities (~90 %), mainly in the lower limbs while ALM of the head and neck region is uncommon (~10 %) [7, 8]. Submucosal ALMs of the sinonasal tract are exceptionally rare. To date, 38 cases have been reported, mostly as single case reports [9–41] (Table 1). In this study, we describe our experience with submucosal ALMs of sinonasal tract and discuss their clinicopathological and immunohistochemical characteristics in light of previously reported cases with special emphasis on the frequent presence of adipocytic differentiation and similarities and differences compared to their cutaneous and soft tissue counterparts.

Materials and Methods

We reviewed our routine and consultation files for lesions coded as angioleiomyoma, angiomyoma, angiomyolipoma and vascular leiomyoma originating in the nose, nasal cavity, or paranasal sinuses. Diagnosis was based on criteria defined for similar lesions in the most recent World Health organization (WHO) classification of tumors of the head and neck and tumors of soft tissue and bone [1, 6]. After review, only tumors arising from the mucosa-lined sinonasal sites (excluding cutaneous lesions) were included in this series. The tumor specimens were fixed in buffered formalin and embedded routinely for light microscopic examination. Immunohistochemical studies were performed on 3–4-μm sections cut from paraffin blocks using a fully automated system ("Benchmark XT System", Ventana Medical Systems Inc, Tucson, Arizona, USA) using the following antibodies: α-smooth muscle actin (clone 1A4, 1:200, Dako), h-caldesmon (clone h-CD, 1:100, Dako), desmin (clone D33, 1:250, Dako), CD34 (clone QBEnd10, 1:200, Immunotech), CD56 (clone MRQ-42, 1:100, CELL MARQUE), HMB45 (clone HMB45, 1:50, Loxo), and podoplanin (clone D2-40, 1:50, Zytomed).

Results

Clinical Features

Sixteen cases were retrieved from our files (Table 1, Cases 39–54). Patients included seven females and nine males aged 25–82 years (mean 58; median 62). Variable combinations of intermittent nasal obstruction, chronic sinusitis-like symptoms and recurrent epistaxis were the presenting symptoms in eight patients with detailed data, respectively. A painful mass was stated in one case. Other cases either lacked detailed history or a slowly growing mass or nodule was the presenting symptom of the disease. The site was stated within different compartments of the nasal cavity (five in turbinates, four in the nasal cavity unspecified, three from the nasal septum, two in the nasal orifices, and one in the lateral nasal wall). One case (the only sinus-based lesion) was found incidentally in a polyposis specimen from the ethmoid sinus. None of the lesions was multifocal or involved more than one subregion of the sinonasal tract. There was no evidence of associated diseases or similar tumors elsewhere in the body. All lesions were removed via simple complete local excision with free albeit close margins.

At last follow-up (range 9–211 months; mean 58 months), no recurrences were recorded.

Pathological Findings

Tumor size ranged from 6 to 25 mm (mean 11) in cases with gross description or as measured from glass slides. Grossly, the lesions were described as tan-whitish with solid whorled cut-surface and firm consistency. Histologically, all lesions were non-encapsulated but well circumscribed (Fig. 1a, b). The tumors were covered by sinonasal mucosa with variable reactive or metaplastic changes (Fig. 1c). Six tumors showed mucosal ulceration/erosion with variable inflammation between the tumor and mucosal surface associated with variable degree of fibromyxoid vascular obliteration (Fig. 1d). The tumors were composed of well differentiated smooth muscle cells having elongated vesicular blunt-ended nuclei with inconspicuous nucleoli and brightly eosinophilic fibrillary cytoplasm without atypia. The cells were arranged in intersecting bundles and whorls encasing or surrounding numerous vascular channels. The smooth musculature of the vessel walls seemed to merge gradually and imperceptibly with the surrounding smooth muscle bundles. There was no cellular pleomorphism and mitotic figures were absent. Twelve of 16 cases showed compact arrangement of the smooth muscle occasionally mimicking leiomyoma but careful assessment revealed the characteristic thick-walled collapsed vascular channels (solid type) (Fig. 2a). Two lesions showed convolutes of thick-walled venous channels closely mimicking venous hemangioma (venous type) (Fig. 2b). Another two cases showed prominent dilated venous vessels within the smooth muscle proliferation corresponding to the cavernous type (Fig. 2c). A variable but generally prominent adipocytic component was appreciated in four cases (25 %). Mature macrovesicular adipocytes were scattered either singly or forming small aggregates and lobules within the lesions. The fatty

Table 1 Clinicopathological features of previously reported sinonasal angioleiomyomas including current series (n = 54)

No.	Author	Age/gender	Site, size cm	Symptoms, duration	Histological pattern	IHC positive markers	IHC negative markers	Associated mucosal changes	Follow up (months)
1	Maesaka et al. [9]	49 F	Vestibule	Facial pain	Vascular	ND	ND	NS	NR
2	Ram [10]	40 M	Right inferior turbinate, 2.5 cm	Nasal obstruction, few mo.	Solid (reported as fibromyoma)	ND	ND	NS	NA
3	Wolfowitz et al. [11]	42 F	Inferior turbinate, 1 cm	Recurrent epistaxis	Vascular leiomyoma	ND	ND	Ulceration	NR (30 mo.)
4	Schwartzman et al. [12]	57 M	Sinuses	Obstruction, headache	Vascular	ND	ND	NS	NR (36 mo.)
5	McCafferey et al. [13]	76 F	Inferior turbinate, 0.5 cm	Epistaxis	Vascular	ND	ND	NS	NA
6	Dawlatly et al. [14]	52 M	Right vestibule, 4 cm	Epistaxis, obstruction, 1 year	Solid with fat	ND	ND	None	NR (12 mo.)
7	Hanna et al. [15]	64 F	Inferior turbinate, 3 cm	Epistaxis, obstruction, pain, 3 wks	Solid, no fat	ND	ND	None	NR (12 mo.)
8	Sawada [16]	41 M	Right nasal cavity/ orifice	Mass, slowly growing for years	Solid with fat	ND	ND	Erythema	NR (12 mo.)
9	Ragbeer et al. [17]	49 F	Right nasal floor, 1.5 cm	Epistaxis, pain, suppuration	Solid with fat	Desmin, MSA, vimentin	S100	None	NR (12 mo.)
10	Harcourt et al. [18]	55 F	Right ethmoid sinus, 2 cm	Right epiphora, 10 years	Venous, no fat	ND	ND	ND	NR
11	Khan et al. [19]	71 F	Left inferior turbinate, 4 cm	Obstruction, 2 years	Solid with fat	NS	NS	NS	NR (12 mo.)
12	Gatalica et al. [20]	64 M	Right vestibule, 2 cm	Obstruction, >1 year	Solid with dominant fat	Muscle-specific actin, vimentin	HMB45, desmin	NS	NA
13	Ardekian et al. [21]	54 F	Left nasal vestibule and septum, 2 cm	Obstruction, pain and bloody discharge	Solid, no fat	NS	NS	Inflammation	NA
14	Nall et al. [22]	43 F	Superior turbinate	Epistaxis, obstruction, facial pain, months	Venous	αSMA	NS	No	NR (21 mo.)
15	Murono et al. [23]	69 F	Right inferior turbinate, 2 cm	Epistaxis, 1 year	Solid with fat	Vimentin, αSMA	NS	No	NA
16	Watanabe et al. [24]	66 M	Right nasal cavity, 2 cm	Mass, after chemotherapy for Hodgkin lymphoma	Solid with fat	αSMA, MSA, focally desmin	S100, HMB45	No	NR (24 mo.)
17	Watanabe et al. [24]	88 F	Vestibule, 2 cm	Mass	Solid with fat	αSMA, MSA, focally desmin	S100, HMB45	No	NR (6 mo.)
18	Marioni et al. [25]	70 F	Right vestibule, 1.5 cm	Obstruction and epistaxis	Solid-venous, no fat	αSMA, PR	ER	No	NR (3 mo.)
19	Tardio et al. [26]	45 M	Right nasal cavity, 1.5 cm	Epistaxis and obstruction, 2 mo.	Solid with fat	αSMA, desmin, MSA	HMB45	No	NR (1 mo.)

Table 1 continued

No.	Author	Age/gender	Site, size cm	Symptoms, duration	Histological pattern	IHC positive markers	IHC negative markers	Associated mucosal changes	Follow up (months)
20	Wang et al. [27]	70 M	Septum, 1.1 cm	Epistaxis	Solid, no fat	SMA	NS	NS	NR
21	Wang et al. [27]	66 F	Inferior turbinate, 0.3 cm	Asymptomatic mass	Venous, with fat	αSMA	NS	NS	NR
22	Bel Hag Salah et al. [28]	50 F	Right middle turbinate	Nasal obstruction + rhinorrhea, 5 mo.	Solid, no fat	αSMA, h-caldesmon	NS	NS	NA
23	Erkilic et al. [29]	52 M	Left nasal cavity, 3.5 cm	Snoring and obstruction, 20 years	Solid with fat	αSMA	S100, HMB45	NS	NA
24	Chen et al. [30]	88 M	Right inferior turbinate, 1.3 cm	Discharge, hearing impairment	Solid with fat	αSMA, desmin	ER, PR, CD34, EBV ISH	Inflammation	NR (12 mo.)
25	Meher et al. [31]	24 F	Right middle turbinate, 2 cm	Epistaxis, 2 mo.	Solid-venous, no fat	NS	NS	NS	NR
26	Campelo et al. [32]	44 F	Left turbinate	Recurrent epistaxis (4 years), obstruction (1 year), itching	Solid, no fat	NS	NS	NS	NR (10 mo.)
27	Vafiadis et al. [33]	68 M	Right nasal vestibule, 2 cm	Nasal obstruction, >6 years	Solid, no fat glands entrapped	NS	NS	No	NR (24 mo.)
28	Singh et al. [34]	31 M	Right nasal cavity septum, 3.2 cm	Nasal obstruction + intermittent epistaxis, 3 years	Solid, no fat	NS	NS	Surface ulceration	NR (18 mo.)
29	Michael et al. [35]	34 M	Left nasal cavity inferior turbinate	Nasal obstruction + intermittent epistaxis, 10 years	Venous	αSMA, desmin	NS	NS	NA
30	He et al. [36]	58 M	Right inferior turbinate, 2 cm	Recurrent epistaxis and obstruction, 10 years	Solid with fat	PR (20–30 %)	ER, HMB45, EBV	Erosion and inflammation	NR (12 mo.)
31	Navarro et al. [37]	62 F	Left septum, 4 cm	Epistaxis, obstruction, pain, mass, 6 years	Solid, no fat	NS	NS	NS	NA
32	Moreira et al. [38]	54 M	Left inferior meatus	Recurrent epistaxis, 20 years	Solid with fat	NS	HMB45	NS	NR
33	Purohit et al. [39]	45 M	Septum	Nasal obstruction, 3 years	Solid, no fat	NS	NS	No	NA
34	Yoon et al. [40]	64 M	Inferior turbinate, 0.8 cm	Mass	Solid	Actin+	NS	NS	NR
35	Yoon et al. [40]	65 M	Nasal mucosa, 1 cm	Mass	Solid	Actin+	NS	NS	NR
36	Yoon et al. [40]	37 M	Nasal septum, 1 cm	Epistaxis	Cavernous	Actin+	NS	NS	NR
37	Yoon et al. [40]	71 F	Nasal septum, 2 cm	Nasal obstruction	Cavernous	ND	NS	NS	NR

Table 1 continued

No.	Author	Age/gender	Site, size cm	Symptoms, duration	Histological pattern	IHC positive markers	IHC negative markers	Associated mucosal changes	Follow up (months)
38	Tseng et al. [41]	48 F	Right inferior turbinate, 1 cm	Recurrent mucous + bloody discharge, 3 mo.	Solid, no fat	αSMA, PR	ER, S100	No	NR (48 mo.)
39	Current study	73 M	Right lateral nasal wall, 1.4 cm	Intermittent nasal obstruction, 10 years.	Solid with fat (<10 %)	Desmin, αSMA, h-caldesmon	HMB45	None	NR (52 mo.)
40	Current study	82 M	Lower left turbinate, 0.8 cm	Recurrent epistaxis for years	Solid with fat (<10 %)	αSMA, h-caldesmon	HMB45, desmin	Erosion with inflammation	NR (43 mo.)
41	Current study	53 M	Left nasal orifice, 0.8 cm	Mass	Venous, no fat	αSMA, h-CD, desmin ±, CD56±	AR, HMB45, D2-40	Erosion with inflammation	NR (34 mo.)
42	Current study	76 F	Right nasal orifice, 0.6 cm	Mass	Solid with fat (40 %)	Desmin, αSMA, h-caldesmon	HMB45, ER, PR, CD56	None	NR (32 mo)
43	Current study	63 M	Right septum, 0.7 cm	Tumor, pyogenic granuloma?	Cavernous with fat (<2 %)	Desmin, αSMA, h-caldesmon	HMB45, CD56, D2-40	None	NR (31 mo.)
44	Current study	25 F	Ethmoidal cells, 0.2 cm	Incidental, recurrent sinusitis	Venous, No fat	Desmin, αSMA, h-caldesmon	HMB45	None	NR (15 mo.)
45	Current study	77 F	Nasal cavity, 0.7 cm	Mass	Solid with fat (<10 %)	αSMA, h-caldesmon, CD56	Desmin, HMB45	Erosion with inflammation	NR (211 mo.)
46	Current study	62 F	Nasal cavity, 1.5 cm	Mass	Solid, no fat	αSMA, desmin F +, h-caldesmon, CD56	HMB45	Ulcerated with inflammation	NR (80 mo.)
47	Current study	48 F	Concha, 1.2 cm	Mass	Solid, no fat	αSMA, desmin, h-caldesmon, CD56	HMB45	Ulcerated with inflammation	NR (161 mo.)
48	Current study	26 M	Right inferior nasal cavity floor, 2.5 cm	Painful mass, increasing in size, 3 mo	Solid, no fat	αSMA, MSA, desmin	S100 protein, pan-cytokeratin, HMB45	None	NR (108 mo.)
49	Current study	55 M	Right septum, 1.0 cm	Multiple polyps, nasal congestion, sneezing, difficulty breathing, pan-sinusitis and anterior septum mass, 1.5 mo.	Solid, no fat	MSA	S100 protein	None	NR (53 mo.)
50	Current study	77 F	Right anterior turbinate, 0.9 cm	Epistaxis with friable mass, 9 mo.	Solid, no fat	Desmin	HMB45	None	NR (46 mo.)
51	Current study	51 F	Left nasal polyp, 1.7 cm	Ear pain, cough, foreign-body sensation, nasal obstruction and epistaxis, 8 mo.	Cavernous, no fat	αSMA, desmin	S100 protein, CD34, pan-cytokeratin	Surface ulceration (excoriation)	NR (26 mo.)
52	Current study	36 M	Right lateral nasal wall (turbinate), 1.7 cm	Mass at the nasal vestibule, showing recent growth, 8 mo.	Solid, no fat	αSMA, SMMHC	Desmin, S100 protein	None	NR (20 mo.)

Table 1 continued

No.	Author	Age/gender	Site, size cm	Symptoms, duration	Histological pattern	IHC positive markers	IHC negative markers	Associated mucosal changes	Follow up (months)
53	Current study	65 M	Right anterior nasal septum, 1.0 cm	Nasal congestion, with a past history of rhinoplasty and difficulty breathing and epistaxis, 20 mo.	Solid, no fat	MSA	none	Squamous metaplasia	NR (18 mo.)
54	Current study	66 M	Right inferior turbinate, 1.2 cm	Right nasal obstruction with epistaxis, 24 mo.	Solid, no fat	MSA, desmin	S100 protein, EBER	Squamous metaplasia	NR (9 mo.)

F female, *M* male, *MO* month, *MSA* muscle-specific actin, *NA* not available, *NR* no recurrence, *PR* progesterone receptor, *SMA* smooth muscle actin, *SMMHC* smooth muscle myosin heavy chain

component ranged from a few cells to 20 % of the lesion (Fig. 3d–h). There were no cytoplasmic vacuoles within the smooth muscle cells or other features suggestive of gradual transition from myogenic to fatty cells. The Elastica stain confirmed the venous nature of the vessels (Fig. 3a).

By immunohistochemistry, all cases tested showed strong expression of alpha smooth muscle actin (12/12), h-caldesmon (9/9), muscle-specific actin (4/4) and variable expression of desmin (11/14; diffuse in nine cases, focal in two and negative in three cases). Six cases were tested for CD56: three showed a diffuse reaction, one was focally positive, and two were negative. No correlation between CD56, desmin, and histological pattern was observed for the cases stained for both markers. Two cases stained with D2-40 showed no lymphatic component. The proliferation fraction (Ki-67) was <2 %. None of the 11 cases tested were reactive for HMB45. Selected immunohistochemistry findings are illustrated in Fig. 3b–d.

Discussion

Head and neck angioleiomyoma (ALM) are rare, comprising 8.5 and 13 % of all ALMs in two larger series [7, 8]. ALMs originating from sinonasal mucosa-covered sites are even rarer. They represented 9.5–12.5 % of head and neck and 1 % of all ALMs, respectively [7, 8, 27]. Only a single case of ALM was identified among 331 consecutive benign sinonasal masses (0.3 %) [42]. Since the first description by Maesaka et al. [9], no more than 38 well documented cases have been reported in the English literature, mainly as single case reports [9–41]. Although a female predilection has been suggested [1], review of previously reported cases combined with this clinical series (total: 54; Table 1) showed that both genders are affected equally (28 males and 26 females). Age range of reported cases was 24–88 years (mean 57 years). Mean age is 56 and 55 years for women and men, respectively. The turbinates are affected most frequently, followed by other subregions of the nasal cavity including nasal orifices, septum and lateral nasal wall. The paranasal sinuses were affected in only three cases. Most sinonasal ALMs present as sessile or polypoid well circumscribed but non-encapsulated masses. Their size ranged from 0.2 to 4 cm (mean 1.7 cm). Seven of 45 cases (15 %) with detailed information measured >2 cm. Pain, a characteristic symptom of cutaneous vascular leiomyoma [1, 6, 7] was reported in 5/54 patients with sinonasal tract ALM. Another three patients reported facial pain/headache, among other symptoms.

An infrequent finding in ALMs in general is the observation of a variable clustered or intermingled component of mature adipocytes, which resulted in the use of the

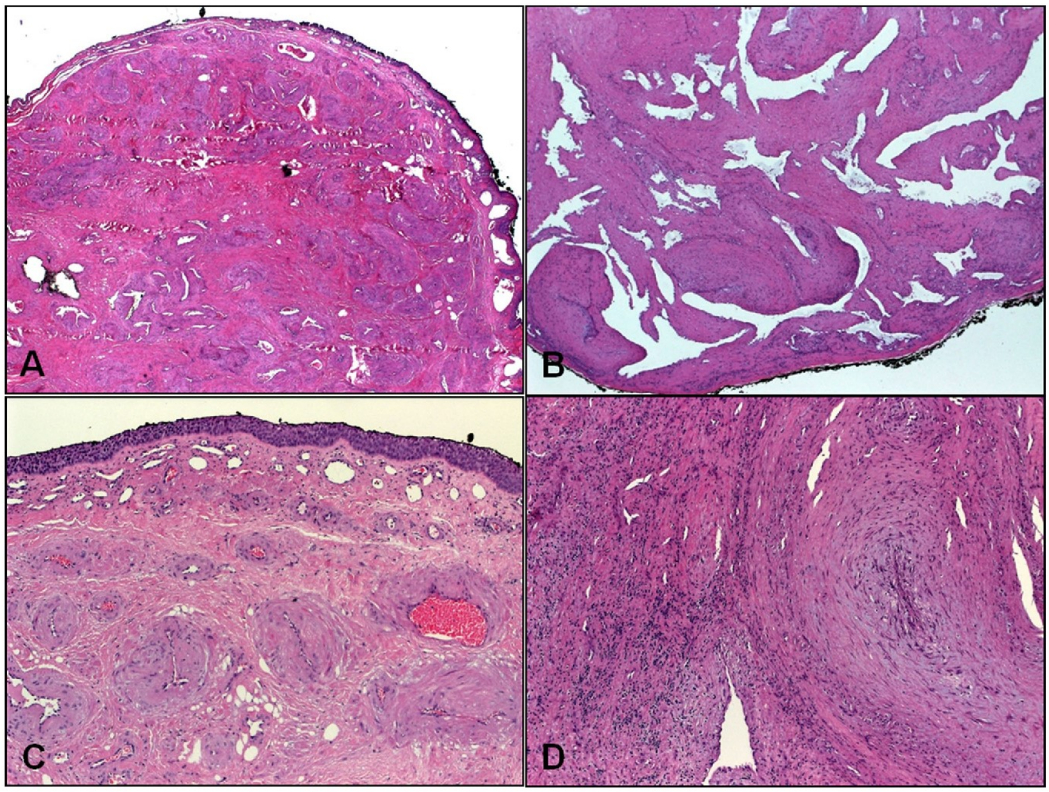

Fig. 1 Low-power findings in sinonasal angioleiomyomas. **a** Compact submucosal growth of haphazardly arranged thick-walled venous vessel with intervening fibromuscular stroma. **b** This example showed ectatic (cavernous) venous channels with their muscular walls blending with background musculature. **c** Surface epithelium showed squamoid metaplasia. **d** Interstitial inflammation with fibromyxoid vascular obliteration in ulcerated lesions may mask the underlying tumor

alternative term *angiomyolipoma* for some of previously reported cases [14, 24, 26, 29]. Among ALMs from all sites, a fatty component was observed in 2.8 % of cases [7]. However, review of reported cases and this clinical series (Table 1) showed a higher frequency of fatty component in sinonasal submucosal ALMs compared to their cutaneous counterparts (35 vs. 2.8 %, respectively). Comparing the subcohorts with (n = 19) and without (n = 35) adipocytic differentiation, ALM with fat tends to affect males more frequently than those without fat (63 vs. 46 % males) and to occur at a higher age (65 vs. 52 years for those with and without fat, respectively). Mean size was similar in both subgroups (18 and 16 mm, respectively).

Given that the presence or absence of a fatty component was not mentioned in several of the previously reported cases, it is possible that the frequency of adipocytic differentiation is even higher. None of the cases with available immunohistochemical findings stained for the melanocytic marker HMB45. The histological features were uniformly those of cutaneous-type ALM with or without adipocytic differentiation [43]. Based on these reported cases, sinonasal ALMs with adipocytic differentiation are histologically identical to their cutaneous/soft tissue counterparts and are distinctly different from renal-type angiomyolipoma. The latter can be associated with tuberous sclerosis complex, shows characteristic granular myogenic cells with frequent perivascular aggregates of epithelioid cells, convoluted thick-walled dysplastic vessels and cells with intermediate or transitional features between mature fatty cells and myogenic cells with cytoplasmic vacuoles indicating continuous differentiation. By immunohistochemistry, angiomyolipoma of renal type characteristically co-expresses myogenic and melanocytic markers (mainly HMB45). On the other hand, sinonasal

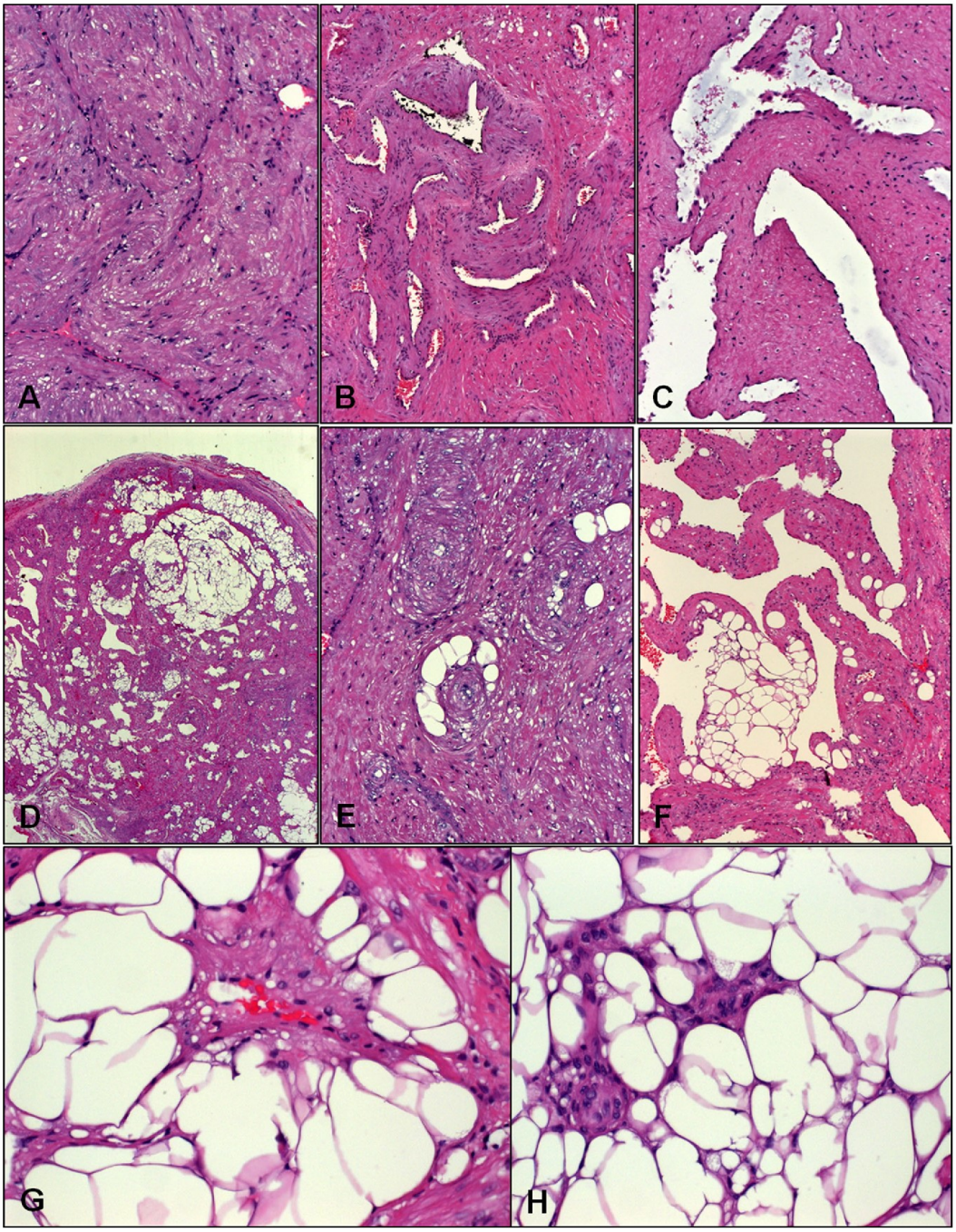
A
B
C
D
E
F
G
H

◀**Fig. 2** Histological spectrum of sinonasal angioleiomyomas. **a** Solid type with collapsed vascular channels amid smooth muscle bundles. **b** Lobule-like convolutes of veins surrounded by smooth muscle stroma. **c** This lesion showed ectatic vascular channels enclosed within smooth muscle bundles without discernible vascular walls. **d** Overview of a fat-rich lesion. **e** This solid lesion contained scattered adipocytes forming ring-like aggregates surrounding vessels. **f** Cavernous lesion with fatty lobules within vascular walls. **g** Perivascular "ring-adipocytes" from another case. **h** This fat-rich lesion showed size variation of adipocytes and can be mistaken for angiomyolipoma or adipocytic neoplasm

ALM shows a mature smooth muscle phenotype (desmin+/α-SMA+/h-caldesmon+/HMB45−). On critical review of the literature, it is evident that many of the reported sinonasal angiomyolipomas were actually "ALM with adipocytic differentiation" [14, 24, 26, 29], but a few cases of genuine renal-type angiomyolipomas and PEComas have been documented in the sinonasal tract as well [44, 45]. Accordingly, ambiguous and misleading terms such as angiomyolipoma and angiolipoleiomyoma should be abandoned. Instead, the term "angioleiomyoma with adipocytic differentiation" should be used for sinonasal ALMs with fatty component, analogous to their cutaneous and soft tissue counterparts [46]. Some ALMs may show focal perivascular concentric myoid cells closely mimicking myopericytoma [43]. On the other hand, the presence of ALM-like myopericytoma is well appreciated [47]. While most myopericytomas are composed of alpha smooth muscle actin+, h-caldesmon+, desmin-negative perivascular myoid cells, 15–20 % of ALMs are desmin-negative as observed in previous studies [43] and in our current series. These observations suggest the presence of lesions with overlapping features of ALM and myopericytoma, at least in a subset of cases [43, 47]. In our current series, none of the cases showed myopericytoma-like features. Albeit rare, Epstein-Barr Virus (EBV)-associated smooth

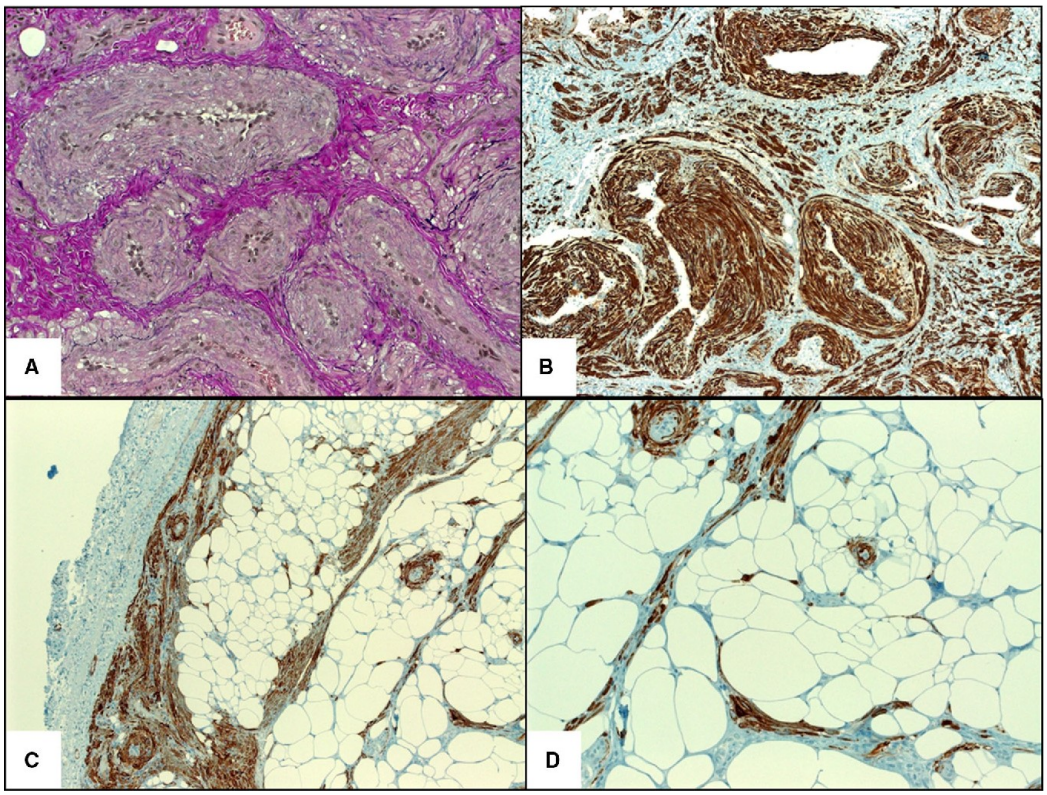

Fig. 3 **a** Elastic van Gieson stain highlighting the venous channels. **b** Strong desmin expression highlighting intervascular smooth muscle bundles. **c** H-caldesmon showed strong reactivity in muscle cells (note peripheral circumscription). **d** Higher magnification of h-caldesmon showed scattered isolated smooth muscle cells amid the fatty component

muscle tumors may on occasion closely mimic ALM. These rare lesions are characteristically multifocal involving different organs and affect patients with acquired or congenital immunodeficiency. Definitionally, they harbor EBV, detectable by in situ hybridization methods for EBER [48].

Review of the previous cases showed that some lesions likely represented other entities (excluded in the current review). In particular, sinonasal glomangiopericytoma/hemangiopericytoma was more commonly confused with ALM, given that both lesions strongly express smooth muscle actin. Sinonasal glomangiopericytoma, however, is a cellular neoplasm composed of monomorphic short spindled or ovoid to glomoid cells with distinctive cytoplasm and characteristic pericytomatous vascular pattern. They usually show a characteristic peritheliomatous hyalinization, lacking in ALM. Further, they lack the cytoplasmic eosinophilia and elongated blunt-ended nuclei of mature smooth muscle cells of ALMs and they are negative for h-caldesmon and desmin [3]. Two recent studies showed uniform nuclear expression of β-catenin in sinonasal glomangiopericytoma as a consequence of β-catenin mutations [49, 50].

In summary, we reported 16 new cases and reviewed 38 previously reported cases of submucosal sinonasal angioleiomyomas emphasizing their benign nature, frequent fatty component, similarity to cutaneous angioleiomyoma and distinctness from renal-type angiomyolipoma and equal gender distribution. Awareness of their histological spectrum is necessary to distinguish them from other potentially recurring or locally aggressive neoplasms.

Conflict of interest None.

References

1. Fanburg-Smith JC, Thompson LDR. Benign soft tissue tumours. In: Barnes L, Eveson JW, Reichart P, Sidransky D, editors. World Health Organization classification of tumours. Pathology and genetics of head and neck tumours. Lyon: IARC Press; 2005. p. 46–50.
2. Azani AB, Bishop JA, Thompson LD. Sinonasal tract neurofibroma: a clinicopathologic series of 12 cases with a review of the literature. Head Neck Pathol. 2014 Dec 13 (Epub ahead of print).
3. Thompson LD, Miettinen M, Wenig BM. Sinonasal-type hemangiopericytoma: a clinicopathologic and immunophenotypic analysis of 104 cases showing perivascular myoid differentiation. Am J Surg Pathol. 2003;27:737–49.
4. Lewis JT, Oliveira AM, Nascimento AG, Schembri-Wismayer D, Moore EA, Olsen KD, Garcia JG, Lonzo ML, Lewis JE. Low-grade sinonasal sarcoma with neural and myogenic features: a clinicopathologic analysis of 28 cases. Am J Surg Pathol. 2012;36:517–25.
5. Wenig BM. Recently described sinonasal tract lesions/neoplasms: considerations for the new world health organization book. Head Neck Pathol. 2014;8:33–41.
6. Hisaoka M, Quade B. Angioleiomyoma. In: Fletcher CDM, Bridge JA, Hogendoorn PCW, Mertens F, editors. World Health Organisation classification of tumours of soft tissue and bone (4th ed). Lyon: IARC Press; 2013. p. 120–121.
7. Hachisuga T, Hashimoto H, Enjoji M. Angioleiomyoma. A clinicopathologic reappraisal of 562 cases. Cancer. 1984;54:126–30.
8. Liu Y, Li B, Li L, Liu Y, Wang C, Zha L. Angioleiomyomas in the head and neck: a retrospective clinical and immunohistochemical analysis. Oncol Lett. 2014;8:241–7.
9. Maesaka A, Keyaki Y, Nakhashi T, Matsubara F. Nasal angioleiomyoma and leiomyosarcoma. Report of two cases. Otologia. 1966;12:42–7.
10. Ram M. Fibromyoma of posterior end of inferior turbinal. J Laryngol Otol. 1971;85:719–21.
11. Wolfowitz BL, Schmaman A. Smooth-muscle tumours of the upper respiratory tract. S Afr Med J. 1973;47:1189–91.
12. Schwartzman J, Schwartzman J. Leiomyoangioma of paranasal sinuses: case report. Laryngoscope. 1973;83:1856–8.
13. McCaffrey TV, McDonald TJ, Unni KK. Leiomyoma of the nasal cavity. Report of a case. J Laryngol Otol. 1978;92:817–9.
14. Dawlatly EE, Anim JT, El-Hassan AY. Angiomyolipoma of the nasal cavity. J Laryngol Otol. 1988;102:1156–8.
15. Hanna GS, Akosa AB, Ali MH. Vascular leiomyoma of the inferior turbinate—report of a case and review of the literature. J Laryngol Otol. 1988;102:1159–60.
16. Sawada Y. Angioleiomyoma of the nasal cavity. J Oral Maxillofac Surg. 1990;48:1100–1.
17. Ragbeer MS, Stone J. Vascular leiomyoma of the nasal cavity: report of a case and review of literature. J Oral Maxillofac Surg. 1990;48:1113–7.
18. Harcourt JP, Gallimore AP. Leiomyoma of the paranasal sinuses. J Laryngol Otol. 1993;107:740–1.
19. Khan MH, Jones AS, Haqqani MT. Angioleiomyoma of the nasal cavity—report of a case and review of the literature. J Laryngol Otol. 1994;108:244–6.
20. Gatalica Z, Lowry LD, Petersen RO. Angiomyolipoma of the nasal cavity: case report and review of the literature. Head Neck. 1994;16:278–81.
21. Ardekian L, Samet N, Talmi YP, Roth Y, Bendet E, Kronenberg J. Vascular leiomyoma of the nasal septum. Otolaryngol Head Neck Surg. 1996;114:798–800.
22. Nall AV, Stringer SP, Baughman RA. Vascular leiomyoma of the superior turbinate: first reported case. Head Neck. 1997;19:63–7.
23. Murono S, Ohmura T, Sugimori S, Furukawa M. Vascular leiomyoma with abundant adipose cells of the nasal cavity. Am J Otolaryngol. 1998;19:50–3.
24. Watanabe K, Suzuki T. Mucocutaneous angiomyolipoma. A report of 2 cases arising in the nasal cavity. Arch Pathol Lab Med. 1999;123:789–92.
25. Marioni G, Marchese-Ragona R, Fernandez S, Bruzon J, Marino F, Staffieri A. Progesterone receptor expression in angioleiomyoma of the nasal cavity. Acta Otolaryngol. 2002;122:408–12.
26. Tardío JC, Martín-Fragueiro LM. Angiomyolipoma of the nasal cavity. Histopathology. 2002;41:174–5.
27. Wang CP, Chang YL, Sheen TS. Vascular leiomyoma of the head and neck. Laryngoscope. 2004;114:661–5.
28. Bel Haj Salah M, Mekni A, Nouira K, Kharrat S, Bellil K, Bellil S, Haouet S, Chelly I, Kchir N, Zitouna MM. Leiomyoma of the nasal cavity. A case report. Pathologica. 2005;97:376–7.
29. Erkiliç S, Koçer NE, Mumbuç S, Kanlikama M. Nasal angiomyolipoma. Acta Otolaryngol. 2005;125:446–8.
30. Chen CJ, Lai MT, Chen CY, Fang CL. Vascular leiomyoma of the nasal cavity: case report. Chin Med J. 2007;120:350–2.
31. Meher R, Varshney S. Leiomyoma of the nose. Singap Med J. 2007;48:e275–6.

2.2.2. SELECTED CASE FROM THE ARKADI M. RYWLIN INTERNATIONAL PATHOLOGY SLIDE SEMINAR: BENIGN WARTHIN TUMOR OF THE THYROID

This case report was published in a journal designated to publish reviews as well as to provide a special section to reports of extraordinary cases circulated among the members of the international slides seminar referred to as “Arkadi M. Rywlin slide seminar”. Herein we described an exceedingly rare lesion of the thyroid probably of a branchial cleft origin, which was not published in the world literature before. A 58-year-old woman underwent a total thyroidectomy for bilateral goiter. Grossly, there was one yellowish nodule sized 15mm in the largest dimension found in the right lobe. Microscopically, the thyroid parenchyma showed signs of Hashimoto thyroiditis. The nodule in the right lobe was composed of a part of solid cell nests appearance, another part resembling a branchial cleft cyst, and a part resembling Warthin tumor. This lesion may belong to the histogenetically similar group of entities in the head and neck region which are derived from branchial cleft derivatives and which, under the inflammatory influence, have the ability to a cystic dilatation and proliferation of the epithelial component. The epithelium can afterwards become papillary and may undergo oncocytic transformation, thus gaining features that impart the resemblance of a Warthin tumor. Club members generally agreed with a submitted diagnosis of benign Warthin tumor of the thyroid.

Selected Case From the Arkadi M. Rywlin International Pathology Slide Seminar: Benign Warthin Tumor of the Thyroid

Kvetoslava Peckova, MD, Ondrej Daum, MD,* Michael Michal, MD,*† Radmila Curcikova, MD,‡ and Michal Michal, MD**

Abstract: We report on an exceedingly rare lesion of the thyroid probably of a branchial cleft origin, which was not published in the world literature before. A 58-year-old woman underwent a total thyroidectomy for bilateral goiter. Grossly, there was one yellowish nodule sized 15 mm in the largest dimension found in the right lobe. Microscopically, the thyroid parenchyma showed signs of Hashimoto thyroiditis. The nodule in the right lobe was composed of a part of solid cell nests appearance, another part resembling a branchial cleft cyst, and a part resembling Warthin tumor. This lesion may belong to the histogenetically similar group of entities in the head and neck region which are derived from branchial cleft derivatives and which, under the inflammatory influence, have the ability to a cystic dilatation and proliferation of the epithelial component. The epithelium can afterwards become papillary and may undergo oncocytic transformation, thus gaining features that impart the resemblance of a Warthin tumor. Club members generally agreed with a submitted diagnosis of benign Warthin tumor of the thyroid.

Key Words: thyroid, Warthin tumor, solid cell nests, branchial cleft cyst, benign

(*Adv Anat Pathol* 2016;23:339–342)

OVERVIEW

Diagnosis

Benign thyroidal tumor of ultimobranchial origin.

CLINICAL HISTORY

A 58-year-old woman underwent a total thyroidectomy for bilateral goiter.

PATHOLOGIC FINDINGS

Gross Features and Conventional Microscopic Examination

Grossly, the right lobe ($54 \times 40 \times 23$ mm in size) was grayish white and of compact parenchymatous structure on cut section, with one yellowish nodule sized 15 mm in the largest dimension. The left lobe ($58 \times 34 \times 24$ mm in size) had the same appearance, but was devoid of nodular lesions. The whole gland was submitted in 48 paraffin blocks. Furthermore, 3 lymph nodes were found and submitted for histologic investigation.

Microscopically, the thyroid parenchyma showed signs of Hashimoto thyroiditis. The nodule in the right lobe described above consisted of 3 distinct components (Fig. 1). The first component had solid cell nests (SCN) appearance characterized by small polygonal, elongated, or spindled cells with distinct borders forming solid structures occasionally with partial cystic transformation. The second part, resembling a branchial cleft cyst, was lined by predominantly squamous epithelium with focal presence of ciliated cells, and surrounded by abundant lymphoid tissue rich in germinal centers. Finally, the third part was identical to Warthin tumor with its typical 2 layers-thick epithelial lining with oncocytes forming the luminal layer. The epithelium was arranged in papillary-cystic pattern and surrounded by dense lymphoid stroma with germinal centers (Fig. 2).

Special Studies

Immunohistochemical study was applied to paraffin sections. The lining cells were thyroglobulin and TTF-1

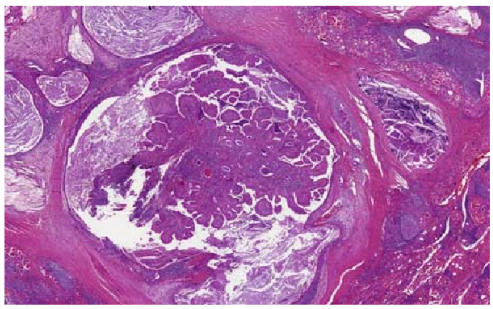

FIGURE 1. The tumor displayed features of Hashimoto thyroiditis with solid cell nests associated with structures resembling branchial cleft cyst and Warthin-like tumor of the thyroid (H&E, ×20).

From the *Department of Pathology, Charles University, Medical Faculty and Charles University Hospital Plzen; †Biomedical Center, Faculty of Medicine in Plzen and Charles University Hospital Plzen, Pilsen; and ‡Department of Pathology, Liberec Regional Hospital, Liberec, Czech Republic.

The case was circulated in the standard AMR Seminar #67 (case number 12, contributed by Michal Michal) and was also presented at Bioptic Seminar SD IAP, on June 20 to 21, 2014, held in Bratislava-Senec, Slovakia.

Supported by the National Sustainability Program I (NPU I) Nr. LO1503 provided by the Ministry of Education Youth and Sports of the Czech Republic.

The authors have no conflicts of interest to disclose.

Reprints: Kvetoslava Peckova, MD, Department of Pathology, Charles University, Medical Faculty and Charles University Hospital Plzen, Alej Svobody 80, 304 60 Pilsen, Czech Republic (e-mail: peckova.kveta@gmail.com).

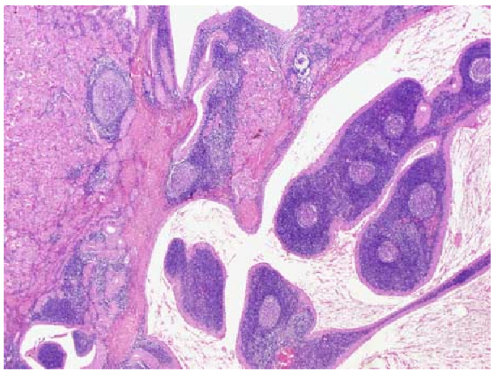

FIGURE 2. The component of the tumor identical to Warthin tumor. The epithelium was arranged in papillary-cystic pattern and surrounded by dense lymphoid stroma with germinal centers (H&E, ×40).

(monoclonal, 8G7G3/1, 1:100; Dako, Glostrup, Denmark) negative (Fig. 3), but positive for p63 and galectin 3. Carcinoembryonic antigen showed only patchy positivity, and Ki-67 was positive only in several individual cells.

Final Diagnosis

Benign Warthin tumor of the thyroid.

Follow-up

The patient is alive and well in 3 years of clinical follow-up.

Club Members' Anonymous Opinions

- Yet another case from Michal peculiar collection of strange cases. Wouldn't this tumor be an oncocytic variant papillary carcinoma with lymphoid stroma? Thinking of your large series of similar metaplastic lesions presented at the USCAP 2014 on same topic and having observed the distinctive bilayered "Warthinoid" epithelium, I agree that such a variant exist in the thyroid, albeit of unsure genetic basis. It would be interesting to look for similar cases unassociated with Hashimoto thyroiditis.
- Benign Warthin tumor of the thyroid. I initially thought it was a Warthin-like variant of papillary carcinoma but it really looks like a true Warthin tumor.
- Michal has very original and interesting "takes" on lesions that could be banalized by mere mortal pathologists. In this lesion there are papillary structures lined by eosinophilic cells that I would have thought were Hurtle cells. Was this the component interpreted as Warthin tumor and were these cells negative for thyroid markers? Is Warthin tumor appearing in the thyroid formed by thyroid cells or by the same cells which compose the tumor in the salivary gland? Is there a connection between the Warthin tumor and the branchial cleft portion?
- Agree. Weird.
- I thought of a peculiar benign cystic lesion with squamous and Warthin-like areas occurring in the background of Hashimoto thyroiditis, but I was not aware of this entity: thanks!

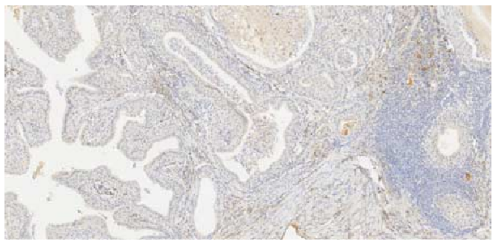

FIGURE 3. TTF-1 (monoclonal, 8G7G3/1, 1:100; Dako) was negative in the epithelial cells of Warthin tumor, branchial cleft-like areas, and solid cell nests.

- Agree with diagnosis. I probably would have simply called this Warthin tumor with some metaplastic changes.
- Yes, the 2 layered eosinophilic columnar cells are the giveaway. Again thank you for this educational case. Not seen this before. Thank you Michal.
- Hashimoto thyroiditis with Warthin tumor, differential diagnosis with Warthin-like papillary carcinoma of the thyroid described years ago by LiVolsi.
- Interesting case. My first association was sclerosing mucoepidermoid carcinoma but closer look is more in line with Warthin with squamous metaplasia. Translocation negative?
- Another "man of Istanbul." Reminds me of a Warthin-like papillary carcinoma submitted many years ago to this seminar. The papillary configuration of this particular case is remarkable.
- Educational case, especially considering the differential diagnosis with an oncocytic variant of papillary thyroid carcinoma (PTC). However, the immunohistochemical profile (p63 +, TTF1−, thyroglobulin−) sustain this diagnosis.
- The relationship with SCN is interesting.
- This case is very interesting. The morphology is focally similar to a Warthin tumor of the parotid, and the p63 positivity, if located to the basal cell layer can confirm it. As all of you know, Warthin-like papillary carcinoma of the thyroid are described and in the present case should be considered in the differential diagnosis. In the present case, TTF1 is reported negative, and the double cell layer is underlined by the presence of p63-positive cells. Nevertheless, the nuclear contour and grooving are quite similar to those of papillary carcinoma. I wonder if the case had been diagnosed by fine needle aspiration before surgery.
- A benign Warthin tumor in the thyroid, I have never seen it.
- Agree with diagnosis. Intriguing at this anatomic location.
- This lesion is, of course, very different from what is known under the name Warthin-like papillary carcinoma of the thyroid that is essentially an oncocytic variant of papillary carcinoma with lymphoid stroma. This type of lesion submitted by you must be extremely rare.
- What an unusual finding!
- Very beautiful Warthin tumor in the thyroid. Thanks so much.
- Yes, there is a strange Warthin tumor–like area in the background of lymphocytic thyroiditis. Also squamous metaplasia.

- Agree. Despite nuclear grooves, other features of PTC not present—also architecture not worrying. Interesting histogenesis. Michal, the "recent" publication was from 2006. Time flies.
- I leave this diagnosis to the thyroid experts but it does remind me of a Warthin tumor. I'm glad that you think of 2006 as "recent." That's really a European perspective, which I appreciate. In the United States that paper would be categorized as "old."
- Interesting lesion! I was not aware of the relation of branchial cleft cysts, Warthin, and SCNs.
- Very rare lesion! It does indeed show some resemblance on scanning magnification to a Warthin tumor of salivary gland. Although some of the papillae are lined by tall columnar granular cells, the more solid portions are clearly squamous and show very well-defined cell membranes and pavement-like architecture. The squamous nature of these cells is supported by the p63 positivity. Don't know how to interpret this lesion. Although it resembles a Warthin tumor it is not really a perfect fit for it (no double cell layer in the papillae, absence of lymphoid follicles in the stroma, foci of squamous metaplasia/differentiation). It looks more like a thyroid cyst with oncocytic and metaplastic changes arising from the cyst lining. Parenthetically, "Warthin-like PTC" does not enter in the differential here due to the absence of the nuclear features of PTC. The latter was initially presented in a platform at USCAP in 1994 as "*Warthin-like tumor* of the thyroid gland," and in the same platform session there was another platform describing the oncocytic variant of PTC. It dawned only later that the 2 platforms were actually presenting the same thing. "Warthin-like PTC" is nothing other than the oncocytic variant of PTC with prominent lymphoid stroma, a feature that was well illustrated in the original platform and paper on oncocytic PTC. Dr LiVolsi later changed the title of her paper to "Warthin-like PTC" at the time of publication in response to the criticism leveled by some of the attendees that the lesions should not be considered benign given that some of her cases had metastasized to lymph nodes.
- It looked familiar, did not know it exists in the thyroid…

AUTHORS' COMMENTS

There is a group of lesions in the head and neck region derived from branchial arches and related structures which, when inflamed, are characterized by the formation of cysts lined by squamous or glandular (sometimes respiratory) epithelium and surrounded by a heavy inflammatory infiltrate rich in germinal centers, and which are called in different ways depending on their localization. These entities include branchial cleft cyst, multilocular thymic cysts, lymphoepithelial cyst of the salivary gland region, and in case of intrathyroidal localization a branchial cleft-like cyst.[1–4]

Regarding the thyroid gland, the majority of cystic lesions herein arise as a degenerative process in multinodular goiter or a neoplasm. However, occurrence of the cyst histogenetically similar to the above-mentioned lesions is also possible, despite the fact, that embryologic origin of the thyroid is traditionally placed to the ductus thyreoglossus. Nevertheless, the intrathyroidal presence of branchial cleft remnants may be explained by a parathyroid or a thymic origin of these lesions, as both thymus and parathyroids are branchial cleft derivatives and can be incidentally found within the thyroid.[2] Another possible origin of such lesions is the ultimobranchial body, an embryological structure which gives rise to the parafollicular C cells and is derived from the fourth and/or fifth branchial pouches. The most well-known morphologic correlate of ultimobranchial body in the thyroid are the so-called SCN.[5] SCN usually represent an incidental finding in the thyroid gland removed for other reasons; however, they may cause diagnostic perplexity, because they may be a source of miscellaneous structures. In their typical form, SCN are small, solid structures which display large polygonal cells with abundant cytoplasm and distinct cell borders. They are sometimes intermingled with C cells, which mirrors their origin in the ultimobranchial body as a progenitor of both cell lines. Sometimes SCN can bear irregular shape and in case they are interspersed with fibrous tissue (eg, in chronic inflammatory background) they can mimic a metastatic process. In some instances the SCN may show some atypical nuclear features including prominent nuclear grooves, enlarged overlapping nuclei, or nuclear clearing and therefore they can be easily mistaken for papillary thyroid microcarcinomas.[6] In other instances they may be confused with medullary carcinoma, squamous metaplasia, or C-cell hyperplasia.[1,4] Positive immunohistochemical staining for galectin 3, CK19, p63, bcl-2, and carcinoembryonic antigen, and negative staining for thyroglobulin, calcitonin, parathyroid hormone, and TTF-1 should distinguish SCN from their mimics.[7] Interestingly, SCN were encountered in association with salivary gland tissue inside of the thyroid, which further points to the common origin of these 2 types of tissues.[8]

The common denominator of these branchial cleft-derived cystic lesions in the head and neck region is that they all arise as an inflammatory process around these vestigial structures, which can lead to cystic dilatation and proliferation of the epithelial component. The epithelium afterwards can become papillary, may undergo oncocytic transformation, consequently acquiring the features of a Warthin tumor. According to this theory, it was suggested that the Warthin tumor is yet another manifestation of the same phenomenon, in sense of being just a lymphoepithelial cyst of salivary gland instead of a real neoplasm. This hypothesis was supported by researchers, who examined the clonal status of the epithelial cells of Warthin tumor by using polymerase chain reaction method based on trinucleotide repeat polymorphism of the X chromosome-linked human androgen receptor gene (HUMARA) and on a random inactivation of the gene by methylation. HUMARA analysis showed, that the epithelial component was a polyclonal population which indicates a nonneoplastic origin of Warthin tumor epithelial component.[9]

CONCLUSIONS

In conclusion, our case raises the question, whether this unique tumor is genuinely composed of 3 individual parts, or whether this phenomenon just represents different stages of cystic dilatation of intrathyroidal branchial remnants induced by Hashimoto thyroiditis. The latter theory is supported by the recent proof of polyclonal nature of epithelial component in Warthin tumor of salivary glands. And the last but not the least, the occurrence of Warthin tumor inside the thyroid as we describe should not be

terminologically confused with rare occurrence of the oncocytic papillary carcinoma of the thyroid associated with lymphoid stroma, a lesion called sometimes as "thyroidal Warthin's tumor" in the past.[10–12]

Authors' Additional Comment

After the slides have been distributed, 1 additional clone of TTF1 (monoclonal, SPT24, 1:400; Novocastra, Newcastle, UK) was performed. Positive nuclear staining for this clone was detected in all 3 components of the tumor, namely in the SCN and in the epithelial part of both branchial cleft-like cyst and Warthin tumor.

As repeatedly reported, the negative staining for TTF1 is generally considered as one of the contributory diagnostic marker of SCN and related lesions and serves to confirm their nonthyroid embryonic nature. Nevertheless, the positive staining for TTF1 of such lesions has been previously published.[7,13] Accordingly, our observations merely remind of notorious rule, that the morphologic features should be in diagnostic process assessed superior than immunohistochemical examination, as the latter might serve inconsistent results.

REFERENCES

1. Suster S, Rosai J. Multilocular thymic cyst: an acquired reactive process. Study of 18 cases. *Am J Surg Pathol*. 1991;15:388–398.
2. Louis DN, Vickery AL Jr, Rosai J, et al. Multiple branchial cleft-like cysts in Hashimoto's thyroiditis. *Am J Surg Pathol*. 1989;13:45–49.
3. Michal M, Kacerovska D, Kazakov DV, et al. Pseudotumors and mimickers of malignancy of the head and neck pathology. *Cesk Patol*. 2012;48:190–197.
4. Michal M, Mukensnabl P, Kazakov DV. Branchial-like cysts of the thyroid associated with solid cell nests. *Pathol Int*. 2006;56:150–153.
5. Cameselle-Teijeiro J, Varela-Duran J, Sambade C, et al. Solid cell nests of the thyroid: light microscopy and immunohistochemical profile. *Hum Pathol*. 1994;25:684–693.
6. Asioli S, Erickson LA, Lloyd RV. Solid cell nests in Hashimoto's thyroiditis sharing features with papillary thyroid microcarcinoma. *Endocr Pathol*. 2009;20:197–203.
7. Rios Moreno MJ, Galera-Ruiz H, De Miguel M, et al. Inmunohistochemical profile of solid cell nest of thyroid gland. *Endocr Pathol*. 2011;22:35–39.
8. Cameselle-Teijeiro J, Varela-Duran J. Intrathyroid salivary gland-type tissue in multinodular goiter. *Virchows Arch*. 1994;425:331–334.
9. Honda K, Kashima K, Daa T, et al. Clonal analysis of the epithelial component of Warthin's tumor. *Hum Pathol*. 2000;31:1377–1380.
10. D'Antonio A, De Chiara A, Santoro M, et al. Warthin-like tumour of the thyroid gland: RET/PTC expression indicates it is a variant of papillary carcinoma. *Histopathology*. 2000;36:493–498.
11. Baloch ZW, LiVolsi VA. Warthin-like papillary carcinoma of the thyroid. *Arch Pathol Lab Med*. 2000;124:1192–1195.
12. Ludvikova M, Ryska A, Korabecna M, et al. Oncocytic papillary carcinoma with lymphoid stroma (Warthin-like tumour) of the thyroid: a distinct entity with favourable prognosis. *Histopathology*. 2001;39:17–24.
13. Nakazawa T, Kondo T, Oishi N, et al. Branchial cleft-like cysts involving 3 different organs: thyroid gland, thymus, and parotid gland. *Medicine (Baltimore)*. 2015;94:e1758.

2.2.3. A NEW HITHERTO UNREPORTED HISTOPATHOLOGIC MANIFESTATION OF MAMMARY ANALOGUE SECRETORY CARCINOMA: "MASKED MASC" ASSOCIATED WITH LOW-GRADE MUCINOUS ADENOCARCINOMA AND LOW-GRADE IN SITU CARCINOMA COMPONENTS

Mammary analogue secretory carcinoma (MASC) is a salivary gland tumor relatively recently described by several of my colleagues [61]. This case report presented a unique manifestation of MASC characterized by a tumor showing a minor conventional MASC component (20%) admixed with an entirely different mucinous adenocarcinoma component comprising 80% of the lesion. This part consisted of morphologically nondescript low-grade intraductal carcinoma (in situ) component. Using FISH, a break in the ETV6 gene was documented in the mucinous adenocarcinomatous, the conventional MASC, and the intraductal (in situ) components. RT-PCR failed to reveal an ETV6-NTRK3 fusion. The entire conventional MASC and only rare mucinous adenocarcinoma tumor cells were mammaglobin positive, whereas the low-grade intraductal carcinoma (in-situ) component was negative. S-100 protein stained only the MASC component.

In the close future, it will be interesting to submit this tumor for NGS analysis and search for the unknown fusion partner as we recently uncovered an alternative fusion partner for cases of MASC that do not show the canonical *ETV6-NTRK3* fusion. Instead, a subset of tumors until recently referred to as ETV6-X MASCs [62] were shown to harbor ETV6-RET fusion (discussed later) [63]. Another group also very recently published a case report of MASC with ETV6-MET fusion [64].

A New Hitherto Unreported Histopathologic Manifestation of Mammary Analogue Secretory Carcinoma: "Masked MASC" Associated With Low-grade Mucinous Adenocarcinoma and Low-grade In Situ Carcinoma Components

Fredrik Petersson, MD, PhD, Michael Michal, MD,† Dmitry V. Kazakov, MD,† Petr Grossmann, PhD,† and Michal Michal, MD†*

Abstract: We present a salivary gland tumor of the parotid gland in a 54-year-old woman, which contained a minor mammary analogue secretory carcinoma (MASC) component (20%) intermixed with a morphologically entirely different mucinous adenocarcinomatous component that comprised 80% of the tumor mass and a morphologically nondescript low-grade intraductal carcinoma (in situ) component. On fluorescence in situ hybridization, a break in the *ETV6* gene was documented in the mucinous adenocarcinomatous, the conventional MASC, and the intraductal (in situ) components. RT-PCR failed to reveal an *ETV6-NTRK3* fusion. The entire conventional MASC and only rare mucinous adenocarcinoma tumor cells were mammaglobin positive, whereas the low-grade intraductal carcinoma (in-situ) component was negative. S-100 protein stained only the MASC component.

Key Words: mammary analogue secretory carcinoma, adenocarcinoma, *ETV6* gene, salivary gland

(*Appl Immunohistochem Mol Morphol* 2016;24:e80–e85)

Mammary analogue secretory carcinoma (MASC) is a relatively new entity in the salivary gland pathology, first described in a series of 16 cases in 2010.[1] The original and subsequent studies have shown that the majority of cases occur in the parotid gland and minor salivary glands of the oral cavity.[2–4] Recently, 1 series of 3 cases, 1 case report, and 1 case in a larger series of MASCs with high-grade transformation have been reported.[5–7] MASC shows histopathologic features that are very similar to its mammary counterpart, and on a molecular genetic level, both MASCs and mammary secretory carcinomas carry the t(12;15)(p13;q25) translocation, resulting in fusion of *ETV6* to *NTRK3*. Recently, however, cases of MASC with no *NRTK3* gene rearrangement (ETV6-X) were reported.[8] Histologically, MASC displays a multinodular or lobular architecture with solid, microcystic, and tubular patterns. The histopathologic spectrum has been expanded to include macrocystic, unicystic, and papillary patterns. Frequently, several patterns coexist in the same tumor. Despite the presence of various patterns, cytologically, the tumors are uniform and composed of 1 cell type. The neoplastic cells in MASC have "low-grade," round to ovoid nuclei with 1 small distinct nucleolus and a small amount of pale-pink, granular to variably vacuolated cytoplasm. Mitotic figures are scarce and generally difficult to find. MASCs contain Periodic acid schiff (PAS)-positive secretory material. In addition to cytokeratins, MASCs coexpress vimentin, S-100 protein (S-100), and mammaglobin (MGL).[1,2]

In this report, we present a unique case of MASC with a hitherto unreported combination of patterns and cell types, including a minor (20%) component of conventional MASC, a predominant component that displayed a mucinous adenocarcinoma that was cytologically entirely different from MASC, and a low-grade intraductal (in situ) carcinoma component with nondescript cytomorphologic features.

MATERIALS AND METHODS

Tissue was fixed in formalin and embedded in paraffin, and 4-μm-thick sections were cut and stained with hematoxylin and eosin, PAS, and mucicarmine. Immunohistochemical studies were performed using commercially available antibodies to cytokeratin 7 (monoclonal, OV-TL 12/30, 1:200; Dako, Glostrup, Denmark), CK5/6 (monoclonal, D5/16 B4, 1:200; Dako), S100-protein (polyclonal, 1:400; Dako), mammaglobin (monoclonal, 304-1A5, prediluted; Cell Marque), smooth-muscle actin (monoclonal,

Received for publication November 10, 2015; accepted November 24, 2015.

From the *Department of Pathology, National University Health System, Singapore, Singapore; and †Department of Pathology, Medical Faculty in Pilsen, Charles University in Prague, Plzen, Czech Republic.

The authors declare no conflict of interest.

Reprints: Fredrik Petersson, MD, PhD, Department of Pathology, National University Health System, 5 Lower Kent Ridge Road, Singapore 119074, Singapore (e-mail: fredrikpetersson@live.se).

1A4, 1:500; Dako), Her2 (monoclonal,4B5, prediluted; Ventana), p53 (monoclonal, DO-7, prediluted; Ventana), GCDFP-15 (monoclonal, EP1582Y, 1:200; Cell Marque), Ki-67 (monoclonal, 30-9, prediluted; Ventana), M-GGMC-1 (monoclonal, HIK1083, 1:100; Cosmo Bio Co Inc.), TTF1 (monoclonal, SPT24, 1:100; Novocastra), GATA3 (monoclonal, L50-823, 1:250; BioCare Medical), and SATB2 (monoclonal, CL0276, 1:100; Sigma).

Molecular Genetic Study

Detection of the *ETV6-NTRK3* Fusion Transcript by RT-PCR

RNA from the formalin-fixed paraffin-embedded tissue was extracted using the RecoverAll Total Nucleic Acid Isolation Kit (Ambion, Austin, TX). cDNA was synthesized using the Transcriptor First Strand cDNA Synthesis Kit (RNA input 1 μg) (Roche Diagnostics, Mannheim, Germany). All procedures were performed according to the manufacturers' protocols. Amplification of a 105-bp and a 133-bp product of the β2-microglobulin gene and a 247-bp product of the PGK gene was used to test the quality of the extracted RNA as described previously.[9–11] The detection of a 110-bp fragment of the ETV6/NTRK3 fusion transcript was performed according to the method described by Bourgeois et al.[12]

In brief, 2 μL of cDNA was added to a reaction consisting of 12.5 μL of HotStart Taq PCR Master Mix (Qiagen, Hilden, Germany), 10 pmol of each primer (TRKC1059 complementary to NTRK3 with the sequence CAGTTCTCGCTTCAGCACGATG and TEL971 complementary to *ETV6* with the sequence ACCACATCATG GTCTCTGTCTCCC), and distilled water up to 25 μL. The amplification program comprised denaturation at 95°C for 14 minutes and then 40 cycles of denaturation at 95°C for 1 minute, annealing at 65°C for 1 minute, and extension at 72°C for 1 minute. The program was finished by incubation at 72°C for 7 minutes.

Successfully amplified PCR products of the *ETV6/NTRK3* fusion gene were purified with a Montage PCR Centrifugal Filter Device (Millipore, Billerica, MA). Then, the PCR products were sequenced on both sides using a Big Dye Terminator Sequencing kit (Applied Biosystems), run on an automated genetic analyzer ABI Prism 3130xl (Applied Biosystems) at a constant voltage of 13.2 kV for 20 minutes, and compared with the GenBank sequence.

Detection of *ETV6*, *NTRK3* Break by FISH

A 4-μm-thick section was placed onto a positively charged slide. The hematoxylin and eosin–stained slide was examined for the determination of areas for cell counting.

The unstained slide was deparaffinized routinely and incubated in the 1× Target Retrieval Solution Citrate pH 6 (Dako) for 40 minutes at 95°C and subsequently cooled for 20 minutes at room temperature in the same solution. The slide was washed in deionized water for 5 minutes and digested in protease solution with Pepsin (0.5 mg/mL) (Sigma Aldrich, St Louis, MO) in 0.01 M HCl at 37°C for 30 minutes. The slide was then placed into deionized water for 5 minutes, dehydrated in a series of ethanol solution (70%, 85%, and 96% for 2 min each), and air dried. Detection of rearrangement of the *ETV6* gene was performed using the Vysis *ETV6* Break Apart FISH Probe Kit (Vysis/Abbott Molecular, IL). The probe was mixed with water and the LSI/WCP (Locus-Specific Identifier/Whole Chromosome Painting) Hybridization buffer (Vysis) in a 1:2:7 ratio, respectively. Probes for the detection of rearrangement of the *NTRK3* gene region were mixed from custom-design SureFISH probes (Agilent Technologies Inc., Santa Clara, CA) with localizations chr15:87501469-88501628 and chr15:88701444-89700343, water, and LSI/WCP Hybridization buffer (Vysis) in a 1:1:1:7 ratio, respectively. An appropriate amount of probe mix was applied on the specimen, covered with a glass coverslip, and sealed with rubber cement. The slide was incubated in the ThermoBrite instrument (StatSpin/Iris Sample Processing, Westwood, MA) with codenaturation parameters of 85°C for 8 minutes and hybridization parameters of 37°C for 16 hours. The rubber-cemented coverslip was then removed, and the slide was placed in the posthybridization wash solution (2× SSC/0.3% NP-40) at 72°C for 2 minutes. The slide was air dried in the dark, counterstained with 4′, 6′-diamidino-2-phenylindole DAPI (Vysis), coverslipped, and examined immediately.

FISH Interpretation

The section was examined with an Olympus BX51 fluorescence microscope (Olympus Corporation, Tokyo, Japan) using a 100× objective and filter sets Triple Band Pass (DAPI/SpectrumGreen/SpectrumOrange), Dual Band Pass (SpectrumGreen/SpectrumOrange), and Single Band Pass (SpectrumGreen or SpectrumOrange).

One hundred randomly selected nonoverlapping tumor cell nuclei were examined for the presence of yellow (normal) or green and orange (chromosomal breakpoint) fluorescent signals. The cut-off value was set to >10% of the nuclei with chromosomal breakpoint signals (mean + 3 SD in normal non-neoplastic control tissues).

CASE REPORT

The patient was a 54-year-old woman with a history of Parkinson disease, left-sided brain stroke, and thyrotoxicosis. In addition, her history included a left parotid lump excised >30 years ago (the tumor is not available for revision). On admission, the patient complained of a slowly growing left-sided parotid lump. Clinical examination revealed a left-sided parotid tumor that was slightly painful on palpation. The facial nerve function was intact. A computerized tomography scan revealed an up to 25 mm large, lobulated and moderately enhancing tumor in the superficial lobe of the left parotid gland (Fig. 1). Neither the clinical examination nor the imaging study yielded any evidence of lymphadenopathy. A frozen section of the tumor was reported as adenocarcinoma, and the patient underwent a parotidectomy with sacrifice of the facial nerve and neck dissection. One intraparotid lymph node harbored a metastasis,

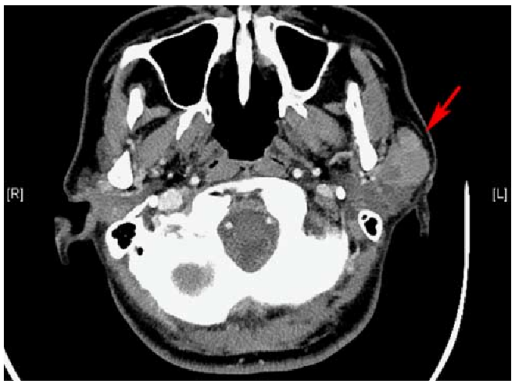

FIGURE 1. A computerized tomography scan revealed an up to 25 mm large, lobulated tumor in the superficial lobe of the left parotid gland (arrow).

whereas no metastases were identified in the neck dissection specimens outside of the parotid gland.

RESULTS

The surgically excised specimen showed a nonencapsulated, partly circumscribed, firm, whitish tumor measuring $2.3 \times 1.7 \times 1.7$ cm.

Histologic examination revealed a tumor with irregular infiltrative borders. The main part of the tumor displayed distinctive mucinous adenocarcinomatous features, where neoplastic cells formed glands, frequently arranged in cribriform arrangements (Fig. 2). This component was morphologically very different from MASC and was composed of cells with abundant eosinophilic cytoplasm filled with mucin and focally formed secretory apocrine snouts on the luminal surface of the glands (Fig. 3). This mucinous component was well differentiated

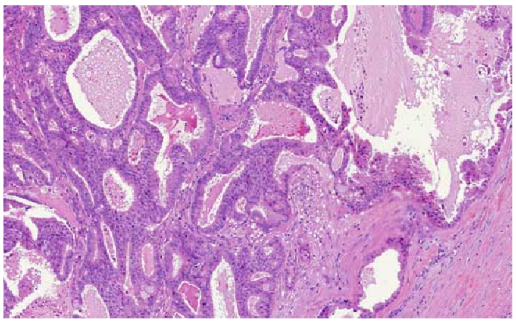

FIGURE 3. The mucinous adenocarcinomatous component composed of cells with an abundant eosinophilic cytoplasm filled with mucin, focally forming secretory apocrine snouts on the luminal surface of the glands.

with a low degree of nuclear pleomorphism and low mitotic activity. No areas of necrosis were present. Mucinous secretions of the tumor glands stained with mucicarmine stain. A second neoplastic component revealed an entirely different morphology, with a distinctively low-grade moiety, exhibiting typical features of conventional MASC featuring reticular to microcystic arrangement with weakly eosinophilic focally bubbly secretions within the lumina (Fig. 4). The tumor cells had small, round to ovoid nuclei with small nucleoli and a small amount of eosinophilic, frequently vacuolated cytoplasm. No mitotic figures were observed. These 2 components were often intermixed without any transitional areas. Interspersed between the 2 components were variably dilated ducts harboring a low-grade, monotonous, multilayered epithelium, representing an intraductal carcinoma (in situ) component of the tumor.

The immunohistochemical study showed that both neoplastic components and the intraductal (in situ)

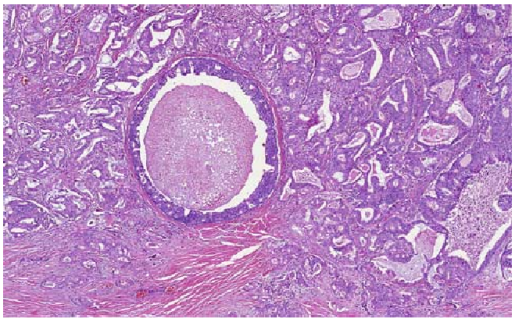

FIGURE 2. The main part of the tumor with distinctive mucinous adenocarcinomatous features characterized by neoplastic cells forming glands, frequently arranged in cribriform arrangements. An intraductal component can be seen in the central part of the lesion.

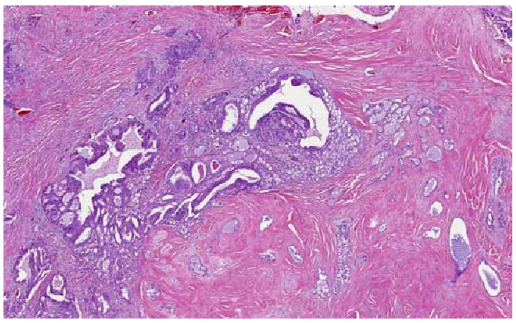

FIGURE 4. A minor component of the tumor consisting of conventional MASC featuring a reticular to microcystic arrangement with a weakly eosinophilic focally bubbly secretion within the lumina. Note that the MASC component intermingles with the mucinous non-MASC component. MASC indicates mammary analogue secretory carcinoma.

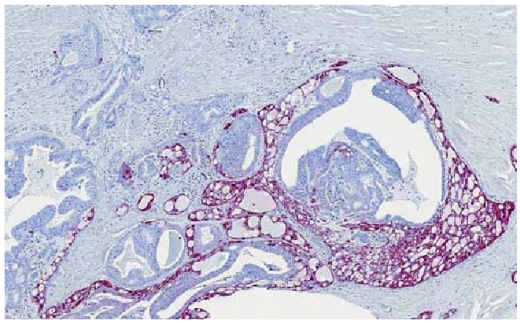

FIGURE 5. The MASC component showed strong cytoplasmic and nuclear expression of the S-100 protein, whereas the mucinous adenocarcinomatous part is completely S-100 protein negative. MASC indicates mammary analogue secretory carcinoma.

component were expressing CK7 strongly and diffusely. In contrast to this diffuse immunoreactivity for CK7, only the MASC component revealed strong cytoplasmic and nuclear expression of S-100, whereas both the mucinous adenocarcinomatous and the intraductal carcinoma components were completely S-100 protein negative (Fig. 5). Neoplastic cells of the MASC component and its secretions were diffusely positive for MGL, whereas only scattered MGL-positive cells were evident in the mucinous adenocarcinomatous component (Fig. 6). CK5/6 and SMA highlighted the myoepithelial layer of the dilated ducts of the intraductal carcinoma component, but the rest of the tumor was negative with these antibodies. Both the MASC and the mucinous adenocarcinomatous component expressed GCDFP-15. There was no expression of HER2, TTF1, GATA3, and SATB2. Ki-67 proliferation was < 5% in the MASC component and 5% to 10% in the adenocarcinomatous component. No strong nuclear expression of p53 was present.

In the molecular genetic study, the *ETV6-NTRK3* fusion transcript was not detected. FISH showed

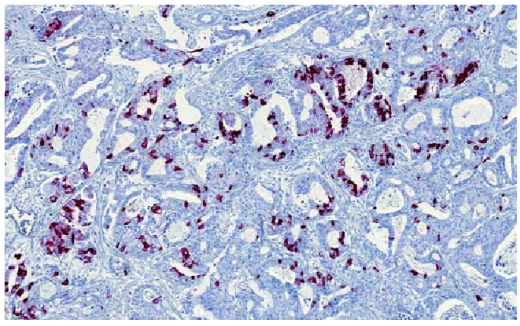

FIGURE 6. Only rare scattered cells in the mucinous adenocarcinomatous component expressed mammaglobin.

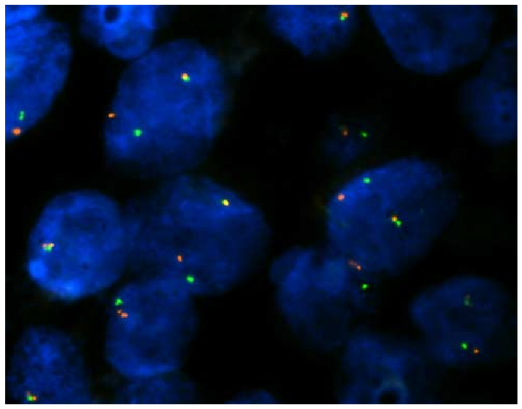

FIGURE 7. The FISH study (split-apart probe) showed rearrangement of *EVT6* in the conventional MASC, adenocarcinomatous, and low-grade intraductal (in situ) components. The photomicrograph is from the adenocarcinomatous component. MASC indicates mammary analogue secretory carcinoma.

rearrangement of *EVT6* in the conventional MASC and adenocarcinomatous components as well as in the intraductal carcinoma (in situ) component (Fig. 7). No rearrangement of *NTRK3* was present in the tumor.

DISCUSSION

The range of histologic patterns in MASC can be variable, encompassing solid, tubular, microcystic, macrocystic, reticular, papillary, and polypoid patterns. Despite the architectural diversity, the cytologic appearance of MASC cells is always uniform. The tumor in our case, in addition to the classic histopathologic features of MASC in a minority of the tumor mass, revealed a low-grade mucinous adenocarcinomatous component. The tumor showing such a combination of MASC and an entirely differently appearing mucinous adenocarcinoma component has never been reported to date, as far as we are aware. The possibility of intermixture of 2 independent tumors (collision tumor) was refuted by the occurrence of *ETV6* rearrangement in both components.

Immunohistochemically, most MASCs display a characteristic immuneprofile with a strong and diffuse expression of CK 7, vimentin, S-100 protein, and MGL,[1,5,13,14] which was the case in the MASC component in the tumor we report. The presence of a mucinous adenocarcinomatous component, as seen in our case, despite being quite remarkable, has not been described in any well-known salivary gland tumors. By showing a conspicuous abundant eosinophilic cytoplasm and well-formed apocrine snouts, the mucinous adenocarcinomatous component remotely resembled the apocrine epithelium seen often in apocrine cysts of mammary glands.

A typical MASC is characterized by a distinctive balanced t(12;15) (p13;q25) chromosomal rearrangement resulting in the fusion of *ETV6* and *NTRK3* genes.[1,2,5] However, some reported cases of MASC have failed to reveal the *ETV6-NTRK3* fusion by RT-PCR.[1,5,15] Recently, Ito et al[16] reported 2 cases of MASC with the *ETV6* gene split detected by FISH, but in which the *ETV6* gene appeared to be fused with a gene partner other than *NTRK3*. Similarly, Skalova and colleagues reported 25 cases of MASCs that displayed the *ETV6* rearrangement, but lacked the classic *ETV6-NTRK3* fusion transcript by RT-PCR. Our case seems to fall into the same group of cases, with the difference that 80% of the tumor mass of our case had a morphology entirely different from MASC and 20% of the tumor mass had the appearance and immunohistochemical properties of classic MASC.

Skalova et al[5] have recently described 3 cases of MASC with a high-grade dedifferentiation component. Our case differs from their cases in that the mucinous adenocarcinoma non-MASC component was not a high-grade or a dedifferentiated tumor. This component appeared as low grade, similar to the conventional MASC component. In fact, we are not aware of any salivary gland tumor with such an appearance in the salivary gland tumor pathology.

Nonetheless, a similar dual neoplastic differentiation phenomenon has been described in other organs. It is well known that tumors in patients with the *CYLD1* germ cell mutation may have various components such as cylindroma, spiradenoma, trichoblastoma, and lymphadenoma within the same tumor mass,[17–19] even if these versatile components seen in 1 tumor mass in these Brooke-Spiegler syndrome patients are otherwise mostly described as independent entities. Another similar example of a neoplasm that can reveal an entirely different differentiation is dermatofibrosarcoma protuberans, which can have a component of giant-cell fibroblastoma.[20,21] By far the best known phenomenon to all pathologists are malignant mixed germ cell tumors of the gonads that may reveal various and entirely different components within that same tumor mass including seminoma, embryonal carcinoma, teratoma, yolk sac tumor, or choriocarcinoma. All the components of malignant mixed germ cell tumors have a different immunohistochemical profile as α-fetoprotein is usually seen only in yolk sac tumor, CD30 in the embryonal carcinoma, and diffuse cytokeratin positivity is seen in most components of malignant germ cell tumors, leaving out a seminoma component. Notwithstanding this, genetically all components of malignant mixed germ cell tumors reveal the presence of the i12 iso-chromosome similar to the presence of a break in the *ETV6* gene in all components of the tumor we report herein.

In summary, we present a hitherto undescribed salivary gland tumor composed of a minor classic MASC component, a major mucinous adenocarcinoma component, and a morphologically nondescript, low-grade intraductal (in situ) component. Despite different immunohistochemical profiles, the presence of a break in the *ETV6* gene in all 3 components points strongly toward the same histogenesis of all tumor parts.

REFERENCES

1. Skalova A, Vanecek T, Sima R, et al. Mammary analogue secretory carcinoma of salivary glands, containing the ETV6-NTRK3 fusion gene: a hitherto undescribed salivary gland tumor entity. *Am J Surg Pathol*. 2010;34:599–608.
2. Bishop JA, Yonescu R, Batista D, et al. Utility of mammaglobin immunohistochemistry as a proxy marker for the ETV6-NTRK3 translocation in the diagnosis of salivary mammary analogue secretory carcinoma. *Hum Pathol*. 2013;44:1982–1988.
3. Bishop JA. Unmasking MASC: bringing to light the unique morphologic, immunohistochemical and genetic features of the newly recognized mammary analogue secretory carcinoma of salivary glands. *Head Neck Pathol*. 2013;7:35–39.
4. Connor A, Perez-Ordonez B, Shago M, et al. Mammary analog secretory carcinoma of salivary gland origin with the ETV6 gene rearrangement by FISH: expanded morphologic and immunohistochemical spectrum of a recently described entity. *Am J Surg Pathol*. 2012;36:27–34.
5. Skalova A, Vanecek T, Majewska H, et al. Mammary analogue secretory carcinoma of salivary glands with high-grade transformation: report of 3 cases with the ETV6-NTRK3 gene fusion and analysis of TP53, beta-catenin, EGFR, and CCND1 genes. *Am J Surg Pathol*. 2014;38:23–33.
6. Jung MJ, Song JS, Kim SY, et al. Finding and characterizing mammary analogue secretory carcinoma of the salivary gland. *Korean J Pathol*. 2013;47:36–43.
7. Luo W, Lindley SW, Lindley PH, et al. Mammary analog secretory carcinoma of salivary gland with high-grade histology arising in hard palate, report of a case and review of literature. *Int J Clin Exp Pathol*. 2014;7:9008–9022.
8. Skalova A, Vanecek T, Simpson RH, et al. Mammary analogue secretory carcinoma of salivary glands: molecular analysis of 25 ETV6 gene rearranged tumors with lack of detection of classical ETV6-NTRK3 fusion transcript by standard RT-PCR: report of 4 cases harboring ETV6-X gene fusion. *Am J Surg Pathol*. 2016;40:3–13..
9. Viswanatha DS, Foucar K, Berry BR, et al. Blastic mantle cell leukemia: an unusual presentation of blastic mantle cell lymphoma. *Mod Pathol*. 2000;13:825–833.
10. Gaffney R, Chakerian A, O'Connell JX, et al. Novel fluorescent ligase detection reaction and flow cytometric analysis of SYT-SSX fusions in synovial sarcoma. *J Mol Diagn*. 2003;5:127–135.
11. Antonescu CR, Kawai A, Leung DH, et al. Strong association of SYT-SSX fusion type and morphologic epithelial differentiation in synovial sarcoma. *Diagn Mol Pathol*. 2000;9:1–8.
12. Bourgeois JM, Knezevich SR, Mathers JA, et al. Molecular detection of the ETV6-NTRK3 gene fusion differentiates congenital fibrosarcoma from other childhood spindle cell tumors. *Am J Surg Pathol*. 2000;24:937–946.
13. Patel KR, Solomon IH, El-Mofty SK, et al. Mammaglobin and S-100 immunoreactivity in salivary gland carcinomas other than mammary analogue secretory carcinoma. *Hum Pathol*. 2013;44:2501–2508.
14. Laco J, Svajdler M Jr., Andrejs J, et al. Mammary analog secretory carcinoma of salivary glands: a report of 2 cases with expression of basal/myoepithelial markers (calponin, CD10 and p63 protein). *Pathol Res Pract*. 2013;209:167–172.
15. Majewska H, Skálová A, Stodulski D, et al. Mammary analogue secretory carcinoma of salivary glands: a new entity associated with ETV6 gene rearrangement. *Virchows Arch*. 2015;466:245–254.
16. Ito Y, Ishibashi K, Masaki A, et al. Mammary analogue secretory carcinoma of salivary glands: a clinicopathological and molecular study including 2 cases harboring *ETV6-X* fusion. *Am J Surg Pathol*. 2015;39:602–610.
17. Kazakov DV, Soukup R, Mukenšnabl P, et al. Brooke-Spiegler syndrome: report of a case with combined lesions containing

cylindromatous, spiradenomatous, trichoblastomatous and sebaceous differentiation. *Am J Dermatopathol*. 2005;27:27–33.
18. Kazakov DV, Kutzner H, Mukensnabl P, et al. Cutaneous malignant adnexal neoplasms with multidirectional differentiation (glandular, trichoblastomatous, spiradenocylindromatous) differentiation. *Am J Dermatopathol*. 2006;28:341–345.
19. Kazakov DV, Zelger B, Rütten A, et al. Morphological diversity of malignant tumors arising in preexisting spiradenoma, cylindroma and spiradenocylindroma based on the study of 24 cases, sporadic or occurring in the setting of Brooke-Spiegler syndrome. *Am J Surg Pathol*. 2009;33:705–719.
20. Michal M, Zámečník M. Giant cell fibroblastoma with a dermatofibrosarcoma protuberans component. *Am J Dermatopathol*. 1992;14:549–552.
21. Zámečník M, Michal M. Giant cell fibroblastoma with pigmented dermatofibrosarcoma protuberans component. *Am J Surg Pathol*. 1994;18:736–740.

2.2.4. SPECTRUM OF LESIONS DERIVED FROM BRANCHIAL ARCHES OCCURRING IN THE THYROID: FROM SOLID CELL NESTS TO TUMORS

The purpose of this manuscript was to review and report the morphological spectrum of thyroid lesions derived from branchial arches and related structures, i.e. in the thyroid mainly from ultimobranchial body. When inflamed, these structures lead to formation of cystic spaces that are lined by squamous or glandular epithelium and surrounded by inflammatory infiltrate which focally forms germinal centers.

To investigate the spectrum of such thyroid lesions, the consultation files were reviewed for thyroid samples containing pathological structures regarded to arise from the ultimobranchial body. Positive reaction with antibodies against CK5/6, p63, galectin 3, and CEA, and negative reaction with antibodies against thyroglobulin, TTF-1, and calcitonin were used to confirm the diagnosis. The specific subtype of the ultimobranchial body-derived lesion was then determined based on histological examination of H&E-stained slides. Twenty-one cases of ultimobranchial body-derived lesions were retrieved from the consultation files, 20 of them along with clinical information (M/F = 6/14,mean age 55 years, range 36–68 years). Lesions derived from the ultimobranchial body were classified as follows: (hyperplastic) solid cell nests (nine cases), solid cell nests with focal cystic change (five cases), cystic solid cell nests (two cases), branchial cleft-like cyst (four cases), and finally a peculiar case of Warthin tumor-like lesion (already reported previously by us in a separate case reported and discussed above. We suggested that the common denominator of these structures is that they all arise due to activation of inflammatory cells around the vestigial structures, which leads to cystic dilatation and proliferation of the epithelial component.

Virchows Arch
DOI 10.1007/s00428-017-2201-4

ORIGINAL ARTICLE

Spectrum of lesions derived from branchial arches occurring in the thyroid: from solid cell nests to tumors

Kristyna Srbecka[1] · Kvetoslava Michalova[1,2] · Radmila Curcikova[2,3] · Michael Michal Jr.[2,4] · Magdalena Dubova[1,2] · Marian Svajdler[1,2] · Michal Michal[1] · Ondrej Daum[1,2]

Received: 24 January 2017 / Revised: 23 June 2017 / Accepted: 10 July 2017

Abstract There is a group of lesions in the head and neck region derived from branchial arches and related structures which, when inflamed, are characterized by the formation of cysts lined by squamous or glandular epithelium and surrounded by a heavy inflammatory infiltrate rich in germinal centers. In the thyroid, the main source of various structures which may cause diagnostic dilemma is the ultimobranchial body. To investigate the spectrum of such thyroid lesions, the consultation files were reviewed for thyroid samples containing pathological structures regarded to arise from the ultimobranchial body. Positive reaction with antibodies against CK5/6, p63, galectin 3, and CEA, and negative reaction with antibodies against thyroglobulin, TTF-1, and calcitonin were used to confirm the diagnosis. The specific subtype of the ultimobranchial body-derived lesion was then determined based on histological examination of H&E-stained slides. Twenty-one cases of ultimobranchial body-derived lesions were retrieved from the consultation files, 20 of them along with clinical information (M/F = 6/14, mean age 55 years, range 36–68 years). Lesions derived from the ultimobranchial body were classified as follows: (hyperplastic) solid cell nests (nine cases), solid cell nests with focal cystic change (five cases), cystic solid cell nests (two cases), branchial cleft-like cyst (four cases), and finally a peculiar Warthin tumor-like lesion (one case). We suggest that the common denominator of these structures is that they all arise due to activation of inflammatory cells around the vestigial structures, which leads to cystic dilatation and proliferation of the epithelial component.

Keywords Thyroid · Branchial arch · Ultimobranchial body · Solid cell nest · Warthin tumor

✉ Ondrej Daum
DAUM@fnplzen.cz

[1] Sikl's Department of Pathology, University Hospital Plzen, Medical Faculty in Plzen, Charles University in Prague, Edvarda Benese 13, Plzen 305 99, Czech Republic

[2] Biopticka laborator s.r.o, Plzen, Czech Republic

[3] Department of Pathology, Liberec Regional Hospital, Liberec, Czech Republic

[4] Biomedical Center, University Hospital Plzen, Medical Faculty in Plzen, Charles University in Prague, Plzen, Czech Republic

Introduction

Remnants of the branchial arches and related structures occurring in the head and neck region, when inflamed, give rise to a group of lesions characterized by the formation of cysts lined by squamous or glandular epithelium and enveloped by a lymphoid cuff rich in germinal centers. These lesions include the branchial cleft cyst [1], lymphoepithelial cyst of the salivary gland region, multilocular thymic cyst [2], and possibly even the enigmatic ectopic hamartomatous thymoma [3].

Furthermore, the ultimobranchial body, derived from the inferior branchial arches, is a source from which various structures such as solid cell nests (SCNs) in the thyroid originate [4]. SCNs and other vestigial structures derived from the branchial arches are prone to cystic dilation and proliferation of the epithelial component with possible epithelial metaplasia when engaged in an inflammatory process. The epithelial proliferation may result in papillary rearrangement of the epithelial lining. Due to this morphological plasticity, lesions in the head and neck region derived from branchial arches and related structures constitute a myriad of morphological patterns.

Published online: 20 July 2017

In most cases, H&E slides suffice to identify the branchial origin of an investigated lesion, while in others, immunohistochemistry provides vital data as it has been recorded that SCNs are CK5/6, p63, p40, CEA, and galectin 3 positive, and calcitonin, thyroglobulin, and TTF-1 negative, although the expression of the latter two has proven to be rather controversial [5].

Our consultation files were reviewed for thyroid cases containing pathological structures assumed to arise from the ultimobranchial body to investigate the morphological spectrum of thyroid lesions derived from vestigia of the branchial arches.

Materials and methods

For the purposes of this study, we reviewed the authors' consultation files to find thyroid cases containing pathological structures regarded to have arisen from the ultimobranchial body. Key words "ultimobranchial body," "solid cell nests," "branchial," and "thyroid" were used to search for the cases in the consultation files. As the consultation files do not represent general archives of a single institution, but were designed to collect difficult and interesting cases originating not only from our institutions, but also sent for consultation from various other departments of pathology, it is impossible to estimate the prevalence of such lesions or their frequency among thyroid resection specimens. The slides, stained with H&E, were assessed for the presence of patterns indicating ultimobranchial origin. This origin was then confirmed immunohistochemically. For the immunohistochemical investigations, the following primary antibodies were used: Thyroglobulin (polyclonal, RTU, Dako, Glostrup, Denmark), Thyroglobulin (2H11+6E1, RTU, Ventana, Tucson, AZ), TTF-1 (8G7G3/1, 1:100, Dako, Glostrup, Denmark), TTF-1 (SPT24, 1:400, Novocastra, Newcastle, UK), calcitonin (polyclonal, RTU, Ventana, Tucson, AZ), Ki-67 (30-9, RTU, Ventana, Tucson, AZ), Galectin 3 (9C4, RTU, Ventana, Tucson, AZ), p63 Protein (4A4, 1:200, Dako, Glostrup, Denmark), Cytokeratin 5/6 (DB5/16B4, 1:50, Dako, Glostrup, Denmark), Carcinoembryonic Antigen (CEA) (II-7, 1:200, Dako, Glostrup, Denmark). No special pre-treatment was used. Appropriate positive and negative control slides were employed. Positive reaction with antibodies against CK5/6, p63, CEA, and galectin 3, and negative reaction with antibodies against thyroglobulin, TTF-1, and calcitonin were used to confirm ultimobranchial origin. The specific subtype of the ultimobranchial body-derived lesion was then determined based on histological examination of H&E-stained slides. "(Hyperplastic) SCNs" were defined as nests larger than 0.1 mm in their greatest dimension and/or aggregated into nodules composed of nests devoid of cystic spaces. "SCNs with subtle (or partial) focal cystic change" contained small cavities sized up to about five times the size of a main cell, the solid component remaining the dominant part of the lesion, while "cystic SCNs" contained larger cystic spaces forming the majority of the lesion's volume. In addition to the steps described above, background changes in the surrounding thyroid gland were evaluated histologically.

Results

Twenty-one cases of ultimobranchial body-derived lesions were retrieved from the consultation files; clinical information was available for 20 of them (M/F = 6/14, mean age 55 years, range 36–68 years). Available clinical and pathological data is shown in Table 1. Briefly, one patient underwent surgery for thyrotoxicosis, eight for nodular goiter, one for goiter with hypothyroidism, one for diffuse goiter, four for Hashimoto thyroiditis, one for Graves' disease, one for suspected follicular neoplasia (based on fine needle aspiration cytology), and one for suspected papillary carcinoma (based on fine needle aspiration cytology); the cause of surgery was not known in three cases. Lesions derived from the ultimobranchial body were classified as follows: (hyperplastic) SCNs (nine cases, Figs. 1, 2, 3), SCNs with subtle focal cystic change (five cases, Fig. 4), cystic SCNs (two cases), branchial cleft-like cysts (four cases, all associated with SCNs, Fig. 5), and finally a tumor 15 mm in size composed of a part containing clusters of SCNs, a part with morphological features of a branchial cleft-like cyst, and finally a part resembling a Warthin tumor (Fig. 6). Details on the ultimobranchial body-related lesions are shown in Table 2. Immunohistochemically, the cells lining the Warthin tumor-like structure, as well as the epithelial lining of branchial cleft-like cysts and the main cells of SCNs, were positive for CK5/6, p63, and galectin 3, focally for CEA, but negative for thyroglobulin and calcitonin, with the exception of case 10, which showed several individual calcitonin-positive C cells scattered within SCNs with subtle focal cystic transformation (Fig. 7). TTF-1 was negative with the Dako antibody but, in 14 cases, weakly positive with the antibody manufactured by Novocastra. In all the cases of branchial cleft-like cysts, SCNs were present in the surrounding thyroid tissue, in one case showing cystic change with cystic spaces communicating with the labyrinth-like cystic structures of the branchial cleft-like cyst, thus representing its most distal outpouchings. In the surrounding thyroid tissue, Hashimoto thyroiditis was found in 16 cases (5 of them representing the fibrous variant of the disease), multinodular colloid goiter was diagnosed in 1 case, and Graves' disease occurred in 1 case. Further histological findings included the following: follicular adenoma (one case), papillary microcarcinoma (one case), papillary thyroid carcinoma (one case), and MALT lymphoma (one case). No parathyroid tissue or thymus-like remnants were found in the proximity of any of the described lesions.

Table 1 Clinical and pathological data

Case	Sex	Age	Clinical diagnosis	Ultimobranchial body-related findings	Other findings
1	F	36	Nodular goiter	Cystic solid cell nests	Hashimoto thyroiditis
2	F	54	Nodular goiter	Solid cell nests	Multinodular colloid goiter
3	F	53	Hashimoto thyroiditis	Solid cell nests, some with cystic change	Fibrous Hashimoto thyroiditis
4	NA	NA	NA	Solid cell nests, branchial cleft-like cyst	Fibrous Hashimoto thyroiditis
5	F	68	Hashimoto thyroiditis with hypothyroidism	Solid cell nests	Hashimoto thyroiditis
6	F	61	Nodular goiter	Solid cell nests, some with cystic change	Hashimoto thyroiditis
7	F	60	Nodular goiter	Solid cell nests, some with cystic change	Hashimoto thyroiditis
8	F	57	Graves' disease	Solid cell nests	Graves' disease
9	M	52	Nodular goiter	Solid cell nests, some with cystic change	Hashimoto thyroiditis
10	M	59	Thyroid nodule suspected to be follicular neoplasia based on FNAC	Solid cell nests with focal cystic change	Follicular adenoma
11	M	65	Goiter with hypothyroidism	Solid cell nests, branchial cleft-like cyst (20 mm)	Fibrous Hashimoto thyroiditis
12	F	50	Probably papillary carcinoma based on FNAC	Solid cell nests	Hashimoto thyroiditis
13	F	64	NA	Solid cell nests	Hashimoto thyroiditis
14	F	40	Thyrotoxicosis	Solid cell nests	Papillary microcarcinoma
15	M	47	NA	Solid cell nests	Fibrous Hashimoto thyroiditis
16	F	42	Hashimoto thyroiditis	Cystic solid cell nests	Hashimoto thyroiditis
17	M	67	Diffuse goiter	Solid cell nests	MALT lymphoma
18	M	52	Hashimoto thyroiditis	Solid cell nests	Hashimoto thyroiditis
19	F	57	Nodular goiter	Solid cell nests, branchial cleft-like cyst	Fibrous Hashimoto thyroiditis
20	F	55	Nodular goiter	Solid cell nests, branchial cleft-like cyst	Hashimoto thyroiditis, PTC
21	F	58	Nodular goiter	Benign Warthin-like tumor (15 mm), ultimobranchial cleft-like cyst, solid cell nests	Hashimoto thyroiditis

NA not available, *FNAC* fine needle aspiration cytology

Discussion

Our series comprised cases of SCNs, branchial cleft-like cysts, and a peculiar Warthin tumor-like lesion intimately associated with a branchial cleft-like cyst and surrounded by SCNs. The most common background diagnosis in our subject group was Hashimoto thyroiditis.

SCNs have been noted to occur incidentally, although not exclusively so [6], in the lateral lobes of the normal thyroid gland as well as having been discovered in association with neoplastic or non-neoplastic lesions [7, 8]; altogether, their presence was recorded in up to 61% of serially sectioned thyroids [9]. However, they were only found in 1.3–6% of routinely processed thyroid surgery specimens [4, 6, 9–12]. It is widely accepted that SCNs are indeed ultimobranchial body remnants [4, 8, 9, 13, 14]. The extent of SCNs' presence in the thyroid appears to be a largely random phenomenon; in examining 1390 thyroids, Martin et al. found no significant correlation between the occurrence of SCNs and either age or thyroid lesion type [8]. The fact that in our study SCNs were found in association to pathological lesions (most often Hashimoto thyroiditis) does not challenge Martin's conclusion, as our sample group was composed of material taken from patients for diagnostic purposes and did not include samples obtained from healthy controls. In our series, Hashimoto thyroiditis, characterized by a diffuse lymphoplasmacytic infiltration, variable in its intensity and effacement of the follicles, with focal formation of germinal centers, commonly seen in association with oncocytic change of thyrocytes, was found in 75% of cases. This is significantly higher than the average frequency of Hashimoto thyroiditis in our general thyroidectomy specimens (8%). We hypothesize that this extraordinarily high frequency may be explained by selection bias; our series is mostly made up of cases consulted because of their eye-catching or difficult-to-interprete, probably reactive changes of SCNs. It is possible that chronic inflammation

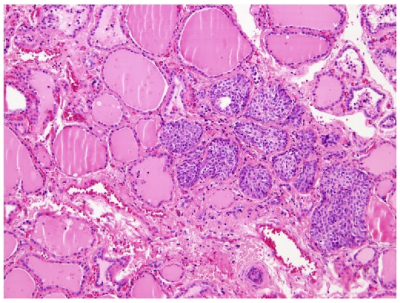

Fig. 1 Case 2. An ordinary focus of solid cell nests found incidentally in a multinodular colloid goiter (H&E, ×100)

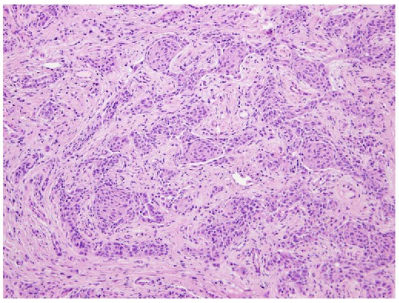

Fig. 3 Case 15. In rare cases, the foci of solid cell nests may reach even grossly visible dimensions and may simulate neoplastic growth (H&E, ×100)

serves as a cofactor in the pathogenesis of these changes, which may explain the frequent finding of Hashimoto thyroiditis in our study group.

SCNs and related structures are readily distinguishable from the follicular architecture of the thyroid parenchyma; they are formed by cells packed together in compact, solid clusters 0.1 mm or less in size. SCNs consist primarily of two populations of cells: main cells and C cells [4]. Main cells, which mainly account for SCN cellularity, are of elongated shape and contain centrally located frequently grooved oval nuclei devoid of pseudoinclusions and surrounded by eosinophilic cytoplasm, in contrast to C cells, which are characterized by clear cytoplasm and round nuclei [4, 5]. It has been suggested that main cells function as pluripotent cells, contributing to the histogenesis of C cells, follicular cells, perhaps even ectopic salivary gland tissue, and tumorigenesis of specific tumors [7, 15–19]. Four distinct types of SCNs have been described: (floret-like) type 1 composed mostly of main cells surrounded by lymphocyte clusters; (epidermoid-like) type 2 made up of large polygonal cells with plentiful cytoplasm and clearly defined cell boundaries; type 3 presenting flat or large polygonal cells enveloping cystic structures; type 4 defined as mixed follicles (structures lined by both main and follicular epithelium) [5, 9, 20]. Parafolicullar C cells are known to express calcitonin, chromogranin, TTF-1, and CEA [21]. Main cells are immunohistochemically characterized by the expression of p63 [5, 22–25], p40 [10], galectin 3 [10, 25, 26], and CK19 [10]. Staining for TTF-1, thyroglobulin, and HBME-1 in SCNs represents a controversial issue; while TTF-1 was reported to be negative by Reis-Filho et al. [24], Rios Moreno et al. detected TTF-1 in some SCN cells, mainly those of type 4 (mixed follicles) [25], and others found weak, but unequivocal diffuse positivity of main cells when stained with clone 8G7G3/1 manufactured by Dako [5, 27]. In our study, all SCNs and SCN-derived lesions were negative with the same Dako antibody, but used in higher dilution, whereas they were weakly positive in reaction with the antibody manufactured by Novocastra. Thyroglobulin is traditionally regarded as a negative marker of SCNs [4, 5, 25]; nevertheless, it has been reported to be focally positive in mixed follicles (type 4 SCN) [28–30]. HBME-1 was reported to be negative by Asioli et al. [5], but found positive in type 1 SCN by Seethala et al. [31], and detected focally in two cases by Manzoni et al. [10]; these findings cast doubt on the usefulness of these immunohistochemical markers in the differential diagnosis between SCNs (mainly type 1) and papillary microcarcinoma typically positive for CK19, galectin 3, and HBME-1.

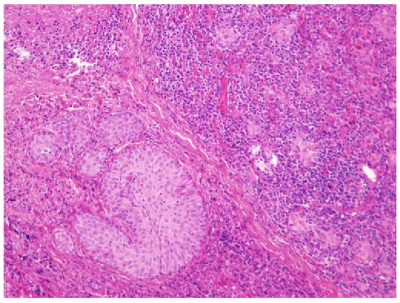

Fig. 2 Case 12. Solid cell nests are quite commonly found on the background of autoimmune thyroiditis (H&E, ×100)

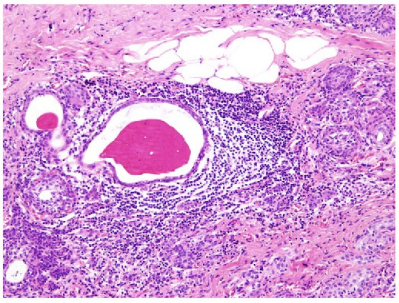

Fig. 4 Case 6. Quite commonly, mainly in association with lymphocytic inflammatory infiltrate, solid cell nests show cystic changes (H&E, ×100)

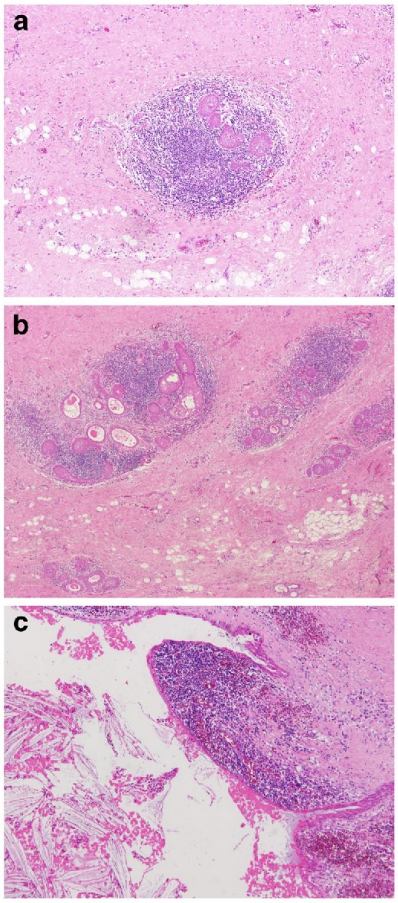

Fig. 5 Case 11. This thyroid contained solid cell nests associated with lymphocytic inflammatory infiltrate (**a**, H&E, ×40), focal discrete cystic changes (**b**, H&E, ×40), and an adjacent branchial cleft-like cyst (**c**, H&E, ×40)

In fact, the distinction between SCNs and papillary (micro)carcinoma is mainly based on the hematoxylin and eosin appearance (SCNs typically present with distinctly lobular architecture, coexistence of cystic areas, and a predominantly oval shape of the nuclei lacking pseudoinclusions) along with negative staining of SCNs for thyroglobulin and TTF-1, and their strong nuclear staining for p63.

C cell hyperplasia and medullary carcinoma are diffusely positive for calcitonin, whereas SCNs are either negative or contain only scattered individual C cells.

Ectopic thymic tissue typically presents as a nodule packed with small lymphocytes, containing cystically dilated Hassall's corpuscles. Even if the islands of thymic tissue are composed almost exclusively of epithelial elements devoid of the typical Hassall's corpuscles, differential diagnosis against SCNs is not of crucial importance, as both lesions are benign. Carcinoma showing thymus-like elements (CASTLE) forms a real neoplastic mass composed of irregular nests of atypical squamoid, spindled, or syncytial cells usually showing strong diffuse membranous CD5 staining.

Metastatic squamous cell carcinoma usually presents some degree of nuclear atypia. Furthermore, personal history may be of vital importance in such cases.

Lymphoepithelial branchial cleft cysts typically occur in the lateral areas of the neck and are lined by predominantly squamous and sometimes columnar epithelium. Their wall contains dense lymphoid tissue that often forms follicles [1]. Similar cysts have been published under various names such

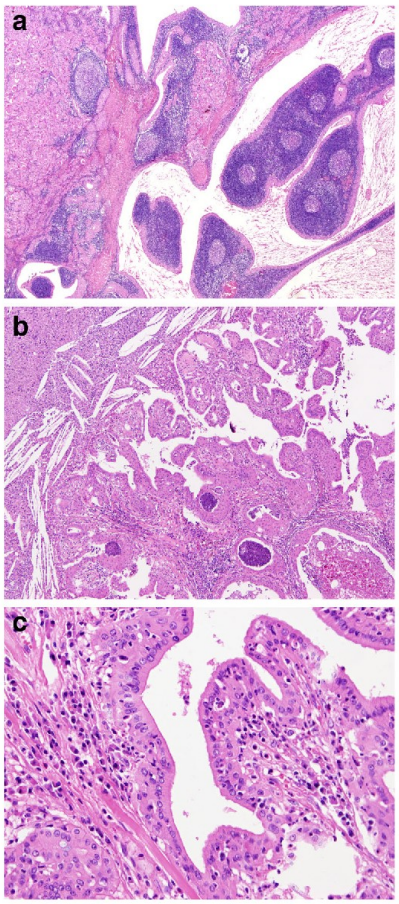

Fig. 6 Case 21. The most interesting case displayed features of Hashimoto thyroiditis with solid cell nests associated with a branchial cleft-like cyst merging with structures reminiscent of the Warthin tumor of salivary glands (**a**, H&E, ×40), (**b**, H&E, ×100), (**c**, H&E, ×200)

Table 2 Details on ultimobranchial body-related lesions

Case	Site	Focality	Size	Cell types	Immunohistochemical findings
1	Right lobe	Unifocal	Nodule sized 15 mm composed of nests sized 0.1–1 mm	Main cells, squamous cells	Positive: p63, CK5/6, galectin 3, focal CEA Negative: thyroglobulin, calcitonin, TTF-1
2	Left lobe	Multifocal	0.1–0.5 mm	Main cells	Positive: p63, CK5/6, galectin 3, focal CEA Negative: thyroglobulin, calcitonin, TTF-1 Dako (but Novocastra weakly positive)
3	Right lobe	Multifocal	0.1–0.9 mm	Main cells	Positive: p63, CK5/6, galectin 3, focal CEA Negative: thyroglobulin, calcitonin, TTF-1 Dako (but Novocastra weakly positive)
4	NA	Unifocal	Cyst 18 mm in size, surrounded by solid cell nests 0.1–0.6 mm	Main cells, squamous cells	Positive: p63, CK5/6, galectin 3, focal CEA Negative: thyroglobulin, calcitonin, TTF-1 Dako (but Novocastra weakly positive)
5	Right lobe	Multifocal	0.2–0.4 mm	Main cells	Positive: p63, CK5/6, galectin 3, focal CEA Negative: thyroglobulin, calcitonin, TTF-1
6	Both lobes	Multifocal	0.1–1 mm	Main cells, squamous cells, columnar cells	Positive: p63, CK5/6, galectin 3, focal CEA Negative: thyroglobulin, calcitonin, TTF-1 Dako (but Novocastra weakly positive)
7	Right lobe	Multifocal	0.1–0,5 mm	Main cells, squamous cells, columnar cells	Positive: p63, CK5/6, galectin 3, focal CEA Negative: thyroglobulin, calcitonin, TTF-1 Dako (but Novocastra weakly positive)
8	Both lobes	Multifocal	0.05–0.3 mm	Main cells, squamous cells	Positive: p63, CK5/6, galectin 3, focal CEA Negative: thyroglobulin, calcitonin, TTF-1 Dako (but Novocastra weakly positive)
9	Right lobe	Multifocal	0.05–0.4 mm	Main cells	Positive: p63, CK5/6, galectin 3, focal CEA Negative: thyroglobulin, calcitonin, TTF-1
10	Right lobe	Unifocal	Cluster 3 mm composed of SCNs sized 0.1–0.3 mm	Main cells, individual scattered C cells	Positive: p63, CK5/6, galectin 3, focal CEA; calcitonin in C-cells Negative: thyroglobulin, TTF-1 Dako (but Novocastra weakly positive)
11	Right lobe	Unifocal	Cyst sized 40 × 40 × 50 mm surrounded by solid cell nests 0.1–0.4 mm	Main cells, squamous cells, columnar cells	Positive: p63, CK5/6, galectin 3, focal CEA Negative: thyroglobulin, calcitonin, TTF-1 Dako (but Novocastra weakly positive)
12	Both lobes	Multifocal	0.05–0.3 mm	Main cells	Positive: p63, CK5/6, galectin 3, focal CEA Negative: thyroglobulin, calcitonin, TTF-1
13	NA	Unifocal	Cluster 2 mm in diameter composed of SCNs sized 0.05–1.5 mm	Main cells	Positive: p63, CK5/6, galectin 3, focal CEA Negative: thyroglobulin, calcitonin, TTF-1 Dako (but Novocastra weakly positive)
14	Left lobe	Multifocal	0.05–0.1 mm	Main cells	Positive: p63, CK5/6, galectin 3, focal CEA Negative: thyroglobulin, calcitonin, TTF-1 Dako (but Novocastra weakly positive)
15	NA	Multifocal	0.1–0.3 mm	Main cells	Positive: p63, CK5/6, galectin 3, focal CEA Negative: thyroglobulin, calcitonin, TTF-1
16	Left lobe	Unifocal	2 mm	Main cells, squamous cells	Positive: p63, CK5/6, galectin 3, focal CEA Negative: thyroglobulin, calcitonin, TTF-1
17	Left lobe	Multifocal	0.05–0.2 mm	Main cells	Positive: p63, CK5/6, galectin 3, focal CEA Negative: thyroglobulin, calcitonin, TTF-1 Dako (but Novocastra weakly positive)
18	NA	Multifocal	0.1–0.3 mm	Main cells	Positive: p63, CK5/6, galectin 3, focal CEA Negative: thyroglobulin, calcitonin, TTF-1 Dako (but Novocastra weakly positive)
19	Right lobe	Unifocal	14 mm	Main cells, squamous cells	Positive: p63, CK5/6, galectin 3, focal CEA Negative: thyroglobulin, calcitonin, TTF-1 Dako (but Novocastra weakly positive)
20	Right lobe	Unifocal	Cyst 13 mm in size surrounded by solid cell nests sized 0.1–0.3 mm	Main cells, squamous cells, columnar cells	Positive: p63, CK5/6, galectin 3, focal CEA Negative: thyroglobulin, calcitonin, TTF-1
21	Right lobe	Unifocal	15 mm	Main cells, squamous cells, columnar cells, oncocytic cells	Positive: p63, CK5/6, galectin 3, focal CEA Negative: thyroglobulin, calcitonin, TTF-1 Dako (but Novocastra weakly positive)

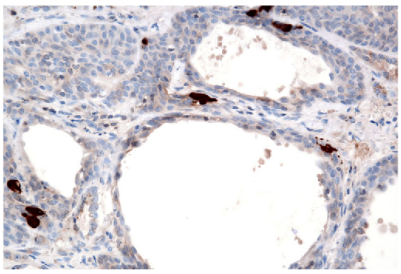

Fig. 7 Case 10. Individual scattered C cells can be found in rare solid cell nests with focal subtle cystic change (calcitonin, polyclonal, Ventana, ×400)

as branchial cleft-like cysts [32–35], lymphoepithelial cysts of the thyroid [36–38], and others [39, 40]. Occasional reports on lymphoepithelial cysts associated with thymic anlage or parathyroid tissue suggest a branchial cleft origin [36, 41]. This suggestion is further supported by reports describing SCNs occurring in close proximity to lymphoepithelial cysts, sparking belief these cysts may share their embryological origin with SCNs, as indeed appears to be true in the cases we examined [33, 35–38, 40]. What is more, in one of our cases, published previously as a case report [42], the labyrinth-like cystic structures of the branchial cleft-like cyst were found to communicate with cystic spaces of the adjacent SCNs showing cystic change, which seems to be an indirect but compelling proof that lymphoepithelial branchial cleft-like cysts and SCNs share a similar embryological origin, namely the ultimobranchial body. In addition, both SCNs and branchial cleft-like cysts may occasionally be found in association with intrathyroid salivary gland tissue [15, 16, 35].

The unique Warthin tumor-like lesion (not to be confused with oncocytic papillary carcinoma with lymphoid stroma) composed of a dense lymphoid cuff surrounding a cystic cavity with papillary projections lined with columnar oncocytes devoid of "papillary" nuclear features, merging with a branchial cleft-like cyst, and associated with SCNs has already been published as a case report [43]. This case led us to hypothesize that all its three distinct regions might simply represent different stages of cystic dilation of the vestiges of branchial arches and related structures induced by Hashimoto thyroiditis [43]. Regardless of its precise neoplastic or non-neoplastic biological nature, from a practical point of view, the SCN-derived Warthin tumor-like lesion of the thyroid broadens the spectrum of thyroid tumors possibly derived from the ultimobranchial body rests (mainly mucoepidermoid carcinoma [17, 18, 44–46] and, although less convincingly, CASTLE [47, 48], small-cell basaloid carcinoma [49], and papillary thyroid carcinoma [7]).

In conclusion, we present a series of thyroid lesions probably derived from the ultimobranchial body, which encompasses a wide spectrum of morphological structures. We hypothesize that all these structures arose from SCNs under the influence of activation of lymphoid tissue surrounding these vestigial structures, leading to cystic dilation, proliferation, and metaplastic changes of the epithelial component, thus enabling the development of cystic SNCs, branchial cleft-like cysts, benign tumors resembling the Warthin tumor of salivary glands, and even malignant tumors, most frequently the mucoepidermoid carcinoma of the thyroid.

Acknowledgments The study was supported by the Ministry of education, youth and sports grant SVV-2017-260 39.

Compliance with ethical standards The study design has been approved by the local ethics committee (Charles University, Medical School Plzen) LEK FN Plzen. For this type of study, formal consent is not required.

Funding This study was supported by the Ministry of education, youth and sports grant SVV-2017-260 39.

Conflict of interest The authors declare that they have no conflict of interest.

References

1. Bhaskar SN, Bernier JL (1959) Histogenesis of branchial cysts; a report of 468 cases. Am J Pathol 35:407–443
2. Suster S, Rosai J (1991) Multilocular thymic cyst: an acquired reactive process. Study of 18 cases. Am J Surg Pathol 15:388–398
3. Weissferdt A, Kalhor N, Petersson F, Moran CA (2016) Ectopic hamartomatous thymoma-new insights into a challenging entity: a clinicopathologic and immunohistochemical study of 9 cases. Am J Surg Pathol 40:1571–1576. doi:10.1097/PAS.0000000000000699
4. Cameselle-Teijeiro J, Varela-Duran J, Sambade C, Villanueva JP, Varela-Nunez R, Sobrinho-Simoes M (1994) Solid cell nests of the thyroid: light microscopy and immunohistochemical profile. Hum Pathol 25:684–693
5. Asioli S, Erickson LA, Lloyd RV (2009) Solid cell nests in Hashimoto's thyroiditis sharing features with papillary thyroid microcarcinoma. Endocr Pathol 20:197–203. doi:10.1007/s12022-009-9095-x
6. Ozaki O, Ito K, Sugino K, Yasuda K, Yamashita T, Toshima K, Hosoda Y (1991) Solid cell nests of the thyroid gland. Virchows Arch A Pathol Anat Histopathol 418:201–205
7. Cameselle-Teijeiro J, Abdulkader I, Perez-Becerra R, Vazquez-Boquete A, Alberte-Lista L, Ruiz-Ponte C, Forteza J, Sobrinho-Simoes M (2009) BRAF mutation in solid cell nest hyperplasia associated with papillary thyroid carcinoma. A precursor lesion? Hum Pathol 40:1029–1035. doi:10.1016/j.humpath.2008.11.015
8. Martin V, Martin L, Viennet G, Challier B, Carbillet J, Fellmann D (2000) "Solid cell nests" et pathologies thyroïdiennes étude retrospective de 1 390 thyroïdes. Ann Pathol 20:196–201
9. Harach HR (1988) Solid cell nests of the thyroid. J Pathol 155:191–200. doi:10.1002/path.1711550303
10. Manzoni M, Roversi G, Di Bella C, Pincelli AI, Cimino V, Perotti M, Garancini M, Pagni F (2016) Solid cell nests of the thyroid gland: morphological, immunohistochemical and genetic features. Histopathology 68:866–874. doi:10.1111/his.12858
11. Yamaoka Y (1973) Solid cell nest (SCN) of the human thyroid gland. Acta Pathol Jpn 23:493–506

12. Janzer RC, Weber E, Hedinger C (1979) The relation between solid cell nests and C cells of the thyroid gland: an immunohistochemical and morphometric investigation. Cell Tissue Res 197:295–312
13. Williams ED, Toyn CE, Harach HR (1989) The ultimobranchial gland and congenital thyroid abnormalities in man. J Pathol 159: 135–141. doi:10.1002/path.1711590208
14. Beckner ME, Shultz JJ, Richardson T (1990) Solid and cystic ultimobranchial body remnants in the thyroid. Arch Pathol Lab Med 114:1049–1052
15. Cameselle-Teijeiro J, Varela-Duran J (1993) Salivary gland tissue associated with solid cell nests of the thyroid gland: a further prove of the ultimobranchial body origin of SCN. Pathol Res Pract 189: 663
16. Cameselle-Teijeiro J, Varela-Duran J (1994) Intrathyroid salivary gland-type tissue in multinodular goiter. Virchows Arch 425:331–334
17. Cameselle-Teijeiro J, Febles-Perez C, Sobrinho-Simoes M (1995) Papillary and mucoepidermoid carcinoma of the thyroid with anaplastic transformation: a case report with histologic and immunohistochemical findings that support a provocative histogenetic hypothesis. Pathol Res Pract 191:1214–1221. doi:10.1016/S0344-0338(11)81129-5
18. Cameselle-Teijeiro J (1996) Mucoepidermoid carcinoma and solid cell nests of the thyroid. Hum Pathol 27:861–863
19. Cameselle-Teijeiro J, Preto A, Soares P, Sobrinho-Simoes M (2005) A stem cell role for thyroid solid cell nests. Hum Pathol 36:590–591. doi:10.1016/j.humpath.2005.02.010
20. Vollenweider I, Hedinger C (1988) Solid cell nests (SCN) in Hashimoto's thyroiditis. Virchows Arch A Pathol Anat Histopathol 412:357–363
21. Chan JK, Tse CH (1988) Parafollicular C-cells do contain carcinoembryonic antigen. Am J Surg Pathol 12:247–248
22. Burstein DE, Nagi C, Wang BY, Unger P (2004) Immunohistochemical detection of p53 homolog p63 in solid cell nests, papillary thyroid carcinoma, and Hashimoto's thyroiditis: a stem cell hypothesis of papillary carcinoma oncogenesis. Hum Pathol 35:465–473
23. Preto A, Cameselle-Teijeiro J, Moldes-Boullosa J, Soares P, Cameselle-Teijeiro JF, Silva P, Reis-Filho JS, Reyes-Santias RM, Alfonsin-Barreiro N, Forteza J, Sobrinho-Simoes M (2004) Telomerase expression and proliferative activity suggest a stem cell role for thyroid solid cell nests. Mod Pathol 17:819–826. doi:10.1038/modpathol.3800124
24. Reis-Filho JS, Preto A, Soares P, Ricardo S, Cameselle-Teijeiro J, Sobrinho-Simoes M (2003) p63 expression in solid cell nests of the thyroid: further evidence for a stem cell origin. Mod Pathol 16:43–48. doi:10.1097/01.MP.0000047306.72278.39
25. Rios Moreno MJ, Galera-Ruiz H, De Miguel M, Lopez MI, Illanes M, Galera-Davidson H (2011) Immunohistochemical profile of solid cell nest of thyroid gland. Endocr Pathol 22:35–39. doi:10.1007/s12022-010-9145-4
26. Faggiano A, Talbot M, Baudin E, Bidart JM, Schlumberger M, Caillou B (2003) Differential expression of galectin 3 in solid cell nests and C cells of human thyroid. J Clin Pathol 56:142–143
27. Ryska A, Ludvikova M, Rydlova M, Cap J, Zalud R (2006) Massive squamous metaplasia of the thyroid gland—report of three cases. Pathol Res Pract 202:99–106. doi:10.1016/j.prp.2005.11.002
28. Harach HR (1985) Solid cell nests of the thyroid. An anatomical survey and immunohistochemical study for the presence of thyroglobulin. Acta Anat (Basel) 122:249–253
29. Harach HR (1987) Mixed follicles of the human thyroid gland. Acta Anat (Basel) 129:27–30
30. Autelitano F, Santeusanio G, Di Tondo U, Costantino AM, Renda F, Autelitano M (1987) Immunohistochemical study of solid cell nests of the thyroid gland found from an autopsy study. Cancer 59: 477–483
31. Seethala RR, Chiosea SI (2010) Solid cell nests, papillary thyroid microcarcinoma, and HBME1. Am J Clin Pathol 134:169–170. doi:10.1309/AJCPRL8M1PTKOUWZ
32. Louis DN, Vickery AL Jr, Rosai J, Wang CA (1989) Multiple branchial cleft-like cysts in Hashimoto's thyroiditis. Am J Surg Pathol 13:45–49
33. Delabie J, De Wolf-Peeters C, Cappelle L, Van Damme B, Desmet V (1990) Branchial cleftlike cysts of the thyroid. Am J Surg Pathol 14:1165–1167
34. Haba R, Miki H, Kobayashi S, Kushida Y, Saoo K, Hirakawa E, Ohmori M (2000) Intrathyroidal branchial cleft-like cyst in chronic thyroiditis. Pathol Int 50:897–900
35. Park JY, Kim GY, Suh YL (2004) Intrathyroidal branchial cleft-like cyst with heterotopic salivary gland-type tissue. Pediatr Dev Pathol 7:262–267. doi:10.1007/s10024-003-3022-9
36. Apel RL, Asa SL, Chalvardjian A, LiVolsi VA (1994) Intrathyroidal lymphoepithelial cysts of probable branchial origin. Hum Pathol 25:1238–1242
37. Ryska A, Vokurka J, Michal M, Ludvikova M (1997) Intrathyroidal lymphoepithelial cyst. A report of two cases not associated with Hashimoto's thyroiditis. Pathol Res Pract 193:777–781
38. Carter E, Ulusarac O (2003) Lymphoepithelial cysts of the thyroid gland. A case report and review of the literature. Arch Pathol Lab Med 127:e205–e208. doi:10.1043/0003-9985(2003)127<e205:LCOTTG>2.0.CO;2
39. Parham DM (1988) Laterally situated neck cysts derived from the embryological remnants of thyroid development. Histopathology 12:95–98
40. Miyauchi A, Matsuzuka F, Kuma K, Katayama S (1992) Piriform sinus fistula and the ultimobranchial body. Histopathology 20:221–227
41. Chetty R, Forder MD (1991) Parathyroiditis associated with hyperparathyroidism and branchial cysts. Am J Clin Pathol 96:348–350
42. Michal M, Mukensnabl P, Kazakov DV (2006) Branchial-like cysts of the thyroid associated with solid cell nests. Pathol Int 56:150–153
43. Peckova K, Daum O, Michal M, Curcikova R (2016) Selected case from the Arkadi M. Rywlin International Pathology Slide Seminar: benign Warthin tumor of the thyroid. Adv Anat Pathol 23:339–342. doi:10.1097/PAP.0000000000000123
44. Harach HR (1985) A study on the relationship between solid cell nests and mucoepidermoid carcinoma of the thyroid. Histopathology 9:195–207
45. Ozaki O, Ito K, Sugino K, Yasuda K, Yamashita T, Toshima K (1992) Solid cell nests of the thyroid gland: precursor of mucoepidermoid carcinoma? World J Surg 16:685–688 discussion 688-689
46. Baloch ZW, Solomon AC, LiVolsi VA (2000) Primary mucoepidermoid carcinoma and sclerosing mucoepidermoid carcinoma with eosinophilia of the thyroid gland: a report of nine cases. Mod Pathol 13:802–807. doi:10.1038/modpathol.3880140
47. Yerly S, Lobrinus JA, Bongiovanni M, Becker M, Zare M, Granger P, Pusztaszeri M (2013) A carcinoma showing thymus-like elements of the thyroid arising in close association with solid cell nests: evidence for a precursor lesion? Thyroid 23:511–516. doi:10.1089/thy.2011.0415
48. Reimann JD, Dorfman DM, Nose V (2006) Carcinoma showing thymus-like differentiation of the thyroid (CASTLE): a comparative study: evidence of thymic differentiation and solid cell nest origin. Am J Surg Pathol 30:994–1001
49. Cruz J, Eloy C, Agrues JM, Vinagre J, Sobrinho-Simoes M (2011) Small-cell (basaloid) thyroid carcinoma: a neoplasm with a solid cell nest histogenesis? Int J Surg Pathol 19:620–626. doi:10.1177/1066896911405320

2.2.5. MOLECULAR PROFILING OF MAMMARY ANALOG SECRETORY CARCINOMA REVEALED A SUBSET OF TUMORS HARBORING A NOVEL ETV6-RET TRANSLOCATION. REPORT OF 10 CASES

As briefly mentioned in the previous sections, MASC, a low-grade salivary gland carcinoma, usually harbors a characteristic *ETV6-NTRK3* gene fusion. However, in a small subset of these tumors, the *ETV6* had an unknown fusion partner, as the *NTRK3* gene rearrangements were not found in this fraction and were provisionally labeled as *ETV6-X* MASCs [62]. In this study, we analyzed altogether 10 such *ETV6-X* cases using NGS methods with the hope of identifying the partner genes. Eventually, all cases were confirmed to harbor the *ETV6-RET* gene fusion.

This finding is very important since some cases of MASC may behave very aggressively and such patients profit from already available targeted therapy. However, the drug, which is currently finishing its clinical trials, is effective only for the *NTRK3*-fused tumors. The detection of *ETV6-RET* fusion allows the use of another drug which is currently also undergoing clinical trials. Therefore, the findings of this study are of utmost clinical importance with the potential to save or prolong lives in a very close future.

Also, another recent report documented a case of MASC with *ETV6-MET* fusion which is another important contribution to this topic [64].

Molecular Profiling of Mammary Analog Secretory Carcinoma Revealed a Subset of Tumors Harboring a Novel *ETV6-RET* Translocation

Report of 10 Cases

Alena Skalova, MD, PhD,† Tomas Vanecek, PhD,‡ Petr Martinek, PhD,‡ Ilan Weinreb, MD,§ Todd M. Stevens, PhD,‖ Roderick H.W. Simpson, MD, MB, ChB, FRCPath,¶ Martin Hyrcza, MD, PhD,# Niels J. Rupp, MD,** Martina Baneckova, MD,*† Michael Michal, Jr, MD,*†† David Slouka, MD, MBA, PhD,‡‡ Tomas Svoboda, MD, PhD,§§ Alena Metelkova, MD, PhD,‖‖ Arghavan Etebarian, DDS, OMP,¶¶ Jaroslav Pavelka, PhD,‡## Steven J. Potts, PhD,*** Jason Christiansen, PhD,*** Petr Steiner, MSc,*‡ and Michal Michal, MD**

Abstract: *ETV6* gene abnormalities are well described in tumor pathology. Many fusion partners of *ETV6* have been reported in a variety of epithelial, mesenchymal, and hematological malignancies. In salivary gland tumor pathology, however, the *ETV6-NTRK3* translocation is specific for (mammary analog) secretory carcinoma, and has not been documented in any other salivary tumor type. The present study comprised a clinical, histologic, and molecular analysis of 10 cases of secretory carcinoma, with typical morphology and immunoprofile harboring a novel *ETV6-RET* translocation.

From the Departments of *Pathology; ‡‡Otorhinolaryngology; §§Oncology and Radiotherapy, Oncological Clinic; ‖‖Clinical Oncology, Oncological Clinic, Faculty of Medicine in Plzen; ††Biomedical Center, Faculty of Medicine in Pilsen, Charles University; †Bioptic Laboratory Ltd; ‡Bioptic Laboratory Ltd, Molecular Pathology Laboratory; ##Faculty of Education, University of West Bohemia, Plzen, Czech Republic; §Department of Pathology, University Health Network, Toronto, ON, Canada; ‖Department of Pathology, University of Alabama at Birmingham, Birmingham, AL; ¶Department of Anatomical Pathology, University of Calgary and Foothills Medical Centre, Calgary, AB; #Department of Pathology and Molecular Medicine, St. Joseph's Healthcare & Hamilton Health Sciences, McMaster University, Vancouver, BC, Canada; **Department of Pathology and Molecular Pathology, University Hospital Zurich, Zurich, Switzerland; ¶¶Department of Oral and Maxillofacial Pathology, School of Dentistry, Tehran University of Medical Sciences, Tehran, Iran; and ***Ignyta Inc. San Diego, California, United States.

Conflicts of Interest and Source of Funding: Supported in parts by the National Sustainability Program I (NPU I) Nr. LO1503 and by the grant SVV–2017 No. 260 391 provided by the Ministry of Education Youth and Sports of the Czech Republic. The NGS analysis was in part supported by Ignyta Inc., San Diego, CA. The authors have disclosed that they have no significant relationships with, or financial interest in, any commercial companies pertaining to this article.

Correspondence: Alena Skalova, MD, PhD, Sikl's Department of Pathology, Medical Faculty of Charles University, Faculty Hospital, E. Benese 13, Plzen 305 99, Czech Republic (e-mail: skalova@fnplzen.cz).

Key Words: salivary, mammary analog secretory carcinoma, MASC, *ETV6-NTRK3*, *ETV6-RET* fusion transcript

(*Am J Surg Pathol* 2018;42:234–246)

(Mammary analog) secretory carcinoma of salivary gland origin is a recently described tumor that harbors a characteristic balanced t(12;15)(p13;q25) chromosomal translocation resulting in an *ETV6-NTRK3* fusion[1] identical to that commonly found in secretory carcinoma (SC) of the breast.[2] The *ETV6-NTRK3* fusion gene encodes a chimeric tyrosine kinase with transforming activity in epithelial and myoepithelial cells in the mouse mammary gland.[3]

Over many years, Skalova et al[1] began to identify a distinctive, hitherto unrecognized neoplasm arising in the salivary glands characterized by morphologic and immunohistochemical features strongly reminiscent of those of SC of the breast. These salivary carcinomas are composed of microcystic and solid areas with abundant vacuolated colloid-like periodic acid-Schiff-positive secretory material within the microcystic spaces. These tumors had previously been categorized as either unusual variants of salivary acinic cell carcinoma (AciCC) or adenocarcinoma not otherwise specified.[1]

Salivary SC was initially recognized as an entity different from AciCC on the basis of 3 major findings.[1] First, SC showed no basophilia in the cytoplasm of any of the constituent cells, which is the hallmark of the serous acinar cells of AciCC resulting from the presence of cytoplasmic zymogen granules. Second, these neoplasms had a completely different immunohistochemical profile, almost always expressing S100 protein, mammaglobin, vimentin, STAT5, and MUC4, all of which are rarely expressed in AciCC. Finally, SCs were found to harbor an

TABLE 1. Antibodies Used for Immunohistochemical Study

Antibody Specificity	Clone	Dilution	Antigen Retrieval/Time (min)	Source
S100 protein	Polyclonal	RTU	CC1/20	Ventana
CK7	OV-TL 12/30	1:200	CC1/36	Dako Cytomation
GCDFP-15	EP1582y	RTU	CC1/64	Cell Marque
Mammaglobin	304-1A5	RTU	CC1/36	Dako Cytomation
STAT 5a	Polyclonal	1:400	CC1/36	Assay Designs Inc.
Ki-67	30-9	RTU	CC1/64	Ventana
P63	4A4	RTU	CC1/64	Ventana
DOG1	SP31	RTU	CC1/36	Cell Marque
GATA3	L50-823	1:200	CC1/52	BioCare Medical
SOX10	Polyclonal	1:100	CC1/64	Cell Marque

CC1 indicates EDTA buffer, pH 8.6; RTU, ready to use (prediluted).

ETV6-NTRK3 fusion gene due to a t(12; 15)(p13,q25) translocation, a finding identical to SC of the breast[2] and absent in AciCCs.[1] Because of the morphologic similarities and identical *ETV6-NTRK3* fusion transcripts, the designation "mammary analog secretory carcinoma of salivary gland" has been proposed,[1] and the name was widely accepted and used in the literature. The most recent version of the World Health Organization Classification of Head and Neck Tumors, however, utilizes the terminology "secretory carcinoma"[4] for consistency, and because SCs have been recently described at other extrasalivary and extramammary sites, such as thyroid gland,[5–8] skin,[9,10] and sinonasal mucosa.[11]

The presence of the *ETV6-NTRK3* fusion gene has not been demonstrated in any other salivary gland tumor, but the same translocation can be seen not only in SC of breast,[2] but also in infantile fibrosarcoma,[12] congenital mesoblastic nephroma,[13] certain hematopoietic malignancies,[14] ALK-negative inflammatory myofibroblastic tumors,[15] a small subset of gastrointestinal stromal tumors,[16] and in radiation-induced papillary thyroid carcinomas.[17] Moreover, *ETV6-NTRK3* translocated papillary thyroid cancers have been recently described in adult patients with no history of radiation exposure.[18]

The near 100% rate of *ETV6* gene rearrangement in SC has been subsequently confirmed by many other studies.[19–25] Detection of *ETV6* rearrangements by fluorescent in situ hybridization (FISH) or the *ETV6-NTRK3* fusion by reverse-transcriptase polymerase chain reaction (RT-PCR) in formalin-fixed paraffin-embedded (FFPE) material is technically relatively straightforward and >300 cases of SC have been published since its original description.

Up until now, in all published cases of SC where the fusion partner is identified, *ETV6* is fused with *NTRK3*, and no other fusion partners have been reported so far. Nevertheless, for several years, we have been aware of several SC cases positive for the *ETV6* gene split as visualized by FISH, but in which the classic *ETV6-NTRK3* fusion transcript (exon 5-exon 15 junction) was not detected by standard RT-PCR. A subset of SCs showing *ETV6* rearrangements with so far unknown partners have been recently reported and provisionally called *ETV6-X* translocated SCs,[26] in agreement with a study of Ito et al,[27] who found 2 such cases. In the present study using the next-generation sequencing (NGS) as a diagnostic platform, we describe 10 cases morphologically and immunohistochemically typical of SC, harboring a novel *ETV6-RET* translocation.

MATERIALS AND METHODS

Among >4500 cases of primary salivary gland tumors, 194 cases of SCs were retrieved from the consultation files of the Salivary Gland Tumor Registry, at

TABLE 2. Primers for Detection of *ETV6-NTRK3* Fusion Transcripts

Original Primer Name	Sequence	Annealing Temperature (°C)	Localization
ETV6-ex4-F3	AGCCGGAGGTCATACTGCAT	55	ETV6 exon 4 inner
ETV6-ex4-F4	CATTCTTCCACCCTGGAAAC	55	ETV6 exon 4 outer
ETV6B†	ACATCATGGTCTCTGTCTCCCCGC	55	ETV6 exon 5 inner
TEL971* (ETV6A†)	ACCACATCATGGTCTCTGTCTCCC	65	ETV6 exon 5 outer
NTRK3-ex14-R1	GTGATGCCGTGGTTGATGT	55	NTRK3 exon 14 inner
NTRK3 ex14-R2	AGTCATGCCAATGACCACAG	55	NTRK3 exon 14 outer
NTRK3B†	TTCTCGCTTCAGCACGATGTCT	55	NTRK3 exon 15 inner
TRKC1059* (NTRK3A†)	CAGTTCTCGCTTCAGCACGATG	65	NTRK3 exon 15 outer
ETV6-Archer1-F1	CGATGGGAGGACAAAGAATC	55	ETV6 exon 6
RET-Archer1-R1	AACCAAGTTCTTCCGAGGGA	55	RET exon 12
ETV6-Archer1-F2	CAACGGACTGGCTCGACTG	55	ETV6 exon 6
RET-Archer1-R2	GACCACTTTTCCAAATTCGCCT	55	RET exon 12

*Bourgeois et al[32]
†Ito et al,[27] Skalova et al[26].

FIGURE 1. A, The result of analysis by NGS with custom-designed ArcherDX Kit of case 3 (case 17 in Skalova et al[26]). Analysis revealed the presence of fusion transcript *ETV6-RET* joining exons 6 and 12, respectively. The red arrows represent position of primers. B, The confirmation of the presence of *ETV6-RET* fusion transcript by RT-PCR followed by Sanger sequencing. The black arrow indicates area of fusion.

the Department of Pathology, Faculty of Medicine in Plzen, and Biopticka Laborator Ltd, Plzen, Czech Republic (A.S. and M.M.).

The histopathologic features of all tumors and the immunohistochemical stains, when available, were reviewed by 2 pathologists (A.S. and M.B.). A diagnosis of SC was confirmed in cases that displayed, at least focally, histologic features consistent with original description[1] in conjunction with the appropriate immunohistochemical profile, that is, coexpression of S100 protein, cytokeratin CK7, and mammaglobin with the absence of p63 and DOG1 staining. For the purpose of this particular study, we have included 4 cases of SC with *ETV6-X* profile from study Skalova et al[26] and 26 cases of SC with *ETV6* gene break found by FISH or with morphologic and immunohistochemical pattern of SC but without analyzable *ETV6* gene break by FISH due to low quality or lack of material. Thus, a total of 30 SC cases were studied by NGS using ArcherDX Fusion Plex Kit.

For conventional microscopy, the excised tissues were fixed in formalin, routinely processed, embedded in paraffin (FFPE), cut, and stained with hematoxylin and eosin. In most cases, additional stains were also performed, including periodic acid-Schiff with and without diastase, mucicarmine, and alcian blue at pH 2.5.

For immunohistochemical studies, 4 μm thick sections were cut from paraffin blocks and mounted on positively charged slides (TOMO, Matsunami Glass Ind., Japan). Sections were processed on a BenchMark ULTRA (Ventana Medical System, Tucson, AZ), deparaffinized, and then subjected to heat-induced epitope retrieval by immersion in a CC1 solution at pH 8.6 at 95°C. After antigen retrieval, sections were stained with a pan-RTK antibody cocktail consisting of rabbit monoclonal antibodies, all obtained from Cell Signaling (Danvers, MA), targeting pan-Trk (A7H6R, active against TrkA, TrkB, and TrkC, 1:50 dilution), ROS1 (D4D6, 1:50), and ALK (D5F3, 1:50), as described previously.[28]

All other primary antibodies used are summarized in Table 1. The bound antibodies were visualized using the ultraView Universal DAB Detection Kit (Roche) and ultraView Universal Alkaline Phosphatase Red Detection Kit (Roche). The slides were counterstained with the Mayer hematoxylin. Appropriate positive and negative controls were used.

Clinical follow-up was obtained from the patients, their physicians, or from referring pathologists.

Molecular Genetic Study

Detection of ETV6-NTRK3 and ETV6-RET Fusion Transcripts by RT-PCR

RNA was extracted using the RecoverAll Total Nucleic Acid Isolation Kit (Ambion, Austin, TX). cDNA was synthesized using the Transcriptor First Strand cDNA Synthesis Kit (RNA input 500 ng; Roche Diagnostics, Mannheim, Germany). All procedures were performed according to the manufacturer's protocols. Amplification of a 105 and 133 bp product of the μ2-microglobulin gene and 247 bp product of the *PGK* gene was used to test the quality of the extracted RNA as previously described.[29–31] A detection of classic exon 5 of *ETV6* gene and exon 15 of *NTRK3* gene,[32] as well as atypical exon 4 of the *ETV6* gene and exon 14 of the *NTRK3* gene (and their combinatorial variants) fusion transcript was performed by RT-PCR. In addition, more sensitive, nested RT-PCR was performed for the detection of classic[26,27] as well as selected atypical junction of transcripts. Except that,

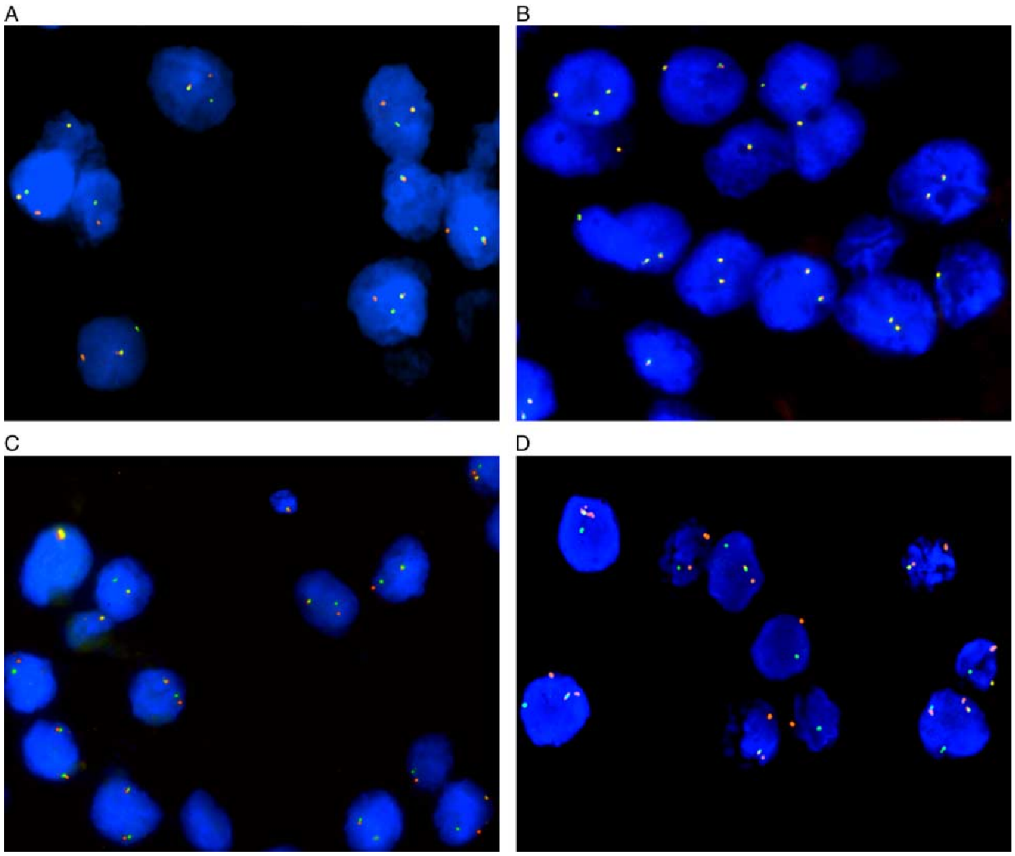

FIGURE 2. Interphase FISH analysis using break-apart probes (A–C) and dual-fusion probe (D). Positive cells with break-apart *ETV6* (A) and *RET* (C) probes contain nucleus with separate (split) orange and (or) green signals indicating a rearrangement (break) of 1 copy of the gene region and also 1 orange/green (yellow) fusion signal representing 1 normal (intact) copy of homolog locus. Negative cells with break-apart *NTRK3* (B) probe contain only normal (not split) yellow signal. Positive cells using fusion probe *ETV6-RET* (D) show orange/green (yellow) fusion signals representing translocation *ETV6-RET* and also separate orange and green signals showing the intact genes.

RT-PCR for *ETV6-RET* fusion transcript detection was also carried out after receiving of the NGS results.

For single-round PCR, 2 L of cDNA was added to reaction consisting of 12.5 µL of HotStar Taq PCR Master Mix (QIAgen, Hilden, Germany), 10 pmol of each primer (Table 2), and distilled water up to 25 µL. The amplification program comprised denaturation at 95°C for 14 minutes and then 45 cycles of denaturation at 95°C for 1 minute, annealing at temperature seen in Table 2 for 1 minute and extension at 72°C for 1 minute. The program was finished by incubation at 72°C for 7 minutes. For nested PCR, the same reaction conditions were utilized. One microliter of PCR product from the first round was used as a template.

Successfully amplified PCR products were purified with magnetic particles of Agencourt AMPure (Agencourt Bioscience Corporation, A Beckman Coulter Company, Beverly, MA). Products were then bidirectionally sequenced using Big Dye Terminator Sequencing Kit (Applied Biosystems, Foster City, CA), and purified with magnetic particles of Agencourt CleanSEQ (Agencourt Bioscience Corporation), all according to the manufacturer's protocol, and run on an automated sequencer ABI Prism 3130xl (Applied Biosystems) at a constant voltage of 13.2 kV for 11 minutes.

Detection of Alteration of ETV6, NTRK3, and RET Genes by FISH Method

Four-micrometer-thick FFPE sections were placed onto positively charged slides. Hematoxylin and eosin–stained slides were examined for determination of areas for cell counting.

TABLE 3. Molecular Genetics Findings in 10 Cases of SC With *ETV6-RET* Fusion

Case #	Case #	NGS Results	Fusion	FISH ETV6ba	FISH NTRK3ba	RT-PCR ETV6-NTRK3	FISH RETba	FISH ETV6-RET	RT-PCR ETV6-RET
1	6*	+	*ETV6-RET*	+	−	−	+	+	+
2	15*	+	*ETV6-RET*	+	−	−	+	ND	+
3	17*	+	*ETV6-RET*	+	−	−	+	+	+
4	20*	+	*ETV6-RET*	+	−	−	+	+	−
5		+	*ETV6-RET*	+	−	−	+	+	+
6		+	*ETV6-RET*	ND	ND	−	ND	+	+
7		+	*ETV6-RET*	+	−	−	+	+	+
8		+	*ETV6-RET*	NA	NA	−	NA	+	+
9		+	*ETV6-RET*	ND	ND	−	ND	ND	−
10	12†	+	*ETV6-RET*	+	−	−	+	+	+

*Skalova et al[26] (Table 6).
†Stevens et al[8] (Table 2).
NA indicates not analyzable; ND, not done due to lack of material.

The unstained slides were routinely deparaffinized and incubated in the ×1 Target Retrieval Solution Citrate pH 6 (Dako, Glostrup, Denmark) at 95°C for 40 minutes and subsequently cooled for 20 minutes at room temperature in the same solution. Slides were washed in deionized water for 5 minutes and digested in protease solution with Pepsin (0.5 mg/mL; Sigma Aldrich, St Louis, MO) in 0.01 M HCl at 37°C for 25 to 60 minutes, according to the sample conditions. Slides were then placed into deionized water for 5 minutes, dehydrated in a series of ethanol solutions (70%, 85%, 96% for 2 min each), and air dried.

Two commercial probes were used for the detection of rearrangement of *ETV6* and *RET* genes, Vysis ETV6 Break Apart FISH Probe Kit (Vysis/Abbott Molecular, IL) and ZytoLight SPEC RET Dual Color Break Apart Probe (ZytoVision GmbH, Bremerhaven, Germany). ETV6 probe was mixed with water and LSI/WCP (Locus-Specific Identifier/Whole Chromosome Painting) Hybridization buffer (Vysis/Abbott Molecular) in a 1:2:7 ratio, respectively. RET probe was factory premixed.

Probes for detection of rearrangement of *NTRK3* gene region and *ETV6-RET* genes fusion were mixed from custom designed SureFISH probes (Agilent Technologies Inc., Santa Clara, CA). Chromosomal regions for *NTRK3* break-apart probe oligos are chr15:87501469-88501628 and chr15:88701444-89700343; for *ETV6-RET* fusion probe, chr12:11675872-12175711 and chr10:43354893-43849282. Probe mixture was prepared from corresponding probes (each color was delivered in a separate well), deionized water, and LSI Buffer (Vysis/Abbott Molecular) in a 1:1:1:7 ratio, respectively.

An appropriate amount of mixed and premixed probes was applied on specimens, covered with a glass coverslip, and sealed with rubber cement. Slides were incubated in the ThermoBrite instrument (StatSpin/Iris Sample Processing, Westwood, MA) with codenaturation at 85°C for minutes and hybridization at 37°C for hours. Rubber cemented coverslip was then removed and the slide was placed in posthybridization wash solution (2×SSC/0.3% NP-40) at 72°C for 2 minutes. The slide was air dried in the dark, counterstained with 4′,6′-diamidino-2-phenylindole DAPI (Vysis/Abbott Molecular), coverslipped, and immediately examined.

FISH Interpretation

The sections were examined with an Olympus BX51 fluorescence microscope (Olympus Corporation, Tokyo, Japan) using a ×100 objective and filter sets Triple Band Pass (DAPI/SpectrumGreen/SpectrumOrange), Dual Band Pass (SpectrumGreen/SpectrumOrange), and Single Band Pass (SpectrumGreen or SpectrumOrange).

TABLE 4. Details of NGS Analysis by the Archer Platform in 10 Cases of SC With *ETV6-RET* Translocation

Case #	Case #	NGS Results	Fusion	Exons Included in Fusion	No. Valid Fusion Read	% of Reads Supporting Fusion	No. Unique Start Sites
1	Case 6*	+	ETV6-RET	6-12	51	100	17
2	Case 15*	+	ETV6-RET	6-12	84	20.1	33
3	Case 17*	+	ETV6-RET	6-12	1126	23.5	183
4	Case 20*	+	ETV6-RET	6-12	15	1.8	10
5		+	ETV6-RET	6-12	163	11.4	63
6		+	ETV6-RET	6-12	21	100	11
7		+	ETV6-RET	6-12	49	14	32
8		+	ETV6-RET	6-12	100	86.2	51
9		+	ETV6-RET	6-12	41	60.3	14
10	Case 12†	+	ETV6-RET	6-12	24	14.8	17

*Skalova et al[26] (Table 6).
†Stevens et al[8] (Table 2).

TABLE 5. Clinical Findings in 10 SCs With *ETV6-RET* Fusion Transcript

Case #	Age/ Sex	Case #	Stadium TNM	Local Recurrence	Length of Symptoms	Metastasis (y, mo)	Treatment	Follow-up	Outcome
1	50/M	Case 6*	NA	NA		NA	NA	NA	NA
2	29/M	Case 15*	pT2pN1M0	No	6 y	LN+	SP and RT, no neck dissection	4 y 6 mo	Alive NED
3	31/M	Case 17*	pT3pN0M0	Residual tumor	7 y	No	Excision radical resection (1 mo)	4 y	Alive NED
4	77/F	Case 20*	pT2N0M0	No	1 y	No	Excision, RT	3 y	DOC
5	51/M		pT3N0M0	Residual tumor	15 mo	No	Excision SP after 3 mo	8 mo	Alive NED
6	20/F		pT3N0M0	No	NA	No	PE	NA	NA
7	55/M		pT3N0M3	No	3 y	Multiple bone meta (pelvic, scapula) at 15 mo	PP, RT, and CHT	2 y	DOD
8	28/F		pT1N0M0	No	1 mo	No	Parotid resection and lymphadenectomy level II: 12 lymph nodes negative	2 y	Alive NED
9	33/M		pT1pN0 (0/2)	No	6 mo	No	PP	3 y 9 mo	Alive NED
10	34/M	Case 12†	pT2N0M0 (0/1)	No	Several months, very slow enlargement	No	SP	4 y 2 mo	Alive NED

*Skalova et al[26] (Table 6).
†Stevens et al[8] (Table 2).
CHT indicates chemotherapy; DOC, dead of other causes; DOD, dead of disease; LN, lymph nodes; NA, not available; NED, no evidence of disease; PE, parotidectomy; PP, partial parotidectomy; RT, radiotherapy; SP, superficial parotidectomy.

For each probe, 100 randomly selected nonoverlapping tumor cell nuclei were examined for the presence of yellow or green and orange fluorescent signals. Regarding break-apart probes, yellow signals were considered negative, and separate orange and green signals were considered positive; conversely, for fusion probe, yellow signals were considered positive, and separate orange and green signals were considered negative.

Cutoff values were set to >10% and 20% of nuclei (break-apart and fusion probes, respectively) with chromosomal breakpoint signals (mean, +3 SD rounded up in normal non-neoplastic control tissues).

Sample Preparation for NGS

For NGS studies, 2 to 3 FFPE sections (10 μm thick) were macrodissected to isolate tumor-rich regions. Samples were extracted for total nucleic acid using Agencourt FormaPure Kit (Beckman Coulter, Brea, CA) following the corresponding protocol with an overnight digest and an additional 80°C incubation as described in modification of the protocol by ArcherDX (ArcherDX Inc., Boulder, CO). Total nucleic acid was quantified using the Qubit Broad Range RNA Assay Kit (Thermo Fisher Scientific) and 2 μL of sample.

RNA Integrity Assessment and Library Preparation for NGS

Unless otherwise indicated, 250 ng of FFPE RNA was used as input for NGS studies. To assess RNA quality, the PreSeq RNA QC Assay using iTaq Universal SYBR Green Supermix (Biorad, Hercules, CA) was performed on all samples during library preparation to generate a measure of the integrity of RNA (in the form of a cycle threshold value). Library preparation and RNA QC were performed following the Archer Fusion Plex Protocol for Illumina (ArcherDX Inc.). A custom primer set with 28 primers spanning regions on 3 specific genes of interest, including all 8 exons of *ETV6* gene in 3′ direction, was designed and used. Final libraries were diluted 1:100,000 and quantified in a 10 μL reaction following the Library Quantification for Illumina Libraries protocol and assuming a 200 bp fragment length (KAPA, Wilmington, MA). The concentration of final libraries was around 200 nM. The threshold representing the minimum molar concentration for which sequencing can be robustly performed was set at 50 nM.

NGS and Analysis

Libraries were sequenced on a MiSeq sequencer (Illumina, San Diego, CA). They were diluted to 4 nM and equal amounts of up to 16 libraries were pooled per run. The optimal number of raw reads per sample was set to 500,000. Library pools were diluted to 16 pM library stock with 5% 12.5 pM PhiX and loaded into the MiSeq cartridge. Analysis of sequencing results was performed using the Archer Analysis software (v5; ArcherDX Inc.). Fusion parameters were set to a minimum of 5 valid fusion reads with a minimum of 3 unique start sites within the valid fusion reads.

RESULTS

Molecular Genetic Findings

Selected 30 cases of SC (as described earlier) were analyzed by NGS using the ArcherDX analysis platform.

TABLE 6. Clinical and Histologic Findings in 10 SCs With *ETV6-RET* Fusion Transcript

Case #	Age/ Sex	Case #	Location	Tumor Size (mm)	Capsule	Surgical Margins	Thick Fibrous Septa	Hyalinized Sclerosis	Invasion (LVI, PN)	Cystic Pattern	Necrosis	Comments
1	50/M	Case 6*	Lip	15	NA	2	No	No	NA	No	−	Fragmented tissue
2	29/M	Case 15*	Parotid	23	No	1	+	++	PN+, LVI +Extraglandular, muscle invasion	No	−	Hyalinized, multilobular, microcystic, and solid growth pattern
3	31/M	Case 17*	Submand	30	No	2	++	++	PN+	No	−	Hyalinized, multilobular, microcystic
4	77/F	Case 20*	Submand	70	Focal		+	+	No	+	−	Multicystic, papillary with apocrine cells
5	51/M		Parotid	10	No	1	++	++	PN+	No	+	Central hyalinized sclerosis, invasive growth pattern
6	20/F		Parotid	40	No	2	+	+	Extraglandular	No	−	Lobular, microcystic
7	55/M		Parotid	70	No	2	+	+	PN+, perivascular	+	+	High grade component
8	28/F		Parotid	12	No	1	+	+	Intraglandular	No	−	Predominantly solid and microcystic
9	33/M		Parotid	17	+	1	No	No	No	+	−	Predominantly cystic
10	34/M	Case 12†	Parotid	19	+	0	No	No	No	+	−	Multicystic with mural nodules

*Skalova et al[26] (Table 6).
†Stevens et al[8] (Table 2).
Surgical margins: free-0; close (means distance from the tumor <0.5 mm) -1; positive-2.
F indicates female; LVI, lymphovascular invasion; M, male; NA, not available; PN, perineural invasion.

This analysis detected a novel *ETV6-RET* fusion transcript joining exon 6 of *ETV6* gene and exon 12 of *RET* gene in 10 cases of salivary gland tumors displaying histologic and immunohistochemical features typical of SC (Fig. 1). All but 1 *ETV6-RET* positive SC case were then tested by at least 1 FISH probe for the presence of *ETV6-RET* rearrangements (Fig. 2). In case 9, there was no residual tissue material for confirmation of the NGS analysis by FISH tests. In addition, RT-PCR for the confirmation of the presence of *ETV6-RET* fusion transcript followed by Sanger sequencing on positive samples was performed in all 10 cases (Fig. 1). The results of the NGS tests, details of the analysis, and results of confirmatory genetic tests are summarized in Tables 3 and 4. In addition, NGS analysis resulted in detection of the *ETV6-NTRK3* fusion in 15 SC cases. In 4 cases, NGS revealed negative results, and 1 case was unanalyzable (detailed data not shown). No other fusion transcripts different from *ETV6-NTRK3* or *ETV6-RET* were found by NGS in any analyzable case of SC.

Clinical and Histologic Characteristics of the Study Group

The clinical and follow-up data of 10 patients with *ETV6-RET* translocated SC of salivary glands are summarized in Table 5. There were 3 female and 7 male patients. The median patient age was 40.8 years, with a range between 20 and 77 years. The most common anatomic site of involvement was the parotid gland, occurring in 7 patients. Other primary sites of the origin included the submandibular gland and minor salivary gland of the upper lip in 2 patients and 1 patient, respectively.

Follow-up Data

Clinical follow-up data were obtained from 8 patients, and ranged from 6 to 50 months (mean, 36 mo); 2 patients were lost to follow-up. Detailed clinical, follow-up, and histologic findings in 10 patients with *ETV6-RET* translocated SC are summarized in Table 5.

All tumors were treated by surgical excision; in 1 patient the excision was radical with clear surgical margins, in 4 cases the surgical margins were positive, and in 4 additional patients, the tumor infiltration was close (<0.5 mm) to the surgical margins. Five patients underwent subtotal conservative parotidectomy, in 3 of them in combination with radiotherapy (cases 2, 4, and 7). Residual tumors were treated by radical reexcision with clear surgical margins in 2 patients. Concomitant chemotherapy and radiotherapy was used in 1 patient with high-grade transformed SC complicated by metastatic

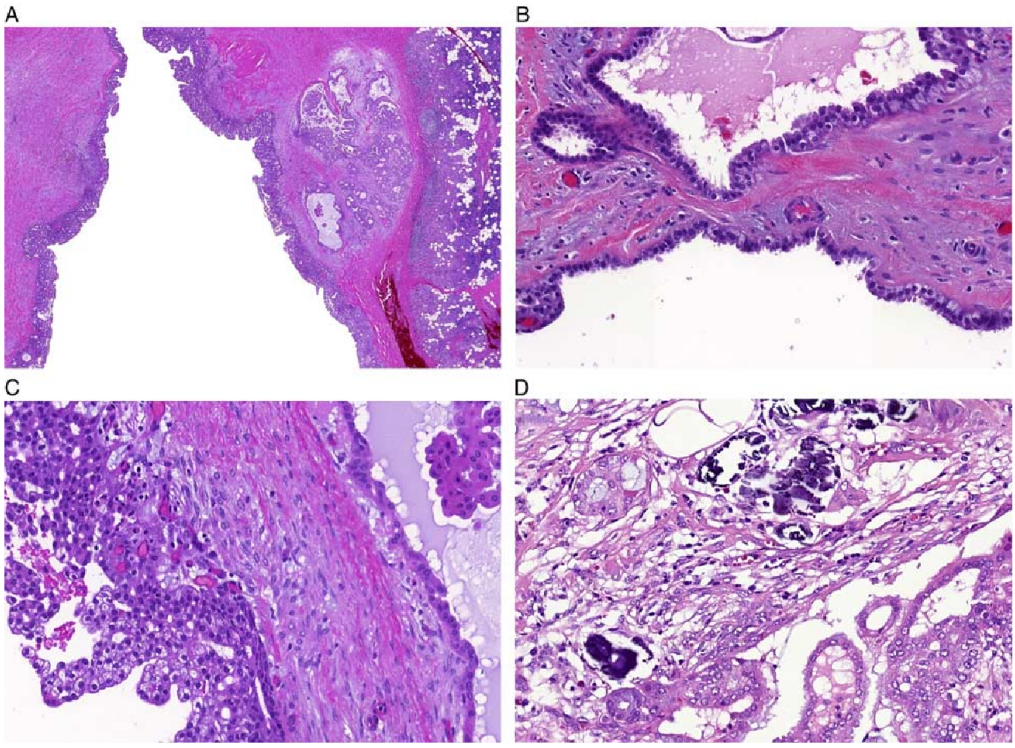

FIGURE 3. A, SC is well circumscribed and surrounded by a thick fibrous capsule enclosing predominantly multicystic growth pattern with multiple mural nodules. The cysts were lined mostly by a single or focally by a double layer of cells with prominent apocrine differentiation including hobnail (B) and vacuolated foamy cells (C). The fibrous capsule and septa comprised psammoma bodies in places (D).

disease at 15 months after surgery (case 7). Clinical and follow-up findings are summarized in Table 5.

Macroscopic Features

Detailed clinical and morphologic findings in 10 patients with *ETV6-RET* translocated SC are summarized in Table 6. The median tumor size was 3.6 cm, with a range of 1.0 to 7.0 cm. Grossly, most tumors were variably invasive: 2 were entirely circumscribed and encapsulated, 1 had focally infiltrative edges, and 7 were predominantly infiltrative.

Microscopic and Immunohistochemical Features

On low power magnification, 3 major growth patterns of SC were identified in our material. First, 3 tumors were well circumscribed and surrounded by a thick, focally uninterrupted, fibrous capsule enclosing a predominantly multicystic growth pattern with multiple mural nodules (Fig. 3A). The cysts were lined mostly by a single or focally by a double layer of cells with prominent apocrine differentiation including hobnail and vacuolated foamy cells (Figs. 3B, C), and contained abundant proteinaceous eosinophilic material. The fibrous capsule and septa comprised psammomatoid calcifications in some places (Fig. 3D). The second pattern was characterized by solid and microcystic growth with a multilobular structure divided by thin fibrous septa (Fig. 4A). The tumors either lacked a capsule or were only partially encapsulated with prominent infiltrative borders (Fig. 4B). These cases were predominantly composed of microcystic and slightly dilated glandular spaces filled with a variable amount of eosinophilic homogenous secretory material (Fig. 4C). The third pattern, prevailing in 3 cases, comprised a prominent fibrosclerotic stroma with isolated tumor cells in small islands or trabeculae, which were seen in the central part of the tumor (Fig. 5A). In case 7, 2 different growth patterns were seen, in particular low-grade components arranged in multiple macrocystic and microcystic lobules with comedo-like necroses, and high-grade components with limited secretory material and high proliferative activity (Fig. 5B).

However, most tumors demonstrated 2 or more architectural patterns, with microcystic, tubular, solid, and papillary patterns often occurring together. Regardless of

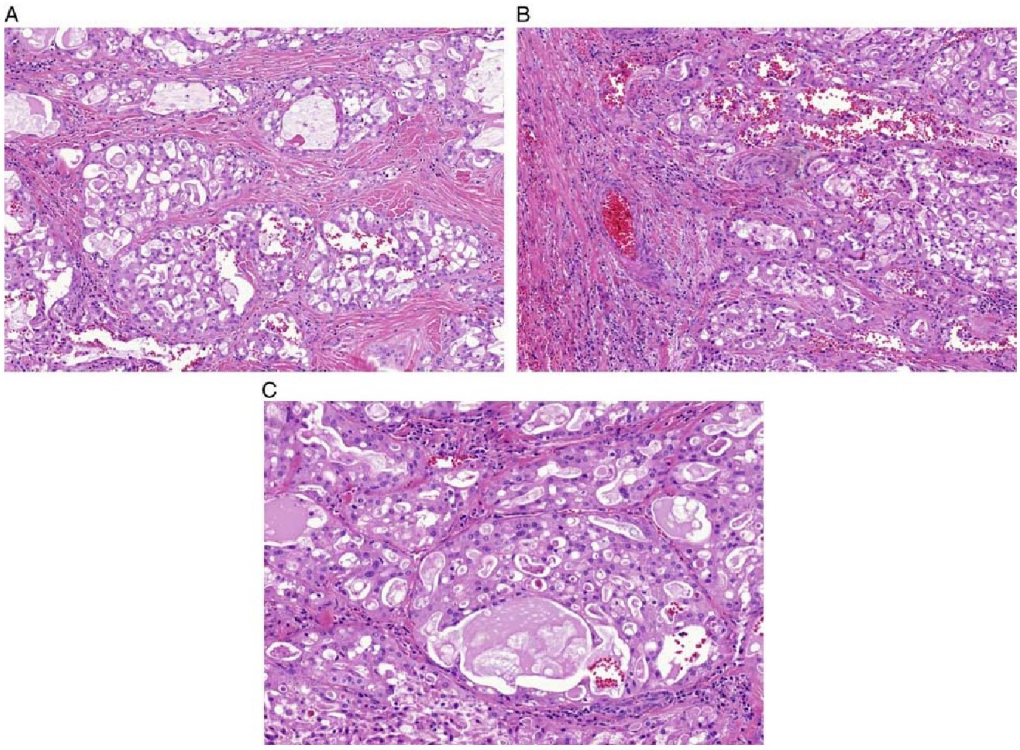

FIGURE 4. A, SC is characterized by solid and microcystic growth with a multilobular structure divided by thin fibrous septa. B, The tumor has a prominent infiltrative border. C, The tumor is predominantly composed of microcystic and slightly dilated glandular spaces filled with a variable amount of eosinophilic homogenous secretory material.

the growth pattern of SC, the tumor cells were often bland looking, with abundant pale pink vacuolated and foamy cytoplasm and with vesicular oval nuclei with a single small but prominent nucleolus. The cytologic features were similar from case to case. The range of nuclear atypia was assessed as grades 1 to 3. Mitotic figures were rare and necrosis was absent. Prominent perineural and intraneural invasion was seen in case 7 (Fig. 5C). Only 1 patient (case 2) presented with a single periparotideal lymph node metastasis at the time of diagnosis.

Immunohistochemical Findings

By immunohistochemistry, all examined SC cases were positive for S100 protein (Fig. 6A), mammaglobin (Fig. 6B), typically in strong and diffuse fashion (secretory material was also positive), and cytokeratin CK7 (Fig. 6C). GATA-3, SOX-10 (Fig. 6D), and STAT5a expression was detected in 3/6, 5/6, and 2/3 cases, respectively. P63 protein was completely negative in most cases, with limited areas of positive peripheral myoepithelial cell staining suggestive of a focal intraductal component in 3 cases. DOG1 was negative in all examined cases. Proliferative activity was generally low, with a mean MIB1 index of 15% (range, 5% to 40%).

DISCUSSION

Salivary gland tumors are increasingly being found to have characteristic chromosomal rearrangements. SC is a salivary gland tumor that recapitulates the histology and genetics of a rare malignancy of the breast SC. These tumors are defined by the t(12;15)(q13;q15) translocation, a fusion of the *ETV6* gene from chromosome 12 and the *NTRK3* gene from chromosome 15. The same translocation has been detected in most cases of the infantile fibrosarcomas, congenital mesoblastic nephromas,[13] chronic eosinophilic leukemias,[33] acute myeloid leukemia,[14] and some papillary carcinomas of the thyroid with and without previous irradiation.[18] These groups of tumors are the focus of interest, because tumors with *ETV6-NTRK3* fusion translocation respond well to treatment by entrectinib, which is a potent inhibitor of tyrosine kinases TRKA/B/C, ROS1, and ALK. The drug entrectinib is administered orally, is safe and well tolerated, and can cross the blood-brain barrier,

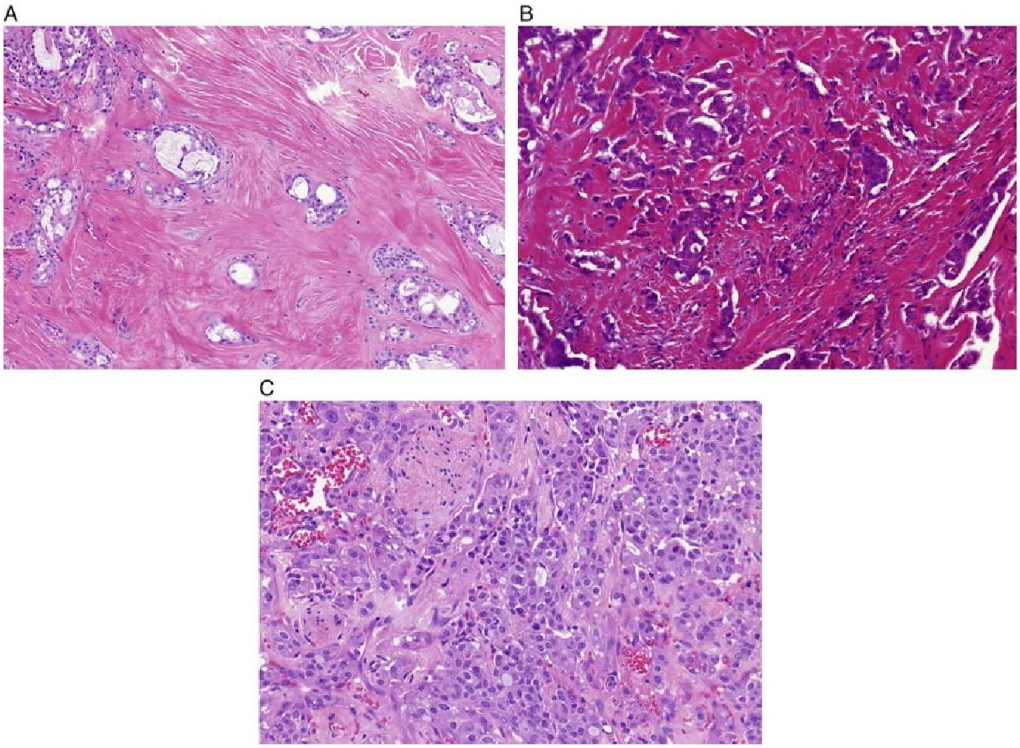

FIGURE 5. A, The third pattern of SC has a prominent fibrosclerotic stroma with isolated tumor cells in small islands or trabeculae were seen in the central part of the tumor. B, High-grade component of SC with limited secretory material and high proliferative activity. C, Prominent perineural and intraneural invasion was seen in 1 tumor.

so that it can be effective for treatment of brain metastases.[34,35]

Originally it appeared that all cases of SC share the same *ETV6-NTRK3* fusion translocation. However, in recent years Ito et al[27] and Skalova et al[26] described altogether 6 cases of SC with the *ETV6* gene split detected by FISH, but in which the *ETV6* gene appeared to be fused with a gene different to *NTRK3*. These cases were marked as SCs with *ETV6-X* fusion.

Herein, we describe a novel *ETV6-RET* fusion in 10 cases of salivary gland carcinomas with histologic features and IHC profile typical of SC, including the 4 *ETV6-X* SC cases published previously.[26] The presence of *ETV6-RET* fusion in SC was proven by at least 3 independent tests (NGS, FISH, RT-PCR), in all but 2 cases (Table 3, cases 4 and 9). In case 4, NGS and FISH confirmed *ETV6-RET* fusion but RT-PCR was negative, probably due to low or focal expression of fusion transcript (Table 4). Case 9 was the only sample unconfirmed by independent analysis. There was a lack of material for FISH analysis and RT-PCR for *ETV6-RET* fusion transcript detection was negative. In this case, low quality of RNA rather than low or focal expression is responsible for this result.

The alternative *ETV6-RET* transcription will be important for treatment of those SCs with uncontrolled regional growth or SCs with metastatic foci, as treatment with entrectinib and similar drugs with the same target specificity will probably be ineffective in these SCs with alternative fusion transcript different from *ETV6-NTRK3*. The alternative fusion partner different from *ETV6-NTRK3* in SC should not be of great surprise, because infantile fibrosarcoma with *ETV6-NTRK3* translocation may have alternative *EML4-NTRK3* translocation,[36] and there are descriptions of acute myeloid leukemias in which the *ETV6* gene fuses with many alternative fusion partners, including *ETV6-ABL1*,[37] *ETV6-LPXN*,[38] *ETV6-RUNX1*,[39] *ETV6-NCOA2*,[40] and many others.

To our knowledge, *ETV6-RET* fusions have not been reported in salivary gland tumors so far. Notably, however, recent studies using RNA sequencing have revealed that salivary duct carcinoma (SDC) may also be added to the growing list of gene fusion-positive salivary

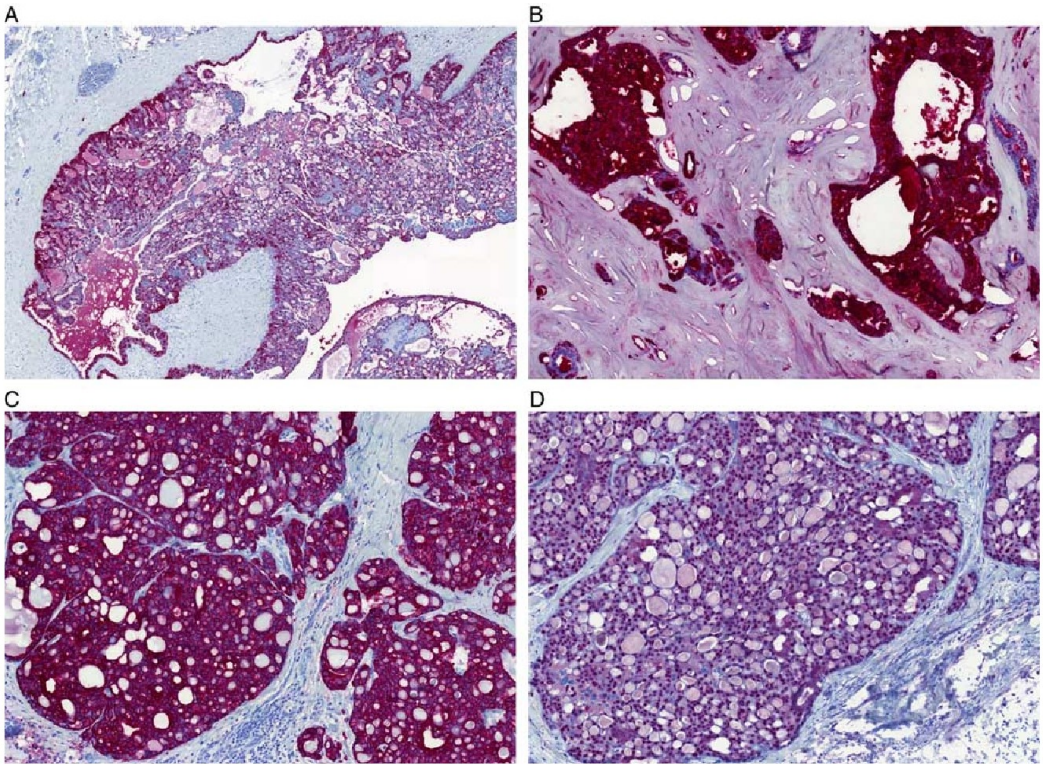

FIGURE 6. SC cases were all positive for S100 protein (A), mammaglobin (B), typically in strong and diffuse fashion (secretory material was also positive), and cytokeratin CK7 (C). SOX-10 positive nuclear expression is present (D).

carcinomas. *NCOA4-RET* fusions have been found in 2 SDCs.[41] Both *NCOA4-RET* translocated SDCs were positive for androgen receptors, and the tumors progressed in spite of undergoing concurrent chemoradiation, combination chemotherapy, and dual androgen deprivation therapy. Both patients with *NCOA4-RET* translocation, however, benefited from *RET*-targeted therapy.[41]

The treatment of SC has varied, ranging from simple excision to radical resection, neck dissection, adjuvant radiotherapy, and/or adjuvant systemic chemotherapy.[1,42,43] For patients presenting with a locally advanced, recurrent, or metastatic disease, the treatment options are currently limited and mainly palliative.[42,43] Therefore, SCs with *ETV6-RET* fusion translocation must be clearly distinguished from SCs with *ETV6-NTRK3* translocation, because the drugs RXDX105 and LOXO 292, effective with various tumors driven with *RET* gene alterations, are being tested for the treatment. SCs with *ETV6-RET* translocation might respond much better to these drugs, whereas entrectinib and similar inhibitors of tyrosine kinases TRKA/B/C will probably be ineffective.[44–47]

In summary, a novel finding in our study has been the discovery of a subset of SC patients with *ETV6-RET* fusions who may benefit from *RET*-targeted therapy. Many salivary gland malignancies are still included in the group of adenocarcinomas not otherwise specified. We believe that detailed genomic profiling and NGS of a large cohort of these unspecified neoplasms may lead to the identification of novel gene fusions and driver mutations characterizing new clinically relevant subgroups of salivary gland carcinomas. This study highlights that further molecular analyses of salivary gland tumors are warranted and deserve special attention to identify new tumor types with possible therapeutic implications.

ACKNOWLEDGMENTS

The authors thank Alos Lucia, MD (Barcelona, Spain), Rychlý B, MD, PhD (Bratislava, Slovac Republic), Vazmitel M, MD, PhD (USA), Dana Cempirková, MD (Jindřichův Hradec, Czech Republic), Ian Cook, MD (Salisbury, UK), and Tiziana Salviati, MD (Italy) for submitting the cases and clinical information about the patients.

REFERENCES

1. Skalova A, Vanecek T, Sima R, et al. Mammary analogue secretory carcinoma of salivary glands, containing the *ETV6-NTRK3* fusion gene: a hitherto undescribed salivary gland tumor entity. *Am J Surg Pathol*. 2010;34:599–608.
2. Tognon C, Knezevich SR, Huntsman D, et al. Expression of the *ETV6-NTRK3* gene fusion as a primary event in human secretory breast carcinoma. *Cancer Cell*. 2002;2:367–376.
3. Li Z, Tognon CE, Godinho FJ, et al. *ETV6-NTRK3* fusion oncogene initiates breast cancer from committed mammary progenitors via activation of AP1 complex. *Cancer Cell*. 2007;12:542–558.
4. Skálová A, Bell D, Bishop JA, et al. Secretory carcinoma. In: El-Naggar A, Chan JKC, Grandis JR, Takata T, Slootweg PJ, eds. *World Health Organization (WHO) Classification of Head and Neck Tumours*, 4th ed. Lyon, France: IARC Press; 2017:177–178.
5. Dogan S, Wang L, Ptashkin RN, et al. Mammary analog secretory carcinoma of the thyroid gland: a primary thyroid adenocarcinoma harboring *ETV6-NTRK3* fusion. *Mod Pathol*. 2016;29:985–995.
6. Reynolds S, Shaheen M, Olson G, et al. A case of primary mammary analog secretory carcinoma (MASC) of the thyroid masquerading as papillary thyroid carcinoma: potentially more than a one off. *Head Neck Pathol*. 2016;10:405–413.
7. Dettloff J, Seethala RR, Stevens TM, et al. Mammary analog secretory carcinoma (MASC) involving the thyroid gland: a report of the first 3 cases. *Head Neck Pathol*. 2007;11:266–267.
8. Stevens TM, Kovalovsky AO, Velosa C, et al. Mammary analog secretory carcinoma, low-grade salivary duct carcinoma, and mimickers: a comparative study. *Mod Pathol*. 2015;28:1084–1100.
9. Hyrcza MD, Ng T, Crawford RI. Detection of the *ETV6-NTRK3* translocation in cutaneous mammary-analogue secretory carcinoma. *Diagn Histopathol*. 2015;21:481–484.
10. Bishop JA, Taube JM, Su A, et al. Secretory carcinoma of the skin harboring *ETV6* gene fusions. A cutaneous analogue to secretory carcinomas of the breast and salivary glands. *Am J Surg Pathol*. 2017;41:62–66.
11. Lurquin E, Jorissen M, Debiec-Rychter M, et al. Mammary analogue secretory carcinoma of the sinus ethmoidalis. *Histopathology*. 2015;67:749–751.
12. Rubin BP, Chen CJ, Morgan TW, et al. Congenital mesoblastic nephroma t(12;15) is associated with ETV6-NTRK3 gene fusion: cytogenetic and molecular relationship to congenital (infantile) fibrosarcoma. *Am J Pathol*. 1998;153:1451–1458.
13. Knezevich SR, Garnett MJ, Pysher TJ, et al. *ETV6- NTRK3* gene fusions and trisomy 11 establish a histogenetic link between mesoblastic nephroma and congenital fibrosarcoma. *Cancer Res*. 1998;15:5046–5048.
14. Kralik JM, Kranewitter W, Boesmueller H, et al. Characterization of a newly identified ETV6-NTRK3 fusion transcript in acute myeloid leukemia. *Diagn Pathol*. 2011;6:19.
15. Alassiri AH, Ali RH, Shen Y, et al. *ETV6-NTRK3* is expressed in a subset of ALK-negative inflammatory myofibroblastic tumor. *Am J Surg Pathol*. 2016;40:1051–1061.
16. Brenca M, Rossi S, Polano M, et al. Transcriptome sequencing identifies *ETV6–NTRK3* as a gene fusion involved in GIST. *J Pathol*. 2016;238:543–549.
17. Leeman-Neill RJ, Kelly LM, Liu P, et al. *ETV6-NTRK3* is a common chromosomal rearrangement in radiation-associated thyroid cancer. *Cancer*. 2014;120:799–807.
18. Seethala RR, Chiosea SI, Liu CZ, et al. Clinical and morphological features of *ETV6-NTRK3* translocated papillary thyroid carcinoma in an adult population without radiation exposure. *Am J Surg Pathol*. 2017;41:446–457.
19. Griffith C, Seethala R, Chiosea SI. Mammary analogue secretory carcinoma: a new twist to the diagnostic dilemma of zymogen granule poor acinic cell carcinoma. *Virchows Arch*. 2011;459:117–118.
20. Fehr A, Loning T, Stenman G. Mammary analogue secretory carcinoma of the salivary glands with *ETV6-NTRK3* gene fusion. Letter to the editor. *Am J Surg Pathol*. 2011;35:1600–1602.
21. Connor A, Perez-Ordoñez B, Shago M, et al. Mammary analog secretory carcinoma of salivary gland origin with the *ETV6* gene rearrangement by FISH: expanded morphologic and immunohistochemical spectrum of a recently described entity. *Am J Surg Pathol*. 2012;36:27–34.
22. Chiosea SI, Griffith C, Assad A, et al. The profile of acinic cell carcinoma after recognition of mammary analog secretory carcinoma. *Am J Surg Pathol*. 2012;36:343–350.
23. Majewska H, Skálová A, Stodulski D, et al. Mammary analogue secretory carcinoma of salivary glands: first retrospective study of a new entity in Poland with special reference to *ETV6* gene rearrangement. *Virchows Arch*. 2015;466:245–254.
24. Pinto A, Nosé V, Rojas C, et al. Searching for mammary analogue secretory carcinoma among their mimicks. *Mod Pathol*. 2014;27:30–37.
25. Bishop JA. Unmasking MASC: bringing to light the unique morphologic, immunohistochemical and genetic features of the newly recognized mammary analogue secretory carcinoma of salivary glands. *Head Neck Pathol*. 2013;7:35–39.
26. Skalova A, Vanecek T, Simpson RHW, et al. Mammary analogue secretory carcinoma of salivary glands. Molecular analysis of 25 *ETV6* gene rearranged tumors with lack of detection of classical *ETV6-NTRK3* fusion transcript by standard rt-pcr: report of 4 cases harboring *ETV6-X* gene fusion. *Am J Surg Pathol*. 2016;40:3–13.
27. Ito Y, Ishibashi K, Masaki A, et al. Mammary analogue secretory carcinoma of salivary glands: a clinicopathological and molecular study including 2 cases harboring *ETV6-X* fusion. *Am J Surg Pathol*. 2015;39:602–610.
28. Murphy DA, Ely HA, Shoemaker R, et al. Detecting gene rearrangements in patient populations through a 2-step diagnostic test comprised of rapid IHC enrichment followed by sensitive next-generation sequencing. *Appl Immunohistochem Mol Morphol*. 2017;25:513–523.
29. Viswanatha DS, Foucar K, Berry BR, et al. Blastic mantle cell leukemia: an unusual presentation of blastic mantle cell lymphoma. *Mod Pathol*. 2000;13:825–833.
30. Gaffney R, Chakerian A, O'Connell JX, et al. Novel fluorescent ligase detection reaction and flow cytometric analysis of SYT-SSX fusions in synovial sarcoma. *J Mol Diagn*. 2003;5:127–135.
31. Antonescu CR, Kawai A, Leung DH, et al. Strong association of SYT-SSX fusion type and morphologic epithelial differentiation in synovial sarcoma. *Diagn Mol Pathol*. 2000;9:1–8.
32. Bourgeois JM, Knezevich SR, Mathers JA, et al. Molecular detection of the ETV6-NTRK3 gene fusion differentiates congenital fibrosarcoma from other childhood spindle cell tumors. *Am J Surg Pathol*. 2000;24:937–946.
33. Su RJ, Jonas BA, Welborn J, et al. Chronic eosinophilic leukemia, NOS with t(5;12)(q31;p13)/ETV6-ACSL6 gene fusion: a novel variant of myeloid proliferative neoplasm with eosinophilia. *Hum Pathol*. 2016;5:6–9.
34. Drilon A, Siena S, Ou SI, et al. Safety and antitumor activity of the multitargeted Pan-TRK, ROS1, and ALK inhibitor Entrectinib: Combined results from two phase I trials ALKA-372-001 and STARTRK-1. *Cancer Discov*. 2017;7:400–407.
35. Drilon A, Li G, Dogan S, et al. What hides behind the MASC: clinical response and acquired resistance to entrectinib after *ETV6-NTRK3* identification in a mammary analogue secretory carcinoma (MASC). *Ann Oncol*. 2016;27:920–926.
36. Tannenbaum-Dvir S, Glade Bender JL, Church AJ, et al. Characterization of a novel fusion gene *EML4-NTRK3* in a case of recurrent congenital fibrosarcoma. *Cold Spring Harb Mol Case Stud*. 2015;1:a000471.
37. Tirado CA, Siangchin K, Shabsovich DS, et al. A novel three-way rearrangement involving *ETV6* (12p13) and *ABL1* (9q34) with an unknown partner on 3p25 resulting in a possible *ETV6-ABL1* fusion in a patient with acute myeloid leukemia: a case report and a review of the literature. *Biomark Research*. 2016;4:16.
38. Abe A, Yamamoto Y, Iba S, et al. *ETV6-LPXN* fusion transcript generated by t(11;12)(q12.1;p13) in a patient with relapsing acute myeloid leukemia with NUP98-HOXA9. *Genes Chromosomes Cancer*. 2016;55:242–250.
39. Garcia DR, Arancibia AM, Ribeiro RC, et al. Intrachromosomal amplification of chromosome 21 (iAMP21) detected by *ETV6/RUNX1* FISH screening in childhood acute lymphoblastic leukemia: a case report. *Rev Bras Hematol Hemoter*. 2013;35:369–371.

40. Strehl S, Nebral K, König M, et al. *ETV6-NCOA2*: a novel fusion gene in acute leukemia associated with coexpression of T-lymphoid and myeloid markers and frequent NOTCH1 mutations. *Clin Cancer Res*. 2008;14:977–983.
41. Wang K, Russell JS, McDermott JD, et al. Profiling of 149 salivary duct carcinomas, carcinoma ex pleomorphic adenomas, and adenocarcinomas, not otherwise specified reveals actionable genomic alterations. *Clin Cancer Res*. 2016;22:6061–6068.
42. Skálová A, Vanecek T, Majewska H, et al. Mammary analogue secretory carcinoma of salivary glands with high-grade transformation: report of 3 cases with the *ETV6-NTRK3* gene fusion and analysis of TP53, beta-catenin, EGFR, and CCND1 genes. *Am J Surg Pathol*. 2014;38:23–33.
43. Luo W, Lindley SW, Lindley PH, et al. Mammary analog secretory carcinoma of salivary gland with high-grade histology arising in palate, report of a case and review of literature. *Int J Clin Exp Pathol*. 2014;7:9008–9022.
44. Li GG, Somwar R, Joseph J, et al. Antitumor activity of RXDX-105 in multiple cancer types with RET rearrangements or mutations. *Clin Cancer Res*. 2017;23:2981–2990.
45. Sabari JK, Siau ED, Drilon A. Targeting RET-rearranged lung cancers with multikinase inhibitors. *Oncoscience*. 2017;4:23–24.
46. Chi HT, Ly BT, Kano Y, et al. *ETV6-NTRK3* as a therapeutic target of small molecule inhibitor PKC412. *Biochem Biophys Res Commun*. 2012;429:87–92.
47. Tognon CE, Somasiri AM, Evdokimova VE, et al. *ETV6-NTRK3*-mediated breast epithelial cell transformation is blocked by targeting the IGF1R signaling pathway. *Cancer Res*. 2011;71:1060–1070.

2.2.6. MAMMARY ANALOG SECRETORY CARCINOMA OF THE NASAL CAVITY: CHARACTERIZATION OF 2 CASES AND THEIR DISTINCTION FROM OTHER LOW-GRADE SINONASAL ADENOCARCINOMAS

MASC is a low-grade salivary gland tumor with majority of cases characterized by a t(12;15)(p13;q25) translocation, resulting in an ETV6-NTRK3 gene fusion. Most MASCs are localized to the parotid gland and intraoral minor salivary glands. Moreover, ETV6-rearranged carcinomas with secretory features have been reported recently in the thyroid (with and without a history of radiation exposure) [65, 66], skin [67], and in very rare instances in the sinonasal tract [68]. In this report, we described 2 cases of primary MASC in the sinonasal tract and provided a detailed clinical and histopathologic characterization of their morphology, immunohistochemical profile, and genetic background and highlighted features allowing its separation from its recently described molecular mimicker, ETV6-rearranged low-grade sinonasal adenocarcinoma [68].

Mammary Analog Secretory Carcinoma of the Nasal Cavity

Characterization of 2 Cases and Their Distinction From Other Low-grade Sinonasal Adenocarcinomas

Martina Baneckova, MD,† Abbas Agaimy, MD,‡ Simon Andreasen, MD,§‖ Tomas Vanecek, PhD,¶ Petr Steiner, Mgr,*¶ David Slouka, MD, MBA, PhD,# Tomas Svoboda, MD, PhD,** Marketa Miesbauerova, MD,*† Michael Michal Jr, MD,*† and Alena Skálová, MD, PhD*†*

Abstract: Secretory carcinoma, originally described as mammary analog secretory carcinoma (MASC), is a low-grade salivary gland tumor characterized by a t(12;15)(p13;q25) translocation, resulting in an *ETV6-NTRK3* gene fusion. Most MASCs are localized to the parotid gland and intraoral minor salivary glands. Moreover, *ETV6*-rearranged carcinomas with secretory features have been reported recently in the thyroid (with and without a history of radiation exposure), skin, and in very rare instances in the sinonasal tract. Here, we describe 2 cases of primary MASC in the sinonasal tract and provide a detailed clinical and histopathologic characterization of their morphology, immunohistochemical profile, and genetic background and highlight features allowing for its separation from its recently described molecular mimicker, *ETV6*-rearranged low-grade sinonasal adenocarcinoma.

Key Words: nasal cavity, mammary analog secretory carcinoma, MASC, low-grade sinonasal adenocarcinoma, *ETV6-NTRK3*

(*Am J Surg Pathol* 2018;00:000–000)

Secretory carcinoma (SC), originally described as mammary analog secretory carcinoma (MASC), is a low-grade salivary gland tumor characterized by a t(12;15)(p13;q25) translocation, resulting in an *ETV6-NTRK3* gene fusion.[1] In addition to having identical genetics with SC, MASC expresses S100 and mammaglobin while being negative for DOG-1 and p63, thus highly resembling SC of the breast.[2] However, these features are unique among tumors of the salivary gland.

Most MASCs are localized in the parotid gland, submandibular gland, and minor salivary glands of the oral cavity, such as soft palate, lips, base of the tongue, and buccal mucosa. Since its description in the major and minor salivary glands,[1] MASC has been described in several other locations, such as skin,[3–5] thyroid,[6–8] and the sinonasal tract.[9,10] The first case of MASC of the sinonasal tract was reported by Lurquin et al,[9] and, very recently, another case with high-grade transformation was reported in the maxillary sinus.[10]

Primary sinonasal adenocarcinomas (SNACs) are uncommon and morphologically heterogenous.[11] These tumors are divided into nonsalivary and salivary types. Non–salivary-type SNACs are further classified into 2 broad categories: intestinal-type adenocarcinoma (ITAC) and the non–intestinal-type adenocarcinoma (non-ITAC).[12] The non–intestinal-type SNAC is of presumed surface epithelium/seromucinous gland origin and accounts for <1% of head and neck cancers.[11–13] It is morphologically a very diverse group, as it can show high-grade or low-grade features, as determined by the proliferative activity and pattern of growth.[14–17] An increasing number of distinct types of non-ITAC has been recognized recently, including a subset with rearrangement of the *ETV6* gene, the so-called *ETV6* gene–rearranged sinonasal low-grade SNAC.[18]

By screening a series of low-grade SNACs with fluorescence in situ hybridization (FISH) and/or reverse transcription polymerase chain reaction (RT-PCR), we identified 2 cases of primary MASC arising in the nasal cavity, and herein we provide a detailed clinical, histopathologic, and molecular characterization. Recognizing MASC in the sinonasal tract among other SNACs of the salivary type, as well as *ETV6*-rearranged low-grade SNAC, is important, as the correct diagnosis is prognostically relevant, and *ETV6*-related fusions serve as therapeutic targets.[19,20]

MATERIALS AND METHODS

Patient Material

Fifteen cases of low-grade non–intestinal-type SNAC with secretory features resembling MASC were identified in a review of the Salivary Gland Tumor Registry, at the

From the Departments of *Pathology; #Otorhinolaryngology; **Oncology and Radiotherapy, Oncological Clinic, Faculty of Medicine in Plzen, Charles University; †Bioptic Laboratory Ltd; ¶Department of Molecular Pathology, Bioptic Laboratory Ltd, Plzen, Czech Republic; ‡Institute of Pathology, Friedrich-Alexander-University, Erlangen, Germany; §Department of Otorhinolaryngology and Maxillofacial Surgery, Køge University Hospital; and ‖Department of Otolaryngology Head & Neck Surgery, Rigshospitalet, Denmark.

Conflicts of Interest and Source of Funding: Supported by the National Sustainability Program I (NPU I) Nr. LO1503 and by the grant SVV–2017 No. 260 391 provided by the Ministry of Education, Youth and Sports of the Czech Republic. The authors have disclosed that they have no significant relationships with, or financial interest in, any commercial companies pertaining to this article.

Correspondence: Alena Skálová, MD, PhD, Sikl's Department of Pathology, Medical Faculty of Charles University, Faculty Hospital, E. Benese 13, Plzen 305 99, Czech Republic (e-mail: skalova@fnplzen.cz).

TABLE 1. Antibodies Used for Immunohistochemical Study

Antibody Specificity	Clone	Dilution	Antigen Retrieval/Time (min)	Source
S100 protein	Polyclonal	RTU	CC1/20	Ventana Medical Systems
Mammaglobin	304-1A5	RTU	CC1/36	DakoCytomation
CK7	OV-TL 12/30	1:200	CC1/36	DakoCytomation
CK20	Ks20.8	1:100	CC1/36	DakoCytomation
CDX2	EPR2764Y	RTU	CC1/64	Cell Marque
GCDFP-15	EP1582y	RTU	CC1/64	Cell Marque
p63	4A4	RTU	CC1/64	Ventana Medical Systems
DOG-1	SP31	RTU	CC1/36	Cell Marque
GATA-3	L50-823	1:200	CC1/52	BioCareMedical
SOX10	Polyclonal	1:100	CC1/64	Cell Marque
Pan-TRK	A7H6R	1:20	CC1/64	Cell Signaling
SATB2	Polyclonal	1:100	CC2/68	Sigma Aldrich
STAT5a	Polyclonal	1:400	CC1/36	AssayDesigns Inc.
MIB1	30-9	RTU	CC1/64	Ventana Medical Systems

CC1 indicates EDTA buffer, pH 8.6; RTU, ready to use.

Department of Pathology, Faculty of Medicine in Plzen, and Biopticka Laboratory Ltd, Plzen, Czech Republic. Two additional cases with features mimicking MASC were retrieved from the files of the Institute of Pathology, Friedrich-Alexander University, Erlangen, Germany, thus amounting to a total of 17 cases. Clinical follow-up was obtained from the patients, their physicians, or from referring pathologists.

Histology and Immunohistochemistry

For conventional microscopy, tissues were fixed in formalin, routinely processed, embedded in paraffin (FFPE), cut, and stained with hematoxylin and eosin. In most cases, additional stains were also performed, including periodic acid-Schiff with and without diastase, mucicarmine, and alcian blue at pH 2.5.

For immunohistochemistry, 4-µm-thick sections were cut from paraffin blocks and mounted on positively charged slides (TOMO; Matsunami Glass Ind., Japan). Sections were processed on a BenchMark ULTRA (Ventana Medical Systems, Tucson, AZ), deparaffinized, and subjected to heat-induced epitope retrieval by immersion in a CC1 solution (pH 8.6) at 95°C. Following antigen retrieval, sections were stained with a pan-TRK antibody cocktail consisting of rabbit monoclonal antibodies, all obtained from Cell Signaling (Danvers, MA), targeting pan-TRK (clone A7H6R, active against TrkA, TrkB, and TrkC, 1:50 dilution), ROS1 (clone D4D6, 1:50), and ALK (clone D5F3, 1:50), as described elsewhere.[21]

All other primary antibodies used are summarized in Table 1. Visualization was performed using the ultraView Universal DAB Detection Kit (Roche Diagnostics, Mannheim, Germany) and ultraView Universal Alkaline Phosphatase Red Detection Kit (Roche Diagnostics). The slides were counterstained with Mayer hematoxylin. Appropriate positive and negative controls were used.

Molecular Genetic Study

Detection of *ETV6-NTRK3* Fusion Transcript by RT-PCR

RNA was extracted using the RecoverAll Total Nucleic Acid Isolation Kit (Ambion, Austin, TX). cDNA was synthesized using the Transcriptor First Strand cDNA Synthesis Kit (RNA input 500 ng) (Roche Diagnostics). All procedures were performed according to the manufacturer's protocols. Amplification of a 105 bp product and a 133 bp product of the β2-microglobulin gene, and a 247 bp product of the *PGK* gene was used to test the quality of the extracted RNA, as previously described.[22–24] This resulted in the detection of the classic fusion transcript of exon 5 of the *ETV6* gene and exon 15 of the *NTRK3* gene.[25]

For PCR, 2 µL of cDNA was added to the reaction, which consisted of 12.5 µL of HotStar Taq PCR Master Mix (Qiagen, Hilden, Germany), 10 pmol of each primer (Table 2), and distilled water up to 25 µL.[26,27] The amplification program comprised denaturation at 95°C for 14 minutes followed by 45 cycles of denaturation at 95°C for 1 minute; annealing at temperatures shown in Table 2 was carried out for 1 minute and extension at 72°C for 1 minute. The procedure was completed by incubation at 72°C for 7 minutes.

Successfully amplified PCR product was purified with magnetic particles using Agencourt AMPure (Agencourt

TABLE 2. Primers for Detection of *ETV6-NTRK3* Fusion Transcripts

Original Primer Name	Sequence	Annealing Tempearture (°C)	Localization
TEL971* (ETV6A†)	ACCACATCATGGTCTCTGTCTCCC	65	*ETV6* exon 5 outer
TRKC1059* (NTRK3A†)	CAGTTCTCGCTTCAGCACGATG	65	*NTRK3* exon 15 outer

*Bourgeois et al.[25]
†Ito et al,[26] Skalova et al.[27]

Bioscience Corporation, A Beckman Coulter Company, Beverly, MA). The product was then bidirectionally sequenced using Big Dye Terminator Sequencing Kit (PE/Applied Biosystems, Foster City, CA) and purified with magnetic particles using Agencourt CleanSEQ (Agencourt Bioscience Corporation); all this was carried out according to the manufacturer's protocols and run on an automated sequencer ABI Prism 3130xl (Applied Biosystems) at a constant voltage of 13.2 kV for 11 minutes.

Detection of *ETV6* and *NTRK3* by FISH Method

Four-µm-thick FFPE sections were placed onto positively charged slides. Hematoxylin and eosin–stained slides were examined for determination of areas for cell counting.

The unstained slides were routinely deparaffinized and incubated in the 1× Target Retrieval Solution Citrate pH 6 (Dako, Glostrup, Denmark) at 95°C/40 minutes and subsequently cooled for 20 minutes at room temperature in the same solution. The slides were washed in deionized water for 5 minutes and digested in protease solution with Pepsin (0.5 mg/mL) (Sigma Aldrich, St Louis, MO) in 0.01 M HCl at 37°C/25 to 60 minutes according to the sample conditions. The slides were then placed in deionized water for 5 minutes, dehydrated in a series of ethanol solution (70%, 85%, 96% for 2 min each), and air-dried.

For the detection of *ETV6* rearrangement, a commercial probe, Vysis *ETV6* Break Apart FISH Probe Kit (Vysis/Abbott Molecular, Illinois), was used. The *ETV6* probe was mixed with water and LSI/WCP (Locus-Specific Identifier/Whole Chromosome Painting) Hybridization buffer (Vysis/Abbott Molecular) in a 1:2:7 ratio, respectively.

The probe for the detection of the rearrangement of the *NTRK3* gene region was mixed from custom-designed SureFISH probes (Agilent Technologies Inc., Santa Clara, CA). Chromosomal regions for *NTRK3* break-apart probe oligos are chr15:87501469-88501628 and chr15:88701444-89700343. The probe mixture was prepared from corresponding probes (each color was delivered in a separated well), deionized water, and LSI Buffer (Vysis/Abbott Molecular) in a 1:1:1:7 ratio, respectively.

An appropriate amount of mixed probe was applied on specimens, covered with a glass coverslip, and sealed with rubber cement. The slides were incubated in the ThermoBrite instrument (StatSpin/Iris Sample Processing, Westwood, MA) with codenaturation at 85°C/8 minutes and hybridization at 37°C/16 hours. The rubber-cemented coverslip was then removed, and the slide was placed in posthybridization wash solution (2× SSC/0.3% NP-40) at 72°C/2 minutes. The slide was air-dried in the dark, counterstained with 4', 6'-diamidino-2-phenylindole (DAPI; Vysis/Abbott Molecular), coverslipped, and immediately examined.

FISH Interpretation

The sections were examined with an Olympus BX51 fluorescence microscope (Olympus Corporation, Tokyo, Japan) using a ×100 objective and filter sets Triple Band Pass (DAPI/SpectrumGreen/SpectrumOrange), Dual Band Pass (SpectrumGreen/SpectrumOrange), and Single Band Pass (SpectrumGreen or SpectrumOrange).

For each probe, 100 randomly selected non-overlapping tumor cell nuclei were examined for the presence of yellow or green and orange fluorescent signals. Yellow signals were considered negative, and separate orange and green signals were considered as positive.

Cutoff values were set to >10% of nuclei with chromosomal breakpoint signals (mean, +3 SD in normal non-neoplastic control tissues).

Sample Preparation for Next-generation Sequencing

For next-generation sequencing (NGS) studies, 2-3 FFPE sections (10 µm thick) were macrodissected to isolate tumor-rich regions. The samples were extracted for total nucleic acid using Agencourt FormaPure Kit (Beckman Coulter, Brea, CA), following the corresponding protocol with overnight digestion and an additional 80°C incubation, as described in the modification of the protocol by ArcherDX (ArcherDX Inc., Boulder, CO). Total nucleic acid was quantified using the Qubit Broad Range RNA Assay Kit (Thermo Fisher Scientific) and 2 µL of sample.

RNA Integrity Assessment and Library Preparation for NGS

Unless otherwise indicated, 250 ng of FFPE RNA was used as an input for NGS studies. To assess RNA quality, the PreSeq RNA QC Assay using iTaq Universal SYBR Green Supermix (Biorad, Hercules, CA) was performed on all samples during library preparation to generate a measure for the integrity of RNA (in the form of a cycle threshold value). Library preparation and RNA QC were performed following the Archer Fusion Plex Protocol for Illumina (ArcherDX Inc.). A custom primer set with 28 primers spanning regions on 3 specific genes of interest including *ETV6* was used. Final libraries were diluted 1:100,000 and quantified in a 10 µL reaction following the Library Quantification for Illumina Libraries protocol and assuming a 200 bp fragment length (KAPA, Wilmington, MA). The concentration of the final libraries was around 200 n. The threshold representing the minimum molar concentration for which sequencing can be robustly performed was set at 50 nM.

NGS and Analysis (Archer)

The libraries were sequenced on an MiSeq sequencer (Illumina, San Diego, CA). The libraries were diluted to 4 nM, and equal amounts of up to 16 libraries were pooled per run. The recommended number of raw reads per sample was set to 500,000. Library pools were diluted to 16 pM library stock with 10% 12.5 pM PhiX and loaded in the MiSeq cartridge. Analysis of sequencing results was performed using the Archer Analysis software (version 5; ArcherDX Inc.). Fusion parameters were set to a minimum of 5 valid fusion reads with a minimum of 3 unique start sites within the valid fusion reads.

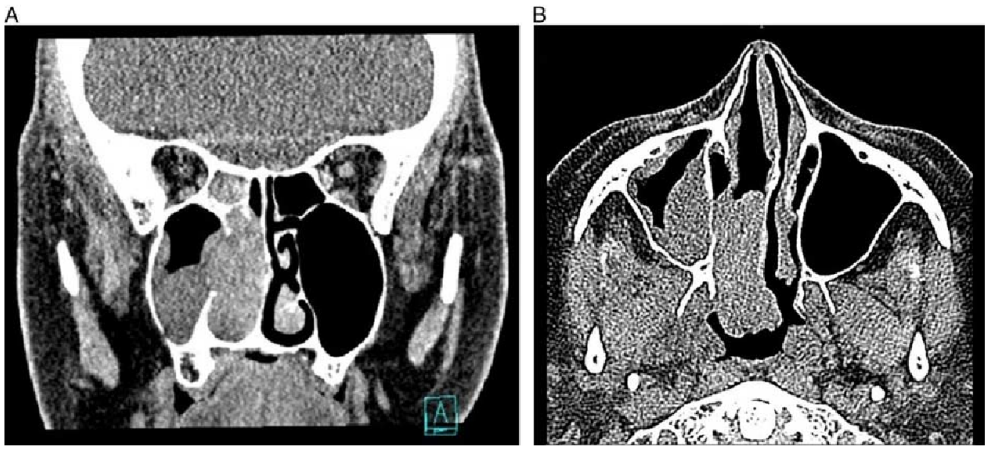

FIGURE 1. Representative imaging of case 2. A, Coronal computed tomography of case 2 demonstrating a right-sided nasal mass. B, The mass extends into the nasopharynx. There was no involvement of the maxillary sinus.

RESULTS

Case Histories

Case 1

A 51-year-old woman, nonsmoker without a prior history of breast cancer, presented with intermittent tenderness or pain behind the right eye and occasional forehead discomfort. A mass was identified on the right side of the nasal septum, and the patient was referred to surgical resection. The resected specimen measured 1.5×1.5×0.4 cm, and the patient was staged as T1N0M0. The patient was alive and showed no evidence of recurrent disease after > 10 years of follow-up.

Case 2

A 65-year-old woman, nonsmoker without prior history of breast cancer, presented with right-sided nasal obstruction, nasopharyngeal secretion, and occasional retrobulbar pain. Past medical history was unremarkable except for a pleomorphic adenoma of the palate 5 years previously. Computed tomography identified a mass in the right nasal cavity extending into the nasopharynx. The patient underwent surgical excision of the mass including the middle turbinate along with maxillary sinus antrostomy, right ethmoidectomy, and partial resection of the nasal septum. The tumor measured 4×4×1.5 cm, and the patient was staged as T2NxM0. The patient received adjuvant radiotherapy and is alive with no evidence of disease after 4 years of follow-up (Figs. 1A, B).

Detailed clinicopathologic findings in these 2 patients are presented in Table 3.

Histopathology and Immunohistochemical Findings

Cases 1 and 2 had histologic features and immunoprofiles identical to salivary gland MASC. The tumors were unencapsulated and composed of tubular, papillary, and microcystic growth patterns with invasive margins (Fig. 2A). The tumor cells had low-grade vesicular and round to oval nuclei with fine, granular chromatin. Abundant eosinophilic homogenous extracellular periodic acid-Schiff with diastase–positive material (Fig. 2B) was present in both cases. The tumors were composed of solid microcystic growth patterns, in places divided by thick hyalinized fibrous septa (Fig. 2C). Focal necrotic areas were present in case 2 (Fig. 2D). In contrast to acinic cell carcinoma (AciCC), both tumors lacked cytoplasmic periodic acid-Schiff with diastase–positive zymogen granules. Mitoses were few, and there was no lymphovascular invasion or perineural growth.

In contrast, cases 3 to 17 displayed histologic features of low-grade tubulopapillary adenocarcinomas or

TABLE 3. Clinical Findings in 2 MASCs of the Nasal Cavity

Cases	Age (y)/Sex	Site	Size (cm)	Stage (TNM)	Local Recurrence	Duration of Symptoms (y)	Treatment	Follow-up (y)	Outcome
1	51/F	Right nasal septum	1.5×1.5×0.4	T1N0M0	No	1-2	Surgery	14	Alive NED
2	65/F	Right nasal cavity	4×4×1.5	pT2pNxM0	No	1	Surgery+RT	4	Alive NED

F indicates female; NED, no evidence of disease; RT, radiotherapy.

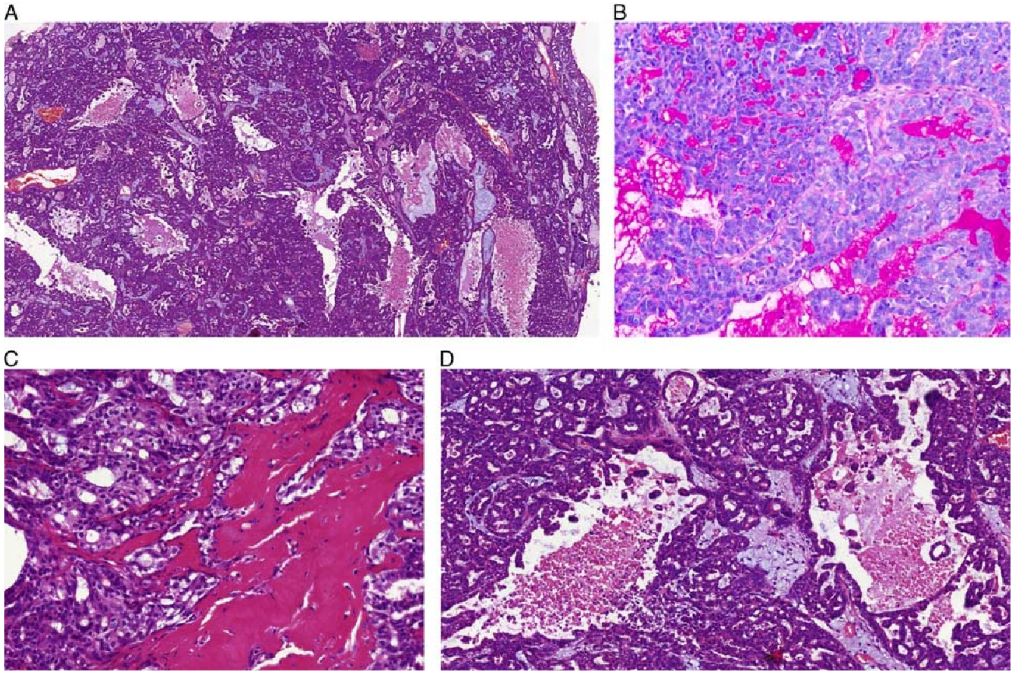

FIGURE 2. Histologic findings of sinonasal MASC. A, MASC shows admixed tubular, papillary, and microcystic growth patterns. B, Abundant periodic acid-Schiff with diastase–positive extracellular material within tubular and cystic spaces. C, The tumors were composed of solid, microcystic growth patterns, occasionally divided by thick hyalinized fibrous septa. D, Focal necrosis was present in case 2.

low-grade non–intestinal-type SNAC, not otherwise specified.[13,16,17]

The immunohistochemical findings are summarized in Tables 4 and 5. Both MASCs were positive for CK7, SOX10, GATA3, STAT5, and S100 (diffuse and strong staining in all tumor cells). Immunohistochemical staining for mammaglobin was diffusely positive in case 1 and focally positive in case 2 (Figs. 3A–D). Both cases were negative for p63 protein, CK20, CDX2, SATB2, and DOG-1 (Table 4). The remaining 15 cases, except for case 13, were negative for mammaglobin. Case 13 was S100 protein/SOX10/GATA3-positive with focal staining for mammaglobin in <5% of the tumor cells. Data from all 17 cases are summarized in Table 5.

TABLE 4. Immunohistochemical Results of 2 Cases of MASC in the Nasal Cavity

Antibody	Case 1	Case 2
CK7	+(D)	+(D)
S100	+(D)	+(F)
Mammaglobin	+(D)	+(F)
GATA3	+(D)	+(D)
SOX10	+(D)	+(D)
Pan-TRK	+	+
Stat5	+	+
p63	Neg	Neg
CK20	Neg	Neg
CDX2	Neg	Neg
DOG-1	Neg	Neg
GCDFP*	+(F)*	+(E)*
MIB1	5%	40%

*Immunochemistry performed at Department of Otorhinolaryngology and Maxillofacial Surgery, Køge University Hospital, and Department of Otolaryngology Head & Neck Surgery Rigshospitalet.

D indicates diffuse staining; E, staining of extracellular material; F, focal staining.

Genetic Findings

After histologic and immunohistochemical characterization, all 17 cases were characterized for the presence of the *ETV6-NTRK3* fusion transcript and/or rearrangement of *ETV6*. These findings are summarized in Table 6. Two cases, cases 1 and 2, showed *ETV6* gene rearrangement by FISH. Case 1 was negative with RT-PCR, but a product was identified with RT-PCR in case 2, and sequencing confirmed an exon 5 to 15 junction. In case 1, NGS identified an atypical exon 5-13 fusion. Cases 3 to 17 were negative or not analyzable with either RT-PCR or FISH, or were negative for both methods (Table 6 and Figs. 4A–C).

TABLE 5. Immunohistochemical Results of All 17 Cases

Case No.	Final Diagnosis	CK7	CK20	DOG-1	GATA3	SOX10	S100	MGA	p63	STAT5	MIB1	CDX2	SATB2
1	MASC	+	Neg	Neg	+	+	+	+	Neg	+	5%	Neg	Neg
2	MASC	+	Neg	Neg	+	+	+	+	Neg	+	40%	Neg	Neg
3	LG SNAC	+	Neg	Neg	+	+	+	Neg	Neg	ND	ND	Neg	ND
4	LG SNAC	Neg	Neg	Neg	+	+	+	Neg	Neg	ND	ND	Neg	ND
5	LG SNAC	+	Neg	Neg	Neg	Neg	Neg	Neg	Neg	ND	20%	Neg	Neg
6	LG SNAC	+	Neg	Neg	Neg	Neg	Neg	Neg	Neg	+	3%	Neg	Neg
7	LG SNAC	+	Neg	Neg	+	+	Neg	Neg	Neg	+	3%	Neg	Neg
8	LG SNAC	+	Neg	Neg	ND	+	+	Neg	Neg	ND	5%	Neg	ND
9	LG SNAC	+	Neg	Neg	Neg	+	+	Neg	Neg	+	3%	Neg	Neg
10	LG SNAC	+	Neg	NA	NA	NA	Neg	NA	NA	NA	NA	NA	Neg
11	LG SNAC	+	Neg	Neg	Neg	Neg	Neg	Neg	Neg	ND	90%	Neg	ND
12	LG SNAC	+	Neg	Neg	Neg	Neg	+	Neg	+	+	5%	Neg	ND
13	LG SNAC	+	Neg	Neg	+	+	+	+(F) 5%	Neg	+	10%	Neg	ND
14	LG SNAC	+	Neg	Neg	Neg	Neg	+(F)	Neg	+	+(F)	2%	Neg	Neg
15	LG SNAC	+	Neg	Neg	Neg	Neg	+	Neg	Neg	Neg	2%	Neg	Neg
16	LG SNAC	+	Neg	Neg	ND	+(F)	+	Neg	Neg	ND	2%	Neg	Neg
17	LG SNAC	+	Neg	Neg	Neg	+	Neg	Neg	Neg	ND	0%	ND	Neg

F indicates focally; LG, low grade; NA, not analyzable; ND, not done; Neg, negative.

DISCUSSION

In contrast to the sinonasal tract, diagnosing MASC in the major salivary glands as well as the oral minor glands is not difficult in most cases. MASC is well characterized not only by histologic and immunohistochemical features but also by the *ETV6-NTRK3* gene fusion.[1] However, if MASC is present in unexpected locations, the differential diagnosis is more challenging. MASC can be confused with other salivary gland tumors, including AciCC and adenocarcinoma not otherwise specified.[28] More than half of cases previously diagnosed as zymogen granule–poor AciCC were positive for *ETV6* translocation on rereview and therefore classified as MASC, and most tumors previously diagnosed as AciCC of the minor salivary glands also represent MASC.[29,30] In contrast to AciCC, MASC shows no basophilic granularity in the cytoplasm of any of the constituent cells, this being the hallmark of the serous acinar cells of AciCC. Moreover, MASC has a completely different immunohistochemical profile than AciCC, almost always strongly expressing

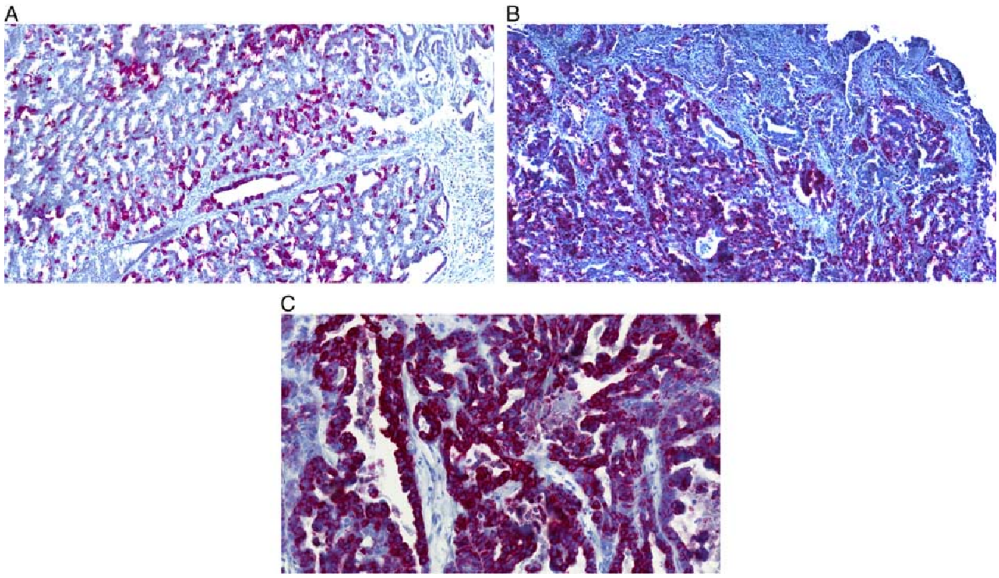

FIGURE 3. Immunohistochemical characteristics of MASC in the sinonasal tract. In both MASCs, tumor cells were intensely and diffusely positive for mammaglobin (A), S100 (B), and CK7 (C).

TABLE 6. Results of Molecular Analysis of 17 Cases of Sinonasal Carcinomas

		FISH		RT-PCR		
Cases	**Final Diagnosis**	***ETV6***	***NTRK3***	**Exons 5-15 Fusion Transcript**	**Archer NGS**	**Gene Status**
1	MASC	Break	NA	Neg	*ETV6-NTRK3* exons 5-13	*ETV6-NTRK3*
2	MASC	Break	Break	+	ND	*ETV6-NTRK3*
3	LG SNAC	NA	Intact	NA	ND	Neg
4	LG SNAC	Intact	Intact	Neg	ND	Neg
5	LG SNAC	Intact	ND	Neg	ND	Neg
6	LG SNAC	Intact	ND	Neg	ND	Neg
7	LG SNAC	Intact	ND	Neg	ND	Neg
8	LG SNAC	NA	ND	Neg	ND	Neg
9	LG SNAC	Intact	ND	ND	ND	Neg
10	LG SNAC	Intact	ND	ND	ND	Neg
11	LG SNAC	Intact	ND	Neg	ND	Neg
12	LG SNAC	NA	ND	NA	ND	NA
13	LG SNAC	NA	ND	Neg	ND	Neg
14	LG SNAC	Intact	ND	Neg	ND	Neg
15	LG SNAC	Intact	ND	Neg	ND	Neg
16	LG SNAC	NA	ND	NA	ND	NA
17	LG SNAC	Intact	ND	Neg	ND	Neg

LG indicates low grade; NA, not analyzable; ND, not done.

S100 protein and mammaglobin,[1,31,32] and lacking DOG-1 expression.[33]

Low-grade SNACs represent a histologically heterogenous group of tumors, including non-ITAC and ITAC subtypes.[13] In recent years, an increasing number of distinct types of SNACs have been recognized, including HPV-related multiphenotypic sinonasal carcinoma, SMARCB1-deficient sinonasal carcinoma, and tubulopapillary low-grade SNAC.[16,34–37] Recently, Andreasen et al[18] reviewed a series of low-grade SNACs of non-ITAC type with tubulopapillary growth pattern and found a subset of tumors harboring *ETV6* rearrangements and the *ETV6-NTRK3* fusion in 2 of 3 cases. From a strictly genetic perspective, *ETV6*-rearranged low-grade SNAC represents a pitfall for identifying true sinonasal MASC. However, despite the identical genetic features of sinonasal MASC and *ETV6*-rearranged low-grade SNAC, the following features allow for accurate separation. First, all 3 *ETV6*-rearranged low-grade SNACs reported were predominantly tubular, composed of cylindrical to cuboidal

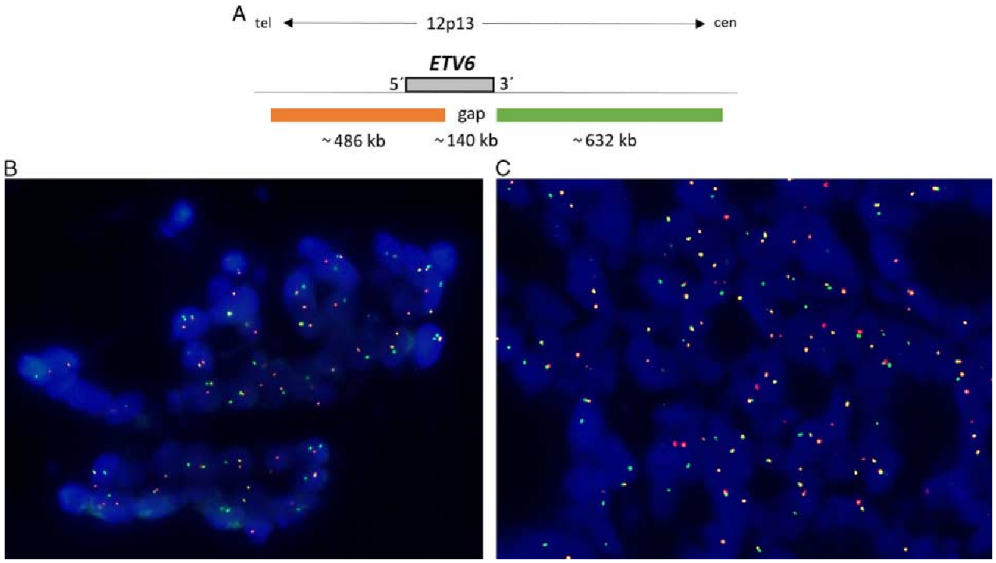

FIGURE 4. FISH. A, Design of the *ETV6* break-apart probe. B, Case 1 showing separate green and orange signals for *ETV6*. C, *NTRK3* indicating concomitant rearrangement of both genes.

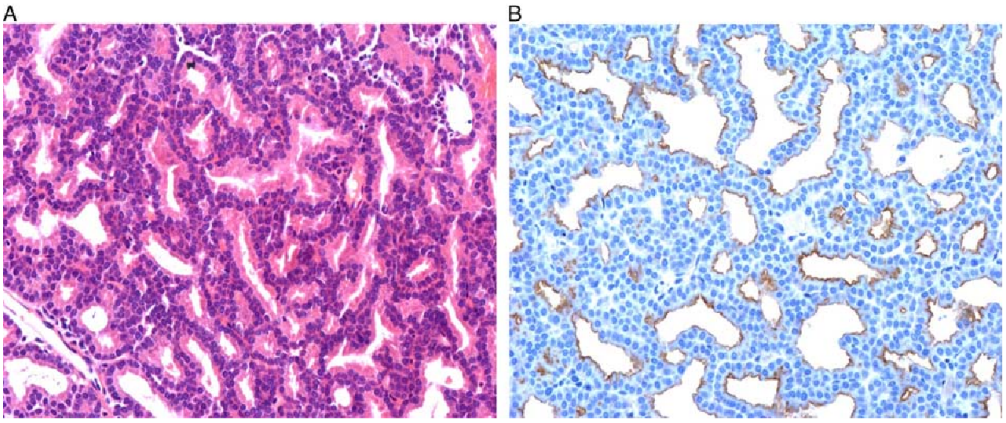

FIGURE 5. Histologic and immunohistochemical findings in *ETV6*-rearranged low-grade SNACs. A, *ETV6*-rearranged low-grade SNACs are composed of glands arranged back-to-back with little intervening stroma and minimal to absent secretory features. B, Tumors are focally DOG-1 positive.

tumor cells with occasional apocrine features and focal trabecular areas, which were not prominent features of sinonasal MASC. Second, tumor cells in *ETV6*-rearranged low-grade SNAC were arranged back-to-back with little intervening stroma with minimal or absent secretory features (Fig. 5A).[18] In contrast, both our MASCs showed abundant hyalinized septae and pronounced secretory features. Third, *ETV6*-rearranged low-grade SNAC is positive for DOG-1, negative for mammaglobin, and negative or patchy positive for S100, with the opposite being the case in MASC (Fig. 5B). Fourth, both MASCs presented here were invasive, whereas this was not seen in *ETV6*-rearranged low-grade SNAC.

The most important reason for separating these 2 entities is the difference in clinical behavior. While low-grade non-ITAC, including *ETV6*-rearranged low-grade SNAC, behaves in an essentially benign manner, MASC is a bona fide malignancy. Awareness of the existence of MASC within this anatomic region is important not only for separating these from the recently described *ETV6*-rearranged low-grade SNAC but also for separating MASC from more aggressive SNACs of non-ITAC and ITAC types.

In conclusion, we report 2 cases of sinonasal MASC and describe its unique features, which are valuable in its separation from *ETV6*-rearranged low-grade SNAC and other low-grade SNACs. Importantly, this separation is merited not only for academic reasons, as the more aggressive nature of MASC could necessitate treatment with TRK inhibitors.[19,20]

REFERENCES

1. Skalova A, Vanecek T, Sima R, et al. Mammary analogue secretory carcinoma of salivary glands, containing the *ETV6-NTRK3* fusion gene: a hitherto undescribed salivary gland tumor entity. *Am J Surg Pathol*. 2010;34:599–608.
2. Tognon C, Knezevich SR, Huntsman D, et al. Expression of the *ETV6-NTRK3* gene fusion as a primary event in human secretory breast carcinoma. *Cancer Cell*. 2002;2:367–376.
3. Amin SM, Beattie A, Ling X, et al. Primary cutaneous mammary analog secretory carcinoma with *ETV6-NTRK3* translocation. *Am J Dermatopathol*. 2016;38:842–845.
4. Bishop JA, Taube JM, Su A, et al. Secretory carcinoma of the skin harboring *ETV6* gene fusions: a cutaneous analogue to secretory carcinomas of the breast and salivary glands. *Am J Surg Pathol*. 2017;41:62–66.
5. Hyrcza MD, Ng T, Crawford RI. Detection of the *ETV6-NTRK3* translocation in cutaneous mammary-analogue secretory carcinoma. *Diagn Histopathol*. 2015;21:481–484.
6. Dogan S, Wang L, Ptashkin RN, et al. Mammary analog secretory carcinoma of the thyroid gland: a primary thyroid adenocarcinoma harboring *ETV6–NTRK3* fusion. *Modern Pathol*. 2016;29:985–995.
7. Dettloff J, Seethala RR, Stevens TM, et al. Mammary analog secretory carcinoma (MASC) involving the thyroid gland: a report of the first 3 cases. *Head Neck Pathol*. 2017;11:124–130.
8. Stevens TM, Kovalovsky AO, Velosa C, et al. Mammary analog secretory carcinoma, low-grade salivary duct carcinoma, and mimickers: a comparative study. *Mod Pathol*. 2015;28:1084–1100.
9. Lurquin E, Jorissen M, Debiec-Rychter M, et al. Mammary analogue secretory carcinoma of the sinus ethmoidalis. *Histopathology*. 2015; 67:749–751.
10. Xu B, Aryeequaye R, Wang L, et al. Sinonasal secretory carcinoma of salivary gland with high grade transformation: a case report of this under-recognized diagnostic entity with prognostic and therapeutic implications. *Head Neck Pathol*. 2017; DOI:10.1007/s12105-017-0855-5.
11. Slootweg PJ, Chan JKC, Stelow EB, et al. Tumours of the nasal cavity, paranasal sinuses and skull base. In: El-Naggar AK, Chan JKC, Grandis JR, Takata T, Slootweg PJ, eds. *WHO Classification of Head and Neck Tumours*, 4th ed. Lyon: IARC Press; 2017:11–76.
12. Leivo I. Sinonasal adenocarcinoma: update on classification, immunophenotype and molecular features. *Head Neck Pathol*. 2016;10:68–74.
13. Skalova A, Bell D, Bishop JA, et al. Secretory carcinoma. In: El-Naggar AK, Chan JKC, Grandis JR, Takata T, Slootweg PJ, eds. *WHO Classification of Head and Neck Tumours*, 4th ed. Lyon: IARC Press; 2017:177–178.
14. Heffner DK, Hyams VJ, Hauck KW, et al. Low-grade adenocarcinoma of the nasal cavity and paranasal sinuses. *Cancer*. 1982;50: 312–322.
15. Wenig B, Hyams VJ, Heffner DK. Nasopharyngeal papillary adenocarcinoma. A clinicopathologic study of a low-grade carcinoma. *Am J Surg Pathol*. 1988;12:946–953.

16. Skálová A, Cardesa A, Leivo I, et al. Sinonasal tubulopapillary low-grade adenocarcinoma. Histopathological, immunohistochemical and ultrastructural features of poorly recognised entity. *Virchows Arch*. 2003;443:152–158.
17. Luna MA. Sinonasal tubulopapillary low-grade adenocarcinoma. A specific diagnosis or just another seromucous adenocarcinoma? *Adv Anat Pathol*. 2015;12:109–115.
18. Andreasen S, Skálová A, Agaimy A, et al. *ETV6* Gene rearrangements characterize a morphologically distinct subset of sinonasal low-grade non–intestinal-type adenocarcinoma. A novel translocation-associated carcinoma restricted to the sinonasal tract. *Am J Surg Pathol*. 2017;41:1552–1560.
19. Drilon A, Li G, Dogan S, et al. What hides behind the MASC: clinical response and acquired resistance to entrectinib after ETV6-NTRK3 identification in a mammary analogue secretory carcinoma (MASC). *Ann Oncol*. 2016;27:920–926.
20. Skalova A, Stenman G, Simpson RHW, et al. The role of molecular testing in the differential diagnosis of salivary gland carcinomas. *Am J Surg Pathol*. 2018;42:e11–e27.
21. Murphy DA, Ely HA, Shoemaker R, et al. Detecting gene rearrangements in patient populations through a 2-step diagnostic test comprised of rapid ihc enrichment followed by sensitive next-generation sequencing. *Appl Immunohistochem Mol Morphol*. 2017;25:513–523.
22. Viswanatha DS, Foucar K, Berry BR, et al. Blastic mantle cell leukemia: an unusual presentation of blastic mantle cell lymphoma. *Mod Pathol*. 2000;13:825–833.
23. Gaffney R, Chakerian A, O'Connell JX, et al. Novel fluorescent ligase detection reaction and flow cytometric analysis of SYT-SSX fusions in synovial sarcoma. *J Mol Diagn*. 2003;5:127–135.
24. Antonescu CR, Kawai A, Leung DH, et al. Strong association of SYT-SSX fusion type and morphologic epithelial differentiation in synovial sarcoma. *Diagn Mol Pathol*. 2000;9:1–8.
25. Bourgeois JM, Knezevich SR, Mathers JA, et al. Molecular detection of the ETV6-NTRK3 gene fusion differentiates congenital fibrosarcoma from other childhood spindle cell tumors. *Am J Surg Pathol*. 2000;24:937–946.
26. Ito Y, Ishibashi K, Masaki A, et al. Mammary analogue secretory carcinoma of salivary glands: a clinicopathological and molecular study including 2 cases harboring *ETV6-X* fusion. *Am J Surg Pathol*. 2015;39:602–610.
27. Skalova A, Vanecek T, Simpson RHW, et al. Mammary Analogue Secretory Carcinoma of Salivary Glands. Molecular Analysis of 25 *ETV6* Gene Rearranged Tumors With Lack of Detection of Classical *ETV6-NTRK3* Fusion Transcript by Standard RT-PCR: Report of 4 Cases Harboring *ETV6-X* Gene Fusion. *Am J Surg Pathol*. 2016;40:3–13.
28. Chiosea SI, Griffith C, Assaad A, et al. Clinicopathological characterization of mammary analogue secretory carcinoma of salivary glands. *Histopathology*. 2012;61:387–394.
29. Chiosea SI, Griffith C, Assaad A, et al. The profile of acinic cell carcinoma after recognition of mammary analog secretory carcinoma. *Am J Surg Pathol*. 2012;36:343–350.
30. Bishop JA, Yonescu R, Batista D, et al. Most nonparotid "acinic cell carcinomas" represent mammary analog secretory carcinomas. *Am J Surg Pathol*. 2013;37:1053–1057.
31. Skálová A. Mammary analogue secretory carcinoma of salivary gland origin: an update and expanded morphologic and immunohistochemical spectrum of recently described entity. *Head Neck Pathol*. 2013;7:S30–S36.
32. Bishop JA. Unmasking MASC: bringing to light the unique morphologic, immunohistochemical and genetic features of the newly recognized mammary analogue secretory carcinoma of salivary glands. *Head Neck Pathol*. 2013;7:35–39.
33. Chenevert J, Duvvuri U, Chiosea S, et al. DOG1: a novel marker of salivary acinar and intercalated duct differentiation. *Mod Pathol*. 2012;25:919–929.
34. Bishop JA. Newly described tumor entities in sinonasal tract pathology. *Head Neck Pathol*. 2016;10:23–31.
35. Bishop JA, Andreasen S, Hang JF, et al. HPV-related multiphenotypic sinonasal carcinoma: an expanded series of 49 Cases of the tumor formerly known as HPV-related carcinoma with adenoid cystic carcinoma-like features. *Am J Surg Pathol*. 2017;41:1690–1701.
36. Andreasen S, Bishop JA, Hansen TV, et al. Human papillomavirus-related carcinoma with adenoid cystic-like features of the sinonasal tract: clinical and morphological characterization of six new cases. *Histopathology*. 2017;70:880–888.
37. Agaimy A, Hartmann A, Antonescu CR, et al. SMARCB1 (INI-1)-deficient sinonasal carcinoma: a series of 39 cases expanding the morphologic and clinicopathologic spectrum of a recently described entity. *Am J Surg Pathol*. 2017;41:458–471.

2.3. TESTICULAR AND PENILE NEOPLASIA

2.3.1.-2.3.4. PANCREATIC ANALOGUE SOLID PSEUDOPAPILLARY NEOPLASM OF THE TESTIS AND PRIMARY SIGNET RING CELL STROMAL TUMOR OF THE TESTIS – A COLLECTIVE COMMENT ON FOUR SEPARATE PAPERS STUDYING A SPECTRUM OF A SINGLE ENTITY.

Two years ago, we received for consultation a peculiar tumor that morphologically looked exactly like the solid pseudopapillary neoplasm of the pancreas (SPN-P). The only problem with this otherwise straightforward case was that the patient was a man and the tumor occurred in his testis/paratestis. We performed the IHC staining with classical SPN-P IHC markers and even these results were completely in concert with the diagnosis of SPN-P. We also performed molecular genetic analysis which revealed an oncogenic mutation in exon 3 of CTNNB1 gene, the same gene that is mutated in SPN-P. This case of course triggered our curiosity. We looked for more such cases in our registry and indeed found more very similar tumors that also shared the same morphology, IHC and mutation. However, they were slightly morphologically different so we decided to leave them for a separate study. The initial case was published only as a case report entitled "Pancreatic analogue solid pseudopapillary neoplasm arising in the paratesticular location. The first case report". Shortly thereafter, another group published a letter to the editor in response to our manuscript basically confirming our results and sharing our notion, that this is a new entity in the testis [69]. We reacted on their letter in response entitled as "Solid pseudopapillary tumor: a new tumor entity in the testis? Reply".

The remaining tumors from our registry as well as several others later received from our colleagues from various institutions were almost identical but featured a high amount of signet ring cells, and in this regard, they were identical to another study published by my colleagues years ago, entitled as "Primary signet-ring stromal tumor of the testis" [70]. However, in many cases, these signet ring cells comingled with non-signet ring cells that were identical to the cellular population found in the case that was reported as "Pancreatic analogue solid pseudopapillary neoplasm arising in the paratesticular location". After a careful morphological review, a clear spectrum was found ranging from cases of pure signet ring morphology (scattered signet ring cells can, however, be present in SPN-P as well), to cases of mixed morphology comprising signet ring and non-signet ring component, the latter being identical to the cells of SPN-P. Altogether, we collected 13 such cases and published them in an article entitled as "Primary signet ring stromal tumor of the testis: a study of 13 cases indicating their phenotypic and genotypic analogy to pancreatic solid pseudopapillary neoplasm".

The problem with this topic is that so called Sertoli cell tumors NOS, a long-established heterogeneous group of mostly benign testicular tumors may, in a subset of cases, have the same phenotype. It was also the problem of one of the reviewers of the latter paper. However, as mentioned, Sertoli cell tumors NOS, are a very heterogeneous group of tumors, with a very

variable and uncharacteristic morphology, immunophenotype and molecular genetic changes including CTNNB1 mutation which is present in only about one half of cases. In fact, what we are attempting is to separate a morphologically, immunohistochemically and molecular genetically completely homogeneous group of tumors from a heterogeneous one. Furhermore we think that a "Sertoli cell tumors" with signet ring cell/SPN-P morphology, IHC staining with classical SPN-P IHC markers and CTNNB1 mutation represent in fact analogues of solid pseudopapillary tumors occurring in the testis and not Sertoli cell tumors of any kind.

Eventually, we published a paper in which we broadened the morphological spectrum of herein described tumors by adding 6 testicular tumors devoid of signer ring cells, thus being very similar/identical to the SPN-P. In order to provide further evidence for our concept we compared them morphologically, immunohistochemically and molecular genetically to 8 SPN-P. This latest paper was entitled "Solid pseudopapillary neoplasm (SPN) of the testis: Comprehensive mutational analysis of 6 testicular and 8 pancreatic SPNs."

Human Pathology (2016) **56**, 52–56

ELSEVIER

Human PATHOLOGY

www.elsevier.com/locate/humpath

Case study

Pancreatic analogue solid pseudopapillary neoplasm arising in the paratesticular location. The first case report☆,☆☆

Michal Michal MD[a], Stela Bulimbasic MD[b], Marijana Coric MD[b], Monika Sedivcova MSc[c], Dmitry V. Kazakov MD[d], Michael Michal MD[a,*], Ondrej Hes MD[d]

[a]*Department of Pathology, Charles University, Biomedical Center, Faculty of Medicine in Plzen and Charles University Hospital, Plzen, Czech Republic, 30460*
[b]*Department of Pathology, University Hospital Centre, Zagreb, Croatia, 100000*
[c]*Biopticka Laborator s.r.o., Plzen, Czech Republic, 32600*
[d]*Department of Pathology, Charles University, Medical Faculty and Charles University Hospital, Plzen, Czech Republic, 30460*

Received 22 January 2016; revised 27 April 2016; accepted 3 June 2016

Keywords:
Testis;
Paratesticular;
Pancreatic analogue solid pseudopapillary neoplasm;
CTNNB1 gene;
Testis;
Paratestis;
Solid pseudopapillary neoplasm;
CTNNB1 gene

Summary We describe the first pancreatic analogue of solid pseudopapillary neoplasm arising in paratesticular location. It was a tumor arising in 32-year-old man adhering closely to the testis. The tumor had several morphologic components. The greatest was represented by signet ring cells which gradually changed into solid, non–signet ring cell areas, often being mixed together. It also formed distinct trabeculae and pseudopapillae frequently adhering to cystic areas of the tumor. Immunohistochemically, the tumor had an identical profile to its pancreatic counterpart. The tumor cells reacted diffusely with S100 protein, β-catenin, cyclin D1, Fli-1, vimentin, CD10, galectin-3, and neuron-specific enolase and focally with synaptophysin. CD56 and E-cadherin reacted only in those parts of the tumor, which formed pseudopapillae. Cytokeratin antibody AE1-AE3 was strongly positive in the areas of trabecular formation of the tumor. The mutational analysis of exon 3 of the *CTNNB1* gene confirmed mutation in this exon.

1. Introduction

Solid pseudopapillary neoplasm (SPN) is an epithelial neoplasm of the pancreas first recognized by Frantz [1] in 1959. It occurs primarily in young women in their 20s. There have been described 4 cases outside the pancreas: a colonic example arising allegedly from ectopic pancreas [2] and in 2010 the first 3 cases arising primarily in the ovary [3]. We describe the first case of pancreatic analogue of SPN arising in the paratesticular location.

2. Case report

2.1. Clinical course

A 32-year-old man presented with a tumor adhering closely to the right testis. Thorough check-up did not reveal any tumor elsewhere in the body including pancreas. Three months after

☆ Competing interests: The authors have no conflicts of interest to disclose.
☆☆ Funding/Support: The study was supported by the Biomedical Center of the Faculty of Medicine in Pilsen, project number CZ.1.05/2.1.00/03.0076.
* Corresponding author at: Department of Pathology, Charles University, Medical Faculty and Charles University Hospital Plzen, Alej Svobody 80, 304 60 Pilsen, Czech Republic.
E-mail address: michael.michal@medima.cz (M. Michal).

http://dx.doi.org/10.1016/j.humpath.2016.06.007
0046-8177/

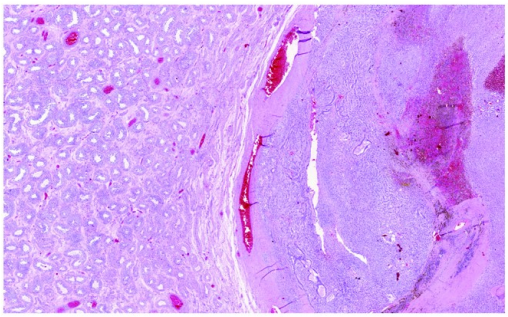

Fig. 1 The tumor was in the paratesticular position. In the septa of the neoplasm, there were deposits of hemosiderin, Gandy-Gamna bodies, and foamy macrophages as remnants of old hemorrhage.

the excision, the patient was without any signs of recurrences and metastases.

2.2. Gross and microscopic examination

The tumor adhered closely to the right testis (Fig. 1). The tumor was 4.8 × 4 × 3 cm in size, lobulated, and gray in color with hemorrhagic spots on cut section.

Microscopically, adjacent testis had normal appearance. There was no intratubular germ cell neoplasia inside the testicular tubules. The tumor had several morphologic components. The greatest one was the signet ring cell component (Fig. 2A). This component gradually changed into the solid, non–signet ring cell areas (Fig. 2B) and these areas often mixed together (Fig. 2C). Another characteristic picture was the formation of distinct trabeculae (Fig. 2C). Small parts revealed oncocytic change, which was reminiscent of endometrial decidual change (Fig. 2D). Focally, periodic acid–Schiff–positive hyaline globules were found in the tumor. In the septa of the neoplasm, there were deposits of hemosiderin, Gandy-Gamna bodies, and foamy macrophages as remnants of old hemorrhage (Fig. 1).

2.3. Immunohistochemistry

The tumor cells reacted strongly and diffusely to antibodies to vimentin (Table), CD10, galectin-3, S-100 protein (Fig. 3), androgen receptors, α-antitrypsin, and neuron-specific enolase (NSE), and focally positively to synaptophysin and progesterone receptors antibody. There was distinct diffuse intranuclear positivity with antibodies to β-catenin and cyclin D1. CD56 and E-cadherin reacted in those parts of the tumor, which formed pseudopapillae. The signet ring cell component was CD56 and E-cadherin negative. Fli-1 reacted diffusely by a weak intranuclear positivity. Cytokeratin antibody AE1-AE3

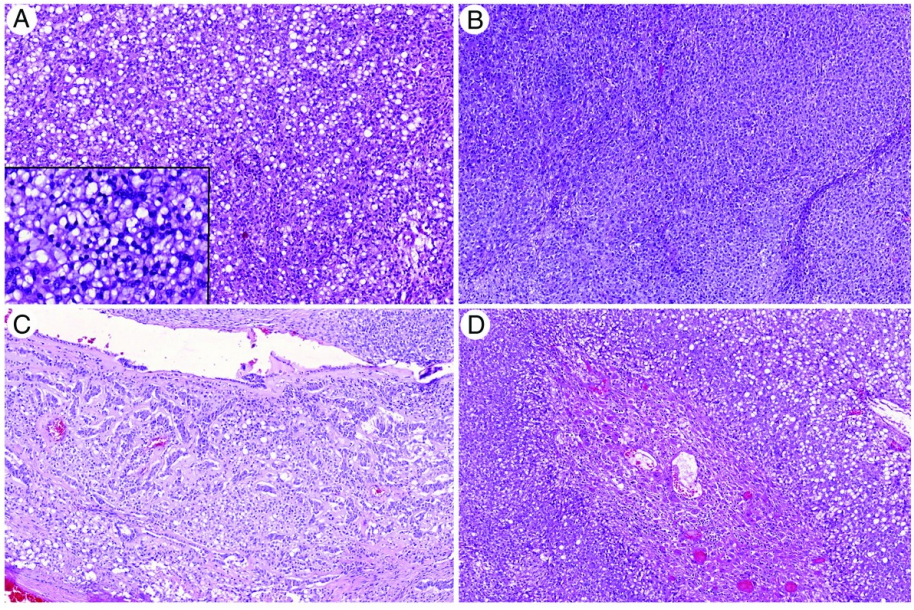

Fig. 2 A, The greatest part of the tumor represented signet ring cell component. This signet ring cell component gradually changed into the solid, non–signet ring cell areas (**B**), or these 2 components were intermixed (**C**). D, Small parts revealed oncocytic change, which was reminiscent of endometrial decidual change.

Table Source of antibodies

Antibody	Clone	Manufacturer	Dilution
Vimentin	V9	Cell Marque, Rocklin, CA	RTU
CD10	SP67	Ventana Medical System, Inc., Tucson, Arizona	RTU
Galectin-3	9C4	Cell Marque	RTU
S-100 protein	Polyclonal	Ventana Medical System, Inc	RTU
α-Antitrypsin	Polyclonal	Cell Marque	1:200
NSE	BBS/NC/VI-H14	Dako, Glostrup, Denmark	1:1000
Synaptophysin	SP11	Ventana Medical System, Inc	RTU
β-Catenin	Polyclonal	Thermo Fischer Scientific, Fremont, CA	1:150
Cyclin D1	Polyclonal	Thermo Fisher Scientific	1:100
CD56	MRQ-42	Cell Marque	RTU
E-Cadherin	36	Ventana Medical System, Inc	RTU
Fli-1	MRQ-1	Cell Marque	1:50
AE1-AE3	AE1/AE3/PCK26	Ventana Medical System, Inc	RTU
Chromogranin	DAK-A3	Dako	1:400
Serotonin	5HT-H209	Dako	1:400
GFAP	6F2	Dako	RTU
NANOG	Polyclonal	Abcam, Cambridge, UK	1:100
SALL4	6E3	Sigma-Aldrich, Saint Louis, MO	1:800
LIN28	Polyclonal	Abcam	1:100
CD57	NK1	Ventana Medical System, Inc	RTU
GATA3	L50–823	BioCare Medical	1:1000
Inhibin	R1	Ventana Medical System, Inc	RTU
Calretinin	SP65	Ventana Medical System, Inc	RTU
α-Fetoprotein	Polyclonal	Cell Marque	1:200
Placental alkaline phosphatase	NB10	Ventana Medical System, Inc	RTU
Androgen receptor	SP107	Ventana Medical System, Inc	RTU
Progesterone receptor	1E2	Ventana Medical System, Inc	RTU

Abbreviation: RTU, ready to use.

reacted patchily, and it was strongly positive in the areas of trabecular formation of the tumor. Tumor cells reacted negatively to antibodies to chromogranin, serotonin, AFP, GFAP, NANOG, SALL4, LIN28, CD57, GATA3, inhibin, calretinin, and placental alkaline phosphatase.

2.4. Molecular pathology

Mutational analysis of exon 3 of the *CTNNB1* gene was performed via polymerase chain reaction and direct sequencing as described previously [4]. The tumor revealed mutation c.101G>T (p.Gly34Val) in exon 3 of the *CTNNB1* gene (Fig. 4).

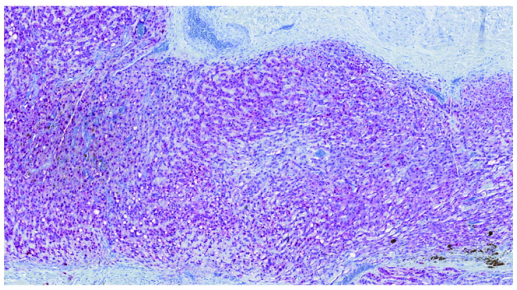

Fig. 3 Strong and diffuse reactivity of the tumor cells with antibody to S100 protein.

3. Discussion

We report a tumor arising in the paratesticular location that resembles SPN of the pancreas morphologically, immunohistochemically, and molecular genetically. We are not aware of any prior reports of SNP in this area. Grossly, SPN of the pancreas can vary from entirely cystic with small mural nodules to entirely solid neoplasms [5]. All areas found in our case are often found in the pancreatic SPN. We reviewed 20 haphazardly selected cases of SPNs from our files, and 16 of 20 showed signet ring cell component as well. And those 4 cases of pancreatic SPN of the pancreas that lacked the signet ring cell component were invariably those cases where only one block was available on review (often received on consultation). Similar signet ring cell component was found in the ovarian samples of this neoplasm. It therefore seems that the signet ring cell component is a characteristic differentiation of SPN of the pancreas and ovary. Only the oncocytic component is found rarely in the SPN of the pancreas, although it is well known and well described in the SPN of both the pancreas and the ovary [3,6]. Another notoriously known feature of SPN present in

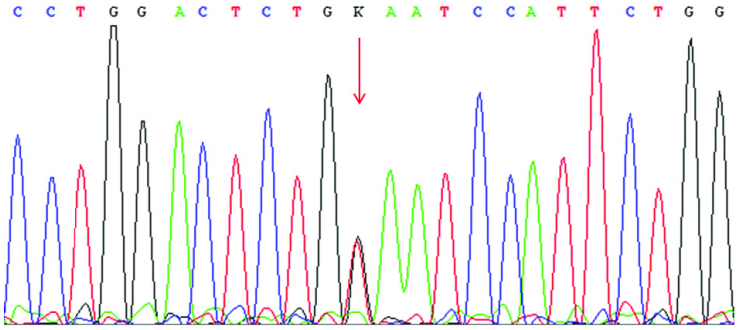

Fig. 4 The arrow shows the mutation c.101G>T/p. Gly34Val in exon 3 of the *CTNNB1* gene.

our tumor was the periodic acid–Schiff–positive hyaline globules [7].

SPNs of the pancreas and ovary invariably show mutation of exon 3 of the *CTNNB1* gene encoding β-catenin. This mutation leads to overexpression of β-catenin protein that escapes intracytoplasmic phosphorylation and subsequent degradation and therefore binds to the T-cell transcription factor (Tcf/Lef) [8]. The β-catenin–Tcf/Lef complex is then abnormally translocated to the nucleus, as indicated by nuclear expression of β-catenin on immunohistochemistry, as in our case. The immunohistochemical profile, namely, positivity to antibodies to cyclin D1, NSE, CD10, galectin-3, Fli-1, E-cadherin, and CD56 as detected in our case, is well known to occur in pancreatic SNPs and well described in the literature [9-13].

The relationship between the signet ring cell component of SPN arising in the paratesticular location (SPNPT) and signet ring cell stromal tumor of the testis (some of which also occur in the paratesticular location) described first by Michal et al [14] and later by Kuo et al [15] should be addressed. We have gathered some 10 cases of signet ring cell stromal tumor of the testis in our consultation files, and all these tumors have similar immunoprofile to the SPNPT and SPN, being immunohistochemically positive with antibodies to β-catenin, CD10, synaptophysin, NSE, and cyclin D1 (unpublished observation). We therefore think that these tumors might be very close or even identical to SPNPT and SPN. Signet ring cell stromal tumor of the testis [14,15] may represent the very incipient growth phase of SPNPT.

In the differential diagnosis, SPN arising in the paratesticular location should be distinguished from sex-cord stromal tumors and neuroendocrine tumors of the testis. Immunohistochemical positivity of antibodies to synaptophysin and NSE is rarely seen in the sex-cord stromal tumors. In addition, sex-cord stromal tumors are in contrast to SPNPT nearly invariably immunohistochemically positive to antibodies to inhibin and calretinin.

Neuroendocrine tumors of the testis show trabecular or insular patterns and practically never reveal signet ring cell component as our case, so that they would be confused with SPNPT [16]. Furthermore, the "salt and pepper type" of chromatin of neuroendocrine tumors of the testis is unlike the pale uniform chromatin seen in SPNPT.

In summary, we describe the first ever reported example of pancreatic analogue SPN arising in the paratesticular location.

References

[1] Frantz VK. Tumors of the Pancreas. Washington, DC: Armed Forces Institute of Pathology; 1959.
[2] Ishikawa JA, Ishiguro S, Ohigashi H, et al. Solid and papillary neoplasm arising from ectopic pancreas in the mesocolon. Am J Gastroenterol 1990;85:597-560.
[3] Deshpande V, Oliva E, Young RH. Solid pseudopapillary neoplasm of the ovary: a report of 3 primary ovarian tumors resembling those of the pancreas. Am J Surg Pathol 2010;34:1514-20.
[4] Kazakov DV, Sima R, Vanecek T, et al. Mutations in exon 3 of the *CTNNB1* gene (beta-catenin gene) in cutaneous adnexal tumors. Am J Dermatopathol 2009;31:248-55.
[5] Nishimori I, Kohsaki T, Tochika N, et al. Non-cystic solid-pseudopapillary tumor of the pancreas showing nuclear accumulation of activating gene mutation of β-catenin. Pathol Int 2006;56:707-11.
[6] Goldstein J, Benharroch D, Sion-Vardy N, et al. Solid cystic and papillary tumor of the pancreas with oncocytic differentiation. J Surg Oncol 1994;56:63-7.
[7] Meriden Z, Shi C, Edil BH, et al. Hyaline globules in neuroendocrine and solid-pseudopapillary neoplasm of the pancreas. Am J Surg Pathol 2011; 35:981-8.
[8] Bosman FT, Carneiro F, Hruban RH, Theise ND. WHO Classification of Tumors of the Digestive System. Lyon: IARC; 2010.
[9] Notohara K, Hamazaki S, Tsukayama C, et al. Solid-pseudopapillary tumor of the pancreas. Immunohistochemical localization of neuroendocrine markers and CD10. Am J Surg Pathol 2000;24:1367-71.
[10] Agaimy A, Haller. CTNNB1 (β-catenin)-altered neoplasia: a review focusing on soft tissue neoplasms and parenchymal lesions of uncertain histogenesis. Adv Anat Pathol 2016;23:1-12.
[11] Tiemann K, Kosmahl M, Ohlendorf J, Krams M, Klöppel G. Solid pseudopapillary neoplasms of the pancreas are associated with FLI-1 expression, but not with EWS/FLI-1 translocation. Mod Pathol 2006;19:1409-13.
[12] Chetty R, Serra S, Salahshor S. Nuclear expression of E-cadherin. Am J Surg Pathol 2008;32:1269-70.
[13] Chu HH, Song JS, Yu HC, Moon WS. Solid-pseudopapillary neoplasm of the pancreas with extensive pleomorphic neuroendocrine differentiation. Pathology 2015;47:468-71.

[14] Michal M, Hes O, Kazakov DV. Primary signet–ring stromal tumor of the testis: a case report and literature review. Virchows Arch 2005;447:107-10.
[15] Kuo CY, Wen MC, Wang J, Jan YJ. Signet-ring stromal tumor of the testis: a case report and literature review. HUM PATHOL 2009;40:584-7.
[16] Reyes A, Moran CA, Suster S, Michal M, Dominguez H. Neuroendocrine carcinomas (carcinoid tumor) of the testis. A clinicopathologic and immunohistochemical study of ten cases. Am J Clin Pathol 2003; 120:182-7.

and diffusely stained with CD10 (Figure F), CD56, CD117, CD99, progesterone receptors, and cyclin D1 (Figure D). Negative staining was observed with α-inhibin, E-cadherin (Figure G), pan-cytokeratins, SALL-4, OCT-4, CDX2, α-fetoprotein, CD30, β-HCG, DOG-1, calretinin, chromogranin, synaptophysin, glypican-3, and SF1. Mutations in the *CTNNB1* gene exon 3 were identified by direct sequencing. An abdominal computed tomographic scan performed in both patients gave a negative result. These features consistently supported the diagnosis of SPT of the testis. No further therapy was performed after surgery, and the patients are alive and well at 15- and 27-month follow-up, respectively.

In 2010, Deshpande et al [2] first described 3 primary ovarian neoplasms histologically and immunohistochemically identical to SPT of the pancreas. Since then, different examples have been reported in the ovary, leading to the introduction of SPT as a distinct tumor entity in the last *WHO Classification of Tumours of Female Reproductive Organs* [3].

The main differential diagnosis in these cases is with Sertoli cell tumor (SCT), including its sclerosing-type variant, with which SPT may share some morphologic and immunohistochemical features. Interestingly, protein nuclear expression and mutations of *β*-catenin gene have been demonstrated in SCT [4], and signet ring cell stromal tumor is generally considered an uncommon variant of SCT [5]. However, we agree with Michal et al [1] that signet ring cell stromal tumor of the testis does represent an "orphan" neoplasm of uncertain histogenesis, possibly representing a peculiar morphologic variant of SPT in the testis. As in the ovary, the exact pathogenesis of SPT remains unclear, and the lack of a teratoma component does not support the possibility of a neoplastic transformation from ectopic pancreatic tissue. Because several other SPTs of the ovary have been published after the initial description by Deshpande et al [2], it will be not surprising to "officially" recognize the occurrence of SPT also in the testis among tumors showing solid, pseudopapillary, and signet ring cell growth pattern and *β*-catenin alterations.

Maria Cecilia Mengoli, MD
Luca Reggiani Bonetti, MD, PhD
Department of Anatomic Pathology, Azienda Ospedaliero-Universitaria Policlinico di Modena
71-41124 Modena, Italy
E-mail address: cecilia.mengoli@gmail.com

Donatella Intersimone, MD
Franco Fedeli, MD
Operative Unit of Pathologic Anatomy
Azienda Ospedaliera S. Andrea, 19121 La Spezia, Italy

Giulio Rossi, MD, PhD
Pathologic Anatomy, Hospital of Aosta, 11100 Aosta, Italy

http://dx.doi.org/10.1016/j.humpath.2016.08.011

References

[1] Michal M, Bulimbasic S, Coric M, et al. Pancreatic analogue solid pseudopapillary neoplasm arising in the paratesticular location. The first case report. Hum Pathol 2016;56:52-6.
[2] Deshpande V, Oliva E, Young RH. Solid pseudopapillary neoplasm of the ovary: a report of 3 primary ovarian tumors resembling those of the pancreas. Am J Surg Pathol 2010;34:1514-20.
[3] Kurman RJ, Carcangiu ML, Herrington CS, Young RH, editors. WHO classification of tumours of female reproductive organs. 4th ed. Lyon: IARC; 2014.
[4] Kuo CY, Wen MC, Wang J, Jan YJ. Signet-ring stromal tumor of the testis: a case report and literature review. Hum Pathol 2009;40:584-7.
[5] Perrone F, Bertolotti A, Montemurro G, et al. Frequent mutation and nuclear localization of *β*-catenin in Sertoli cell tumors of the testis. Am J Surg Pathol 2014;38:66-70.

Solid pseudopapillary tumor: a new tumor entity in the testis? Reply

To the Editor,

We would like to thank Dr Mengoli et al for their letter to the editor concerning our previously published article [1]. Their observations are valuable, and the authors confirm our suggestion that most signet ring cell tumors of testis [2] are an "orphan neoplasm" representing a peculiar variant of solid pseudopapillary neoplasm (SPN) known for the long time to occur in the pancreas and recently described in the ovary as well [3].

In the meantime, we have collected 13 cases of testicular tumors being entirely (Fig. 1) or partly composed of signet ring cells. Interestingly, the non–signetring cell component in some of these tumors appeared very distinctive. It contained areas characteristically seen in pancreatic SPN including solid, pseudopapillary, oncocytic (oxyphilic) areas, foamy cells, deposits of hemosiderin, trabecular areas, and hyaline globules (Fig. 2A-D). In addition, the immunohistochemical profile comprising CD10, synaptophysin, CD56, *β*-catenin, and neuron-specific enolase positivity and chromogranin, inhibin, calretinin, SF1, and FOXL2 negativity is entirely identical to SPN of the pancreas.

Signet ring cell stromal tumors of the testis were likely misdiagnosed as Sertoli cell tumors, not otherwise specified in the past [4]. It is our view that tumors with such an immunoprofile can hardly be regarded as any tumor with Sertoli cell differentiation, and a much simpler explanation is to consider them as the testicular analogue of SPN.

Kvetoslava Michalova, MD
Department of Pathology, Charles University Medical Faculty and Charles University Hospital Plzen
Pilsen 30460, Czech Republic

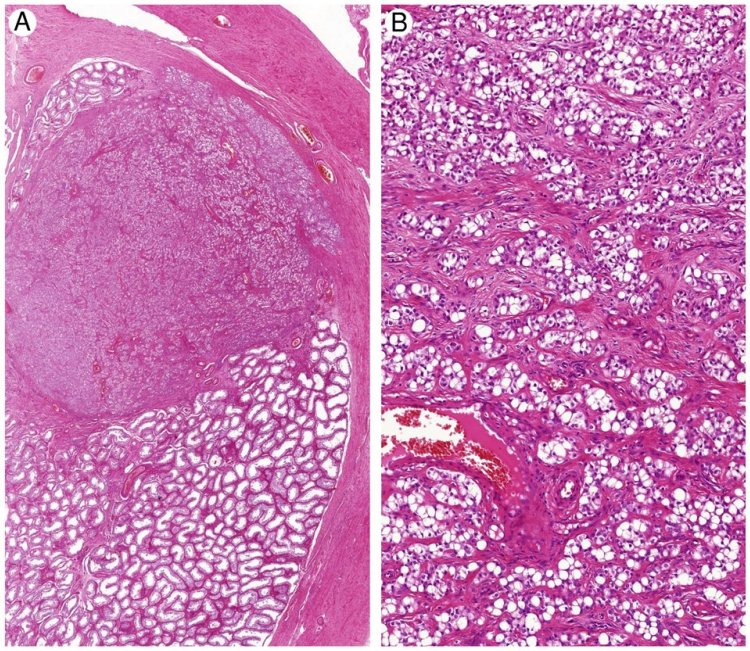

Fig. 1 Small tumors were composed entirely of signet ring cell component.

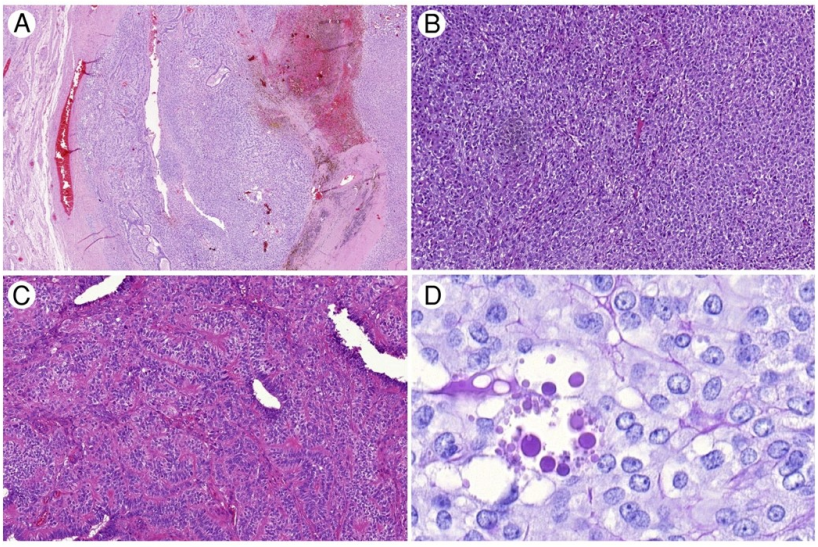

Fig. 2 Larger tumors often contained a large component that, in addition to signet ring cells, contained pseudopapillary (A), solid (B), and trabecular areas (C) and hyaline globules (D).

Michael Michal, MD
Biomedical Center of the Faculty of Medicine in Plzen and Charles University Hospital Plzen
Pilsen 30460, Czech Republic
E-mail address: michael.michal@seznam.cz

Ondrej Hes, MD
Dmitry V. Kazakov, MD
Michal Michal, MD
Department of Pathology, Charles University Medical Faculty and Charles University Hospital Plzen
Pilsen 30460, Czech Republic

http://dx.doi.org/10.1016/j.humpath.2016.08.012

References

[1] Michal M, Bulimbasic S, Coric M, et al. Pancreatic analogue solid pseudopapillary neoplasm arising in the paratesticular location. The first case report. Hum Pathol 2016;56:52-6.
[2] Michal M, Hes O, Kazakov DV. Primary signetring stromal tumor of the testis: a case report and literature review. Virchows Arch 2005;447:107-10.
[3] Deshpande V, Oliva E, Young RH. Solid pseudopapillary neoplasm of the ovary: a report of 3 primary ovarian tumors resembling those of the pancreas. Am J Surg Pathol 2010;34:1514-20.
[4] Moch H, Humphrey PA, Ulbright TM, Reutzer VE. WHO Classification of Tumours of the Urinary System and Male Genital Organs. Lyon: IARC; 2016. p. 228-30.

Azzopardi phenomenon reported in metal-on-metal arthroplasties is in fact iron encrustation of blood vessels

Dear Sirs,

It is with great interest that we have read the case study, "Azzopardi phenomenon in cystic pseudotumours associated with retrieved metal-on-metal arthroplasty" by Zustin et al [1]. The authors describe an unusual phenomenon of deposition of basophilic material in the vessel walls of soft tissues from metal-on-metal (MoM) cystic pseudotumours. (See Figure)

Grossly, the authors describe gray metallic-colored tissues that are divided from a deeper fibrous joint capsule by a thin linear "ferruginous rim" of tissue. It is at the interface of viable and necrotic tissue that the authors have identified dark-blue coloration of the blood vessel walls and fibers of extracellular matrix. Metal wear particle–laden macrophages and siderophages surround the blood vessels. The material is proven to be DNA on the basis of positive Feulgen reaction and lack of Von-Kossa and Alizarin red S stain for calcium. Furthermore, they have reported a lack of excess of lymphocytes in the vicinity.

Have the authors considered performing Prussian blue stain for this material? There does not appear to be a reference made to Prussian blue stain in their article. In our experience, this material shows strong Prussian blue reaction due to iron encrustation of the vessels and extracellular matrix material (Figure). This is more commonly seen in MoM joints with hemarthrosis in the setting of adverse reaction to metal debris. The iron encrustation is blue/black, rather homogeneous in appearance, as opposed to the coarse, granular, dark-blue, almost black smearing of blood vessels derived from DNA of fragile nuclei of malignant tumors like small cell carcinoma of the lung with high proliferative index [2]. The iron encrustation is typically seen at the interface of viable and necrotic material. Prussian blue also stains hemosiderin granules within siderophages in the vicinity. Occasionally, iron encrustation is seen around metal corrosion products coating large metal particles forming "ferruginous bodies," similar to asbestos. The authors do describe a ferruginous layer grossly, and it would be worth performing Prussian blue stain to confirm or refute our findings. Photomicrograph B demonstrates formation of Gamna-Gandy body–like structures (classically seen in congestive splenomegaly). It can also be seen in long-standing hemarthrosis. The authors also state that there is a lack of excess of lymphocytes in the area with this change. The lymphocytes could be a potential source of cells with

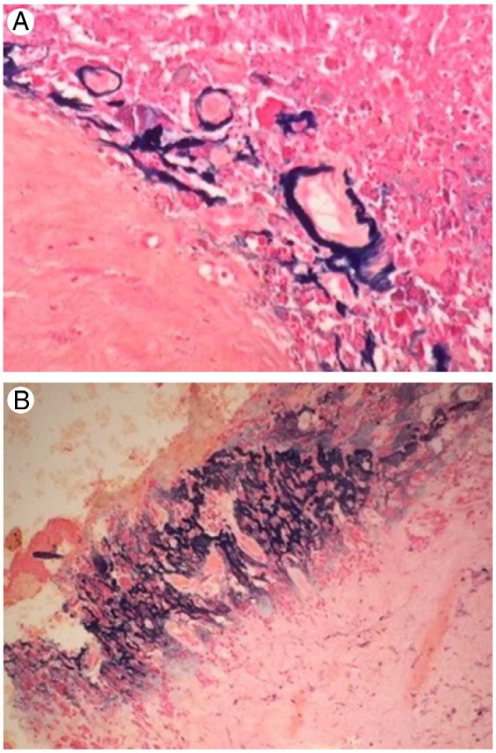

Figure A and B, Positive Prussian blue staining reaction due to iron encrustation of blood vessels. A, original magnification ×200; B, ×100.

Human Pathology (2017) 67, 85–93

ELSEVIER

Human PATHOLOGY

www.elsevier.com/locate/humpath

Original contribution

Primary signet ring stromal tumor of the testis: a study of 13 cases indicating their phenotypic and genotypic analogy to pancreatic solid pseudopapillary neoplasm☆,☆☆

Kvetoslava Michalova MD[a,*], Michael Michal Jr MD[a,b], Dmitry V. Kazakov MD[a], Monika Sedivcova MSc[c], Ondrej Hes MD[a], Ladislav Hadravsky MD[d], Abbas Agaimy MD[e], Maria Tretiakova MD[f], Carlos Bacchi MD[g], Arndt Hartmann MD[e], Naoto Kuroda MD[h], Stela Bulimbasic MD[i], Marijana Coric MD[i], Tatjana Antic MD[j], Michal Michal MD[a]

[a]*Department of Pathology, Faculty of Medicine in Plzen, 30460, Charles University in Prague, 11636, Biopticka laborator s.r.o., Plzen, 30100, Czech Republic*
[b]*Biomedical Center, Faculty of Medicine in Plzen, 30460, Charles University, Czech Republic*
[c]*Biopticka laborator s.r.o., Plzen, 30100, Czech Republic*
[d]*Department of Pathology, Charles University, 3rd Medical Faculty and Charles University Hospital Royal Vineyards, Prague, 10034, Czech Republic*
[e]*Institute of Pathology, University Hospital Erlangen, Friedrich-Alexander University Erlangen-Nürnberg, Erlangen, 91054, Germany*
[f]*Department of Pathology, University of Washington, Seattle, 98195, USA*
[g]*Consultoria em Patologia, Botucatu, SP, 18602-010, Brazil*
[h]*Department of Diagnostic Pathology, Kochi Red Cross Hospital, Kochi, 780-8562, Japan*
[i]*Department of Pathology, University Hospital Centre, Zagreb, 100000, Croatia*
[j]*Department of Pathology, The University of Chicago, Chicago, 60637, USA*

Received 14 April 2017; revised 11 June 2017; accepted 4 July 2017

Keywords:
Testis;
Pancreas;
Primary signet ring stromal tumor;
Solid pseudopapillary neoplasm;
Analogue

Summary Primary signet ring stromal tumor of the testis (PSRSTT) is an extremely rare tumor described only twice in the literature. Pancreatic-analogue solid pseudopapillary neoplasm (SPN) of the testis is a recently reported entity with morphological overlap with PSRSTT. We reviewed our files to find all cases of PSRSTT to better characterize this entity. We studied 13 cases of PSRSTTs using histological, immunohistochemical (IHC), and molecular genetic methods and compared the results with pancreatic SPN. Grossly, the size of PSRSTTs ranged from 0.5 to 2 cm (mean 1.1). Microscopically, PSRSTTs predominantly showed a proliferation of low-grade epithelioid cells containing characteristic cytoplasmic vacuole dislodging the nucleus (signet ring cells) separated by fibrous septa into trabeculae and nests. The immunoprofile was characterized by immunoreactivity for β-catenin, cyclin D1 (nuclear positivity for both antibodies), CD10,

☆ Competing interests: The authors have no conflict of interest to disclose. Neither ethics approval nor informed consent was required for our study.
☆☆ Funding/Support: This study was partly supported by the National Sustainability Program I (NPU I) Nr. LO1503 and by the grant SVV–2017 No. 260 391 provided by the Ministry of Education Youth and Sports of the Czech Republic, Prague, 11800, Czech Republic.
* Corresponding author at: Department of Pathology, Charles University, Medical Faculty and Charles University Hospital Plzen, Alej Svobody 80, 304 60 Plzen, Czech Republic.
E-mail address: kveta.michalova@biopticka.cz (K. Michalova).

http://dx.doi.org/10.1016/j.humpath.2017.07.010

vimentin, galectin-3, claudin 7, α-1-antitrypsin, CD56, and neuron-specific enolase and negativity for chromogranin, inhibin, calretinin, SF-1, NANOG, OCT3/4, and SALL4. In some cases, the IHC panel was restricted because of a limited amount of tissue. Molecular genetic analysis revealed mutations within exon 3 of the *CTNNB1* encoding β-catenin in all analyzable cases. Based on histological similarities between pancreatic SPN and PSRSTT and their identical IHC and molecular genetic features, we assume that both neoplasms share the same pathogenesis, and thus, PSRSTT can be considered as a testicular analogue of pancreatic SPN.

1. Introduction

Primary signet ring stromal tumor of the testis (PSRSTT) was first described in 2005 by Michal et al [1] and subsequently by Kuo et al [2] as single case reports. Microscopically, both tumors were characterized by the proliferation of low-grade epithelioid cells containing characteristic cytoplasmic vacuole dislodging the nucleus to the periphery of the cells (signet ring cells), which were separated by fibrous septa resulting in a trabecular and/or nested architecture [1]. Pancreatic solid pseudopapillary neoplasm (SPN) is a rare tumor with uncertain histogenesis traditionally encountered in the pancreas [3]. However, recent small series and several case reports have described an ovarian tumor identical to that seen in the pancreas [4-8], and most recently, a pancreatic analogue solid pseudopapillary neoplasm of the testis (PA-SPN) has been described by our group [9]. Microscopically, PA-SPN consisted of 2 distinct components: a signet ring cell component histologically identical to that seen in the PSRSTT blending with a component identical to pancreatic SPN by showing a solid (and in minor parts also pseudopapillary) component comprised by poorly cohesive low-grade cells with eosinophilic cytoplasm. The purpose of this study is to morphologically, immunohistochemically, and molecular genetically investigate 13 cases of PSRSTT and compare their features with pancreatic SPN and with 1 published case of PA-SPN [9] to establish their possible pathogenetic relationship.

2. Materials and methods

Cases cross-matching the keywords *testis*, *signet ring stromal tumor*, *unclassified sex cord tumor*, *male adnexal tumor of probable Wolffian origin*, and *Sertoli cell tumor, benign, NOS* were retrieved from the Plzen tumor registry; they came from the period 1993-2017. Additional cases were retrieved from the routine and consultation files of the authors. Upon reevaluation, 13 cases of primary testicular tumors that fulfilled the diagnostic criteria for this study were selected. The clinical information was extracted from the registry records, and follow-up data were obtained from attending clinicians. In all but 2 cases, paraffin blocks or unstained reserve slides were available for the study. To compare PSRSTT with SPN, we reviewed 20 pancreatic cases from the Plzen tumor registry. For conventional microscopy, tissues were fixed in formalin, routinely processed, and stained with hematoxylin-eosin.

2.1. Immunohistochemistry

The immunohistochemical (IHC) analysis was performed using a Ventana BenchMark ULTRA (Ventana Medical System, Inc, Tucson, AZ). The list of antibodies and the basic technical specifications are summarized in Table 1. Because of the limited amount of tissue blocks or reserve slides, the utilization of the entire immunohistochemical panel was restricted. The following stains were performed on most cases: β-catenin, CD10, CD56, neuron-specific enolase (NSE), inhibin, calretinin, S100, and OSCAR. These additional stains were applied in only a few of them: vimentin, synaptophysin, chromogranin, SF-1, OCT3/4, SALL4, NANOG, cyclin D1, AE1/3, galectin-3, MIB-1, claudin 5, claudin 7, and α-1-antitrypsin. Antibodies were visualized using the enzymes alkaline phosphatase or peroxidase as detecting systems (both purchased from Ventana Medical System, Inc).

2.2. Molecular genetic analysis of the β-catenin gene

Mutational analysis of exon 3 of the *CTNNB1* gene was performed via polymerase chain reaction and direct sequencing as described previously [10].

3. Results

3.1. Clinical features

The clinical features are summarized in Table 2. The age of the patients at the time of diagnosis ranged from 23 to 58 years (mean 39, median 35). Follow-up was available for 5 patients. One patient died of unrelated disease (prostatic adenocarcinoma). The remaining patients were alive and well without progression, recurrence, or evidence of metastatic disease. None of the patients had a tumor in the pancreas and/or suffered from familiar adenomatous polyposis.

3.2. Gross and microscopic findings

Grossly, the tumors were predominantly well circumscribed and encapsulated, solid, and gray in color. No cystic or necrotic foci were noted. The size of the tumors ranged from 0.5 to 2 cm (mean 1.1, median 1). Twelve of 13 tumors were located in the testis (Fig. 1A); the remaining tumor was paratesticular. All

Table 1 List of antibodies

Antibody	Clone	Manufacturer	Dilution
β-Catenin	Polyclonal	Thermo Fischer Scientific, Freemont, CA	1:150
CD10	SP67	Ventana Medical System, Inc., Tucson, AZ	RTU
Vimentin	V9	Cell Marque, Rocklin, CA	RTU
CD56	MRQ-42	Cell Marque, Rocklin, CA	RTU
Synaptophysin	SP11	Ventana Medical System, Inc., Tucson, AZ	RTU
Chromogranin	DAK-A3	Dako, Glostrup, Denmark	1:400
NSE	BBS/NC/VI-H14	Dako, Glostrup, Denmark	1:1000
Inhibin	R1	Ventana Medical System, Inc., Tucson, AZ	RTU
Calretinin	SP65	Ventana Medical System, Inc., Tucson, AZ	RTU
SF-1	N1665	R + D Systems, Minneapolis, MN	1:100
OCT3/4	N1NK	Novocastra, Newcastle, UK	RTU
SALL4	6,00E+ 03	Sigma-Aldrich, Saint Louis, MO	1:800
NANOG	Polyclonal	Abcam, Cambridge, UK	1:100
Cyclin D1	Polyclonal	Thermo Fisher Scientific, Fremont, CA	1:100
S-100 protein	Polyclonal	Ventana Medical System, Inc., Tucson, AZ	RTU
AE1-AE3	AE1/AE3/PCK26	Ventana Medical System, Inc., Tucson, AZ	RTU
OSCAR	IsoType:IgG2a	Covance, Emeryville, CA	1:100
Galectin-3	9C4	Cell Marque, Rocklin, CA	RTU
MIB 1	Ki-67	Dako, Glostrup, Denmark	1:400
Claudin 5	4C3C2	Invitrogen Corporation, Camarillo, CA	1:100
Claudin 7	LS-B2918	LSBio, Seattle, WA	1:200
α-1-Antitrypsin	Polyclonal	Cell Marque, Rocklin, CA	1:200

tumors were unilateral. Microscopically, all of them showed a signet ring cell population. Signet ring cells were characterized as monomorphic rounded epithelioid cells, which contained single, large cytoplasmic vacuoles (Fig. 1B). These vacuoles compressed and displaced the nuclei, which caused some nuclei to acquire a crescent shape, whereas others retained an original round shape. Signet ring cells were separated by fibrous septa into trabeculae and nests, which sometimes resulted in a single-file appearance reminiscent of metastatic signet ring cell carcinomas. Beside the signet ring cell proliferation, 6 tumors contained a trabecular, nested or solid, non–signet ring cell component consisting of benign-looking cells with eosinophilic cytoplasm (Fig. 2A-E). Both components were often intermixed, with the signet ring cell component gradually blending with non–signet ring areas (Fig. 2F). The smallest tumor containing both components measured 0.9 cm in largest dimension.

Cellular atypia was absent, and mitoses were extremely rare in both components. Nuclei were uniform, with finely dispersed chromatin and occasional grooves. Focally, hyaline

Table 2 Clinicopathologic features

Case	Age	Size (cm)	Localization	Follow-up
PA-SPN	32	4.8 × 4 × 3	Paratestis	AW in 1-y FU
1	34	Diam 0.9	Testis	NA
2	NA	Diam 0.5	Testis	NA
3	NA	NA	Testis	NA
4	55	2 × 1 × 1	Paratestis	AW in 4-y FU
5	43	NA	Testis	AW in 4-y FU
6	32	Diam 0.9	Testis	AW in 6-y FU
7	57	NA	Testis	NA
8	23	Diam 1	Testis	NA
9	35	Diam 1	Testis	NA
10	29	Diam 1.2	Testis	AW in 5-y FU
11	58	Diam 1	Testis	Died from prostatic adenocarcinoma in 2001
12	29	Diam 2	Testis	NA
13	35	0.8 × 0.7 × 0.6	Testis	NA

NOTE. PA-SPN reported previously by our group.
Abbreviations: AW, alive and well; Diam, diameter; FU, follow-up; NA, not available.

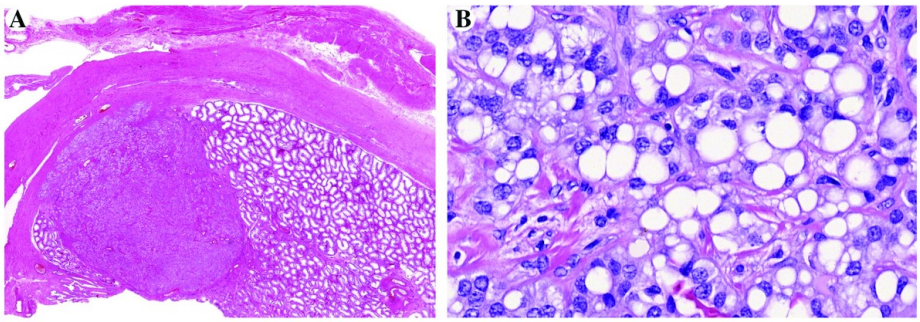

Fig. 1 A, The tumors were well circumscribed and small in size. B, Signet ring cells were characterized as monomorphic rounded epithelioid cells, which contained single, large, and clear cytoplasmic vacuole compressing and displacing the nucleus, which caused some nuclei to acquire a crescent shape, whereas others retained an original round shape.

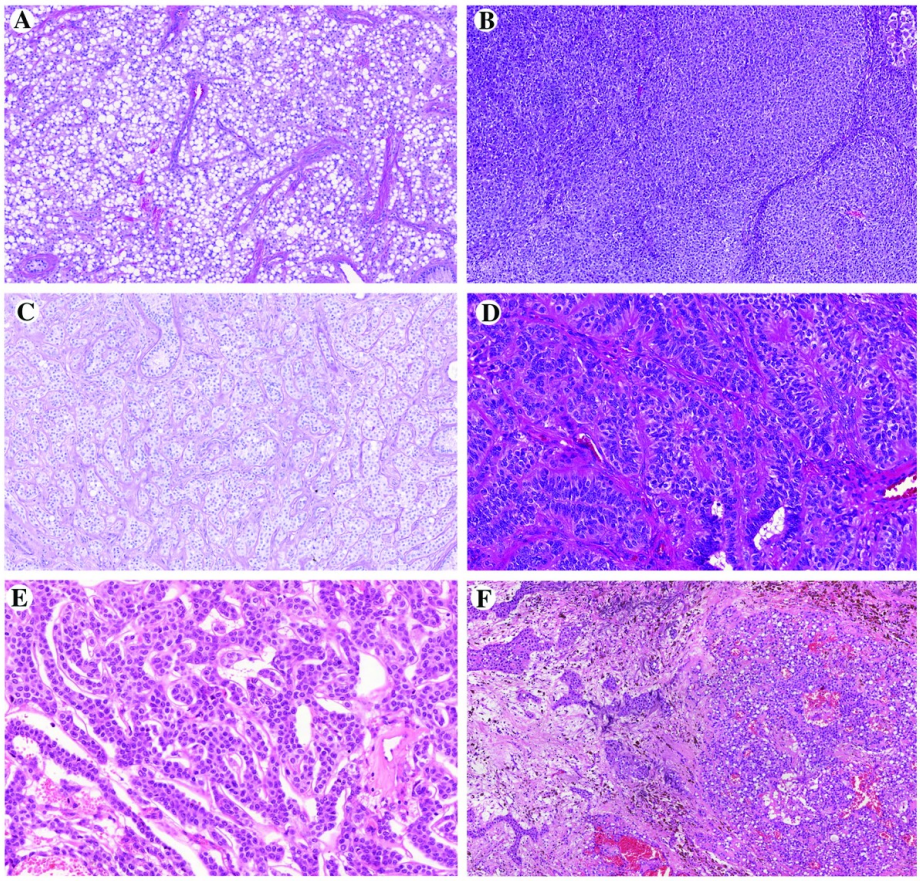

Fig. 2 Signet ring cell component was a characteristic feature of every case. Small tumors were composed entirely of signet ring cells (A). Beside the signet ring cell proliferation, larger tumors contained additional non–signet ring cell component arranged in solid (B), nested (C), or trabecular (D and E) fashion. The components were often intermixed, with the signet ring cell component gradually blending with a non–signet ring area (F).

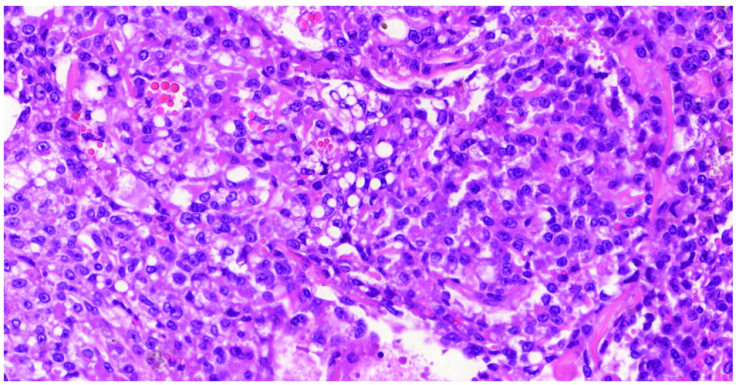

Fig. 3 Focally, hyaline PAS-positive globules were intermingled within tumors in 4 cases.

PAS-positive globules were intermingled within tumors in 4 cases (Fig. 3). The adjacent nonneoplastic testis was devoid of germ cell neoplasia in situ or any other pathologic changes.

After reviewing 20 cases of pancreatic SPN, we found a signet ring cell component in 17 neoplasms, and it was morphologically identical to the one seen in PSRSTT.

3.3. Immunohistochemistry

The IHC findings are summarized in Table 3. Neoplastic cells in all studied tumors reacted diffusely with antibodies to β-catenin, cyclin D1 (nuclear positivity for both antibodies), CD10, vimentin, galectin-3, claudin 7, and α-1-antitrypsin (Fig. 4A-C). CD56 was diffusely positive in 5 of 9 analyzable cases, whereas in the remaining 4 cases, immunoreactivity was focal. NSE was diffusely positive in 6 of 7 cases and reacted focally in the remaining case. Expression of synaptophysin, S100 protein, pan-cytokeratins (AE1/3, OSCAR), and claudin 5 was variable, and there was no expression of chromogranin, inhibin, calretinin, SF-1, NANOG, OCT3/4, and SALL4 (Fig. 4D).

3.4. Mutations in exon 3 of the *CTNNB1* gene

The molecular genetic features are summarized in Table 4, and examples are depicted in Fig. 5A-C. In all (10/10) analyzable cases, a mutation was detected in exon 3 of the *CTNNB1*. Two cases revealed mutation c.98C>G (p.Ser33Cys), 2 cases c.110C>T (p.Ser37Phe), 1 case c.110C>G (p.Ser37Cys), 1 case c.94G>T (p.Asp32Tyr), 1 case c.94G>C (p.Asp32His), 1 case c.94G>A (p.Asp32Asn), 1 case c.122C>T (p.Thr41Ile), and 1 case featured c.88_99del12 (p.Tyr30_Ser33del). The remaining 3 cases were not analyzable.

4. Discussion

PSRSTT is an extremely rare tumor, with only 2 cases published so far. Both reported neoplasms were asymptomatic, unilateral, and small in size (1 and 0.7 cm) and followed a benign clinical course without recurrence or metastasis [1,2]. Histologically, both tumors were well circumscribed and demonstrated a monomorphic population of bland signet ring cells separated by fibrous septae into trabeculae and nests [1,2]. Immunohistochemically, the tumor cells in both cases reacted with vimentin and were negative with cytokeratin, epithelial membrane antigen, inhibin, and estrogen and progesterone receptors.

Pancreatic SPN is a rare tumor [11] usually affecting young adults (mean age 28 years) with a striking female predominance (female-to-male ratio 10:1). When clinically apparent, it is usually large. Pancreatic SPN is generally considered as a tumor with an indolent behavior, although some neoplasms may pursue an aggressive course, causing on rare occasions death of the patients [12]. Microscopically, they are characterized by poorly cohesive monomorphic bland tumor cells growing in a solid and focally pseudopapillary fashion (as a result of cellular discohesion and necrosis). The diagnosis can be confirmed by the typical coexpression of β-catenin (nuclear positivity), CD10, vimentin, galectin-3, CD56, NSE, cyclin D1 (nuclear positivity), and α-1-antitrypsin in addition to the negative reaction with chromogranin in most cases. Sex cord markers and smooth muscle markers are not expressed by pancreatic SPN [13].

Extrapancreatic primary SPN is a rare entity. There have been few isolated case reports and 1 small series of SPN arising outside the pancreas and without the presence of an ectopic pancreatic tissue at the site of occurrence: 9 cases were recorded arising primarily in the ovary [4-7,14], and 1 case of testicular tumor has recently been reported by our group [9]. The tumor was described under the name *pancreatic analogue solid pseudopapillary neoplasm arising in paratesticular location*. In fact, although the bulk of the tumor originally seemed to

Table 3 Immunohistochemical results

Case	β-cat	CD 10	Vim	CD 56	Syna	Chro	NSE	Inh	Calret	SF-1	OCT 3/4	SALL 4	NAN	Cyc D1	S100	AE1/3	OSC	Gal 3	MIB-1	Clau 5	Clau 7	α-1-antitr
PA-SPN	+	+	+	Foc +	Foc +	–	+	–	–	–	NP	–	–	+	+	Foc +	+	+	NP	+	+	+
1	+	+	NP	Foc +	+	NP	+	–	–	NP	NP	NP	NP	+	–	Foc +	Foc +	+	low	weak +	+	+
2	+	+	NP	Foc +	–	–	NP	NP	NP	–	NP	NP	NP	NP	–	–	NP	NP	NP	NP	NP	NP
3	+	+	NP	Foc +	–	NP	+	–	–	NP	NP	NP	NP	NP	–	NP	–	NP	NP	NP	NP	NP
4	+	+	NP	NP	–	NP	+	–	–	NP	NP	NP	NP	+	–	NP	Foc +	NP	low	NP	NP	NP
5	NP	NP	NP	NP	NP	NP	NP	–	–	NP	–	–	–	NP	–	NP	NP	NP	NP	NP	NP	NP
6	+	+	+	+	NP	–	+	–	–	NP	NP	–	–	+	Foc +	NP	Foc +	NP	NP	NP	NP	NP
7	+	+	+	NP	+	NP	Foc +	–	–	–	NP	NP	NP	NP	NP	NP	NP	NP	low	NP	NP	NP
8	NP	NP	NP	NP	NP	NP	NP	NP	NP	NP	NP	NP	NP	NP	NP	NP	NP	NP	NP	NP	NP	NP
9	+	+	NP	Foc +	NP	NP	NP	–	–	NP	NP	NP	NP	NP	NP	NP	–	NP	NP	NP	NP	NP
10	+	+	+	+	NP	NP	NP	–	–	–	NP	NP	NP	NP	NP	NP	–	NP	NP	NP	NP	NP
11	+	+	+	+	–	NP	+	–	–	NP	NP	NP	NP	+	–	–	–	NP	NP	NP	NP	NP
12	+	weak +	+	+	NP	NP	NP	–	–	NP	NP	NP	NP	+	Foc +	–	–	+	NP	–	+	+
13	+	+	NP	+	NP	NP	+	–	–	–	–	–	–	NP	NP	NP	Foc +	NP	NP	NP	NP	NP

Abbreviations: α-1-antitr, α-1-antitrypsin; β-cat, β-catenin; Calret, calretinin; Chro, chromogranin; Clau 5, claudin 5; Clau 7, claudin 7; Cyc D1, cyclin D1; Foc, focal; Gal 3, galectin-3; Inh, inhibin; NAN, NANOG; NP, not performed; OSC, OSCAR; SF-1, steroidogenic factor 1; Syn, synaptophysin; Vim, vimentin.

be paratesticular in location, recently, after making a large amount of recuts for educational purposes, in the deeper levels, it was evident that it originated in testicular parenchyma. Accordingly, we will use the name *pancreatic analogue solid pseudopapillary neoplasm of the testis* (PA-SPN) instead of the original term. Microscopically, PA-SPN exhibits 2 distinct components, namely, a signet ring cell component indistinguishable from that occurring in the aforementioned PSRSTT and a solid (and in minor parts also pseudopapillary) component of poorly cohesive low-grade cells with eosinophilic cytoplasm identical to that seen in pancreatic SPN. Clusters of foamy macrophages, deposits of hemosiderin, and small foci of oncocytic change were sporadically found within the solid areas, and hyaline PAS-positive globules were scattered between tumor cells in both components. Such features are well described in the pancreatic SPN [15,16]. Owing to the very pronounced signet ring cell component in the PA-SPN, we came to the idea that the PSRSTT might belong in the same category.

For this purpose, we have collected 13 cases of PSRSTT, which are included in this study. Although 7 of them featured only the signet ring component, the remaining 6 cases exhibited both signet ring cell and solid non–signet ring cell components in various proportions. These cases with both components were morphologically similar to the PA-SPN. The immunoprofile of PSRSTT included positivity for β-catenin, cyclin D1 (both nuclear), CD10, NSE, CD56, α-1-antitrypsin, vimentin, galectin-3, and claudin 7 and negativity for chromogranin, sex cord markers, and germ cell markers. In some cases, the IHC panel was restricted because of a limited amount of tissue. These striking IHC similarities between PSRSTT and PA-SPN provide indirect evidence that these tumors are very closely related if not entirely identical.

An oncogenic somatic mutation in exon 3 of the *CTNNB1* (β-catenin) gene has been found in pancreatic SPN [17] and recently detected in ovarian solid pseudopapillary neoplasm [14] and PA-SPN [9], thus linking them at the molecular genetic level, in addition to morphological similarities. β-Catenin is a key regulatory molecule of the Wnt signaling pathway, which is important for cell homeostasis, differentiation, and proliferation, and its activity is tightly regulated [18]. β-Catenin is activated by Wnt binding, after which it is transferred to the nucleus where it works as a transcriptional cofactor. In the absence of Wnt, β-catenin remains in the cytoplasm where it is rapidly degraded by the destruction complex containing, among others, adenomatous polyposis coli protein [18]. Missense mutations of β-catenin lead to an abnormal stabilization and nuclear overexpression of its protein, which can be highlighted immunohistochemically. In the current study, all analyzable cases of PSRSTT revealed a mutation in exon 3 of the *CTNNB1* gene. The family of β-catenin–driven neoplasia is gradually growing and includes a variety of epithelial neoplasms, a continuously enlarging group of soft tissue neoplasms, and also parenchymal lesions of uncertain histogenesis. To the former category belong neuromuscular choristomas [19], and to the latter belong sclerosing hemangioma of

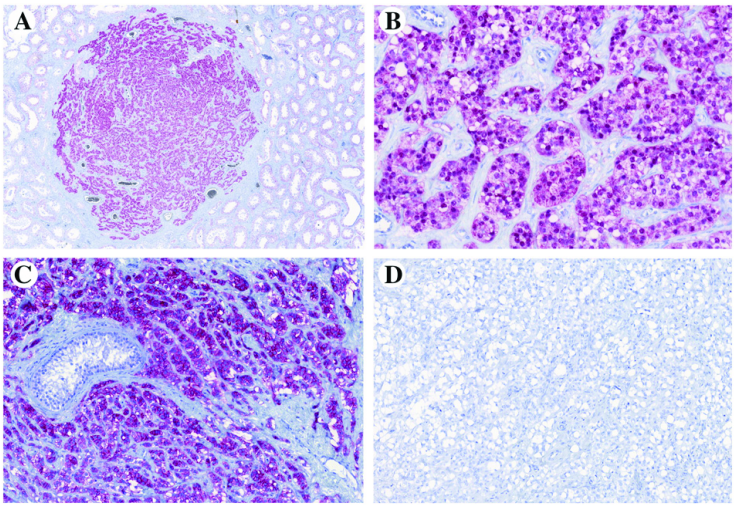

Fig. 4 The immunoreaction with β-catenin was relatively strong and diffuse (A), and the positivity with this antibody was nuclear (B). All tested cases were positive with CD10 (C) and negative with calretinin (D).

the lung, calcifying nested stromal epithelial tumor of the liver, microcystic stromal tumor of the ovary [20,21], and pancreatic SPN together with SPN of the ovary [18]. Our study adds PSRSTT and PA-SPN to this list.

We retrieved 20 pancreatic SPN from our files to determine the frequency of a signet ring cell component in these tumors. This was found in 17 of 20 cases, indicating that this feature is one of the morphological characteristics of pancreatic SPNs. Because all pure PSRSTTs were the smallest tumors in our series, we hypothesize that testicular examples that have mostly a signet ring cell component represent neoplasms in the incipient growth phase, and as the lesions grow, solid areas with trabecular or pseudopapillary arrangement typical for pancreatic SPN develop. This hypothesis can be further supported by the PA-SPN, as its size (nearly 5 cm) was significantly larger than PSRSTTs, and the solid, SPN-like component was here very well developed.

Table 4 Molecular genetic features

Case	Mutations in exon 3 of the *CTNNB1* gene
PA-SPN	c.101G>T (p.Gly34Val)
1	c.110C>T, p.Ser37Phe
2	c.88_99del12, p.Tyr30_Ser33del
3	c.122C>T, p.Thr41Ile
4	c.98C>G, p.Ser33Cys
5	c.110C>T, p.Ser37Phe
6	c.98C>G, p.Ser33Cys
7	NA
8	NA
9	c.110C>G, p.Ser37Cys
10	c.94G>T, p.Asp32Tyr
11	c.94G>C, p.Asp32His
12	NA
13	c.94G>A, p.Asp32Asn

Abbreviations: NA, not analyzable; Wt, wild type.

There is no consensus regarding the line of differentiation of pancreatic SPN. It is traditionally classified as an epithelial neoplasm; however, the cytokeratin expression is rare and mostly absent. Thus, the origin and phenotypic relationship of pancreatic SPN tumor cells to the pancreatic tissue still remain enigmatic [13]. Kosmahl et al [13] in their study suggested an extrapancreatic origin of solid pseudopapillary neoplasms. Genital ridges are very close to the pancreatic anlage during embryogenesis, allowing the possibility that cells from the primitive gonads may migrate to the developing pancreas [13]. This theory has been discussed for mucinous cystic neoplasms and serous microcystic adenomas of the pancreas and may be also valid for pancreatic SPN [22,23]. The occurrence of the herein discussed cases in the testicular area together with the previously published cases in the ovary may serve as arguments in favor of this theory.

In the differential diagnosis, distinction from Sertoli cell tumor NOS is the most interesting. It is our view that, in the past, PSRSTTs were diagnosed as Sertoli cell tumor NOS, as this category included even cases that were immunohistochemically negative for sex cord markers inhibin, calretinin, and SF-1 [24]. It seems to us that, immunohistochemically, inhibin-, calretinin-, and SF-1–negative testicular tumors with signet ring cell histology that featured positive immunoreactivity for β-catenin, cyclin D1 (both nuclear), CD10, NSE, CD56, α-1-antitrypsin, vimentin, galectin-3, and claudin 7 and negativity for chromogranin represented in fact PSRSTTs and not Sertoli cell tumors of any kind. Real testicular tumors with Sertoli cell differentiation are in our view mostly

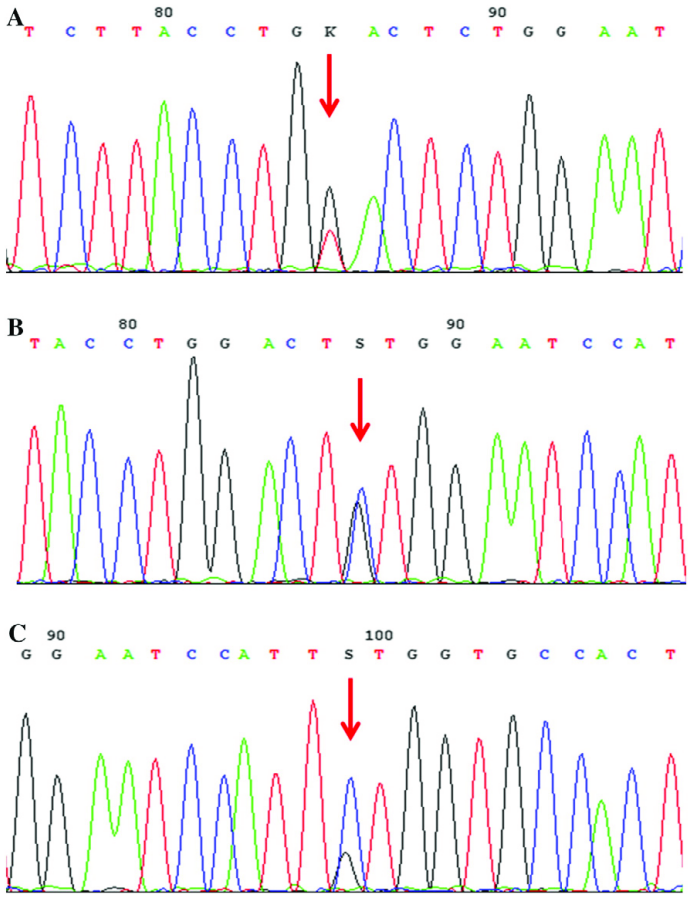

Fig. 5 The sequenogram data involving mutations in exon 3 of *CTNNB1* gene; used nomenclature NM_001904.3. Substitution c.94G>T, p.Asp32Tyr (A), substitution c.98C>G, p.Ser33Cys (B), substitution c.110C>G, p.Ser37Cys (C).

immunohistochemically positive for sex cord markers such as inhibin and calretinin, SF-1, or FOXL2 [25].

It is not our intention to question the entity of Sertoli cell tumors but rather to set apart a morphologically well-defined group of tumors with consistent IHC and molecular characteristics, which we think deserves separation from the rather heterogeneous category of Sertoli cell tumors NOS.

In conclusion, we have described a series of primary signet ring stromal tumors of the testicular region showing morphologic, immunohistochemical, and molecular genetic overlap with PA-SPN. We believe that PSRSTT and SPN of the pancreas, ovary, and pancreatic analogue SPN of the testis are similar tumors probably representing a single entity occurring in different organs. We further think that the recently published case of a 1.1-cm large signet ring stromal cell tumor of the ovary with *CTNNB1* mutation and vimentin, cyclin D1, CD10, and β-catenin immunohistochemical positivity and cytokeratins, calretinin, epithelial membrane antigen, and inhibin negativity is the ovarian counterpart of PSRSTT and represents incipient growth phase of ovarian SPN [26].

Our concept was further strengthened by a recently published letter to the editor by Mengoli et al. The authors reported another 2 identical cases with the same results and conclusion [27,28]. Notwithstanding, we acknowledge that the final proof that PSRSTT is identical to pancreatic SPN will bring only the genetic comparison of these 2 entities.

References

[1] Michal M, Hes O, Kazakov DV. Primary signet-ring stromal tumor of the testis. Virchows Arch 2005;447:107-10.
[2] Kuo CY, Wen MC, Wang J, Jan YJ. Signet-ring stromal tumor of the testis: a case report and literature review. Hum Pathol 2009;40:584-7.

[3] Seo HE, Lee MK, Lee YD, et al. Solid-pseudopapillary tumor of the pancreas. J Clin Gastroenterol 2006;40:919-22.
[4] Deshpande V, Oliva E, Young RH. Solid pseudopapillary neoplasm of the ovary: a report of 3 primary ovarian tumors resembling those of the pancreas. Am J Surg Pathol 2010;34:1514-20.
[5] Cheuk W, Beavon I, Chui DT, Chan JK. Extrapancreatic solid pseudopapillary neoplasm: report of a case of primary ovarian origin and review of the literature. Int J Gynecol Pathol 2011;30:539-43.
[6] Stoll LM, Parvataneni R, Johnson MW, et al. Solid pseudopapillary neoplasm, pancreas type, presenting as a primary ovarian neoplasm. Hum Pathol 2012;43:1339-43.
[7] He S, Yang X, Zhou P, Cheng Y, Sun Q. Solid pseudopapillary tumor: an invasive case report of primary ovarian origin and review of the literature. Int J Clin Exp Pathol 2015;8:8645-9.
[8] Syriac S, Kesterson J, Izevbaye I, et al. Clinically aggressive primary solid pseudopapillary tumor of the ovary in a 45-year-old woman. Ann Diagn Pathol 2012;16:498-503.
[9] Michal M, Bulimbasic S, Coric M, et al. Pancreatic analogue solid pseudopapillary neoplasm arising in the paratesticular location. The first case report. Hum Pathol 2016;56:52-6.
[10] Kazakov DV, Sima R, Vanecek T, et al. Mutations in exon 3 of the *CTNNB1* gene (beta-catenin gene) in cutaneous adnexal tumors. Am J Dermatopathol 2009;31:248-55.
[11] Klimstra DS, Wenig BM, Heffess CS. Solid-pseudopapillary tumor of the pancreas: a typically cystic carcinoma of low malignant potential. Semin Diagn Pathol 2000;17:66-80.
[12] Estrella JS, Li L, Rashid A, et al. Solid pseudopapillary neoplasm of the pancreas: clinicopathologic and survival analyses of 64 cases from a single institution. Am J Surg Pathol 2014;38:147-57.
[13] Kosmahl M, Seada LS, Janig U, Harms D, Kloppel G. Solid-pseudopapillary tumor of the pancreas: its origin revisited. Virchows Arch 2000;436:473-80.
[14] Kominami A, Fujino M, Murakami H, Ito M. Beta-catenin mutation in ovarian solid pseudopapillary neoplasm. Pathol Int 2014;64:460-4.
[15] Goldstein J, Benharroch D, Sion-Vardy N, et al. Solid cystic and papillary tumor of the pancreas with oncocytic differentiation. J Surg Oncol 1994;56:63-7.
[16] Meriden Z, Shi C, Edil BH, et al. Hyaline globules in neuroendocrine and solid-pseudopapillary neoplasms of the pancreas: a clue to the diagnosis. Am J Surg Pathol 2011;35:981-8.
[17] Abraham SC, Klimstra DS, Wilentz RE, et al. Solid-pseudopapillary tumors of the pancreas are genetically distinct from pancreatic ductal adenocarcinomas and almost always harbor beta-catenin mutations. Am J Pathol 2002;160:1361-9.
[18] Agaimy A, Haller F. *CTNNB1* (beta-catenin)-altered neoplasia: a review focusing on soft tissue neoplasms and parenchymal lesions of uncertain histogenesis. Adv Anat Pathol 2016;23:1-12.
[19] Carter JM, Howe BM, Hawse JR, et al. *CTNNB1* mutations and estrogen receptor expression in neuromuscular choristoma and its associated fibromatosis. Am J Surg Pathol 2016;40:1368-74.
[20] Irving JA, Young RH. Microcystic stromal tumor of the ovary: report of 16 cases of a hitherto uncharacterized distinctive ovarian neoplasm. Am J Surg Pathol 2009;33:367-75.
[21] Irving JA, Lee CH, Yip S, et al. Microcystic stromal tumor: a distinctive ovarian sex cord-stromal neoplasm characterized by FOXL2, SF-1, WT-1, cyclin D1, and beta-catenin nuclear expression and *CTNNB1* mutations. Am J Surg Pathol 2015;39:1420-6.
[22] Compagno J, Oertel JE. Microcystic adenomas of the pancreas (glycogen-rich cystadenomas): a clinicopathologic study of 34 cases. Am J Clin Pathol 1978;69:289-98.
[23] Compagno J, Oertel JE. Mucinous cystic neoplasms of the pancreas with overt and latent malignancy (cystadenocarcinoma and cystadenoma). A clinicopathologic study of 41 cases. Am J Clin Pathol 1978;69:573-80.
[24] Moch H, Humphrey PA, Ulbright TM, Reuter VE. WHO classification of tumours of the urinary system and male genital organs. 4th ed. Lyon: IARC; 2016.
[25] Perrone F, Bertolotti A, Montemurro G, et al. Frequent mutation and nuclear localization of beta-catenin in Sertoli cell tumors of the testis. Am J Surg Pathol 2014;38:66-71.
[26] Kopczynski J, Kowalik A, Chlopek M, et al. Oncogenic activation of the Wnt/beta-catenin signaling pathway in signet ring stromal cell tumor of the ovary. Appl Immunohistochem Mol Morphol 2016;24:e28-3.
[27] Mengoli MC, Bonetti LR, Intersimone D, Fedeli F, Rossi G. Solid pseudopapillary tumor: a new tumor entity in the testis? Hum Pathol 2017;62:242-3.
[28] Michalova K, Michal M, Kazakov DV, Michal M. Solid pseudopapillary tumor: a new tumor entity in the testis?—reply. Hum Pathol 2017;62:243-5.

Annals of Diagnostic Pathology 35 (2018) 42–47

Contents lists available at ScienceDirect

Annals of Diagnostic Pathology

journal homepage: www.elsevier.com/locate/anndiagpath

Solid pseudopapillary neoplasm (SPN) of the testis: Comprehensive mutational analysis of 6 testicular and 8 pancreatic SPNs

Kvetoslava Michalova[a,*], Michael Michal[a,b], Monika Sedivcova[c], Dmitry V. Kazakov[a], Carlos Bacchi[d], Tatjana Antic[e], Marketa Miesbauerova[a], Ondrej Hes[a], Michal Michal[a]

[a] Department of Pathology, Faculty of Medicine in Pilsen, Charles University, 323 00 Pilsen, Czech Republic
[b] Biomedical Center, Faculty of Medicine in Pilsen, Charles University, 323 00 Pilsen, Czech Republic
[c] Bioptical Laboratory, Ltd., Plzen 301 00, Czech Republic
[d] Consultoria em Patologia, Botucatu, SP, Brazil
[e] Department of Pathology, The University of Chicago, Chicago, USA

ARTICLE INFO

Keywords:
Solid pseudopapillary neoplasm
Primary signet ring cell stromal tumor
Testis
Pancreas
SPN
Analogue

ABSTRACT

Background: Recently, we came with the theory of a possible relationship between a group of testicular and pancreatic tumors. We used one case of a pancreatic analogue solid pseudopapillary neoplasm of the testis composed partially of areas reminiscent of solid pseudopapillary neoplasm (SPN) of the pancreas and partially of structures identical to primary signet ring stromal tumor of the testis (PSRSTT) as a connecting link between these two entities. After demonstrating that PSRSTT and pancreatic analogue SPN of the testis share the same immunoprofile and genetic features characteristic for pancreatic SPN, we came to the conclusion that pancreatic analogue SPN of the testis and PSRSTT represent a morphological spectrum of a single entity and that both are related to the pancreatic SPN.

Design: The aim of this study is to present a series of 6 cases of testicular tumors, which lacked the signet ring cell component and were thus morphologically very similar to the SPN of the pancreas. The goal of this study is to compare the genetic background of these testicular tumors that are obviously related to the PSRSTT/pancreatic analogue SPN of the testis with the series of 8 pancreatic SPN.

Results: The mutational analysis revealed an oncogenic somatic mutation in the exon 3 of the *CTNNB1* (β-catenin) gene in all analyzable (5/6) testicular and all pancreatic (8/8) tumors. The immunoprofile (positivity with β-catenin, CD10, vimentin, NSE, CD56, and negativity with inhibin, calretinin, chromogranin) was identical in all testicular and pancreatic tumors.

Conclusion: This study expanded the morphological spectrum of the PSRSTT/pancreatic analogue SPN of the testis by adding 6 cases without the signet ring cell component. Considering the obvious analogy of PSRSTT/pancreatic analogue SPN of the testis/SPN of the testis and their relationship to the pancreatic SPN we propose the collective term "solid pseudopapillary neoplasm of the testis" for these tumors. The mutational profile of the SPN of the testis and pancreas was the same in both groups of tumors which we consider as a final proof that SPN of the testis is identical to the SPN of the pancreas.

1. Introduction

Very recently, we have described pancreatic analogue solid pseudopapillary neoplasm (SPN) of the testis [1], a peculiar tumor demonstrating a morphological, immunohistochemical and genetic overlap with pancreatic SPN. Histologically, it showed biphasic features represented by the signet ring cell component and the solid component. Subsequently, we noticed that the signet ring cell component is virtually identical to the primary signet ring stromal tumor of the testis (PSRSTT) and based on this observation, we published a study comparing these two entities. The identical immunohistochemical and mutational profile led us to the conclusion that PSRSTT and pancreatic analogue SPN of the testis represent a morphological spectrum of a single entity and that both seem to be related to the pancreatic SPN [2-4]. However, to further reinforce our theory, we decided to directly compare the mutational profiles of both the testicular and pancreatic tumors. Herein, we present 6 testicular tumors which histologically showed only the solid component of the pancreatic analogue SPN of the

* Corresponding author at: Department of Pathology, Charles University, Medical Faculty and Charles University Hospital Plzen, 304 60, Czech Republic.
E-mail address: kveta.michalova@medima.cz (K. Michalova).

https://doi.org/10.1016/j.anndiagpath.2018.04.003

testis. They also had immunohistochemical features identical to PSRSTT/pancreatic analogue SPN of the testis and to those of SPN of the pancreas [1,5-7]. Morphologically, they were highly reminiscent of the pancreatic SPN and therefore we called them "solid pseudopapillary neoplasm of the testis".

The objective of this study was the comparison of mutational profiles of both testicular and pancreatic SPN. It is obvious that the testicular SPN presented herein are akin to PSRSTT and pancreatic analogue SPN of the testis and we expected the analogic mutational profile of the testicular SPN with the latter as previously published [1,2]. Therefore, we consider the mutational profile analysis of SPN of the testis sufficient for the whole group of tumors comprising PSRSTT, pancreatic analogue SPN of the testis and testicular SPN.

2. Materials and methods

To retrieve the testicular cases, our tumor registry was searched using the keywords "testis", "unclassified sex-cord tumor", "male adnexal tumor of probable Wolffian origin", "Sertoli cell tumor", "benign", "NOS" and "signet ring stromal tumor". Only cases morphologically and immunophenotypically similar to the pancreatic SPN were selected. Cases having a prominent signet ring cell component (more than 5% of the tumor area) were excluded. Upon reevaluation, 6 cases of primary testicular tumors which met the diagnostic criteria were selected for further investigation. Reserve slides (16 and 35) or paraffin tissue blocks (1 to 6) were available for the cases 1 and 2 and for the cases 3–6, respectively.

The cases of solid pseudopapillary neoplasm (SPN) of the pancreas were retrieved from our registry using keywords "pancreas" and "solid pseudopapillary neoplasm". This search altogether yielded 22 specimens. Only cases with available tissue blocks and sufficient DNA quality allowing the molecular analysis were selected for the study (8 cases). One representative block from each case was used for the immunohistochemical study and another one for the genetic analysis.

The cases of both testicular and pancreatic tumors came from the period between 1993 and 2018. None of them has been reported previously. The clinical information was extracted from the registry records, and follow-up data were obtained from attending clinicians. Tissues for light microscopy were fixed in 4% formaldehyde and embedded in paraffin using the routine procedure. Three-μm-thick sections were cut from tissue blocks and stained with hematoxylin and eosin (H &E).

2.1. Immunohistochemistry

The immunohistochemical analysis was performed using a Ventana BenchMark ULTRA (Ventana Medical System Inc., Tucson, AZ). The primary antibodies used are shown in Table 1. They were visualized using the enzymes alkaline phosphatase or peroxidase as detecting systems (both purchased from Ventana Medical System Inc.).

2.2. Molecular genetic analysis of the β-catenin gene

Mutational analysis of the exon 3 of the *CTNNB1* (β-catenin) gene was performed using polymerase chain reaction and direct sequencing as described previously [8].

3. Results

3.1. Clinicopathologic features

3.1.1. Testicular tumors

The clinicopathologic characteristics are summarized in Table 2. The age of the patients at the time of diagnosis ranged from 24 to 82 years (mean 47, median 37.5). Follow-up was available for 5/6 patients with average duration 2.1 years (range 5 months–5 years). All patients with the available clinical information are alive and well with no signs of an aggressive clinical course. None of the patients have had any other intraabdominal tumor, and the pancreas was unremarkable. Except for one paratesticular tumor, all were located in the testis. All tumors were unilateral, well circumscribed and encapsulated. The tumor size ranged from 0.5 cm to 3 cm in the largest dimension, with an average size of 1.7 cm (median 1.8). The adjacent non-neoplastic testis showed no signs of germ cell neoplasia in situ or any other pathologic alterations.

Table 1
List of antibodies.

Antibody	Clone	Manufacturer	Dilution
β-Catenin	Polyclonal	Thermo Fischer Scientific, Freemont, CA, USA	1:150
CD10	SP67	Ventana Medical System, Inc., Tucson, Arizona, USA	RTU
Vimentin	V9	Cell Marque, Rocklin, CA, USA	RTU
CD56	MRQ-42	Cell Marque, Rocklin, CA, USA	RTU
Synaptophysin	SP11	Ventana Medical System, Inc., Tucson, Arizona, USA	RTU
Chromogranin	DAK-A3	Dako, Glostrup, Denmark	1:400
NSE	BBS/NC/VI-H14	Dako, Glostrup, Denmark	1:1000
Inhibin	R1	Ventana Medical System, Inc., Tucson, Arizona, USA	RTU
Calretinin	SP65	Ventana Medical System, Inc., Tucson, Arizona, USA	RTU

Cases 1, 2, 4 and 6 grew in a solid fashion (Fig. 1A–D), whereas Cases 3 and 5 were entirely (Fig. 2A, B) or partially cystic (Fig. 3A, B), respectively. Neoplastic cells were arranged in nests and sheets, cords or trabeculae, in most cases set in a fibrotic stroma which presented either as fibrous septa of varying thickness (Cases 1, 4, 5, 6) or as a marked sclerotic background (Case 2) (Fig. 1C, D). Pseudopapillary structures were focally presented in 3 cases. The tumor cells had a uniform epithelioid appearance with bland looking nuclei and eosinophilic cytoplasm, devoid of marked vacuolation or signet ring cells. Cellular atypia and mitoses as well as necrotic areas were absent.

3.1.2. Pancreatic tumors

The clinicopathological features are shown in Table 3. All patients were women: age at the time of diagnosis ranged between 15 and 58 years (mean 31, median 26). Follow-up data were available for 6 patients and ranged from 1 to 18 years (mean 12.5, median 14). The tumors followed a favorable clinical course, and no patient with the available clinical information suffered from a metastatic spread or died of the disease. The size of the tumors ranged from 2.7 to 18 cm (mean 8.5, median 6). Histologically, the tumors were composed of monomorphic epithelioid cells variably arranged in sheets and nests or exhibiting post-degenerative changes characterized by pseudopapillae and cysts. Scattered epithelioid cells with large and clear intracytoplasmic vacuole (signet ring cells) were focally found in most cases. Pleomorphism and mitotic figures were not found.

3.2. Immunohistochemistry and molecular genetic analysis of the β-catenin gene

Both immunohistochemical and mutational profile was essentially the same in both testicular and pancreatic tumors. For the sake of clarity, each organ is discussed in a separate paragraph.

3.2.1. Testicular tumors

The IHC and molecular genetic results are shown in Table 4. All tumors reacted with β-catenin (nuclear positivity), CD10, vimentin and NSE (the positivity was focal in 4 cases), 5/6 tumors were positive or focally positive for CD56 and synaptophysin. Inhibin was uniformly

Table 2
SPN of the testis: clinicopathologic features.

Case	Age (years)	Size (cm)	Localisation	Histology	Follow-up
1	67	Diam. 0.5	testis	Solid, fibrous bands of various thickness, tumor cells arranged in nests and sheets	AW, 6 years
2	38	Diam. 2.1	Testis	Solid, marked sclerotic background, occasional pseudopapillae, tumor cells arranged in cords and trabeculae	AW, 3 years
3	33	Diam. 0.5	Paratestis	Multicystic (cysts and microcysts), no fibrosis, tumor cells arranged in cords and trabeculae	AW, 3 years
4	24	3 × 3 × 2.5	Testis	Solid, fibrous bands of various thickness, occasional, pseudopapillae, tumor cells arranged in nests and sheets	AW, 2 year
5	82	2 × 2 × 2.5	Testis	Solid, cystic and microcystic, fibrous bands of various thickness, focal pseudopapillae, tumor cells arranged in cords and trabeculae	NA
6	37	1 × 1 × 1.5	Testis	Solid, fibrous bands of various thickness, tumor cells arranged in nests and sheets	AW, 3 months

SPN: solid pseudopapillary neoplasm; Diam diameter; AW alive and well, NA: not available.

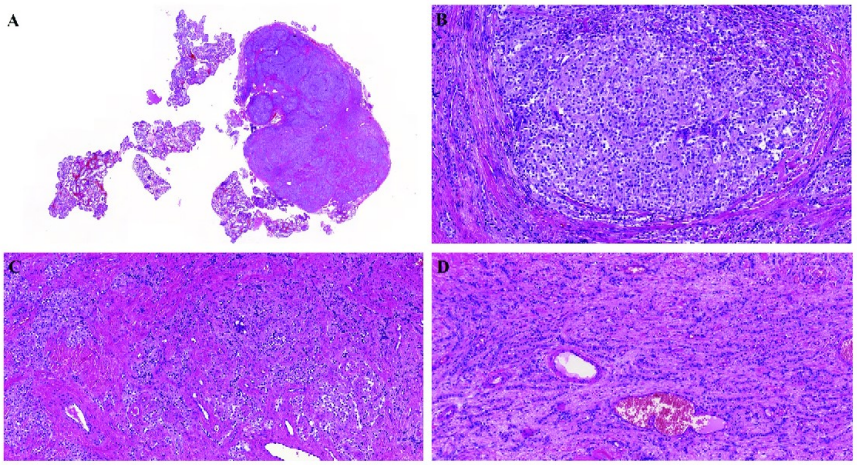

Fig. 1. Case 6 was entirely solid in arrangement (A, B). Areas where the tumor grew in thin cords set in a fibrotic stroma were found (C, D).

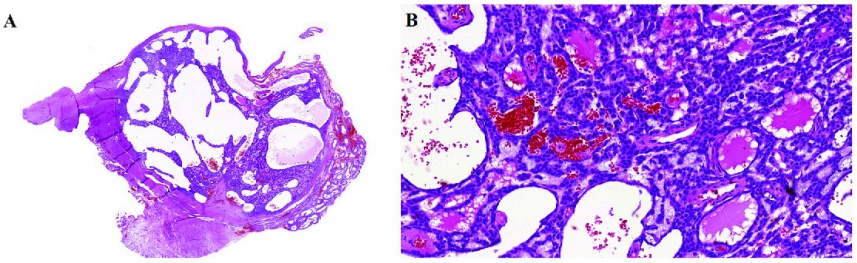

Fig. 2. Case 3. Arrangement of this case was entirely cystic and microcystic and lacked fibrosis (A, B).

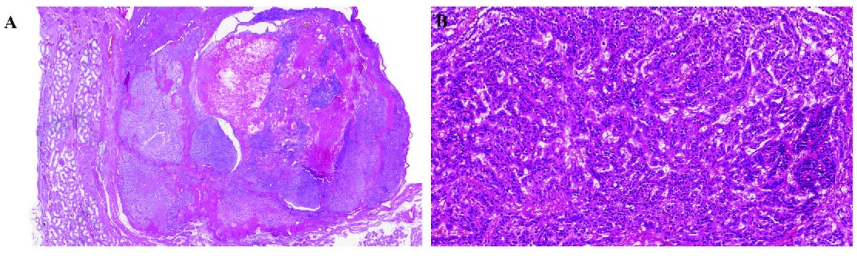

Fig. 3. Case 5. This case had an arrangement identical to the analogous tumor in pancreas, containing large areas of pseudocystic and focally pseudopapillary arrangement (A). Most of the tumor cells grew in cords (B).

Table 3
SPN of the pancreas: clinicopathologic features.

Case	Age (years)/sex	Size (cm)	Histology	Follow-up
1	27/F	14 × 11 × 7.5	Solid, pseudopapillary, signet ring cells	AW, 1 year
2	22/F	18 × 15 × 15	Solid, pseudopapillary, fibrous bands, signet ring cells	AW, 18 years
3	25/F	5.5 × 5 × 4.5	Solid, pseudopapillary, nests, sheets, fibrous bands, signet ring cells	NA
4	28/F	13 × 12 × 8	Solid sheets, pseudopapillary, fibrous bands, signet ring cells	NA
5	57/F	Diam 2.7	Solid, trabecular, fibrous bands, hyaline globules, no pseudopapillae, no signet ring cells	AW, 14 years
6	15/F	6 × 5.5 × 5	Solid, cystic, pseudopapillary, signet ring cells	AW, 18 years
7	15/F	6 × 5.5 × 5	Solid, cystic, pseudopapillary, signet ring cells	AW, 10 years
8	58/F	Diam 3	Solid, trabecular, fibrous bands, no pseudopapillae, no signet ring cells	AW, 14 years

SPN: solid pseudopapillary neoplasm; Diam: diameter; AW: alive and well, NA: not available.

Table 4
SPN of the testis: IHC and molecular genetic features.

Case	β-cat	CD 10	Vim	CD 56	Synapt	Chrom	NSE	Inhib	Calret	Mutational analysis
1	+	+	+	+	−	NP	NP	−	−	c.98C > G, p.Ser33Cys
2	+	+	NP	−	Focal +	−	Focal +	−	−	c.109T > G, p.Ser37Ala
3	+	+	+	+	+	NP	+	−	−	c.110C > G, p.Ser37Cys
4	+	+	+	Focal +	Focal +	−	Focal +	−	−	c.98C > G, p.Ser33Cys
5	+	+	NP	Focal +	+	−	Focal +	−	−	NA
6	+	+	+	Focal +	+	−	+	−	−	c.98C > T, p.Ser33Phe

SPN: solid pseudopapillary neoplasm; β-cat: β-catenin; Vim: vimentin; Synapt: synaptophysin; Chrom: chromogranin; NSE: neuron specific enolase; Inhib: inhibin; Calret: calretinin; NP: not performed, +: positive, −: negative, NA: not analyzable.

negative in all cases. None of the tumors reacted with chromogranin or calretinin.

A mutation in exon 3 of the *CTNNB1* (β-catenin) gene was detected in 5/6 cases; the remaining case was not analyzable. 2 cases revealed mutation c.98C > G p.Ser33Cys, 1 case c.98C > T, p.Ser33Phe, 1 case c.110C > G p.Ser37Cys and the remaining case c.109T > G, p.Ser37Ala.

3.2.2. Pancreatic tumors

The immunoprofile and the results of molecular genetic testing are depicted in Table 5. Immunohistochemically, all tumors showed a positive reaction with β-catenin (nuclear positivity), CD10, vimentin, CD56 and NSE. 1/8 tumors was focally positive with synaptophysin, while there was no reactivity with chromogranin, inhibin, and calretinin in any of the tumors.

All tested tumors (8/8) revealed a mutation in exon 3 of the *CTNNB1* (β-catenin) gene. 2 cases featured c.101G > A, p.Gly34Glu, 2 cases c.100G > C, p.Gly34Arg, 1 case c.95A > T, p.Asp32Val, 1 case c.95A > G, p.Asp32Gly, 1 case c.94G > T, p.Asp32Tyr and finally 1 case c.110C > T, p.Ser37Phe.

4. Discussion

Pancreatic analogue solid pseudopapillary neoplasm (SPN) of the testis [1] may be composed of two components, namely the signet ring and the solid. Recently, we showed that the primary signet ring stromal tumor of the testis (PSRSTT) [5,9] which contains an indistinguishable signet ring component, is a closely related tumor and that both are probably akin to the pancreatic SPN [2].

In this study, we expand the morphological spectrum of pancreatic analogue SPN of the testis/PSRSTT by adding 6 cases of testicular tumors which morphologically contained only the solid component of the pancreatic analogue SPN of the testis lacking signet ring cell component. These areas were morphologically identical to analogous areas of SPN of the pancreas. Specifically, it consisted of nests, sheets, cords and trabeculae of epithelioid cells devoid of marked vacuolation or signet ring cells. Occasionally, it also showed areas with poor intercellular cohesivity resulting in the formation of pseudopapillae, surrounded by hyalinized stromal and fibrous tissue of various thickness. These features have been well described in the SPN of the pancreas [10]. Case 3 had entirely a cystic and microcystic architecture and lacked fibrosis (Fig. 2A, B). Case 5 featured a cystic and microcystic arrangement in some areas and fibrosis was present (Fig. 3A, B). Although, as the name implies, pancreatic SPN typically grows in solid or pseudopapillary fashion, the microcystic arrangement has recently been recognized as part of its morphologic spectrum by Abe et al. [11]. In their paper, the Fig. 1B and C closely resembled Case 3 from our series.

In our recent study on PSRSTT [2], we divided the cases into two groups: the first one composed of signet ring cells only (pure signet ring cell tumors) and the second one displaying biphasic features (signet

Table 5
SPN of the pancreas: IHC and molecular genetic features.

Case	β-cat	CD 10	Vim	CD 56	Chrom	Synapt	NSE	Inhib	Calret	Mutational analysis
1	+	Focal +	+	+	−	−	+	−	−	c.94G > T, p.Asp32Tyr
2	+	+	+	+	−	−	+	−	−	c.95A > T, p.Asp32Val
3	+	+	+	+	−	−	+	−	−	c.100G > C, p.Gly34Arg
4	+	+	+	+	−	Focal +	+	−	−	c.95A > G, p.Asp32Gly
5	+	+	+	+	−	−	+	−	−	c.101G > A, p.Gly34Glu
6	+	+	+	Focal +	−	−	Focal +	−	−	c.100G > C, p.Gly34Arg
7	+	+	+	+	−	−	+	−	−	c.110C > T, p.Ser37Phe
8	+	+	+	+	−	−	Focal +	−	−	c.101G > A, p.Gly34Glu

SPN: solid pseudopapillary neoplasm; +: positive, −: negative, β-cat: β-catenin; Vim: vimentin; Synapt: synaptophysin; Chrom: chromogranin; NSE: neuron specific enolase; Inhib: inhibin; Calret: calretinin;

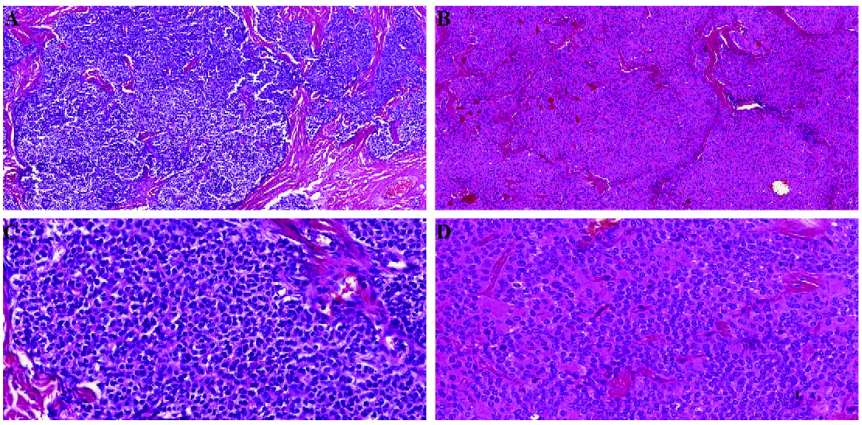

Fig. 4. The morphologic comparison between small pancreatic and testicular tumors. Architecturally, in most cases, both testicular (A) and pancreatic (B) SPNs were arranged in a solid fashion with intersecting fibrous septa of various thickness. The neoplastic cells of testicular (C) and pancreatic (D) tumors had a uniform epithelioid appearance with round to oval nuclei and eosinophilic cytoplasm, in all testicular and two small pancreatic tumors devoid of marked vacuolation.

ring and solid, non-signet ring component) as previously described in pancreatic analogue SPN of the testis. We hypothesized that the pure signet ring tumors represent an incipient growth phase of SPN and as the tumor increases in size, the solid component gradually emerges. This theory followed the observation that the pure signet ring stromal tumors were the smallest tumors in our series (up to 0.9 cm), biphasic tumors were slightly larger (up to 2 cm), and pancreatic analogue SPN of the testis measured nearly 5 cm and exhibited the most conspicuous solid component. Testicular SPN presented herein were of a similar size as PSRSTT (measured 0.5–3 cm, median 1.75) and essentially lacked signet ring cells. Thus, it is obvious that certain cases grow as solid tumors from the very beginning.

Summarizing the morphological features, most of the tumors did not appear like the classical example of pancreatic SPN, e.g., pseudopapillary structures occurred occasionally or focally only in 3 cases. This can be explained by the considerable difference in tumor size between the testicular (mean size 1.6 cm) and pancreatic tumors (mean size 8.5 cm). Taking into account that pseudopapillae are regarded as a result of secondary degenerative changes, it is understandable that such changes are more common in larger (pancreatic) tumors and less prominent in smaller and incipient (testicular) tumors. In addition, we noticed that it were the smallest pancreatic tumors that resembled the testicular cases at most. There were 2 small pancreatic tumors in our series (diameter 3 and 2.7 cm) which grew in a solid fashion and also almost lacked postdegenerative pseudopapillary changes. The morphologic comparison between testicular and small pancreatic SPN is depicted on Fig. 4.

The IHC features of the current cohort were identical to the pancreatic analogue SPN of the testis/PSRSTT as well. Based on the histomorphology and immunoprofile, the testicular tumors presented herein were collectively termed “solid pseudopapillary neoplasm of the testis”. It is obvious that the testicular SPNs belong to the same group of tumors as PSRSTT and pancreatic analogue SPN of the testis. As we demonstrated in the previous study [2], the former proved to have an analogous mutational profile as the latter, namely the oncogenic somatic mutation in exon 3 of the *CTNNB1* (β-catenin) gene. However, the pancreatic tumors were evaluated only morphologically in this study, and neither immunohistochemical nor molecular analysis was performed; the IHC and molecular features of pancreatic SPN were derived only from the literature [12-14]. One of the goals of the current study was the molecular comparison of SPN of the testis and pancreas which we consider as a final proof that this kind of testicular tumors (comprising pancreatic analogue SPN of the testis, SPN of the testis and PSRSTT) belong into the same category as pancreatic SPN. As a result, the oncogenic somatic mutation in exon 3 of the *CTNNB1* (β-catenin) gene was detected in both testicular (5/5 cases) and pancreatic (8/8 cases) SPNs.

Nine cases of ovarian SPN have already been reported in the English literature [15-21]. SPN of the ovary is histopathologically even more reminiscent of its pancreatic counterpart since owing to its location, it frequently presents as a large tumor mass [15] and the degenerative changes thus occur more commonly. Both ovarian and pancreatic SPN can grow imperceptibly for a long time, as opposed to its testicular counterpart which is visible/palpable earlier in the course of the disease and thus more likely to be resected in the incipient stage. The association of ovarian SPN with the β-catenin mutation has been identified [20] and very recently, the same mutation was detected in primary signet ring stromal tumor of the ovary [22]. Mengoli et al. suggested to cluster primary signet ring stromal tumor of the ovary, ovarian SPN and microcystic stromal tumor (MST) of the ovary to the category of the “family of β-catenin ovarian tumors” [23]. We agree with the authors and in fact, we propose the same approach for the testicular tumors. MST of the ovary is histologically characterized by three features occurring in a various proportion, namely conspicuous microcysts, solid cellular areas, and hyalinized fibrous stroma. Immunohistochemically it stains with CD10, β-catenin (nuclear), FOXL2, SF-1 and vimentin and is negative with inhibin and calretinin [24]. The oncogenic somatic mutation in exon 3 of the *CTNNB1* (β-catenin) gene defines it genetically [25]. Its first description is dated back to 2009 [26], and since then, it has been known to occur only in the ovary. Very recently, Zhu et al. described the first case of testicular MST with a confirmed β-catenin somatic mutation [27]. Interestingly, in our present study, two cases showed a predominant or focal microcystic change (Figs. 2, 3). When compared with Fig. 2B from Zhu et al. [27], it seems plausible that these are identical tumors and that the hypothesis suggested by Mengoli [23] can be applied to the testicular location as well. However, immunohistochemically, MST expresses FOXL2 and SF-1 antibodies while being negative with CD56. This currently supports the classification of MST as a sex cord stromal tumor [24]. On the contrary, the primary signet ring stromal tumor of the testis shows an inversed reaction with these antibodies. Since the antibodies against FOXL2 and SF-1 failed to work in our laboratory, we could assess only the positive reaction with CD56. However, we expect the same results as published for PSRSTT [2] recently. Therefore, we cannot confirm the relationship between the testicular MST and the PSRSTT/SPN with certainty.

The most important differential diagnostic consideration is Sertoli cell tumor. The arguments against the notion, that SPN of the testis (and PSRSTT) are in fact a subgroup of Sertoli cell tumors are fully discussed elsewhere [2]. Suffice to say that although we are aware of some similarities between these two entities, we consider testicular SPN/pancreatic analogue SPN of the testis/PSRSTT as clearly defined tumors with consistent morphology, IHC and molecular background in contrast to the miscellaneous group of Sertoli cell tumors. In our opinion, testicular SPN/pancreatic analogue SPN of the testis/PSRSTT are relatively common tumors but most of them are currently diagnosed as Sertoli cell tumors, NOS.

It should be noted that one case of testicular SPN has already been published by Mengoli et al. [3,4]. The authors presented two cases, one of which was PSRSTT and the second one case was identical to the cases presented herein (see Figures A and B in their paper [3]).

In summary, we expanded the morphological spectrum of the recently described PSRSTT/pancreatic analogue SPN of the testis by adding 6 cases histologically similar to the SPN of the pancreas. Considering the obvious analogy of PSRSTT/pancreatic analogue SPN of the testis/SPN of the testis and their relationship to the pancreatic SPN, we propose the collective term “solid pseudopapillary neoplasm of the testis”. The genetic comparison between these cases and pancreatic SPN revealed the same oncogenic somatic mutation in exon 3 of the *CTNNB1* (β-catenin) gene, which we consider a final proof that SPN of the testis is identical to the SPN of the pancreas.

Compliance with ethical standards

Neither ethics approval nor informed consent was required for our study.

Funding

This study was supported by the National Sustainability Program I (NPU I) Nr. LO1503 provided by the Ministry of Education Youth and Sports of the Czech Republic and by Charles University Fund SVV 2017-260391.

Conflict of interest

All authors declare no conflict of interest.

References

[1] Michal M, Bulimbasic S, Coric M, Sedivcova M, Kazakov DV, Michal M, et al. Pancreatic analogue solid pseudopapillary neoplasm arising in the paratesticular location. The first case report. Hum Pathol 2016;56:52–6.
[2] Michalova K, Michal M, Jr., Kazakov DV, Sedivcova M, Hes O, Hadravsky L, Agaimy A, Tretiakova M, Bacchi C, Hartmann A, Kuroda N, Bulimbasic S, Coric M, Antic T, Michal M. Primary signet ring stromal tumor of the testis: a study of 13 cases indicating their phenotypic and genotypic analogy to pancreatic solid pseudopapillary neoplasm. Hum Pathol 2017; 67, 85–93.
[3] Mengoli MC, Bonetti LR, Intersimone D, Fedeli F, Rossi G. Solid pseudopapillary tumor: a new tumor entity in the testis? Hum Pathol 2017;62:242–3.
[4] Michalova K, Michal M, Hes O, Kazakov DV, Michal M. Solid pseudopapillary tumor: a new tumor entity in the testis? Reply. Hum Pathol 2017;62:243–5.
[5] Michal M, Hes O, Kazakov DV. Primary signet-ring stromal tumor of the testis. Virchows Arch 2005;447:107–10.
[6] Kosmahl M, Seada LS, Janig U, Harms D, Kloppel G. Solid-pseudopapillary tumor of the pancreas: its origin revisited. Virchows Arch 2000;436:473–80.
[7] McCluney S, Wijesuriya N, Sheshappanavar V, Chin-Aleong J, Feakins R, Hutchins R, et al. Solid pseudopapillary tumour of the pancreas: clinicopathological analysis. ANZ J Surg 2018.
[8] Kazakov DV, Sima R, Vanecek T, Kutzner H, Palmedo G, Kacerovska D, et al. Mutations in exon 3 of the CTNNB1 gene (beta-catenin gene) in cutaneous adnexal tumors. Am J Dermatopathol 2009;31:248–55.
[9] Kuo CY, Wen MC, Wang J, Jan YJ. Signet-ring stromal tumor of the testis: a case report and literature review. Hum Pathol 2009;40:584–7.
[10] Estrella JS, Li L, Rashid A, Wang H, Katz MH, Fleming JB, et al. Solid pseudopapillary neoplasm of the pancreas: clinicopathologic and survival analyses of 64 cases from a single institution. Am J Surg Pathol 2014;38:147–57.
[11] Abe A, Ohishi Y, Miyazaki T, Ozono K, Mochidome N, Saeki K, et al. ‘Microcystic pattern’ should be recognised as part of the morphological spectrum of solid-pseudopapillary neoplasm of the pancreas. Histopathology 2018;72:216–26.
[12] Tanaka Y, Kato K, Notohara K, Hojo H, Ijiri R, Miyake T, et al. Frequent beta-catenin mutation and cytoplasmic/nuclear accumulation in pancreatic solid-pseudopapillary neoplasm. Cancer Res 2001;61:8401–4.
[13] Notohara K, Hamazaki S, Tsukayama C, Nakamoto S, Kawabata K, Mizobuchi K, et al. Solid-pseudopapillary tumor of the pancreas: immunohistochemical localization of neuroendocrine markers and CD10. Am J Surg Pathol 2000;24:1361–71.
[14] Serra S, Chetty R. Revision 2: an immunohistochemical approach and evaluation of solid pseudopapillary tumour of the pancreas. J Clin Pathol 2008;61:1153–9.
[15] Deshpande V, Oliva E, Young RH. Solid pseudopapillary neoplasm of the ovary: a report of 3 primary ovarian tumors resembling those of the pancreas. Am J Surg Pathol 2010;34:1514–20.
[16] Cheuk W, Beavon I, Chui DT, Chan JK. Extrapancreatic solid pseudopapillary neoplasm: report of a case of primary ovarian origin and review of the literature. Int J Gynecol Pathol 2011;30:539–43.
[17] He S, Yang X, Zhou P, Cheng Y, Sun Q. Solid pseudopapillary tumor: an invasive case report of primary ovarian origin and review of the literature. Int J Clin Exp Pathol 2015;8:8645–9.
[18] Stoll LM, Parvataneni R, Johnson MW, Gui D, Dorigo O, Sullivan P. Solid pseudopapillary neoplasm, pancreas type, presenting as a primary ovarian neoplasm. Hum Pathol 2012;43:1339–43.
[19] Syriac S, Kesterson J, Izevbaye I, de Mesy Bentley KL, Lele S, Mhawech-Fauceglia P. Clinically aggressive primary solid pseudopapillary tumor of the ovary in a 45-year-old woman. Ann Diagn Pathol 2012;16:498–503.
[20] Kominami A, Fujino M, Murakami H, Ito M. Beta-catenin mutation in ovarian solid pseudopapillary neoplasm. Pathol Int 2014;64:460–4.
[21] Singh K, Patel N, Patil P, Paquette C, Mathews CA, Lawrence WD. Primary ovarian solid pseudopapillary neoplasm with CTNNB1 c.98C > G (p.S33C) point mutation. Int J Gynecol Pathol Mar 2018;37(2):110–6.
[22] Kopczynski J, Kowalik A, Chlopek M, Wang ZF, Gozdz S, Lasota J, et al. Oncogenic activation of the Wnt/beta-catenin signaling pathway in signet ring stromal cell tumor of the ovary. Appl Immunohistochem Mol Morphol 2016;24:e28–33.
[23] Mengoli MC, Valli R, Zannoni GF. The family of beta-catenin ovarian tumors. Appl Immunohistochem Mol Morphol 2017;25:e95–9.
[24] Irving JA, Lee CH, Yip S, Oliva E, McCluggage WG, Young RH. Microcystic stromal tumor: a distinctive ovarian sex cord-stromal neoplasm characterized by FOXL2, SF-1, WT-1, cyclin D1, and beta-catenin nuclear expression and CTNNB1 mutations. Am J Surg Pathol 2015;39:1420–6.
[25] Maeda D, Shibahara J, Sakuma T, Isobe M, Teshima S, Mori M, et al. Beta-catenin (CTNNB1) S33C mutation in ovarian microcystic stromal tumors. Am J Surg Pathol 2011;35:1429–40.
[26] Irving JA, Young RH. Microcystic stromal tumor of the ovary: report of 16 cases of a hitherto uncharacterized distinctive ovarian neoplasm. Am J Surg Pathol 2009;33:367–75.
[27] Zhu P, Duan Y, Ao Q, Wang G. Microcystic stromal tumor of testicle: first case report and literature review. Cancer Res Treat 2017.

2.3.5. DIFFERENTIATED SQUAMOUS INTRAEPITHELIAL LESION (DSIL)-LIKE CHANGES IN THE EPIDERMIS OVERLYING ANOGENITAL MELANOCYTIC NEVI: A DIAGNOSTIC PITFALL

Differentiated squamous intraepithelial lesion (dSIL) is a premalignant lesion occurring in the skin of the anogenital area that is frequently misinterpreted histopathologically as a benign dermatosis. In this paper, we described a peculiar change in the basal cell layer of the epidermis/epithelium overlying anogenital melanocytic nevi that may histopathologically imitate dSIL. The aim of this study was to familiarize the pathologists with this pitfall to avoid its possible overdiagnosis as dysplasia. Further, we tried to explore the biological characteristics of the dSIL-like changes and to focus on the differential diagnostic aspects.

Annals of Diagnostic Pathology 26 (2016) 43–46

Contents lists available at ScienceDirect

Annals of Diagnostic Pathology

Differentiated squamous intraepithelial lesion (dSIL)-like changes in the epidermis overlying anogenital melanocytic nevi: A diagnostic pitfall

Kvetoslava Michalova, M.D. [a,*], Dmitry V. Kazakov, M.D. [a], Michael Michal, M.D. [a,b], Ladislav Hadravsky, M.D. [c], Denisa Kacerovska, M.D. [a], Boris Rychly, M.D. [d], Marketa Miesbauerova, M.D. [a], Michal Michal, M.D. [a]

[a] Department of Pathology, Charles University, Medical Faculty and Charles University Hospital Plzen, Czech Republic
[b] Biomedical Center, Faculty of Medicine in Plzen and Charles University Hospital Plzen, Czech Republic
[c] Department of Pathology, Charles University, 3rd Medical Faculty and Charles University Hospital Royal Vineyards, Prague, Czech Republic
[d] Cytopathos, Bratislava, Slovakia

ARTICLE INFO

Available online xxxx

ABSTRACT

Background: Differentiated squamous intraepithelial lesion (dSIL) is morphologically and immunohistochemically analogous in the whole anogenital region. dSIL is a premalignant lesion frequently misinterpreted histopathologically as a benign dermatosis. The authors describe a peculiar change in the basal cell layer of the epidermis/epithelium overlying anogenital melanocytic nevi that may histopathologically imitate dSIL. The aim of this study is to familiarize the pathologists with this pitfall to avoid its possible overdiagnosis as dysplasia. Further, we tried to explore the biological characteristics of the dSIL-like changes and to focus on the differential diagnostic aspects.

Design: Seventy cases of anogenital nevi were retrieved from our registry. All cases were stained with hematoxylin and eosin (H&E) and reviewed. Cases in which the epidermis overlying nevi featured atypical appearing basal keratinocytes in otherwise fully differentiated epithelium, variable degrees of acanthosis and parakeratosis were selected for additional investigation.

Results: Thirty cases meeting the above described criteria were identified. The patients were 8 males and 22 females, with age at the time of diagnosis ranging from 4 to 68 years. Follow-up data were available for 28 patients (range 0.5–19 years, mean 5.1), and to date, no signs of epithelial malignancy have been recorded. Immunohistochemically (IHC), the epidermis overlying nevi showed insignificant positivity for p53 in all tested cases. Melanocytic markers (S-100 protein, SOX10, Melan A) and cytokeratin AE1/3 labeled melanocytes and keratinocytes, respectively, enabling their distinction, especially in nevi featuring a junctional component.

Conclusions: Differentiated squamous intraepithelial lesion-like changes seem to occur relatively often in the epidermis overlying anogenital melanocytic nevi. Since morphologically they are virtually identical to the "true" dSIL, their distinction largely depends on p53 expression in basal keratinocytes with normal p53 expression in dSIL-like changes and diffuse nuclear/p53-null immunostaining in the "true" dSIL serving as an essential differential diagnostic tool. dSIL-like alterations seem to have no malignant potential, as to date, none of the patients included in this study have shown any signs of epithelial malignancy.

1. Introduction

Differentiated squamous intraepithelial lesion (dSIL) was originally described in the vulva and subsequently in the whole anogenital region, i.e. penis, anus, and perianal region [1,2,7,10,13]. dSIL, usually associated with lichen sclerosus et atrophicus, represents one of two main distinct pathways of anogenital squamous cell carcinoma development (SCC) [4]. Due to its inconspicuous histological appearance, this lesion is frequently misinterpreted and underdiagnosed as a benign dermatosis, mostly lichen simplex or lichen planus or simply overlooked. This problem has been acknowledged in recent studies focusing on early recognition of differentiated vulvar intraepithelial neoplasia (dVIN) [11-13].

In our routine practice, we have recently received a vulvar specimen with an intradermal melanocytic nevus, above which the epidermis manifested changes morphologically similar if not identical to dVIN, while the adjacent epidermis was normal. The immunohistochemical (IHC) analysis showed a normal p53 expression in the whole epidermis, including the atypical part above the nevus. Therefore, we considered the epithelial changes as nondysplastic, only mimicking dVIN. This finding prompted us to find out whether this was a unique case or similar epidermal aberrations above nevi were previously overlooked by us.

* Corresponding author at: Department of Pathology, Charles University, Medical Faculty and Charles University Hospital Plzen, Alej Svobody 80, 304 60 Pilsen, Czech Republic.
E-mail address: peckova.kveta@gmail.com (K. Michalova).

http://dx.doi.org/10.1016/j.anndiagpath.2016.11.002
1092-9134/

In this study, we describe a peculiar alteration in the epidermis above melanocytic nevi in the anogenital area that occasions a close resemblance to dSIL and thus potentially represents a diagnostic pitfall to the unaware.

2. Materials and methods

Cases cross-matching the keywords "vulva" "penis" "anus" and "nevus" were retrieved from the Pilsner consultation tumor registry and the routine biopsy archive. The 70 cases of melanocytic nevi occurring in anogenital area came from the period between 1993–2016. For conventional microscopy, tissues were fixed in formalin, routinely processed, embedded in paraffin, cut into 4 μm-thick sections, and stained with hematoxylin-eosin (H&E). All cases were reviewed and 30 cases in which the epidermis overlying the nevi featured atypical basal keratinocytes in otherwise fully differentiated epithelium, variable degrees of acanthosis, and parakeratosis were selected for further investigation. The clinical information was extracted from the registry records, and follow-up data were obtained from the attending clinicians. To determine if dSIL-like changes in the epidermis overlying melanocytic nevi can occur at body sites other than anogenital region, 25 specimens with nevi located elsewhere were randomly retrieved and reviewed.

2.1. Immunohistochemistry

Out of the 30 included cases, 27 cases were investigated immunohistochemically with the whole panel of antibodies (vide infra), whereas in 2 cases, the complete IHC analysis could not be performed due to limited available material and no tissues were available for IHC studies for the remaining case. The immunohistochemical analysis was performed using a Ventana BenchMark ULTRA (Ventana Medical System, Inc., Tucson, Arizona). The following primary antibodies were used: p53 (monoclonal, DO-7, RTU, Ventana Medical Systems, Tucson, Arizona), p16 (Monoconal, E6H4, RTU, Ventana Medical Systems), Melan A (monoclonal, A 103, 1:100, Dako, Glostrup, Denmark), SOX 10 (polyclonal, 1:100, Cell Marque, Rocklin, CA), S-100 protein (polyclonal, RTU, Ventana Medical Systems), AE1/3 (monoclonal, AE1/AE3 & PCK26, RTU, Ventana Medical Systems). The primary antibodies were visualized employing the enzymes alkaline phosphatase or peroxidase as detecting systems (both purchased from Ventana Medical Systems, Inc.). Appropriate positive controls were used. The immunoreactions were assessed separately for the nevi and for the epidermal layers.

3. Results

The main clinicopathological data are summarized in Table 1. There were 8 males and 22 females, with the age ranging from 4 to 68 years (mean 32 yrs, median 29 yrs). Locations included vulva (19 cases), penis (4 cases), anus (3 cases), perianal region (3 cases) and scrotum (1 case). Follow-up was available for 28 patients, ranging from 0.5 to 19 yrs (mean 5.1 yrs, median 3,5 yrs). None of the patients showed any signs of epithelial malignancy or disease progression from a clinical perspective (no repeated biopsies were performed).

3.1. Gross and microscopic findings

All anogenital nevi included in this study were removed by a simple excision and all were generally small in size, up to 1.2 cm in the largest dimension.

In all 30 lesions, the epidermis above the nevi showed changes resembling dSIL, namely atypical basal keratinocytes (Figs. 1–4). In addition, the epidermis occasionally manifested parakeratosis, prominent intercellular bridges (mild spongiosis) and irregular acanthosis, with branching and elongated rete ridges. In one case (Case 3), apart from dSIL-like changes above the melanocytic lesion, authentic dSIL was detected in the skin adjacent to the nevus in conjunction with lichen sclerosus et atrophicus and in another case (Case 19), a condyloma accuminatum was found near the nevus and dSIL-like change.

Table 1
Clinicopathological data.

Case no	Age/sex	Localisation	Type of melanocytic nevus	Follow-up
1	26/F	Vulva	Compound, special site	AW 2 yrs
2	50/F	Vulva	Intradermal, special site	AW 2 yrs
3	16/F	Vulva	Compound, special site	AW 3 yrs
4	38/F	Vulva	Compound, atypical special site	NA
5	35/F	Vulva	Intradermal	AW 8 yrs
6	19/F	Vulva	Intradermal, congenital	NA
7	24/F	Vulva	Compound, congenital	AW 6 yrs
8	48/F	Vulva	Intradermal	AW 6 yrs
9	4/F	Vulva	Atypical special site	AW 4 yrs
10	29/F	Vulva	Intradermal	AW 14 yrs
11	39/F	Vulva	Microalveolar intradermal	AW 15 yrs
12	60/F	Vulva	Intradermal	AW 12 yrs
13	29/F	Vulva	Intradermal, special site	AW 3 yrs
14	63/F	Vulva	Intradermal, special site	AW 5 yrs
15	8/F	Vulva	Compound, special site	AW 2 yrs
16	26/F	Vulva	Compound, special site	AW 2 yrs
17	23/F	Vulva	Compound, special site	AW 4 yrs
18	68/F	Vulva	Junctional	AW 4 yrs
19	58/F	Vulva	Intradermal	AW 5 yrs
20	17/M	Scrotum	Atypical intradermal	AW 17 yrs
21	15/M	Penis	Compound, special site	AW 0,5 yr
22	18/M	Penis	Compound	AW 0,5 yr
23	44/M	Penis	Intradermal	AW 1 yr
24	36/M	Penis	Compound	AW 4 yrs
25	27/F	Perianal	Intradermal	AW 1 yr
26	38/M	Perianal	Intradermal	AW 0,5 yr
27	34/F	Perianal	Intradermal	AW 0,5 yr
28	31/M	Anus	Intradermal	AW 19 yrs
29	13/F	Anus	Intradermal	AW 1 yr
30	24/M	Anus	Intradermal	AW 1 yr

AW alive and well; NA not available.

The nevi were classified as follows: intradermal (18), compound (10), and junctional (1). The remaining case of a compound nevus exhibited significant architectural atypia (special site nevus).

3.2. Immunohistochemistry

All tested nevi were immunoreactive for S-100 protein, SOX10, Melan A and p16, although the positivity was occasionally focal and were immunonegative for AE1/3. The epidermis above the nevi stained negatively for p16 and the melanocytic markers. The staining for p53 protein showed "normal" expression (occasional dot-like positivity) in the basal cell layer overlying a nevus in all 29 cases. In the case where authentic dSIL was present adjacent to the nevus and dSIL-like area, p53 labeled the dysplastic areas diffusely.

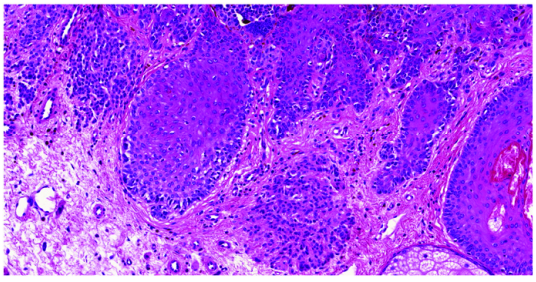

Fig. 1. The epidermis above the nevi showed changes resembling dSIL, namely atypical basal keratinocytes.

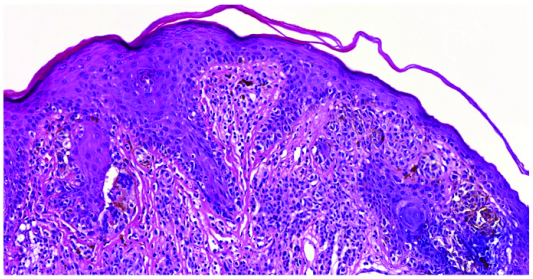

Fig. 2. The epidermis showed features resembling aberrant maturation with basal atypia, consisting of cells with enlarged, angulated, hyperchromatic nuclei.

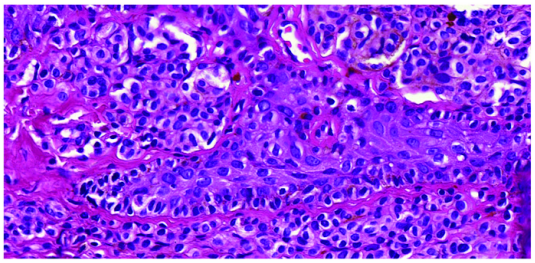

Fig. 4. At higher magnification, the basal cells which featured significant atypical morphology can be appreciated.

4. Discussion

According to the WHO 2014, there are two different pathways participating in the development of squamous intraepithelial neoplasia [5]. Their distinction is based on the epidemiological, clinical, pathological and molecular differences, which allow to view them as two different entities [4,5]. dSIL represents the human papilloma virus (HPV)-independent and unique pathway originally described in vulva [1]. Subsequent research revealed that this process is morphologically and immunohistochemically analogous to lesions on the penis, in the anal and perianal region [2,7,10,13,14]. In anogenital area, dSIL is most frequently associated with lichen sclerosus et atrophicus [4]. Since it has been demonstrated that dSIL accompanies the majority of HPV-negative SCCs, its role as a straight precursor has been accepted [12]. One of the main histological characteristics of dSIL is the presence of atypical keratinocytes in the basal layer of otherwise fully differentiated squamous epithelium [14]. The differentiated histological appearance implies that dSIL can be easily overlooked or misinterpreted as a benign dermatosis.

Immunostaining for the p53 protein is generally considered as an effective tool for the diagnosis of dSIL. It is important to note that patchy and irregular immunohistochemical positivity in approximately 10% of basal keratinocytes or less is considered as a normal result [11]. p53 is normally present in cells, but at extremely low levels because the protein is very rapidly degraded following synthesis [6]. Mutations of the *TP53* gene are the hallmark of the dSIL and the HPV-independent SCC [11]. Two different variants of the *TP53* gene mutation and likewise two different immunostaining patterns of the basal keratinocytes are recognized. The first and more common variant is a missense mutation that leads to the translation of a mutant protein, which, due to the mutation, becomes more stable and resists degradation. As a result, the protein persists in the nucleus of most of the keratinocytes. This is consequently reflected in a diffuse and linear (in uninterrupted row) immunostaining of the basal keratinocyte's nuclei which is seen in most cases of dSIL.

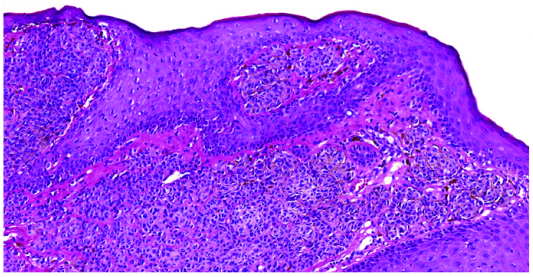

Fig. 3. In addition, the epidermis occasionally manifested irregular acanthosis, with branching and elongated rete ridges.

The second and less common pathway is characterized by a nonsense mutation or deletion of the *TP53* gene which leads to a damage or loss of its function. As a result, no p53 protein expression can be detected immunohistochemically, the so-called p53-null pattern [11]. The appropriate positive control is mandatory for the evaluation of the p53-null pattern. In very rare cases of so-called HPV-negative VIN/PeIN with basaloid features, a third pattern, namely diffuse p53 staining in all epidermal dysplastic layers is encountered [9].

Our study of 70 cases of anogenital nevi revealed that dSIL-like changes were detected in nearly half (43%) of them. There was no correlation between the occurrence of this alteration and type of the nevus, however, the dSIL-like areas were better appreciated intradermal nevi. In junctional and compound nevi, atypical keratinocytes were intermingled with melanocytes at the dermoepidermal junction, complicating interpretation and their separation. The differentiation between these two cell types in H&E staining was challenging and therefore, we used several melanocytic markers and a cytokeratin antibody to highlight the exact boundaries between the melanocytic and keratinocytic population.

In our control group of melanocytic nevi located at other anatomic areas, no dSIL-like abnormalities were noted suggesting that dSIL-like changes overlying the nevi might be characteristic of the anogenital region. In addition to the melanocytic nevus and dSIL-like changes in the overlying epidermis, one lesion (Case 3) manifested authentic dSIL in the adjacent epidermis associated with lichen sclerosus et atrophicus. In contrast to dSIL-like areas with occasional p53 immunoreactivity, a diffuse, linear staining for p53 was noted in the dysplastic area. In another case of vulvar nevus (Case 19), the melanocytic nevus with the dSIL-like reaction was associated with condyloma accuminatum. These two cases illustrate that the presence of an anogenital melanocytic nevus with dSIL-like reaction does not exclude the possibility of synchronous occurrence of another lesion, including those characteristic for this area.

A variety of reactive epidermal changes accompanying melanocytic nevi have been described in the literature [8]. As far as we are aware, dSIL-like changes in the epidermis overlying anogenital melanocytic lesions have not been previously reported but similar histopathological appearances can be recognized in illustrations of some published articles. For example, Figs. 2 and 3 in the work of Carlson et al. on melanocytic lesions associated with lichen sclerosus et atrophicus illustrate areas with changes suspicious for dSIL [3]. The authors discussed a shared keratinocytic and melanocytic response to stromal fibrosis or sclerosis denoted by increased proliferation and inverse expression of envelope proteins (e.g., involucrin) by keratinocytes and HMB-45 expression and increased proliferation of melanocytes, while emphasizing the similarities of melanocytic nevi associated with lichen sclerosus et atrophicus to persistent melanocytic nevi. Indeed, we have seen occasionally atypical basal keratinocytes in so-called recurrent/persistent

nevi, including those outside the anogenital area (our unpublished observation).

In conclusion, we present a simulator of dVIN/PeIN/AIN/PaIN seen in anogenital melanocytic nevi and appearing histopathologically as atypical basal keratinocytes. In contrast to authentic dSIL, the atypical parts do not show abnormal p53 staining. dSIL-like alterations accompanying anogenital melanocytic nevi seem to have no malignant potential. Although no repeated biopsies were performed in our patients, from the clinical standpoint, none of the patients included in this study have developed SCC to date and all have unremarkable clinical course, which are arguments for the reactive nature of the epidermal change we report on. It is important to be aware of this feature to avoid a possible overdiagnosis of dysplasia and to prevent unnecessary overtreatment of the patients.

Conflict of interest

The authors have no conflicts of interest to disclose.

References

[1] Abell MR. Intraepithelial carcinomas of epidermis and squamous mucosa of vulva and perineum. Surg Clin North Am 1965;45:1179–98.
[2] Arsenic R, Kurrer MO. Differentiated dysplasia is a frequent precursor or associated lesion in invasive squamous cell carcinoma of the oral cavity and pharynx. Virchows Arch 2013;462:609–17.
[3] Carlson JA, Mu XC, Slominski A, et al. Melanocytic proliferations associated with lichen sclerosus. Arch Dermatol 2002;138:77–87.
[4] Del Pino M, Rodriguez-Carunchio L, Ordi J. Pathways of vulvar intraepithelial neoplasia and squamous cell carcinoma. Histopathology 2013;62:161–75.
[5] Kurman RJ, Carcangiu ML, Herrington CS, Young RH. WHO Classification of Tumours of Female Reproductive Organs4th ed. ; 2014.
[6] Liu Y, Kulesz-Martin M. P53 regulation and function in normal cells and tumors. Medicina 2000;60(Suppl. 2):9–11.
[7] Michal M, OH, Kacerovská D, Hora M, Rotter L, Švajdler M, et al. Classification of the penile intraepithelial neoplasias preceding invasive squamous cell carcinomas and their analogy with precancerous lesions of vulvar squamous cell carcinoma. Czech Urol 2014;18.
[8] Mooi WJ. In: Mooi WJ, Krausz T, editors. Pathology of Melanocytic Disorders. London: Hodder Arnold; 2007.
[9] Ordi J, Alejo M, Fuste V, et al. HPV-negative vulvar intraepithelial neoplasia (VIN) with basaloid histologic pattern: an unrecognized variant of simplex (differentiated) VIN. Am J Surg Pathol 2009;33:1659–65.
[10] Paliga A, Mai KT. Squamous cell carcinomas of the anterior oral cavity are commonly associated with simplex (or differentiated) oral intraepithelial neoplasia: clinical and pathologic significance. Int J Surg Pathol 2014;22:231–40.
[11] Singh N, Leen SL, Han G, et al. Expanding the morphologic spectrum of differentiated VIN (dVIN) through detailed mapping of cases with p53 loss. Am J Surg Pathol 2015;39:52–60.
[12] van de Nieuwenhof HP, Bulten J, Hollema H, et al. Differentiated vulvar intraepithelial neoplasia is often found in lesions, previously diagnosed as lichen sclerosus, which have progressed to vulvar squamous cell carcinoma. Mod Pathol 2011;24:297–305.
[13] Wasserman JK, Bateman J, Mai KT. Differentiated squamous intraepithelial neoplasia associated with squamous cell carcinoma of the anal canal. Histopathology 2016;68:834–42.
[14] Yang B, Hart WR. Vulvar intraepithelial neoplasia of the simplex (differentiated) type: a clinicopathologic study including analysis of HPV and p53 expression. Am J Surg Pathol 2000;24:429–41.

2.3.6. PENILE WARTY MUCOEPIDERMOID CARCINOMA WITH FEATURES OF STRATIFIED MUCIN-PRODUCING INTRAEPITHELIAL LESION AND INVASIVE STRATIFIED MUCIN-PRODUCING CARCINOMA

As discussed in the section on first authored manuscripts, we described a penile lesion that was histologically identical to the Stratified mucin-producing intra-epithelial lesion (SMILE) of the uterine cervix. Invasive stratified mucin-producing carcinoma (ISMC) is another recently described cervical lesion [71], whereas SMILE of the cervix is its precursor. In this case report, we reported an unusual case of mixed variant of penile squamous cell carcinomas with warty, usual and mucoepidermoid SMILE/ISMC features.

Histopathology

Histopathology 2018, **72**, 867–873. DOI: 10.1111/his.13438

SHORT REPORT

Penile warty mucoepidermoid carcinoma with features of stratified mucin-producing intra-epithelial lesion and invasive stratified mucin-producing carcinoma

Kenji Yorita,[1] Naoto Kuroda,[1] Takushi Naroda,[2] Masato Tamura,[2] Chisato Ohe,[3] Mukul Divatia,[3] Mahul B Amin,[4] Antonio L Cubilla,[5] Dimitry V Kazakov,[6] Ondrej Hes,[6] Michael Michal[6] & Michal Michal[6]

[1]*Department of Diagnostic Pathology, Japanese Red Cross Kochi Hospital,* [2]*Department of Urology, Japanese Red Cross Kochi Hospital, Kochi-city, Kochi, Japan,* [3]*Department of Pathology and Laboratory Medicine, Cedars-Sinai Medical Center, Los Angeles, CA,* [4]*Department of Pathology and Laboratory Medicine, University of Tennessee Health Sciences Center, Memphis, TN, USA,* [5]*Instituto de Patologia e Investigacion, Universidad Nacional de Asuncion, Asuncion, Paraguay, and* [6]*Department of Pathology, Charles University, Medical Faculty and Charles University Hospital Plzen, Pilsen, Czech Republic*

Date of submission 25 July 2017
Accepted for publication 10 November 2017
Published online *Article Accepted* 16 November 2017

Yorita K, Kuroda N, Naroda T, Tamura M, Ohe C, Divatia M, Amin M B, Cubilla A L, Kazakov D V, Hes O, Michal M & Michal M

(2018) *Histopathology* **72**, 867–873. https://doi.org/10.1111/his.13438

Penile warty mucoepidermoid carcinoma with features of stratified mucin-producing intra-epithelial lesion and invasive stratified mucin-producing carcinoma

Aims: Stratified mucin-producing intra-epithelial lesion (SMILE) and invasive stratified mucin-producing carcinoma (ISMC) are recently described cervical and penile lesions. We report an unusual case of mixed variant of penile squamous cell carcinomas with warty, usual and mucoepidermoid SMILE/ISMC features.

Methods and results: A 62-year-old Japanese man had a glans penis lesion of one-and-a-half years' duration, suggesting malignancy. Partial penectomy and left inguinal lymphadenectomy were performed. Pathological evaluation revealed a mixed squamous cell carcinoma with warty, mucinous and usual features. The mucinous component resembled mucoepidermoid carcinoma (MEC) and SMILE/ISMC. Glandular differentiation was absent. All the diverse tumour components were negative for p16, which was confirmed by negative human papillomavirus (HPV) genotyping. The mucinous component was diffusely positive for cytokeratin 7 and largely negative for cytokeratin 5 and p63. Fluorescence *in-situ* hybridisation did not detect rearrangement in the *MAML2* or *EWSR1* genes. The tumour was pathological stage pT2, pN1 (AJCC prognostic stage group IIIA) and was disease-free 26 months after surgery.

Conclusions: The lack of glands in the mucinous areas suggested that MEC should be separated from adenosquamous carcinoma (ASC). Penile SMILE/ISMC may occur without dependence upon HPV status. Further studies will be necessary to determine the pathogenesis and definition of penile SMILE/ISMC, the presence of true MEC arising from the glans penis and the clinicopathological differences of penile ASC, MEC and SMILE/ISMC. Herein, we refer to the SMILE-like penile lesion as 'mucinous penile intra-epithelial neoplasia'.

Address for correspondence: K Yorita MD, PhD, Department of Diagnostic Pathology, Japanese Red Cross Kochi Hospital, 2-13-51, Shinhon-machi, Kochi-city, Kochi 780-8562, Japan. e-mail: kenjiyorita@gmail.com

Keywords: adenosquamous carcinoma, invasive stratified mucin-producing carcinoma, mucoepidermoid carcinoma, penile cancer, penile intraepithelial neoplasia, stratified mucin-producing intra-epithelial lesion, warty carcinoma

Introduction

Most penile cancers are squamous cell carcinoma (SCC), but mucin-producing penile cancers, such as adenosquamous carcinoma (ASC)[1–4] or mucoepidermoid carcinoma (MEC),[5–7] are rarely reported. Penile ASCs are gland-forming mucinous tumours, with only 11 cases having been documented.[4] Penile MEC, which are solid tumours without overt gland formation, are even less common.[5–7] In the 2016 World Health Organisation (WHO) classification of penile cancers,[4] primary penile mucinous tumours with or without glands were considered adenosquamous, and the mucoepidermoid terminology was a synonym. Previously reported penile ASCs have shown glandular differentiation.[1–3] ASC of other organs, such as those in the hypopharynx,[8] larynx,[8] trachea,[8] gallbladder,[9] extrahepatic bile ducts,[9] pancreas,[10] uterine cervix,[11] vagina,[12] vulva[13] and prostate,[14] manifest with glandular differentiation. In addition, ASC and MEC are categorised as different entities in other organs, such as the lungs,[15,16] thymus,[17,18] hypopharynx,[8] larynx[8] and trachea.[8] Therefore, considering the different histology of both ASC and MEC, these penile tumours may be classified as separate clinicopathological entities in the future.

MEC occurs mainly in the salivary glands and is characterised by a cystic and solid growth of mucinous, intermediate and squamous tumour cells.[19] Most MECs are characterised genetically by a t(11;19)(q21;p13) translocation and *CRTC1–MAML2* gene fusion, MEC with t(11;15)(q21;q26) translocation and *CRTC3–MAML2* gene fusion, or t(6;22)(p21;q12) translocation and *EWSR1–POU5F1* gene fusion.[19] However, previously reported penile MECs[5–7] have not shown the presence of chromosomal translocations.

Recently, Michal *et al.*[20] proposed a new type of mucin-producing penile tumour, the penile analogue of stratified mucin-producing intra-epithelial lesions (SMILEs) of the uterine cervix. SMILE and invasive stratified mucin-producing carcinoma (ISMC), with morphological features identical to SMILE, have been reported as uterine cervix mucin-producing tumours.[21–24] SMILE is postulated to be induced by high-risk human papillomavirus (HPV) and is characterised histologically by a stratified epithelium with atypical cells containing varying quantities of intracytoplasmic mucin throughout the majority of the epithelium. In addition, SMILE is associated with various types of non-invasive and invasive cervical tumours, such as high-grade stratified intra-epithelial lesions, *in-situ* and invasive adenocarcinoma, ASC and SCC.[21–24]

We report herein an undescribed mixed penile carcinoma consisting of an intra-epithelial and invasive mucin-producing tumour, which was similar histologically to previously published cases of penile MEC/SMILE[5–7,20] and SMILE/ISMC of the uterine cervix.[21–24] To confirm the tumour subtype in our case, we evaluated the chromosomal translocations of *MAML2* and *EWSR1* genes with fluorescence *in-situ* hybridisation (FISH), p16 immunoreactivity and HPV genotyping.

Materials and methods

CLINICAL AND RADIOLOGICAL FINDINGS

A 62-year-old uncircumcised Japanese man, with a history of hypertension and hyperuricaemia, was referred to our hospital for a penile lesion. The patient noticed a small nodule on the glans penis one-and-a-half years prior to admission. No history of malignant tumour was found. The glans penis showed a reddened irregular surface focally with white keratinous portions. Serum levels of SCC antigen were normal.[18]F-2-fluoro-2-deoxyglucose-positron emission tomography revealed significant uptake in both the penile lesion and a 13-mm left inguinal lymph node. The clinical diagnosis of carcinoma of the glans penis was considered and a partial penectomy with left inguinal lymphadenectomy were performed. The patient is disease-free 26 months after surgery.

PATHOLOGICAL SPECIMENS AND IMMUNOHISTOCHEMISTRY

Whole-mount preparation of the resected penile tissue was performed, and sections were stained with haematoxylin and eosin, as well as periodic acid-Schiff (PAS) and Alcian blue (AB) stains. Immunohistochemistry was performed on a BenchMark Ultra

autostainer (Ventana Medical Systems, Inc., Tucson, AZ, USA), using commercially available antibodies (Table S1).

FISH AND HPV GENOTYPING

Tissue FISH analysis for *MAML2* gene and *EWSR1* gene rearrangements was performed. A 4-μm-thick formalin-fixed paraffin-embedded section of the tumour was placed on a glass slide, pretreated with a VP-2000 Processor (Abbott Molecular, Tokyo, Japan) and incubated with a *MAML2* dual-colour break-apart probe (ZytoVision, Bremerhaven, Germany) or an LSI *EWSR1* dual-colour break-apart probe (Abbott Molecular, Des Plaines, IL, USA). Fluorescence data were observed using the Axio Imager 2 Upright Microscope (Zeiss, Tokyo, Japan) and were analysed using the Isis FISH imaging system version 5.5 (MetaSystems, Altlussheim, Germany). At least 100 nuclei were scored automatically. Positive rearrangement of the *EWSR1* and *MAML2* genes was defined by the presence of more than 20%[25] and 10%[26] of tumour cells with split signals, respectively.

HPV genotyping was performed using the following primer systems: CPSGB, $GP5^+/GP6^+$ and type-specific primers for HPV 16, 18, 31, 33, 35 and 45, as described elsewhere.[27]

Results

PATHOLOGICAL AND IMMUNOHISTOCHEMICAL FINDINGS

The tumour partially involved the glans, coronal sulcus and the inner foreskin layer (Figure 1A–C). Microscopically the appearance was variegated: mucin-producing carcinoma (Figure 1D–F), warty carcinoma (Figure 1G) and usual SCC. Each component was associated with intra-epithelial mucin-producing tumour (Figure 2A–F), warty penile intra-epithelial neoplasia (PeIN) and differentiated PeIN, respectively. The mucin-producing carcinoma and the associated intra-epithelial lesion occupied 40% of the tumour and consisted of solid nests or sheets of cells with eccentric nuclei, distinct nucleoli and voluminous cytoplasm (Figures 1D–E and 2A, B). The cells occasionally had abundant PAS- and Alcian blue-positive cytoplasm (Figures 1F and 2C, D). In addition, the mucinous cells were present throughout the tumour epithelium, but without true glandular structures. The mucin-producing carcinoma was similar histologically to MEC and ISMC and the intra-epithelial lesion was similar to uterine cervix SMILE. The SMILE-like lesion (Figure 1A–C) was found largely in the glans mucosa involving the coronal sulcus, and connected to warty PeIN, warty carcinoma and differentiated PeIN. The warty carcinoma occupied 50% of the tumour, invaded the corpus spongiosum and was partly intermixed with the mucin-producing carcinoma (Figure 1H, I). The typical SCC was detected in the inner foreskin layer, with this component connected only to the differentiated PeIN. Dysplastic epithelium was absent in the urethral epithelium. Metastatic carcinoma consisting of a mixture of warty and mucin-producing carcinoma was found in one of the left inguinal lymph nodes. The tumour was pathological stage pT2, pN1 (AJCC prognostic stage group IIIA).[28]

Immunohistochemically, the mucin-producing carcinoma and the SMILE-like lesion were diffusely positive for cytokeratin 7 (CK7, Figures 1H and 2E), mucin core protein 1 (MUC1), MUC5AC and MUC6; partly positive for carcinoembryonic antigen (CEA), CK5 (Figure 1I), CK14, p40 and p63 (Figure 2F) and negative for p16, gross cystic disease fluid protein 15 (GCDFP-15), S-100 protein, CDX2, MUC2 and HPV. Immunoreactivity of CK5, CK14, p40 and p63 was observed focally in the peripheral or basal cells of the mucin-producing carcinoma and SMILE-like lesion. However, warty carcinoma and SCC were diffusely positive for CK5 (Figure 1I), CK14, p40 and p63 and negative for CK7 (Figure 2H), p16, CEA, GCDFP-15, S-100 protein, CDX2, mucin core proteins and HPV. Tumour components were negative for anaplastic lymphoma kinase (ALK) and c-Ros oncogene 1 receptor tyrosine kinase (ROS-1).

FISH AND HPV GENOTYPING

Split signals of the *MAML2* and *EWSR1* genes were less than the cut-off value in all tumour components. HPV was not detected.

Discussion

We presented a unique variant of penile SCC with warty, mucoepidermoid and usual features. The pathogenesis of the mucin-producing tumour of our case is unknown. In the reported tumour, p16 was negative. The HPV genotyping was also negative, although the primers used can detect only the following HPV types: 1–9, 10a, 11–13, 14a, 16–22, 24, 25, 30–33, 35–40, 43, 45, 46, 51, 52, 54–56, 58, 59 and 66.[29,30] The morphology of the warty carcinoma, however, was typical. It is known that among the HPV-related variants of penile SCCs, warty

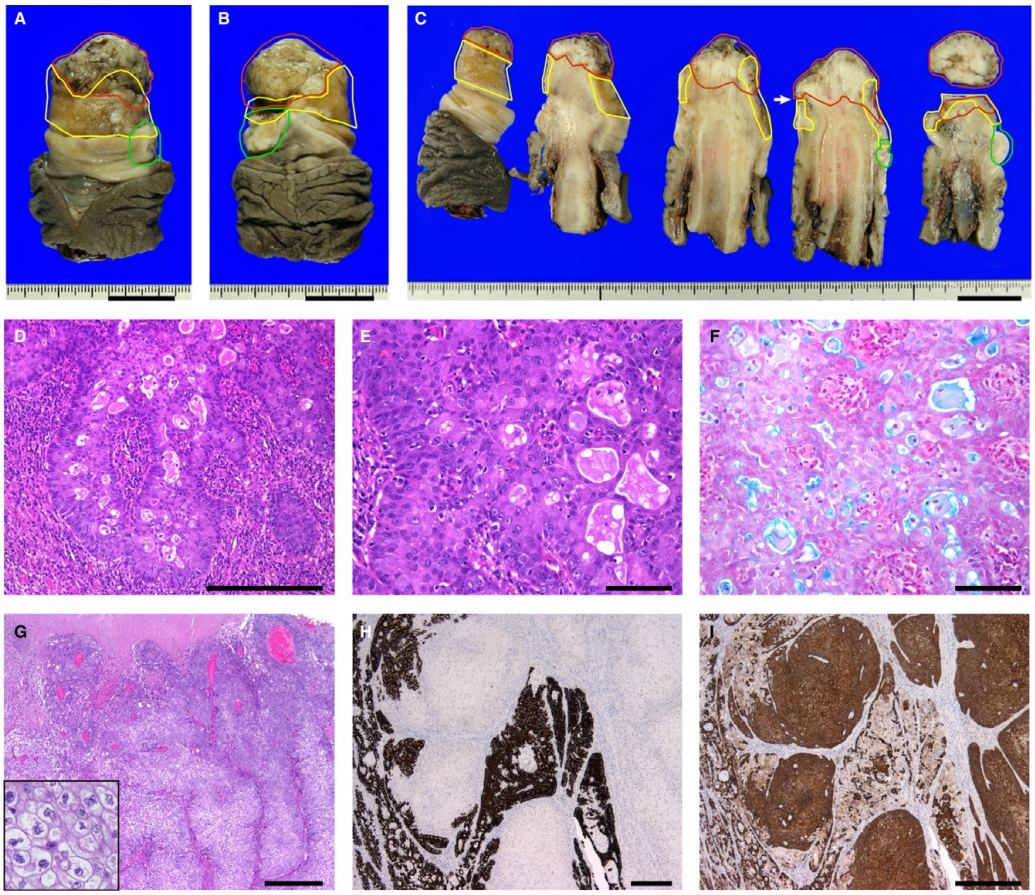

Figure 1. Gross and microscopic features of the penile tumour. **A–C**, Gross features of the tumour. Dorsal portion (**A**), ventral portion (**B**) and cut sections (**C**) of the penis reveal the tumour lesion; areas lined in red represent warty carcinoma and warty penile intra-epithelial neoplasia (PeIN); areas in yellow represent the invasive mucin-producing carcinoma and intra-epithelial mucin-producing tumour; and areas in green represent usual squamous cell carcinoma (SCC) and differentiated PeIN. The meatal opening is indicated by an arrow. **D–F**, Low (**D**) and high (**E**) magnification photographs and an Alcian blue-stained section (**F**) show that the invasive mucin-producing carcinoma component consists of sheets of voluminous and mucinous cells, with pseudoglandular structures containing myxoid substances. This component resembles mucoepidermoid carcinoma (MEC). **G**, The warty carcinoma component proliferates with fibrovascular cores. The inset shows the tumour cells with wrinkled nuclei, containing perinuclear cytoplasmic clearings. **H**, **I**, Immunohistochemistry of the mixed portion of MEC and warty carcinoma. Cytokeratin 7 (**H**) shows that the MEC is diffusely positive and the warty carcinoma portion is negative. Cytokeratin 5 (**I**) shows the opposite result. Peripheral immunoreactivity to cytokeratin 5 is seen in the MEC component. **D**, **E** and **G** represent haematoxylin and eosin-stained sections. Bars represent 2 cm in **A–C**, 200 μm in **D–F** and 500 μm in **G–I**.

carcinoma, and especially warty carcinoma mixed with other tumour subtypes, show the lowest HPV detection rate and the reasons are unknown, with some tumours possibly being related to unknown subtypes of HPV genotypes.[31,32]

A novel finding in this study was the mucin-producing pattern of PeIN involving the entire epithelial thickness. This feature of PeIN has not been reported previously in cases of penile ASCs[1–3] and MECs,[5–7] for which we suggest the name 'mucinous PeIN'. The 2016 World Health Organisation (WHO) publication classifies PeIN as: (i) non-HPV-related (differentiated); (ii) HPV-related (warty, basaloid and warty basaloid); and (iii) other. The last category of PeIN includes rare

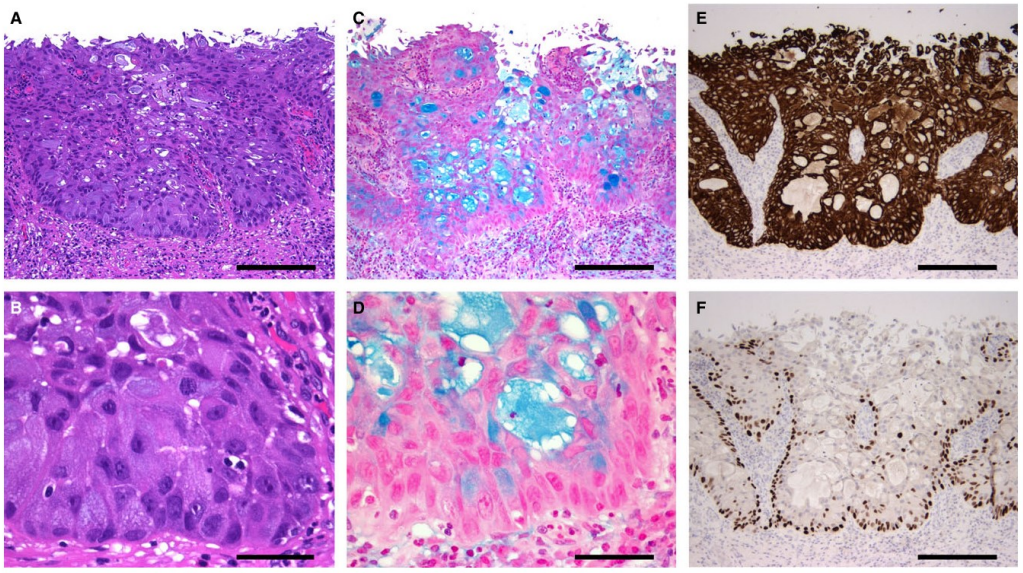

Figure 2. Microscopic features of mucinous penile intra-epithelial neoplasia. **A**, **B**, The haematoxylin and eosin-stained section shows an atypical stratified epithelium of the glans penis. Low (**A**) and high (**B**) lower portion of the epithelium magnification images show the epithelium consisting of sheets of atypical cells with eccentric nuclei, distinct nucleoli and voluminous cytoplasm. Loss of polarity is observed. **C**, **D**, An Alcian blue-stained section (**C**, low magnification; **D**, high magnification and lower portion of the epithelium) reveals that the mucinous cells and deposits are present throughout the atypical epithelium. **E**, **F**, Immunohistochemistry of the atypical epithelium. The epithelium is diffusely positive for cytokeratin 7 (**E**). Pseudoglandular spaces are noted. The basal portion of the atypical epithelium was stained for p63 expression (**E**). The atypical epithelium resembles histologically and immunohistochemically stratified mucin-producing intra-epithelial lesion of the uterine cervix. The bars in **A**, **C**, **E** and **F** represent 200 μm, and the bars in **B** and **D** represent 100 μm.

morphological presentations, such as pleomorphic, spindle, clear cell and pageoid.[33] Mucinous PeIN should be included in this rare category.

The differential diagnoses of the mucin-producing component include: mucinous metaplasia, extramammary Paget disease (EMPD), secretory carcinoma, ALK- or ROS1-related cancer, MEC and a penile analogue of uterine cervix SMILE/ISMC.

The mucosal epithelium of the glans penis and foreskin may show mucinous metaplasia.[34–38] Mucinous metaplasia is characterised histologically by the focal replacement of the stratified squamous epithelium, with non-atypical goblet cell-like mucinous cells in the superficial portion. In our case, mucinous cells showed cellular atypia and random location within the epithelium, which excluded mucinous metaplasia.

EMPD is included in the differential diagnosis of our case, and primary EMPD cells can be positive for CK7, CEA, MUC1 and MUC5AC,[39] which was true in our case. However, primary EMPD is more frequent in the penile shaft and scrotum, with glans involvement being rare. Moreover, sweat glands are not present in the glans penis,[40] thereby making primary EMPD improbable. Furthermore, the glans surface can be involved infrequently with pagetoid spread of mucin-producing tumour cells, such as bladder urothelial carcinoma[41] or prostatic carcinoma,[42] which were not observed. Therefore, primary or secondary EMPD is unlikely in our case.

Secretory carcinoma occurring in the mammary gland, salivary gland or skin[43] may be histologically similar to this case, but this tumour was diffusely negative for the S-100 protein. In lung adenocarcinomas, the presence of mucin-rich tumour cells intermixed in solid tumour nests may be related to *ALK* and *ROS1* gene rearrangements, which can show a diffuse immunoreactivity for ALK and ROS1. However, the present case was negative for both markers.

The mucin-producing component of this case was similar to the previous cases of penile MEC.[5–7] However, characteristic chromosomal translocations of MECs of the salivary gland were absent according to FISH. MEC of the salivary glands is postulated to originate from the submucosal glands,[8] but the penile

tissues relevant in our case do not typically have glandular tissue.[40] Therefore, these characteristics of MEC originating from other sites may not apply to penile cancers.

The mucinous components, *in-situ* and invasive, of our case were morphologically indistinguishable from the recently reported SMILE/ISMC of the uterine cervix[21,24] and penile SMILE.[20] Our case accompanied various *in-situ* and invasive penile tumours, as was seen in reported cases of SMILE.[20–24] However, SMILE/ISMC is typically HPV-related, with p16-negative SMILE/ISMC having been unreported.[20,22–24] Penile warty carcinomas may be HPV-negative for unknown reasons, despite their distinctive condylomatous appearance.[31,32]

In summary, we present a case of unusual penile cancer. The lack of glands in the mucinous areas suggested that MECs should be separated from ASCs. Penile SMILE/ISMC may occur without dependence upon HPV status. Further studies will be necessary to determine the pathogenesis and definition of penile SMILE/ISMC, the presence of true MEC arising from the glans penis and the clinicopathological differences of penile ASC, MEC and SMILE/ISMC.

Acknowledgements

We thank Ms Keiko Mizuno, Mr Masahiko Ohara, Ms Kaori Yasuoka, Ms Yukari Wada and Ms Yoshiko Agatsuma for preparing the specimens for histological and immunohistochemical analysis and FISH. We would like to thank Editage (www.editage.jp) for English language editing. The case study was supported partly by the Grant-in-Aid from the Life Fund of Kochi Shimbun and Kochi broadcast in 2015.

Conflicts of interest

The authors state that they have no conflicts of interest to declare.

References

1. Jamieson NV, Bullock KN, Barker TH. Adenosquamous carcinoma of the penis associated with balanitis xerotica obliterans. *Br. J. Urol.* 1986; **58**; 730–731.
2. Cubilla AL, Ayala MT, Barreto JE, Bellasai JG, Noel JC. Surface adenosquamous carcinoma of the penis. A report of three cases. *Am. J. Surg. Pathol.* 1996; **20**; 156–160.
3. Masera A, Ovcak Z, Volavsek M, Bracko M. Adenosquamous carcinoma of the penis. *J. Urol.* 1997; **157**; 2261.
4. Cubilla AL, Amin MB, Ayala A *et al.* Malignant epithelial tumours. In Moch H, Humphrey PA, Ulbright TM, Reuter VE eds. *World Health Organisation classification of tumours of the urinary system and male genital organs*. Lyon, France: IARC, 2016; 262–276.
5. Shrikhande SS, Sirsat MV. Muco-epidermoid carcinoma of the penis. Report of an unusual case. *Br. J. Urol.* 1974; **46**; 233–235.
6. Layfield LJ, Liu K. Mucoepidermoid carcinoma arising in the glans penis. *Arch. Pathol. Lab. Med.* 2000; **124**; 148–151.
7. Froehner M, Schobl R, Wirth MP. Mucoepidermoid penile carcinoma: clinical, histologic, and immunohistochemical characterization of an uncommon neoplasm. *Urology* 2000; **56**; 154.
8. Parasad ML, Cardesa A, Helliwell T, Hille J, Nadal A. Adenosquamous carcinoma. In El-Naggar AK, Chan JKC, Grandis JR, Takata T, Slootweg PJ eds. *World Health Organisation classification of head and neck tumours*. Lyon, France: IARC, 2017; 89.
9. Albrores-Saavedra J, Kloppel G, Adsay NV *et al.* Carcinoma of the gallbladder and extrahepatic bile ducts. In Bosman FT, Carneiro F, Hruban RH, Theise ND eds. *World Health Organisation classification of tumours of the digestive system*. Lyon, France: IARC, 2010; 266–273.
10. Fukushima N, Hruban RH, Kato Y *et al.* Ductal adenocarcinoma variants and mixed neoplasms of the pancreas. In Bosman FT, Carneiro F, Hruban RH, Theise ND eds. *World Health Organisation classification of tumours of the digestive system*. Lyon, France: IARC, 2010; 292–295.
11. Colgan TJ, Kim KR, Hirschowitz L, McCluggage WG. Other epithelial tumours. In Kurman RJ, Carcangiu ML, Herrington CS, Young RH eds. *World Health Organisation classification of tumours of female reproductive organs*. Lyon, France: IARC, 2014; 194–196.
12. Ferenczy AS, Park KJ, Colgan TJ *et al.* Epithelial tumours. In Kurman RJ, Carcangiu ML, Herrington CS, Young RH eds. *World Health Organisation classification of tumours of female reproductive organs*. Lyon, France: IARC, 2014; 210–217.
13. Crum CP, McCluggage WG, Herrington CS, Regauer S, Wilkinson EJ. Epithelial tumours. In Kurman RJ, Carcangiu ML, Herrington CS, Young RH eds. *World Health Organisation classification of tumours of female reproductive organs*. Lyon, France: IARC, 2014; 232–241.
14. Epstein JI, Algaba F. Squamous neoplasms. In Moch H, Humphrey PA, Ulbright TM, Reuter VE eds. *World Health Organisation classification of tumours of the urinary system and male genital organs*. Lyon, France: IARC, 2016; 170.
15. Yatabe Y, Nicholson AG, Brambilla E *et al.* Adenosquamous carcinoma. In Travis WD, Brambilla E, Burke AP, Marx A, Nicholson AG eds. *World Health Organisation classification of tumours of the lung, pleura, thymus and heart*. Lyon, France: IARC, 2015; 86–87.
16. Ishikawa Y, Dacic S, Alvarez-Fernandez E, Nicholson AG, Aubry MC. Mucoepidermoid carcinoma. In Travis WD, Brambilla E, Burke AP, Marx A, Nicholson AG eds. *World Health Organisation classification of tumours of the lung, pleura, thymus and heart*. Lyon, France: IARC, 2015; 99–100.
17. Matsuno Y, Marom EM, Chan JKC, Wick M, Detterbeck F. Mucoepidermoid carcinoma. In Travis WD, Brambilla E, Burke AP, Marx A, Nicholson AG eds. *World Health Organisation classification of tumours of the lung, pleura, thymus and heart*. Lyon, France: IARC, 2015; 218–219.
18. Nonaka D, Tateyama H. Other rare thymic carcinomas. In Travis WD, Brambilla E, Burke AP, Marx A, Nicholson AG eds. *World Health Organisation classification of tumours of the lung, pleura, thymus and heart*. Lyon, France: IARC, 2015; 233.

19. Brandwein-Gensler M, Bell D, Inagaki H *et al.* Mucoepidermoid carcinoma. In El-Naggar AK, Chan JKC, Grandis JR, Takata T, Slootweg PJ eds. *World Health Organisation classification of head and neck tumours*. Lyon, France: IARC, 2017; 163–164.
20. Michal M, Michal M, Miesbauerova M, Hercogova J, Skopalikova B, Kazakov DV. Penile analogue of stratified mucin-producing intraepithelial lesion of the cervix: the first described case. A diagnostic pitfall. *Am. J. Dermatopathol.* 2016; **38**; e64–e67.
21. Park JJ, Sun D, Quade BJ *et al.* Stratified mucin-producing intraepithelial lesions of the cervix: adenosquamous or columnar cell neoplasia? *Am. J. Surg. Pathol.* 2000; **24**; 1414–1419.
22. Boyle DP, McCluggage WG. Stratified mucin-producing intraepithelial lesion (SMILE): report of a case series with associated pathological findings. *Histopathology* 2015; **66**; 658–663.
23. Lastra RR, Park KJ, Schoolmeester JK. Invasive stratified mucin-producing carcinoma and stratified mucin-producing intraepithelial lesion (smile): 15 cases presenting a spectrum of cervical neoplasia with description of a distinctive variant of invasive adenocarcinoma. *Am. J. Surg. Pathol.* 2016; **40**; 262–269.
24. Onishi J, Sato Y, Sawaguchi A *et al.* Stratified mucin-producing intraepithelial lesion with invasive carcinoma: 12 cases with immunohistochemical and ultrastructural findings. *Hum. Pathol.* 2016; **55**; 174–181.
25. Antonescu CR, Katabi N, Zhang L *et al.* EWSR1–ATF1 fusion is a novel and consistent finding in hyalinizing clear-cell carcinoma of salivary gland. *Genes Chromosom. Cancer* 2011; **50**; 559–570.
26. Skalova A, Vanecek T, Simpson RH *et al.* CRTC1–MAML2 and CRTC3–MAML2 fusions were not detected in metaplastic Warthin tumour and metaplastic pleomorphic adenoma of salivary glands. *Am. J. Surg. Pathol.* 2013; **37**; 1743–1750.
27. Kazakov DV, Nemcova J, Mikyskova I, Belousova IE, Vazmitel M, Michal M. Human papillomavirus in lesions of anogenital mammary-like glands. *Int. J. Gynecol. Pathol.* 2007; **26**; 475–480.
28. Pettaway CA, Srigley JR, Brookland RK *et al.* Penis. In Amin MB (Editor-in-Chief), Edge SB, Greene FL *et al.* eds. *AJCC cancer staging manual*, 8th ed. New York: Springer, 2017; 701–714.
29. de Roda Husman AM, Walboomers JM, van den Brule AJ, Meijer CJ, Snijders PJ. The use of general primers GP5 and GP6 elongated at their 3′ ends with adjacent highly conserved sequences improves human papillomavirus detection by PCR. *J. Gen. Virol.* 1995; **76**; 1057–1062.
30. Tieben LM, ter Schegget J, Minnaar RP *et al.* Detection of cutaneous and genital HPV types in clinical samples by PCR using consensus primers. *J. Virol. Methods* 1993; **42**; 265–279.
31. Gregoire L, Cubilla AL, Reuter VE, Haas GP, Lancaster WD. Preferential association of human papillomavirus with high-grade histologic variants of penile-invasive squamous cell carcinoma. *J. Natl Cancer Inst.* 1995; **87**; 1705–1709.
32. Cubilla AL, Lloveras B, Alejo M *et al.* The basaloid cell is the best tissue marker for human papillomavirus in invasive penile squamous cell carcinoma: a study of 202 cases from paraguay. *Am. J. Surg. Pathol.* 2010; **34**; 104–114.
33. Velazquez EF, Moch H, Amin MB *et al.* Precursor lesions. In Moch H, Humphrey PA, Ulbright TM, Reuter VE eds. *World Health Organisation classification of tumours of the urinary system and male genital organs*. Lyon, France: IARC, 2016; 277–279.
34. Val-Bernal JF, Hernandez-Nieto E. Benign mucinous metaplasia of the penis. A lesion resembling extramammary Paget's disease. *J. Cutan. Pathol.* 2000; **27**; 76–79.
35. Fang AW, Whittaker MA, Theaker JM. Mucinous metaplasia of the penis. *Histopathology* 2002; **40**; 177–179.
36. Ruiz-Genao DP, Dauden-Tello E, Adrados M, Fraga J, Garcia-Diez A. Mucinous metaplasia of the glans penis. *Histopathology* 2004; **44**; 90–91.
37. Garcia-Abos M, Fraga J, Dauden E. Mucinous metaplasia of the penis associated with Zoon's balanitis. *Actas Dermosifiliogr* 2010; **101**; 362–364.
38. Boer-Auer A, August C, Falk TM, Jung JE, Kohl K, Metze D. Benign mucinous metaplasia of the genital mucosa: histomorphological and immunohistochemical features and criteria for differentiation from extramammary Paget disease. *Br. J. Dermatol.* 2011; **165**; 1263–1272.
39. Yoshii N, Kitajima S, Yonezawa S, Matsukita S, Setoyama M, Kanzaki T. Expression of mucin core proteins in extramammary Paget's disease. *Pathol. Int.* 2002; **52**; 390–399.
40. Velazquez EF, Barreto JE, Cubilla AL. Penis and distal urethra. In Mills SE ed. *Histology for pathologists*, 4th ed. China: Lippincott Williams & Wilkins, 2012; 1027–1042.
41. Salamanca J, Benito A, Garcia-Penalver C, Azorin D, Ballestin C, Rodriguez-Peralto JL. Paget's disease of the glans penis secondary to transitional cell carcinoma of the bladder: a report of two cases and review of the literature. *J. Cutan. Pathol.* 2004; **31**; 341–345.
42. Suzuki T, Togo Y, Yasuda K, Yamamoto H, Kokura K, Nagareda T. Prostatic duct adenocarcinoma with pagetoid spread on the glans penis: a case report. *Hinyokika kiyo Acta Urol. Jap.* 2006; **52**; 887–890.
43. Bishop JA, Taube JM, Su A *et al.* Secretory carcinoma of the skin harboring ETV6 gene fusions: a cutaneous analogue to secretory carcinomas of the breast and salivary glands. *Am. J. Surg. Pathol.* 2017; **41**; 62–66.

Supporting Information

Additional Supporting Information may be found in the online version of this article:

Table S1. The antibodies used for immunohistochemical analysis.

2.4. THE REST

2.4.1. ENDOMETRIAL ENDOMETRIOID CARCINOMA WITH LARGE CYSTIC GROWTH CONFIGURATION AND DECEPTIVE PATTERN OF INVASION ASSOCIATED WITH ABUNDANT NODULAR FASCIITIS-LIKE STROMA: A UNIQUE HITHERTO UNREPORTED HISTOLOGY IN ENDOMETRIOID CARCINOMA

This case report presented a case of an unusual endometrial endometrioid carcinoma occurring in a 67-year-old woman which was microscopically characterized by two components. The first consisted of broad zones of cytologically bland fibromyxoid stroma resembling nodular fasciitis, showing vaguely nodular architecture. The second component was represented by neoplastic glands that were characterized by interconnected elongated slit-like and large cystic profiles, mostly lined by flattened epithelium with variable squamous differentiation, whereas typical columnar endometrioid cells were only focally present. Voluminous nodules of the stroma produced phyllodes-like appearance of the tumor. The myofibroblastic proliferation was present throughout the tumor and the neoplastic glands showed anastomosing “large cystic” rather than “small cystic” profiles. Some of the neoplastic glands presented almost complete or complete squamous differentiation, with relatively bland-looking squamous cells and no hint of endometrioid differentiation, which resulted in initial misdiagnosis of Müllerian adenofibroma. We believe that nodular fasciitis-like pattern represents yet undescribed, and diagnostically challenging pattern of invasion in endometrial endometrioid carcinoma.

Endometrial Endometrioid Carcinoma With Large Cystic Growth Configuration and Deceptive Pattern of Invasion Associated With Abundant Nodular Fasciitis-like Stroma: A Unique Hitherto Unreported Histology in Endometrioid Carcinoma

Marián Švajdler, MD,† Michael Michal, MD,*† Pavol Dubinský, MD, PhD,‡ Peter Švajdler, MD,§ Ondrej Ondič, MD,*† and Michal Michal, MD*†*

Abstract: We describe a case of an unusual endometrial endometrioid carcinoma occurring in a 67-year-old woman. The tumor involved uterine corpus as well as lower uterine segment and presented as polypoid tumor protruding through the cervical orifice. Microscopically, the tumor was characterized by broad zones of cytologically bland fibromyxoid stroma resembling nodular fasciitis, showing vaguely nodular architecture. Neoplastic glands were characterized by interconnected elongated slit-like and large cystic profiles, mostly lined by flattened epithelium with variable squamous differentiation, whereas typical columnar endometrioid cells were only focally present. Voluminous nodules of the stroma produced phyllodes-like appearance of the tumor. The tumor showed some resemblance to the microcystic, elongated, and fragmented (MELF) glands growth pattern, but in contrast with MELF pattern, where fibromyxoid change occurs focally, in the presented case abundant myofibroblastic proliferation was present throughout the tumor and the neoplastic glands showed anastomosing "large cystic" rather than "small cystic" profiles. Some of the neoplastic glands presented almost complete or complete squamous differentiation, with relatively bland-looking squamous cells and no hint of endometrioid differentiation, which resulted in initial misdiagnosis of Müllerian adenofibroma. We believe that nodular fasciitis-like pattern represents yet undescribed, and diagnostically challenging pattern of invasion in endometrial endometrioid carcinoma.

Key Words: uterus, endometrioid carcinoma, large cysts, fibromyxoid stroma, nodular fasciitis-like, MELF

(*Adv Anat Pathol* 2016;23:381–384)

CASE ID AND SOURCE

The case was circulated in the standard AMR Seminar #67 (case number 11, contributed by Michal Michal).

CLINICAL HISTORY

A 67-year-old woman presented with postmenopausal uterine bleeding. Clinical examination revealed a polypoid tumor of the uterine cervix protruding through the cervical orifice. Diagnostic biopsy was performed at another institution and was interpreted as cervical Müllerian adenofibroma. Abdominal hysterectomy and bilateral adnexectomy was performed.

PATHOLOGIC FINDINGS

Gross Features and Conventional Microscopic Examination

Hysterectomy specimen showed markedly enlarged and dilated lower uterine segment and cervical canal filled by a polypoid firm solid white tumor, measuring $10.0 \times 7.5 \times 8.5$ cm. The tumor partly protruded through the cervical orifice. In the uterine corpus, just proximally and in continuity with the above described polypoid mass, there was a much softer tan exophytic tumorous mass, measuring $3.5 \times 3.0 \times 1.5$ cm, macroscopically invading more than one half of myometrium and reaching 3 mm under the serous surface. The adnexa were found to be normal.

Histologically, sections from the upper portion of the tumor (from the uterine corpus) and some parts of the polypoid mass in the lower uterine segment showed classic well-differentiated endometrioid endometrial adenocarcinoma, with broad front (pushing) pattern of myoinvasion and none to minimal stromal reaction (Fig. 1A). Most of the tumor in the lower uterine segment and the cervix showed, however, completely different growth pattern. This was characterized by large zones of fibromyxoid stroma reminiscent of nodular fasciitis, showing vaguely nodular architecture, variable cellularity, myxoid change, and collagen deposition (Fig. 1B). Focally, voluminous nodules of the stroma produced phyllodes-like appearance of the tumor (Fig. 1C). Cells of the stromal component were plump and spindle shaped, but bland looking, lacking nuclear atypia, pleomorphism, or mitotic activity (Fig. 1D).

Neoplastic glands were characterized by interconnected elongated slit-like (Fig. 2A) or large cystic profiles (Fig. 2B), mostly lined by flattened epithelium with variable squamous differentiation. However, typical columnar endometrioid cells were focally present (Fig. 2C). Some glands showed almost complete or complete squamous differentiation, with relatively bland-looking squamous cells and no hint of endometrioid differentiation (Fig. 2D). Importantly, fragmentation of neoplastic glands into small cell clusters or single cells, typical of microcystic, elongated, and fragmented (MELF) pattern, was not present. Vascular invasion was not found.

From the *Šikl's Department of Pathology, The Faculty of Medicine and Faculty Hospital in Pilsen, Charles University, Prague; †Bioptická laboratoř, s.r.o., Pilsen, Czech Republic ; ‡Department of Radiation Oncology, Oncology Institute; and §Department of Pathology, Louis Pasteur University Hospital, Košice, Slovakia.

The authors have no NIH funding or conflicts of interest to disclose.

Reprints: Marián Švajdler, MD, Bioptická laboratoř, s.r.o., Mikulášske nám. 4, 326 00 Pilsen, Czech Republic (e-mail: svajdler@yahoo.com).

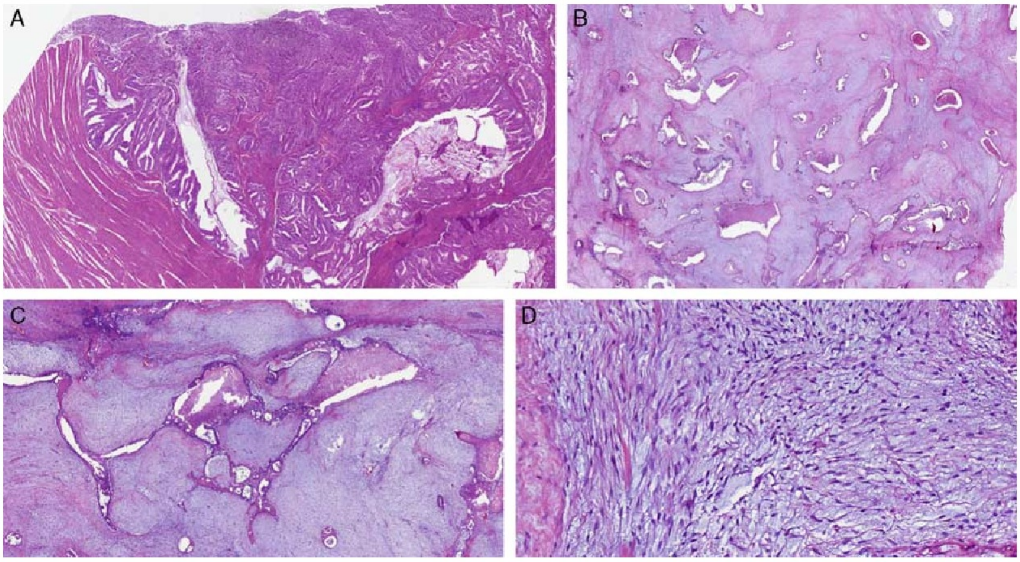

FIGURE 1. A, Broad front (pushing) myoinvasion of the well-differentiated endometrioid adenocarcinoma showing minimal stromal reaction. B, Large zones of fibromyxoid stroma, showing vaguely nodular architecture. Note the peculiar anastomosing elongated and large cystic profiles of neoplastic glands. C, Voluminous nodules of the myxoid stroma imparting phyllodes-like appearance to the tumor. D, High-power view demonstrating bland fibroblasts of the stromal component, set in a loose myxoid matrix. This picture is indistinguishable from that seen in nodular fasciitis.

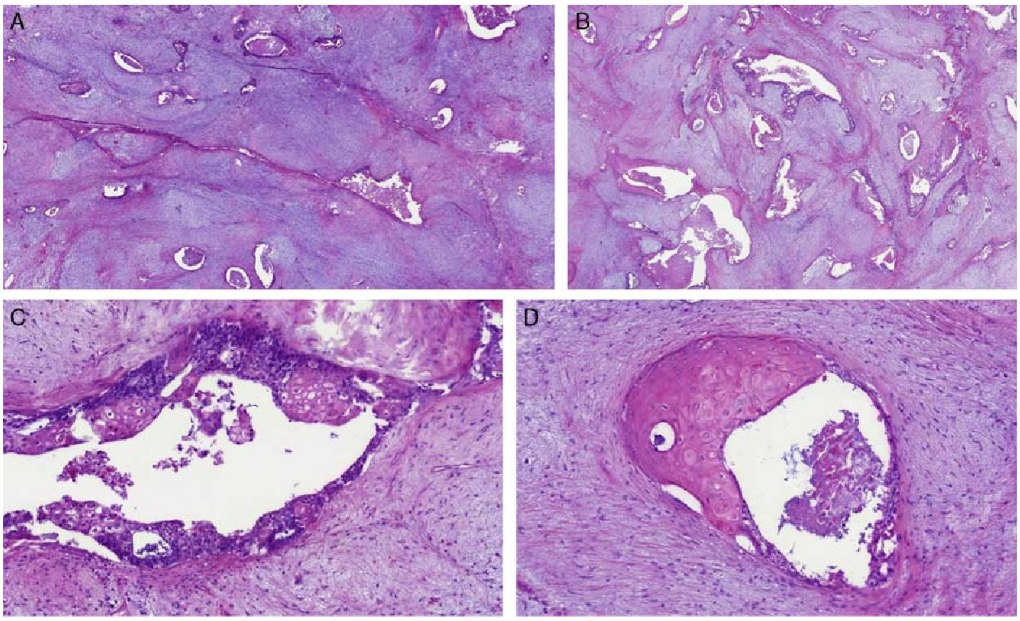

FIGURE 2. A, Interconnected elongated slit-like gland profiles with attenuated epithelium and squamous differentiation. B, Neoplastic glands forming large and anastomosing cystic profiles. C, Columnar endometrioid cells were at least focally present in some glands. D, Neoplastic gland showing attenuated epithelium and almost complete squamous differentiation and no hint of endometrioid differentiation. Note the bland appearance of the squamous cells.

Special Studies

Immunohistochemically, neoplastic glands were p16 negative, estrogen and progesterone receptor positive, and showed retained expression of the DNA mismatch repair proteins (MLH, PMS2, MSH2, and MSH6). Squamous nests showed p63 expression. Stromal component was characterized by focal expression of smooth muscle actin and CD10, and by negative expression of cytokeratins (AE1/AE3), EMA, p63, desmin, h-caldesmon, hormone receptors, S100 protein, myogenin, and β-catenin. Proliferation index of the stromal component was very low (< 1% of Mib-1-positive cells).

DIAGNOSIS

Endometrial endometrioid carcinoma (EEC) with nodular fasciitis-like stroma and large cystic growth pattern.

COMMENTS

Five different patterns of endometrioid endometrial adenocarcinoma (EEC) myoinvasion have been described so far, including "traditional" diffusely infiltrating, broad front, adenoma malignum, adenomyosis-like, and MELF pattern. Each of these patterns can cause diagnostic problems, especially when assessing depth of invasion of EEC.[1–3] Moreover EEC may have a variety of unusual appearances that can cause problems in differential diagnosis. These patterns include sertoliform endometrial adenocarcinoma,[4] endometrioid carcinoma with prominent spindle-cell component,[5] low-grade metaplastic adenocarcinoma (low-grade Müllerian carcinosarcoma),[6] and "corded and hyalinized" endometrioid carcinoma.[7] Our case does not fit the description of any of the above-mentioned myoinvasive patterns or unusual morphologic variants of EEC, and we are not aware of any similar case of EEC reported in the literature so far. Presented lesion shows some resemblance to the MELF pattern, described first by Murray et al.[3] This pattern of myoinvasion is best appreciated at low power as a focal fibromyxoid change within the myometrium, usually along the leading edge of the tumor.[1,3] The glandular changes in MELF pattern were characterized by pseudopods of neoplastic epithelium that budded off typical glands of the endometrioid carcinoma, and when became detached, showed a degenerative phenomenon that took 3 major forms: (i) microcysts lined by cells that often had conspicuous eosinophilic cytoplasm and that sometimes appeared vaguely squamoid and that occasionally formed intraluminal tufts or were flattened; (ii) elongated structures with a compressed, sometimes slit-like lumen lined by cells that also often had conspicuous eosinophilic cytoplasm or were flattened and endothelial-like; and (iii) clusters of detached cells or individual cells sometimes lying in edematous or myxoid tissue. The lumens of microcysts and other epithelial-lined spaces of the tumor often contained neutrophils and occasionally eosinophils.[3] In contrast with MELF pattern, where fibromyxoid change occurs focally, in our case abundant myofibroblastic proliferation was present throughout the tumor, and showed vaguely nodular architecture. Histologically, this stromal component was identical to nodular fasciitis. Similar misleading phenomenon was described in a variant of thyroid papillary carcinoma, namely thyroid papillary carcinoma with exuberant nodular fasciitis-like stroma, described originally by Chan and colleagues.[8,9]

The pattern of glandular proliferation in the reported case was also quite different from typical changes seen in MELF pattern. Unlike in MELF pattern, neoplastic glands formed interconnected elongated or large cystic profiles, with resemblance to a phyllodes tumor of the breast. Fragmentation of the glands or single cells was not found. Another intriguing and potentially misleading feature was the presence of benign-looking glands showing almost complete or complete squamous differentiation, which were not diagnostic of EEC by itself. Eventually this resulted in the initial diagnosis of Müllerian adenofibroma.

Carcinosarcoma (malignant mixed Müllerian tumor) is the most important and the only differential diagnosis in this case. However, carcinosarcoma is typically composed of high-grade carcinomatous and sarcomatous elements (mostly a high-grade, nondescript spindle-cell sarcoma with frequent heterologous differentiation),[10] none of which were seen in our case. Very rarely, epithelial and stromal components of Müllerian carcinosarcoma may show low-grade features.[6] The stromal component of this low-grade carcinosarcoma appears to arise from epithelial cells through a metaplastic process, as a gradual transition between epithelial and stromal cells. Immunohistochemically, the cells of both components express cytokeratins.[6] Endometrioid carcinoma with prominent spindle-cell component, described first in the ovary, and probably closely related to the above-described low-grade carcinosarcoma, shows extensive spindle-cell component, which is intimately admixed with the glands. The nuclear features of the spindle cells and the glands are similar and spindle cells are keratin positive.[5,11] In contrast, the stromal component in our case showed keratin negativity, was morphologically distinct from the glandular component, and showed no zones of transition from the glands. We believe that the nodular fasciitis-like stroma in the reported case is non-neoplastic and reactive phenomenon in its nature.

We have reported a rare case of EEC showing yet undescribed, and diagnostically challenging growth pattern, characterized by prominent nodular fasciitis-like stroma, elongated slit-like, and large cystic proliferation of neoplastic glands resembling phyllodes tumor, and foci of very bland squamous differentiation.

FOLLOW-UP

The patient died of surgical complications 1 month after the surgery. She did not receive any oncological treatment.

CLUB MEMBERS' ANONYMOUS OPINIONS

- Thank you for sharing this unique and interesting case, Michal. At first glance, I thought the stroma is somewhat inherent to the tumor suggesting a biphasic pattern as seen in Müllerian adenosarcomas, etc. The spatial relationship between the epithelial and stromal component in this case seems unique. The endometrioid component is clear-cut and squamoid differentiation prominent, so the case is unique in several aspects including site.
- Endometrioid adenocarcinoma of the uterus with minimally atypical, copious myxoid stroma. To me, the myxoid stroma is not quite the same as myxoid nodular fasciitis or the nodular fasciitis-like stroma of some papillary thyroid carcinomas or the occasional metaplastic breast carcinoma, which can almost exactly

mimic nodular fasciitis except that the spindle cells are keratin positive. On the other hand, I agree that it is not a malignant mixed Mullerian tumor. I will be very interested to hear what other club members think. I do not think I have seen a tumor quite like this before.

- This epithelial tumor is very squamous looking. The myxoid stroma is impressive but while on its own it is on the bland side, it otherwise seems to merge with the epithelium. By Occam's razor I would think of mixed Mullerian, but I can't deny the logic of Michal's diagnosis.
- I found the endometrial carcinoma very subtle, at least on my slide, mostly I have squamous metaplasia. I wasn't so convinced the stroma was benign and was concerned for MMMT.
- I agree, the stroma looks myofibroblastic/reactive to me.
- Agree with diagnosis. I was trying to make this into a peculiar MMMT but I like the idea of fasciitis-like stroma.
- This diagnosis seems very plausible Michal, since the MMMTs usually have high-grade carcinoma and sarcoma. Thank you, I have not seen this entity before neither in uterus nor thyroid.
- The stroma has a peculiar appearance, it shows myxoid nodules pushing the glandular structures like in fibroadenoma and some odontogenic tumors. Could it represent a biphasic neoplasm of the family of mixed Mullerian tumors? There are adenofibromas, carcinosarcomas etc. The name could be carcinofibroma.
- Seems like a plausible but rare explanation.
- Quite remarkable loose, spindle-cell stroma which suggests at a glance a biphasic neoplasm. Squamous morulae are also prominent. Great case, Michal, as always!
- Thank you for sharing this case. To me it's possible to observe this stromal reaction in a wide set of tumors; first of all I remember the papillary thyroid carcinoma with exuberant nodular fasciitis-like stroma.
- Important for the differential diagnosis with a sarcoma.
- Endometrioid adenocarcinoma of the uterus, with fasciitis-like stroma. This is a fascinating and rare case. I do not understand if there can be a relation with low-grade Mullerian carcinosarcoma affecting the uterus (Michal published a case in *Ann Diagn Pathol.* 2005;9(6):335–339).
- I agree endometrioid adenocarcinoma with fasciitis-like stroma. I have never seen it before. There are no atypia and no mitotic figures.
- Carcinoma with fasciitis-like stroma is a great idea, provided the spindle cells are keratin/p63 negative.
- I think that cases in which the fasciitis-like stroma is predominant are very difficult.
- Has a weird "adamantinoid" appearance with squamous differentiation and tooth matrix-like stroma. Very unique as a uterine tumor. Even wondered if this was the right slide (but it was numbered AMR67 Case 11).
- This is really fascinating with this strange stroma.
- I cannot relieve myself from the possibility of the stromal component being neoplastic, albeit low grade. Clonality analysis—HUMARA?
- Very interesting case, Michal. The stromal component type fasciitis is benign and even a cartilaginous component is seen in my slide.
- Very interesting case. I'm really out of my element here but I think there are a couple of possibilities besides the suggested diagnosis of endometrioid adenocarcinoma with fasciitis-like stroma. Some of the more myxoid lobules look neoplastic to me, not just reactive, so it may be some sort of MMMT, but the stroma looks much lower grade than usual. I also wondered if the lesion could be metastatic. Since metastatic lesions frequently cause desmoplastic stroma, is it possible that the adenocarcinoma metastasized from somewhere else? That would be in keeping with cases 3 and 5, which would be ironic if true.
- I was not aware of this variant of endometrioid carcinoma with fasciitis-like stroma. Thank you!
- Not familiar with this phenomenon in endometrial carcinoma—but I don't see much GYN pathology to begin with!
- Thank you for this unusual case.

REFERENCES

1. Cole AJ, Quick CM. Patterns of myoinvasion in endometrial adenocarcinoma: recognition and implications. *Adv Anat Pathol*. 2013;20:141–147.
2. Zaino RJ. Unusual patterns of endometrial carcinoma including MELF and its relation to epithelial mesenchymal transition. *Int J Gynecol Pathol*. 2014;33:357–364.
3. Murray SK, Young RH, Scully RE. Unusual epithelial and stromal changes in myoinvasive endometrioid adenocarcinoma: a study of their frequency, associated diagnostic problems, and prognostic significance. *Int J Gynecol Pathol*. 2003;22:324–333.
4. Eichhorn JH, Young RH, Clement PB. Sertoliform endometrial adenocarcinoma: a study of four cases. *Int J Gynecol Pathol*. 1996;15:119–126.
5. Clement PB, Young RH. Endometrioid carcinoma of the uterine corpus: a review of its pathology with emphasis on recent advances and problematic aspects. *Adv Anat Pathol*. 2002;9:145–184.
6. Zamecnik M, Sokol L, Michal M. Low-grade metaplastic adenocarcinoma (carcinosarcoma) of the uterus: report of an unusual case. *Ann Diagn Pathol*. 2005;9:335–339.
7. Murray SK, Clement PB, Young RH. Endometrioid carcinomas of the uterine corpus with sex cord-like formations, hyalinization, and other unusual morphologic features: a report of 31 cases of a neoplasm that may be confused with carcinosarcoma and other uterine neoplasms. *Am J Surg Pathol*. 2005;29:157–166.
8. Chan JK, Carcangiu ML, Rosai J. Papillary carcinoma of thyroid with exuberant nodular fasciitis-like stroma. Report of three cases. *Am J Clin Pathol*. 1991;95:309–314.
9. Michal M, Chlumska A, Fakan F. Papillary carcinoma of thyroid with exuberant nodular fasciitis-like stroma. *Histopathology*. 1992;21:577–579.
10. Wells M, Oliva E, Palacios J, et al. Mixed epithelial and mesenchymal tumours. In: Kurman JR, Carcangiu ML, Herrington CS, You-ng RH, eds. *WHO Classification of Tumours of Female Reproductive Organs*. Lyon: IARC; 2014:148–152.
11. Tornos C, Silva EG, Ordonez NG, et al. Endometrioid carcinoma of the ovary with a prominent spindle-cell component, a source of diagnostic confusion: a report of 14 cases. *Am J Surg Pathol*. 1995;19:1343–1353.

CONCLUSION

This dissertation finalizes the postgraduate study of MUDr. Michael Michal. All the objectives were fulfilled over the course of the study. With the help of the colleagues, the student presented altogether 13 research papers as the first author and participated as a co-author on another 20 studies, all aimed at the use and correlation of IHC and molecular genetic methods in the diagnosis of tumors.

ACKNOWLEDGEMENTS

I would like to thank my supervisor Prof. MUDr. Alena Skalova for her help and assistance over the course of my postgraduate study. I would also like to thank to Prof. MUDr. Michal Michal and Prof. MUDr. Dmitry Kazakov, particularly for their help with my initial studies as well as to all my other colleagues that guide me through my pathology residency. I also very much appreciate the help and patience of my wife MUDr. Kveta Michalova, PhD and of the other members of my family. The acknowledments also goes to my alma mater for providing me with the chance to attend a well organized postgraduate study.

REFERENCES

1. Montgomery EA, Devaney KO, Giordano TJ, Weiss SW. Inflammatory myxohyaline tumor of distal extremities with virocyte or Reed-Sternberg-like cells: a distinctive lesion with features simulating inflammatory conditions, Hodgkin's disease, and various sarcomas. Mod Pathol 1998; 11, 384-391.
2. Michal M. Inflammatory myxoid tumor of the soft parts with bizarre giant cells. Pathol Res Pract 1998; 194, 529-533.
3. Meis-Kindblom JM, Kindblom LG. Acral myxoinflammatory fibroblastic sarcoma: a low-grade tumor of the hands and feet. Am J Surg Pathol 1998; 22, 911-924.
4. Sakaki M, Hirokawa M, Wakatsuki S, Sano T, Endo K, Fujii Y, et al. Acral myxoinflammatory fibroblastic sarcoma: a report of five cases and review of the literature. Virchows Arch 2003; 442, 25-30.
5. Hassanein AM, Atkinson SP, Al-Quran SZ, Jain SM, Reith JD. Acral myxoinflammatory fibroblastic sarcomas: are they all low-grade neoplasms? J Cutan Pathol 2008; 35, 186-191.
6. Laskin WB, Fetsch JF, Miettinen M. Myxoinflammatory fibroblastic sarcoma: a clinicopathologic analysis of 104 cases, with emphasis on predictors of outcome. Am J Surg Pathol 2014; 38, 1-12.
7. Hallor KH, Sciot R, Staaf J, Heidenblad M, Rydholm A, Bauer HC, et al. Two genetic pathways, t(1;10) and amplification of 3p11-12, in myxoinflammatory fibroblastic sarcoma, haemosiderotic fibrolipomatous tumour, and morphologically similar lesions. J Pathol 2009; 217, 716-727.
8. Zreik RT, Carter JM, Sukov WR, Ahrens WA, Fritchie KJ, Montgomery EA, et al. TGFBR3 and MGEA5 rearrangements are much more common in "hybrid" hemosiderotic fibrolipomatous tumor-myxoinflammatory fibroblastic sarcomas than in classical myxoinflammatory fibroblastic sarcomas: a morphological and fluorescence in situ hybridization study. Hum Pathol 2016; 53, 14-24.
9. Kao YC, Ranucci V, Zhang L, Sung YS, Athanasian EA, Swanson D, et al. Recurrent BRAF Gene Rearrangements in Myxoinflammatory Fibroblastic Sarcomas, but Not Hemosiderotic Fibrolipomatous Tumors. Am J Surg Pathol 2017; 41, 1456-1465.
10. Gaetke-Udager K, Yablon CM, Lucas DR, Morag Y. Myxoinflammatory fibroblastic sarcoma: spectrum of disease and imaging presentation. Skeletal Radiol 2016; 45, 347-356.
11. Carter JM, Sukov WR, Montgomery E, Goldblum JR, Billings SD, Fritchie KJ, et al. TGFBR3 and MGEA5 rearrangements in pleomorphic hyalinizing angiectatic tumors and the spectrum of related neoplasms. Am J Surg Pathol 2014; 38, 1182-1992.
12. Kazakov DV, Pavlovsky M, Mukensnabl P, Michal M. Pleomorphic hyalinizing angiectatic tumor with a sarcomatous component recurring as high-grade myxofibrosarcoma. Pathol Int 2007; 57, 281-284.
13. Capovilla M, Birembaut P. Primary cutaneous myxofibrosarcoma mimicking pleomorphic hyalinizing angiectatic tumor (PHAT): a potential diagnostic pitfall. Am J Dermatopathol 2006; 28, 276-277; author reply 277-278.
14. Val-Bernal JF, Mayorga M, Teran-Villagra N. Extracutaneous intravascular histiocytosis of the aortic valve: Report of two cases. Pathol Res Pract 2016; 212, 258-263.
15. Antonescu CR SB, Woodruff JM. AFIP atlas of tumor pathology (series 4): tumors of the peripheral nervous system. Silver Spring, Maryland: ARP Press, 2013.
16. McCarron KF, Goldblum JR. Plexiform neurofibroma with and without associated malignant peripheral nerve sheath tumor: a clinicopathologic and immunohistochemical analysis of 54 cases. Mod Pathol 1998; 11, 612-617.
17. Lazarus SS, Trombetta LD. Ultrastructural identification of a benign perineurial cell tumor. Cancer 1978; 41, 1823-1829.
18. Zamecnik M, Michal M. Malignant peripheral nerve sheath tumor with perineurial cell differentiation (malignant perineurioma). Pathol Int 1999; 49, 69-73.

19. Michal M, Fanburg-Smith JC, Lasota J, Fetsch JF, Lichy J, Miettinen M. Minute synovial sarcomas of the hands and feet: a clinicopathologic study of 21 tumors less than 1 cm. Am J Surg Pathol 2006; 30, 721-726.
20. Goldblum JR FA, Weiss SW. Enzinger and Weiss soft tissue tumors Elsevier Saunders, 2014.
21. Billings SD, Walsh SV, Fisher C, Nusrat A, Weiss SW, Folpe AL. Aberrant expression of tight junction-related proteins ZO-1, claudin-1 and occludin in synovial sarcoma: an immunohistochemical study with ultrastructural correlation. Mod Pathol 2004; 17, 141-149.
22. Fetsch JF, Miettinen M. Sclerosing perineurioma: a clinicopathologic study of 19 cases of a distinctive soft tissue lesion with a predilection for the fingers and palms of young adults. Am J Surg Pathol 1997; 21, 1433-1442.
23. Feany MB, Anthony DC, Fletcher CD. Nerve sheath tumours with hybrid features of neurofibroma and schwannoma: a conceptual challenge. Histopathology 1998; 32, 405-410.
24. Hirose T, Tani T, Shimada T, Ishizawa K, Shimada S, Sano T. Immunohistochemical demonstration of EMA/Glut1-positive perineurial cells and CD34-positive fibroblastic cells in peripheral nerve sheath tumors. Mod Pathol 2003; 16, 293-298.
25. Erlandson RA, Woodruff JM. Peripheral nerve sheath tumors: an electron microscopic study of 43 cases. Cancer 1982; 49, 273-287.
26. Hirose T, Sano T, Hizawa K. Ultrastructural localization of S-100 protein in neurofibroma. Acta Neuropathol 1986; 69, 103-110.
27. Creytens D, Mentzel T, Ferdinande L, Lecoutere E, van Gorp J, Atanesyan L, et al. "Atypical" Pleomorphic Lipomatous Tumor: A Clinicopathologic, Immunohistochemical and Molecular Study of 21 Cases, Emphasizing its Relationship to Atypical Spindle Cell Lipomatous Tumor and Suggesting a Morphologic Spectrum (Atypical Spindle Cell/Pleomorphic Lipomatous Tumor). Am J Surg Pathol 2017; 41, 1443-1455.
28. Kao YC, Flucke U, Eijkelenboom A, Zhang L, Sung YS, Suurmeijer AJH, et al. Novel EWSR1-SMAD3 Gene Fusions in a Group of Acral Fibroblastic Spindle Cell Neoplasms. Am J Surg Pathol 2018; 42, 522-528.
29. Boyle DP, McCluggage WG. Stratified mucin-producing intraepithelial lesion (SMILE): report of a case series with associated pathological findings. Histopathology 2015; 66, 658-663.
30. McCluggage WG, Jamison J, Boyde A, Ganesan R. Vulval intraepithelial neoplasia with mucinous differentiation: report of 2 cases of a hitherto undescribed phenomenon. Am J Surg Pathol 2009; 33, 945-949.
31. Monda L, Warnke R, Rosai J. A primary lymph node malignancy with features suggestive of dendritic reticulum cell differentiation. A report of 4 cases. Am J Pathol 1986; 122, 562-572.
32. Perez-Ordonez B, Erlandson RA, Rosai J. Follicular dendritic cell tumor: report of 13 additional cases of a distinctive entity. Am J Surg Pathol 1996; 20, 944-955.
33. Raymond I, Al Saati T, Tkaczuk J, Chittal S, Delsol G. CNA.42, a new monoclonal antibody directed against a fixative-resistant antigen of follicular dendritic reticulum cells. Am J Pathol 1997; 151, 1577-1585.
34. Chan JK, Fletcher CD, Nayler SJ, Cooper K. Follicular dendritic cell sarcoma. Clinicopathologic analysis of 17 cases suggesting a malignant potential higher than currently recognized. Cancer 1997; 79, 294-313.
35. Soriano AO, Thompson MA, Admirand JH, Fayad LE, Rodriguez AM, Romaguera JE, et al. Follicular dendritic cell sarcoma: a report of 14 cases and a review of the literature. Am J Hematol 2007; 82, 725-728.
36. Pang J, Mydlarz WK, Gooi Z, Waters KM, Bishop J, Sciubba JJ, et al. Follicular dendritic cell sarcoma of the head and neck: Case report, literature review, and pooled analysis of 97 cases. Head Neck 2016; 38 Suppl 1, E2241-2249.

37. Perez-Ordonez B, Rosai J. Follicular dendritic cell tumor: review of the entity. Semin Diagn Pathol 1998; 15, 144-154.
38. Pai VD, Desai S, Desouza A, Saklani AP. Extranodal follicular dendritic cell sarcoma: a frequently misdiagnosed entity. J Postgrad Med 2015; 61, 55-56.
39. Bisceglia M, Sickel JZ, Giangaspero F, Gomes V, Amini M, Michal M. Littoral cell angioma of the spleen: an additional report of four cases with emphasis on the association with visceral organ cancers. Tumori 1998; 84, 595-599.
40. Chung EB, Enzinger FM. Infantile myofibromatosis. Cancer 1981; 48, 1807-1818.
41. Oudijk L, den Bakker MA, Hop WC, Cohen M, Charles AK, Alaggio R, et al. Solitary, multifocal and generalized myofibromas: clinicopathological and immunohistochemical features of 114 cases. Histopathology 2012; 60, E1-11.
42. Cheung YH, Gayden T, Campeau PM, LeDuc CA, Russo D, Nguyen VH, et al. A recurrent PDGFRB mutation causes familial infantile myofibromatosis. Am J Hum Genet 2013; 92, 996-1000.
43. Linhares ND, Freire MC, Cardenas RG, Bahia M, Puzenat E, Aubin F, et al. Modulation of expressivity in PDGFRB-related infantile myofibromatosis: a role for PTPRG? Genet Mol Res 2014; 13, 6287-6292.
44. Martignetti JA, Tian L, Li D, Ramirez MC, Camacho-Vanegas O, Camacho SC, et al. Mutations in PDGFRB cause autosomal-dominant infantile myofibromatosis. Am J Hum Genet 2013; 92, 1001-1007.
45. Hung YP, Fletcher CDM. Myopericytomatosis: Clinicopathologic Analysis of 11 Cases With Molecular Identification of Recurrent PDGFRB Alterations in Myopericytomatosis and Myopericytoma. Am J Surg Pathol 2017; 41, 1034-1044.
46. Chen BJ, Marino-Enriquez A, Fletcher CD, Hornick JL. Loss of retinoblastoma protein expression in spindle cell/pleomorphic lipomas and cytogenetically related tumors: an immunohistochemical study with diagnostic implications. Am J Surg Pathol 2012; 36, 1119-1128.
47. Howitt BE, Fletcher CD. Mammary-type Myofibroblastoma: Clinicopathologic Characterization in a Series of 143 Cases. Am J Surg Pathol 2016; 40, 361-367.
48. Iwasa Y, Fletcher CD. Cellular angiofibroma: clinicopathologic and immunohistochemical analysis of 51 cases. Am J Surg Pathol 2004; 28, 1426-1435.
49. Folpe AL, Fanburg-Smith JC, Billings SD, Bisceglia M, Bertoni F, Cho JY, et al. Most osteomalacia-associated mesenchymal tumors are a single histopathologic entity: an analysis of 32 cases and a comprehensive review of the literature. Am J Surg Pathol 2004; 28, 1-30.
50. Lee JC, Jeng YM, Su SY, Wu CT, Tsai KS, Lee CH, et al. Identification of a novel FN1-FGFR1 genetic fusion as a frequent event in phosphaturic mesenchymal tumour. J Pathol 2015; 235, 539-545.
51. Lee JC, Su SY, Changou CA, Yang RS, Tsai KS, Collins MT, et al. Characterization of FN1-FGFR1 and novel FN1-FGF1 fusion genes in a large series of phosphaturic mesenchymal tumors. Mod Pathol 2016; 29, 1335-1346.
52. Shon W, Folpe AL, Fritchie KJ. ERG expression in chondrogenic bone and soft tissue tumours. J Clin Pathol 2015; 68, 125-129.
53. Coindre JM, Mariani O, Chibon F, Mairal A, De Saint Aubain Somerhausen N, Favre-Guillevin E, et al. Most malignant fibrous histiocytomas developed in the retroperitoneum are dedifferentiated liposarcomas: a review of 25 cases initially diagnosed as malignant fibrous histiocytoma. Mod Pathol 2003; 16, 256-262.
54. Thway K, Jones RL, Noujaim J, Zaidi S, Miah AB, Fisher C. Dedifferentiated Liposarcoma: Updates on Morphology, Genetics, and Therapeutic Strategies. Adv Anat Pathol 2016; 23, 30-40.
55. Agaimy A, Daum O, Markl B, Lichtmannegger I, Michal M, Hartmann A. SWI/SNF Complex-deficient Undifferentiated/Rhabdoid Carcinomas of the Gastrointestinal Tract: A Series of 13 Cases Highlighting Mutually Exclusive Loss of SMARCA4 and SMARCA2 and Frequent Co-inactivation of SMARCB1 and SMARCA2. Am J Surg Pathol 2016; 40, 544-553.

56. Hoffman A, Lazar AJ, Pollock RE, Lev D. New frontiers in the treatment of liposarcoma, a therapeutically resistant malignant cohort. Drug Resist Updat 2011; 14, 52-66.
57. Makise N, Yoshida A, Komiyama M, Nakatani F, Yonemori K, Kawai A, et al. Dedifferentiated Liposarcoma With Epithelioid/Epithelial Features. Am J Surg Pathol 2017; 41, 1523-1531.
58. Doyle LA, Marino-Enriquez A, Fletcher CD, Hornick JL. ALK rearrangement and overexpression in epithelioid fibrous histiocytoma. Mod Pathol 2015; 28, 904-912.
59. Jedrych J, Nikiforova M, Kennedy TF, Ho J. Epithelioid cell histiocytoma of the skin with clonal ALK gene rearrangement resulting in VCL-ALK and SQSTM1-ALK gene fusions. Br J Dermatol 2015; 172, 1427-1429.
60. Dickson BC, Swanson D, Charames GS, Fletcher CD, Hornick JL. Epithelioid fibrous histiocytoma: molecular characterization of ALK fusion partners in 23 cases. Mod Pathol 2018.
61. Skalova A, Vanecek T, Sima R, Laco J, Weinreb I, Perez-Ordonez B, et al. Mammary analogue secretory carcinoma of salivary glands, containing the ETV6-NTRK3 fusion gene: a hitherto undescribed salivary gland tumor entity. Am J Surg Pathol 2010; 34, 599-608.
62. Skalova A, Vanecek T, Simpson RH, Laco J, Majewska H, Baneckova M, et al. Mammary Analogue Secretory Carcinoma of Salivary Glands: Molecular Analysis of 25 ETV6 Gene Rearranged Tumors With Lack of Detection of Classical ETV6-NTRK3 Fusion Transcript by Standard RT-PCR: Report of 4 Cases Harboring ETV6-X Gene Fusion. Am J Surg Pathol 2016; 40, 3-13.
63. Skalova A, Vanecek T, Martinek P, Weinreb I, Stevens TM, Simpson RHW, et al. Molecular Profiling of Mammary Analog Secretory Carcinoma Revealed a Subset of Tumors Harboring a Novel ETV6-RET Translocation: Report of 10 Cases. Am J Surg Pathol 2018; 42, 234-246.
64. Rooper LM, Karantanos T, Ning Y, Bishop JA, Gordon SW, Kang H. Salivary Secretory Carcinoma With a Novel ETV6-MET Fusion: Expanding the Molecular Spectrum of a Recently Described Entity. Am J Surg Pathol 2018.
65. Dogan S, Wang L, Ptashkin RN, Dawson RR, Shah JP, Sherman EJ, et al. Mammary analog secretory carcinoma of the thyroid gland: A primary thyroid adenocarcinoma harboring ETV6-NTRK3 fusion. Mod Pathol 2016; 29, 985-995.
66. Leeman-Neill RJ, Kelly LM, Liu P, Brenner AV, Little MP, Bogdanova TI, et al. ETV6-NTRK3 is a common chromosomal rearrangement in radiation-associated thyroid cancer. Cancer 2014; 120, 799-807.
67. Bishop JA, Taube JM, Su A, Binder SW, Kazakov DV, Michal M, et al. Secretory Carcinoma of the Skin Harboring ETV6 Gene Fusions: A Cutaneous Analogue to Secretory Carcinomas of the Breast and Salivary Glands. Am J Surg Pathol 2017; 41, 62-66.
68. Andreasen S, Skalova A, Agaimy A, Bishop JA, Laco J, Leivo I, et al. ETV6 Gene Rearrangements Characterize a Morphologically Distinct Subset of Sinonasal Low-grade Non-intestinal-type Adenocarcinoma: A Novel Translocation-associated Carcinoma Restricted to the Sinonasal Tract. Am J Surg Pathol 2017; 41, 1552-1560.
69. Mengoli MC, Bonetti LR, Intersimone D, Fedeli F, Rossi G. Solid pseudopapillary tumor: a new tumor entity in the testis? Hum Pathol 2017; 62, 242-243.
70. Michal M, Hes O, Kazakov DV. Primary signet-ring stromal tumor of the testis. Virchows Arch 2005; 447, 107-110.
71. Lastra RR, Park KJ, Schoolmeester JK. Invasive Stratified Mucin-producing Carcinoma and Stratified Mucin-producing Intraepithelial Lesion (SMILE): 15 Cases Presenting a Spectrum of Cervical Neoplasia With Description of a Distinctive Variant of Invasive Adenocarcinoma. Am J Surg Pathol 2016; 40, 262-269.